frontiers | Research Topics

Tertiary lymphoid structures (TLS) in the tumor immune microenvironment

Edited by
Ying Ma and Hui Zhao

Published in
Frontiers in Immunology
Frontiers in Oncology

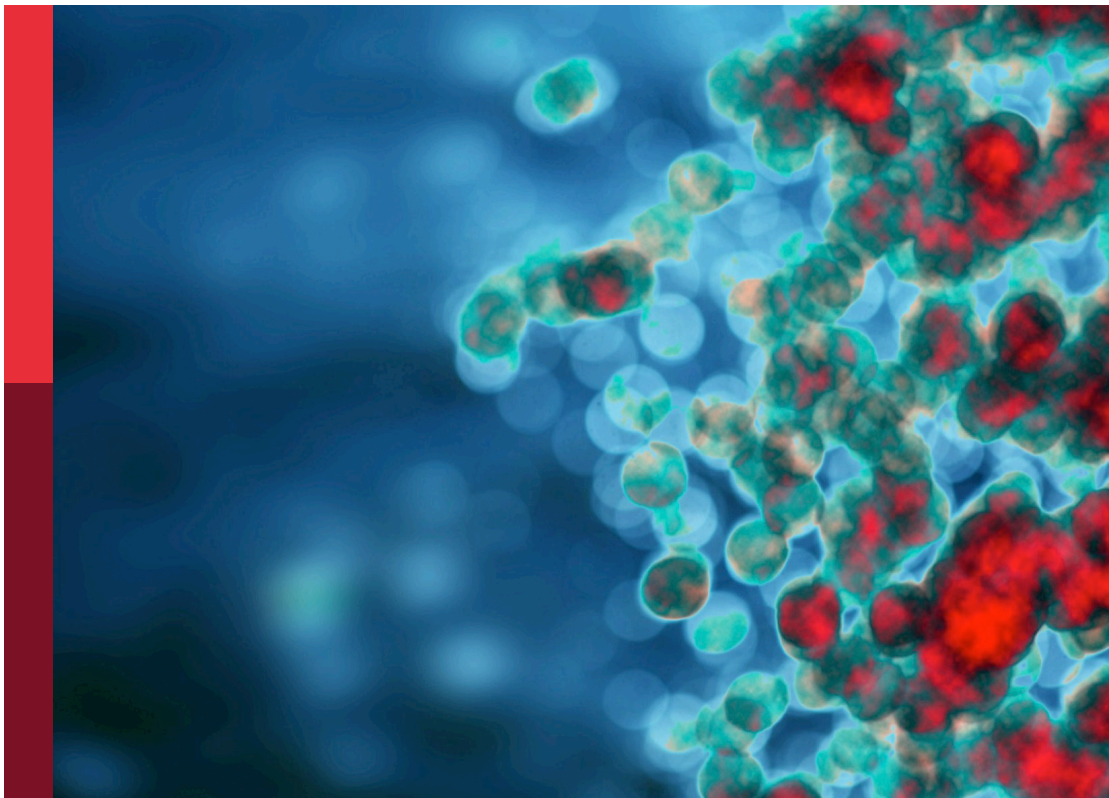

ISSN 1664-8714
ISBN 978-2-8325-5971-0
DOI 10.3389/978-2-8325-5971-0

About Frontiers

Frontiers is more than just an open access publisher of scholarly articles: it is a pioneering approach to the world of academia, radically improving the way scholarly research is managed. The grand vision of Frontiers is a world where all people have an equal opportunity to seek, share and generate knowledge. Frontiers provides immediate and permanent online open access to all its publications, but this alone is not enough to realize our grand goals.

Frontiers journal series

The Frontiers journal series is a multi-tier and interdisciplinary set of open-access, online journals, promising a paradigm shift from the current review, selection and dissemination processes in academic publishing. All Frontiers journals are driven by researchers for researchers; therefore, they constitute a service to the scholarly community. At the same time, the *Frontiers journal series* operates on a revolutionary invention, the tiered publishing system, initially addressing specific communities of scholars, and gradually climbing up to broader public understanding, thus serving the interests of the lay society, too.

Dedication to quality

Each Frontiers article is a landmark of the highest quality, thanks to genuinely collaborative interactions between authors and review editors, who include some of the world's best academicians. Research must be certified by peers before entering a stream of knowledge that may eventually reach the public - and shape society; therefore, Frontiers only applies the most rigorous and unbiased reviews. Frontiers revolutionizes research publishing by freely delivering the most outstanding research, evaluated with no bias from both the academic and social point of view. By applying the most advanced information technologies, Frontiers is catapulting scholarly publishing into a new generation.

What are Frontiers Research Topics?

Frontiers Research Topics are very popular trademarks of the *Frontiers journals series*: they are collections of at least ten articles, all centered on a particular subject. With their unique mix of varied contributions from Original Research to Review Articles, Frontiers Research Topics unify the most influential researchers, the latest key findings and historical advances in a hot research area.

Find out more on how to host your own Frontiers Research Topic or contribute to one as an author by contacting the Frontiers editorial office: frontiersin.org/about/contact

Tertiary lymphoid structures (TLS) in the tumor immune microenvironment

Topic editors

Ying Ma — Tianjin Medical University Cancer Institute and Hospital, China

Hui Zhao — University of Texas MD Anderson Cancer Center, United States

Citation

Ma, Y., Zhao, H., eds. (2025). *Tertiary lymphoid structures (TLS) in the tumor immune microenvironment*. Lausanne: Frontiers Media SA.

doi: 10.3389/978-2-8325-5971-0

Table of contents

frontiers | Frontiers in Immunology

TYPE Editorial
PUBLISHED 23 January 2025
DOI 10.3389/fimmu.2025.1555677

OPEN ACCESS

EDITED AND REVIEWED BY
Peter Brossart,
University of Bonn, Germany

*CORRESPONDENCE
Ying Ma
yingma@tmu.edu.cn;
yingma_maying@hotmail.com
Hui Zhao
huizhao_liu@yahoo.com;
huizhao@mdanderson.org

RECEIVED 05 January 2025
ACCEPTED 08 January 2025
PUBLISHED 23 January 2025

CITATION
Gao X, Zhao X, Li X, Zhang J, Zhao H and Ma Y (2025) Editorial: Tertiary lymphoid structures (TLS) in the tumor immune microenvironment.
Front. Immunol. 16:1555677.
doi: 10.3389/fimmu.2025.1555677

Editorial: Tertiary lymphoid structures (TLS) in the tumor immune microenvironment

Xinbo Gao[1], Xiangqin Zhao[1], Xuesong Li[2], Jin Zhang[3], Hui Zhao[4]* and Ying Ma[1]*

[1]Department of Pancreatic Cancer, Tianjin Medical University Cancer Institute and Hospital, National Clinical Research Center for Cancer, Tianjin's Clinical Research Center for Cancer, Tianjin Key Laboratory of Digestive Cancer, Key Laboratory of Cancer Prevention and Therapy, Tianjin, China, [2]Department of Pediatric Oncology, Shandong Cancer Hospital and Institute, Shandong First Medical University and Shandong Academy of Medical Sciences, Jinan, Shandong, China, [3]Department of Orthopedics, Nanjing First Hospital, Nanjing Medical University, Nanjing, Jiangsu, China, [4]Department of Health Services Research, The University of Texas MD Anderson Cancer Center, Houston, TX, United States

KEYWORDS

tertiary lymphoid structures (TLSs), tumor microenvironment (TME), immunotherapy, immune checkpoint inhibitors (ICI), solid tumors (ST), biomarkers, prognosis

Editorial on the Research Topic
Tertiary lymphoid structures (TLS) in the tumor immune microenvironment

Tertiary lymphoid structures (TLSs) (1, 2) are organized clusters of immune cells that develop within non-lymphoid tissues under specific conditions, including autoimmunity, chronic infections, and cancer. These structures resemble lymphoid follicles, typically featuring a core of B cells surrounded by T cells, along with dendritic cells, a supporting network of extracellular matrix, and specialized high endothelial venules facilitating lymphocyte entry. TLSs are thought to recruit and activate naive T and B cells within the tumor microenvironment (TME) via chemokine signaling, contributing significantly to the complex interplay of immune cells and tumor cells within the TME.

The TME in solid tumors comprises a complex ecosystem of tumor cells, stromal components, blood vessels, and immune cells. This environment plays a crucial role in tumor progression and its interaction with surrounding tissues. Tumor-infiltrating lymphocytes (TILs) exert a powerful influence within the TME, with cytotoxic TILs inhibiting tumor growth while certain suppressive or exhausted lymphocyte populations can promote it. TLS have been recognized as a significant source of TILs, and their presence often correlates with improved patient prognosis. However, our understanding of TLS function within the TME remains incomplete. Factors like TLS location, density, and maturity likely influence clinical outcomes, including survival and treatment response, across different cancer types. Furthermore, research into methods of manipulating TLS for therapeutic benefit is an area of active investigation, exploring their potential as immune niches to enhance existing and future cancer therapies. This Research Topic introduces a collection of articles in our Research Topic focused on TLS in solid tumors, exploring their anatomy, key features, immunological roles, and future research directions.

The fourteen articles in this Research Topic explore TLS across a range of solid tumors, including non-small cell lung cancer (Xu F. et al., Xin et al., Berthe et al., and Luo et al.), melanoma (Zhao et al.), gastrointestinal cancers (Yu et al.), colorectal cancer (Feng et al. and Xu Z. et al.), pancreatic adenocarcinoma (Gao et al.), cholangiocarcinoma (Shang et al.), and a meta-analysis across many types of solid tumors in 19 clinical trials (Jiang et al.). Several articles provide broader perspectives: You et al. and Ding et al. offer a comprehensive overview of TLS formation, maturation, localization, and heterogeneity, emphasizing the clinical implications of TLS heterogeneity in cancer patients. Zhao et al. elucidate the impact of immunogenic cell death-inducing chemotherapeutics on immune cell activation and TLS formation in melanoma.

These studies collectively highlight three key areas: the significance of TLS in predicting immunotherapy response and patient prognosis; the importance of assessing TLS maturity and density across different tissue types and spatial locations; and the crucial link between immune checkpoint pathways and TLS formation and maturation, with implications for understanding the mechanism of immune checkpoint inhibitors.

1 TLS in predicting immunotherapy response and patient prognosis

1.1 TLS and prognostic value in cholangiocarcinoma and pancreatic cancer

Cholangiocarcinoma (CCA), a malignancy of the biliary epithelium, carries a poor prognosis, hampered by the lack of reliable biomarkers for predicting treatment response and survival. Recognizing the role of tertiary lymphoid structures (TLS) as crucial microenvironments for anti-tumor immunity, Shang et al. investigated their prognostic value in a cohort of 471 CCA patients. Using H&E and immunohistochemical (IHC) staining to assess TLS maturity and composition, they observed varying degrees of TLS maturity and identified a four-gene signature (PAX5, TCL1A, TNFRSF13C, and CD79A) strongly expressed within TLS regions. High intratumoral TLS density correlated with improved overall survival (OS), while, interestingly, high peritumoral TLS density was associated with shorter OS. Similarly, a previous study (3) analyzed pancreatic cancer samples, identifying TLS-associated marker genes and developing a risk score model. This model stratified patients into high- and low-risk groups, with the low-risk group exhibiting increased immune cell infiltration and improved prognosis.

1.2 TLS in colorectal cancer: challenges and opportunities

While TLS are generally associated with favorable outcomes in several cancers, their role in colorectal cancer (CRC) is more nuanced. Although some studies have linked TLS presence to improved OS, progression-free survival (PFS), disease-free survival (DFS), and recurrence-free survival (RFS), Yu et al. highlight the lack of significant association between TLS and OS in CRC-specific subgroup analyses. This discrepancy may stem from the presence of pre-existing lymphoid tissues like GALT or Peyer's patches, which could be misidentified as TLS. This approach could potentially enhance the prognostic utility of TLS in CRC. Furthering this line of inquiry, Xu Z. et al. developed a 14-gene TLS-related prognostic risk model, validated in TCGA and GEO datasets. They identified TLS-related subclusters and characterized hub genes, including PRRX1, a potential immunomodulatory factor and therapeutic target, whose expression was elevated in the TLS-positive CRC group. Their work showcases the combined power of bioinformatics, IHC, and multiplex immunofluorescence (MIF) for characterizing TLS and identifying clinically relevant markers.

1.3 TLS in non-small cell lung cancer: prognostic value and immunotherapy

Non-small cell lung cancer (NSCLC) remains a leading cause of cancer-related death, and while immunotherapy offers promising treatment avenues, robust prognostic markers are needed. Xin et al. revealed TLS in the current landscape of NSCLC and emerging immunotherapy strategies. Focusing on neoadjuvant chemoimmunotherapy, Xu F. et al. identified the platelet-to-lymphocyte ratio (PLR) as an independent predictor of TLS expression, with lower PLR correlating with higher TLS levels. Both systemic immune-inflammation index (SII) and TLS were independent prognostic factors, with high TLS and low SII associated with improved prognosis. Combining SII and TLS provided greater prognostic accuracy than either alone. Berthe et al. developed a multiplex IF panel to evaluate TLS maturity in NSCLC, finding that TLS relative area and CD21 positivity were strong prognostic indicators. Their TLS scoring system, incorporating TLS relative area, B cell density, and CD21+CD23-FDC density, demonstrated significant prognostic value.

1.4 TLS in pancreatic ductal adenocarcinoma and the complexity of TLS characterization

Pancreatic ductal adenocarcinoma (PDAC) is a highly aggressive subtype of pancreatic cancer, characterized by an immunosuppressive TME that contributes to immunotherapy resistance. While immune checkpoint inhibitors (ICIs) have shown limited efficacy in PDAC, other immunotherapeutic approaches are under development. Interestingly, the density of small nerve fibers within TLS aggregates has been linked to improved OS in PDAC. The complex architecture of TLS, comprising diverse immune and stromal cell populations, is essential for effective anti-tumor immune responses. However, the lack of a standardized TLS definition and the variety of assessment methods (H&E, IHC, MIF, gene expression profiling) contribute to

variability in TLS classification and clinical interpretation. Characterizing TLS at a higher resolution, considering their functional, compositional, and spatial heterogeneity, is crucial for understanding their impact on patient survival.

2 TLS maturity and density across different tissue types and spatial locations

2.1 TLS formation, maturation, and characterization

TLS development is a multi-stage process involving fibroblast activation, immune cell recruitment, and maturation, as detailed by Gao et al. (4) Cytokines like IL-13, IL-17, and IL-22 play a role in the initial fibroblast priming by immune cells under inflammatory stress (5, 6). Histologically, TLS maturity was primarily distinguished by the presence or absence of germinal centers (GCs), crucial sites for B cell maturation and affinity maturation. Mature TLS, containing GCs, exhibit proliferating B cells, follicular dendritic cells (FDCs) expressing DC-LAMP, and markers like Ki67, AID, and BCL6. More recently, a three-tiered maturity model for lung cancer TLS has been proposed, classifying TLS as early (dense lymphocytic clusters without FDCs or GCs), intermediate ("primary follicle-like" with CD21 +CD23- FDCs), and mature ("secondary follicle-like" with GCs) (7). This model underscores the importance of B cell maturation and humoral immunity in anti-tumor responses. However, TLS definitions vary across studies, with some relying on basic histological examination (H&E staining) and markers like PNAd or Ki67 (8, 9), while others employ more rigorous characterization based on distinct T and B cell zones, FDCs, and high endothelial venules (HEVs) (10, 11). This lack of standardization highlights the need for consistent criteria for defining and classifying TLS maturity.

2.2 Spatial heterogeneity of TLS in NSCLC

Xin et al. investigated the spatial distribution of TLS in non-small cell lung cancer (NSCLC), dividing tumor samples into intratumoral (IT), invasive margin (IM), and peritumoral (PT) regions. They further categorized TLS as early (E-TLS) or follicular (F-TLS). TLS density and the proportion of F-TLS were highest in the IT region, decreasing towards the IM and PT regions. Surprisingly, lower E-TLS density in the IM region correlated with better prognosis, possibly due to the suppressive immune environment at the tumor margin inhibiting TLS maturation. The IM region also showed increased infiltration of B cells, T cells, cytotoxic T cells, and macrophages, potentially explaining the correlation between these cell types and E-TLS density. E-TLS density in the IM region and TNM stage emerged as independent prognostic factors.

2.3 Contrasting TLS distribution and prognostic significance

In contrast to the findings in NSCLC, Feng et al.'s immunotherapy response scoring model in colorectal cancer revealed a different pattern of TLS distribution and maturation. A higher proportion of patients with higher scores, based on TLS characteristics, was observed in the peritumoral region compared to the intratumoral region. This scoring system, incorporating TLS distribution, quantity, and maturity, positively correlated with immunotherapy efficacy. This highlights the context-dependent nature of TLS and its prognostic significance. Furthermore, the role of TLS can vary across cancer types. While increased intratumoral TLS density is often associated with improved outcomes in intrahepatic cholangiocarcinoma, studies in other liver cancers have reported conflicting results. Both for hepatocellular carcinoma, Finkin et al. suggested that intratumoral TLS (12) could promote tumor progression, while Li et al. (25) linked peritumoral TLS to better prognosis. Similar discrepancies exist in breast cancer, bladder cancer, and gastric cancer, emphasizing the functional heterogeneity of lymphoid aggregates and the need for refined criteria to define functional TLS.

2.4 Spatial distribution and functional significance of TLS in different cancer types

The maturation state and density of TLS vary based on tumor type and spatial location, leading to diverse prognostic implications. This spatial heterogeneity is further exemplified in melanoma, where increased peritumoral mature TLS density is associated with improved survival (13). In PDAC, TLS are more frequently found at the invasive margin than in the tumor core (14). While one study showed a predominance of peritumoral TLS in PDAC samples (8), a more recent study highlighted the enhanced maturity, immune cell infiltration, and pro-inflammatory profile of the less abundant intratumoral TLS, associating them with improved survival (8). The dense, fibrotic stroma characteristic of PDAC may necessitate the close proximity of TLS to tumor cells for effective anti-tumor activity (15–17). These findings underscore the complex interplay between TLS location, maturation, and the tumor microenvironment in shaping clinical outcomes. Further research is needed to fully elucidate the factors influencing TLS function and their relationship with tumor progression in different cancer types.

3 Link between immune checkpoint pathways and TLS

3.1 The interplay between immune checkpoints and TLS formation

Immune checkpoint inhibitors (ICIs) targeting pathways like PD-1/PD-L1 and CTLA-4/CD80 have shown promise in cancer

10.3389/fimmu.2025.1555677

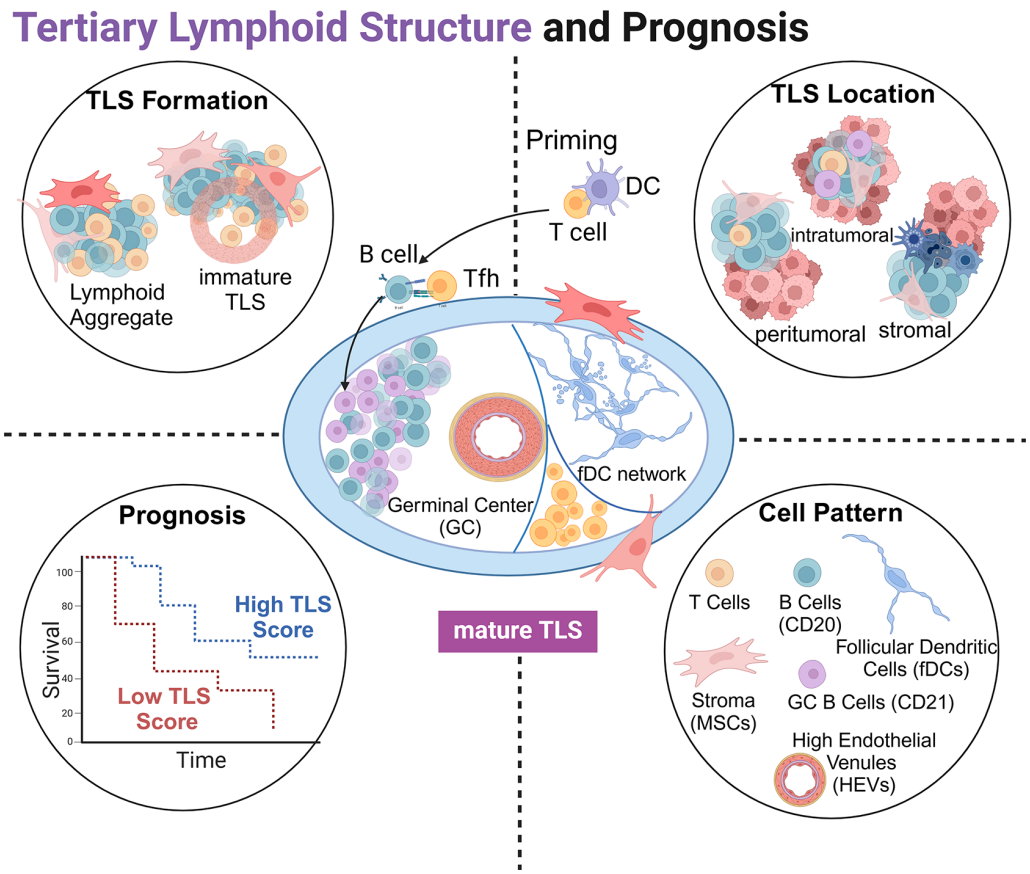

FIGURE 1
Schematic representation of tertiary lymphoid structures (TLSs): the structure of a mature TLS (center), the formation of TLS (top left), the relative positional relationship with tumor tissue (top right), TLS score with tumor prognosis (bottom left), and cell components involved in TLSs (bottom right).

treatment. Studies have linked TLS abundance and spatial distribution to ICI response in cholangiocarcinoma (CCA). A previous study (3) stratified pancreatic cancer patients into high- and low-risk groups based on TLS marker gene expression. The low-risk group exhibited higher expression of both co-stimulatory immune checkpoints (e.g., CD28, TNFRSF4, CTLA4, CD40LG, ICOSLG, LAG3, PDCD1, TIGIT) and the inhibitory checkpoint CD276. This suggests that patients with abundant and well-distributed TLS might respond more favorably to ICIs.

3.2 TLS as a predictive biomarker and target for ICI therapy

Feng et al.'s work supports the link between TLS and ICI response. TLS presence could predict anti-PD-1 immunotherapy response in various cancers, including esophageal carcinoma, bladder cancer, melanoma, and head and neck squamous cell carcinoma (HNSCC), and may even be a direct target of PD-1 blockade (18–20). The association between high PD-1 expression at the invasive margin and TLS presence further suggests that context-specific PD-1 targeting within the tumor microenvironment may enhance efficacy (21). Xu Z. et al. also discussed a positive correlation between TLS and PD-L1 expression in colorectal cancer (CRC). These findings, along with evidence linking TLS to improved outcomes and immunotherapy efficacy in melanoma and breast cancer (22, 23), suggest that TLS can convert "cold" tumors to "hot" by enhancing immune recognition and clearance (24). Furthermore, recent research suggests that combining immunotherapy with strategies to promote TLS formation or maturation could amplify treatment efficacy.

3.3 Mechanisms of ICI influence on TLS

The abundance and maturity of TLS reflect a patient's immune infiltration status, and ICIs have been shown to increase TLS abundance in several cancers. Ding et al. found that ICI response is linked to CXCL13-mediated recruitment of CXCR5+ B cells with high clonal diversity. Their *in vitro* data showed increased CXCL13 production in human peripheral blood mononuclear cells after anti-PD-1 treatment. This enhanced B cell infiltration and B cell receptor (BCR) diversity facilitates tumor antigen presentation, activating follicular helper CD4 T cells (Tfh) and tumor-reactive CD8 T cells. This influx of immune cells into the tumor microenvironment contributes to TLS abundance, maturation, and spatial organization.

In essence, one mechanism of ICI action involves promoting antigen presentation by CXCR5+ B cells to activate CD4+ and CD8+ T cells.

3.4 The role of HEVs and immune checkpoint ligands

Luo et al. 's research on NSCLC revealed another ICI mechanism related to high endothelial venules (HEVs). Mature HEVs facilitate CD8+ T cell trafficking into the tumor, but immune checkpoint ligands (ICLs) expressed on these HEVs can hinder this process. Their ICL total score model demonstrated that HEV ICL expression predicts both CD8+ T cell infiltration and patient survival, with higher scores indicating poorer infiltration and prognosis. This suggests that ICIs can restore the function of specialized vasculature within TLS, enabling lymphocyte delivery into the tumor microenvironment and supporting TLS formation.

4 Future directions and limitations

Further research with large, prospective cohorts is needed to validate these findings and address limitations of previous retrospective studies, such as limited sample sizes and potential biases. Future studies should also incorporate more immunotherapy subgroups and address the challenge of comprehensively assessing TLS across the entire tumor. Larger sample sizes will help provide robust prognostic data and minimize the influence of individual differences and geographic variation. These efforts will advance the understanding of the complex relationship between TLS and ICI therapy, paving the way for more effective cancer immunotherapies.

5 Summary

The articles in this Research Topic provide a meaningful overview of the crucial relationship between TLS and ICI immunotherapy, highlighting the clinical significance of TLS in promoting anti-tumor immunity and predicting its prognostic value in solid tumors (Figure 1). Future mechanistic studies are needed to further explore this complex interplay.

Author contributions

XG: Investigation, Writing – original draft. XZ: Writing – review & editing. XL: Writing – review & editing. JZ: Writing – review & editing. HZ: Investigation, Project administration, Supervision, Writing – review & editing. YM: Conceptualization, Funding acquisition, Investigation, Project administration, Supervision, Writing – review & editing.

Funding

The author(s) declare financial support was received for the research, authorship, and/or publication of this article. This research was funded by National Natural Science Foundation of China grants 82272767 and 82072691 to YM.

Acknowledgments

The authors thank their team members for discussion and cooperation. While using ChatGPT and Claude-3 for language editing, the authors carefully reviewed and validated the words and sentences generated by ChatGPT or Claude-3 before including them in the article.

Conflict of interest

The authors declare that the research was conducted in the absence of any commercial or financial relationships that could be construed as a potential conflict of interest.

Publisher's note

References

1. MacFawn IP, Magnon G, Gorecki G, Kunning S, Rashid R, Kaiza ME, et al. The activity of tertiary lymphoid structures in high grade serous ovarian cancer is governed by site, stroma, and cellular interactions. *Cancer Cell.* (2024) 42:1864–81. doi: 10.1016/j.ccell.2024.09.007

2. Ruffin AT, Cillo AR, Tabib T, Liu A, Onkar S, Kunning SR, et al. B cell signatures and tertiary lymphoid structures contribute to outcome in head and neck squamous cell carcinoma. *Nat Commun.* (2021) 12:3349. doi: 10.1038/s41467-021-23355-x

3. Ma Y, Li X, Zhang J, Zhao X, Lu Y, Shen G, et al. Integrating tertiary lymphoid structure-associated genes into computational models to evaluate prognostication and immune infiltration in pancreatic cancer. *J Leukoc Biol.* (2024) 116:589–600. doi: 10.1093/jleuko/qiae067

4. Gago da Graça C, van Baarsen LGM, Mebius RE. Tertiary lymphoid structures: diversity in their development, composition, and role. *J Immunol.* (2021) 206:273–81. doi: 10.4049/jimmunol.2000873

5. Pikor Natalia B, Astarita Jillian L, Summers-Deluca L, Galicia G, Qu J, Ward Lesley A, et al. Integration of th17- and lymphotoxin-derived signals initiates meningeal-resident stromal cell remodeling to propagate neuroinflammation. *Immunity.* (2015) 43:1160–73. doi: 10.1016/j.immuni.2015.11.010

6. Nayar S, Campos J, Smith CG, Iannizzotto V, Gardner DH, Mourcin F, et al. Immunofibroblasts are pivotal drivers of tertiary lymphoid structure formation and local pathology. *Proc Natl Acad Sci.* (2019) 116:13490–7. doi: 10.1073/pnas.1905301116

7. Posch F, Silina K, Leibl S, Mündlein A, Moch H, Siebenhüner A, et al. Maturation of tertiary lymphoid structures and recurrence of stage II and III colorectal cancer. *OncoImmunology*. (2017) 7:e1378844. doi: 10.1080/2162402X.2017.1378844

8. Hiraoka N, Ino Y, Yamazaki-Itoh R, Kanai Y, Kosuge T, Shimada K. Intratumoral tertiary lymphoid organ is a favourable prognosticator in patients with pancreatic cancer. *Br J Cancer*. (2015) 112:1782–90. doi: 10.1038/bjc.2015.145

9. Kuwabara S, Tsuchikawa T, Nakamura T, Hatanaka Y, Hatanaka KC, Sasaki K, et al. Prognostic relevance of tertiary lymphoid organs following neoadjuvant chemoradiotherapy in pancreatic ductal adenocarcinoma. *Cancer Science*. (2019) 110:1853–62. doi: 10.1111/cas.2019.110.issue-6

10. Delvecchio FR, Fincham REA, Spear S, Clear A, Roy-Luzarraga M, Balkwill FR, et al. Pancreatic cancer chemotherapy is potentiated by induction of tertiary lymphoid structures in mice. *Cell Mol Gastroenterol Hepatology*. (2021) 12:1543–65. doi: 10.1016/j.jcmgh.2021.06.023

11. Gunderson AJ, Rajamanickam V, Bui C, Bernard B, Pucilowska J, Ballesteros-Merino C, et al. Germinal center reactions in tertiary lymphoid structures associate with neoantigen burden, humoral immunity and long-term survivorship in pancreatic cancer. *OncoImmunology*. (2021) 10:1900635. doi: 10.1080/2162402X.2021.1900635

12. Finkin S, Yuan D, Stein I, Taniguchi K, Weber A, Unger K, et al. Ectopic lymphoid structures function as microniches for tumor progenitor cells in hepatocellular carcinoma. *Nat Immunol*. (2015) 16:1235–44. doi: 10.1038/ni.3290

13. Ladányi A, Kiss J, Somlai B, Gilde K, Fejős Z, Mohos A, et al. Density of DC-LAMP+ mature dendritic cells in combination with activated T lymphocytes infiltrating primary cutaneous melanoma is a strong independent prognostic factor. *Cancer Immunology Immunother*. (2007) 56:1459–69. doi: 10.1007/s00262-007-0286-3

14. Papalampros A, Vailas M, Ntostoglou K, Chiloeches ML, Sakellariou S, Chouliari NV, et al. Unique spatial immune profiling in pancreatic ductal adenocarcinoma with enrichment of exhausted and senescent T cells and diffused CD47-SIRPα Expression. *Cancers*. (2020) 12:1825. doi: 10.3390/cancers12071825

15. Binkley CE, Zhang L, Greenson JK, Giordano TJ, Kuick R, Misek D, et al. The molecular basis of pancreatic fibrosis: common stromal gene expression in chronic pancreatitis and pancreatic adenocarcinoma. *Pancreas* (2024) 29:254–63. doi: 10.1097/00006676-200411000-00003

16. Bachem MG, Schünemann M, Ramadani M, Siech M, Beger H, Buck A, et al. Pancreatic carcinoma cells induce fibrosis by stimulating proliferation and matrix synthesis of stellate cells. *Gastroenterology*. (2005) 128:907–21. doi: 10.1053/j.gastro.2004.12.036

17. Armstrong T, Packham G, Murphy LB, Bateman AC, Conti JA, Fine DR, et al. Type I collagen promotes the Malignant phenotype of pancreatic ductal adenocarcinoma. *Clin Cancer Res*. (2004) 10:7427–37. doi: 10.1158/1078-0432.CCR-03-0825

18. Hayashi Y, Makino T, Sato E, Ohshima K, Nogi Y, Kanemura T, et al. Density and maturity of peritumoral tertiary lymphoid structures in oesophageal squamous cell carcinoma predicts patient survival and response to immune checkpoint inhibitors. *Br J Cancer*. (2023) 128:2175–85. doi: 10.1038/s41416-023-02235-9

19. Zhou L, Xu B, Liu Y, Wang Z. Tertiary lymphoid structure signatures are associated with survival and immunotherapy response in muscle-invasive bladder cancer. *OncoImmunology*. (2021) 10:1915574. doi: 10.1080/2162402X.2021.1915574

20. Cabrita R, Lauss M, Sanna A, Donia M, Skaarup Larsen M, Mitra S, et al. Tertiary lymphoid structures improve immunotherapy and survival in melanoma. *Nature*. (2020) 577:561–5. doi: 10.1038/s41586-019-1914-8

21. Mokhtari Z, Rezaei M, Sanei MH, Dehghanian A, Faghih Z, Heidari Z, et al. Tim3 and PD-1 as a therapeutic and prognostic targets in colorectal cancer: Relationship with sidedness, clinicopathological parameters, and survival. *Front Oncol*. (2023) 13. doi: 10.3389/fonc.2023.1069696

22. Di Caro G, Bergomas F, Grizzi F, Doni A, Bianchi P, Malesci A, et al. Occurrence of tertiary lymphoid tissue is associated with T-cell infiltration and predicts better prognosis in early-stage colorectal cancers. *Clin Cancer Res*. (2014) 20:2147–58. doi: 10.1158/1078-0432.CCR-13-2590

23. Germain C, Gnjatic S, Tamzalit F, Knockaert S, Remark R, Goc J, et al. Presence of B cells in tertiary lymphoid structures is associated with a protective immunity in patients with lung cancer. *Am J Respir Crit Care Med*. (2014) 189:832–44. doi: 10.1164/rccm.201309-1611OC

24. Helmink BA, Reddy SM, Gao J, Zhang S, Basar R, Thakur R, et al. B cells and tertiary lymphoid structures promote immunotherapy response. *Nature*. (2020) 577:549–55. doi: 10.1038/s41586-019-1922-8

25. Li H, Liu H, Fu H, Li J, Xu L, Wang G, et al. Peritumoral Tertiary Lymphoid Structures Correlate With Protective Immunity and Improved Prognosis in Patients With Hepatocellular Carcinoma. *Front Immunol*. (2021) 12:648812.

frontiers | Frontiers in Immunology

TYPE Original Research
PUBLISHED 10 May 2023
DOI 10.3389/fimmu.2023.1166497

OPEN ACCESS

EDITED BY
Ying Ma,
Tianjin Medical University Cancer Institute and Hospital, China

REVIEWED BY
Toshihiko Torigoe,
Sapporo Medical University, Japan
Dan Merrick,
University of Colorado Anschutz Medical Campus, United States

*CORRESPONDENCE
Feiling Feng
ffeiling@163.com
Hui Dong
huidongwh@126.com
Hongyang Wang
hywangk@vip.sina.com
Liwei Dong
dlw@smmu.edu.cn

†These authors have contributed equally to this work

RECEIVED 15 February 2023
ACCEPTED 28 April 2023
PUBLISHED 10 May 2023

CITATION
Shang T, Jiang T, Lu T, Wang H, Cui X, Pan Y, Xu M, Pei M, Ding Z, Feng X, Lin Y, Li X, Tan Y, Feng F, Dong H, Wang H and Dong L (2023) Tertiary lymphoid structures predict the prognosis and immunotherapy response of cholangiocarcinoma. *Front. Immunol.* 14:1166497. doi: 10.3389/fimmu.2023.1166497

Tertiary lymphoid structures predict the prognosis and immunotherapy response of cholangiocarcinoma

Taiyu Shang[1,2†], Tianyi Jiang[1†], Tao Lu[3†], Hui Wang[4†], Xiaowen Cui[1], Yufei Pan[1], Mengyou Xu[1], Mengmiao Pei[1,5], Zhiwen Ding[1], Xiaofan Feng[1], Yunkai Lin[1], Xin Li[4], Yexiong Tan[1], Feiling Feng[5*], Hui Dong[3*], Hongyang Wang[1,2,6*] and Liwei Dong[1,6*]

[1]National Center for Liver Cancer, Naval Medical University, Shanghai, China, [2]School of Life Sciences, Institute of Metabolism and Integrative Biology, Fudan University, Shanghai, China, [3]Department of Pathology, Eastern Hepatobiliary Surgery Hospital, Naval Medical University, Shanghai, China, [4]Department of Hepatobiliary Diseases, Eastern Hepatobiliary Surgery Hospital, Naval Medical University, Shanghai, China, [5]Department of Hepatic Surgery, Eastern Hepatobiliary Surgery Hospital, Naval Medical University, Shanghai, China, [6]International Cooperation Laboratory on Signal Transduction, Eastern Hepatobiliary Surgery Hospital, Shanghai, China

Introduction: Cholangiocarcinoma (CCA) is a malignant tumor of the biliary epithelium with a poor prognosis. The lack of biomarkers to predict therapeutic response and prognosis is one of the major challenges for CCA treatment. Tertiary lymphoid structures (TLS) provide a local and pivotal microenvironment for tumor immune responses. The prognostic value and clinical relevance of TLS in CCA remain unclear. We aimed to explore the characteristics and clinical significance of TLS in CCA.

Methods: We investigated the prognostic value and clinical relevance of TLS in CCA using a surgery cohort containing 471 CCA patients (cohort 1) and an immunotherapy cohort containing 100 CCA patients (cohort 2). Hematoxylin and eosin (H&E) and immunohistochemical (IHC) staining were used to evaluate the maturity of TLS. Multiplex IHC (mIHC) was employed to characterize the composition of TLS.

Results: Different maturity of TLS were observed in CCA tissue sections. Strong staining of the four-gene signature including PAX5, TCL1A, TNFRSF13C, and CD79A were found in TLS regions. A high density of intra-tumoral TLS (T-score high) were significantly correlated with longer overall survival (OS) both in CCA cohort 1 ($p = 0.002$) and cohort 2 ($p = 0.01$), whereas a high density of peri-tumoral TLS (P-score high) were associated with shorter OS in these two cohorts ($p = 0.003$ and $p = 0.03$, respectively).

Conclusion: The established four-gene signature efficiently identified the TLS in CCA tissues. The abundance and spatial distribution of TLS were significantly correlated with the prognosis and immune checkpoint inhibitors (ICIs) immunotherapy response of CCA patients. The presence of intra-tumoral TLS are positive prognostic factors for CCA, which provide a theoretical basis for the future diagnosis and treatment of CCA.

KEYWORDS

cholangiocarcinoma, tertiary lymphoid structures, tumor microenvironment, immune checkpoint inhibitors, prognosis

Introduction

Cholangiocarcinoma (CCA) is an epithelial cell malignancy arising from varying locations within the biliary tree, with rising mortality worldwide over the past few decades (1, 2). It can be classified as intrahepatic, perihilar and distal carcinomas in terms of the anatomical location of the tumor in the bile duct tree. Despite the tremendously high postoperative recurrence rate of CCA, surgery remains the prior treatment for patients diagnosed at an early stage. Unfortunately, most CCA patients are afflicted with advanced-stage diseases at initial diagnosis, and neither radiotherapy nor chemotherapy regimens (Gemcitabine and Cisplatin) can significantly improve survival (3). Currently, several studies have attempted to identify the molecular subtypes of CCA and have revealed the critical role of the tumor immune microenvironment (TME) in CCA progression (4–6). Therefore, the direct characterization of TME may contribute to developing novel and effective personalized therapeutic approaches.

A typical histopathological feature of CCA is the presence of abundant stroma, which surrounds and infiltrates tumor structures containing lymphatics, fibrogenic cells, and several immune cells (7). The crosstalk between tumor cells and cells populating the TME contributes to the progression and metastases of CCA. Immunotherapy using antibodies to target immune checkpoints (immune checkpoint inhibitors, ICIs), including the PD-1/PD-L1 and CTLA-4/CD80 pathways, has shown promising anti-cancer effects in a variety of cancers (8–10). Tertiary lymphoid structures (TLS) have been recognized as ectopic aggregated lymphocytes which develop in inflammatory tissues or tumors. TLS is composed of a B-cell zone containing germinal centers and a surrounding T-cell zone comprising several types of T cells, dendritic cells, and high endothelial venules (HEVs) (11, 12). Generally, TLS represents a state of local immune infiltration in the TME since it provides a privileged site for lymphocyte differentiation and antigen presentation, thus providing a crucial environment for both humoral and cellular immune responses against cancer. By modulating immune trafficking and immune response, TLS participates in regulating immune microenvironment and has been associated with better prognosis and elevated immunotherapeutic response in several tumors, such as melanoma, breast cancer, and lung cancer (13–15). However, few studies have demonstrated the prognostic value and immunotherapy relevance of TLS in CCA.

In this study, we aimed to explore the characteristics and clinical significance of TLS in CCA. We investigated and classified TLS in two CCA cohorts, cohort 1 contained 471 cases who received surgery and were treated with standard chemotherapy after postoperative progress, and cohort 2 contained 100 cases who received first-line chemotherapy combined with immune checkpoint inhibitors (ICIs) to prevent postoperative recurrence. Our findings reveal the opposite roles of intra-tumoral and peri-tumoral TLS in predicting the prognosis of CCA and establish new biomarkers for TLS identification.

Materials and methods

CCA surgery cohort

The CCA surgery cohort was composed of 471 patients with histologically verified CCA who were surgically resected from 2012 to 2017 at the Eastern Hepatobiliary Surgery Hospital (EHBH), the Naval Medical University, Shanghai, with the approval of the EHBH Research Ethics Committee. All diagnoses were confirmed by pathological analyses. Informed consent was obtained from all patients. The inclusion criteria were as follows: 1) no history of other malignant tumors within 5 years before surgery; 2) no other history of anti-tumor therapy before surgery; 3) between 20 and 75 years of age; 4) no history of immunotherapy and chemotherapy; 5) no perioperative death occurred. The exclusion criteria were: 1) incomplete clinicopathological data; 2) incomplete follow-up information. The data cutoff date for the final analysis was May 3, 2020. Patient characteristics, including age, gender, primary tumor size, primary tumor number, and other tumor parameters relevant to the study, are shown in Supplementary Table S1.

CCA immunotherapy cohort

The CCA immunotherapy cohort was composed of 100 patients who received first-line chemotherapy combined with ICIs to prevent

postoperative recurrence from 2017 to 2020 at EHBH, with the approval of the EHBH Research Ethics Committee. All of the patients received R1 and R2 resection, none patients received radical resection. All diagnoses were confirmed by pathological analyses. Patients with Karnofsky Performance Scores (KPS) ≥ 70 were enrolled for further treatment. The first-line chemotherapy was a regimen of GC treatment (1000 mg/m2 gemcitabine and 25 mg/m2 cisplatin in a three-weekly cycle with administrations on days one and eight). The PD-1 inhibitor (anti-PD-1, Sintilimab, Daboshu) is a recombinant fully human monoclonal antibody against programmed death receptor 1, which is independently developed by Innovent Biologics (Suzhou) Co. Ltd. Sintilimab was administered by intravenous infusion at a recommended dose of 200 mg once every three weeks for up to 2 years or until disease progression, intolerable toxicity. Clinical information is shown in Supplementary Table S2.

Evaluation of tumor microenvironment composition

Transcriptomic data were downloaded from the Gene Expression Omnibus (GEO) database (accession code: GSE26566) for a total of 70 samples, including 32 CCA tissues, 32 surrounding liver (SL) tissues, and 6 normal intrahepatic bile duct tissues. The raw microarray data were normalized using R-package *limma* (16). The tumor immune microenvironment (TME) of each sample was then estimated using the MCP-counter tool (17), giving abundance scores of eight immune cells (B cells, T cells, $CD8^+$ T cells, NK cells, cytotoxic lymphocytes, neutrophils, myeloid dendritic cells, and monocyte lineage) and two stromal populations (fibroblasts and endothelial cells). Cell composition scores are based on the analysis of specific transcriptomic markers that are specifically and stably expressed in unique cell populations. The relevant characteristics of the cell populations estimated by the MCP counter have been reported in a previous study (18). In addition, the expression of TLS-associated chemokines was explored between CCA and surrounding liver and normal intrahepatic samples. These data sets displayed transcriptional estimates at the gene level, as in $\log_2$ (x +1) transformed RSEM normalized counts. Genes were mapped to human genome coordinates.

Differential gene expression analysis of TCGA data, genetic mutation analysis

The mRNA-seq and clinical information of the TCGA CHOL cohort were downloaded from the UCSC Xena platform (http://xena.ucsc.edu/). Data used for tumor genetic mutation analysis were downloaded from cholangiocarcinoma (TCGA, PanCancer Atlas) datasets of cBioPortal (http://www.cbioportal.org/datasets). TLS was quantified using H&E images of the TCGA CHOL cohort (https://portal.gdc.cancer.gov/repository). Tissues containing TLS were considered as "TLS-positive" cases, while tissues with no TLS observed were considered as "TLS-negative" cases. Differential gene analysis was performed between TLS-positive and TLS-negative cases by DESeq2 (version 1.34.0).

Immunohistochemistry

Formalin-fixed paraffin-embedded tissues were sectioned (4 μm) and stained with hematoxylin and eosin (H&E) for histological analysis or used for immunohistochemistry (IHC). For IHC, endogenous peroxidases were inactivated by 3% hydrogen peroxide and nonspecific signals were blocked by 1% BSA. Sections were incubated with the primary antibody: CD20 (1:200, #MA5-13141, Invitrogen), CD3 (1:200, #ab16669, Abcam), MECA-79 (1:100, #sc-19602, Santa Cruz), CD21 (1:100, #sc-13135, Santa Cruz), CD23 (1:100, #MA5-14572, Invitrogen), TCL1A (1:500, #ab108978, Abcam), PAX5 (1:1000, #ab109443, Abcam), TNFRSF13C (1:300, #ab168389, Abcam), CD79A (1:200, #ab79414, Abcam) at 4°C overnight, HRP-conjugated secondary antibody at 37°C for 1 h, and subsequently stained with DAB substrate. Counterstaining was performed with hematoxylin and mounted with a mounting medium.

Multiplex immunohistochemistry (mIHC) staining

The slides were dewaxed in xylene, rehydrated through a decreasing ethanol series and fixed in NBF (10% neutral buffered formalin) for 10 min. Slides were stained to enable the simultaneous visualization of four markers: anti-CD23, anti-CD20, anti-CD68, and anti-CD56. At the beginning of each staining cycle, the slides were immersed in Tris-EDTA buffer to perform heat-induced antigen retrieval. After blocking proteins for 10 min, these four primary antibodies were sequentially incubated for 60 min at 37°C. Then the incubation of HRP-conjugated secondary antibody and tyramide signal amplification (TSA) with Opal was followed. Microwave treatment was performed at each cycle of staining to remove the Ab TSA complex. Finally, all slides were stained with 4'-6'-diamidino-2-phenylindole (DAPI, SIGMA-ALDRICH) for 8 min and enclosed with a mounting medium. A full slice scan was performed using Scanner (Pannoramic MIDI, 3DHISTECH).

Characterization and quantification of TLS

The H&E staining sections of each patient were scanned for whole slide images (WSIs), including tissues from both the tumor and adjacent surrounding liver. TLS was blindly quantified by two pathologists without the knowledge of clinicopathological data. The presence and location of TLS were assessed based on morphology in H&E staining sections. To determine the spatial distribution of TLS, each WSI was subdivided into 2 subregions: intra-tumor (T) and peri-tumor (P) regions. Different abundances and heterogeneous arrangements of TLS were observed in different subregions, and TLS were divided into intra-tumoral TLS and peri-tumoral TLS based on their location to tumor invasive margins. The TLS scoring system was performed as described previously (19). 4 categories for characterization of TLS in the T region (T-score): 1) score 0 for no TLS in the T region (TLS negative CCA); 2) score 1 for 1 or 2 TLS within T region; 3) score 2 for at least 3 TLS in the T region but does

not meet the criteria of score 3; 4) score 3 for massive TLS distributed throughout the T region which converges with each other. TLS abundance in the P region (P-score) was scored as follows: 1) score 0 for no TLS in the P region; 2) score 1 for TLS distributed in a localized area of the P region (less than 50%); 3) score 2 for TLS distribution in the majority of the P region (more than 50%); 4) score 3 for massive TLS distributed in the P region (encompassing the entire P region). Granulocytes in necrotic areas were excluded in the assessment. In this study, T-score 0-1 cases were considered as the "T-score low" group, while T-score 2-3 cases were considered as the "T-score high" group. Similarly, P-score 0-1 cases were considered as the "P-score low" group, and P-score 2-3 cases were considered as the "P-score high" group.

TLS maturation stages were investigated using IHC staining. Especially, early TLS contained primary clusters of B and T cells without FDC network and germinal centers (GC centers); primary TLS contained FDC network (CD21) without GC centers; Secondary TLS was identified by $CD20^+$ B cells and $CD23^+$ FDC cells.

Statistical analysis

Statistical analyses were performed using SPSS version 21 (IBM, Armonk, NY, USA), GraphPad Prism (version 9.3.0), and Rstudio (version 4.1.3). Categorical variables were compared using Chi-square or Fisher's exact tests. Kaplan-Meier and log-rank survival analyses were used to compare overall survival (OS) and progression-free survival (PFS). All statistical analyses were two-sided and p-value < 0.05 was considered statistically significant.

Results

Immune microenvironment composition of CCA

We first performed an immune infiltration analysis of 32 CCA and 32 surrounding liver (SL) tissues (GSE26566) with overtly available gene expression profiles by MCP counter. The results showed significant differences in the composition of the immune microenvironment between CCA and SL tissues (Figure 1A). Specifically, most samples in the CCA group were enriched with B cells, T cells, monocytic lineage, and cytotoxic lymphocytes, suggesting that TLS may exist. Since multiple chemokines are associated with the presence of TLS, we also investigated the expression of chemokines in the two groups. As expected, chemokines and TLS-related factors including CCL5, CCL8, CCL18, CCL19, CXCL11, LTB, CD79A, and CD79B were remarkably up-regulated in the CCA group compared to the SL group (Figure 1B). In addition, higher expression of CCL5, CCL18, CXCL9, and CXCL11 was also detected in CCA tissues compared with the other 6 normal intrahepatic bile duct tissues enrolled in this cohort (Figure 1C). In conclusion, these results indicate a high aggregation of tumor-infiltrating immune cells in CCA tissues and also suggest CCA tumor has an immune microenvironment adapted to TLS.

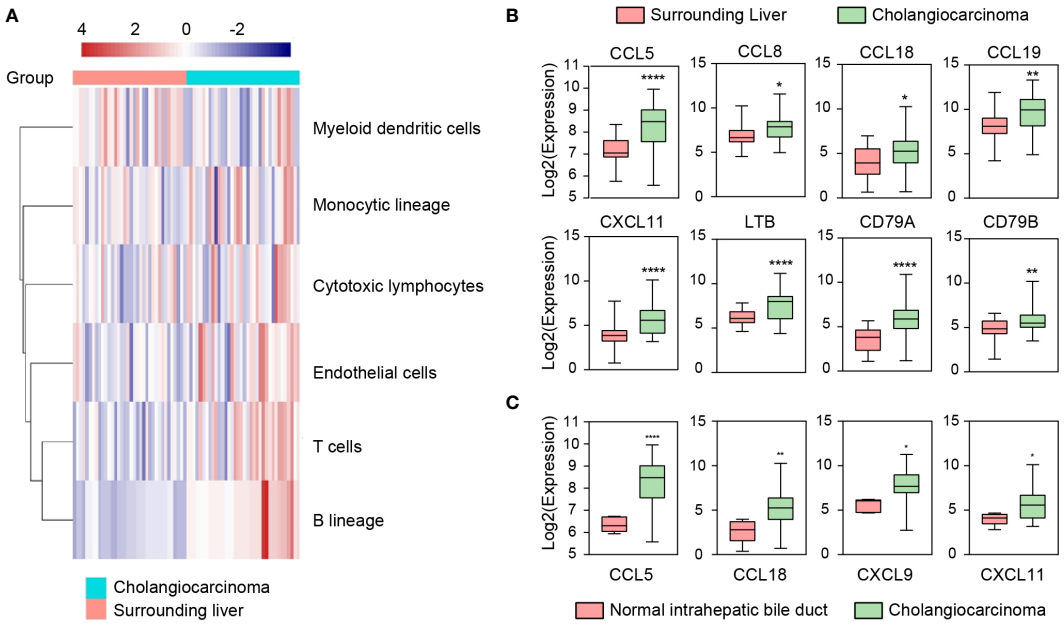

FIGURE 1
Immune microenvironment (IME) compositions of CCA, surrounding liver, and normal intrahepatic bile duct tissues in GSE26566. **(A)** IME compositions between CCA and surrounding liver tissues detected by MCP-counter. **(B, C)** Expressions of TLS-related factors and chemokines in CCA, surrounding liver, and normal intrahepatic bile duct tissues. Indicators for P values: **** P ≤ 0.0001, ** P ≤ 0.01, * P ≤ 0.05.

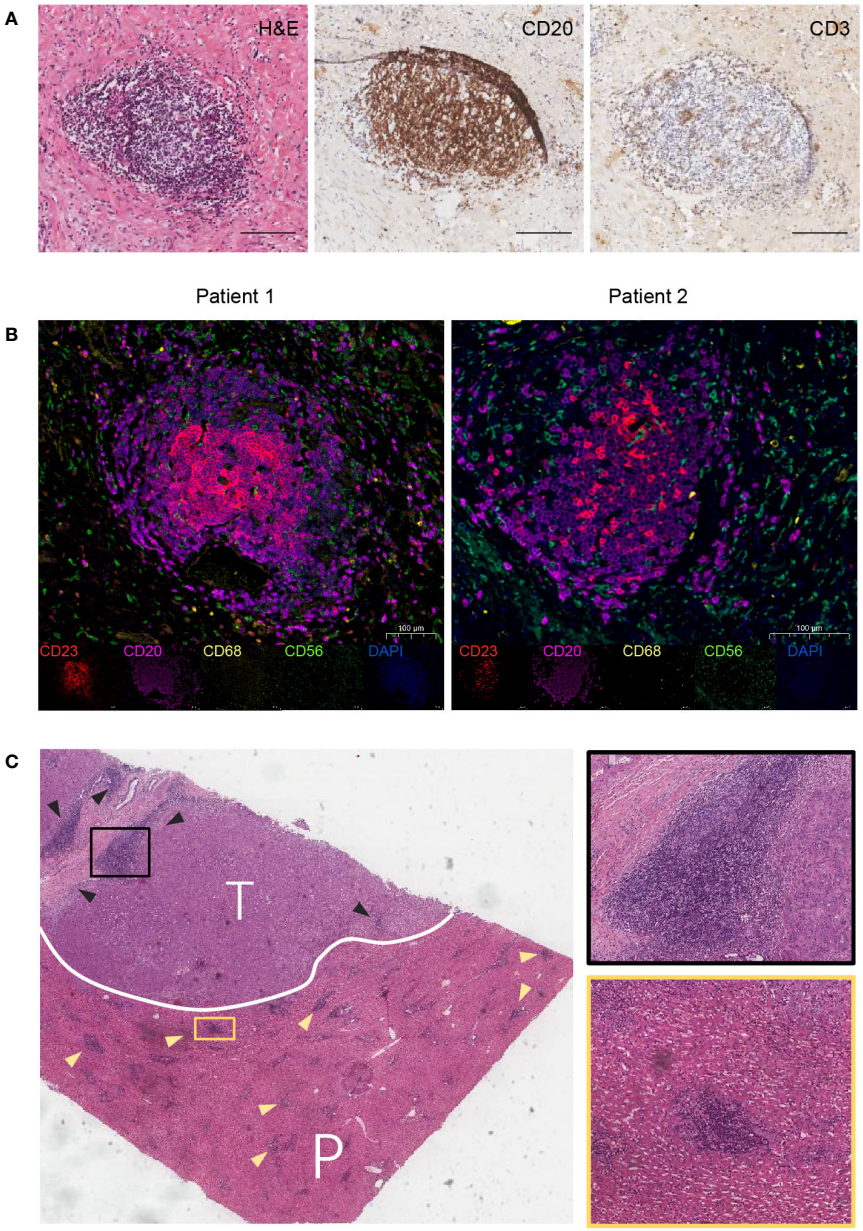

FIGURE 2
Features of TLS in CCA. **(A)** H&E and IHC staining for a typical TLS in CCA tissue. TLS appeared as clusters of B-cell follicles surrounded by T-cell zones. Scale bars, 100 μm. **(B)** Multiplex immunohistochemistry (mIHC) staining for TLS identification. Markers for follicular dendritic cells (CD23), B cells (CD20), macrophages (CD68), and natural killer cells (CD56) are used. **(C)** H&E staining for intra-tumoral (T) and peri-tumoral (P) regions. Triangles indicate TLS.

Different maturity of tertiary lymphoid structures in CCA

Hematoxylin and eosin (H&E) and immunohistochemical (IHC) staining were performed to validate the presence of TLS in CCA tissues. The results showed that TLS consisted of clusters for a $CD20^+$ B cell zone and a $CD3^+$ T cell zone, with follicular structures formed by B cells as the main TLS component (Figure 2A). Then, TLS was identified using multiplex immunohistochemistry staining (mIHC) in tissue sections of CCA patients. The agglomeration of $CD23^+$ follicular dendritic cells (FDCs) and $CD20^+$ B cells indicated the presence of TLS, along with $CD68^+$ macrophages and $CD56^+$ natural killer cell (NK cells) sparsely distributed around the aggregates (Figure 2B). TLS were found in both intra-tumoral (T) and peri-tumoral (P) tissues in CCA (Figure 2C).

TLS has been reported to present in multiple solid tumors and evolves through different stages of maturation (20). Generally, lymphoid aggregates were considered the typical structure of TLS. The presence of multistage maturation of TLS (early TLS, primary TLS, and secondary TLS) could be observed in the H&E-staining sections of CCA (Figure 3A). Subsequently, we confirmed the immune cells with cell type-specific surface markers by IHC

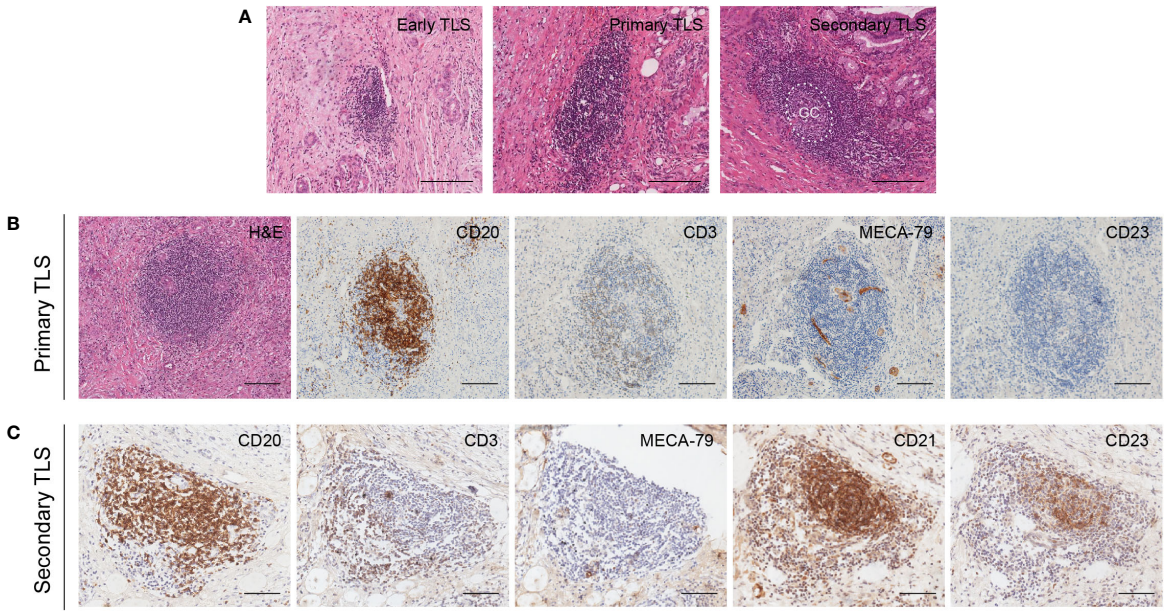

FIGURE 3
Different maturity and corresponding features of TLS in CCA. **(A)** Different maturity of TLS present in CCA. GC center can be found in the secondary TLS in H&E staining sections. **(B)** Primary TLS. $CD20^+$ B cells were diffusely distributed without $CD23^+$ follicular structures formation. **(C)** Secondary TLS. $CD20^+$ B cells and $CD23^+$ FDCs were formed into a follicular structure, with many T cells aggregated around and within the follicles. Scale bars, 200 μm.

staining. The results showed that $CD20^+$ B cells, $CD3^+$ T cells, and $MECA\text{-}79^+$ HEV were distributed on both primary and secondary TLS in CCA (Figures 3B, C). A follicular structure centered on B cells in the network of $CD21^+CD23^+$ FDCs was found in secondary TLS, with multiple T cells clustered around the follicles. In contrast, T cells were dispersed in the TLS without $CD23^+$ follicular structures formation, so they were classified as primary TLS.

Discovery of potential TLS markers for CCA

Next, we quantified TLS using H&E-stained tissue sections from the Cancer Genome Atlas (TCGA) cholangiocarcinoma cohort (Figure 4A). We divided samples into two groups (TLS-negative group and TLS-positive group) and the relationship between the existence of TLS and genetic mutations was explored. However, no significant difference in genetic mutations was enriched within these two groups harboring distinct TLS status (Figure 4B). Consistently, a previous study also showed immune subtypes were irrelevant to genetic mutations (5), suggesting that gene mutation may not be the main factor affecting the presence of TLS in tumors.

To explore the potential markers for TLS, we analyzed the differential gene expression profiles of TLS-positive and TLS-negative CCA cases in the TCGA database. The results showed a higher expression of genes related to B and T cell immunity in the TLS-positive group (Supplementary Table S3). The expression of four genes was remarkably elevated in the TLS-positive group: PAX5, TCL1A, TNFRSF13C, and CD79A (Figure 4C). We further evaluated the ability of these four molecules to characterize TLS by IHC and found that they all displayed strong staining in the TLS region, indicating a broad application prospect of these four molecules in characterizing TLS (Figures 4D, E). These four molecules were also observed in early TLS and primary TLS (Supplementary Figure 1).

TLS in different regions predicts a distinct prognosis of CCA

We next set out to explore the relevance between TLS and clinical features in CCA. A total of 471 CCA patients were enrolled and the clinical characteristics are shown in Tables 1 and 2. The median age of the cohort was 56, ranging from 20 to 85 years old, with 160 female patients (34.0%) and 311 male patients (66.0%). The majority of patients had tumors with a diameter of more than 5 cm (303, 64.3%), and a single tumor was observed in most cases (314, 66.7%).

A TLS scoring system was employed to characterize the TLS in this cohort according to the scoring criteria described before. The TLS scores of the intra-tumoral region (T-score) and peri-tumoral region (P-score) were assessed in each case. TLS abundance in intra-tumoral tissues (T-score) was graded into 4 categories, and the TLS in peri-tumoral tissues (P-score) was also scored by another quaternary category. As a result, TLS was found in 438/471 (93.0%) CCA tissues. According to the TLS scoring system, 471 CCA cases

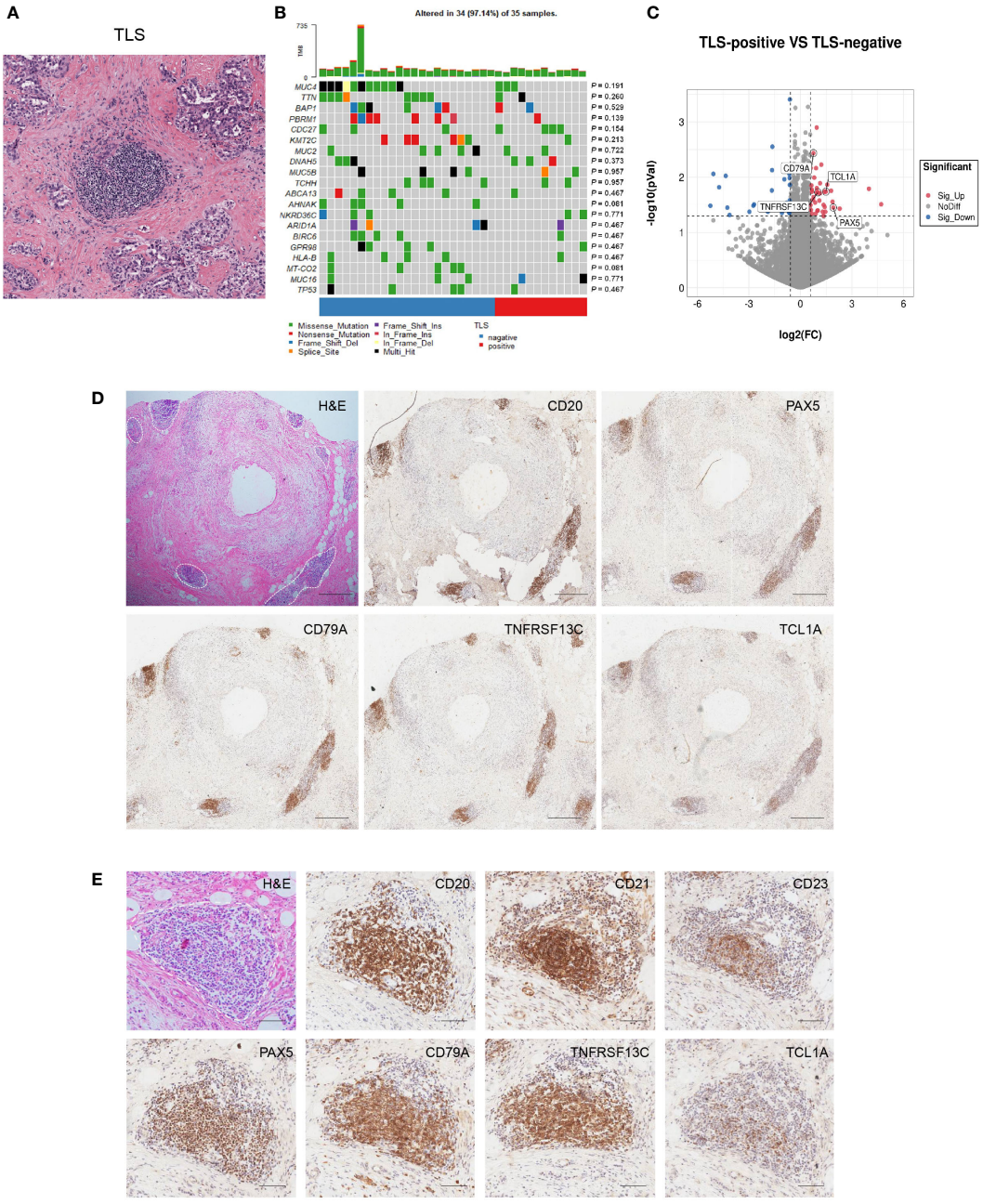

FIGURE 4
Discovery and validation of four-gene signature for TLS identification. **(A)** Representative H&E image of TLS in CCA. **(B)** Correlation between TLS presence and genetic mutation. The p values were assessed by chi-square tests. **(C)** Differential gene expression of TLS-positive versus TLS-negative CCA cases in the TCGA database. **(D, E)** Representative images of PAX5, TCL1A, TNFRSF13C, and CD79A staining in CCA sections. Scale bars in D, 300 μm. Scale bars in E, 100 μm.

could be classified into four groups: T_{high} P_{high} group (Group 1, 31/471, 6.6%), T_{high} P_{low} group (Group 2, 79/471, 16.8%), T_{low} P_{high} group (Group 3, 152/471, 32.3%), and T_{low} P_{low} group (Group 4, 209/471, 44.4%).

The correlations between the TLS score and the clinicopathological characteristics were listed in Tables 1 and 2. The results showed that the tumor diameter of the samples with high T-scores was smaller than those with low T-scores (p = 0.010). There were no significant differences in tumor metastasis and differentiated pathology grade between the high T-score and low T-score groups. Patients with high P-score possessed higher incidences of satellite lesions (p = 0.048) and lymphatic metastasis (p = 0.040) than those with low P-score. A higher P-score was also found to be positively associated with fatty liver in patients in this cohort (p = 0.022). Taken together, we discovered that T-score was associated with reduced tumor size, whereas the P-

TABLE 1 Correlation analyses between the T-score and the clinicopathological characteristics of 471 CCA patients.

Characteristics		Number n (%)	TLS T-score		χ^2	P value
			High n (%)	Low n (%)		
Gender	Female	160(34.0)	36(32.7)	124(34.3)	0.099	0.423
	Male	311(66.0)	74(67.3)	237(65.7)		
Age	<65	350(74.3)	86(78.2)	264(73.1)	1.127	0.175
	≥65	121(25.7)	24(21.8)	97(26.9)		
Fatty liver	Negative	411(87.3)	94(85.5)	317(87.8)	0.421	0.308
	Positive	60(12.7)	16(14.5)	44(12.2)		
Tumor size(cm)	<5	168(35.7)	50(45.5)	118(32.7)	5.989	0.010*
	≥5	303(64.3)	60(54.5)	243(67.3)		
Tumor number	Single	314(66.7)	76(69.1)	238(65.9)	0.380	0.310
	Multiple	157(33.3)	34(30.9)	123(34.1)		
Satellite lesions	Absent	311(66.0)	77(70.0)	234(64.8)	1.009	0.187
	Present	160(34.0)	33(30.0)	127(35.2)		
Lymphatic metastasis	Absent	390(82.8)	90(81.8)	300(83.1)	0.098	0.427
	Present	81(17.2)	20(18.2)	61(16.9)		
Distant metastasis	Absent	448(95.1)	104(94.5)	344(95.3)	0.101	0.458
	Present	23(4.9)	6(5.5)	17(4.7)		
Differentiation	Poorly	25(5.3)	7(6.4)	18(5.0)	0.318	0.361
	Well	446(94.7)	103(93.6)	343(95.0)		
Portal vein invasion	Absent	438(93.0)	102(92.7)	336(93.1)	0.016	0.522
	Present	33(7.0)	8(7.3)	25(6.9)		

*P < 0.05

score was associated with a high occurrence of satellite lesions, lymphatic metastasis, and fatty liver (all $p < 0.05$). These different clinicopathological correlations between T and P scores suggested an essential discrepancy between intra- and peri-tumoral TLS.

Next, we asked whether TLS score affected the survival of CCA patients. Since TLS in different locations showed distinct functions, we assessed the predictive effects of the T-score and P-score, respectively. We found that a higher P-score was significantly related to reduced PFS ($p = 0.001$) and OS ($p = 0.003$) in CCA patients, as the median PFS was 5 months (95% CI: 4.562-5.438) and the median OS was 14 months (95% CI: 12.103-15.897) in the P-score high group, while the median PFS was 6 months (95% CI: 4.845-7.155) and the median OS was 22 months (95% CI: 19.036-24.964) in the P-score low group (Figures 5A, B). In contrast, a higher T-score was significantly related to increased PFS ($p = 0.038$) and OS ($p = 0.002$), as the median PFS was 7.567 months (95% CI: 5.454-9.679) and the median OS was 29 months (95% CI: 24.931-33.069) in the T-score high group, whereas the median PFS was 5 months (95% CI: 4.297-5.703) and the median OS was 17 months (95% CI: 14.735-19.265) in the T-score low group (Figures 5C, D). These data suggest that a diverse abundance of TLS in different regions predicts a distinct prognosis for CCA patients.

A high T-score was associated with better prognosis in patients with immune checkpoint inhibitors therapy

Next, we examined whether TLS can predict the response to ICIs therapy from a cohort of 100 patients who received first-line chemotherapy combined with immune checkpoint inhibitors (ICIs) to prevent postoperative recurrence. H&E staining and IHC staining were performed and the TLS scores were evaluated in the resected tumor sections. Here we discovered that patients in the P-score high group had a relatively shorter PFS ($p = 0.042$) and OS ($p = 0.003$) than those in the P-score low group, with a median PFS of 5 months (95% CI: 3.734-6.266) and a median OS of 7 months (95% CI: 5.621-8.379) (Figures 6A, B). However, patients in the T-score high group had a significantly longer PFS ($p = 0.021$) and OS ($p = 0.010$) compared to those in the T-score low group, with a median PFS of 14 months (95% CI: 10.038-17.962) and a median OS of 23 months (95% CI: 19.917-26.083) (Figures 6C, D). The expression of four-gene TLS signature was found not to correlate with patient survival, and there was no significant relevance between tumor cell PDL1 expression and the spatial distribution and abundance of TLS (Supplementary Figures 2, 3). In summary, these data indicate that a

10.3389/fimmu.2023.1166497

TABLE 2 Correlation analyses between the P-score and the clinicopathological characteristics of 471 CCA patients.

Characteristics		Number n (%)	TLS P-score		χ^2	P value
			High n (%)	Low n (%)		
Gender	Female	160(34.0)	63(34.4)	97(33.7)	0.028	0.472
	Male	311(66.0)	120(65.6)	191(66.3)		
Age	<65	350(74.3)	140(76.5)	210(72.9)	0.754	0.224
	≥65	121(25.7)	43(23.5)	78(27.1)		
Fatty liver	Negative	411(87.3)	152(83.1)	259(89.9)	4.752	0.022*
	Positive	60(12.7)	31(16.9)	29(10.1)		
Tumor size(cm)	<5	168(35.7)	68(37.2)	100(34.7)	0.289	0.330
	≥5	303(64.3)	115(62.8)	188(65.3)		
Tumor number	Single	314(66.7)	114(62.3)	200(69.4)	2.574	0.067
	Multiple	157(33.3)	69(37.7)	88(30.6)		
Satellite lesions	Absent	311(66.0)	112(61.2)	199(69.1)	3.110	0.048*
	Present	160(34.0)	71(38.8)	89(30.9)		
Lymphatic metastasis	Absent	390(82.8)	144(78.7)	246(85.4)	3.557	0.040*
	Present	81(17.2)	39(21.3)	42(14.6)		
Distant metastasis	Absent	448(95.1)	172(94.0)	276(95.8)	0.819	0.244
	Present	23(4.9)	11(6.0)	12(4.2)		
Differentiation	Poorly	25(5.3)	8(4.4)	17(5.9)	0.522	0.309
	Well	446(94.7)	175(95.6)	271(94.1)		
Portal vein invasion	Absent	438(93.0)	170(92.9)	268(93.1)	0.004	0.543
	Present	33(7.0)	13(7.1)	20(6.9)		

*P < 0.05

high T-score of pre-treatment tumor tissues predicts a better prognosis in patients with immunotherapy, as the presence of intra-tumoral TLS was associated with a prolonged OS and PFS.

Discussion

CCA are aggressive tumors characterized by highly connective tissue hyperplasia and genetic heterogeneity with a high risk of morbidity and mortality. Available evidence suggests that TME plays a crucial role in CCA progression and metastasis (21, 22). Targeting the components of TME or the crosstalk between CCA cells and TME may create a novel therapeutic approach (23). As an ectopic lymphoid structure, TLS has been detected in multiple tumors and has shown favorable prognostic values (24, 25). Therefore, TLS may be a practicable biomarker to assess the prognosis and immunotherapeutic efficacy of CCA.

By performing the immune infiltration analysis from the GSE26566 database using MCP-counter, a high level of immune cell infiltration was observed in CCA, accompanied by a remarkable up-regulation of chemokines associated with TLS. Then we assessed the features of TLS in CCA sections by H&E and IHC staining. Consistent with previous reports, we found different maturity of TLS presented in CCA such as immature TLS, primary TLS, and secondary TLS. For immature TLS, it is still unknown whether these lymphoid aggregates can participate in further TLS maturation or only remain in an immature state. Fully mature TLS has been reported to contain $CD21^+CD23^+$ FDCs, which distinguishes them from immature or primary TLS (20). Antigen presentation and maturation of B cells may occur in the mature TLS in CCA, leading to the immune response *in situ*. Indeed, the participation of TLS within anti-tumor immune responses has been reported in recent studies (13, 26, 27).

By quantifying TLS using H&E-stained sections from the TCGA cholangiocarcinoma cohort, we found that 28.9% (13/45) cases contained significant clusters of lymphoid aggregates, some of which contained GC centers, which we defined here as "TLS-positive" samples. We further explored the correlation of TLS with high-prevalent genetic mutations, but the results showed no significant relevance, which was consistent with a previous report (5). However, considering the limited number of cases available for analysis, the role of genetic mutations in tumor immunity and TLS maturation requires further investigation. Through profiling the differential gene expression in TLS-negative and -positive groups, we identified four genes, including TNFRSF13C, PAX5, CD79A, and TCL1A, as potential molecules for TLS identification. Among

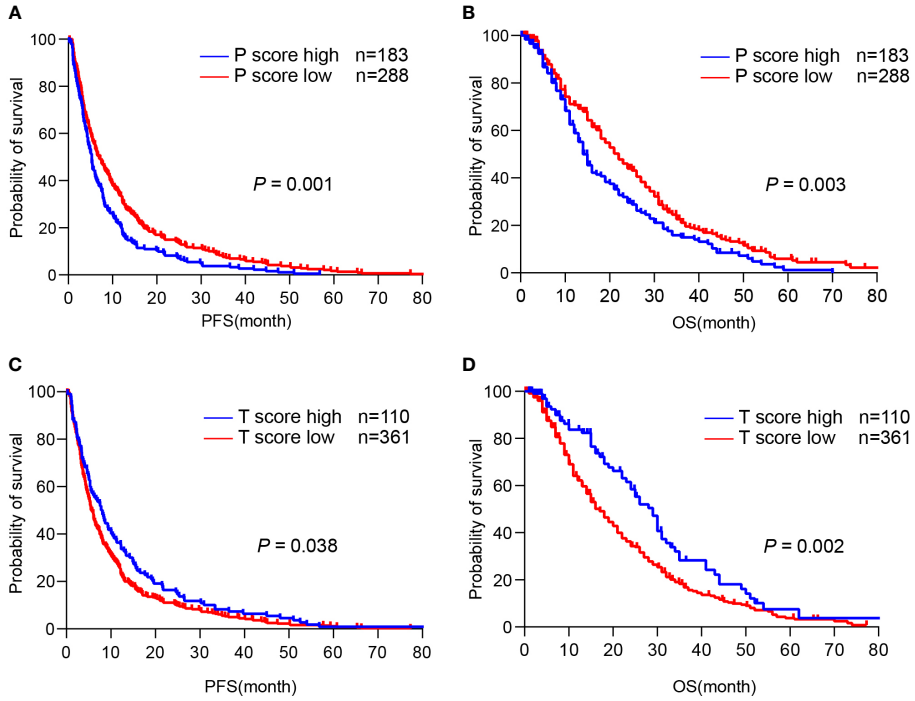

FIGURE 5
TLS in different regions predicts a distinct prognosis of CCA. **(A, B)** Kaplan-Meier analyses of PFS and OS according to P-score in CCA surgery cohort (n = 471). **(C, D)** Kaplan-Meier analyses of PFS and OS according to T-score in CCA surgery cohort. P values were determined by log-rank tests. OS, overall survival; PFS, progression-free survival.

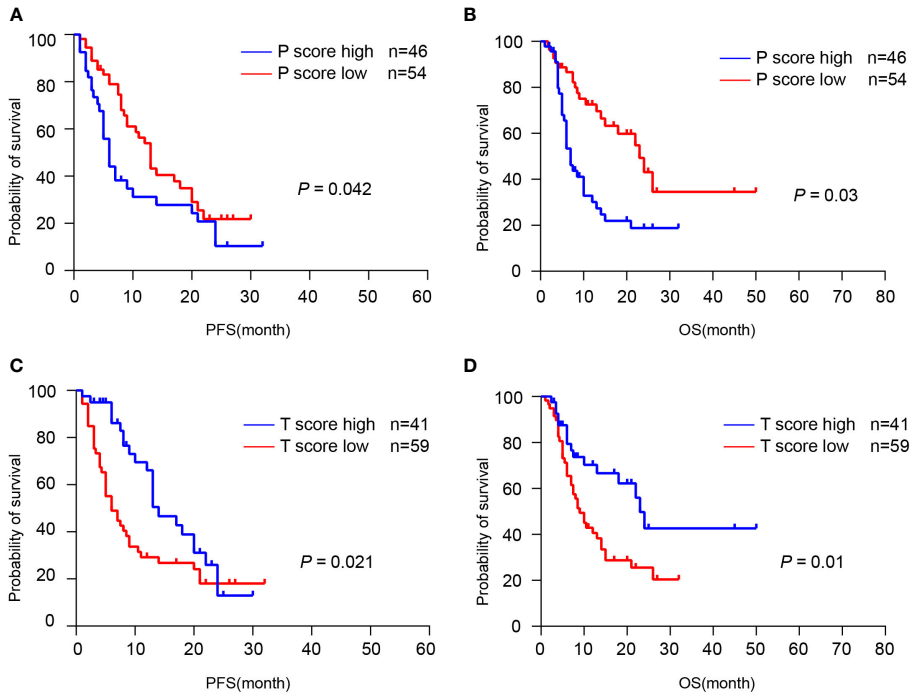

FIGURE 6
TLS was associated with the response to immunotherapy. **(A, B)** Kaplan-Meier analyses of PFS and OS according to P-score in CCA immunotherapy cohort (n = 100). **(C, D)** Kaplan-Meier analyses of PFS and OS according to T-score in CCA immunotherapy cohort. P values were determined by log-rank tests.

them, TNFRSF13C and PAX5 were associated with B cell lineage commitment (28, 29), and PAX5 also reportedly participated in CCA progression (30). CD79A was suggested to be a marker of activated B cells (31). TCL1A was considered an oncogene, whose up-regulation was observed in B cell malignancies (32). However, the anti-tumor role of TCL1A has also been reported recently (33). In our study, these molecules displayed strong staining in the TLS regions, indicating the feasibility of using them to characterize TLS in CCA. Whether these genes influence the presence and maturation of TLS is currently unknown, but this four-gene signature may contribute to TLS identification by combining with other available markers of TLS.

Studies have shown that TLS is associated with longer overall survival and serves as a prognostic marker in pancreatic cancer and colorectal cancer (34, 35). Our study revealed the prognostic role of TLS based on spatial localization and density in CCA patients. Intra-tumoral TLS is a potent predictor of good prognosis, whereas the presence of peri-tumoral TLS is associated with poor prognosis in CCA. This discrepancy of TLS has been verified in hepatocellular carcinoma and breast cancer (36–38), but the underlying mechanisms remain unclear.

Recent studies have shown that B cells and TLS significantly affected the efficacy of immune checkpoint inhibitors (ICIs). Specifically, the presence of TLS along with B cells in the tissues of non-small cell lung cancer (39), melanoma (13), and urothelial carcinoma (40) increased the efficacy of ICIs. Our result confirmed that intra-tumoral TLS is usually associated with better efficacy of anti-PD-1 treatment. In contrast, a high abundance of peri-tumoral TLS is associated with low immune response and poor prognosis. The different maturation and function of TLS located in different regions in CCA may contribute to this discrepancy. A reliable explanation is that B cells and TLS in the tumor microenvironment were complex, which would exert pro- or anti-tumorigenic functions depending on their maturity to secret antibodies, regulate T cell functions, or present antigens. In immature TLS, B cells secrete molecules that inhibit immune responses and reduce interactions with T cells. In contrast, mature TLS may activate T cells, release antibodies, and further induce antibody-dependent cellular cytotoxicity (ADCC) of tumor cells (20). Actually, intra-tumoral TLS were usually tended to oval-shaped with well-formed maturation, while the peri-tumoral TLS usually displayed as squished, slender, or simply lymphatic aggregates in our H&E staining sections.

In summary, our study established a four-gene TLS signature as practicable biomarker for TLS identification and demonstrated that the spatial distribution and abundance of TLS profoundly affect the prognosis and the immunotherapy response in CCA, providing new perspectives for TLS function and possible clinical intervention.

Data availability statement

The original contributions presented in the study are included in the article/Supplementary Material. Further inquiries can be directed to the corresponding author.

Ethics statement

Written informed consent was obtained from the individual(s) for the publication of any potentially identifiable images or data included in this article.

Author contributions

TS, TJ, LD, and HYW designed the study, directed the study, and wrote the manuscript. TS, TJ, TL, and HW performed most of the experiments. YP, MX, MP, ZD, XF, XC, YL, XL, and YT intellectually contributed throughout the project. FF, HD, HYW, and LD guided the project, revised the manuscript, and obtained funding. All authors contributed to the article and approved the submitted version.

Funding

This work was supported by grants from the National Natural Science Foundation of China (32270814, 81830054, 81988101, 82172895, and 91859205), the National Key R&D Program of China (2022YFC2503704), the Shanghai Sailing Program (21YF1457900), the Clinical Research Plan of SHDC (SHDC2020CR2011A), Key project of Jiading District Health Construction Commission of Shanghai (No.2020-ZD-01), and the Basic Medical Research Foundation of the Naval Medical University (2021MS03 and 2021MS15).

Acknowledgments

The authors thank the patients participating in this study, and their families. The authors thank the staff at each participating institution that assisted with the study. The authors also acknowledge Dan Cao and Linna Guo for their technical assistance.

Conflict of interest

The authors declare that the research was conducted in the absence of any commercial or financial relationships that could be construed as a potential conflict of interest.

Publisher's note

All claims expressed in this article are solely those of the authors and do not necessarily represent those of their affiliated organizations, or those of the publisher, the editors and the reviewers. Any product that may be evaluated in this article, or

claim that may be made by its manufacturer, is not guaranteed or endorsed by the publisher.

Supplementary material

The Supplementary Material for this article can be found online at: https://www.frontiersin.org/articles/10.3389/fimmu.2023.1166497/full#supplementary-material

SUPPLEMENTARY FIGURE 1
IHC staining of four-gene signature in early TLS and primary TLS. Scale bars, 100 μm.

SUPPLEMENTARY FIGURE 2
The correlation between patient survival and expression of four-gene signature in the CCA immunotherapy cohort. **(A, B)** Kaplan-Meier analyses of PFS and OS according to PAX5-score in CCA immunotherapy cohort (n = 58). **(C, D)** Kaplan-Meier analyses of PFS and OS according to CD79A-score in CCA immunotherapy cohort (n = 58). **(E, F)** Kaplan-Meier analyses of PFS and OS according to TNFRSF13C-score in CCA immunotherapy cohort (n = 58). **(G, H)** Kaplan-Meier analyses of PFS and OS according to TCL1A-score in CCA immunotherapy cohort (n = 58).

SUPPLEMENTARY FIGURE 3
(A) The correlation between TLS score and expression of four-gene signature in the CCA immunotherapy cohort (n=58). **(B)** The correlation between TLS score and expression of PDL1 in the CCA immunotherapy cohort (n=58).

References

1. Razumilava N, Gores GJ. Cholangiocarcinoma. *Lancet* (2014) 383(9935):2168–79. doi: 10.1016/S0140-6736(13)61903-0

2. Banales JM, Marin JJG, Lamarca A, Rodrigues PM, Khan SA, Roberts LR, et al. Cholangiocarcinoma 2020: the next horizon in mechanisms and management. *Nat Rev Gastroenterol Hepatol* (2020) 17(9):557–88. doi: 10.1038/s41575-020-0310-z

3. Valle J, Wasan H, Palmer DH, Cunningham D, Anthoney A, Maraveyas A, et al. Cisplatin plus gemcitabine versus gemcitabine for biliary tract cancer. *N Engl J Med* (2010) 362(14):1273–81. doi: 10.1056/NEJMoa0908721

4. Lin J, Dai Y, Sang C, Song G, Xiang B, Zhang M, et al. Multimodule characterization of immune subgroups in intrahepatic cholangiocarcinoma reveals distinct therapeutic vulnerabilities. *J Immunother Cancer* (2022) 10(7):e004892. doi: 10.1136/jitc-2022-004892

5. Job S, Rapoud D, Dos Santos A, Gonzalez P, Desterke C, Pascal G, et al. Identification of four immune subtypes characterized by distinct composition and functions of tumor microenvironment in intrahepatic cholangiocarcinoma. *Hepatology* (2020) 72(3):965–81. doi: 10.1002/hep.31092

6. Xue R, Chen L, Zhang C, Fujita M, Li R, Yan S-M, et al. Genomic and transcriptomic profiling of combined hepatocellular and intrahepatic cholangiocarcinoma reveals distinct molecular subtypes. *Cancer Cell* (2019) 35 (6):932–47.e8. doi: 10.1016/j.ccell.2019.04.007

7. Fabris L, Sato K, Alpini G, Strazzabosco M. The tumor microenvironment in cholangiocarcinoma progression. *Hepatology* (2021) 73 Suppl 1(Suppl 1):75–85. doi: 10.1002/hep.31410

8. Zhang Y, Zhang Z. The history and advances in cancer immunotherapy: understanding the characteristics of tumor-infiltrating immune cells and their therapeutic implications. *Cell Mol Immunol* (2020) 17(8):807–21. doi: 10.1038/s41423-020-0488-6

9. Guo X-J, Lu J-C, Zeng H-Y, Zhou R, Sun Q-M, Yang G-H, et al. CTLA-4 synergizes with PD1/PD-L1 in the inhibitory tumor microenvironment of intrahepatic cholangiocarcinoma. *Front Immunol* (2021) 12:705378. doi: 10.3389/fimmu.2021.705378

10. Vogel A, Bridgewater J, Edeline J, Kelley RK, Klümpen HJ, Malka D, et al. Biliary tract cancer: ESMO clinical practice guideline for diagnosis, treatment and follow-up. *Ann Oncol* (2022) 34(2):127–140. doi: 10.1016/j.annonc.2022.10.506

11. Schumacher TN, Thommen DS. Tertiary lymphoid structures in cancer. *Science* (2022) 375(6576):eabf9419. doi: 10.1126/science.abf9419

12. Gago da Graça C, van Baarsen LGM, Mebius RE. Tertiary lymphoid structures: diversity in their development, composition, and role. *J Immunol* (2021) 206(2):273–81. doi: 10.4049/jimmunol.2000873

13. Cabrita R, Lauss M, Sanna A, Donia M, Skaarup Larsen M, Mitra S, et al. Tertiary lymphoid structures improve immunotherapy and survival in melanoma. *Nature* (2020) 577(7791):561–5. doi: 10.1038/s41586-019-1914-8

14. Wang B, Liu J, Han Y, Deng Y, Li J, Jiang Y. The presence of tertiary lymphoid structures provides new insight into the clinicopathological features and prognosis of patients with breast cancer. *Front Immunol* (2022) 13:868155. doi: 10.3389/fimmu.2022.868155

15. Tang J, Ramis-Cabrer D, Curull V, Wang X, Mateu-Jiménez M, Pijuan L, et al. B cells and tertiary lymphoid structures influence survival in lung cancer patients with resectable tumors. *Cancers (Basel)* (2020) 12(9):2644. doi: 10.3390/cancers12092644

16. Ritchie ME, Phipson B, Wu D, Hu Y, Law CW, Shi W, et al. Limma powers differential expression analyses for RNA-sequencing and microarray studies. *Nucleic Acids Res* (2015) 43(7):e47. doi: 10.1093/nar/gkv007

17. Becht E, Giraldo NA, Lacroix L, Buttard B, Elarouci N, Petitprez F, et al. Estimating the population abundance of tissue-infiltrating immune and stromal cell populations using gene expression. *Genome Biol* (2016) 17(1):218. doi: 10.1186/s13059-016-1070-5

18. Bruno TC. New predictors for immunotherapy responses sharpen our view of the tumour microenvironment. *Nature* (2020) 577(7791):474–6. doi: 10.1038/d41586-019-03943-0

19. Ding G-Y, Ma J-Q, Yun J-P, Chen X, Ling Y, Zhang S, et al. Distribution and density of tertiary lymphoid structures predict clinical outcome in intrahepatic cholangiocarcinoma. *J Hepatol* (2022) 76(3):608–18. doi: 10.1016/j.jhep.2021.10.030

20. Fridman WH, Meylan M, Petitprez F, Sun C-M, Italiano A, Sautès-Fridman C. B cells and tertiary lymphoid structures as determinants of tumour immune contexture and clinical outcome. *Nat Rev Clin Oncol* (2022) 19(7):441–57. doi: 10.1038/s41571-022-00619-z

21. Zheng Y, Huang N, Kuang S, Zhang J, Zhao H, Wu J, et al. The clinicopathological significance and relapse predictive role of tumor microenvironment of intrahepatic cholangiocarcinoma after radical surgery. *Cancer* (2022) 129(3):393–404. doi: 10.1002/cncr.34552

22. Toshida K, Itoh S, Harada N, Morinaga A, Yugawa K, Tomiyama T, et al. Cancer-associated fibroblasts promote tumor cell growth via miR-493-5p in intrahepatic cholangiocarcinoma. *Cancer Sci* (2022) 114(3):937–947. doi: 10.1111/cas.15644

23. Cao H, Huang T, Dai M, Kong X, Liu H, Zheng Z, et al. Tumor microenvironment and its implications for antitumor immunity in cholangiocarcinoma: future perspectives for novel therapies. *Int J Biol Sci* (2022) 18 (14):5369–90. doi: 10.7150/ijbs.73949

24. Liu Z, Meng X, Tang X, Zou W, He Y. Intratumoral tertiary lymphoid structures promote patient survival and immunotherapy response in head neck squamous cell carcinoma. *Cancer Immunol Immunother* (2022). doi: 10.1007/s00262-022-03310-5

25. Zhan Z, Shi-Jin L, Yi-Ran Z, Zhi-Long L, Xiao-Xu Z, Hui D, et al. High endothelial venules proportion in tertiary lymphoid structure is a prognostic marker and correlated with anti-tumor immune microenvironment in colorectal cancer. *Ann Med* (2023) 55(1):114–26. doi: 10.1080/07853890.2022.2153911

26. Helmink BA, Reddy SM, Gao J, Zhang S, Basar R, Thakur R, et al. B cells and tertiary lymphoid structures promote immunotherapy response. *Nature* (2020) 577 (7791):549–55. doi: 10.1038/s41586-019-1922-8

27. Meylan M, Petitprez F, Becht E, Bougoüin A, Pupier G, Calvez A, et al. Tertiary lymphoid structures generate and propagate anti-tumor antibody-producing plasma cells in renal cell cancer. *Immunity* (2022) 55(3):527–41.e5. doi: 10.1016/j.immuni.2022.02.001

28. Cobaleda C, Schebesta A, Delogu A, Busslinger M. Pax5: the guardian of b cell identity and function. *Nat Immunol* (2007) 8(5):463–70. doi: 10.1038/ni1454

29. Smulski CR, Eibel H. BAFF and BAFF-receptor in b cell selection and survival. *Front Immunol* (2018) 9:2285. doi: 10.3389/fimmu.2018.02285

30. Sun D, Li F, Liu L, Yu S, Wang H, Gao X, et al. PSMA3-AS1 induced by transcription factor PAX5 promotes cholangiocarcinoma proliferation, migration and invasion by sponging miR-376a-3p to up-regulate LAMC1. *Aging (Albany NY)* (2022) 14(1):509–25. doi: 10.18632/aging.203828

31. Mason DY, Cordell JL, Brown MH, Borst J, Jones M, Pulford K, et al. CD79a: a novel marker for b-cell neoplasms in routinely processed tissue samples. *Blood* (1995) 86(4):1453–9. doi: 10.1182/blood.V86.4.1453.bloodjournal8641453

32. Stachelscheid J, Jiang Q, Aszyk CM, Warner K, Bley N, Müller TA, et al. The proto-oncogene TCL1A deregulates cell cycle and genomic stability in CLL. *Blood* (2022) 141(12):1425–41. doi: 10.1182/blood.2022015494

33. Hao J, Mei H, Luo Q, Weng J, Lu J, Wen Y. TCL1A acts as a tumour suppressor by modulating gastric cancer autophagy via miR-181a-5p-TCL1A-Akt/mTOR-c-MYC loop. *Carcinogenesis* (2022). doi: 10.1093/carcin/bgac085

34. Hiraoka N, Ino Y, Yamazaki-Itoh R, Kanai Y, Kosuge T, Shimada K. Intratumoral tertiary lymphoid organ is a favourable prognosticator in patients with pancreatic cancer. *Br J Cancer* (2015) 112(11):1782–90. doi: 10.1038/bjc.2015.145

35. Wang Q, Shen X, An R, Bai J, Dong J, Cai H, et al. Peritumoral tertiary lymphoid structure and tumor stroma percentage predict the prognosis of patients with non-metastatic colorectal cancer. *Front Immunol* (2022) 13:962056. doi: 10.3389/fimmu.2022.962056

36. Calderaro J, Petitprez F, Becht E, Laurent A, Hirsch TZ, Rousseau B, et al. Intratumoral tertiary lymphoid structures are associated with a low risk of early recurrence of hepatocellular carcinoma. *J Hepatol* (2019) 70(1):58–65. doi: 10.1016/j.jhep.2018.09.003

37. Finkin S, Yuan D, Stein I, Taniguchi K, Weber A, Unger K, et al. Ectopic lymphoid structures function as microniches for tumor progenitor cells in hepatocellular carcinoma. *Nat Immunol* (2015) 16(12):1235–44. doi: 10.1038/ni.3290

38. Sofopoulos M, Fortis SP, Vaxevanis CK, Sotiriadou NN, Arnogiannaki N, Ardavanis A, et al. The prognostic significance of peritumoral tertiary lymphoid structures in breast cancer. *Cancer Immunol Immunother* (2019) 68(11):1733–45. doi: 10.1007/s00262-019-02407-8

39. Patil NS, Nabet BY, Müller S, Koeppen H, Zou W, Giltnane J, et al. Intratumoral plasma cells predict outcomes to PD-L1 blockade in non-small cell lung cancer. *Cancer Cell* (2022) 40(3):289-300.e4. doi: 10.1016/j.ccell.2022.02.002

40. Smith ME, Farahani SJ, Chao T, Palmer M, Arriola A, Lal P. PD-L1 positivity associated with presence of tertiary lymphoid structures and high-stage disease in upper tract urothelial carcinoma. *Am J Clin Pathol* (2020) 154(6):802–10. doi: 10.1093/ajcp/aqaa105

frontiers | Frontiers in Immunology

TYPE Original Research
PUBLISHED 26 June 2023
DOI 10.3389/fimmu.2023.1176994

OPEN ACCESS

EDITED BY
Hui Zhao,
University of Texas MD Anderson Cancer Center, United States

REVIEWED BY
Hunter Shain,
University of California, San Francisco, United States
Ali Roghanian,
University of Southampton, United Kingdom

*CORRESPONDENCE
Melissa G. Lechner
mlechner@mednet.ucla.edu
Willy Hugo
hwilly@mednet.ucla.edu

RECEIVED 01 March 2023
ACCEPTED 22 May 2023
PUBLISHED 26 June 2023

CITATION
Ding L, Sun L, Bu MT, Zhang Y, Scott LN, Prins RM, Su MA, Lechner MG and Hugo W (2023) Antigen presentation by clonally diverse CXCR5+ B cells to CD4 and CD8 T cells is associated with durable response to immune checkpoint inhibitors. *Front. Immunol.* 14:1176994. doi: 10.3389/fimmu.2023.1176994

Antigen presentation by clonally diverse CXCR5+ B cells to CD4 and CD8 T cells is associated with durable response to immune checkpoint inhibitors

Lizhong Ding[1,2], Lu Sun[2,3], Melissa T. Bu[1], Yanjun Zhang[1,4], Lauren N. Scott[5], Robert M. Prins[2,3,6,7], Maureen A. Su[2,7,8,9], Melissa G. Lechner[5,8*] and Willy Hugo[1,2,8*]

[1]Department of Medicine, Division of Dermatology, University of California, Los Angeles, Los Angeles, CA, United States, [2]Parker Institute for Cancer Immunotherapy, University of California, Los Angeles, Los Angeles, CA, United States, [3]Department of Neurosurgery, University of California, Los Angeles, Los Angeles, CA, United States, [4]State Key Laboratory of Experimental Hematology, Institute of Hematology and Blood Diseases Hospital, Chinese Academy of Medical Sciences and Peking Union Medical College, Beijing, China, [5]Department of Medicine, Division of Endocrinology, Diabetes, and Metabolism, University of California, Los Angeles, Los Angeles, CA, United States, [6]Department of Molecular and Medical Pharmacology, University of California, Los Angeles, Los Angeles, CA, United States, [7]Jonsson Comprehensive Cancer Center, University of California, Los Angeles, Los Angeles, CA, United States, [8]Department of Microbiology, Immunology, and Molecular Genetics, University of California, Los Angeles, Los Angeles, CA, United States, [9]Department of Pediatrics, Division of Pediatric Endocrinology, University of California, Los Angeles, Los Angeles, CA, United States

Introduction: Increased T cell infiltration and interferon gamma (IFNγ) pathway activation are seen in tumors of melanoma patients who respond to ICI (immune checkpoint inhibitor) or MAPK pathway inhibitor (MAPKi) therapies. Yet, the rate of durable tumor control after ICI is almost twice that of MAPKi, suggesting that additional mechanisms may be present in patients responding to ICI therapy that are beneficial for anti-tumor immunity.

Methods: We used transcriptional analysis and clinical outcomes from patients treated with ICI or MAPKi therapies to delineate immune mechanisms driving tumor response.

Results: We discovered response to ICI is associated with CXCL13-driven recruitment of CXCR5+ B cells with significantly higher clonal diversity than MAPKi. Our *in vitro* data indicate that CXCL13 production was increased in human peripheral blood mononuclear cells by anti-PD1, but not MAPKi, treatment. Higher B cell infiltration and B cell receptor (BCR) diversity allows presentation of diverse tumor antigens by B cells, resulting in activation of follicular helper CD4 T cells (Tfh) and tumor reactive CD8 T cells after ICI therapy. Higher BCR diversity and IFNγ pathway score post-ICI are associated with significantly longer patient survival compared to those with either one or none.

Conclusions: Response to ICI, but not to MAPKi, depends on the recruitment of CXCR5+ B cells into the tumor microenvironment and their productive tumor antigen presentation to follicular helper and cytotoxic, tumor reactive T cells. Our study highlights the potential of CXCL13 and B cell based strategies to enhance the rate of durable response in melanoma patients treated with ICI.

KEYWORDS

melanoma, immunotherapy, checkpoint inhibitors, interferon gamma pathway, tertiary lymphoid structure (TLS), T cell, B cell, antigen presentation

Introduction

Metastatic melanoma used to have a dismal median overall survival of only nine months after diagnosis (1, 2). However, the advent of immune and targeted therapies (3, 4) has significantly improved the survival of patients with metastatic melanoma. The highly immunogenic nature of melanoma has made it the model cancer to study response to immune checkpoint inhibitors (ICI), such as the blocking antibodies against T cell inhibitory receptors (T cell "checkpoints") such as cytotoxic T lymphocyte antigen (CTLA)-4 and programmed death protein (PD)-1 (5–8). Despite the remarkable success of ICIs in many patients with melanoma, their clinical response remains difficult to predict (9–12). Previous work highlighted the association of T cell infiltration and patient response to ICI; ICI-treated tumors displayed a higher number of infiltrating T cells accompanied by expression of genes related to interferon pathway activities, demonstrating increased production of interferon gamma (IFNγ) of these T cells (13–17).

The discovery of constitutive activation of RAF/MEK/ERK signaling *via* the BRAF V600 mutation in nearly half of all cutaneous melanoma cases also revolutionized cancer therapy (18). MAPK pathway inhibitor (MAPKi) treatment significantly prolonged the survival of metastatic melanoma patients with BRAF V600 mutation ($BRAF^{V600}$ mutant melanoma) (19–21). In addition to its direct tumor suppressive effect through MAPK pathway inhibition, MAPKi treatment also increases the infiltration of antitumor T cells into the tumor microenvironment (TME), suggesting immune modulatory effects (22, 23).

Intriguingly, despite MAPKi therapy having a higher rate of initial response than ICI (MAPKi (dabrafenib+ trametinib): 67% (19), MAPKi (vemurafenib+cobimetinib): 68% (20) vs ICI (nivolumab and ipilimumab): 58% (8)), the 5-year survival rate of $BRAF^{V600}$ mutant subset of melanoma patients treated with MAPKi is only around half that of ICI (34% using dabrafenib and trametinib (24), 31% using vemurafenib and cobimetinib (25) vs. 60% after nivolumab and ipilimumab (26)). Furthermore, a matching-adjusted study found that ICI treatment improved overall survival (OS) of BRAF-mutant melanoma patients when compared to MAPKi (27). While acknowledging some differences among these studies, this consistent and significant difference in durable survival between ICI and MAPKi treated melanoma patients suggests that there may be fundamental differences in the anti-tumor responses induced by these therapies.

To discover such differences, this study analyzes the changes in immune related gene expressions that are significantly associated with survival of melanoma patients after ICI or MAPKi treatment. Previous work compared on-treatment tumors (i.e., these tumor samples were biopsied after treatment) of patients responding to ICI (ICI OT-R) compared with those from patients not responding to ICI (ICI OT-NR) to nominate immune factors/pathways associated with response to ICI (15–17). However, this comparison is not necessarily informative. Since ICI OT-NR tumors generally have less immune infiltration compared to ICI OT-R, most immune cell-related markers will be upregulated in ICI OT-R group. Which of these are drivers of ICI's durable response vs. insignificant bystanders is therefore unclear. Since MAPKi OT-R tumors also have more immune infiltration than MAPKi OT-NR tumors, yet MAPKi OT-R patients are less likely to achieve a durable response than ICI OT-R patients, we posit that immune genes/pathways that are upregulated/enriched in ICI OT-R, but not in MAPKi OT-R tumors, can help explain the higher rate of durable responses in ICI treated patients.

In this report, we used transcriptional analysis and clinical outcomes from patients treated with ICI or MAPKi therapies to delineate immune mechanisms driving tumor response. We discovered higher expression of genes related to B cell recruitment in the ICI OT-R tumor, such as the ligand/receptor pair *CXCL13* and *CXCR5*. Anti-PD1 antibody treatment of human immune cells upregulated CXCL13 while MAPKi inhibited CXCL13 production, suggesting that differential regulation of CXCL13 by these two treatments may dictate treatment outcomes. Single cell RNA-seq analysis of ICI-treated melanoma confirmed that response to ICI increased the number of germinal center-like B cells and its associated T follicular helper CD4 T cells, indicative of tertiary lymphoid structure (TLS) formation as reported previously (28–31). These cells were recruited into the TME by CXCL13-producing, cytotoxic CD8 T cell population that was specific to ICI. Importantly, BCR diversity, but not clonality, was significantly associated with extended overall survival after ICI but not MAPKi. The significant association between BCR diversity and survival after ICI suggests that ICI-induced B cells serve as antigen presenting cells, which will be able to cover more tumor

antigens with more diversified BCR clones. Indeed, patients whose tumors display both higher BCR diversity and IFNγ signaling pathway scores after ICI, which suggest successful antigen presentation by B cells to T cells, have significantly longer overall survival than those with either one or none. Our results suggest a combination of ICI with therapies that enhance immigration of and antigen presentation by clonally diverse B cells can result in a more durable antitumor immune response.

Materials and methods

Datasets used

In order to perform a comparative analysis on transcriptomic response to ICI and MAPKi, we analyzed two batches of immunotherapy data and two batches of targeted therapy data. The two immunotherapy datasets are from Riaz N, et al. (32) (named 2017_Cell_NR) and Abril-Rodriguez G, et al. (16) (named 2020_NC_GA). The patients from the two cohorts were treated with antibodies against PD-1 receptor (anti-PD-1) including nivolumab and pembrolizumab. The two targeted therapy datasets are derived from Hugo W, et al. (23, 33) (named 2015_Cell_WH) and from Kwong LN, et al. (34) (named 2015_JCI_LK). Two microarray datasets of MAPKi-treated tumors were used as validation cohort (35, 36). Patients in the targeted therapy datasets were treated with either BRAF inhibitor monotherapy or BRAF and MEK inhibitors combination therapy (BRAFi: vemurafenib, dabrafenib, encorafenib; MEKi: cobimetinib, trametinib, binimetinib; one patient was treated with trametinib monotherapy). All samples were classified into three groups: pre-treatment (PT), on-treatment responding (OT-R), and on-treatment non-responding (OT-NR). OT-R is defined by clinical benefit after therapy (CR, PR, or SD by RECIST criteria). OT-NR is defined by no clinical benefit (PD) (Supp. Table 1A). For single cell transcriptome analysis, we utilized the data from Sade-Feldman et al. (37). The data profiled 16,291 immune cells (CD45+ cells) from 48 tumor samples of melanoma patients treated with ICI. All samples were classified into four groups: pre-treatment responding (PT-R), pre-treatment non-responding (PT-NR), on-treatment responding (OT-R), and on-treatment non-responding (OT-NR). The PFS and OS data of MAPKi treated patients were extracted from the above-mentioned two microarray datasets (Supp. Table 2).

The bulk RNA-seq data were downloaded from the following online repositories. 2017_Cell_NR (ICI) was from PRJNA356761; 2020_NC_GA (ICI) was from PRJNA578193; 2015_Cell_WH (MAPKi) was from PRJNA273359, PRJNA303170, PRJNA403850; 2015_JCI_LK (MAPKi) was from EGAD00001001306. The single cell RNA-seq data were downloaded from the GEO database (accession ID: GSE120575). Instead of the TPM normalized expression values, we started from the raw counts provided by the authors in personal communications. The raw count expression values were included in the source code of this study. Two microarray data sets of MAPKi-treated melanoma were downloaded from GEO (accession ID: GSE61992 and GSE50509).

Gene expression analysis

The bulk RNA-seq data was re-aligned to hg38 human reference genome using HiSAT2 (v2.1.0), then processed using samtools (v1.10, RRID : SCR_002105) and picard (v2.25.0). The gene expression count was calculated using htseq-count (v0.11.2). The gene expression was normalized using trimmed mean of M-values (TMM) and converted to count per million (cpm) expression value using the R package edgeR (v3.32.1, RRID : SCR_012802). Batch effect was corrected using removeBatchEffect function in the R package limma (v3.46.0).

Differential gene expression analysis

We first computed the expression change of each gene (in $\log_2$ FC) between the PT and OT samples of each patient (the OT samples can be OT-R or OT-NR). Thus, each gene will have a list of $\log_2$ FC values associated with therapy response (OT-R with respect to their respective PT) and resistance/non-response (OT-NR w.r.t their respective PT) (Figure 1A). Differentially expressed genes (DEGs) between the OT-R and OT-NR groups were defined by:

1. two-fold difference between the arithmetic average of $\log_2$ FCs in OT-R and arithmetic average of $\log_2$ FCs in OT-NR ($\Delta\log_2$ FC ≥ 1 where $\Delta\log_2$ FC = mean($\log_2$ FC(OT-R)) - mean($\log_2$ FC(OT-NR))), and,
2. FDR-adjusted t-test p value < 0.05 between the $\log_2$ FCs of the OT-R and OT-NR groups.

The sets of DEGs upregulated in the OT-R groups of either therapy were shown in Figure 1B. The gene sets/ontologies that are enriched in the ICI-specific, MAPKi-specific and ICI and MAPKi shared DEGs were computed using Enrichr (38) (see the **gene set analysis** section). Other than comparing the list of DEGs, we also directly computed the difference of $\log_2$ FC difference between the OT-R and OT-NR groups across the two therapies. For instance, to find the genes that are upregulated at least two-fold higher in ICI's responder when compared to MAPKi responders (after adjusting with their respective non-responder groups), we selected genes satisfying:

1. $\Delta\Delta FC_{ICI\text{-}MAPKi} \geq 1$, where $\Delta\Delta FC_{ICI\text{-}MAPKi} = \Delta\log_2 FC_{ICI} - \Delta\log_2 FC_{MAPKi}$, and,
2. $\Delta\log_2 FC_{ICI} \geq 1$

Conversely, the genes upregulated in MAPKi's responders were computed in the same manner.

Gene sets analysis

Shortlisted genes from DEG analysis were analyzed for overlap-based gene set enrichment using Enrichr (38). Top enriched gene sets from Human_Gene_Atlas and HuBMAP_ASCT_plus_B_

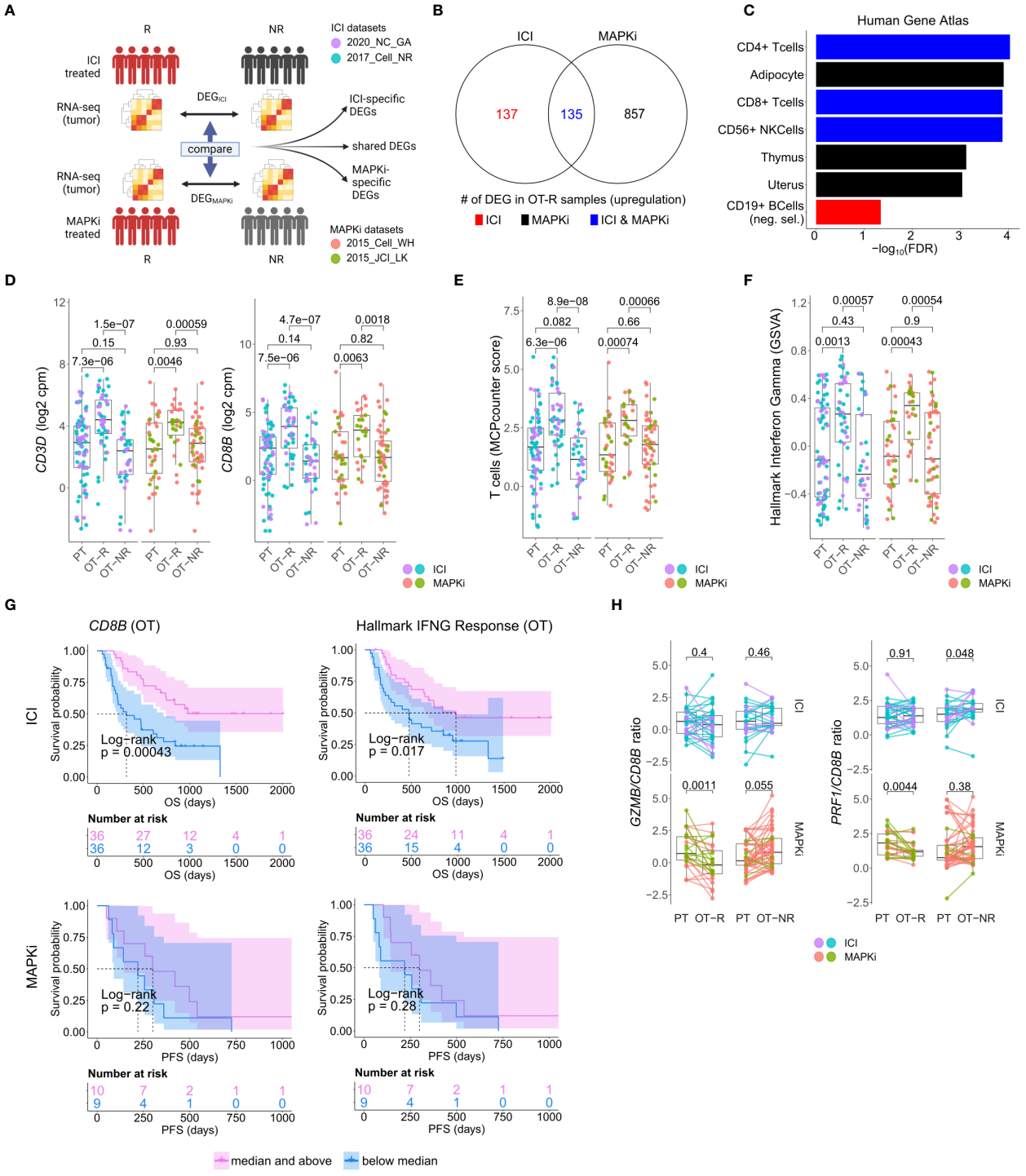

FIGURE 1
Response to ICI or MAPKi therapy is associated with increased T cell infiltration and enhanced interferon gamma (IFNγ) pathway activity in the tumor. **(A)** Schematic of comparative analysis between transcriptomic response to ICI or MAPKi therapy. **(B)** The number of differentially upregulated genes in ICI OT-R (on treatment-responding) tumors (red), MAPKi OT-R (black) or both (blue). The differentially expressed genes (DEGs) are computed with respect to the OT-NR (on treatment-non responding) tumors of each group. **(C)** Enriched cell marker genes (based on Human Gene Atlas using Enrichr tool) in ICI-specific, MAPKi-specific, and ICI and MAPKi-shared upregulated DEGs in **(B)**. **(D)** Normalized expression of T cell marker genes *CD3D* and *CD8B* in the PT (pre-treatment), OT-R and OT-NR tumors of patients treated with ICI or MAPKi therapy. **(E)** T cell enrichment scores computed by MCPcounter in the PT, OT-R and OT-NR tumors of patients treated with ICI or MAPKi therapy. **(F)** GSVA gene set enrichment scores of hallmark interferon gamma downstream gene set from the Molecular Signature database. **(G)** Kaplan-Meier survival curves of ICI- or MAPKi-treated melanoma patients stratified by either *CD8B* expression (left) or hallmark interferon gamma response gene set scores (right) in their OT tumors. **(H)** *CD8B*-normalized normalized expression of T cell cytotoxicity genes *GZMB* and *PRF1* in the PT, OT-R and OT-NR samples of patients treated with ICI or MAPKi therapy.

augmented_w_RNAseq_Coexpression collections are visualized in Figure 1C and listed in Supp. Table 1C. Score based, single sample gene set enrichments was computed using Gene Set Variation Analysis (GSVA) (39) through R packages GSVA (v1.38.2), GSVAdata (v1.26.0), and GSEABase (v1.52.1).

We used the interferon gene sets from the Molecular Signatures Database (MSigDB) (40, 41). Specifically, we collected gene sets containing the keyword "IFN" or "interferon" from the H: hallmark gene sets, C2 CGP: chemical and genetic perturbations, C6: oncogenic signatures, and C7: immunologic signatures (Supp. Table 1E). The gene set of TLS signatures were manually curated in gmt file format. Cabrita et al. developed two gene sets that reflected the presence of TLS in melanoma. One TLS signature of nine genes (*CD79B, CD1D, CCR6, LAT, SKAP1, CETP, EIF1AY, RBP5, PTGDS*) was found using differential expression analysis. The other TLS signature of seven genes (*CCL19, CCL21, CXCL13, CCR7, CXCR5, SELL, LAMP3*) was constructed from a compendium of TLS hallmark genes (29).

Clonotype analysis

As for the TCR clonotyping, the raw output of clonotypes was derived from the raw FASTQ reads of the bulk RNA-seq data using TRUST4 (v1.0.4) (42) with default settings. Nonproductive CDR3aa were removed from the raw output. Clonotypes are separated by chain names such as TRA, TRB, TRD, TRG, IGH, IGK, IGL. Convergent clonotypes, which possess the same amino acid sequences but different nucleotide sequences, were merged. As for the BCR clonotyping, considering the somatic hypermutation (SHM) mechanism of germinal center (GC) B cells, productive IGH chains were selected from the raw AIRR standard format output derived from the bulk RNA-seq data using TRUST4 (v1.0.4). Then the hierarchicalClones() function in the R package SCOPer (43) (v1.2.0) was used to infer—based on the nucleotide sequence—the germline BCR clones that arise from V(D)J recombination (in the bone marrow) and mature (SHM-generated) BCR clones that are derived from germline BCR clones after somatic hypermutation process in the germinal center (44). The R package SHazaM (45) (v1.1.0) was used to automatically calculate the threshold for the bimodal distribution from the hierarchicalClones() function as defined by the SCOPer pipeline. Consequently, the SHM occurrence frequency can be calculated using the count of germline BCR clones associated with more than one mature BCR clone divided by total count of the germline BCR clones. The clonotype repertoire metrics of TCR and BCR, including count, diversity, and clonality were calculated using the custom R package rTCRBCRr (v0.1.0) and other custom R scripts.

Cell population abundance estimation

The R package MCPcounter (v1.2.0) was applied to the normalized $\log_2$ cpm expression matrix from the bulk RNA-seq data in order to estimate the absolute abundance of eight immune and two stromal cell populations in each sample, including T cells, CD8 T cells, cytotoxic lymphocytes, B lineage, NK cells, monocytic lineage, myeloid dendritic cells, neutrophils, endothelial cells, and fibroblasts (Supp. Table 1D).

Overlap-based gene set enrichment

The enrichment of specific biological process or gene ontologies were analyzed using Enrichr, which is implemented in enrichR R package (v3.0) (38). Specifically, lists of DEGs were tested for significant overlaps with pre-curated gene sets within the Enrichr based on fisher exact test. The P values we utilized were the ones adjusted for multiple tests using the FDR method and the cutoff of enriched gene set term is adjusted P value < 0.05.

Survival analysis

The Kaplan-Meier curves were used to visualize differences in survival between patient groups. Cox proportional hazard (Cox PH) regression was used to assess the effect of single or multiple variables on hazard ratio. These analyses were performed using the R packages survival (v3.2.13) and visualized using survminer (v0.4.9), and survivalAnalysis (v0.3.0). For PFS analysis in the MAPKi-treated cohort, we only included OT tumors biopsied prior to progression (giving a total 25 OT tumors from 19 MAPKi-treated patients).

Single cell analysis

The single cell data was processed using the R package Seurat (v4.0.2). The raw count data were provided by the authors. We first normalized the raw counts using the NormalizeData() function with normalization.method="LogNormalize" and scale.factor=10000. 17 clusters were identified at resolution=0.5. Cell types of the clusters were manually annotated based on each cluster's gene markers, which were computed using FindAllMarkers() (min.pct=0.25 and logfc.threshold=0.585). The R package AUCell (v1.12.0) was used to identify gene set enrichments in the single cell transcriptome. The R package CellChat (v1.1.3) was used to visualize cell-cell communication network, grouped by different signaling pathways, among different cell types.

Statistical analysis

All the statistical analysis were performed using R programming language version 4.0.5. Unless otherwise stated, all the statistical tests were two tailed. In all boxplots, including gene expression, GSVA score, and gene expression ratio, P values were calculated using a two-sided Wilcoxon rank sum test. In all boxplots, the median is indicated by the line within the box and the 25th and 75th percentiles indicated by the lower and upper bounds of the box. The upper and lower lines above and below the boxes represent the whiskers. Pearson's R correlation coefficient was computed using

R's *cor.test* function. The P values of the Pearson's R correlation coefficient were computed using two-sided t-test as described in the documentation. In the Kaplan-Meier survival curves, the P value is the log-rank test P value. In the Cox PH analysis, the P value shown for each variable in the graph is the result of Wald test.

In vitro assessment of primary human immune cells

Peripheral blood mononuclear cells (PBMC) from healthy donors were isolated from blood by density gradient centrifugation (Ficoll-Hypaque). PBMC were cultured at 10^6 cells/well in 12 well plates in complete media with 2ME. Stimulation was provided by anti-CD3/CD28 Dynabeads (Invitrogen), as well as anti-human PD-1 (clone pembrolizumab, BioXcell, RRID: AB_2894731), MEKi trametinib (LSBiosciences) and BRAFi dabrafenib (BioVision), or vehicle. Supernatants were collected on day 5. Secreted CXCL13 was quantified in supernatants by ELISA (R&D Systems). The concentrations chosen for dabrafenib and trametinib was based on reported maximum plasma concentration in patients, which were 2.4 μM and 0.03 μM, respectively (46). To avoid overactivation of the T cells in the PBMC, we chose a lower PD-1 antibody concentrations (1 and 10 μg/mL) than the median C_{max} and C_{trough} of pembrolizumab (89.1 and 27.6μg/mL) (47).

Results

ICI and MAPKi treatment induce comparable levels of T cell infiltration

To perform a comparative analysis of transcriptomic response to ICI and MAPKi, we analyzed three separate immunotherapy datasets (16, 32, 37) and three targeted therapy datasets (23, 33, 34) (Supp. Figure 1A; Supp. Table 1A). All samples were classified into three groups: pre-treatment (PT), on-treatment responding (OT-R), and on-treatment non-responding (OT-NR). OT-R is defined by clinical benefit after therapy (CR, PR, or SD by RECIST criteria). OT-NR is defined by no clinical benefit (PD) (Supp. Table 1A). Gene expression in samples across the datasets were integrated and batch normalized (see Methods).

We asked whether the set of differentially expressed genes (DEG) between ICI and MAPKi could reveal any cell populations or biological processes that may explain ICI's more durable antitumor response. To this end, we selected genes upregulated in the OT-R compared to the OT-NR samples for each therapy (Figure 1A, see Methods for details). The upregulated DEG were grouped into either ICI-specific, MAPKi-specific, or ICI and MAPKi-shared (Figure 1B; Supp. Table 1B), and gene sets enriched by these DEGs were computed using Enrichr (38). We first noted gene sets related to T cells being enriched in the OT-R groups of both therapies (Figure 1C; Supp. Tables 1C, D). Indeed, increased T cell infiltration and activity are important for both ICI and MAPKi response (13, 15, 17, 22, 32, 37, 48) and the levels of general T cell marker (*CD3D*), cytotoxic CD8 T cells (*CD8B*), T cell signature and IFNγ pathway score were significantly higher in the OT-R tumors of MAPKi or ICI compared to PT and OT-NR tumors (Figures 1D–F; Supp. Tables 1D, E). T cell marker expressions and IFNγ pathway score were not significantly different between ICI and MAPKi in either PT, OT-R or OT-NR samples (Supp. Figures 1B, C). Our data suggests that response to ICI or MAPKi induces a robust increase in T cell infiltration and IFNγ pathway activation in the TME.

Intriguingly, only higher normalized expression of CD8 T cell marker *CD8B* or higher IFNγ gene set enrichment in ICI OT tumors, but not MAPKi OT tumors, was significantly correlated with longer survival (Figure 1G). Neither *CD8B* expression nor IFNγ pathway score in PT biopsies was significantly correlated with survival (Supp. Figure 1D), indicating the importance of T cell infiltration and activity after therapy. Using a separate microarray dataset of MAPKi OT tumors (35, 36), we confirmed that neither higher *CD8B* nor higher IFNγ gene set enrichment was correlated with OS and PFS after MAPKi therapy (Supp. Figure 1E). Since the MAPKi RNA-seq datasets only have progression free survival (PFS) information available and since melanoma patients' PFS is significantly correlated with their OS in the MAPKi microarray data (Supp. Figure 1F), we will use PFS differences in the MAPKi cohort as a surrogate of OS differences in later analysis of the MAPKi RNA-seq datasets.

We noted higher total expression of T cell cytotoxicity-related genes, *GZMB* and *PRF1*, in ICI OT-R than MAPKi OT-R (Supp. Figure 1G). We further estimated the levels of these cytotoxicity-related genes on a per T cell basis by computing the ratio between normalized expression of the markers and *CD8B*. On this approximated per-CD8 basis, MAPKi-treated responders had lower *GZMB* and *PRF1* expression than their patient-matched PT tumors while ICI-treated responders did not show such a decrease (Figure 1H). Overall, our analysis demonstrated that ICI treatment induces the infiltration of more cytotoxic CD8 T cells into the TME compared to MAPKi and such increase in T cell activity is significantly correlated with patient OS after ICI therapy.

B cells are more abundant in ICI On Treatment Responding tumors and are correlated with improved survival after ICI therapy

We next examined ICI-specific DEGs to discover additional cell populations or pathways that are significantly associated with response to ICI therapy. On one hand, genes related to B cells and DC gene sets (Figures 1C; 2A; Supp. Table 1C) were upregulated in ICI OT-R tumors compared to MAPKi OT-R tumors (after adjusting against the average expression of the same genes in the respective OT-NR groups, see Methods). On the other

10.3389/fimmu.2023.1176994

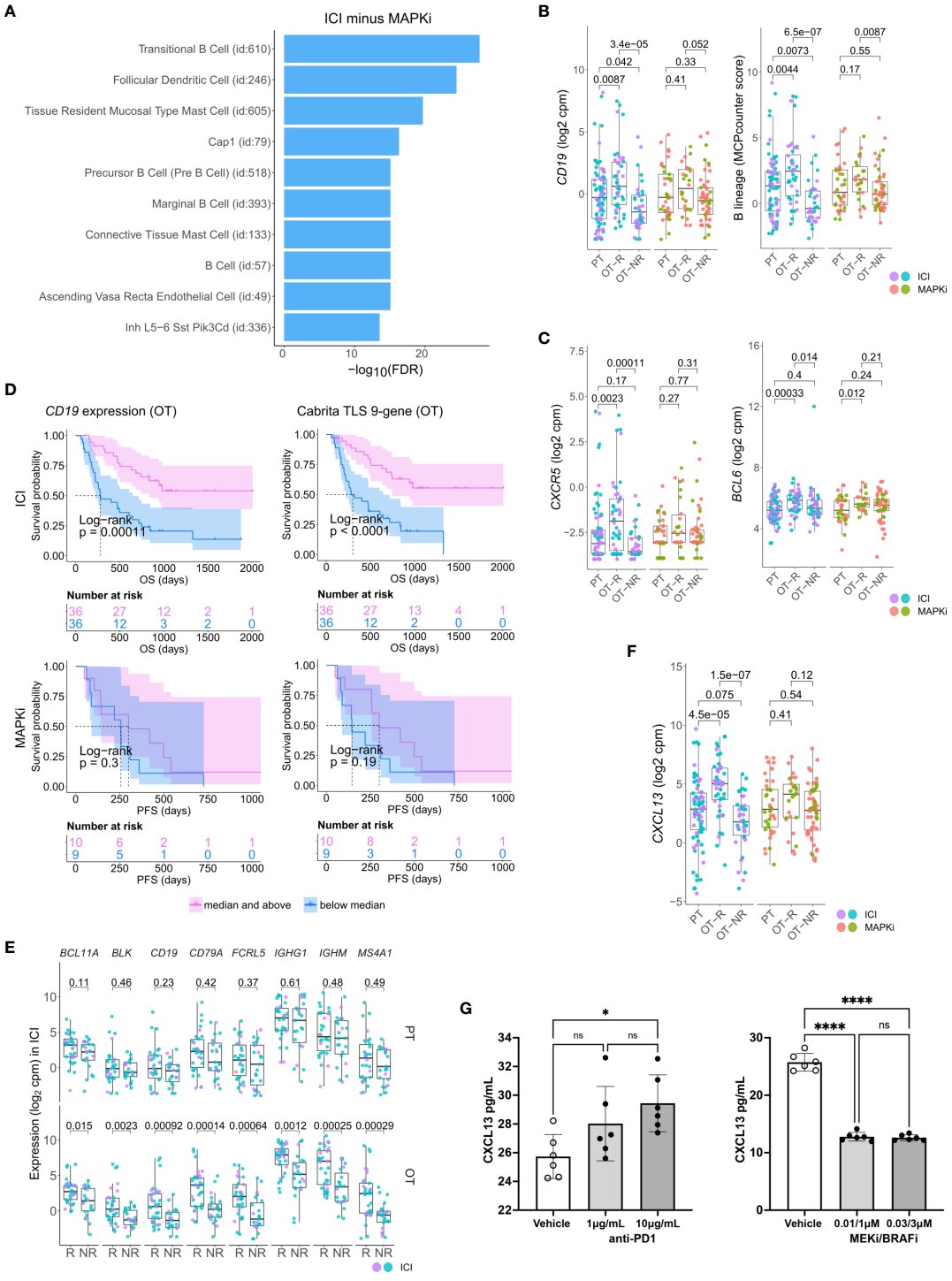

FIGURE 2
Relative increase of B cell and tertiary lymphoid structure (TLS) marker genes in response to ICI therapy compared to MAPKi. **(A)** Enriched tissue specific gene sets in DEGs upregulated in ICI OT-R tumors with respect to MAPKi OT-R tumors (after adjustment by respective therapy group's OT-NR tumors; see Methods). **(B)** Normalized expression of B cell marker genes and enrichment of B cell lineage gene set among the PT, OT-R and OT-NR tumors in the ICI or MAPKi therapy group. **(C)** Normalized expression of TLS-related genes, *CXCR5* and *BCL6*, among the PT, OT-R and OT-NR tumors in the ICI or MAPKi therapy group. **(D)** Kaplan-Meier survival curves of ICI- or MAPKi-treated melanoma patients stratified by either *CD19* expression (left) or TLS gene set enrichment score (right) of their OT tumors. **(E)** Pairwise expression comparison of the listed B cell-related genes between PT (top) or OT (bottom) samples of melanoma patients stratified by response (R) or no response (NR) to ICI. **(F)** Normalized expression of *CXCL13* among the PT, OT-R and OT-NR tumors in the ICI or MAPKi therapy group. **(G)** CXCL13 secretion by human peripheral blood mononuclear cells is increased by anti-PD-1 antibody treatment but decreased by trametinib (MEK inhibitor) + dabrafenib (BRAF V600E inhibitor) *in vitro*. The six points in each bar graph across represent the same PBMC samples from six donors; these were treated with the indicated amount of antibody/inhibitor or vehicle. Significance of pairwise comparisons was computed using t-test, * p<0.05, ****p<0.0001, ns, not significant.

hand, MAPKi OT-R tumors showed enrichment of non-immune related gene sets such as neuron, melanocyte and adipocyte related genes (Supp. Figure 2A; Supp. Table 1C).

There were more prominent upregulations of B cell gene markers, B cell signature and immunoglobulin genes in OT-R tumors, with respect to either OT-NR or PT tumors after ICI compared to MAPKi therapy (Figure 2B; Supp. Figure 2B; Supp. Tables 1C, D). Importantly, the expression of TLS-associated, germinal center B cell (GC B cells) and follicular helper T cell (Tfh) markers, *CXCR5* and *BCL6*, were significantly upregulated only in response to ICI but not MAPKi (Figure 2C). The presence of TLS has been correlated with improved survival after ICI therapy in melanoma (28, 29) and other cancers (30, 31). ICI treatment also induced a more significant increase of gene set scores of two TLS signatures (29) compared to MAPKi (Supp. Figure 2C; Supp. Table 1E). The magnitude of *CD19* expression and TLS signature score both significantly correlated with survival after ICI but not MAPKi therapy (Figure 2D; Supp. Figure 2D). On the other hand, the level of B cell marker or the TLS signature in the PT samples is not associated with survival after ICI treatment (Supp. Figure 2E). In agreement with the survival data, B cell marker expression was positively correlated with tumor response to ICI in OT but not PT tumors (Figure 2E), suggesting that the expression of B cell and TLS marker genes pre-therapy are relatively weak predictors of ICI response and survival in melanoma patients.

Among ICI-specific differentially expressed of cytokines and chemokines was *CXCL13*, which is the ligand for *CXCR5* and a key chemokine for the formation of TLS (Figure 2F). The upregulation of *CXCL13* after ICI treatment is expected to recruit *CXCR5*+ B cells and *CXCR5*+ Tfh cells. We tested if ICI can directly increase CXCL13 expression in human immune cells. Incubation of anti-CD3/28 activated peripheral blood mononuclear cells (PBMC) with anti-PD-1 antibody increased the secretion of CXCL13 protein (Figure 2G, left). In contrast, treatment with BRAF and MEK inhibitors (MAPKi) significantly inhibited CXCL13 secretion (Figure 2G, right). Thus, CXCL13 production is promoted by anti-PD1 antibody, but impaired by BRAF and MEK inhibitors. The increase in CXCL13 was associated with increased expression of B cell and TLS-associated markers (*CXCR5*, *BCL6*) in ICI OT-R tumors.

Enrichment of B cell and Tertiary Lymphoid Structure gene markers in single cell transcriptome of ICI responding melanoma

To analyze potential connections between enhanced CD8 T cell cytotoxicity and increased presence of TLS-associated B cells in ICI OT-R tumors, we examined single cell transcriptomic data of tumors from an independent cohort of ICI-treated melanoma patients (37). Since this scRNA-seq is done on a sampling of sorted CD45+ cells, we can only compare the relative abundances of immune populations within the samples. Nonetheless, we were able to analyze significantly increased/decreased expression of gene markers within each immune population, allowing us to identify the cellular source of DEGs in the bulk RNA-seq analysis.

After normalization and scaling of the gene expression values (see Methods), we re-clustered the single cells and identified the cell types based on differentially upregulated immune gene markers in each cluster (Figures 3A–C; Supp. Table 3A). Clusters of known immune populations, such as memory T cell (*CD4/8*+ *CCR7*+ *TCF7*+), activated CD8 T cell (*IFNG*+ or high in interferon downstream genes (ISGs)), activated/exhausted CD8 T cell (*PDCD1*+ *CTLA4*+ *TOX*+) with high expression of *CXCL13*, B cell (*CD19*+ *MS4A1*+), plasma cell (*SDC1*+ *IGHG/A*+), NK cell (*FCGR3A*+ *GNLY*+), Treg (*FOXP3*+ *CTLA4*+), monocyte/macrophage (Mφ) (*CD14*+ *CD163*+), monocyte-derived dendritic cells (monocytic DC: *CD14*+ *CLEC10A*+), plasmacytoid DC (*LILRA4*+) and proliferating immune cell (*MKI67*+), were marked accordingly. We identified a *CXCR5*+ *BCL6*+ *CXCL13*+ follicular helper T cell (Tfh) population in a subset of *PDCD1*+ *CXCL13*+ *CTLA4*+ *TOX*+ *TCF7*+ *CD4*+ T cells (Figure 3B). We also noted the expression of *BCL6* and *REL* in the B cell population (Figure 3C); along with *BCL6*, *REL* is a transcription factor that is upregulated in GC B cells (44).

Corroborating the B cell marker up-expression in ICI OT-R tumors in bulk RNA-seq, we noted a significantly higher proportion of B cells in ICI OT-R samples compared to OT-NR samples (Figure 3D, red boxplots, bottom, Supp. Table 3B). We also noted that, in this scRNA-seq cohort, the proportion of B cells was already higher in the PT-R samples (Figure 3D, red boxplots, top, Supp. Table 3B). However, only B cell abundance in ICI OT tumors was significantly correlated with the patients' OS (Figure 3E; Supp. Table 3C).

Looking at the other cell populations, the proportion of *CCR7*+ *TCF7*+ memory T cells per sample were higher in the PT-R and OT-R samples (Figure 3D, leftmost boxplot, Supp. Table 3B), in line with the original publication (37). Populations with a higher proportion in the OT-NR biopsies were the proliferating cluster and CD14+ CD163+ Mφ clusters (Supp. Figure 3A; Supp. Table 3B). The proliferative cluster showed high expression of *CD3D*, *CD8A*, *PDCD1*, *CTLA4* and *TOX* (Figure 3B, rightmost boxplot); this population matches the phenotype of an intermediate exhausted cytotoxic T cells, which are expected to differentiate into terminally exhausted T cells (49). The CD14+ CD163+ Mφ fraction was associated with worse OS after ICI (Supp. Figure 3B), suggesting that this is an immunosuppressive Mφ population.

In each cell population, we analyzed genes increased in expression in ICI OT-R tumors compared to OT-NR tumors (Supp. Table 3D). Consistent with evidence for GC B cells and Tfh in ICI-responders from the bulk RNA-seq cohort above, CXCR5+ B cells in OT-R showed increased expression of *BCL6* and *REL* (Figure 3F). We also confirmed that expression of *CXCR5* was significantly increased in Tfh/Tph population of ICI OT-R patients (Figure 3G, green boxplots), implying a higher proportion of Tfh cells in ICI OT-R tumors. The bulk RNA-seq cohorts showed an increased overall expression of *CXCL13*, which is the chemotactic factor for the CXCR5+ GC B and Tfh cells in ICI OT-R tumors. The scRNA-seq data allowed us to trace the source of *CXCL13* expression; *CXCL13* was significantly upregulated in the *PDCD1*+ *TOX*+ CD8 T cell in ICI OT-R tumors (Figure 3G). Of note, *CXCL13*+ *PD1*+ *TOX*+ CD8 T cell population was recently reported to comprise a high fraction of tumor antigen-specific CD8 T cells (50).

10.3389/fimmu.2023.1176994

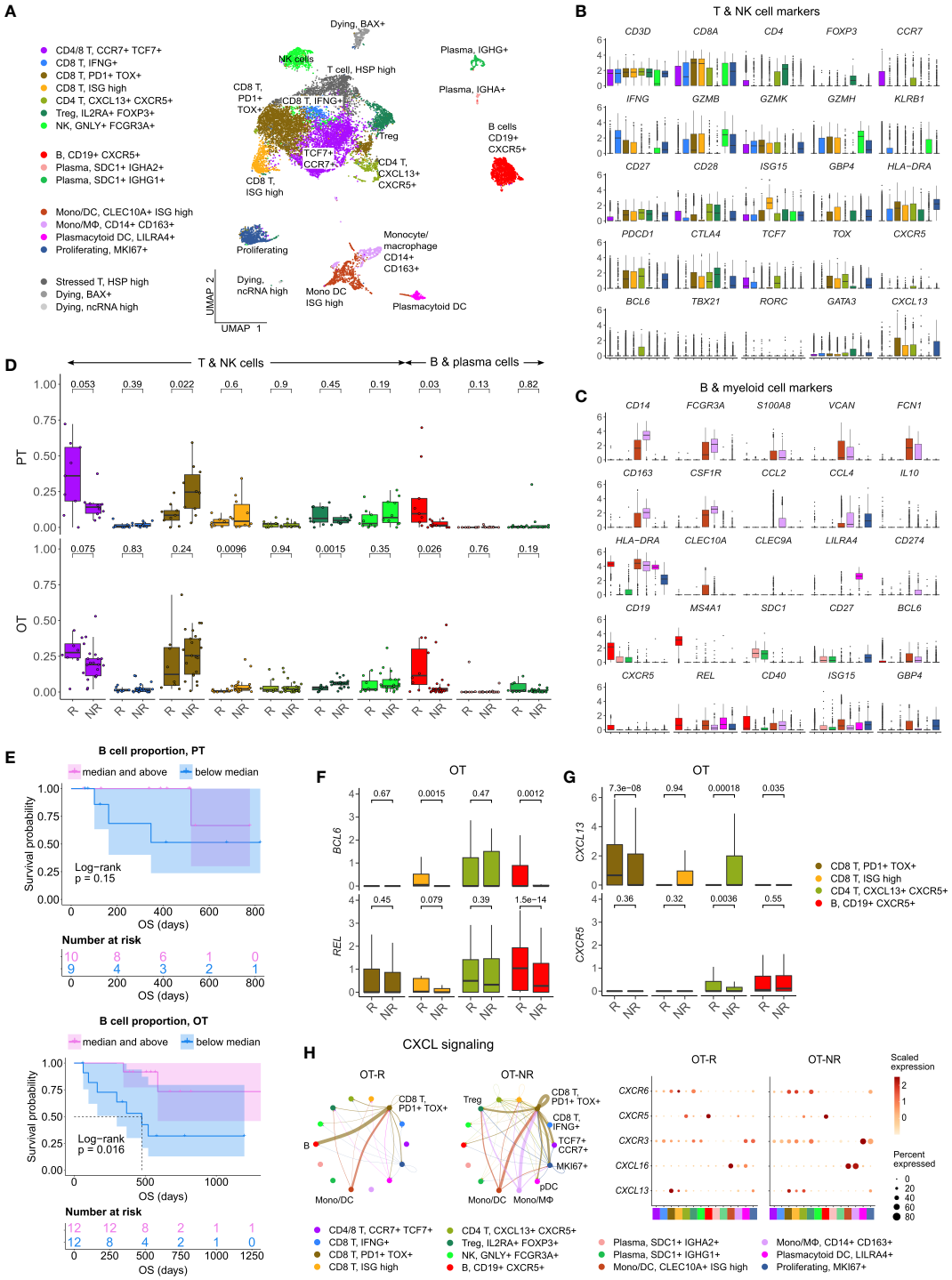

FIGURE 3
Increased B cell proportion is associated with TLS marker enrichments and improved OS in an independent cohort of ICI treated melanoma. **(A)** UMAP projection of intratumoral CD45+ cells of ICI-treated melanoma. The cell type annotation of each cell cluster was inferred from the DEGs of each cluster. Mono/DC: monocytic DCs, Mono/Mφ: monocytes/macrophages. **(B, C)** Normalized expression of markers of cell type/activity among different T and NK cell **(B)** or B cell and myeloid cell populations **(C)**. **(D)** The fraction of the T, NK, B and plasma cell populations in stratified by response vs. non-response to ICI in PT (top) and OT tumors (bottom). The boxplots are colored to match the cell clusters in **(A)**. **(E)** Kaplan-Meier survival curves of ICI-treated patients stratified by the proportion of B cells within either their PT (top) or OT tumors (bottom). **(F, G)** Normalized expression of germinal center (GC) B cell markers, *BCL6* and *REL*, or follicular helper T cell (Tfh) markers, *CXCR5* and *CXCL13*, within the listed T/B cell populations from the scRNA-seq. **(H)** Predicted enrichment of receptor-ligand interaction involving the CXCL chemokine signaling in the ICI OT samples (left; the color of the connecting edge is the source cell's) and the normalized expression of the chemokine and their receptors in each immune population (right). The interaction involving the CXCL13-CXCR5 pair between tumor reactive *PDCD1+ TOX+* CD8 T cells and B cells was more enriched in ICI OT-R tumors.

CXCL chemokine-receptor interaction analysis using CellChat predicted that *CXCL13* expressed by *PD1+ TOX+* CD8 T cells (source) mainly engaged CXCR5+ B cells (target) (Figure 3H, left). On the other hand, ICI OT-NR tumors show a mixture of CXCL16-CXCR6 and CXCL13-CXCR3 interaction among the monocytic DCs, macrophages and T cells (with weak CXCL13-CXCR5 interaction involving B cells). Although the relative fractions and normalized expression of *CXCL13* and *CXCR5* were similar between ICI OT-R and OT-NR (Figure 3H, dot plots), the CXCL13-CXCR5 interaction is expected to be stronger in ICI OT-R group since it has a larger fraction of CXCR5+ B cells among the CD45+ immune cells. Finally, AUCell analysis (51) showed enrichments of TLS gene sets specifically in B and Tfh cell clusters (Supp. Figure 3C), indicative of TLS formation within which CD8+ T, CD4+ Tfh and GC B cells interact with one another. Overall, our analyses illustrate ICI-mediated release of T cell checkpoint engagement of tumor-specific, PD1+ TOX+ CD8 T cells upregulates CXCL13, which subsequently recruits CXCR5+ B cells and Tfh to form TLS in the TME.

B cells and Tfh in ICI-responding tumors upregulate markers of productive antigen presentation

Using their B cell receptor (BCR), B cells can selectively capture antigens and present them to Tfh cells in through the MHC II antigen presentation pathway (52–54). For this interaction to happen, antigen-specific B cell clones must encounter cognate antigen-specific T cells in the T cell zones of the lymphoid follicle in secondary lymphoid organs or TLS. Indeed, our receptor-ligand interaction analysis suggests that intratumoral B cells in ICI OT-R tumors present antigens to *CXCR5+* Tfh and Tregs through MHC II pathway (Figure 4A; Supp. Figure 4A). In OT-NR tumors, MHC II interaction was observed mostly between Tregs and multiple MHC II+ populations, including B cells, DC and the immunosuppressive Mφ (Figure 4A; Supp. Figure 4A).

Antigen recognition by Tfh results in the activation of their T helper function, providing stimulatory signal to CD40+ B cells through upregulation of CD40L (52). BCR ligation and CD40/CD40L pathway activation of B cells stimulates expression of APC maturation marker, *CD83*, which further strengthen the antigen presentation activity of B cells (55). Accordingly, we observed the upregulation of *CD40LG* and *CD83* transcripts in the Tfh and B cell populations, respectively (Figure 4B; Supp. Table 3D). Receptor-ligand interaction analysis on the genes in CD40 pathway also showed enrichment of the pathway only in ICI OT-R tumors (Figure 4C; Supp. Figure 4A). CD40L and IFNγ-induced activation can drive B cells to cross present antigens to CD8 T cells (56). Indeed, we confirmed that both CD40L and IFNγ pathways were active in the TME of ICI OT-R tumors and CellChat analysis predicted a significant MHC I pathway interaction between B cells and the tumor reactive *CXCL13+ PD1+ TOX+* CD8 T cells (Supp. Figure 4B).

Taken together, our single cell transcriptome analysis of ICI-treated melanoma demonstrated upregulation of gene markers and enrichment of pathways associated with a productive antigen presentation by B cells to T cells in the TME of ICI OT-R tumors.

Diversity but not clonality of B cell population correlates with survival after ICI therapy

After a productive antigen presentation to T cells, antigen specific B cells can undergo class switch recombination (CSR), somatic hypermutation (SHM) and differentiation into long-lived plasma cells or memory B cells (52). It is unclear if ICI response in melanoma is associated with the formation of tumor-specific, antibody producing cells, as seen in clear cell renal cell carcinoma (31). We did not observe association between the relative abundances of plasma cells and response to ICI in the scRNA-seq cohort (Figure 3D). There were also very few cells expressing *CD19* or *MS4A1* within the *KI67+* proliferating cell cluster, indicating a rarity of proliferating B cells in this dataset (Figure 3C, based on the levels of the *CD19* or *MS4A1* in the rightmost proliferating cell cluster).

We applied TRUST4 to reconstruct the CDR3 regions within mRNA transcripts of immunoglobulin heavy (IGHA/M/G) chain in the bulk RNA-seq and scRNA-seq data (42). By defining each distinct IGH CDR3 sequence as a B cell clone, we can obtain an estimate of the B cells' clonal dynamics after ICI or MAPKi therapy. Response to ICI exhibited statistically significant increase of BCR diversity in ICI OT-R tumors (with respect to both PT and OT-NR) but not in MAPKi OT-R tumors (Figure 4D; Supp. Table 4A). SCOPer (43) analysis predicted an increased somatic hypermutation (SHM) in ICI OT-R tumors, which may have contributed to the increase of BCR diversity in ICI OT-R tumors (Figure 4E). We observed that most B cell clones in the ICI OT-R tumors were newly infiltrating clones after the therapy (Supp. Figure 4C). The same predominance of OT tumor specific clones can also be observed in the T cell populations (Supp. Figure 4D). The clonal dynamics of both T and B cells after ICI treatment matches the "T cell clonal replacement" event reported in basal/squamous cell carcinoma patients who responded to ICI (57).

Higher BCR diversity was associated with improved survival after ICI but not MAPKi therapy (Figure 4F). The significant correlation between BCR diversity and OS after ICI therapy was also confirmed in the scRNA-seq cohort (Figure 4G and Supp. Table 3E; Supp. Table 4B). BCR clonality was not associated with patient survival after ICI nor MAPKi therapy (Figures 4F, G). The observation of increased BCR diversity in response to ICI therapy suggests that B cells' role in the TME is to present T cells with a broad variety of tumor antigens. Since B cells present tumor antigens to T cells through BCR-specific internalization of extracellular tumor antigens (54), a more diverse BCR repertoire will improve the chance of a successful antigen presentation. The strong association between patient survival after ICI and BCR diversity, but not clonality, further implies that ICI response depends on successful tumor antigen presentation to T cells and not on the subsequent clonal expansion and differentiation of B cells into long lived antibody producing plasma cells.

10.3389/fimmu.2023.1176994

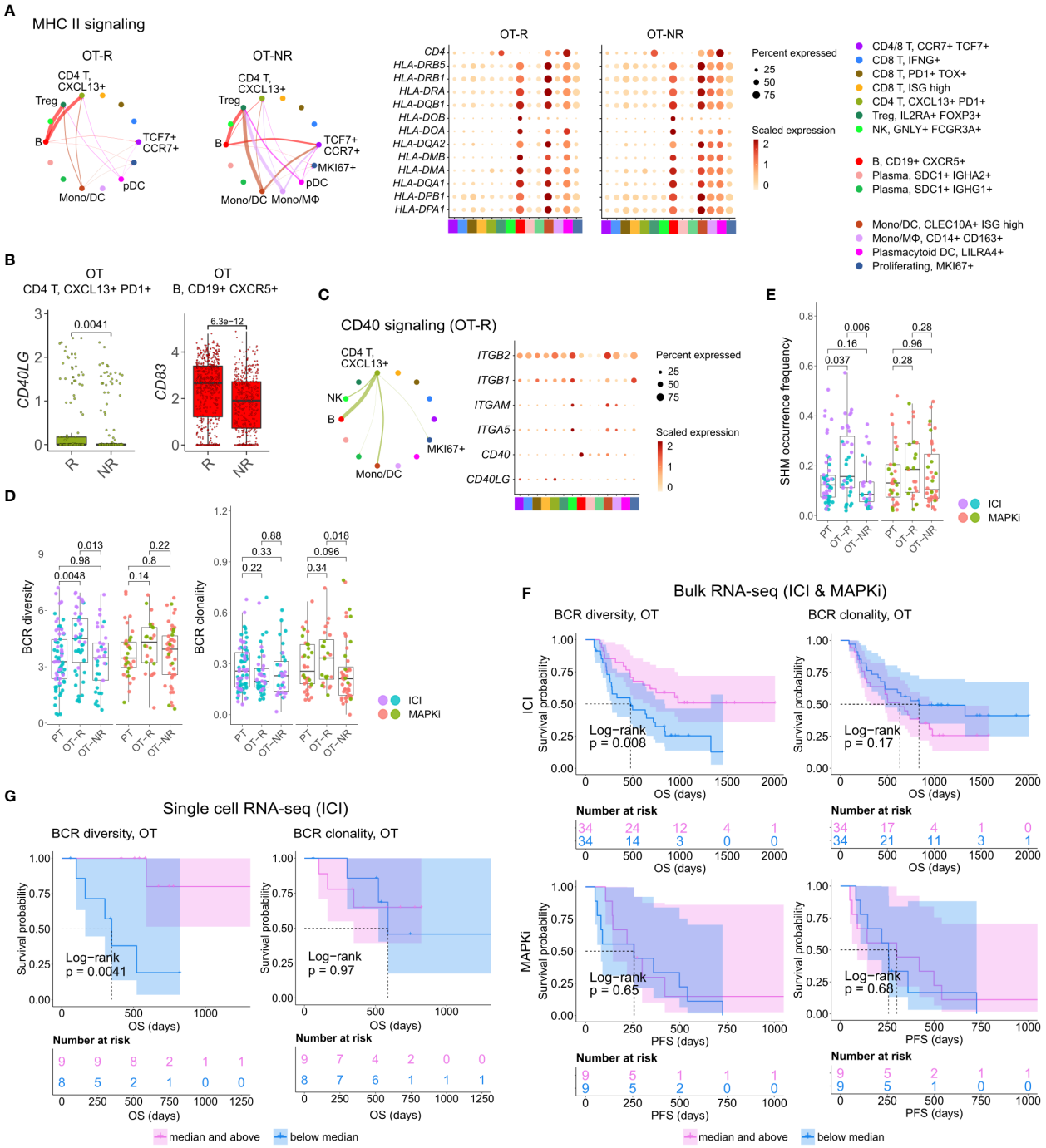

FIGURE 4
B cells in ICI OT-R tumors present antigens to *PDCD1*+ *TOX*+ tumor-reactive CD8 T and CD4 Tfh cells *via* the MHC I and II pathways. **(A)** Predicted enrichment of cell-to-cell interaction through MHC II antigen presentation pathway (left) and the normalized expression of MHC II-related genes (right). The expressions of MHC II genes are similar between ICI OT-R and OT-NR but, because of the higher proportion of B cells in ICI OT-R, the predicted MHC II interaction is (relatively) dominated by B cells in ICI OT-R. The interaction is more evenly distributed among the monocytic DCs, macrophages, and B cells in ICI OT-NR tumors. **(B)** Normalized expression of *CD40LG* and *CD83* in follicular helper T cell (Tfh) and CXCR5+ B cell populations, respectively. **(C)** Predicted enrichment of cell-to-cell interaction through CD40L/CD40 pathway specific to ICI OT-R tumors (left) and the normalized expression of CD40 pathway related genes (right). **(D)** BCR clonotype diversity and clonality among the PT, OT-R and OT-NR tumors in the ICI or MAPKi therapy group. The BCR clones are based on TRUST4's predicted CDR3 sequences of the immunoglobulin heavy (IGH) chains in each RNA-seq sample (see Methods). **(E)** Somatic hypermutation (SHM) frequencies based on predicted germline (i.e., prior to SHM) BCR clones by SCOPer (see Methods). **(F)** Kaplan-Meier survival curves of ICI- or MAPKi-treated melanoma patients in the bulk RNA-seq datasets stratified by either the BCR diversity (left) or clonality (right) of their OT tumors. **(G)** Kaplan-Meier survival curves of ICI-treated patients in the scRNA-seq dataset stratified by either the BCR diversity (left) or clonality (right) of their OT tumors.

Combined increase in BCR diversity and IFNγ pathway activity correlates with the greatest long-term survival after ICI therapy

Successful antigen recognition by CD8 T cells increased the overall IFNγ expression (Supp. Figure 5A), which subsequently induced IFNγ pathway activation in the TME of ICI OT-R tumors (Figure 1F). IFNγ expression by multiple CD8 T cell populations mostly activated the IFNγ pathway in B cells and monocytic DCs from ICI OT-R tumors (Figure 5A). The activation of IFNγ pathway in these immune populations is expected to boost their antigen presentation activity, resulting in additional Tfh and CD8 T cell activation. In OT-NR tumors, IFNγ pathway interaction mainly involved the immunosuppressive CD14+ CD163+ Mφ and monocytic DCs (Figure 5A).

When stratified by the enrichment of hallmark interferon gamma gene set and BCR diversity of their tumors (high: median and above, and, low: below median), ICI-treated patients with the best survival were those with high hallmark interferon gamma gene set and BCR diversity in their OT samples (Figure 5B, log-rank P=0.0072). Cox proportional hazard analyses suggested that hallmark interferon gamma gene set score and BCR diversity in the OT samples are independent predictors of survival in ICI treated patients (Figure 5C; Supp. Table 4C). Stratification of the patients by the expression of CD8 T cell marker *CD8B* and B cell marker *CD19* show a similar trend where patients with high expression of both *CD19* and *CD8B* had better survival after ICI treatment (Supp. Figure 5B), which is in agreement with a recent report on a separate cohort of melanoma patients (29). Curiously, our analysis also revealed an interaction/dependency between BCR diversity and hallmark interferon gamma gene set scores in relation with the patients' OS (Supp. Figure 5C; Supp. Table 4D, HR of interaction = 0.55, P = 0.054). Indeed, the combined positive effect of clonally diverse B cells and high IFNγ signaling pathway activity (indicating successful antigen presentation to T cells) on patients' OS is significantly greater the sum of their individual effects (Figure 5B). Thus, higher clonal diversity of intratumoral B cells and IFNγ signaling pathway activity in the TME may act synergistically to drive a durable ICI response.

Discussion

To discover immune factors and pathways associated with durable response to ICI-based immunotherapy, we analyzed the transcriptomic profiles of melanoma biopsies taken before and after ICI treatment. Unique to our study is the use of transcriptomic profiles of melanoma biopsied pre- and post-MAPKi therapy. Since MAPKi therapy also induces significant immune infiltration, yet MAPKi-treated patients are less likely to achieve a durable response than ICI-treated patients, comparing immune infiltration associated with ICI against MAPKi allowed us to separate drivers of durable response from immune "bystanders" in ICI OT-R tumors. Genes that are upregulated in ICI OT-R tumors highlighted enrichment of B cell and Tfh gene markers, strongly hinting the presence of TLS in the tumor. This observation confirms previous studies reporting positive association between TLS and ICI response in multiple cancer histologies (28–31).

In ICI OT-R tumors, the increase of TLS-associated CXCR5+ B and Tfh cells were correlated with increased mRNA expression of CXCR5's ligand, *CXCL13*, by activated, tumor reactive CXCL13+ CD8 T cells (50). We propose a model where an effective response to ICI is marked with CXCL13+ CD8 T cell-driven recruitment of highly diversified, CXCR5+ B cell clones whose subsequent (tumor) antigen presentation activities induce and sustain the activation of tumor-reactive CD4 Tfh and CD8 T cells (Figure 5D). Notably, our model resembles the cancer-immunity cycle initially proposed by Chen and Mellman (58) with the important distinctions of the cycle happening directly in the TME and CXCR5+ B cells functioning as its major APC.

Our cell-cell interaction analysis highlighted CXCR5+ B cells as the dominant antigen presenting cells in ICI OT-R TME, presenting antigens to both tumor-reactive CD8 T cells and CD4 Tfh cells and through MHC I and MHC II pathways, respectively. We observed a concomitant overexpression of *CD40LG* in the Tfh population, reflecting a productive antigen presentation by B cells to Tfh (53, 54). CD40L up-expression in Tfh then activated the CD40 signaling pathway in B cells, as shown by upregulation of *CD83* in the B cells (55). CD83 is a marker of light zone-specific, antigen presenting GC B cells (52) and its expression is crucial for B cell longevity after antigen stimulation (59). Overall upregulation of IFNγ expression in ICI OT-R tumors (bulk RNA-seq) was predicted to significantly activate the IFNγ pathway of B cells and DC in ICI OT-R tumors. Notably, simultaneous activation of IFNγ and CD40 signaling pathways in B cells can increase their antigen cross presentation to CD8 T cells (56, 60). Successful cross-presentation to tumor reactive CD8 T cells is expected to drive their cytotoxic activity against the tumor.

Another support of B cells' antigen presenting role in ICI response comes from the clonal dynamics of B cells in ICI OT-R tumors. Higher BCR diversity, which is expected to increase the chance of tumor antigen uptake and presentation to T cells, is significantly correlated with longer OS after ICI therapy both in the bulk and single-cell RNA-seq cohorts of melanoma patients. However, higher BCR clonality is not associated with improved OS after ICI. This suggests that B cells' subsequent clonal expansion and differentiation into long-lived plasma/memory B cells are less correlated with response to ICI than the diversity of their presented antigens. Finally, we demonstrated that BCR diversity and IFNγ signaling pathway scores are both significant and synergistic variables that are correlated with patient survival after ICI therapy.

Our study has several limitations. First, it is a correlative, retrospective study of combined cohorts of ICI-treated tumors. To overcome this, we ensured that the most important observations from one dataset are corroborated an independent dataset. For instance, the increased expression of TLS markers in ICI OT-R tumors and the association between BCR diversity/clonality with survival were confirmed in both bulk and scRNA-seq datasets of ICI treated melanoma. We also validated the differential effects of ICI (using a PD-1 antibody) and MAPKi on CXCL13 expression by activated T cells, albeit in an *in vitro* context. Another limitation is

10.3389/fimmu.2023.1176994

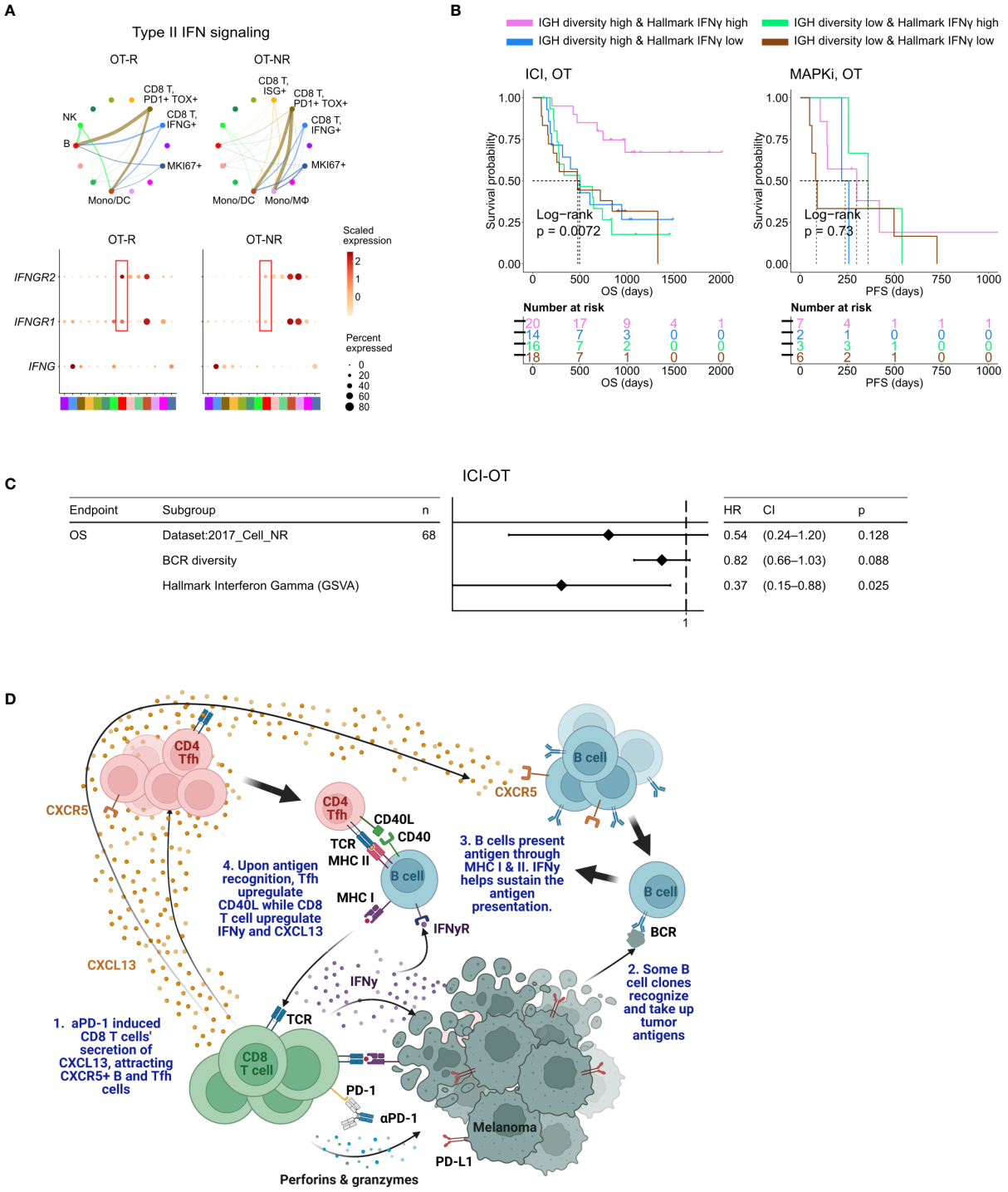

FIGURE 5
BCR diversity and IFNγ signaling pathway activation are significant factors associated with enhanced OS after ICI therapy. **(A)** Predicted enrichment of receptor-ligand interaction involving type II IFN signaling between *IFNG* expression CD8 T cell clusters and B cells in ICI OT-R tumors (top). Increased expression of *IFNGR1/R2* in the B cells of ICI-responders (bottom) is expected to further enhance B cells' antigen presentation activity. **(B)** Kaplan-Meier survival curves of patients stratified by BCR diversity and hallmark interferon gamma gene set score in OT tumors of the ICI or MAPKi therapy group. **(C)** Multivariate Cox proportional hazards analysis assessing the hazard ratios of BCR diversity and hallmark interferon gamma gene set score in ICI OT tumor samples. **(D)** The schematic of our proposed model of productive ICI response. First, tumor-reactive CD8 T cells produce CXCL13 in response to ICI to recruit TLS-associated CXCR5+ Tfh and B cells. B cells pick up tumor antigens from tumor cells debris, potentially killed by ICI-activated CD8 T cells. Successful tumor antigen presentation by B cells, expected to highly correlate with their BCR repertoire diversity, results in the activation of the Tfh and (additional) tumor reactive CD8 T cells. Tfh and CD8 T cells upregulates CD40L and IFNγ, respectively, resulting in enhancement of B cell antigen presentation activity. Finally, newly activated, tumor reactive CD8 T cells kill more tumor cells and secrete more CXCL13 to recruit additional CXCR5+ Tfh and B cells, thus completing an *in situ* cancer immunity cycle. Image created with BioRender.com.

that the use of RNA-seq to reconstruct the CDR3 regions of the TCR or BCR may have limited sensitivity. Additional studies using more samples in general and using direct TCR/BCR sequencing of ICI-treated tumors to measure T/B cell diversity and clonality are necessary to confirm our observations.

Our results demonstrate that an effective immune response to ICI involves activation of tumor reactive CD4 and CD8 T cells by antigen presenting B cells, in the context of TLS in the TME. Our finding is in line with a recent scRNA-seq study of ICI-treated triple negative breast cancer patients, which highlighted an enrichment of antigen presentation activity, rather than antibody production, in B cells of ICI-responding tumors (61). The next logical question is how to leverage this observation in the clinic. Several studies have attempted direct TLS formation using secreted factors such as CXCL13 (62). However, TLS formation may not be sufficient to ensure B cell and T cell activation and the subsequent antitumor immunity (63). Strategies to pre-load tumor antigens on B cells to generate B cell vaccine may be more promising as a combinatorial therapy with ICI. B cell-based tumor antigen vaccine was reported to promote ICI efficacy in animal models of melanoma (60), lung cancer (54) and glioblastoma (56). Thus, there is a pressing need for additional pre-clinical and, ultimately, clinical studies to test the most optimal B cell-vaccine approach that can enhance the rate of durable ICI response.

Data availability statement

The original contributions presented in the study are included in the article/Supplementary Material. All the source codes used in this study were uploaded to GitHub repository at https://github.com/sciencepeak/TCR_BCR_project. Further inquiries can be directed to the corresponding authors.

Ethics statement

Ethical review and approval was not required for the study on human participants in accordance with the local legislation and institutional requirements. Written informed consent for participation was not required for this study in accordance with the national legislation and the institutional requirements.

Author contributions

LD, LS, ML, and WH designed the experiments and analyses. LD implemented of the overall computational analyses unless specified otherwise. LS developed the single cell analysis pipeline. LD, LS, and MB performed single cell analysis. LNS and ML designed and performed the *in vitro* experiments. YZ contributed to this study as a visiting scientist at Division of Dermatology, Department of Medicine, UCLA. LD, RP, MS, ML, and WH wrote and edited the manuscript. All authors contributed to the article and approved the submitted version.

Funding

This study was funded in part by the NIH/NCI grant (1R01CA236910) and a grant from Parker Institute for Cancer Immunotherapy. LD is supported by grant from Parker Institute for Cancer Immunotherapy at UCLA and a postdoctoral fellowship from National Cancer Center. WH is supported by grants from NIH/NCI (1R01CA236910), the Jonnson Comprehensive Cancer Center, the Melanoma Research Alliance, the Margaret E. Early Medical Research Trust, and the Parker Institute for Cancer Immunotherapy at UCLA. ML is supported by grants from the NIH/NIDDK (K08DK129829) and the Aramont Charitable Foundation.

Acknowledgments

We thank Moshe Sade-Feldman and Nir Hacohen for generously providing the raw count expression data of single cell RNA-seq used in their publication.

Conflict of interest

The authors declare that the research was conducted in the absence of any commercial or financial relationships that could be construed as a potential conflict of interest.

The reviewer HS declared a shared affiliation with the authors to the handling editor at the time of review.

Publisher's note

Supplementary material

The Supplementary Material for this article can be found online at: https://www.frontiersin.org/articles/10.3389/fimmu.2023.1176994/full#supplementary-material

SUPPLEMENTARY FIGURE 1
Shared and therapy-specific transcriptomic changes after ICI or MAPKi therapy. **(A)** Schematic of the bulk RNA-seq data sets of ICI- and MAPKi-treated melanoma used in this study. **(B, C)** Normalized expression of T cell marker genes (*CD3D*, *CD8B*) **(B)** and GSVA gene set enrichment scores of interferon gamma gene sets from the Molecular Signature database **(C)** in the PT, OT-R and OT-NR samples of patients treated with ICI or MAPKi therapy (inter therapy comparison). **(D)** Kaplan-Meier survival curves of ICI- or MAPKi-treated melanoma patients stratified by either *CD8B* expression (left) or hallmark interferon gamma response gene set scores (right) in their PT tumors. **(E)** Kaplan-Meier survival curves of overall (top) or progression free survival (bottom) of MAPKi-treated melanoma patients stratified by either *CD8B* expression (left) or hallmark interferon gamma response gene set scores

(right) in their OT tumors (two independent microarray datasets of MAPKi-treated melanoma patients). **(F)** Correlation between PFS and OS after MAPKi therapy across two separate melanoma microarray datasets. **(G)** Normalized expression of T cell cytotoxicity genes *GZMB* and *PRF1* in the PT, OT-R and OT-NR samples of patients treated with ICI or MAPKi therapy.

SUPPLEMENTARY FIGURE 2

Characterization of B cell and TLS-related gene expression changes after ICI and MAPKi therapy. **(A)** Enriched tissue specific gene sets in DEGs upregulated in MAPKi OT-R tumors with respect to ICI OT-R tumors (after adjustment by respective therapy group's OT-NR tumors). **(B)** Normalized expression of the listed B cell-related genes among the PT, OT-R and OT-NR tumors in the ICI or MAPKi therapy group. **(C)** Enrichment scores of a recently published TLS 7-gene and 9-gene gene sets among the PT, OT-R and OT-NR tumors in the ICI or MAPKi therapy group. **(D)** Kaplan-Meier survival curves of overall (top) or progression free survival (bottom) of MAPKi-treated melanoma patients stratified by either *CD19* expression (left) or TLS gene set enrichment score (right) in their OT tumors. **(E)** Kaplan-Meier survival curves of ICI- or MAPKi-treated melanoma patients stratified by either *CD19* expression (left) or TLS gene set enrichment score (right) in their PT tumors.

SUPPLEMENTARY FIGURE 3

Single cell analysis of ICI-treated melanoma. **(A)** The fraction of the myeloid and proliferating cell populations in stratified by response vs. non-response to ICI in PT (top) and OT tumors (bottom). **(B)** Kaplan-Meier survival curves of ICI-treated patients stratified by the proportion of monocyte/macrophages within either their PT (left) or OT tumors (right). **(C)** Single cell-based gene set enrichment score of the TLS 7-gene and 9-gene signatures projected on the UMAP (left) or presented in boxplot across all cell types (right). The scores were separated into quartiles to assist the visualization of high and low gene set enrichments in different cell populations.

SUPPLEMENTARY FIGURE 4

B cell-associated antigen presentation and clonotype analyses. **(A)** Inferred cell-cell communication among intratumoral immune populations of pre- and post-ICI treated melanoma across curated signaling pathways in CellChat. The interactions are grouped based on response vs. no-response to ICI in either PT or OT tumors. **(B)** Predicted enrichment of cell-to-cell interaction through MHC I antigen presentation pathway. **(C, D)** Change in BCR **(C)** or TCR **(D)** clonal fraction in grouped by clones found only in the OT sample (OT-specific), only in the PT (PT-specific) and both in the PT and OT samples (overlapping, see illustration on the left). These fractions are calculated with respect to the union of all BCR/TCR clones found in the PT and OT samples of each patient; this analysis is done only on patients with PT and OT tumors.

SUPPLEMENTARY FIGURE 5

Multivariate analysis of survival examining the association among T cell and B cell related variables to patient OS after ICI therapy. **(A)** Normalized bulk RNA-seq expression of *IFNG* in the PT, OT-R and OT-NR samples of patients treated with ICI or MAPKi therapy. **(B)** Kaplan-Meier survival curves of patients stratified by normalized expressions of *CD8B* and *CD19* in either PT or OT tumors of the ICI or MAPKi therapy group. **(C)** Multivariate Cox proportional hazards analysis assessing the hazard ratios of BCR diversity, hallmark interferon gamma gene set score, and their interaction in ICI OT tumor samples.

SUPPLEMENTARY TABLE 1

Clinical characteristics, gene expression and gene set enrichments in the bulk RNA-seq datasets. **(A)** Summary of clinical data associated with the tumor samples (bulk and scRNA-seq datasets). **(B)** Difference in fold changes of OT-R vs. OT-NR samples after ICI or MAPKi therapy. **(C)** Gene sets/cell markers enriched in tumors responding to ICI, MAPKi or both (Enrichr analysis). **(D)** The relative abundance of immune and stromal cell populations in each sample in bulk RNA-seq dataset (MCPcounter analysis). **(E)** GSVA score matrix of selected gene sets of the bulk RNA-seq data of ICI or MAPKi-treated tumors.

SUPPLEMENTARY TABLE 2

PFS and OS correlation in MAPKi-treated melanoma patients. **(A)** OS and PFS data from two MAPKi treated gene expression microarray datasets (Rizos et al CCR 2014 and Long et al Nat. Comm. 2014).

SUPPLEMENTARY TABLE 3

Cell type fraction, DEGs and survival analysis of scRNA-seq data set of ICI-treated melanoma. **(A)** Differentially upregulated genes in each single cell cluster of CD45+ cells from ICI-treated tumors. **(B)** The fraction of immune cell populations in each PT/OT tumor sample of ICI-treated melanoma patients. **(C)** The association between the fraction each immune population (in PT or OT tumors) and OS after ICI therapy. **(D)** Differentially expressed genes in PT and OT tumors based on response (R) vs. no-response (NR) to ICI. **(E)** The association between TCR/BCR clonality or diversity in PT or OT tumors and OS after ICI therapy.

SUPPLEMENTARY TABLE 4

Univariate and multivariate survival analyses of B cell, T cell and TLS-related gene/gene sets. **(A)** TCR and BCR clonotype repertoire metrics of the ICI and MAPKi datasets (bulk and scRNA-seq). **(B)** Univariate CoxPH analysis of survival of B cell, T cell and TLS-related gene/gene sets (bulk RNA-seq cohorts). **(C)** Multivariate CoxPH analysis of survival of significant B cell, T cell and TLS-related gene/gene sets (ICI-OT only, pairwise independent). **(D)** Multivariate CoxPH analysis of survival of significant B cell, T cell and TLS-related gene/gene sets (ICI-OT only, with pairwise interaction term).

References

1. Luke JJ, Schwartz GK. Chemotherapy in the management of advanced cutaneous malignant melanoma. *Clinics Dermatol* (2013) 31:290–7. doi: 10.1016/j.clindermatol.2012.08.016

2. Luke JJ, Flaherty KT, Ribas A, Long GV. Targeted agents and immunotherapies: optimizing outcomes in melanoma. *Nat Rev Clin Oncol* (2017) 14:463–82. doi: 10.1038/nrclinonc.2017.43

3. Curti BD, Faries MB. Recent advances in the treatment of melanoma. *New Engl J Med* (2021) 384:2229–40. doi: 10.1056/NEJMra2034861

4. Tawbi HA, Schadendorf D, Lipson EJ, Ascierto PA, Matamala L, Castillo Gutiérrez E, et al. Relatlimab and nivolumab versus nivolumab in untreated advanced melanoma. *New Engl J Med* (2022) 386:24–34. doi: 10.1056/NEJMoa2109970

5. Hodi FS, O'Day SJ, McDermott DF, Weber RW, Sosman JA, Haanen JB, et al. Improved survival with ipilimumab in patients with metastatic melanoma. *New Engl J Med* (2010) 363:711–23. doi: 10.1056/NEJMoa1003466

6. Robert C, Schachter J, Long GV, Arance A, Grob JJ, Mortier L, et al. Pembrolizumab versus ipilimumab in advanced melanoma. *New Engl J Med* (2015) 372:2521–32. doi: 10.1056/NEJMoa1503093

7. Robert C, Long GV, Brady B, Dutriaux C, Maio M, Mortier L, et al. Nivolumab in previously untreated melanoma without BRAF mutation. *New Engl J Med* (2014) 372:320–30. doi: 10.1056/NEJMoa1412082

8. Larkin J, Chiarion-Sileni V, Gonzalez R, Grob JJ, Cowey CL, Lao CD, et al. Combined nivolumab and ipilimumab or monotherapy in untreated melanoma. *New Engl J Med* (2015) 373:23–34. doi: 10.1056/NEJMoa1504030

9. Kalbasi A, Ribas A. Tumour-intrinsic resistance to immune checkpoint blockade. *Nat Rev Immunol* (2020) 20:25–39. doi: 10.1038/s41577-019-0218-4

10. Schoenfeld AJ, Hellmann MD. Acquired resistance to immune checkpoint inhibitors. *Cancer Cell* (2020) 37:443–55. doi: 10.1016/j.ccell.2020.03.017

11. Nowicki TS, Hu-Lieskovan S, Ribas A. Mechanisms of resistance to PD-1 and PD-L1 blockade. *Cancer J* (2018) 24:47–53. doi: 10.1097/PPO.0000000000000303

12. Bruni D, Angell HK, Galon J. The immune contexture and immunoscore in cancer prognosis and therapeutic efficacy. *Nat Rev Cancer* (2020) 20:662–80. doi: 10.1038/s41568-020-0285-7

13. Tumeh PC, Harview CL, Yearley JH, Shintaku IP, Taylor EJM, Robert L, et al. PD-1 blockade induces responses by inhibiting adaptive immune resistance. *Nature* (2014) 515:568–71. doi: 10.1038/nature13954

14. Ayers M, Lunceford J, Nebozhyn M, Murphy E, Loboda A, Kaufman DR, et al. IFN-γ–related mRNA profile predicts clinical response to PD-1 blockade. *J Clin Invest* (2017) 127:2930–40. doi: 10.1172/JCI91190

15. Chen P-L, Roh W, Reuben A, Cooper ZA, Spencer CN, Prieto PA, et al. Analysis of immune signatures in longitudinal tumor samples yields insight into biomarkers of response and mechanisms of resistance to immune checkpoint blockade. *Cancer Discovery* (2016) 6:827–37. doi: 10.1158/2159-8290.CD-15-1545

16. Abril-Rodriguez G, Torrejon DY, Liu W, Zaretsky JM, Nowicki TS, Tsoi J, et al. PAK4 inhibition improves PD-1 blockade immunotherapy. *Nat Cancer* (2020) 1:46–58. doi: 10.1038/s43018-019-0003-0

17. Grasso CS, Tsoi J, Onyshchenko M, Abril-Rodriguez G, Ross-Macdonald P, Wind-Rotolo M, et al. Conserved interferon-γ signaling drives clinical response to immune checkpoint blockade therapy in melanoma. *Cancer Cell* (2020) 38:500–15.e3. doi: 10.1016/j.ccell.2020.08.005

18. Davies H, Bignell GR, Cox C, Stephens P, Edkins S, Clegg S, et al. Mutations of the BRAF gene in human cancer. *Nature* (2002) 417:949–54. doi: 10.1038/nature00766

19. Long GV, Stroyakovskiy D, Gogas H, Levchenko E, de Braud F, Larkin J, et al. Combined BRAF and MEK inhibition versus BRAF inhibition alone in melanoma. *New Engl J Med* (2014) 371:1877–88. doi: 10.1056/NEJMoa1406037

20. Larkin J, Ascierto PA, Dréno B, Atkinson V, Liszkay G, Maio M, et al. Combined vemurafenib and cobimetinib in BRAF-mutated melanoma. *New Engl J Med* (2014) 371:1867–76. doi: 10.1056/NEJMoa1408868

21. Dummer R, Ascierto PA, Gogas HJ, Arance A, Mandala M, Liszkay G, et al. Encorafenib plus binimetinib versus vemurafenib or encorafenib in patients with BRAF-mutant melanoma (COLUMBUS): a multicentre, open-label, randomised phase 3 trial. *Lancet Oncol* (2018) 19:603–15. doi: 10.1016/S1470-2045(18)30142-6

22. Knight DA, Ngiow SF, Li M, Parmenter T, Mok S, Cass A, et al. Host immunity contributes to the anti-melanoma activity of BRAF inhibitors. *J Clin Invest* (2013) 123:1371–81. doi: 10.1172/JCI66236

23. Song C, Piva M, Sun L, Hong A, Moriceau G, Kong X, et al. Recurrent tumor cell–intrinsic and –extrinsic alterations during MAPKi-induced melanoma regression and early adaptation. *Cancer Discov* (2017) 7:1248–65. doi: 10.1158/2159-8290.CD-17-0401

24. Robert C, Grob JJ, Stroyakovskiy D, Karaszewska B, Hauschild A, Levchenko E, et al. Five-year outcomes with dabrafenib plus trametinib in metastatic melanoma. *New Engl J Med* (2019) 381:626–36. doi: 10.1056/NEJMoa1904059

25. Ascierto PA, Dréno B, Larkin J, Ribas A, Liszkay G, Maio M, et al. 5-year outcomes with cobimetinib plus vemurafenib in BRAFV600 mutation–positive advanced melanoma: extended follow-up of the coBRIM study. *Clin Cancer Res* (2021) 27:5225–35. doi: 10.1158/1078-0432.CCR-21-0809

26. Larkin J, Chiarion-Sileni V, Gonzalez R, Grob JJ, Rutkowski P, Lao CD, et al. Five-year survival with combined nivolumab and ipilimumab in advanced melanoma. *N Engl J Med* (2019) 381:1535–46. doi: 10.1056/NEJMoa1910836

27. Atkins MB, Tarhini A, Rael M, Gupte-Singh K, O'Brien E, Ritchings C, et al. Comparative efficacy of combination immunotherapy and targeted therapy in the treatment of BRAF-mutant advanced melanoma: a matching-adjusted indirect comparison. *Immunotherapy* (2019) 11:617–29. doi: 10.2217/imt-2018-0208

28. Helmink BA, Reddy SM, Gao J, Zhang S, Basar R, Thakur R, et al. B cells and tertiary lymphoid structures promote immunotherapy response. *Nature* (2020) 577:549–55. doi: 10.1038/s41586-019-1922-8

29. Cabrita R, Lauss M, Sanna A, Donia M, Skaarup Larsen M, Mitra S, et al. Tertiary lymphoid structures improve immunotherapy and survival in melanoma. *Nature* (2020) 577:561–5. doi: 10.1038/s41586-019-1914-8

30. Petitprez F, de Reyniès A, Keung EZ, Chen TW-W, Sun C-M, Calderaro J, et al. B cells are associated with survival and immunotherapy response in sarcoma. *Nature* (2020) 577:556–60. doi: 10.1038/s41586-019-1906-8

31. Meylan M, Petitprez F, Becht E, Bougoüin A, Pupier G, Calvez A, et al. Tertiary lymphoid structures generate and propagate anti-tumor antibody-producing plasma cells in renal cell cancer. *Immunity* (2022) 55:527–41.e5. doi: 10.1016/j.immuni.2022.02.001

32. Riaz N, Havel JJ, Makarov V, Desrichard A, Urba WJ, Sims JS, et al. Tumor and microenvironment evolution during immunotherapy with nivolumab. *Cell* (2017) 171:934–49.e16. doi: 10.1016/j.cell.2017.09.028

33. Hugo W, Shi H, Sun L, Piva M, Song C, Kong X, et al. Non-genomic and immune evolution of melanoma acquiring MAPKi resistance. *Cell* (2015) 162:1271–85. doi: 10.1016/j.cell.2015.07.061

34. Kwong LN, Boland GM, Frederick DT, Helms TL, Akid AT, Miller JP, et al. Co-Clinical assessment identifies patterns of BRAF inhibitor resistance in melanoma. *J Clin Invest* (2015) 125:1459–70. doi: 10.1172/JCI78954

35. Rizos H, Menzies AM, Pupo GM, Carlino MS, Fung C, Hyman J, et al. BRAF inhibitor resistance mechanisms in metastatic melanoma: spectrum and clinical impact. *Clin Cancer Res* (2014) 20:1965–77. doi: 10.1158/1078-0432.CCR-13-3122

36. Long GV, Fung C, Menzies AM, Pupo GM, Carlino MS, Hyman J, et al. Increased MAPK reactivation in early resistance to dabrafenib/trametinib combination therapy of BRAF-mutant metastatic melanoma. *Nat Commun* (2014) 5:5694. doi: 10.1038/ncomms6694

37. Sade-Feldman M, Yizhak K, Bjorgaard SL, Ray JP, de Boer CG, Jenkins RW, et al. Defining T cell states associated with response to checkpoint immunotherapy in melanoma. *Cell* (2018) 175:998–1013.e20. doi: 10.1016/j.cell.2018.10.038

38. Kuleshov MV, Jones MR, Rouillard AD, Fernandez NF, Duan Q, Wang Z, et al. Enrichr: a comprehensive gene set enrichment analysis web server 2016 update. *Nucleic Acids Res* (2016) 44:W90–W7. doi: 10.1093/nar/gkw377

39. Hänzelmann S, Castelo R, Guinney J. GSVA: gene set variation analysis for microarray and RNA-seq data. *BMC Bioinf* (2013) 14:7. doi: 10.1186/1471-2105-14-7

40. Subramanian A, Tamayo P, Mootha VK, Mukherjee S, Ebert BL, Gillette MA, et al. Gene set enrichment analysis: a knowledge-based approach for interpreting genome-wide expression profiles. *Proc Natl Acad Sci* (2005) 102:15545–50. doi: 10.1073/pnas.0506580102

41. Liberzon A, Birger C, Thorvaldsdóttir H, Ghandi M, Mesirov Jill P, Tamayo P. The molecular signatures database hallmark gene set collection. *Cell Syst* (2015) 1:417–25. doi: 10.1016/j.cels.2015.12.004

42. Song L, Cohen D, Ouyang Z, Cao Y, Hu X, Liu XS. TRUST4: immune repertoire reconstruction from bulk and single-cell RNA-seq data. *Nat Methods* (2021) 18:627–30. doi: 10.1038/s41592-021-01142-2

43. Nouri N, Kleinstein SH. Somatic hypermutation analysis for improved identification of b cell clonal families from next-generation sequencing data. *PloS Comput Biol* (2020) 16:e1007977. doi: 10.1371/journal.pcbi.1007977

44. De Silva NS, Klein U. Dynamics of b cells in germinal centres. *Nat Rev Immunol* (2015) 15:137–48. doi: 10.1038/nri3804

45. Gupta NT, Vander Heiden JA, Uduman M, Gadala-Maria D, Yaari G, Kleinstein SH. Change-O: a toolkit for analyzing large-scale b cell immunoglobulin repertoire sequencing data. *Bioinformatics* (2015) 31:3356–8. doi: 10.1093/bioinformatics/btv359

46. Flaherty KT, Infante JR, Daud A, Gonzalez R, Kefford RF, Sosman J, et al. Combined BRAF and MEK inhibition in melanoma with BRAF V600 mutations. *N Engl J Med* (2012) 367:1694–703. doi: 10.1056/NEJMoa1210093

47. Freshwater T, Kondic A, Ahamadi M, Li CH, de Greef R, de Alwis D, et al. Evaluation of dosing strategy for pembrolizumab for oncology indications. *J Immunother Cancer* (2017) 5:43. doi: 10.1186/s40425-017-0242-5

48. Hong A, Piva M, Liu S, Hugo W, Lomeli SH, Zoete V, et al. Durable suppression of acquired MEK inhibitor resistance in cancer by sequestering MEK from ERK and promoting antitumor T-cell immunity. *Cancer Discovery* (2021) 11:714–35. doi: 10.1158/2159-8290.CD-20-0873

49. Beltra J-C, Manne S, Abdel-Hakeem MS, Kurachi M, Giles JR, Chen Z, et al. Developmental relationships of four exhausted CD8+ T cell subsets reveals underlying transcriptional and epigenetic landscape control mechanisms. *Immunity* (2020) 52:825–41.e8. doi: 10.1016/j.immuni.2020.04.014

50. Lowery FJ, Krishna S, Yossef R, Parikh NB, Chatani PD, Zacharakis N, et al. Molecular signatures of antitumor neoantigen-reactive T cells from metastatic human cancers. *Science* (2022) 375:877–84. doi: 10.1126/science.abl5447

51. Aibar S, González-Blas CB, Moerman T, Huynh-Thu VA, Imrichova H, Hulselmans G, et al. SCENIC: single-cell regulatory network inference and clustering. *Nat Methods* (2017) 14:1083–6. doi: 10.1038/nmeth.4463

52. Cyster JG, Allen CDC. B cell responses: cell interaction dynamics and decisions. *Cell* (2019) 177:524–40. doi: 10.1016/j.cell.2019.03.016

53. Crotty S. T Follicular helper cell biology: a decade of discovery and diseases. *Immunity* (2019) 50:1132–48. doi: 10.1016/j.immuni.2019.04.011

54. Cui C, Wang J, Fagerberg E, Chen P-M, Connolly KA, Damo M, et al. Neoantigen-driven b cell and CD4 T follicular helper cell collaboration promotes anti-tumor CD8 T cell responses. *Cell* (2021) 184:6101–18.e13. doi: 10.1016/j.cell.2021.11.007

55. Kretschmer B, Kuhl S, Fleischer B, Breloer M. Activated T cells induce rapid CD83 expression on b cells by engagement of CD40. *Immunol Lett* (2011) 136:221–7. doi: 10.1016/j.imlet.2011.01.013

56. Lee-Chang C, Miska J, Hou D, Rashidi A, Zhang P, Burga RA, et al. Activation of 4-1BBL+ b cells with CD40 agonism and IFNγ elicits potent immunity against glioblastoma. *J Exp Med* (2020) 218(1):e20200913. doi: 10.1084/jem.20200913

57. Yost KE, Satpathy AT, Wells DK, Qi Y, Wang C, Kageyama R, et al. Clonal replacement of tumor-specific T cells following PD-1 blockade. *Nat Med* (2019) 25:1251–9. doi: 10.1038/s41591-019-0522-3

58. Chen DS, Mellman I. Oncology meets immunology: the cancer-immunity cycle. *Immunity* (2013) 39:1–10. doi: 10.1016/j.immuni.2013.07.012

59. Prazma CM, Yazawa N, Fujimoto Y, Fujimoto M, Tedder TF. CD83 expression is a sensitive marker of activation required for b cell and CD4+ T cell longevity in vivo. *J Immunol* (2007) 179:4550–62. doi: 10.4049/jimmunol.179.7.4550

60. Wennhold K, Weber TM, Klein-Gonzalez N, Thelen M, Garcia-Marquez M, Chakupurakal G, et al. CD40-activated b cells induce anti-tumor immunity in vivo. *Oncotarget* (2017) 8:27740–53. doi: 10.18632/oncotarget.7720

61. Zhang Y, Chen H, Mo H, Hu X, Gao R, Zhao Y, et al. Single-cell analyses reveal key immune cell subsets associated with response to PD-L1 blockade in triple-negative breast cancer. *Cancer Cell* (2021) 39:1578–93 e8. doi: 10.1016/j.ccell.2021.09.010

62. Ukita M, Hamanishi J, Yoshitomi H, Yamanoi K, Takamatsu S, Ueda A, et al. CXCL13-producing CD4+ T cells accumulate in the early phase of tertiary lymphoid structures in ovarian cancer. *JCI Insight* (2022) 7(12):e157215. doi: 10.1172/jci.insight.157215

63. van Hooren L, Vaccaro A, Ramachandran M, Vazaios K, Libard S, van de Walle T, et al. Agonistic CD40 therapy induces tertiary lymphoid structures but impairs responses to checkpoint blockade in glioma. *Nat Commun* (2021) 12:4127. doi: 10.1038/s41467-021-24347-7

frontiers | Frontiers in Immunology

TYPE Systematic Review
PUBLISHED 06 October 2023
DOI 10.3389/fimmu.2023.1256355

OPEN ACCESS

EDITED BY
Ying Ma,
Tianjin Medical University Cancer Institute and Hospital, China

REVIEWED BY
Kevin M. Mcbride,
University of Texas MD Anderson Cancer Center, United States
Kin Israel Notarte,
Johns Hopkins University, United States
Andrew Gunderson,
The Ohio State University, United States

*CORRESPONDENCE
Zhengxiang Han
cnhzxyq@163.com
Hongmei Wang
wanghongmei8179@126.com

RECEIVED 10 July 2023
ACCEPTED 25 September 2023
PUBLISHED 06 October 2023

CITATION
Yu A, Cao M, Zhang K, Yang Y, Ma L, Zhang X, Zhao Y, Ma X, Fan Z, Han Z and Wang H (2023) The prognostic value of the tertiary lymphoid structure in gastrointestinal cancers.
Front. Immunol. 14:1256355.
doi: 10.3389/fimmu.2023.1256355

The prognostic value of the tertiary lymphoid structure in gastrointestinal cancers

Aoyang Yu, Menghan Cao, Kaile Zhang, Yule Yang, Luyao Ma, Xinran Zhang, Yang Zhao, Xiao Ma, Zhixiang Fan, Zhengxiang Han* and Hongmei Wang*

Department of Oncology, The Affiliated Hospital of Xuzhou Medical University, Jiangsu, China

Background: Numerous studies and research papers have provided evidence suggesting that tertiary lymphoid structures (TLS) play a crucial role in combating and suppressing tumor growth and progression. Despite the wealth of information on the significance of TLS in various types of cancer, their prognostic value in gastrointestinal (GI) cancers remains uncertain. Therefore, this meta-analysis investigated the prognostic value of TLS in GI cancers.

Methods: We searched Web of science, Pubmed, Embase and Cochrane Library for studies that met the requirements as of May 1, 2023, and the hazard ratio (HR) and the corresponding 95% confidence interval (CI) were included in the analysis. The bioinformatics analysis results based on the TCGA database are used to supplement our research.

Results: The meta-analysis included 32 studies involving 5778 patients. The results of comprehensive analysis showed that TLS-High is associated with prolonged OS (HR=0.525,95%CI:0.447-0.616 (P < 0.001), RFS (HR=0.546,95% CI:0.461-0.647, P < 0.001), DFS (HR=0.519,95%CI:0.417-0.646, P < 0.001) and PFS (HR=0.588,95%CI:0.406-0.852, P=0.005) in GI cancer. Among the patients who received immunotherapy, TLS-High is associated with significantly prolonged OS (HR=0.475, 95%CI:0.282-0.799, P=0.005) and PFS(HR=0.576, 95%CI:0.381-0.871, P=0.009). It is worth noting that subgroup analysis showed that there was no significant relationship between TLS and OS(HR=0.775, 95% CI:0.570-1.053,P=0.103) in CRC. And when Present is used as the cut-off criteria of TLS, there is no significant correlation between TLS and OS (HR=0.850, 95% CI:0.721-1.002, P=0.053)in HCC.

Conclusion: TLS is a significant predictor of the prognosis of GI cancers and has the potential to become a prognostic biomarker of immunotherapy-related patients.

Systematic review registration: https://www.crd.york.ac.uk/PROSPERO/#recordDetails, identifier CRD42023443562.

KEYWORDS

tertiary lymphoid structure (TLS), gastrointestinal (GI) cancers, meta-analysis, prognosis, biomarkers

Introduction

Gastrointestinal (GI) cancers, including esophageal, gastric, liver, biliary system, pancreatic, and colorectal tumors, account for more than a quarter of all cancer incidences worldwide. These types of cancers are responsible for one-third of all cancer-related deaths (1). Some previous studies have indicated that there is a correlation between the occurrence of GI cancers and factors such as smoking, diet, and potential pathogens like EBV (Epstein-Barr virus) and Escherichia coli that produces colibactin (2–5). These factors are linked to the escalating burden of GI cancers. In the past decade, immunotherapy such as anti-PD-1/PD-L1 has greatly improved the prognosis of cancer patients. However, this efficacy is largely limited to patients who have high microsatellite instability (MSI-H) or positive PD-L1 expression. Patients with GI cancers have a relatively low overall response rate to current immunotherapy, and the existing prognostic markers are insufficient to determine which patients can benefit from immunotherapy (6, 7). In addition, the heterogeneity of GI cancers has led to a wide range of clinical, pathological, and molecular characteristics. This diversity poses greater challenges in personalized diagnosis and treatment (8). TLS are formed as ectopic lymph node-like structures within non-lymphoid tissues. Typically, TLS consists of T cells, B cells, fibroblastic reticular cells (FRC) network, high endothelial venules (HEV), and follicular dendritic cells (FDC) (9). Recent literature suggests that the presence of TLS is associated with the prognosis of various gastrointestinal (GI) cancers (10–13). However, there is currently no unified way to evaluate TLS. Some studies classify TLS as positive or negative based on density (11, 14, 15), while other studies consider the presence or absence of TLS as a criterion for evaluation (14, 16). Furthermore, some studies assess the maturity level of TLS (17). These different grouping approaches based on TLS may impact the predictive value of TLS for prognosis. In addition, it has been observed that TLS (Tumor-Localized Immune Response) is not correlated with patient prognosis in certain advanced colorectal cancer cohorts (14, 18). Due to the existence of these controversial conclusions, it is necessary to conduct an analysis to elucidate the role of TLS in GI cancer under different grouping methods. This study performed a systematic review and meta-analysis on the relationship between TLS and the survival outcomes of patients with GI cancer.

Methods

Literature search strategies

The meta-analysis was designed and conducted based on the Preferred Reporting Items for Systematic Reviews and Meta-Analyses (PRISMA) reporting guidelines, which are considered the gold standard for reporting systematic reviews and meta-analyses. The specific search strategy is Tertiary Lymphoid Structures OR Lymphoid Structure, Tertiary OR Lymphoid Structures, Tertiary OR Tertiary Lymphoid Structure OR Ectopic Lymphoid-Like Structures OR Lymphoid-Like Structure, Ectopic OR Ectopic Lymphoid Tissues. The protocol for this meta-analysis study can be found in PROSPERO (19).

Inclusion and exclusion criteria

The eligible studies should meet the following criteria (1): GI cancers confirmed by pathological diagnosis (2); Detection of the expression levels of TLS in human tumor tissues (3); Providing survival data, including hazard ratio (HR) and 95% confidence interval (CI) measurements for OS, RFS, PFS, or PFS, or providing Kaplan-Meier curves based on TLS grouping (4); Providing the methods for TLS detection and evaluation. The following studies have been excluded from consideration due to various reasons (1): Comment, animal studies, letter, edit, reviews and meta-analysis (2); Conducting multiple studies using the same set of samples or participants (3); No insufficient data or no prognostic information.

Data extraction and quality assessment

Extract the following data from the included studies: year of publication, region, sample size, sex, cancer type, TLS cut-off criteria, follow-up time(months), survival analysis (OS, RFS, DFS or PFS), HR and 95%CI. If HR and 95% CI are not provided, Engauge Digitizer software version 4.1 was used to plot the Kaplan–Meier curves and extract the multiple survival rates to estimate the HRs and 95% CIs (20). Quality assessment was performed using the Newcastle–Ottawa quality assessment scale (NOS). NOS criteria scores range from 0 (lowest) to 9 (highest), and a NOS score ≥6 is considered a high-quality study. Two reviewers (Kaile Zhang and Yule Yang) independently assessed the quality of the eligible studies and extracted the data, and any disagreement was resolved through discussion with the third (Menghan Cao) (21).

Bioinformatics analysis

In this study, the gene expression and clinical information of gastrointestinal cancer patients were downloaded from the TCGA database (https://portal.gdc.cancer.gov/). The patients were divided into two groups based on the scores of 9 TLS-related genes (CCR6, CD1D, CD79B, CETP, EIF1AY, LAT, PTGDS, RBP5, and SKAP1), namely the TLSscore high group (upper tertile) and the TLSscore low group (lower tertile) (22). The ESTIMATE algorithm was used to analyze the immune, stromal, and ESTIMATE scores. The differences in survival between the two groups were compared using the logarithmic rank test, and visualized using Kaplan-Meier.

The proportion of 28 immune cells in the tumor microenvironment is determined using the single-sample gene set enrichment analysis (ssGSEA) method.

Statistical analysis

The statistical analysis was performed using Stata 15.0. It involved calculating the correlations between TLS and OS, RFS, PFS, and DFS. If $P<0.05$ and I^2 >50%, it indicated high heterogeneity, and a random-effects model was applied. Otherwise, a fixed-effects model was used. Egger's and Begg's tests

were employed to assess publication bias. If significant publication bias was detected, the trim and fill method was utilized to adjust the results. Additionally, a sensitivity analysis was conducted by systematically excluding individual studies in order to evaluate the robustness of the meta-analysis. $P<0.05$ was considered statistically significant.

Results

Characteristics of studies

After the initial search, we eliminated a total of 4435 duplicate articles. Then, we carefully read the titles and abstracts of the remaining articles and excluded 3286 of them. Subsequently, we obtained the full text of the remaining 64 articles and conducted a thorough evaluation. Finally, we selected and included 25 articles for our study (12–18, 23–40). These 25 articles encompassed 32 individual studies and involved a total of 5778 patients. The PRISMA flowchart depicting the entire selection process can be seen in the provided (Figure 1).

The included studies in this research are summarized in (Table 1), which consists of 8 studies on gastric cancer (GC), 6 studies on colorectal cancer (CRC), 7 studies on hepatocellular carcinoma (HCC), 4 studies on esophageal cancer (EC), 4 studies on pancreatic cancer (PC), and 3 studies on intrahepatic cholangiocarcinoma (ICC). Among these studies, 20 were conducted in China, 7 were from Japan, and 2 each were from Finland, the United States, Australia, and Germany. Moreover, 10 studies only provided overall survival (OS) data, 1 study reported only disease-free survival (DFS) data, 1 study solely focused on relapse-free survival (RFS) data, and another study presented progression-free survival (PFS) data exclusively. Interestingly, 11 studies provided both OS and RFS data, while 4 studies included both OS and DFS data, as well as OS and PFS data. The incorporated studies employed four cut-off criteria to designate TLS: namely, Presence, Density, Degree of maturation, and Maximum dimension. The NOS scores of the 32 studies ranged from 6 to 8, signifying an exceptional standard of the encompassed research. Every study embraced pertinent insights regarding TLS within malignant growths in this article.

TLS is divided into TLS-high and TLS-low based on different cut-off criteria. Among the 31 studies included in this paper, different cut-off criteria correspond to different HR. In the subsequent investigation of the relationship between TLS and OS, RFS, PFS, and DFS, we have established inclusion criteria. When a study includes two different TLS cut-off criteria, we prioritize the HR corresponding to Density, Degree of maturity, or Maximal diameter. If a study simultaneously uses Density and Degree of

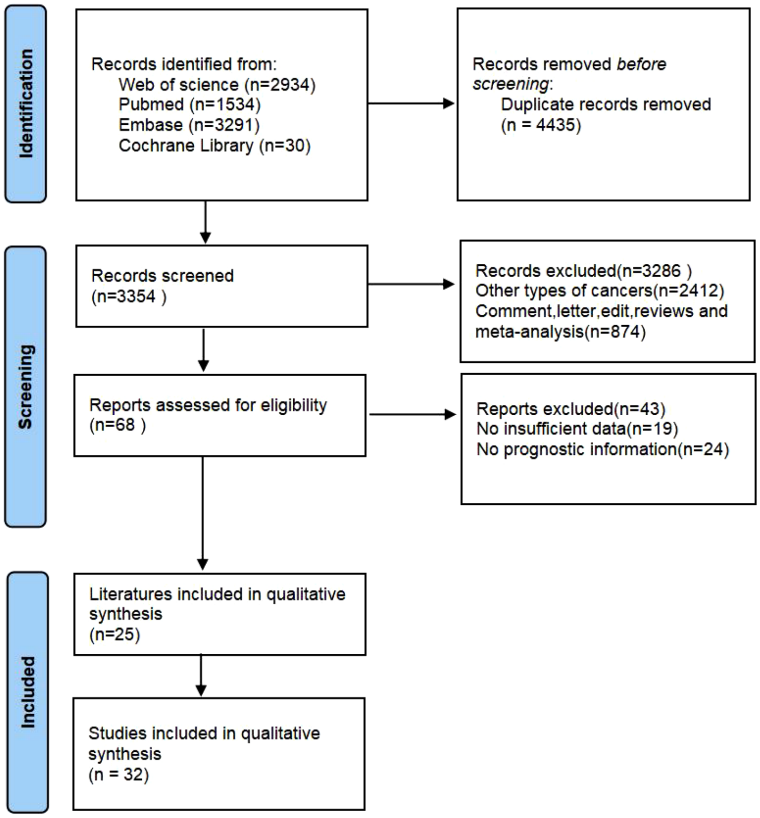

FIGURE 1
The flow diagram of identifying eligible studies.

TABLE 1 Characteristics of included studies.

Study	region	Sample size	Male/ Female	Cancer types	Cut-off crite-ria	Follow-up time (months)	Survival analysis	NOS score
Cheng N.2021 (16)	China	846	585/261	GC	Presence	22.1 (1–99)	OS	8
Yu J.2022 (15)	China	118	82/36	GC	Density	(0-120)	OS,DFS	7
Kemi N.2023 (23)	Finland	583	425/296	GC	maximal diameter	28(1,432)	OS	8
Yin Y.2022(Training) (17)	China	148	131/17	GC	Degree of maturity	(0-60)	OS	8
Yin Y.2022 (Validation) (17)	China	76	NR	GC	Degree of maturity	NR	OS	8
Mori Y.2021 (24)	Japan	261	182/92	GC	Density	(0-70)	OS	7
Mori Y.2022(ICIs) (25)	Japan	19	12/7	GC	Density	(0-27)	OS,PFS	7
Yamakoshi Y.2020 (12)	Japan	226	162/64	GC	Density	(0-90)	DFS	8
Ahmed A.2020 (18)	German	21	14/7	CRC	Density	(0-70)	OS	6
Zhan Z.2023 (26)	China	203	128/75	CRC	Density	50(0-70)	OS,DFS	8
Schweiger T.2016 (14)	Austria	57	33/24	CRC	Presence	(1-140)	OS,RFS	7
Karjula T.2023 (27)	Finland	67	34/33	CRC	Density, maximal diameter	40.2(5-233)	OS	7
Wang Q. 2022 (Training) (40)	China	114	65/49	CRC	Presence	(0-60)	OS,RFS	8
Wang Q. 2022 (Validation) (40)	China	60	37/23	CRC	Presence	(0-60)	OS,RFS	8
Wen S.2021 (28)	China	85	75/13	HCC	Density	44(0-60)	OS	8
Li H.2021(Training) (29)	China	240	202/38	HCC	Density, Presence	60.3(2.4-111.7)	OS,RFS	8
Li H.2021 (Validation) (29)	China	120	99/21	HCC	Density, Presence	NR	OS,RFS	8
Li J.2022 (30)	China	150	125/25	HCC	Presence	(0-80)	OS,RFS	7
Li H.2020(Training) (31)	China	303	251/52	HCC	Presence	61.3(1.5-119.4)	OS,RFS	8
Li H.2020 (Validation) (31)	China	159	132/27	HCC	Presence	NR	OS,RFS	8
Zhang T.2022 (32)	China	170	143/27	HCC	Density	(0-70)	OS,DFS	7
Hayashi Y.2023 (33)	Japan	316	255/61	EC	Density	(0-120)	OS,PFS	7
Hayashi Y.2023(ICIs) (33)	Japan	34	27/7	EC	Density	(0-41)	PFS	7
Deguchi S.2022 (35)	Japan	84	NR	EC	Presence	51(0-100)	RFS	7
Li R.2022(Training) (34)	China	122	102/20	EC	Density, Presence	(0-50)	OS,DFS	8
Zhang W.(Training) (13)	China	182	87/95	PC	Presence	39 (1.5-95)	OS,RFS	7
Zhang W.(Validation) (13)	China	125	60/65	PC	Presence	58 (10–96)	OS,RFS	7
Gunderson A.2021 (36)	America	63	37/26	PC	Density	(0–64)	OS	8

(Continued)

TABLE 1 Continued

Study	region	Sample size	Male/ Female	Cancer types	Cut-off crite-ria	Follow-up time (months)	Survival analysis	NOS score
Tanaka T.2023 (37)	Japan	162	90/72	PC	Presence	26 (1–122)	OS	8
Shang T.2023 (38)	China	471	160/311	ICC	Density	(0–80)	OS,PFS	8
Shang T.2023(ICIs) (38)	China	100	NR	ICC	Density	(0–50)	OS,PFS	8
Zhang P.2022 (39)	China	93	53/40	ICC	Degree of maturity, Presence	(0-108)	OS,RFS	8

GC Gastric cancer, CRC Colorectal cancer, EC Esophageal cancer, HCC Hepatocellular carcinoma, PC Pancreatic cancer, ICC Cholangiocarcinoma.
Follow-up time(months):medians(ranges).
NR, Not available.

maturity or Density and Maximal diameter as the grading methods for TLS, we select the HR corresponding to Density.

TLS and OS

Based on a comprehensive analysis of 29 studies evaluating the association between TLS and OS in GI cancer, it was found that TLS-high is significantly correlated with longer OS (HR=0.525, 95%CI:0.447-0.616, P<0.001)(Figure 2A). However, it should be noted that this analysis showed significant heterogeneity, and a random effects model was used to account for this(I^2 = 65.7%, P<0.001)(Figure 2A). Moreover, subgroup analysis based on different cancer types revealed that TLS-high is closely associated with extended OS in GC(HR=0.422, 95% CI:0.283-0.627,P<0.001), HCC(HR=0.532, 95%CI:0.391-0.726, P=0.003), EC(HR=0.393, 95%CI:0.271-0.570,P<0.001), PC (HR=0.390, 95%CI:0.290-0.525,P<0.001), and ICC(HR=0.493, 95%CI:0.421-0.577,P<0.001), while no significant relationship was found between TLS and OS in CRC(HR=0.775, 95% CI:0.570-1.053,P=0.103) (Figure 2B). Interestingly, significant heterogeneity was observed in GC(I^2 = 80.6%,P<0.001) and HCC(I^2 = 78.0%,P<0.001) (Figure 2B).

TLS and RFS, DFS, PFS

Moving on to the assessment of TLS in relation to RFS, DFS, and PFS, 12, 6, and 5 studies were included, respectively. The analysis showed a significant association between TLS-high and extended RFS(HR=0.546, 95%CI:0.461-0.647, P<0.001)(Figure 3A), DFS(HR=0.519, 95%CI:0.417-0.646, P<0.001)(Figure 3B), and PFS (HR=0.588, 95%CI:0.406-0.852, P=0.005)(Figure 3C). Notably, the analysis of RFS(I^2 = 16.8%, P=0.279)(Figure 3A)and DFS I^2 = 5.7%, P=0.380)(Figure 3B) did not exhibit significant heterogeneity, and a fixed effects model was used, whereas significant heterogeneity was observed in the analysis of PFS[I^2 = 61.2%, P=0.036)](Figure 3C), requiring the use of a random effects model.

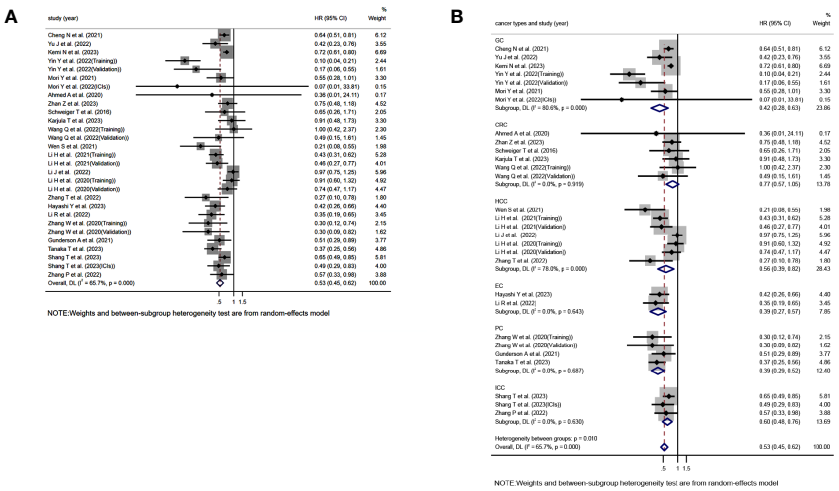

FIGURE 2
Forest plot showing the relationship between TLS and OS in GI cancers. **(A)** OS; **(B)** OS subgroup analysis for different cancer types.HR, hazard ratio; CL, confidence interval.

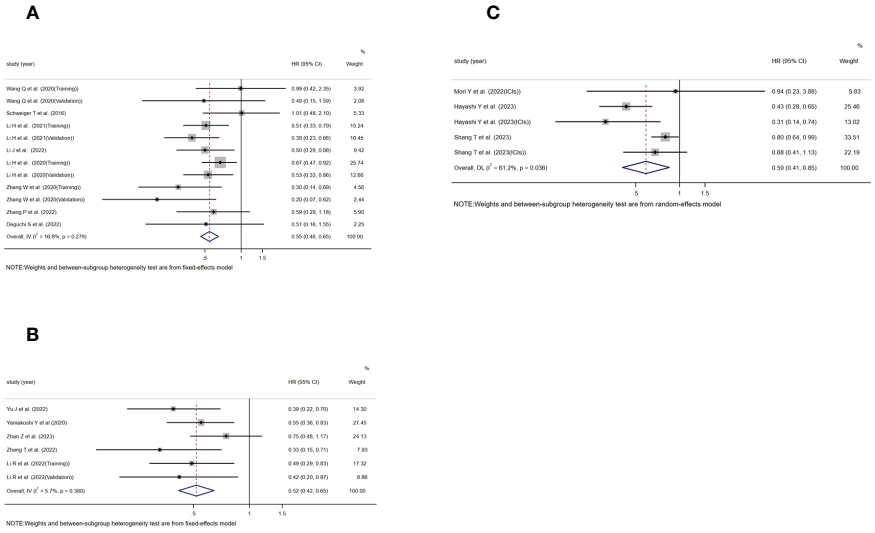

FIGURE 3
Forest plot showing the relationship between TLS and RFS, DFS, PFS in GI cancers. **(A)** RFS; **(B)** DFS; **(C)** PFS.

TLS and ICIs

In addition, two studies assessing the relationship between TLS and OS in the context of using ICIs for treatment were included, as well as three studies evaluating the relationship between TLS and PFS. The study conducted by Mori Y et al. and Hayashi Y et al. included patients who received treatment with anti-PD-1 monoclonal antibodies. On the other hand, the study conducted by Shang T et al. did not explicitly specify the type of ICIs used in their research. The results consistently showed a significant association between TLS-positive and extended OS[HR=0.475, 95%CI:0.282-0.799, P=0.005)](Figure 4A) and PFS[HR=0.576, 95%CI:0.381-0.871, P=0.009)](Figure 4B). No significant heterogeneity was found in any of these studies, and a fixed effects model was applied(I^2 = 0.0%, P=0.352)(Figure 4A), (I^2 = 33.4%, P=0.223)(Figure 4B).

TLS and cut-off criteria

Notably, in previous studies examining the relationship between TLS and OS, significant heterogeneity was still observed in the GC and HCC subgroups. This may be attributed to the use of different TLS cut-off criteria in some studies, resulting in different conclusions. Therefore, to ascertain the potential impact of cut-off criteria on the evaluation of TLS prognosis, studies using different criteria such as Presence, Density, Degree of maturity, and Maximal diameter were included. However, due to the limited number of included studies, further investigation on the impact of cut-off criteria on DFS and PFS was not possible. Firstly, we included 15 studies that used presence as a cut-off criterion to study the relationship between TLS and OS. The evaluation showed a significant correlation between TLS-high and prolonged OS in the included studies(HR=0.590, 95%CI:0.474-0.733, P<0.001)(Figure S1A). However, there was significant heterogeneity observed, so a random-effects model was used(I^2 = 62.7%, P=0.001)(Figure S1A). Subgroup analysis based on cancer types revealed no significant association between TLS and OS in HCC(HR=0.850, 95%CI:0.721-1.002, P=0.053)and CRC(HR=0.731, 95%CI:0.417-1.282, P=0.272), while a significant correlation was found in PC (HR=0.351, 95% CI:0.248-0.498, P<0.001)and other tumors(HR=0.629, 95% CI:0.508-0.778, P<0.001)(Figure S1B). Next, we included 15 studies that used density as a cut-off criterion to study the relationship between TLS and OS. The evaluation showed a significant correlation between TLS positivity and prolonged OS in the included studies(HR= 0.516, 95%CI:0.450-0.591, P<0.001) (Figure S1C). No significant heterogeneity was found, so a fixed-effects model was used(I^2 = 23.3%, P=0.195)(Figure S1C). Subgroup analysis based on cancer types showed a close correlation between TLS-high and OS prolongation in GC(HR=0.466, 95%CI:0.302-

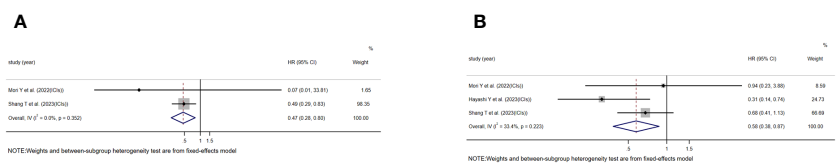

FIGURE 4
Forest plot showing the relationship between TLS and OS, PFS in GI cancers undergoing treatment with immune ICIs. **(A)** OS; **(B)** PFS.

0.719,P<0.001), HCC(HR=0.401, 95%CI:0.307-0.524, P<0.001),EC (HR=0.393, 95%CI:0.271-0.570,P<0.001),PC(HR=0.510, 95% CI:0.291-0.893,P=0.019) and ICC(HR=0.612, 95%CI:0.479-0.781, P<0.001) (Figure S1D). However, no significant relationship was observed in CRC(HR=0.794, 95%CI:0.550-1.145,P=0.217) (Figure S1D). Furthermore, after including 3 studies that used maturity as a criteria to study the relationship between TLS and OS, we found a similar significant correlation between TLS-high and prolonged OS (HR=0.222, 95%CI:0.068-0.0730, P=0.013)(Figure S1E). Due to significant heterogeneity observed in the studies, a random-effects model was used(I^2 = 84.7%, P=0.001)(Figure S1E). Moving on to the relationship between TLS and RFS, we included 10 studies that used presence as a cut-off criterion. We found a significant correlation between TLS and prolonged RFS in these studies(HR=0.591, 95% CI:0.495-0.705, P<0.001)(Figure S2A). No significant heterogeneity was observed, so a fixed-effects model was used [(I^2 = 33.5%, P<0.122](Figure S2A). Subgroup analysis based on cancer types revealed no significant association between TLS and RFS in CRC (HR=0.874, 95%CI:0.527-1.450, P=0.602)(Figure S2B), while a significant correlation was found in HCC(HR=0.638, 95% CI:0.518-0.787, P<0.001), PC(HR=0.260, 95%CI:0.137-0.496, P<0.001), and other tumors HR=0.365, 95%CI:0.200-0.665, P=0.001)(Figure S2B). In the 2 studies that evaluated the relationship between TLS and RFS using density as a cut-off criteria, we found a significant correlation between TLS and RFS (HR=0.457, 95%CI:0.327-0.640, P<0.001)(Figure S2C). No significant heterogeneity was found in these studies, so a fixed-effects model was used(I^2 = 0.0%, P=0.442)(Figure S2C).

We found that different studies have used various criteria such as ROC curves, medians, and other ambiguous methods to divide the Density of TLS into two parts, namely TLS-high and TLS-low, when using Density as the cut-off for TLS. We conducted a meta-regression to determine if different criteria would affect the predictive value of TLS. The different criteria used to divide Density can affect the predictive value of TLS(P=0.023). Further sub-analysis demonstrates that TLS has a significant correlation with OS across various criteria (Figure S3).

Sensitivity analysis and publication bias

To assess sensitivity, we employed the leave-one-out method for statistical analysis. After systematically excluding each individual study, the overall (HR) for OS, RFS, DFS, and PFS did not show any significant changes, indicating the stability and reliability of our findings (Figure S4).

Next, we employed a funnel plot (Figure S5), Begg's test (Figure S6), and Egger's test (Figure S6) to evaluate publication bias in the included studies. We found evidence of publication bias in OS (Begg's test:P=0.063, Egger's test: P=0.001)(Figures S6 A, H). However, no publication bias was observed in RFS(Begg's test: P=0.732, Egger's test:P=0.430)(Figures S6 B, I), DFS(Begg's test: P=0.060, Egger's test:P=0.063)(Figures S6 C, J), and PFS(Begg's test: P=1.000, Egger's test: P=0.364)(Figures S6 D, K). Further analysis of the cut-off criteria for TLS revealed publication bias in OS (Begg's test:P=0.322, Egger's test:P=0.033)in the "Density group"(Figures S6 F, M). There was no publication bias in OS(Begg's test:P=0.235, Egger's test:P=0.064) in the "Presence group"(Figures S6 E, L), and RFS(Begg's test:P=0.210, Egger's test:P=0.125) in the "Presence group"(Figures S6 F, N). All remaining studies from the subgroups mentioned above were included in our analysis. Subsequently, we applied the trim and fill method to fill in the missing data from studies that had zero items missing. This approach ensured that our results remained robust and reliable.

TLS and bioinformatics analysis

We studied the relationship between TLSscore and the immune microenvironment. In the ESTIMATE algorithm, patients in the high TLSscore group showed higher immune, stromal, and ESTIMATE scores (Figure S7). Single-sample gene set enrichment analysis (ssGSEA) revealed a significantly higher degree of infiltration of various immune-related cells in the TLSscore high group compared to the TLSscore low group (Figures 5, 6). Additionally, we further investigated the relationship between TLSscore and prognosis. In HCC, we found a significant improvement in overall survival (OS) associated with TLSscore high, while no significant association between TLSscore and OS was found in other gastrointestinal cancers (Figure S8).

Discussion

Compared to TLS-low tumors, TLS-high tumors exhibit overexpression of a set of genes that promote T cell activation, T helper 1 (TH-1) cell skewing, T cell chemotaxis, and T cell cytotoxicity (41). Moreover, the unique spatial structure of TLS facilitates the presentation of antigen peptides by mature dendritic cells (DC) and potential B cells in the T cell zone, activating them to generate a response against tumor cells presenting the same antigen (9, 42). The Phase 2 PEMBROSARC trial cohort has provided evidence that TLS serves as a novel biological biomarker improving treatment selection for patients with advanced soft tissue sarcoma (STS) undergoing pembrolizumab therapy (43). This reflects the important predictive role of TLS in tumor immunotherapy response. Some studies suggest that the presence of TLS may be associated with the activation of anti-tumor immune responses and further contribute to the anti-tumor effects (44–48). There is a significant variation in clinical prognosis among patients with GI cancer, even within the same TMN stage. Additionally, there is a scarcity of prognostic markers for cancer immunotherapy and they are often difficult to meet clinical needs (49). Therefore, the search for biomarkers that can be used for early detection and prognosis assessment in cancer is of urgent importance.

The purpose of this study is to investigate the relationship between TLS (Tertiary Lymphoid Structures) and prognosis of GI (Gastrointestinal) cancer (50). While previous literature has explored the association between TLS and prognosis of solid tumors, there is still relatively limited information regarding GI cancer. In this study, we updated the information on GI cancer and conducted subgroup analysis to clarify the relationship between

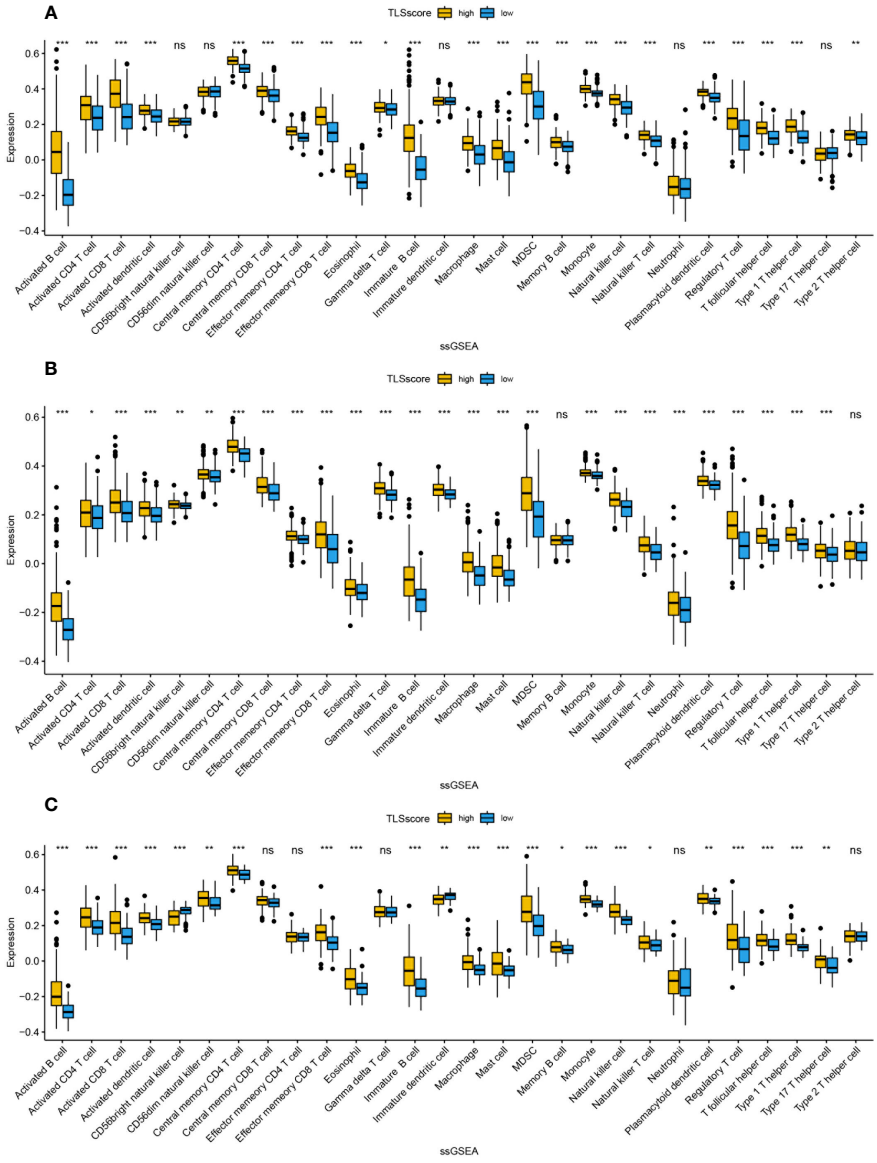

FIGURE 5
The abundance of infiltrating cells in each tumor microenvironment based on ssGSEA analysis of two groups of TLSscore. **(A)** GC, **(B)** CRC, **(C)** EC. *: P<0.05, **: P<0.01, ***: P<0.001, ns: P≥0.05 non-significant.

TLS and overall survival (OS), progression-free survival (PFS), disease-free survival (DFS), and recurrence-free survival (RFS). The results indicated that TLS was significantly associated with prolonged OS, PFS, DFS, and RFS. However, in the subgroup analysis specifically focusing on colorectal cancer, TLS was not significantly associated with OS. A possible explanation may be due to the presence of GALT tissue or Peyer's patches that preexist TLS and are considered as TLS due the inclusion of these genes in those normal lymphoid tissues (51, 52). Wang Q and colleagues suggested that the higher proportion of regulatory T cells (Treg) within TLS in tumors might be one of the mechanisms that undermine its prognostic value in CRC (40). Additionally, TLS was significantly associated with OS and PFS in patients receiving immunotherapy. Furthermore, we investigated whether different cut-off criteria would affect the predictive value of TLS for prognosis in GI cancer. In hepatocellular carcinoma (HCC), TLS positivity did not improve patient OS when using "Presence" as the cut-off criteria, whereas it was significantly associated with prolonged OS when using "Density" as the cut-off criteria. This suggests that different cut-off criteria can influence the predictive value of TLS for prognosis in GI cancer, especially in HCC where "Density" is more suitable as the cut-off criteria for TLS. Moreover, in CRC, three studies using "Density" as the cut-off criteria showed no significant association between TLS and OS, and three studies using "Presence" as the cut-off criteria also did not yield meaningful results. Wang Q and colleagues found that TLS density in the surrounding normal tissue could predict the prognosis of CRC patients (40). Additionally, Yamaguchi K and colleagues' research indicated that a T helper (Th) cell-dominant composition within TLS was an independent risk factor for postoperative recurrence of CRC

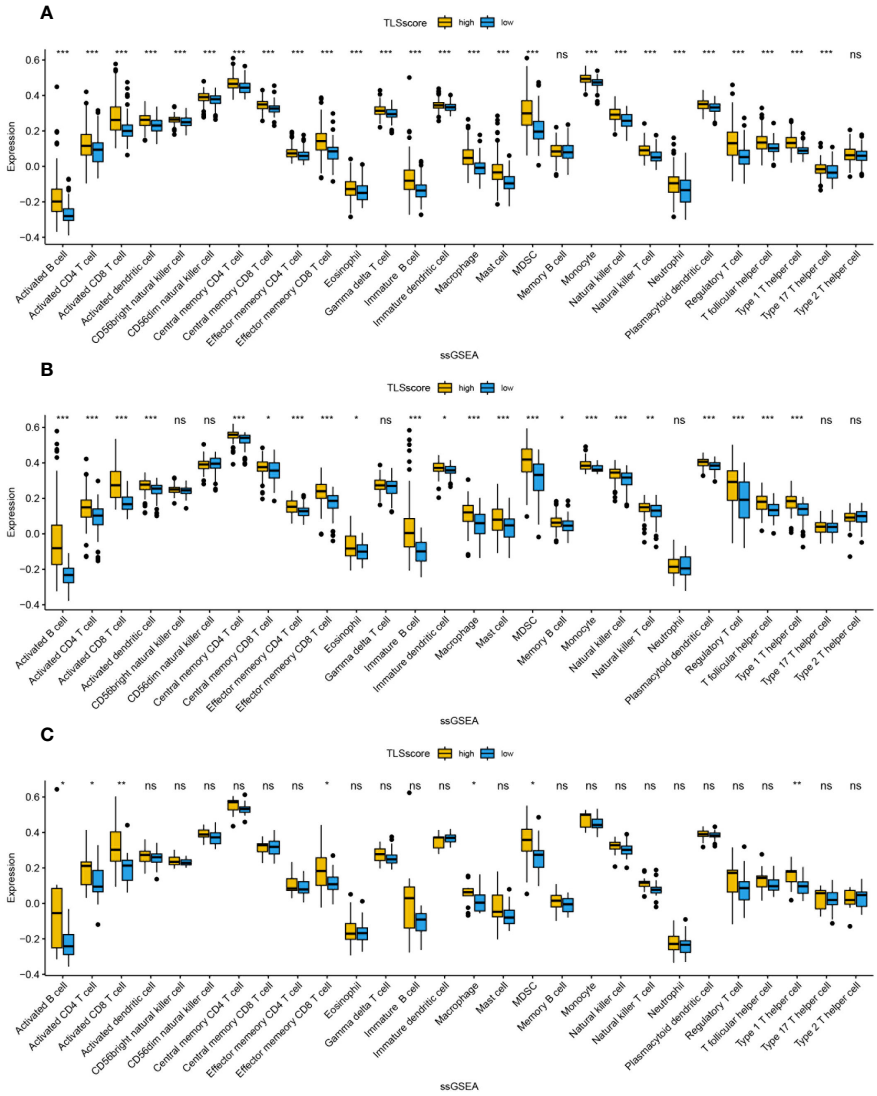

FIGURE 6
The abundance of infiltrating cells in each tumor microenvironment based on ssGSEA analysis of two groups of TLSscore. **(A)** HCC, **(B)** PC, **(C)** ICC. *: P<0.05, **: P<0.01, ***: P<0.001, ns: P≥0.05 non-significant.

(53). Li Q and his team have linked the presence of TLS with the density of tumor-infiltrating lymphocytes, and discovered that this combination acts as a prognostic biomarker for oral cancer. The results of their research, as depicted by the Receiver Operating Characteristic (ROC) curve, demonstrated that this combined marker exhibits a remarkably high predictive accuracy for 5-year OS (54). These novel detection methods have the potential to expand the prognostic value of TLS and make TLS a biological marker for CRC prognosis.

In addition, due to significant heterogeneity among TLS identification methods, we further investigated the relationship between the immune microenvironment and TLS in gastrointestinal cancer in the TCGA database using the method proposed by Cabrita et al. to quantify TLSscore based on 9 TLS-related genes. We found that patients in the TLSscore high group had higher levels of immune cell infiltration compared to those in the TLSscore low group. Recent studies have shown that the formation of TLS is mediated by certain pro-inflammatory cytokines and TNF receptor family members, and involves the participation of fibroblasts, perivascular myofibroblasts, and stromal cells (55). However, in gastrointestinal cancer, a large number of patients have low tumor mutation burden and lack immune cell infiltration, making their tumor microenvironment "cold" and resulting in poor response to emerging therapies targeting the tumor immune microenvironment, such as immunotherapy (56, 57). Hooren et al. discovered the formation of TLS during the process of transforming the solid tumor immune microenvironment from "cold" to "hot" using a CD40 agonist, and TLS was found to be correlated with increased infiltration of T cells (58). We speculate that appropriate immune cell infiltration may be associated with the formation of TLS, and the presence of TLS also promotes the infiltration of local immune cells. Numerous studies have shown a significant prolongation of survival time with high density of immune cell infiltration (59–61), which partially explains

the improvement in prognosis with TLS. However, our survival analysis based on the TCGA database showed that only liver cancer exhibited a predictive value of TLSscore for prognosis in gastrointestinal cancer, which suggests that we need to consider the applicability of the "9-gene method" in gastrointestinal cancer and further investigate the consistency of different methods such as IHC, HE, and gene markers in TLS evaluation in gastrointestinal cancer in real-world studies. Jiang et al. divided gastric cancer patients in the GSE84437 and TCGA cohorts into two groups based on unsupervised clustering analysis of 39 TLS-related genes, and significant differences in prognosis and immune scores were observed between the two groups (62). We look forward to future validation of the accuracy of the TLS biomarker assessment proposed by them in the real world.

There are several limitations in this meta-analysis. Firstly, some articles did not provide sufficient prognostic data, and some survival statistics data calculated from survival curves using Engauge Digitizer may have biases. Secondly, the majority of included studies were from Asia, which may result in a publication bias to some extent. Additionally, there were fewer studies included in some subgroup analyses, especially in the subgroup of immunotherapy, with only 3 immunotherapy studies included in the analysis and a relatively small sample size (153 cases in total), which may affect the evaluation of the role of TLS in prognosis. Lastly, this meta-analysis only included data related to intratumoral TLS, which cannot fully reflect its predictive role in prognosis.

Conclusion

Despite its limitations, we can conclude that TLS can serve as an excellent prognostic factor for GI cancer, and appropriate cut-off criteria should be selected for different cancer subtypes. In CRC, the focus can be on TLS in the surrounding normal tissue of the tumor or in combination with other predictive indicators to serve as prognostic markers. Furthermore, high-quality and multicenter clinical studies, especially in immunotherapy cohorts, are needed to further elucidate the impact of TLS on the survival outcomes of GI cancer.

Data availability statement

The original contributions presented in the study are included in the article/Supplementary Material. Further inquiries can be directed to the corresponding authors.

Author contributions

AY: Writing – original draft. MC: Data curation, Writing – original draft. KZ: Data curation, Methodology, Writing – original draft. YY: Data curation, Formal Analysis, Writing – original draft. LM: Data curation, Formal Analysis, Writing – original draft. XZ: Data curation, Writing – original draft. YZ: Writing – original draft. XM: Writing – original draft. ZF: Writing – original draft. ZH: Writing – review & editing, Conceptualization. HW: Writing – review & editing.

Conflict of interest

The authors declare that the research was conducted in the absence of any commercial or financial relationships that could be construed as a potential conflict of interest.

Publisher's note

Supplementary material

The Supplementary Material for this article can be found online at: https://www.frontiersin.org/articles/10.3389/fimmu.2023.1256355/full#supplementary-material

SUPPLEMENTARY FIGURE 1
Forest plot showing the relationship between TLS and OS in GI cancers under different cut-off criteria. **(A)** OS when presence is used as a cut-off criterion; **(B)** OS subgroup analysis for different cancer types when presence is used as a cut-off criterion. **(C)** OS when density is used as a cut-off criterion. **(D)** OS subgroup analysis for different cancer types when density is used as a cut-off criterion. **(E)** OS when maturity is used as a cut-off criterion.

SUPPLEMENTARY FIGURE 2
Forest plot showing the relationship between TLS and RFS in GI cancers under different cut-off criteria. **(A)** RFS when presence is used as a cut-off criterion; **(B)** RFS subgroup analysis for different cancer types when presence is used as a cut-off criterion. **(C)** RFS when density is used as a cut-off criterion.

SUPPLEMENTARY FIGURE 3
Forest plot showing the relationship between TLS and OS in GI cancers under different criteria.

SUPPLEMENTARY FIGURE 4
Sensitivity analysis. **(A)**OS; **(B)**RFS; **(C)**DFS; **(D)**PFS; **(E)** OS when presence is used as a cut-off criterion;**(F)** OS when density is used as a cut-off criterion; **(G)** RFS when presence is used as a cut-off criterion.

SUPPLEMENTARY FIGURE 5
Funnel plots for detecting publication bias in terms of survival data. **(A)** OS; **(B)** RFS; **(C)** DFS; **(D)** PFS; **(E)** OS when presence is used as a cut-off criterion; **(F)** OS when density is used as a cut-off criterion; **(G)** RFS when presence is used as a cut-off criterion.

SUPPLEMENTARY FIGURE 6
Begg's and Egger's funnel plots for detecting publication bias in terms of survival data. **(A)** Begg's test of OS;**(B)** Begg's test of RFS; **(C)** Begg's test of

DFS; **(D)** Begg's test of PFS; **(E)** Begg's test of OS when presence is used as a cut-off criterion; **(F)** Begg's test of OS when density is used as a cut-off criterion; **(G)**Begg's test of RFS when presence is used as a cut-off criterion; **(H)** Egger's test of OS; **(I)** Egger's test of RFS; **(J)** Egger's test of DFS; **(K)** Egger's test of PFS; **(L)** Egger's test of OS when presence is used as a cut-off criterion; **(M)** Egger's test of OS when density is used as a cut-off criterion; **(N)** Egger's test of RFS when presence is used as a cut-off criterion.

SUPPLEMENTARY FIGURE 7

Two groups of TLSscore immunity, matrix, and ESTIMATE scores based on the analysis using the ESTIMATE algorithm. **(A)** GC, **(B)** CRC, **(C)** EC, **(D)** HCC, **(E)** PC, **(F)** ICC.

SUPPLEMENTARY FIGURE 8

Survival analysis of GI cancers based on TLSscore grouping. **(A)** GC, **(B)** CRC, **(C)** EC, **(D)** HCC, **(E)** PC, **(F)** ICC.

References

1. Huang J, Lucero-Prisno DE, Zhang L, Xu W, Wong SH, Ng SC, et al. Updated epidemiology of gastrointestinal cancers in East Asia. *Nat Rev Gastroenterol Hepatol* (2023) 20(5):271–87. doi: 10.1038/s41575-022-00726-3

2. Kayamba V. Nutrition and upper gastrointestinal cancers: An overview of current understandings. *Semin Cancer Biol* (2022) 83:605–16. doi: 10.1016/j.semcancer.2021.03.004

3. Kashyap S, Pal S, Chandan G, Saini V, Chakrabarti S, Saini NK, et al. Understanding the cross-talk between human microbiota and gastrointestinal cancer for developing potential diagnostic and prognostic biomarkers. *Semin Cancer Biol* (2022) 86(Pt 3):643–51. doi: 10.1016/j.semcancer.2021.04.020

4. Villariba-Tolentino C, Cariño AM, Notarte KI, Macaranas I, Fellizar A, Tomas RC, et al. pks+ Escherichia coli more prevalent in benign than Malignant colorectal tumors. *Mol Biol Rep* (2021) 48(7):5451–8. doi: 10.1007/s11033-021-06552-1

5. Notarte KI, Senanayake S, Macaranas I, Albano PM, Mundo L, Fennell E, et al. MicroRNA and other non-coding RNAs in epstein-barr virus-associated cancers. *Cancers (Basel)* (2021) 13(15):2. doi: 10.3390/cancers13153909

6. Wang Z-X, Pan Y-Q, Li X, Tsubata T, Xu R-H. Immunotherapy in gastrointestinal cancers: advances, challenges, and countermeasures. *Sci Bull (Beijing).* (2023) 68(8):763–6. doi: 10.1016/j.scib.2023.03.036

7. Shen X, Zhao B. Efficacy of PD-1 or PD-L1 inhibitors and PD-L1 expression status in cancer: meta-analysis. *BMJ* (2018) 362:k3529. doi: 10.1136/bmj.k3529

8. Chen Y, Sun Z, Wan L, Chen H, Xi T, Jiang Y. Tumor microenvironment characterization for assessment of recurrence and survival outcome in gastric cancer to predict chemotherapy and immunotherapy response. *Front Immunol* (2022) 13:890922. doi: 10.3389/fimmu.2022.890922

9. Fridman WH, Meylan M, Petitprez F, Sun C-M, Italiano A, Sautès-Fridman C. B cells and tertiary lymphoid structures as determinants of tumour immune contexture and clinical outcome. *Nat Rev Clin Oncol* (2022) 19(7):441–57. doi: 10.1038/s41571-022-00619-z

10. Vanhersecke L, Brunet M, Guégan J-P, Rey C, Bougouin A, Cousin S, et al. Mature tertiary lymphoid structures predict immune checkpoint inhibitor efficacy in solid tumors independently of PD-L1 expression. *Nat Cancer.* (2021) 2(8):794–802. doi: 10.1038/s43018-021-00232-6

11. Posch F, Silina K, Leibl S, Mündlein A, Moch H, Siebenhüner A, et al. Maturation of tertiary lymphoid structures and recurrence of stage II and III colorectal cancer. *Oncoimmunology.* (2018) 7(2):e1378844. doi: 10.1080/2162402X.2017.1378844

12. Yamakoshi Y, Tanaka H, Sakimura C, Deguchi S, Mori T, Tamura T, et al. Immunological potential of tertiary lymphoid structures surrounding the primary tumor in gastric cancer. *Int J Oncol* (2020) 57(1):171–82. doi: 10.3892/ijo.2020.5042

13. Zhang W-H, Wang W-Q, Han X, Gao H-L, Xu S-S, Li S, et al. Infiltrating pattern and prognostic value of tertiary lymphoid structures in resected non-functional pancreatic neuroendocrine tumors. *J Immunother Cancer* (2020) 8(2):6. doi: 10.1136/jitc-2020-001188

14. Schweiger T, Berghoff AS, Glogner C, Glueck O, Rajky O, Traxler D, et al. Tumor-infiltrating lymphocyte subsets and tertiary lymphoid structures in pulmonary metastases from colorectal cancer. *Clin Exp Metastasis* (2016) 33(7):727–39. doi: 10.1007/s10585-016-9813-y

15. Yu J-S, Huang W-B, Zhang Y-H, Chen J, Li J, Fu H-F, et al. The association of immune cell infiltration and prognostic value of tertiary lymphoid structures in gastric cancer. *Neoplasma.* (2022) 69(4):886–98. doi: 10.4149/neo_2022_220128N123

16. Cheng N, Li P, Cheng H, Zhao X, Dong M, Zhang Y, et al. Prognostic value of tumor-infiltrating lymphocytes and tertiary lymphoid structures in epstein-barr virus-associated and -negative gastric carcinoma. *Front Immunol* (2021) 12:692859. doi: 10.3389/fimmu.2021.692859

17. Yin Y-X, Ling Y-H, Wei X-L, He C-Y, Wang B-Z, Hu C-F, et al. Impact of mature tertiary lymphoid structures on prognosis and therapeutic response of Epstein-Barr virus-associated gastric cancer patients. *Front Immunol* (2022) 13:973085. doi: 10.3389/fimmu.2022.973085

18. Ahmed A, Halama N. Tertiary lymphoid structures in colorectal cancer liver metastases: association with immunological and clinical parameters and chemotherapy response. *Anticancer Res* (2020) 40(11):6367–73. doi: 10.21873/anticanres.14657

19. Liberati A, Altman DG, Tetzlaff J, Mulrow C, Gøtzsche PC, Ioannidis JPA, et al. The PRISMA statement for reporting systematic reviews and meta-analyses of studies that evaluate health care interventions: explanation and elaboration. *PloS Med* (2009) 6(7):e1000100. doi: 10.1371/journal.pmed.1000100

20. Parmar MK, Torri V, Stewart L. Extracting summary statistics to perform meta-analyses of the published literature for survival endpoints. *Stat Med* (1998) 17(24):2815–34. doi: 10.1002/(SICI)1097-0258(19981230)17:24<2815::AID-SIM110>3.0.CO;2-8

21. Stang A. Critical evaluation of the Newcastle-Ottawa scale for the assessment of the quality of nonrandomized studies in meta-analyses. *Eur J Epidemiol.* (2010) 25(9):603–5. doi: 10.1007/s10654-010-9491-z

22. Cabrita R, Lauss M, Sanna A, Donia M, Skaarup Larsen M, Mitra S, et al. Tertiary lymphoid structures improve immunotherapy and survival in melanoma. *Nature.* (2020) 577(7791):561–5. doi: 10.1038/s41586-019-1914-8

23. Karjula T, Kemi N, Niskakangas A, Mustonen O, Puro I, Pohjanen V-M, et al. The prognostic role of tumor budding and tumor-stroma ratio in pulmonary metastasis of colorectal carcinoma. *Eur J Surg Oncol* (2023) 49(7):1298–306. doi: 10.1016/j.ejso.2023.02.009

24. Mori T, Tanaka H, Suzuki S, Deguchi S, Yamakoshi Y, Yoshii M, et al. Tertiary lymphoid structures show infiltration of effective tumor-resident T cells in gastric cancer. *Cancer Sci* (2021) 112(5):1746–57. doi: 10.1111/cas.14888

25. Mori T, Tanaka H, Deguchi S, Yamakoshi Y, Miki Y, Yoshii M, et al. Clinical efficacy of nivolumab is associated with tertiary lymphoid structures in surgically resected primary tumors of recurrent gastric cancer. *PloS One* (2022) 17(1):e0262455. doi: 10.1371/journal.pone.0262455

26. Zhan Z, Shi-Jin L, Yi-Ran Z, Zhi-Long L, Xiao-Xu Z, Hui D, et al. High endothelial venules proportion in tertiary lymphoid structure is a prognostic marker and correlated with anti-tumor immune microenvironment in colorectal cancer. *Ann Med* (2023) 55(1):114–26. doi: 10.1080/07853890.2022.2153911

27. Karjula T, Niskakangas A, Mustonen O, Puro I, Elomaa H, Ahtiainen M, et al. Tertiary lymphoid structures in pulmonary metastases of microsatellite stable colorectal cancer. *Virchows Arch* (2023) 483:27–9. doi: 10.1007/s00428-023-03577-8

28. Wen S, Chen Y, Hu C, Du X, Xia J, Wang X, et al. Combination of tertiary lymphoid structure and neutrophil-to-lymphocyte ratio predicts survival in patients with hepatocellular carcinoma. *Front Immunol* (2021) 12:788640. doi: 10.3389/fimmu.2021.788640

29. Li H, Liu H, Fu H, Li J, Xu L, Wang G, et al. Peritumoral tertiary lymphoid structures correlate with protective immunity and improved prognosis in patients with hepatocellular carcinoma. *Front Immunol* (2021) 12:648812. doi: 10.3389/fimmu.2021.648812

30. Li J, Nie Y, Jia W, Wu W, Song W, Li Y. Effect of tertiary lymphoid structures on prognosis of patients with hepatocellular carcinoma and preliminary exploration of its formation mechanism. *Cancers (Basel)* (2022) 14(20):7–9. doi: 10.3390/cancers14205157

31. Li H, Wang J, Liu H, Lan T, Xu L, Wang G, et al. Existence of intratumoral tertiary lymphoid structures is associated with immune cells infiltration and predicts better prognosis in early-stage hepatocellular carcinoma. *Aging (Albany NY).* (2020) 12(4):3451–72. doi: 10.18632/aging.102821

32. Zhang T, Lei X, Jia W, Li J, Nie Y, Mao Z, et al. Peritumor tertiary lymphoid structures are associated with infiltrating neutrophils and inferior prognosis in hepatocellular carcinoma. *Cancer Med* (2023) 12(3):3068–78. doi: 10.1002/cam4.5227

33. Hayashi Y, Makino T, Sato E, Ohshima K, Nogi Y, Kanemura T, et al. Density and maturity of peritumoral tertiary lymphoid structures in oesophageal squamous cell carcinoma predicts patient survival and response to immune checkpoint inhibitors. *Br J Cancer* (2023) 128(12):2175–85. doi: 10.1038/s41416-023-02235-9

34. Li R, Huang X, Yang W, Wang J, Liang Y, Zhang T, et al. Tertiary lymphoid structures favor outcome in resected esophageal squamous cell carcinoma. *J Pathol Clin Res* (2022) 8(5):422–35. doi: 10.1002/cjp2.281

35. Deguchi S, Tanaka H, Suzuki S, Natsuki S, Mori T, Miki Y, et al. Clinical relevance of tertiary lymphoid structures in esophageal squamous cell carcinoma. *BMC Cancer.* (2022) 22(1):699. doi: 10.1186/s12885-022-09777-w

36. Gunderson A J, Rajamanickam V, Bui C, Bernard B, Pucilowska J, Ballesteros-Merino C, et al. Germinal center reactions in tertiary lymphoid structures associate with neoantigen burden, humoral immunity and long-term survivorship in pancreatic cancer. *Oncoimmunology* (2021) 10(1):1900635. doi: 10.1080/2162402X.2021.1900635

37. Tanaka T, Masuda A, Inoue J, Hamada T, Ikegawa T, Toyama H, et al. Integrated analysis of tertiary lymphoid structures in relation to tumor-infiltrating lymphocytes and patient survival in pancreatic ductal adenocarcinoma. *J Gastroenterol* (2023) 58 (3):277–91. doi: 10.1007/s00535-022-01939-8

38. Shang T, Jiang T, Lu T, Wang H, Cui X, Pan Y, et al. Tertiary lymphoid structures predict the prognosis and immunotherapy response of cholangiocarcinoma. *Front Immunol* (2023) 14:1166497. doi: 10.3389/fimmu.2023.1166497

39. Zhang F-P, Zhu K, Zhu T-F, Liu C-Q, Zhang H-H, Xu L-B, et al. Intra-tumoral secondary follicle-like tertiary lymphoid structures are associated with a superior prognosis of overall survival of perihilar cholangiocarcinoma. *Cancers (Basel)* (2022) 14(24). doi: 10.3390/cancers14246107

40. Wang Q, Shen X, An R, Bai J, Dong J, Cai H, et al. Peritumoral tertiary lymphoid structure and tumor stroma percentage predict the prognosis of patients with non-metastatic colorectal cancer. *Front Immunol* (2022) 13:962056. doi: 10.3389/fimmu.2022.962056

41. Sautès-Fridman C, Petitprez F, Calderaro J, Fridman WH. Tertiary lymphoid structures in the era of cancer immunotherapy. *Nat Rev Cancer* (2019) 19(6):307–25. doi: 10.1038/s41568-019-0144-6

42. Petitprez F, de Reyniès A, Keung EZ, Chen TW-W, Sun C-M, Calderaro J, et al. B cells are associated with survival and immunotherapy response in sarcoma. *Nature* (2020) 577(7791):556–60. doi: 10.1038/s41586-019-1906-8

43. Italiano A, Bessede A, Pulido M, Bompas E, Piperno-Neumann S, Chevreau C, et al. Pembrolizumab in soft-tissue sarcomas with tertiary lymphoid structures: a phase 2 PEMBROSARC trial cohort. *Nat Med* (2022) 28(6):1199–206. doi: 10.1038/s41591-022-01821-3

44. Schumacher TN, Thommen DS. Tertiary lymphoid structures in cancer. *Science* (2022) 375(6576):eabf9419. doi: 10.1126/science.abf9419

45. Engelhard V, Conejo-Garcia JR, Ahmed R, Nelson BH, Willard-Gallo K, Bruno TC, et al. B cells and cancer. *Cancer Cell* (2021) 39(10):1293–6. doi: 10.1016/j.ccell.2021.09.007

46. Hu X, Liu XS. A high-resolution view of intra-tumoral B cell immunity. *Immunity*. (2022) 55(3):387–9. doi: 10.1016/j.immuni.2022.02.009

47. Paijens ST, Vledder A, de Bruyn M, Nijman HW. Tumor-infiltrating lymphocytes in the immunotherapy era. *Cell Mol Immunol* (2021) 18(4):842–59. doi: 10.1038/s41423-020-00565-9

48. Rodriguez AB, Engelhard VH. Insights into tumor-associated tertiary lymphoid structures: novel targets for antitumor immunity and cancer immunotherapy. *Cancer Immunol Res* (2020) 8(11):1338–45. doi: 10.1158/2326-6066.CIR-20-0432

49. Ye Z, Zeng D, Zhou R, Shi M, Liao W. Tumor microenvironment evaluation for gastrointestinal cancer in the era of immunotherapy and machine learning. *Front Immunol* (2022) 13:819807. doi: 10.3389/fimmu.2022.819807

50. Zhao Z, Ding H, Lin Z-B, Qiu S-H, Zhang Y-R, Guo Y-G, et al. Relationship between tertiary lymphoid structure and the prognosis and clinicopathologic characteristics in solid tumors. *Int J Med Sci* (2021) 18(11):2327–38. doi: 10.7150/ijms.56347

51. Le Rochais M, Hémon P, Ben-Guigui D, Garaud S, Le Dantec C, Pers J-O, et al. Deciphering the maturation of tertiary lymphoid structures in cancer and inflammatory diseases of the digestive tract using imaging mass cytometry. *Front Immunol* (2023) 14:1147480. doi: 10.3389/fimmu.2023.1147480

52. Jørgensen PB, Fenton TM, Mörbe UM, Riis LB, Jakobsen HL, Nielsen OH, et al. Identification, isolation and analysis of human gut-associated lymphoid tissues. *Nat Protoc* (2021) 16(4):2051–67. doi: 10.1038/s41596-020-00482-1

53. Yamaguchi K, Ito M, Ohmura H, Hanamura F, Nakano M, Tsuchihashi K, et al. Helper T cell-dominant tertiary lymphoid structures are associated with disease relapse of advanced colorectal cancer. *Oncoimmunology* (2020) 9(1):1724763. doi: 10.1080/2162402X.2020.1724763

54. Li Q, Liu X, Wang D, Wang Y, Lu H, Wen S, et al. Prognostic value of tertiary lymphoid structure and tumour infiltrating lymphocytes in oral squamous cell carcinoma. *Int J Oral Sci* (2020) 12(1):24. doi: 10.1038/s41368-020-00092-3

55. Pipi E, Nayar S, Gardner DH, ColaFrancesco S, Smith C, Barone F. Tertiary lymphoid structures: autoimmunity goes local. *Front Immunol* (2018) 9:1952. doi: 10.3389/fimmu.2018.01952

56. Xu M, Chang J, Wang W, Wang X, Wang X, Weng W, et al. Classification of colon adenocarcinoma based on immunological characterizations: Implications for prognosis and immunotherapy. *Front Immunol* (2022) 13:934083. doi: 10.3389/fimmu.2022.934083

57. Wang X, Xu Y, Dai L, Yu Z, Wang M, Chan S, et al. A novel oxidative stress- and ferroptosis-related gene prognostic signature for distinguishing cold and hot tumors in colorectal cancer. *Front Immunol* (2022) 13:1043738. doi: 10.3389/fimmu.2022.1043738

58. van Hooren L, Vaccaro A, Ramachandran M, Vazaios K, Libard S, van de Walle T, et al. Agonistic CD40 therapy induces tertiary lymphoid structures but impairs responses to checkpoint blockade in glioma. *Nat Commun* (2021) 12(1):4127. doi: 10.1038/s41467-021-24347-7

59. Kim Y, Rhee Y-Y, Wen X, Cho N-Y, Bae JM, Kim WH, et al. Combination of L1 methylation and tumor-infiltrating lymphocytes as prognostic marker in advanced gastric cancer. *Gastric Cancer* (2020) 23(3):464–72. doi: 10.1007/s10120-019-01025-8

60. Laghi L, Negri F, Gaiani F, Cavalleri T, Grizzi F, De' Angelis GL, et al. Prognostic and predictive cross-roads of microsatellite instability and immune response to colon cancer. *Int J Mol Sci* (2020) 21(24):5–7. doi: 10.3390/ijms21249680

61. Ku YJ, Kim HH, Cha JH, Shin HJ, Baek SH, Lee HJ, et al. Correlation between MRI and the level of tumor-infiltrating lymphocytes in patients with triple-negative breast cancer. *AJR Am J Roentgenol* (2016) 207(5):1146–51. doi: 10.2214/AJR.16.16248

62. Jiang Q, Tian C, Wu H, Min L, Chen H, Chen L, et al. Tertiary lymphoid structure patterns predicted anti-PD1 therapeutic responses in gastric cancer. *Chin J Cancer Res* (2022) 34(4):365–82. doi: 10.21147/j.issn.1000-9604.2022.04.05

frontiers | Frontiers in Immunology

TYPE Review
PUBLISHED 04 December 2023
DOI 10.3389/fimmu.2023.1286850

OPEN ACCESS

EDITED BY
Hui Zhao,
University of Texas MD Anderson Cancer Center, United States

REVIEWED BY
Bin Wang,
Sichuan University, China
Walter J. Storkus,
University of Pittsburgh, United States

*CORRESPONDENCE
Andreas Weigert
weigert@biochem.uni-frankfurt.de
Kristina Koop
Kristina.Koop@uk-erlangen.de

RECEIVED 31 August 2023
ACCEPTED 20 November 2023
PUBLISHED 04 December 2023

CITATION
You X, Koop K and Weigert A (2023) Heterogeneity of tertiary lymphoid structures in cancer.
Front. Immunol. 14:1286850.
doi: 10.3389/fimmu.2023.1286850

Heterogeneity of tertiary lymphoid structures in cancer

Xin You[1], Kristina Koop[2*] and Andreas Weigert[1,3,4,5*]

[1]Goethe-University Frankfurt, Faculty of Medicine, Institute of Biochemistry I, Frankfurt, Germany, [2]First Department of Medicine, Universitätsklinikum Erlangen, Friedrich-Alexander-Universität Erlangen-Nürnberg, Erlangen, Germany, [3]Frankfurt Cancer Institute, Goethe-University Frankfurt, Frankfurt, Germany, [4]German Cancer Consortium (DKTK), Partner Site Frankfurt, Frankfurt, Germany, [5]Cardiopulmonary Institute (CPI), Frankfurt, Germany

The success of immunotherapy approaches, such as immune checkpoint blockade and cellular immunotherapy with genetically modified lymphocytes, has firmly embedded the immune system in the roadmap for combating cancer. Unfortunately, the majority of cancer patients do not yet benefit from these therapeutic approaches, even when the prognostic relevance of the immune response in their tumor entity has been demonstrated. Therefore, there is a justified need to explore new strategies for inducing anti-tumor immunity. The recent connection between the formation of ectopic lymphoid aggregates at tumor sites and patient prognosis, along with an effective anti-tumor response, suggests that manipulating the occurrence of these tertiary lymphoid structures (TLS) may play a critical role in activating the immune system against a growing tumor. However, mechanisms governing TLS formation and a clear understanding of their substantial heterogeneity are still lacking. Here, we briefly summarize the current state of knowledge regarding the mechanisms driving TLS development, outline the impact of TLS heterogeneity on clinical outcomes in cancer patients, and discuss appropriate systems for modeling TLS heterogeneity that may help identify new strategies for inducing protective TLS formation in cancer patients.

KEYWORDS

immunity, cancer, antigens, mouse models, tertiary lymphoid structures

Introduction

Cancer development is an evolutionary, multi-step process that can take several decades in humans. Throughout this period, the transformed cells continually interact with their local microenvironment, including the immune system. It is now firmly established that this interaction comprises several hallmarks of cancer that initially appear contradictory, as tumor-associated immune responses can either result in the rejection or progression of tumors (1, 2). On one hand, chronic inflammation triggered by environmental and lifestyle factors can give tissues enough plasticity to suppress their

default tumor-suppressive nature and induce somatic mutations in local cells (3–5). Moreover, continuous low-grade inflammation may sustain tumor growth. Through this, several processes, including hypoxia, metabolic adaptations, interaction with dying cells or cellular debris, and negative feedback signals that physiologically limit autoimmunity during infection, educate immune cells to actively support tumor growth (4, 6, 7). On the other hand, altered self-cues, including neo-epitopes and stress-related cell surface molecules, can be recognized by the immune system, leading to tumor rejection (8–10). This process is likely the rule rather than the exception in humans, leading to the eradication of early cancerous lesions or keeping them in check. Tumors that survive these interactions often develop a highly immunosuppressive phenotype, enabling them to progress towards clinically relevant stages (8, 9, 11–15).

Evidence of active anti-tumor immunity was long debated but is now unchallenged due to clinical efficacy of immune checkpoint blockade (ICB), at least in some tumor entities (16, 17). Even in tumors where ICB shows low efficacy, bioinformatic analyses have demonstrated the prognostic and predictive relevance of the immune response in cancer patients (18, 19). Here, immune cell populations and activation states that correlate with positive or poor prognosis across different tumor types have been defined (20). Both, the density and anti-tumor activity of cytotoxic lymphocytes such as γδ T cells, CD8+ T cells, T helper 1 (TH1)-polarized CD4+ T cells, memory T cells or NK cells, as well as tumor-associated B cells, and some activated myeloid cell subsets, are associated with a favorable outcome for patients. In contrast, immunosuppressive myeloid cells including macrophages and immature myeloid-derived suppressor cells, as well as lymphocytes such as regulatory T cells (Treg) or TH17-polarized $CD4^+$ T cells, often indicate poor prognosis (21–23). Given this association of immune quality with patient prognosis, mechanisms that shape protective versus tumor-promoting immunity are being intensively investigated. Besides counteracting tumor-promoting immunosuppressive cells, it is crucial to understand the characteristics determining if protective immunity is induced and persists in cancer patients. It is undisputed that cancer is a systemic disease and that the education of the immune system by cancer antigens in the periphery is an important requirement to induce anti-tumor adaptive immune responses both at baseline and during immunotherapy (24, 25). The generation of an efficient adaptive immune response against cancer typically occurs in secondary lymphoid organs (SLO), where antigens are presented to CD4+ T and CD8+ T cells by mature dendritic cells (DCs) (26, 27). However, when applying spatial analysis criteria to the determine prognostic role of immune cells in cancer, the concept emerged that adaptive immunity can, to a significant degree, also develop locally in newly formed TLS (27, 28). Understanding the principles guiding the formation of these structures and understanding their heterogeneity across cancer types may, thus, be instrumental to harness the full power of the immune system in the fight against cancer. This will be particularly important in patients that currently do not benefit from cancer immunotherapy.

What are TLS

TLS are ectopic hematopoietic aggregates that emerge in sites normally lacking lymphoid organs. TLS have certain developmental and structural similarities with SLO such as lymph nodes, the spleen, tonsils, Peyer's patches, and mucosa-associated lymphoid tissues, but they also exhibit important differences (Figure 1). SLO are encapsulated, and therefore physically separated from their neighborhood, while TLS lack a solid capsule and are directly exposed to the inflammatory milieu in which they develop. Additionally, TLS development pathways seem to be more versatile. Unlike SLO, TLS form in response to chronic inflammation though a process called lymphoid neogenesis (29). This occurs in various disease settings including infection, anti-transplant immunity, autoimmunity and cancer, usually in an antigen-dependent manner. Importantly, TLS seem to necessitate sustained inflammation and may disassemble once inflammation resolves (30–32). Antigen-dependent immune responses within TLS, under the conditions described above, can be both protective and detrimental for the host, depending on the quality of the immune response within TLS. However, the latter seems to dominate during auto-immunity and anti-transplant immunity (33). Particularly in cancer, this contrast seems to hinge on the balance between regulatory T cells and effector lymphocytes, although this relationship is not yet fully understood (34–37). TLS exhibit varying cellular compositions, even within a single tissue, reflecting their maturation status, which appears to be disease-relevant, as outlined in more detail below (32, 38). TLS predominantly consist of B cells, T cells, DCs, follicular dendritic cells (FDCs), and sometimes high endothelial venules (HEVs). Their composition can range from loose clusters of lymphocytes and occasional myeloid cells to highly organized structures with distinct T and B cell zones and the formation of germinal centers (GCs), where high-affinity antibodies are generated (39). There is still much left to be understood regarding the processes guiding TLS formation and composition, and how the outcome of these processes is associated with disease activity and therapy response. Various challenges, such as limited human tissue availability, especially during the early stages of TLS formation, and the scarcity of robust and reproducible mouse models of TLS development, complicate investigations into these matters. These issues impede the design of longitudinal studies to precisely monitor the stages of TLS formation in cancer. Furthermore, there is still a lack of standardized markers useful for determining disease-relevant determinants of TLS heterogeneity. Additionally, while their role as disease biomarkers and their prognostic value for therapy response is evident, it is not fully understood if they directly impact on disease activity, particularly in cancer. Despite these limitations, TLS appear to exemplify the connection between auto-inflammation and anti-tumor immunity. Therefore, understanding TLS formation in cancer may not only benefit cancer patients by serving as biomarkers and therapeutic targets but may also be essential in modulating their formation during infection and chronic inflammatory reactions. In the following pages, we will

10.3389/fimmu.2023.1286850

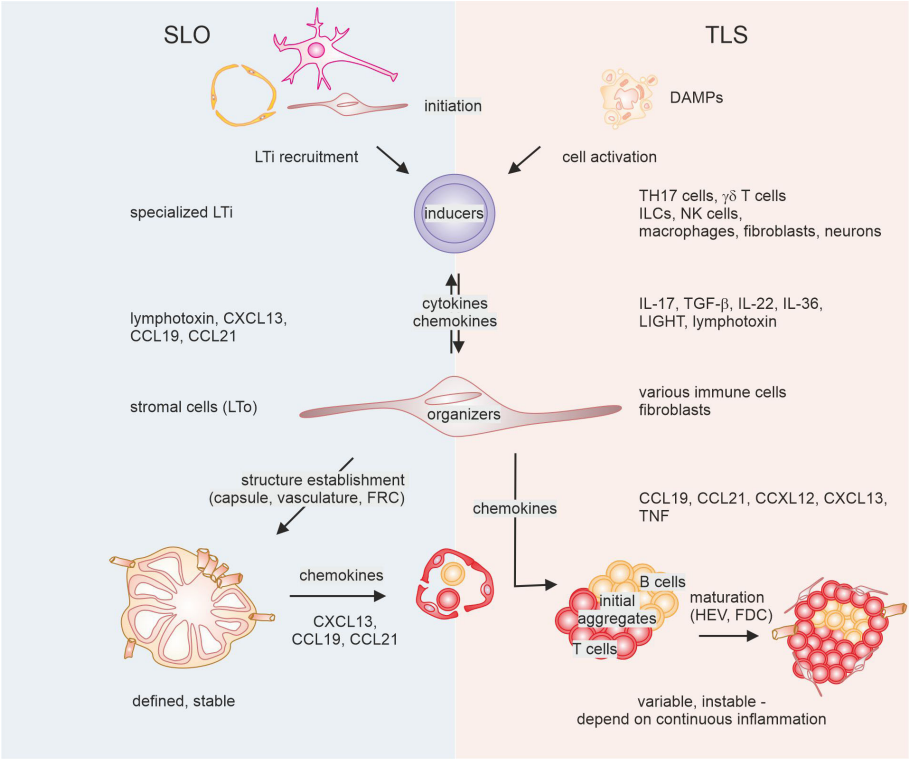

FIGURE 1
Mechanisms of secondary lymphoid organ (SLO) versus tertiary lymphoid structure (TLS) formation. The development of SLO (left) requires interaction between initial lymphoid tissue organizer (LTo) cells and lymphoid tissue inducer (Lti) cells, followed by activation of further LTO cells, and feed-forward recruitment of LTi cells. This ultimately leads to the establishment of a reticular and vascular structure that is populated by lymphocytes. In the case of TLS, diverse cells can fulfill the task of LTi cells, triggered by factors in the tumor microenvironment. These cells interact with diverse other cells that show LTO functionality and recruit lymphocytes. Eventually, such lymphoid aggregates may or may not be supplemented with follicular dendritic cells (FDC) and high endothelial venules (HEV) that are instrumental for the formation of a germinal center reaction. DAMPs, danger-associated molecular patterns; TH17, T helper 17; ILCs, innate lymphocytes; NK cells, natural killer cells; FRC, fibroblastic reticular cells, TGF, transforming growth factor; TNF, tumor necrosis factor.

summarize the current knowledge concerning TLS development, the impact of TLS heterogeneity on cancer development and therapy, and outline and discuss suitable models to study lymphoid neogenesis in cancer.

TLS development

To understand the degree of heterogeneity observed in recent studies regarding TLS formation, a comparison with SLO formation can be instrumental. While there are evident similarities in the sequential events leading to SLO and TLS formation, the diversity at each stage is notably amplified in the case of TLS 31, 32) (Figure 1). This is illustrated by findings showing that TLS can develop in mice and humans, even in the absence of SLO (40–42).

Even though SLO formation is not uniform due to variations in the tissue environment where they develop, common patterns haven been identified by studying genetically modified mice lacking SLO (43–46). Elaborate mechanistic hypotheses explaining SLO development have been extensively reviewed elsewhere (47–49). In brief, SLO formation requires a stepwise interaction between lymphoid tissue organizer (LTo) and lymphoid tissue inducer (LTi) cells. The latter belong to the innate lymphocyte lineage and differentiate from CD3- CD4+/- CD127+ CD45+ innate lymphoid progenitors in the fetal liver, regulated by the nuclear hormone receptor retinoic acid related orphan receptor γt (RORγt) and the transcription inhibitor Id2 (45, 50). During embryogenesis, LTi cells are initially recruited to lymph node Anlagen by CCL21-expressing lymphatic endothelial cells and/or mesenchymal cells that produce CXCL13 under the influence of retinoic acid, which can itself be produced by nerve cells (46, 51). Juxtacrine signaling between lymphotoxin expressed on LTi cells and the LT-β receptor expressed on LTo cells further induces chemokine production and adhesion molecule expression by LTo cells, leading to the recruitment of more LTi cells. This initiates a positive feedback loop, resulting in the remodeling of the lymphatic vasculature (52) and the stromal compartment, along with the formation of a capsule. Only after these structures are formed, lymphocytes are abundantly recruited through newly formed high endothelial venules (HEV), and a stable cellular architecture is established (31, 51).

The initial stages of TLS formation parallel SLO development in the sense that interaction between inducer and organizing cells, which then recruit lymphocytes, appears critical. However, both

inducer as well as organizing cells are not as strictly defined as during SLO generation. In TLS, the role of organizing cells is often assumed by activated local fibroblasts producing chemokines such as CCL19, CCL21, CXCL12, and CXCL13, along with adhesion molecules that recruit B cells and T cells to form initial loose aggregates (31, 32, 53, 54). Moreover, other cells, including macrophages, DCs, and CD8+ T cells, have been shown to produce CXCL13 for recruitment of lymphocytes as well (55–57). Additionally, CCL19+ DCs have been correlated with the presence of TLS and other lymphoid aggregates in breast cancer (58). The activation of these diverse LTo-like cells in TLS can occur *via* various sources and mediators other than specialized innate lymphocyte LTi cells. Several mediators derived from such cells have been identified, although what triggers the activation of LTi-like cells initially remains largely unknown. Factors in the tumor micromilieu, such as DAMPs and mediators from dying cells, likely play a role. Various cytokines such as IL-13, IL-17, IL-22, and type 1 interferons from cells substituting for LTi can activate stromal cells to support TLS formation (53, 59–62). In colorectal tumor models, IL-36 production by macrophages and endothelial cells has been shown to be involved in TLS formation (63, 64). IL-36 activates fibroblasts during intestinal inflammation (65). Whether IL-36 acts *via* fibroblasts to promote TLS development is yet to be determined. Conversely, fibroblasts were observed to induce CXCL13 in T cells through TGF-β production (66, 67).

Finally, similar to SLO formation, activation of the LT-β receptor on stromal cells by both, lymphotoxin and and alternative ligand, LIGHT, promote TLS development (61, 68–73). However, the early events during lymphoid neogenesis can occur independently of LT-β receptor signaling (53, 61, 74). Similar to SLO, signals from nerve cells may play a role in activating stromal cells (74). LT-β receptor signaling seems particularly necessary for later stages of TLS maturation. For instance, a combination of antiangiogenic and immune-modulating therapies provoked the generation of HEV *via* lymphotoxin/LT-β receptor interaction (75). The formation of HEV is viewed as a sign of TLS maturation (31). However, the maintenance of HEV can occur independently of LT-β receptor, requiring the presence of T and NK cells and/or cytokines such as IL-36 (63, 75, 76). Also the generation of FDCs, involved in GC reactions for optimized antibody production (77), was found to depend on LT-β receptor signaling (78).

These findings indicate that key principles and cellular interactions are similar between TLS and SLO formation. The relative heterogeneity of involved cells and mechanisms for TLS formation in cancer may still be underestimated, given the diversity of immune environments even within a single tumor. Although TLS were shown to form 3D intercommunicating networks in colorectal tumors, individual networks within a single tumor exhibited different cellular compositions (38). Given the multitude of signals that are able to induce TLS formation, the question remains why TLS are not always formed during carcinogenesis. One explanation would be the presence of TLS-restricting signals in cancer, as is the case under homeostatic conditions. Identifying such signals in the future may open new avenues for TLS induction. The potential predictive and therapeutic value of such strategies is summarized in the following chapters.

TLS in cancer

The majority of current literature suggests that a high density of TLS is associated with favorable outcomes in solid tumors. However, some investigations have identified TLS density as a marker of disease progression with adverse prognostic implications. There is a lack of systemic studies to define the heterogeneity of TLS, further exacerbated by the absence of uniform scoring criteria (79), hampering the evaluation of TLS in cancer. To perform a rigorous assessment of TLS, certain elements should be carefully considered at the very least: the composition and maturation of TLS, the size of TLS, the density of TLS, and the location of TLS.

The cellular heterogeneity of TLS

Typically, TLS are believed to promote anti-tumor immunity by recruiting immune cells and activating adaptive immunity. As a result, TLS are highly correlated with improved survival outcomes in many cancers, such as breast cancer (80–82), hepatocellular cancer (HCC) (83), colorectal cancer (CRC) (84, 85), melanoma (86), gastric cancer (87, 88), head and neck squamous cell cancer (HNSCC) (89, 90), lung cancer (79, 91) and sarcoma (92). However, it has also been reported that TLS show little correlation with overall survival or are even correlated with high pathologic grade and poor outcomes in malignant diseases, such as breast cancer (80) and HCC (93), posing an obvious contradiction to the previously mentioned studies in these entities. Recent studies indicated that the discrepancy was attributed to the heterogeneity and spatial distribution of TLS in these tumors. As mentioned earlier, unlike SLO, in most tissues, TLS are characterized by CD20+ B cells (B-cell zone) surrounded by CD3+ T cells (T-cell zone), with no capsular involvement (94, 95). This specific anatomical structure facilitates direct interactions between immune cells and the tumor microenvironment. The composition of immune cells in TLS may vary in different tumors or even within single tumors (38). The complex lymphoid aggregates which make up TLS are composed of various immune cells and stromal cells. The immune cells include B cells, T cells, FDCs, and myeloid cells such as other DC subsets and macrophages. The stromal cells, such as follicular reticular cells, fibroblasts and vascular cells (e.g. forming HEVs), are believed to maintain the integrity of the non-capsulated structure and mediate the recruitment of immune cells. We will primarily focus our discussion on the role of B cells, T cells and HEVs from TLS in solid tumors.

B cells and TLS maturation

Extensive clinical and experimental evidence suggests that B cells play a crucial role in the cancer microenvironment, indicating a positive correlation with patient outcomes in various tumors (96–99). It is speculated that B cells in TLS also play a beneficial role by mediating antigen presentation, facilitating T cell activation and development, and producing tumor-specific antibodies in GC

reactions, while contributing to GC formation themselves. GC formation appears as a potent criterion for predicting if TLS are prognostically relevant, serving as a marker for TLS maturation. The maturation of TLS is believed to be essential for activating immunity in cancer and indicating immune therapy efficiency in solid tumors (100). The maturation of TLS has been categorized into three phases: early TLS (eTLS, lymphocyte aggregates), primary follicle-like TLS (pTLS, immature TLS without GCs), secondary follicle-like TLS (sTLS, well-developed lymphoid structures with GCs) (101, 102). An immunostaining panel, including CD20, CD21 and CD23, has been devised to identify the status of TLS in metastatic melanoma. Mature TLS were defined as the presence of CD20+, CD21+ and CD23+ lymphoid aggregates (101). Recent mass cytometry studies confirmed this classification: early lymphoid aggregates lacking organization or GC function were CD20+CD21-CD23-, non-GC TLS were CD20+CD21+CD23- (organized but lacked GC functionality), and GC-containing TLS showed GC organization and functionality associated with the expression of all three markers (CD20+CD21+CD23+) (103). CD23 was even suggested as a useful single marker for mature TLS, at least in breast cancer (104). Interestingly, in a lung cancer cohort, lymph node (LN) metastasis was associated with reduced B cell infiltration and fewer GC formations in TLS. GC+ TLS, rather than non-GC TLS, predicted better outcomes in lung cancer (105). So far, the maturation status of TLS, particularly GC formation (38), has been investigated in various solid tumors, such as esophageal cancer (102), CRC (106), lung cancer (107) and melanoma (101, 108), with the presence of GC+ TLS predominantly associated with a favorable outcome in cancer patients. The relevance of GC formation indicates a strong contribution of B cells to the beneficial impact of TLS in cancer. Although growing evidence suggests an important role of B cells in anti-tumor immunity and immunotherapy (109–111), the role of B cells in TLS towards clinical relevance is still understudied. Helmink and colleagues found that in an immune checkpoint blockade (ICB) trial in melanoma patients, B cells and TLS were more abundant in responders than non-responders. Similar B cell enrichment together with TLS abundancy pattern were validated in a renal cell carcinoma (RCC) ICB trial (109). In a lung adenocarcinoma cohort, a TLS-linked B-cell signature predicted beneficial outcomes in patients treated with PD-1 or PD-L1 inhibitors (112). In summary, mature TLS correlated with B cell presence appears to be involved in anti-tumor immunity and may confer beneficial immunotherapy response and favorable prognosis, although causality remains to be determined. Further studies investigating B cell heterogeneity in TLS may yield even better markers compared to the three-gene (CD20, CD21, CD23) signature. Hereby, establishment of a memory B cell response is likely required to confer long-lasting protection (105).

Divergent role of T cells in TLS

In addition to B cells, the presence of TLS is highly associated with tumor-infiltrating T cells (113). These cells have been extensively studied in the context of basic tumor biology and treatment response, especially in cancers such as CRC (114, 115), breast cancer (116, 117), and lung cancer (118–120). It is well documented that intraepithelial CD8+ T cells, in particular, are associated with a favorable prognosis in solid tumors, including ovarian cancer (121), breast cancer (122), and CRC (123). Additionally, tumor-infiltrating T cells in the stroma also correlate with improved survival in cancer patients. A standardized methodology for assessing stromal tumor-infiltrating T cells in breast cancer was first proposed in 2014 by the International TILs Working Group (124). The model was subsequently modified to evaluate tumor-infiltrating T cells in other cancers as well (125, 126). These studies demonstrated that the presence of tumor-infiltrating T cells remained a powerful predictive factor for most malignancies. Chaurio and colleagues identified that TLS formation was dependent on the CXCL13 pathway in CD4+ T cells, with blocking CXCL13 hindering TLS assembly and subsequently promoting tumor growth (127). Additionally, CD8+ T cells were found to be an important source of CXCL13, mediating immune cell recruitment into TLS and enhancing the sensitivity to immunotherapy in lung cancer (56). Similarly, in another six cohorts of human cancer, a high density of CD8+ tumor-infiltrating T cells was associated with increased B cell recruitment and TLS formation (128). These studies emphasized that T cells play a crucial role for TLS formation and anti-tumor immunity, two phenomena which may, but do not necessarily have to be functionally connected. However, in a cohort of advanced CRC (129), a high ratio of tumor-infiltrating T cells in TLS was associated with tumor recurrence, suggesting a potential deleterious role of tumor-infiltrating T cells in tumor progression. Interestingly, in advanced lung adenocarcinoma, Tregs in TLS were found to suppress anti-tumor immune responses, despite TLS promoting T cells trafficking and activation of the tumor microenvironment (34). In non-small cell lung cancer patients, stromal Tregs suppressed the proliferation of other CD4+ T cells, and a high density of stromal Tregs and Treg cells in TLS correlated with poor outcomes (36). In a prospective study on sarcoma, high Treg numbers in TLS predicted poor responses to ICB treatment, and patients with Treg-enriched TLS had worse survival outcomes (130). These results suggest that not only the functional polarization of tumor-infiltrating T cells *per se* but also within TLS is an important criterion in tumor immunogenicity during tumor progression. Comprehensive quantification of tumor-infiltrating T cell subsets in TLS should be considered to evaluate their prognostic value in different cancer types. Additionally, the phenotypes and functional properties of suppressive Tregs in TLS and their potential association with TLS maturation require further investigation. Interestingly, in tumors of pancreatic ductal adenocarcinoma (PDAC) patients that had received neoadjuvant chemotherapy, a lower proportion of B cells and a higher proportion of regulatory T cells within intratumoral TLS were observed. These TLS were smaller with a reduced maturation level and immune cell activation, leading to a lack of prognostic value of TLS presence in this cohort. (131). Importantly, not only Tregs but also T cell exhaustion phenotypes may be linked to TLS maturation. In breast cancer, while tumors with enhanced exhausted-like T cells contained higher levels of CXCL13-expressing T cells, their presence correlated with more immature rather than mature TLS (132).

Role of HEV in TLS formation

HEVs play an active role in the formation of TLS, boosting anti-tumor immunity by facilitating immune cell trafficking from the peripheral blood to the tumor microenvironment (133–136). A recent study demonstrated that around 40% of lymphocytes entered tumor sites through HEVs during ICB treatment, highlighting HEVs as the primary route for lymphocyte entry into tumor lesions (137). Furthermore, HEVs have been identified as a positive factor for immunotherapy and have shown correlation with improved survival outcomes for melanoma patients. Another study in melanoma and NSCLC indicated that a high HEV score was among patients responding better to ICB, supporting the significance of HEV as an important prognostic factor for immunotherapy (75). However, HEVs also promote tumor metastasis by providing exit points for disseminating tumor cells in murine models and human cancers (138–141). LN metastasis is among the strongest prognostic indicators for clinical outcome of malignant tumors. Regional LN irradiation improves the survival outcome for both early-stage and advanced tumors (142, 143). A recent study indicated that HEV-associated genes were not only linked to high aggregates of T cells and B cells in TLS but also correlated with longer survival in breast cancer (144). Zhan and colleagues performed immunohistochemistry on 203 CRC samples, categorizing them into high and low HEV/TLS groups based on the average area of HEV/TLS (145). A high proportion of HEVs in TLS was associated with a favorable prognosis of CRC suggesting enhanced anti-tumor immunity in the high HEV/TLS groups. HEVs remain an important and complex component in TLS, and further research is necessary to understand the mechanisms of immune cell trafficking and tumor cell dissemination through HEVs. Moreover, studies addressing the molecular mechanisms of HEV generation in TLS are required. In conclusion, markers for the cellular composition of TLS that are linked to TLS maturation and offer insights into their prognostic and therapeutic potential are emerging. However, to utilize to full potential of these markers, further issues need addressing, including standardized protocols for TLS quantification.

Quantification of TLS

Numerous studies have attempted to investigate the size and number of TLS that predict outcomes in solid tumors. However, most studies face limitations due to inconsistent definitions of TLS, distinct quantification methods, retrospective approaches, and single-center experiences. Consequently, the development of an integrative methodology and standardized scoring system to identify the size and density of TLS remains a subject of debate. Pathological evaluations, including Hematoxylin and Eosin (H&E) staining (102, 146–151), fluorescence immunohistochemistry (f-IHC) (53, 152) and multiplex IHC (101, 109), have been shown to be the most straightforward and reliable methods to quantify TLS in tumors. Of note, the majority of studies involved both quantitative and qualitative analyses (153–156). Rakaee and colleagues established three models to quantify TLS in NSCLC. The semi-quantitative method categorized the TLS into four groups based on the number of TLS in the tumor. The quantitative method counted the absolute number of TLS in the tumor and adjacent tissues. The final model compared the GC+ TLS group with the GC- TLS group (79). In a human melanoma study, the counts and area of TLS were normalized to tissue area for quantifying the density of TLS in tumor sections (157). In a cohort of 1924 gastrointestinal cancer patients, a machine-learning model was developed based on histopathology images. The overall TLS score was defined as the sum of a weighted linear eTLS area, pTLS area and sTLS area normalized by tumor area (155). Considering the relative value of maturation of TLS, the final weights of TLS were optimized by Cox regression analysis in the TCGA stomach adenocarcinoma cohort. Patients with high TLS scores exhibited significantly improved overall and disease-free survival compared to those with low TLS scores.

Recently, large scale gene expression analyses, such as RNA-sequencing and spatial transcriptomics, have been implemented to study the landscape of TLS in cancer. TLS-signature genes, including CD79B, CD1D, CCR6, LAT, SKAP1, CETP, EIF1AY, RBP5, and PTGDS, were identified through significance analysis of microarrays, underlining the importance of TLS in melanoma metastasis and immunotherapy (158). High expression of these nine-gene TLS signatures correlated with better overall survival and positive responses to ICB in melanoma. More importantly, the nine-gene TLS gene signature has been recently validated in high-grade serous ovarian cancer, demonstrating better disease-free survival for patients with high TLS scores (159). In CRC and metastatic CRC, 12 chemokines including CCL2, CCL3, CCL4, CCL5, CCL8, CCL18, CCL19, CCL21, CXCL9, CXCL10, CXCL11, and CXCL13, were closely associated with TLS formation. The geometric mean of the above 12 genes was calculated to evaluate TLS in tumor (156, 160). Single cell RNA-sequencing combined with bulk RNA-sequencing of HNSCC revealed CXCR3, CCR7, CCR6, CXCR5, and CCR1 as TLS-associated chemokine receptors, largely dentifying the receptor counterparts to the identified chemokine signature (161). Similar TLS gene signatures have been defined for other solid tumors to predict survival and responses to immunotherapy (89, 162–164). Presently, there is no standardized methodology for quantifying TLS in cancer. However, it is believed that a combination of histology and gene expression analysis would provide a better understanding of TLS composition and function in cancer. Emerging markers, such as the presence of Tregs or HEVs, might also be considered for such analyses. Yet, distinguishing “high” and “low” or defining a specific “cut-off” point in the data is often not objective and challenging to apply uniformly across different sites.

Location of TLS

Besides precise quantification, the spatial distribution of TLS within tumors might add another layer of complexity. Hereby, TLS can be distributed across tumor nests (T-TLS), the peritumoral area (P-TLS) and tumor stroma (S-TLS) (95). The prognostic value of TLS density in solid tumors has been shown, though inconsistently.

Discordance in prognosis may be partially due to different spatial distributions of TLS. However, results across multiple studies were mixed: some studies demonstrated that P-TLS rather than T-TLS were positively correlated with favorable prognosis, while others showed contradictory results. Moreover, the exact delimitation of the three regions remains controversial. An evaluation of the prognostic value of TLS in patients with non-metastatic CRC revealed that high P-TLS contributed to favorable outcomes for patients with CRC, while T-TLS did not significantly correlate with clinical outcomes. The TLS and tumor stroma percentage, representing S-TLS, showed a negative correlation with overall survival for patients (85). Conversely, in CRC liver metastasis, P-TLS were negatively correlated with relapse-free and overall survival, whereas T-TLS were significantly correlated with better outcomes (156). Similarly, Ding et al. found in a cohort of 962 intrahepatic cholangiocarcinomas (CCA) patients from three cancer centers across China that T-TLS were associated with a favorable prognosis, whereas P-TLS indicated a worse outcome (165). Additionally, a high T-TLS score correlated with better prognosis and response to immunotherapy in CCA patients (166).For breast cancer patients, the presence of P-TLS was linked to worse clinical outcomes (167). It has been reported that T-TLS indicated a lower risk of early recurrence in HCC (83), and an enhanced response of ICB in resistant tumors (168). In summary, the majority of literature supports the notion that T-TLS are associated with positive prognostic effect in cancer. Notably, variable definitions and cut-offs may cause confusion when discussing P-TLS and S-TLS. Studies have tended to conflate P-TLS and S-TLS, resulting in limited reports on S-TLS in tumor-immune contexture. However, definitions of P-TLS and S-TLS in cancers remain underexplored. Researchers have adopted a similar definition of P-TLS in CRC, defining the area up to 7 mm from the infiltrative edge (106, 156, 169). Sofopoulos and colleagues defined P-TLS in the area 5 mm away from the tumor invasive margin (167). In the CCA cohort, the peri-tumor region was defined as a normal tissue area 5 mm away from the tumor edge (165). In HCC, the peritumoral area was also considered as the region 5 mm distant from the invasive tumor border (170). These studies again suggest that P-TLS do not always play a protective role in solid tumors, which can be attributed to factors such as tumor types, heterogeneity, status, and staging.

In summary, T-TLS provide an important niche for supporting anti-tumor immunity and are associated with improved clinical outcomes in many tumors. However, the value of P-TLS and S-TLS in determining prognosis remains a subject of debate. Standardized scoring systems of T-TLS, P-TLS and S-TLS are critical to evaluate their functions across different cancer types and cancer stages. Moreover, the reasons for the association of spatial distribution of TLS with clinical outcome in cancer patients need to be studied. The influence of the highly suppressive stromal microenvironment may be at work. Recent multiplexed 3D reconstructed imaging in CRC has revealed that TLS can form interconnected, graded networks, suggesting communication in such larger networks. Additionally, within a single tumor, these networks show diverse cellular compositions (38). Thus, not only the 2D localization but also the interconnectedness of TLS might become an important criterion in the future. Whole-body imaging techniques applied to analysis of TLS in mouse models might aid in studying this aspect (171). Finally, TLS have been shown not only to form at primary but also secondary metastatic sites, which likely significantly affects patient prognosis.

TLS in metastatic cancers

Metastases continue to be the primary cause of cancer mortality, accounting for nearly 90% of cancer-related deaths (172). Studies have shown the formation of TLS at metastatic sites such as the liver and lungs (173). While the majority of literature supports the theory that TLS in metastatic sites contribute to anti-tumor immunity (27), it remains unclear whether there is TLS heterogeneity between primary tumors and metastatic sites. Reliable data concerning the role of TLS at metastatic sites are scarce. In a cohort of CRC and RCC metastases, metastasis-associated TLS exhibited a high degree of similarity with TLS in primary tumors, including their density and cellular composition (174). This suggests either a dominant role of the primary tumor cells in TLS formation, or alternatively suggests a prominent role of systemic tumor-associated immunity in TLS development at different sites. The former assumption is supported by the fact that CRC lung metastases exhibited more abundant TLS in lung stroma compared to RCC lung metastases, which was in line with increased TLS formation in primary CRC lesions. Furthermore, both CRC and CRC lung metastases displayed a significant increase of CD3+, CD8+ T cells, and DCs in TLS. In CRC liver metastases, TLS at the tumor-liver interface, characterized by CD45+CD20+ B cell aggregates, indicated a reduced risk of tumor relapse and a favorable overall survival (175). Similarly, Ahmed and colleagues found that TLS at invasive margins, rather than tumor lesions, were correlated with better survival in CRC liver metastases (176). In a cohort of patients with omental metastases from high-grade serous ovarian cancer, B cells in lymphoid aggregates showed enhanced anti-tumor immunity, particularly boosted by chemotherapy (177). In cutaneous melanoma metastases, patients with positive TLS exhibited improved overall survival. Interestingly, the maturation of TLS was not related to survival outcome, while CD20+CD21+ B cells in TLS correlated with a worse prognosis in metastatic melanoma (101). In a cohort of patients with breast cancer metastases consisting of 355 metastatic samples from the lung, liver, brain, and ovary, no TLS were found in brain and ovarian metastases. The presence of TLS at metastatic sites was an independent factor for a favorable prognosis (178). However, two studies on lung metastases from CRC indicated that the presence of TLS at metastatic sites had no prognostic value (84, 179). These studies suggest that the complex immune contexture of TLS in metastatic cancers is determined by both primary tumor and metastatic lesions. While the majority of data indicate that TLS play a beneficial role in metastatic cancers, some uncertainties and controversies persist. Taken together, TLS formation appears to be relevant in the tumor microenvironment of metastatic cancers.

Further research is required to enhance our understanding of the mechanisms behind TLS formation and their action in metastatic cancers, and the interrelationship between TLS at primary and secondary sites.

Clinical trials related to TLS

A range of clinical trials have underscored the viability of immunotherapy in enhancing patient outcomes, encompassing ICB, cancer vaccines, adoptive cellular therapy, and small molecule-based immunomodulators (180, 181). It is well documented and validated that the combination of immunotherapy and chemotherapy can lead to an improved pathological complete response and enhanced surgical feasibility post neoadjuvant treatment (182–185). Furthermore, adjuvant chemotherapy and immunotherapy substantially improved postoperative DFS and have been considered as a standard of care for select patients (186–188). The induction of TLS during chemoimmunotherapy and its positive effect on patients has raised particular interest (189, 190). However, the significance of TLS in cancer treatment has long been overlooked because studies typically focused on a single cell population, such as lymphocytes, macrophages, and fibroblasts, rather than lymphoid aggregates. Although much remains unknown about TLS in cancer treatment, recent clinical trials suggest TLS as a crucial participant in the tumor microenvironment and demonstrate a close correlation between the presence of TLS and sustained clinical benefits (Table 1) (198, 201, 202).

Lutz and colleagues conducted a phase 2 study of neoadjuvant and adjuvant vaccines with irradiated, granulocyte-macrophage colony-stimulating factor–secreting, allogeneic PDAC vaccine (GVAX) +/- low dose cyclophosphamide. They found that TLS formed in 85% of participants two weeks after vaccination. Inhibition of the Treg pathway and activation of the IL-17 pathway within the TLS were associated with improved survival for PDAC patiens (191). Notably, PDAC with intratumoral TLS formation exhibited an enhanced PD-1/PD-L1 pathway, suggesting that vaccine-treated PDAC was converted into an immunogenic tumor, potentially benefitting from anti-PD-1/PD-L1 ICB. Similarly, in a phase 1, open-labeled clinical trial on high-grade cervical intraepithelial neoplasias, patients received a DNA vaccine targeting HPV16 E7, followed by a boost injection of vaccinia targeting HPV16 and HPV18 E6 and E7. Abundance of organized TLS was noticed in the proximity of vaccinated intraepithelial lesions rather than unvaccinated lesions (192). More importantly, histological alterations were closely associated with a gene signature of immune activation, indicating the induction of a robust tissue-localized immune response. TLS formation was also observed in neoadjuvant chemoimmunotherapy in patients with operable malignancies. A pilot study of metastatic RCC showed that tremelimumab with and without cryoablation increased TLS formation in patients with clear cell histology compared with baseline (196). In another study using nivolumab in patients with metastatic RCC, a significant enrichment of TLS was observed in responders rather than non-responders, showing a trend for improved outcomes (199). Similarly, Ho et al. reported the results of a single-arm phase 1b trial of neoadjuvant cabozantinib and nivolumab in patients with locally advanced HCC. They confirmed that enriched TLS formation was associated with improved responses to neoadjuvant treatments (197). Cascone and colleagues designed a neoadjuvant clinical trial comparing nivolumab + chemotherapy given as a dual therapy or in combination with ipilimumab as a means to estimate the major pathological response in NSCLC patients. Among 22 patients in the dual-therapy group, 7 patients exhibited a major pathologic response (32.1%), whereas 11 patients had a major pathologic response in the triple-therapy group consisting of 22 patients (50%). Increased TLS formation was observed in the triple-therapy group, suggesting immune activity and a close correlation with enhanced pathologic response (200). Since the major pathologic response was defined as more than 90% tumor regression in the context of chemotherapy, Cottrell et al. proposed to establish novel immune-related pathologic response criteria that highlighted the quantification of TLS in neoadjuvant chemoimmunotherapy (193). Importantly, the new criteria were shown to be reproducible and consistent among pathologists. In a single-arm trial of advanced urothelial cancer, 24 participants were treated with 2 doses of ipilimumab and 2 doses of nivolumab, and were evaluated for surgical resection within 12 weeks after initiation of neoadjuvant treatment. A pathological complete response occurred in 46% patients, and TLS were observed upon immunotherapy in responding patients (190). In-depth analysis of the immune contexture of resected samples was conducted to assess the significance of TLS for predicting responses to immunotherapy in urothelial cancer. Compared with deeper TLS, superficial submucosal tissue was characterized by enhanced T-helper cell infiltrations, abundant early TLS, and rare occurence of mature TLS. Interestingly, an increased enrichment of Foxp3+ T-cell-low TLS cluster was observed in unresponsive tumors, whereas a high abundance of macrophage-low TLS cluster was identified in treated tumors (194). The heterogenic TLS clusters were considered as promising biomarkers for predicting responses to immunotherapy in urothelial cancer. Furthermore, the composition of TLS was altered after neoadjuvant immunotherapy in patients with high-risk prostate cancer. Both B and T-cell densities in TLS were significantly reduced in patients receiving one dose of rituximab before prostatectomy (195). The studies mentioned above determined TLS formation as one among various parameters. Notably, a multi-cohort phase 2 study of pembrolizumab combined with chemotherapy in patients with sarcoma specifically assessed the prognostic significance of TLS and showed substantially improved outcomes in a cohort of sarcoma patients positive for TLS. The 6-month non-progression rate and objective response rate were 40% and 30%, respectively, in the cohort of TLS-positive patients, which were approximately 10-fold higher than in all-comer cohorts (92). Undoubtedly, the presence of TLS may provide a new perspective to assess the response to chemoimmunotherapy and the prognosis of patients. However, determining TLS formation in cancer patients remains a long way from being adopted in clinical practice, despite the evidence that it is

intrinsic to immune responses to neoadjuvant and adjuvant treatment in clinical trials. A limited number of clinical trials specifically investigating the role of TLS in cancer are currently ongoing or under development (Table 1). The data emerging from these studies are expected to facilitate the clinical translation of TLS towards patient management. Future trials should consider the complex aspects of TLS biology outlined above, including TLS composition, size, maturation, localization, interconnectedness and appearance at different sites. However, determining which of these above-mentioned parameters are the most promising will need to be established in pre-cinical studies, for which reliable mouse models for studying TLS formation are needed. The currently available models and their suitability are discussed in the following paragraphs.

Modelling TLS formation

The arsenal of experimental models for studying cancer has significantly expanded in recent years, thanks to improved mathematical and bioinformatics modeling tools and human tissue cultures, such as tumor slice cultures or patient-derived organoids (203–205). However, these techniques currently have clear limitations when attempting to model the spatiotemporal and cellular complexity of TLS formation. For instance, modelling TLS in organoid cultures would not only require the population of these cultures with patient-derived PBMCs to avoid alloreactions, but also a pre-population with fibroblasts and potentially endothelial cells. While these steps have been realized individually, combining

TABLE 1 Clinical trials related to TLS.

Study duration	Patient No.	Study type	Phase	Trial ID	Treatment	Cancer type	Reference
Concluded trials							
2008.07-2019.02	87	Interventional	phase 2	NCT00727441	GVAX vaccine	PDAC	(191)
2008.11-2023.08	75	Interventional	phase 1	NCT00788164	HPV vaccine	cervical intraepithelial neoplasia	(192)
2014.09-	45	Interventional	phase 2	NCT02259621	neoadjuvant anti-PD-1	NSCLC	(193)
2018.01-2021.09	54	Interventional	phase 1	NCT03387761	neoadjuvant anti-PD-1 and anti-CTLA-4	urothelial cancer	(190, 194)
2013.07-2019.04	18	Interventional	phase 1	NCT01804712	neoadjuvant anti-CD20	prostate cancer	(195)
2016.03-2022.06	29	Interventional	phase 1	NCT02626130	anti-CTLA-4 and cryoablation	Metastatic RCC	(196)
2018.05-2021.10	15	Interventional	phase 1	NCT03299946	neoadjuvant anti-PD-1 and tyrosine kinase inhibitor	HCC	(197)
2015.06-2021.08	227	Interventional	phase 2	NCT02406781	anti-PD-1 and chemotherapy	sarcoma	(92)
2016.11-2022.03	45	Interventional	phase 2	NCT02901899	anti-PD-1 and chemotherapy	ovarian cancer	(198)
2016.01-2021.06	730	Interventional	phase 2	NCT03013335	anti-PD-1	Metastatic RCC	(199)
2017.06-	101	Interventional	phase 2	NCT03158129	neoadjuvant anti-PD-1, anti-CTLA-4 and chemotherapy	NSCLC	(200)
2016.05-2022.09	24	Interventional	phase 2	NCT02592551	neoadjuvant anti-PD-L1 and anti-CTLA-4	malignant pleural mesothelioma	(201)
2015.11-2019.06	87	Interventional	phase 1/2	NCT02541604	anti-PD-L1	multiple tumors from pediatric patients	(202)
Ongoing trials							
2023.09-	102	Interventional	phase 2	NCT05888857	anti-PD-1 and anti-CTLA-4	solid tumors	N.A.
2024.01-	120	Interventional	phase 2	NCT06084689	MDM2 inhibitor and anti-PD1	solid tumors	N.A.
2022.03-	80	Interventional	phase 2	NCT04874311	anti-PD-L1 and chemotherapy	sarcoma	N.A.
2022.12-	66	Interventional	phase 2	NCT04968106	anti-PD-1 and chemotherapy	sarcoma	N.A.
2020.02-	67	Interventional	phase 2	NCT04095208	anti-PD-1 and anti-LAG-3	sarcoma	N.A.
2021.07-	173	Interventional	phase 2	NCT04705818	anti-PD-L1 and EZH2 inhibitor	solid tumors	N.A.

MDM2, mouse double minute 2 homolog; LAG-3, lymphocyte-activation gene 3; EZH2, enhancer of zeste homolog 2; N.A., not applicable.

them poses major logistical and technical challenges (206). Therefore, we focus our attention on mouse models of TLS formation in the following chapters.

The generation of murine models that mimic the development of solid cancer is complex. If the tumor cells exhibit rapid growth kinetics, the tumor burden will likely reach unacceptable levels before TLS can develop. Conversely, if the mutational burden is low and tumors develop slower, the availability of tumor antigens necessary for activation of the adaptive immune system and the development of TLS is limited (207). Nevertheless, there are autochthonous tumor models with spontaneous development of carcinomas, including mature TLS within the tumor or in close proximity, resembling lung adenocarcinoma (208, 209), PDAC (210), and HCC (93). To mimic the human situation, such genetically engineered mouse models (GEMMs) contain multiple mutations, such as overexpression of oncogenes (e.g. Kras) or deletion of tumor suppressors (e.g. p53), which are also present in the corresponding human cancer. Most importantly, tumor growth in these models can be modified *via* TLS-associated factors. These models are also suitable for developing new immune-based therapy options utilizing the power of TLS, including sensitizing tumors to ICB or CAR-T cell therapy (73). Autochthonous animal models that allow a stringent analysis of organized TLS formation for CRC, breast cancer, and melanoma have not been reported so far.

Besides autochthonous models, orthotopic tumor models have been used to study TLS development. This involves the injection of cancer cells from murine or human origin into recipient mice, either WT or immunodeficient, specifically into the tissue the tumor originated from. A more frequent approach is the heterotopic transplantation of tumor cells into recipient mice, such as the s.c. or i.p. injection of B16 melanoma cells. However, evidence that the localization or transplantation site of a tumor matters emerged from the finding that orthotopic transplantation of murine lung adenocarcinoma cells into C57BL/6 mice resulted in the activation of the adaptive immune system, while s.c failed to induce activated CD8+ T cells (208). Moreover, s.c. transplantation of tumor cells led to the accumulation of immune cells but did not allow the formation of mature TLS (210). GEMM models have already enabled the identification of factors necessary for TLS formation including lymphotoxin and CXCL13 (209, 211). Additionally, genetic modification of tumor cells *in vitro* enables the adaption of (orthotopic) transplantable models to a specific question, for example, the addition of artificial antigens such as OVA to increase immunogenicity and/or TLS formation. Through these means, tailored mouse models specifically for investigating TLS biology may be developed in the future.

TLS in lung adenocarcinoma models

The investigation of lung adenocarcinoma (LUAD) using GEMMs showed the necessity for multiple genetic alterations to resemble the human disease, including TLS formation. Initially, a mouse model with a Lox-Stop-Lox Kras G12D mutation was used in combination with an intranasal or intratracheal application of an adenovirus or lentivirus containing a Cre recombinase for targeted mutation in the lung (K mice) (212). DuPage et al. observed enhanced tumor growth upon an additional deletion of p53 (KP mice) within 2-3 weeks (213, 214). Using the KP mice, Joshi et al. detected low- and high-grade lung adenocarcinomas after 20-24 weeks, but without TLS formation or TLS precursor (34). After depletion of regulatory T cells, the tumor burden was significantly increased, coinciding with TLS detection, emphasizing the significance of intrinsic anti-inflammatory mechanisms. In 2022, Boumelha et al. further developed the KP mice by introducing an overexpression of the APOBEC family of single-stranded deaminases (APOBEC3B) to generate mice with enhanced mutational burden (KPA mice) (208). Increased mutations produce neoantigens, enabling the immune system to recognize the tumor. Consistent with Joshi et al., there was no observed ectopic immune cell accumulation in KP, nor in the KPA mice, at least in proximity to the tumor. To assess whether immune cells altered tumor growth, they created a KPA mouse line on a Rag1-/- background (KPAR mice), but the tumor load remained unchanged and even led to a lethal tumor load in about 14 weeks without activating an anti-tumor response (208). The authors attributed the absent immunogenicity to the subclonal mutations caused by ectopic APOBEC expression. Therefore, they subsequently generated single-cell cloned lines from KPAR tumors and found that upon i.v. injection KPAR tumors developed in the lungs of C57BL/6 mice. Most importantly, the orthotopic tumors induced an anti-tumor response, including CD4+ and CD8+ T cells, as well as NK-cell infiltration. Interestingly, the authors observed the expression of a viral glycoprotein from the murine leukemia retrovirus in the KPAR cells and concluded that endogenous retroviral antigens can trigger effective CD8+ T cell responses. Finally, the tumor growth of KPAR tumors was reduced upon ICB. In a recently published study, the KPAR orthotopic model was used to demonstrate B cell accumulation near the tumor (209). Ng et al. detected mature TLS containing GCs and serum antibodies against KPAR cells expressing endogenous retrovirus envelope glycoproteins. Furthermore, the titer against the virus antigens increased upon ICB with anti-PD-L1 antibodies, shedding light on the dependence of effective anti-tumor B cell responses on viral antigens. The expression of retroviral antigen was also detected in LUAD patients as a prerequisite for response to ICB therapy. In addition, they demonstrated the curative effect of CXCL13 therapy in combination with ICB to enhance anti-tumor immunity in the KPAR orthotopic model. In summary, GEMMs, which contain multiple mutations similar to human LUAD tumors, have been highly useful in investigating the effect of immunotherapy concepts such as ICB in combination with soluble factors that enhance TLS formation. In addition to GEMMs, the i.v. injection of B16 melanoma cells is widely used as a model for melanoma metastasis in the lung, as most, if not all, injected tumor cells accumulate in the lung and induce the formation of lymph node-like structures that include HEVs (215). The B16 melanoma cell line originated from a spontaneous tumor in a C57BL/6J mouse (216). Nevertheless, this transplantation model may not actually be a model for LUAD or lung metastasis, as all B16 tumors should be considered as primary tumors that do not accurately mimic human LUAD (217).

Pancreatic ductal adenocarcinoma TLS models

To model PDAC, either GEMMs or orthotopic transplantation models have been employed. Much like the KP model in the lung, a mouse strain expressing the mutated Kras G12D in pancreatic ductal cells (LSL-KrasG12D/+;Pdx-1-Cre; KC mice) was developed, resulting in a low tumor load after 5 months (218). Subsequently, after the additional depletion of p53 (LSL-KrasG12D/+;LSL-Trp53R172H/+;Pdx-1-Cre; KPC mice), KPC mice developed tumor-associated TLS, including GC B cells (219, 220). Interestingly, Spear et al. did not observe TLS formation in an orthotopic PDAC model where a KPC-derived cell line from liver metastasis was injected into the pancreas (220). This absence was likely due to the highly proliferative nature of this model, resulting in tumor formation within two weeks. Tseng et al. implanted KPC-tumor cells into the pancreas of syngeneic mice without detecting prominent TLS (221). However, transplantation of KPC-tumor cells into Rag-deficient recipients resulted in lower survival compared to immunocompetent mice, suggesting anti-tumor responses by B and T cells primed in SLOs. The KP model, involving spontaneous tumor formation, was combined with DNA vaccination against α-enolase, whose expression is increased in PDAC cells. This vaccination induced the formation of GC B cells and recruitment of T cells into the tumor, thereby fostering TLS formation (222). Additionally, in a model of s.c. transplantation of a human PDAC cell line, coupled with intratumoral injection of CCL21, Turnquist et al. observed increased accumulation of T cells, DCs, and NK cells, forming a pre-TLS structure. This indicated the importance of chemokine guided migration into the tumor, which may show potential for immunotherapy (210). Of note, the overexpression of lymphotoxin in the pancreas during steady-state successfully induced the formation of TLS, suggesting potential for including this construct in KP and KPC models in the future (223). Using an orthotopic transplantation of KPC tumor cells, the i.v. treatment with nanoparticles containing the antifibrotic compound α-mangostin and a plasmid encoding LIGHT resulted in reduced tumor growth. This was accompanied by reduced activated fibroblast numbers, decreased collagen deposition, normalized tumor vasculature, and most importantly, the induction of organized TLS in the tumor (224). These results highlight the intriguing role of extracellular matrix organization in TLS formation. In summary, KP and KPC mice are valuable tools for studying TLS formation, especially concerning DNA vaccines and chemokine therapy. Future studies will reveal if these models can be utilized to study the interplay between TLS and ICB.

Hepatocellular carcinoma models show immunosuppressive features of TLS

The tumorigenesis of HCC was investigated in GEMM by Finkin et al. (93). The authors developed two models of inflammation-driven HCC in mice with an overactive NF-κB signaling pathway, a typical feature of human HCC. IKKβ(EE) Hep mice display a hepatocyte-targeted, constitutively active NF-κB pathway after breeding them with a suitable deleter strain (Albumin-Cre mice). Within 7 months, typical hallmarks of liver inflammation, including an accumulation of macrophages, liver damage, hepatocyte proliferation, and structured TLS with B and T cells as well as HEVs, were detected. After 20 months, all mice developed HCC, indicating that TLS were formed prior to tumorigenesis. Next, the authors generated Alb-IKKβ(EE) mice with constitutively active NF-κB signaling in hepatocytes without the requirement of a Cre recombinase. These mice showed accelerated tumor and TLS growth within 9 months. Interestingly, on a Rag1-/- immunodeficient background, Alb-IKKβ(EE) mice showed a drastically reduced tumor burden, illustrating the pro-tumorigenic effect of the adaptive immune system. In fact, TLS, located in proximity to the tumor but not within the tumor, served as a niche for forming HCC progenitor cells that later egressed and developed into HCC. In summary, the overexpression of the NF-κB signaling pathway in a spontaneous model of HCC mimicked human disease and was suitable for analyzing new concepts of immunotherapy, including interference with TLS formation (225). Future studies are required to develop a relevant model for intratumoral TLS formation that does not show the tumor-supportive features discussed above.

TLS formation in colorectal carcinoma models

To investigate spontaneous tumorigenesis in the intestine, the APCmin model carrying a mutant allele of the APC locus, similar to the mutation in humans, is frequently used, and the accumulation of immune cells in proximity to adenomas and/or tumors is described (our own observations and (226)). In addition, the (repetitive) i.p. injection of the carcinogen azoxymethane (AOM) can be used to induce colon tumorigenesis in mice harboring different alterations in intestinal epithelial cells, such as the deletion of p53 (227). However, a targeted analysis of TLS formation in such models is currently lacking.

The most common model used to investigate inflammation-driven tumor formation that mimics tumorigenesis in patients with inflammatory bowel diseases is the AOM/DSS model, where the animals receive one injection of AOM and three repetitive cycles of dextran sodium sulfate salt (DSS) in the drinking water (228). Our own observations (Figure 2A) clearly show the formation of organized TLS in the AOM/DSS model, but information how TLS formation occurs and whether it can be manipulated, e.g., by ICB in this model, is lacking. Interestingly, a recent study showed that the intestinal microbiota plays an important role during tumorigenesis and can also affect TLS formation in the AOM/DSS model (229). The authors detected increased anti-tumor immunity and reduced tumor growth upon the introduction of *Helicobacter hepaticus (Hhep)* into C57BL/6 animals in the AOM/DSS model. In fact, *Hhep* induced the expansion of T follicular helper cells, leading to the formation of organized TLS in proximity to the tumor. These

results indicate that the microbiota has the power to induce the formation of TLS in an inflammatory environment. Importantly, the formation of TLS appeared to be rather independent of tumorigenesis *per se* but was still useful in inducing an anti-tumor immune reaction.

In addition to the models indicated above, the orthotopic injection or enema of genetically engineered tumor organoids is a novel approach to mimic the mutational cascade in human CRC. These models overcome the limitation of AOM and AOM/DSS tumors, which do not induce metastases (230). Again, TLS formation in orthotopic colon tumors has not been described so far. However, patient-derived organoids (PDO) transplanted into the caecum of humanized mice generated tumors that formed metastases in the liver and peritoneum, but only the growth of the primary tumor and liver metastases were diminished upon ICB treatment (anti-CTLA4, anti-PD-1), a phenomenon also observed in CRC patients (231). The authors detected structured TLS in the primary tumor and the liver metastases but not in the peritoneum. The TLS contained T cells and B cells, showing an IFN-γ signature and CXCL13 expression. Therefore, alterations in tumor growth upon ICB were correlated with the presence of TLS. In summary, although many GEMMs and GEMM-derived organoids are available to model CRC, they are presently underused to investigate TLS during tumorigenesis *in vivo*.

Evidence for early TLS formation in breast cancer models

For investigating the development of breast cancer an autochthonous mouse was developed in 1992 by fusing the mouse mammary tumor virus (MMTV) long terminal repeat promotor with the polyomavirus middle T antigen (PyMT), resulting in tumor formation in mammary glands and lung metastasis (232). While PyMT is not a human oncogene, MMTV-PyMT mice develop similar features, especially compared to end-stage human breast tumors: such as the loss of estrogen receptor and progesterone receptor expression, as well as overexpression of ErbB2 and Cyclin D1 (233). Our own observations (Figure 2B) suggest the formation B and T cell aggregates at the tumor margins but not within tumors. A detailed investigation of structured TLS formation in this model is currently lacking. Interestingly, a combined anti-angiogenic and anti-PD-L1 therapy approach in PyMT mice induced the formation of intratumoral HEVs, which might serve as a prerequisite for TLS formation (234). Furthermore, a more recent detailed analysis of this model with anti-angiogenic and anti-PD-L1 treatment showed the transition from tumor endothelial cells into HEVs based on LT-β receptor signaling by NK and CD8 T cells, thus promoting the expansion of anti-tumor effector T cells (75). Future investigations are essential to confirm the formation of TLS in the PyMT model, as well as in other breast cancer models, such as the inducible expression of viral antigens in mammary epithelial cells (235), aiming to mimic human breast cancer. The PyMT model produces immunologically rather cold tumors that do not respond well to ICB (236, 237), despite frequent mutations in this model (233). Therefore, strategies to overcome immunosuppressive mechanisms in this model are likely necessary to enable the investigation of TLS formation.

TLS formation in models of melanoma

An autochthonous model for melanoma was established in 2009 by inducing the expression of a constitutively active BRAF mutation at position 600 ($BRAF^{V600E/+}$) under the control of the inducible keratinocyte-specific Cre recombinase Tyr::CreERT2 (238). These animals showed highly pigmented lesions, but did not develop malignant melanoma. Therefore, the authors generated a new mouse line by introducing the tumor suppressor Pten with floxed Exon 4 and 5 ($BRAF^{V600E/+}$ PTEN-/- Tyr::CreERT2). Upon repetitive topic application of Tamoxifen, these mice developed melanoma with metastases in lymph nodes and lungs (238). In these melanomas, tumor infiltrating lymphocytes, including CD4+ T cells, CD8+ T cells, Tregs, and DCs, were found, but organized lymphoid structures *in situ* were not investigated (239). Another group observed the early influx of Tregs at the onset of melanoma development, followed by CD8+ T cells (240). Upon the depletion of Tregs, they observed an increased activity and clustering of tumor-infiltrating lymphocytes. This illustrates that Tregs can prevent the development of anti-tumor immunity and the formation of TLS. For the development of differentiated TLS, the formation of PNAd+ HEVs is crucial as they enable the influx of immune cells directly into the TLS. Peske et al. did not detect HEV formation in the $BRAF^{V600E/+}$ PTEN-/- Tyr::CreERT2 mouse model

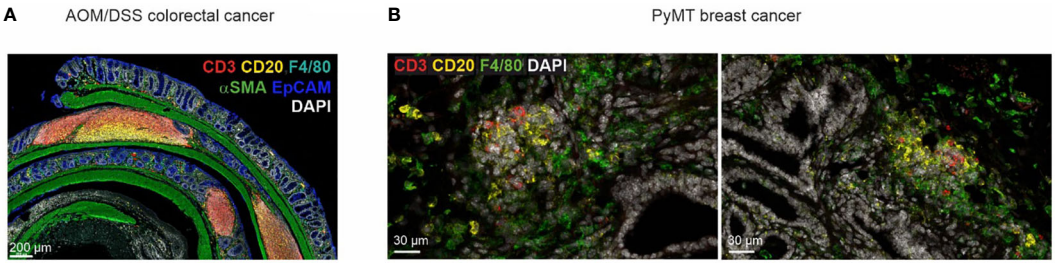

FIGURE 2
TLS heterogeneity in cancer mouse models. **(A)** TLS in different maturation stages in a tumor-bearing mouse in the AOM/DSS model of CRC. **(B)** Early lymphocyte aggregates in the PyMT mouse model of invasive mammary carcinoma.

(76). In summary, this autochthonous melanoma model in its current form is not suitable for a comprehensive analysis of TLS. Integrating a strategy for inducible depletion of Tregs might optimize the model towards this goal.

Using transplantation models to study TLS formation

The transplantation of tumor cells i.p, i.v., or s.c. into immunocompetent as well as in immune-deficient animals has proven to be a useful method for investigating anti-tumor immune mechanisms, including ICB (241), and the formation of TLS. Various cell lines have been used, depending on the specific research question. The most frequently used cancer cell line is the B16 melanoma cell line that was isolated from a spontaneous melanoma in a C57BL/6 mouse (216). B16 cells produce melanin, making them easy to track in the host. Numerous sublines were created expressing artificial antigens or tumor-associated antigens. In general, transplantation of tumor cells offers several advantages, as tumors develop rapidly within two weeks and can be transfected to induce model antigen expression or harbor mutations that are similar to human cancers. The choice of the recipient mouse line allows the investigation of the role of different immune cells. For example, Rag1-/- mice lack B and T cells, whereas μMT mice lack only B cells. Furthermore, the choice of immunocompetent mouse lines harboring a specific knockout, such as deficiency to produce lymphotoxin, can help analyze the role of individual factors during TLS formation (211). It may be surprising that such rapid models are suitable to study TLS formation. However, rapid development of TLS in mice triggered by chronic inflammation that is not related to tumor formation is well established (31, 32). Often, s.c. injection of tumor cells into mice may trigger acute inflammatory reactions rather than mirror the tumor immune co-evolution seen in humans. Therefore, it remains to be determined if TLS emerging under such conditions accurately reflect the situation in human tumors. Along these lines, the method of application appears to be crucial in investigating TLS formation in transplantation models. Two studies reported TLS formation upon B16-OVA melanoma cell transplantation i.p., but not s.c (76, 242). It was further described that fibroblasts in B16-OVA i.p. and s.c. tumors showed differential expression of adhesion molecules. When Icam1+Vcam+ fibroblasts were transplanted together with B16-OVA cells s.c., TLS formed, but not when Icam1+Vcam- fibroblasts were used (54). Most importantly, organized TLS were only detected after ICB, confirming the importance of reducing anti-inflammatory pathways to induce effective anti-tumor immunity (54). The importance of CCL21 for TLS formation was demonstrated in the B16 melanoma model upon s.c. transplantation with different sublines over- or under-expressing CCL21 (243). B16 tumors with high CCL21 expression induced TLS formation but a successful anti-tumor response was prevented due to the infiltration of suppressive immune cells such as Tregs. This illustrates the complex interplay of chemokines required for the formation of immunogenic TLS. In another study, B16 cells were modified to express the tumor-specific sphingolipid GD2 and injected i.v. into syngenic mice, resulting in the formation of pulmonary tumors (215). The authors created a fusion protein of a chimeric anti-GD2 antibody fused to lymphotoxin and demonstrated its effectiveness in reducing the growth of lung tumors by inducing peritumoral TLS, including T cells, B cells, and HEVs. Interestingly, tumor-specific T cells were detected, indicating the effective activation of naïve T cells within the TLS. The potency of lymphotoxin was further highlighted by transplantation of B16 cells expressing GD2 into lymphotoxin-deficient mice (211). Despite the absence of secondary lymphoid organs, TLS were formed upon treatment with the fusion protein.

In a different approach, genetic manipulation of DCs to produce Tbet (DC.Tbet) was reported as a useful tool to induce TLS (63). The authors induced tumors by s.c transplantation of MCA205 sarcoma cells. After seven days, they performed a therapeutic injection of DC.Tbet cells i.t. and observed reduced tumor growth and the development of anti-tumor immunity in association with TLS formation, including the accumulation of T cells, B cells, NK cells, DCs, and PNAd+ HEVs. Interestingly, DC.Tbet cells already secreted CCL19, CCL21, LIGHT/TNFSF14, and lymphotoxin, thereby inducing TLS formation even in lymphotoxin-deficient mice transplanted with MCA205 sarcoma cells and treated with DC.Tbet cells. DC.Tbet cells further produced high levels of IL36γ, and upon transplantation of MC38 colorectal cancer cells into IL36 receptor-deficient mice, the formation of TLS was impaired. These studies indicated a novel role for IL36 in anti-tumor immunity during TLS formation.

We do not offer a complete list of all transplantable tumor models that develop TLS, but rather aim at highlighting models that are particularly useful for investigating TLS formation. While many studies describe the induction of successful anti-tumor immune responses without focusing on TLS formation (244, 245), the diversity of tumor cells and recipient mice, particularly when considering genetic modification of one or both, makes s.c. and i.p. transplantation models valuable tools to investigate at least early mechanisms of TLS formation.

Conclusions

The data summarized above establishes the prognostic relevance of TLS for cancer patients, while outlining the challenges that lie ahead when considering TLS formation as a reliable prognostic and therapeutic goal. While the suitability of TLS as biomarkers in different tumor entities is solidifying, the signals to initiate, sustain, but also prevent TLS formation, and the cellular interactions within TLS, are poorly understood. Such knowledge would be necessary to envision targeted induction of TLS in cancer and prevent their undesired formation in other contexts. Along these lines, an important aspect to consider is the potential auto-immune reactions that may be triggered when TLS are therapeutically induced. While the antigen-dependence of TLS formation may be a limiting factor for such side-effects, recent studies have indicated that TLS may also form due to chronic

inflammation and aging without the requirement of specific antigens (32). The requirement of a sufficient degree of ongoing inflammation for TLS formation not only emerges from cancer mouse models, such as the PyMT model discussed earlier, but also from clinical observations. For instance, tobacco exposure, which triggers inflammatory reactions, has been connected to increased TLS abundance and CCL21 in lung adenocarcinoma patients, correlating with the response to immunotherapy (246). Moreover, cancer patients undergoing corticosteroid treatment exhibited impaired TLS maturation or formation (190, 247). Other inflammatory triggers, such as dying cells or related DAMPs commonly found in tumors and induced in response to tumor therapy, may also affect TLS development (69).

There are critical questions in the TLS field that we feel need specific attention (Figure 3). Particularly TLS heterogeneity concerning maturation state, location, interconnectivity, and cellular composition, both globally and in discrete tumor niches at primary and metastatic sites, needs consideration. The impact of these parameters on anti-tumor immunity and disease progression requires further clinical and pre-clinical investigation. Moreover, standardized, clinically applicable methods of TLS detection need to be established. Importantly, it is not entirely clear if TLS are simply indicative of the local immune response in a tumor or if they represent relevant anti- or pro-tumor entities by themselves. Understanding this issue is vital not only for targeted TLS induction but may also be of interest when aiming at avoiding auto-inflammatory side-effects of immune activation against tumors. Suppressing TLS may, in some cases, reduce auto-immune side-effects rather than affecting anti-tumor immune responses.

Addressing these questions requires longitudinal and spatial analyses to compare intra- and extra-tumoral immune responses, preferably in suitable mouse models that closely replicate tumor development in humans. Such experiments would yield strategies to selectively induce or deplete TLS without hampering local extra-TLS immune responses as well as SLO-dependent adaptive immunity. Another pressing question is identifying the signals and cellular composition that render TLS activating versus suppressive. Understanding the signals that induce or suppress Treg formation/activity in TLS and targeting these mechanisms could potentially revert suppressive TLS into immune-stimulatory powerhouses. Phenotypes and functional properties of suppressive Tregs in TLS and their putative association with TLS maturation require further investigation.

Finally, not all tumors seem permissive for TLS formation, suggesting that homeostatic signals may limit TLS induction even in the presence of inflammatory stimuli. Cytokine receptor antagonists, as shown for IL-36RA (63), or cytokine and chemokine decoy receptors (248) might be potential candidates. Blocking these mediators and receptors may, thus, trigger TLS formation even in non-permissive environments. However, the potential risk of auto-inflammatory side-effects also requires

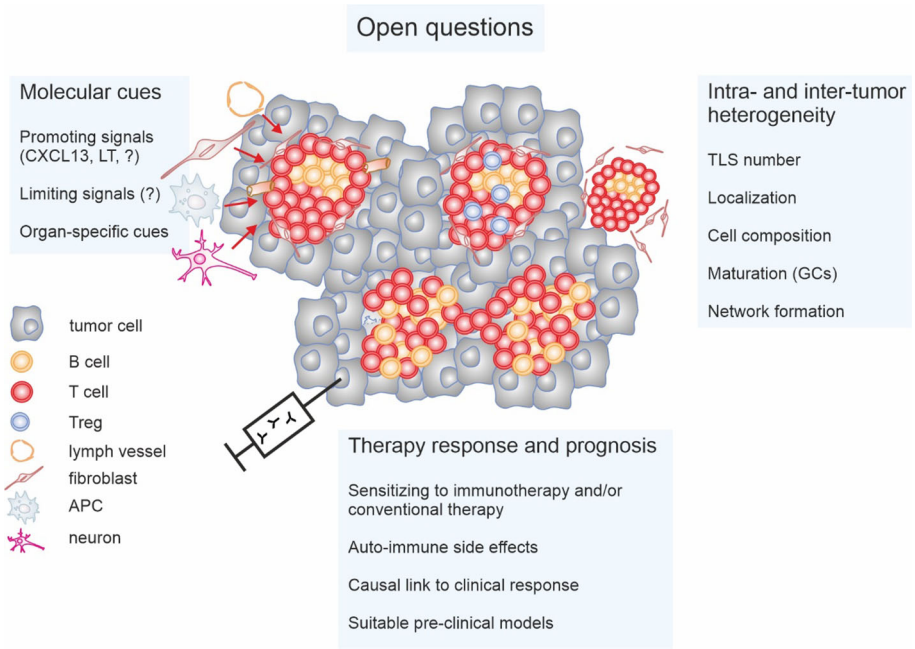

FIGURE 3
Open questions concerning tertiary lymphoid structures (TLS) in cancer. The impact of the intra- and inter-tumor heterogeneity of TLS on anti-tumor immunity and patient prognosis is not fully understood. Important parameters appear to be not only the number of TLS and their localization. Cellular composition such as the relative abundance of regulatory T cells (Tregs) and maturation status such as the presence or absence of germinal centers (GCs) as well as interconnectivity throughout tumors may play a role. Moreover, signals that on the one hand induce and on the other restrict TLS formation, and the cells providing these signals, need to be identified and/or better characterized. This is also relevant on the context of organ specificity. Finally, the fundamental question if TLS are causally involved in anti-tumor immunity or represent a bystander phenomenon is still unanswered. This is only relevant to be able to understand the impact of TLS on anti-cancer therapy responses, and if induction of TLS formation would induce unacceptable auto-immune side-effects. Research towards answering these open questions will require suitable pre-clinical models.

investigation. To this end, optimal tumor (mouse) models to study TLS formation that mimic both, the time scale and cellular complexity of tumor formation in humans need to be developed and cross-validated. Such studies will reveal the true benefit of interfering with TLS formation in cancer patients.

Author contributions

XY: Data curation, Investigation, Writing – original draft, Writing – review & editing. KK: Funding acquisition, Writing – original draft, Writing – review & editing. AW: Data curation, Funding acquisition, Supervision, Visualization, Writing – original draft, Writing – review & editing.

Funding

The author(s) declare financial support was received for the research, authorship, and/or publication of this article. XY is supported by a CSC scholarship funded by the Chinese Government. KK is supported by Deutsche Forschungsgemeinschaft (DFG, German Research Foundation): SFB-TRR241-375876048 B04, and the Interdisciplinary Centre for Clinical Research (IZKF) Erlangen at Universitätsklinikum Erlangen, Friedrich-Alexander-Universität Erlangen-Nürnberg (Junior Project J85). AW is supported by Deutsche Krebshilfe (70114051), Deutsche Forschungsgemeinschaft (SFB 1039, TP B06; GRK 2336, TP1), and the LOEWE Center Frankfurt Cancer Institute (FCI), funded by the Hessen State Ministry for Higher Education, Research and the Arts.

Conflict of interest

The authors declare that the research was conducted in the absence of any commercial or financial relationships that could be construed as a potential conflict of interest.

Publisher's note

References

1. Hanahan D, Weinberg RA. Hallmarks of cancer: the next generation. *Cell* (2011) 144:646–74. doi: 10.1016/j.cell.2011.02.013

2. Trinchieri G. Cancer and inflammation: an old intuition with rapidly evolving new concepts. *Annu Rev Immunol* (2012) 30:677–706. doi: 10.1146/annurev-immunol-020711-075008

3. Coussens LM, Zitvogel L, Palucka AK. Neutralizing tumor-promoting chronic inflammation: a magic bullet? *Science* (2013) 339:286–91. doi: 10.1126/science.1232227

4. Greten FR, Grivennikov SI. Inflammation and cancer: triggers, mechanisms, and consequences. *Immunity* (2019) 51:27–41. doi: 10.1016/j.immuni.2019.06.025

5. Hou J, Karin M, Sun B. Targeting cancer-promoting inflammation - have anti-inflammatory therapies come of age? *Nat Rev Clin Oncol* (2021) 18:261–79. doi: 10.1038/s41571-020-00459-9

6. Weigert A, Mora J, Sekar D, Syed S, Brune B. Killing is not enough: how apoptosis hijacks tumor-associated macrophages to promote cancer progression. *Adv Exp Med Biol* (2016) 930:205–39. doi: 10.1007/978-3-319-39406-0_9

7. Kaymak I, Williams KS, Cantor JR, Jones RG. Immunometabolic interplay in the tumor microenvironment. *Cancer Cell* (2021) 39:28–37. doi: 10.1016/j.ccell.2020.09.004

8. Boon T, Cerottini JC, Van Den Eynde B, van der Bruggen P, Van Pel A. Tumor antigens recognized by T lymphocytes. *Annu Rev Immunol* (1994) 12:337–65. doi: 10.1146/annurev.iy.12.040194.002005

9. Schreiber RD, Old LJ, Smyth MJ. Cancer immunoediting: integrating immunity's roles in cancer suppression and promotion. *Science* (2011) 331:1565–70. doi: 10.1126/science.1203486

10. Olesch C, Bruene B, Weigert A. Keep a little fire burning-the delicate balance of targeting sphingosine-1-phosphate in cancer immunity. *Int J Mol Sci* (2022) 23. doi: 10.3390/ijms23031289

11. Boon T, van der Bruggen P. Human tumor antigens recognized by T lymphocytes. *J Exp Med* (1996) 183:725–9. doi: 10.1084/jem.183.3.725

12. Matsushita H, Vesely MD, Koboldt DC, Rickert CG, Uppaluri R, Magrini VJ, et al. Cancer exome analysis reveals a T-cell-dependent mechanism of cancer immunoediting. *Nature* (2012) 482:400–4. doi: 10.1038/nature10755

13. Joseph CG, Darrah E, Shah AA, Skora AD, Casciola-Rosen LA, Wigley FM, et al. Association of the autoimmune disease scleroderma with an immunologic response to cancer. *Science* (2014) 343:152–7. doi: 10.1126/science.1246886

14. Galon J, Bruni D. Tumor immunology and tumor evolution: intertwined histories. *Immunity* (2020) 52:55–81. doi: 10.1016/j.immuni.2019.12.018

15. Martin TD, Patel RS, Cook DR, Choi MY, Patil A, Liang AC, et al. The adaptive immune system is a major driver of selection for tumor suppressor gene inactivation. *Science* (2021) 373:1327–35. doi: 10.1126/science.abg5784

16. Sharma P, Hu-Lieskovan S, Wargo JA, Ribas A. Primary, adaptive, and acquired resistance to cancer immunotherapy. *Cell* (2017) 168:707–23. doi: 10.1016/j.cell.2017.01.017

17. Wei SC, Duffy CR, Allison JP. Fundamental mechanisms of immune checkpoint blockade therapy. *Cancer Discovery* (2018) 8:1069–86. doi: 10.1158/2159-8290.CD-18-0367

18. Bruni D, Angell HK, Galon J. The immune contexture and Immunoscore in cancer prognosis and therapeutic efficacy. *Nat Rev Cancer* (2020) 20:662–80. doi: 10.1038/s41568-020-0285-7

19. Mlecnik B, Bindea G, Van Den Eynde M, Galon J. Metastasis immune-based scores predict patient survival. *Oncoimmunology* (2020) 9:1806000. doi: 10.1080/2162402X.2020.1806000

20. Mascaux C, Angelova M, Vasaturo A, Beane J, Hijazi K, Anthoine G, et al. Immune evasion before tumour invasion in early lung squamous carcinogenesis. *Nature* (2019) 571:570–5. doi: 10.1038/s41586-019-1330-0

21. Fridman WH, Pages F, Sautes-Fridman C, Galon J. The immune contexture in human tumours: impact on clinical outcome. *Nat Rev Cancer* (2012) 12:298–306. doi: 10.1038/nrc3245

22. Gentles AJ, Newman AM, Liu CL, Bratman SV, Feng W, Kim D, et al. The prognostic landscape of genes and infiltrating immune cells across human cancers. *Nat Med* (2015) 21:938–45. doi: 10.1038/nm.3909

23. Fridman WH, Zitvogel L, Sautes-Fridman C, Kroemer G. The immune contexture in cancer prognosis and treatment. *Nat Rev Clin Oncol* (2017) 14:717–34. doi: 10.1038/nrclinonc.2017.101

24. Spitzer MH, Carmi Y, Reticker-Flynn NE, Kwek SS, Madhireddy D, Martins MM, et al. Systemic immunity is required for effective cancer immunotherapy. *Cell* (2017) 168:487–502 e415. doi: 10.1016/j.cell.2016.12.022

25. Hiam-Galvez KJ, Allen BM, Spitzer MH. Systemic immunity in cancer. *Nat Rev Cancer* (2021) 21:345–59. doi: 10.1038/s41568-021-00347-z

26. Chen DS, Mellman I. Oncology meets immunology: the cancer-immunity cycle. *Immunity* (2013) 39:1–10. doi: 10.1016/j.immuni.2013.07.012

27. Sautes-Fridman C, Petitprez F, Calderaro J, Fridman WH. Tertiary lymphoid structures in the era of cancer immunotherapy. *Nat Rev Cancer* (2019) 19:307–25. doi: 10.1038/s41568-019-0144-6

28. Dieu-Nosjean MC, Antoine M, Danel C, Heudes D, Wislez M, Poulot V, et al. Long-term survival for patients with non-small-cell lung cancer with intratumoral lymphoid structures. *J Clin Oncol* (2008) 26:4410–7. doi: 10.1200/JCO.2007.15.0284

29. Drayton DL, Liao S, Mounzer RH, Ruddle NH. Lymphoid organ development: from ontogeny to neogenesis. *Nat Immunol* (2006) 7:344–53. doi: 10.1038/ni1330

30. Corsiero E, Delvecchio FR, Bombardieri M, Pitzalis C. B cells in the formation of tertiary lymphoid organs in autoimmunity, transplantation and tumorigenesis. *Curr Opin Immunol* (2019) 57:46–52. doi: 10.1016/j.coi.2019.01.004

31. Da Graca CG, Van Baarsen LGM, Mebius RE. Tertiary lymphoid structures: diversity in their development, composition, and role. *J Immunol* (2021) 206:273–81. doi: 10.4049/jimmunol.2000873

32. Sato Y, Silina K, Van Den Broek M, Hirahara K, Yanagita M. The roles of tertiary lymphoid structures in chronic diseases. *Nat Rev Nephrol* (2023) 19:525–37. doi: 10.1038/s41581-023-00706-z

33. Bery AI, Shepherd HM, Li WJ, Krupnick AS, Gelman AE, Kreisel D. Role of tertiary lymphoid organs in the regulation of immune responses in the periphery. *Cell Mol Life Sci* (2022) 79. doi: 10.1007/s00018-022-04388-x

34. Joshi NS, Akama-Garren EH, Lu YS, Lee DY, Chang GP, Li A, et al. Regulatory T cells in tumor-associated tertiary lymphoid structures suppress anti-tumor T cell responses. *Immunity* (2015) 43:579–90. doi: 10.1016/j.immuni.2015.08.006

35. Germain C, Devi-Marulkar P, Knockaert S, Biton J, Kaplon H, Letaief L, et al. Tertiary lymphoid structure-B cells narrow regulatory T cells impact in lung cancer patients. *Front Immunol* (2021) 12. doi: 10.3389/fimmu.2021.626776

36. Devi-Marulkar P, Fastenackels S, Karapentiantz P, Goc J, Germain C, Kaplon H, et al. Regulatory T cells infiltrate the tumor-induced tertiary lymphoid structures and are associated with poor clinical outcome in NSCLC. *Commun Biol* (2022) 5. doi: 10.1038/s42003-022-04356-y

37. Briem O, Kallberg E, Kimbung S, Veerla S, Stenstrom J, Hatschek T, et al. CD169(+) macrophages in primary breast tumors associate with tertiary lymphoid structures, T-regs and a worse prognosis for patients with advanced breast cancer. *Cancers* (2023) 15. doi: 10.3390/cancers15041262

38. Lin JR, Wang S, Coy S, Chen YA, Yapp C, Tyler M, et al. Multiplexed 3D atlas of state transitions and immune interaction in colorectal cancer. *Cell* (2023) 186:363–+. doi: 10.1016/j.cell.2022.12.028

39. Klein U, Dalla-Favera R. Germinal centres: role in B-cell physiology and Malignancy. *Nat Rev Immunol* (2008) 8:22–33. doi: 10.1038/nri2217

40. Moyron-Quiroz JE, Rangel-Moreno J, Kusser KR, Hartson L, Sprague F, Goodrich S, et al. Role of inducible bronchus associated lymphoid tissue (iBALT) in respiratory immunity. *Nat Med* (2004) 10:927–34. doi: 10.1038/nm1091

41. Moyron-Quiroz JE, Rangel-Moreno J, Hartson L, Kusser K, Tighe MP, Klonowski KD, et al. Persistence and responsiveness of immunologic memory in the absence of secondary lymphoid organs. *Immunity* (2006) 25:643–54. doi: 10.1016/j.immuni.2006.08.022

42. Berteloot L, Molina TJ, Bruneau J, Picard C, Barlogis V, Secq V, et al. Alternative pathways for the development of lymphoid structures in humans. *Proc Natl Acad Sci United States America* (2021) 118. doi: 10.1073/pnas.2108082118

43. Futterer A, Mink K, Luz A, Kosco-Vilbois MH, Pfeffer K. The lymphotoxin beta receptor controls organogenesis and affinity maturation in peripheral lymphoid tissues. *Immunity* (1998) 9:59–70. doi: 10.1016/S1074-7613(00)80588-9

44. Dougall WC, Glaccum M, Charrier K, Rohrbach K, Brasel K, De Smedt T, et al. RANK is essential for osteoclast and lymph node development. *Genes Dev* (1999) 13:2412–24. doi: 10.1101/gad.13.18.2412

45. Eberl G, Marmon S, Sunshine MJ, Rennert PD, Choi YW, Littman DR. An essential function for the nuclear receptor ROR gamma t in the generation of fetal lymphoid tissue inducer cells. *Nat Immunol* (2004) 5:64–73. doi: 10.1038/ni1022

46. Van De Pavert SA, Olivier BJ, Goverse G, Vondenhoff MF, Greuter M, Beke P, et al. Chemokine CXCL13 is essential for lymph node initiation and is induced by retinoic acid and neuronal stimulation. *Nat Immunol* (2009) 10:1193–U1178. doi: 10.1038/ni.1789

47. Randall TD, Carragher DM, Rangel-Moreno J. Development of secondary lymphoid organs. *Annu Rev Immunol* (2008) 26:627–50. doi: 10.1146/annurev.immunol.26.021607.090257

48. Van De Pavert SA, Mebius RE. New insights into the development of lymphoid tissues. *Nat Rev Immunol* (2010) 10:664–U624. doi: 10.1038/nri2832

49. Onder L, Ludewig B. A fresh view on lymph node organogenesis. *Trends Immunol* (2018) 39:775–87. doi: 10.1016/j.it.2018.08.003

50. Cherrier M, Sawa S, Eberl G. Notch, Id2, and ROR gamma t sequentially orchestrate the fetal development of lymphoid tissue inducer cells. *J Exp Med* (2012) 209:729–40. doi: 10.1084/jem.20111594

51. Onder L, Morbe U, Pikor N, Novkovic M, Cheng HW, Hehlgans T, et al. Lymphatic endothelial cells control initiation of lymph node organogenesis. *Immunity* (2017) 47:80–+. doi: 10.1016/j.immuni.2017.05.008

52. Bovay E, Sabine A, Prat-Luri B, Kim S, Son K, Willrodt AH, et al. Multiple roles of lymphatic vessels in peripheral lymph node development. *J Exp Med* (2018) 215:2760–77. doi: 10.1084/jem.20180217

53. Nayar S, Campos J, Smith CG, Iannizzotto V, Gardner DH, Mourcin F, et al. Immunofibroblasts are pivotal drivers of tertiary lymphoid structure formation and local pathology. *Proc Natl Acad Sci United States America* (2019) 116:13490–7. doi: 10.1073/pnas.1905301116

54. Rodriguez AB, Peske JD, Woods AN, Leick KM, Mauldin IS, Meneveau MO, et al. Immune mechanisms orchestrate tertiary lymphoid structures in tumors *via* cancer-associated fibroblasts. *Cell Rep* (2021) 36. doi: 10.1016/j.celrep.2021.109422

55. Geurtsvankessel CH, Willart M, Bergen IM, Van Rijt LS, Muskens F, Elewaut D, et al. Dendritic cells are crucial for maintenance of tertiary lymphoid structures in the lung of influenza virus-infected mice. *J Exp Med* (2009) 206:2339–49. doi: 10.1084/jem.20090410

56. Thommen DS, Koelzer VH, Herzig P, Roller A, Trefny M, Dimeloe S, et al. A transcriptionally and functionally distinct PD-1(+) CD8(+) T cell pool with predictive potential in non-small-cell lung cancer treated with PD-1 blockade. *Nat Med* (2018) 24:994–+. doi: 10.1038/s41591-018-0057-z

57. Koscso B, Kurapati S, Rodrigues RR, Nedjic J, Gowda K, Shin C, et al. Gut-resident CX3CR1(hi) macrophages induce tertiary lymphoid structures and IgA response in situ. *Sci Immunol* (2020) 5. doi: 10.1126/sciimmunol.aax0062

58. Wu SY, Zhang SW, Ma D, Xiao Y, Liu Y, Chen L, et al. CCL19(+) dendritic cells potentiate clinical benefit of anti-PD-(L)1 immunotherapy in triple-negative breast cancer. *Med* (2023) 4:373–393 e378. doi: 10.1016/j.medj.2023.04.008

59. Rangel-Moreno J, Carragher DM, Garcia-Hernandez MD, Hwang JY, Kusser K, Hartson L, et al. The development of inducible bronchus-associated lymphoid tissue depends on IL-17. *Nat Immunol* (2011) 12:639–U195. doi: 10.1038/ni.2053

60. Barone F, Nayar S, Campos J, Cloake T, Withers DR, Toellner KM, et al. IL-22 regulates lymphoid chemokine production and assembly of tertiary lymphoid organs. *Proc Natl Acad Sci United States America* (2015) 112:11024–9. doi: 10.1073/pnas.1503315112

61. Pikor NB, Astarita JL, Summers-Deluca L, Galicia G, Qu J, Ward LA, et al. Integration of th17- and lymphotoxin-derived signals initiates meningeal-resident stromal cell remodeling to propagate neuroinflammation. *Immunity* (2015) 43:1160–73. doi: 10.1016/j.immuni.2015.11.010

62. Denton AE, Innocentin S, Carr EJ, Bradford BM, Lafouresse F, Mabbott NA, et al. Type I interferon induces CXCL13 to support ectopic germinal center formation. *J Exp Med* (2019) 216:621–37. doi: 10.1084/jem.20181216

63. Weinstein AM, Chen L, Brzana EA, Patil PR, Taylor JL, Fabian KL, et al. Tbet and IL-36gamma cooperate in therapeutic DC-mediated promotion of ectopic lymphoid organogenesis in the tumor microenvironment. *Oncoimmunology* (2017) 6:e1322238. doi: 10.1080/2162402X.2017.1322238

64. Weinstein AM, Giraldo NA, Petitprez F, Julie C, Lacroix L, Peschaud F, et al. Association of IL-36gamma with tertiary lymphoid structures and inflammatory immune infiltrates in human colorectal cancer. *Cancer Immunol Immunother* (2019) 68:109–20. doi: 10.1007/s00262-018-2259-0

65. Scheibe K, Kersten C, Schmied A, Vieth M, Primbs T, Carle B, et al.). Inhibiting interleukin 36 receptor signaling reduces fibrosis in mice with chronic intestinal inflammation. *Gastroenterology* (2019) 156:1082–1097 e1011. doi: 10.1053/j.gastro.2018.11.029

66. Kinker GS, Vitiello G, Diniz AB, Cabral-Piccin MP, Pereira PHB, Carvalho MLR, et al. Mature tertiary lymphoid structures are key niches of tumour-specific immune responses in pancreatic ductal adenocarcinomas. *Gut* (2023) 72:1927–1941. doi: 10.1136/gutjnl-2022-328697

67. O'connor RA, Martinez BR, Koppensteiner L, Mathieson L, Akram AR. Cancer-associated fibroblasts drive CXCL13 production in activated T cells *via* TGF-beta. *Front Immunol* (2023) 14:1221532. doi: 10.3389/fimmu.2023.1221532

68. Grabner R, Lotzer K, Dopping S, Hildner M, Radke D, Beer M, et al. Lymphotoxin beta receptor signaling promotes tertiary lymphoid organogenesis in the aorta adventitia of aged ApoE(-/-) mice. *J Exp Med* (2009) 206:233–48. doi: 10.1084/jem.20080752

69. Dieude M, Kaci I, Hebert MJ. The impact of programmed cell death on the formation of tertiary lymphoid structures. *Front Immunol* (2021) 12. doi: 10.3389/fimmu.2021.696311

70. Johansson-Percival A, Ganss R. Therapeutic induction of tertiary lymphoid structures in cancer through stromal remodeling. *Front Immunol* (2021) 12. doi: 10.3389/fimmu.2021.674375

71. Ramachandran M, Vaccaro A, Van De Walle T, Georganaki M, Lugano R, Vemuri K, et al. Tailoring vascular phenotype through AAV therapy promotes anti-tumor immunity in glioma. *Cancer Cell* (2023) 41:1134–+. doi: 10.1016/j.ccell.2023.04.010

72. Wen ZF, Liu H, Qiao DD, Chen HL, Li LY, Yang ZY, et al. Nanovaccines fostering tertiary lymphoid structure to attack mimicry nasopharyngeal carcinoma. *ACS Nano* (2023) 17:7194–206. doi: 10.1021/acsnano.2c09619

73. Zhang N, Liu X, Qin J, Sun Y, Xiong H, Lin B, et al. LIGHT/TNFSF14 promotes CAR-T cell trafficking and cytotoxicity through reversing immunosuppressive tumor microenvironment. *Mol Ther* (2023) 31(9):2575–2590. doi: 10.1016/j.ymthe.2023.06.015

74. Olivier BJ, Cailotto C, van der Vliet J, Knippenberg M, Greuter MJ, Hilbers FW, et al. Vagal innervation is required for the formation of tertiary lymphoid tissue in colitis. *Eur J Immunol* (2016) 46:2467–80. doi: 10.1002/eji.201646370

75. Hua YC, Vella G, Rambow F, Allen E, Martinez AA, Duhamel M, et al. Cancer immunotherapies transition endothelial cells into HEVs that generate TCF1(+) T

lymphocyte niches through a feed-forward loop. *Cancer Cell* (2022) 40:1600–+. doi: 10.1016/j.ccell.2022.11.002

76. Peske JD, Thompson ED, Gemta L, Baylis RA, Fu YX, Engelhard VH. Effector lymphocyte-induced lymph node-like vasculature enables naive T-cell entry into tumours and enhanced anti-tumour immunity. *Nat Commun* (2015) 6. doi: 10.1038/ncomms8114

77. Victora GD, Nussenzweig MC. Germinal centers. *Annu Rev Immunol* (2022) 40:413–42. doi: 10.1146/annurev-immunol-120419-022408

78. Fu YX, Huang GM, Wang Y, Chaplin DD. B lymphocytes induce the formation of follicular dendritic cell clusters in a lymphotoxin alpha-dependent fashion. *J Exp Med* (1998) 187:1009–18. doi: 10.1084/jem.187.7.1009

79. Rakaee M, Kilvaer TK, Jamaly S, Berg T, Paulsen EE, Berglund M, et al. Tertiary lymphoid structure score: a promising approach to refine the TNM staging in resected non-small cell lung cancer. *Br J Cancer* (2021) 124:1680–9. doi: 10.1038/s41416-021-01307-y

80. Zhang NN, Qu FJ, Liu H, Li ZJ, Zhang YC, Han X, et al. Prognostic impact of tertiary lymphoid structures in breast cancer prognosis: a systematic review and meta-analysis. *Cancer Cell Int* (2021) 21:536. doi: 10.1186/s12935-021-02242-x

81. Wang B, Liu J, Han Y, Deng Y, Li J, Jiang Y. The presence of tertiary lymphoid structures provides new insight into the clinicopathological features and prognosis of patients with breast cancer. *Front Immunol* (2022) 13:868155. doi: 10.3389/fimmu.2022.868155

82. Bertucci F, De Nonneville A, Finetti P, Mamessier E. Predictive power of tertiary lymphoid structure signature for neoadjuvant chemotherapy response and immunotherapy benefit in HER2-negative breast cancer. *Cancer Commun (Lond)* (2023) 43:943–6. doi: 10.1002/cac2.12447

83. Calderaro J, Petitprez F, Becht E, Laurent A, Hirsch TZ, Rousseau B, et al. Intra-tumoral tertiary lymphoid structures are associated with a low risk of early recurrence of hepatocellular carcinoma. *J Hepatol* (2019) 70:58–65. doi: 10.1016/j.jhep.2018.09.003

84. Schweiger T, Berghoff AS, Glogner C, Glueck O, Rajky O, Traxler D, et al. Tumor-infiltrating lymphocyte subsets and tertiary lymphoid structures in pulmonary metastases from colorectal cancer. *Clin Exp Metastasis* (2016) 33:727–39. doi: 10.1007/s10585-016-9813-y

85. Wang Q, Shen X, An R, Bai J, Dong J, Cai H, et al. Peritumoral tertiary lymphoid structure and tumor stroma percentage predict the prognosis of patients with non-metastatic colorectal cancer. *Front Immunol* (2022) 13:962056. doi: 10.3389/fimmu.2022.962056

86. Romero D. B cells and TLSs facilitate a response to ICI. *Nat Rev Clin Oncol* (2020) 17:195. doi: 10.1038/s41571-020-0338-6

87. Mori T, Tanaka H, Suzuki S, Deguchi S, Yamakoshi Y, Yoshii M, et al. Tertiary lymphoid structures show infiltration of effective tumor-resident T cells in gastric cancer. *Cancer Sci* (2021) 112:1746–57. doi: 10.1111/cas.14888

88. Kemi N, Ylitalo O, Vayrynen JP, Helminen O, Junttila A, Mrena J, et al. Tertiary lymphoid structures and gastric cancer prognosis. *APMIS* (2023) 131:19–25. doi: 10.1111/apm.13277

89. Liu Z, Meng X, Tang X, Zou W, He Y. Intratumoral tertiary lymphoid structures promote patient survival and immunotherapy response in head neck squamous cell carcinoma. *Cancer Immunol Immunother* (2023) 72:1505–21. doi: 10.1007/s00262-022-03310-5

90. Wang M, Zhai R, Wang M, Zhu W, Zhang J, Yu M, et al. Tertiary lymphoid structures in head and neck squamous cell carcinoma improve prognosis by recruiting CD8(+) T cells. *Mol Oncol* (2023) 17:1514–30. doi: 10.1002/1878-0261.13403

91. Tang J, Ramis-Cabrer D, Curull V, Wang X, Mateu-Jimenez M, Pijuan L, et al. B cells and tertiary lymphoid structures influence survival in lung cancer patients with resectable tumors. *Cancers (Basel)* (2020) 12. doi: 10.3390/cancers12092644

92. Italiano A, Bessede A, Pulido M, Bompas E, Piperno-Neumann S, Chevreau C, et al. Pembrolizumab in soft-tissue sarcomas with tertiary lymphoid structures: a phase 2 PEMBROSARC trial cohort. *Nat Med* (2022) 28:1199–206. doi: 10.1038/s41591-022-01821-3

93. Finkin S, Yuan D, Stein I, Taniguchi K, Weber A, Unger K, et al. Ectopic lymphoid structures function as microniches for tumor progenitor cells in hepatocellular carcinoma. *Nat Immunol* (2015) 16:1235–44. doi: 10.1038/ni.3290

94. Ruddle NH. Lymphatic vessels and tertiary lymphoid organs. *J Clin Invest* (2014) 124:953–9. doi: 10.1172/JCI71611

95. Schumacher TN, Thommen DS. Tertiary lymphoid structures in cancer. *Science* (2022) 375:eabf9419. doi: 10.1126/science.abf9419

96. Ladanyi A, Kiss J, Mohos A, Somlai B, Liszkay G, Gilde K, et al. Prognostic impact of B-cell density in cutaneous melanoma. *Cancer Immunol Immunother* (2011) 60:1729–38. doi: 10.1007/s00262-011-1071-x

97. Mahmoud SM, Lee AH, Paish EC, Macmillan RD, Ellis IO, Green AR. The prognostic significance of B lymphocytes in invasive carcinoma of the breast. *Breast Cancer Res Treat* (2012) 132:545–53. doi: 10.1007/s10549-011-1620-1

98. Nielsen JS, Sahota RA, Milne K, Kost SE, Nesslinger NJ, Watson PH, et al. CD20 + tumor-infiltrating lymphocytes have an atypical CD27- memory phenotype and together with CD8+ T cells promote favorable prognosis in ovarian cancer. *Clin Cancer Res* (2012) 18:3281–92. doi: 10.1158/1078-0432.CCR-12-0234

99. Lohr M, Edlund K, Botling J, Hammad S, Hellwig B, Othman A, et al. The prognostic relevance of tumour-infiltrating plasma cells and immunoglobulin kappa C indicates an important role of the humoral immune response in non-small cell lung cancer. *Cancer Lett* (2013) 333:222–8. doi: 10.1016/j.canlet.2013.01.036

100. Vanhersecke L, Brunet M, Guegan JP, Rey C, Bougouin A, Cousin S, et al. Mature tertiary lymphoid structures predict immune checkpoint inhibitor efficacy in solid tumors independently of PD-L1 expression. *Nat Cancer* (2021) 2:794–802. doi: 10.1038/s43018-021-00232-6

101. Lynch KT, Young SJ, Meneveau MO, Wages NA, Engelhard VH, Slingluff CL Jr., et al. Heterogeneity in tertiary lymphoid structure B-cells correlates with patient survival in metastatic melanoma. *J Immunother Cancer* (2021) 9. doi: 10.1136/jitc-2020-002273

102. Hayashi Y, Makino T, Sato E, Ohshima K, Nogi Y, Kanemura T, et al. Density and maturity of peritumoral tertiary lymphoid structures in oesophageal squamous cell carcinoma predicts patient survival and response to immune checkpoint inhibitors. *Br J Cancer* (2023) 128:2175–85. doi: 10.1038/s41416-023-02235-9

103. Le Rochais M, Hemon P, Ben-Guigui D, Garaud S, Le Dantec C, Pers JO, et al. Deciphering the maturation of tertiary lymphoid structures in cancer and inflammatory diseases of the digestive tract using imaging mass cytometry. *Front Immunol* (2023) 14:1147480. doi: 10.3389/fimmu.2023.1147480

104. Wang Q, Sun K, Liu R, Song Y, Lv Y, Bi P, et al. Single-cell transcriptome sequencing of B-cell heterogeneity and tertiary lymphoid structure predicts breast cancer prognosis and neoadjuvant therapy efficacy. *Clin Transl Med* (2023) 13:e1346. doi: 10.1002/ctm2.1346

105. He M, He QH, Cai XY, Liu J, Deng HS, Li F, et al. Intratumoral tertiary lymphoid structure (TLS) maturation is influenced by draining lymph nodes of lung cancer. *J Immunotherapy Cancer* (2023) 11. doi: 10.1136/jitc-2022-005539

106. Posch F, Silina K, Leibl S, Mundlein A, Moch H, Siebenhuner A, et al. Maturation of tertiary lymphoid structures and recurrence of stage II and III colorectal cancer. *Oncoimmunology* (2018) 7:e1378844. doi: 10.1080/2162402X.2017.1378844

107. Silina K, Soltermann A, Attar FM, Casanova R, Uckeley ZM, Thut H, et al. Germinal centers determine the prognostic relevance of tertiary lymphoid structures and are impaired by corticosteroids in lung squamous cell carcinoma. *Cancer Res* (2018) 78:1308–20. doi: 10.1158/0008-5472.CAN-17-1987

108. Cipponi A, Mercier M, Seremet T, Baurain JF, Theate I, Van Den Oord J, et al. Neogenesis of lymphoid structures and antibody responses occur in human melanoma metastases. *Cancer Res* (2012) 72:3997–4007. doi: 10.1158/0008-5472.CAN-12-1377

109. Helmink BA, Reddy SM, Gao J, Zhang S, Basar R, Thakur R, et al. B cells and tertiary lymphoid structures promote immunotherapy response. *Nature* (2020) 577:549–55. doi: 10.1038/s41586-019-1922-8

110. Fridman WH, Meylan M, Petitprez F, Sun CM, Italiano A, Sautes-Fridman C. B cells and tertiary lymphoid structures as determinants of tumour immune contexture and clinical outcome. *Nat Rev Clin Oncol* (2022) 19:441–57. doi: 10.1038/s41571-022-00619-z

111. Fridman WH, Siberil S, Pupier G, Soussan S, Sautes-Fridman C. Activation of B cells in Tertiary Lymphoid Structures in cancer: Anti-tumor or anti-self? *Semin Immunol* (2023) 65:101703. doi: 10.1016/j.smim.2022.101703

112. Budczies J, Kirchner M, Kluck K, Kazdal D, Glade J, Allgauer M, et al. A gene expression signature associated with B cells predicts benefit from immune checkpoint blockade in lung adenocarcinoma. *Oncoimmunology* (2021) 10:1860586. doi: 10.1080/2162402X.2020.1860586

113. Couillault C, Germain C, Dubois B, Kaplon H. Identification of tertiary lymphoid structure-associated follicular helper T cells in human tumors and tissues. *Methods Mol Biol* (2018) 1845:205–22. doi: 10.1007/978-1-4939-8709-2_12

114. Koch M, Beckhove P, Op Den Winkel J, Autenrieth D, Wagner P, Nummer D, et al. Tumor infiltrating T lymphocytes in colorectal cancer: Tumor-selective activation and cytotoxic activity in situ. *Ann Surg* (2006) 244:986–992; discussion 992-983. doi: 10.1097/01.sla.0000247058.43243.7b

115. Bai Z, Zhou Y, Ye Z, Xiong J, Lan H, Wang F. Tumor-infiltrating lymphocytes in colorectal cancer: the fundamental indication and application on immunotherapy. *Front Immunol* (2021) 12:808964. doi: 10.3389/fimmu.2021.808964

116. Savas P, Virassamy B, Ye C, Salim A, Mintoff CP, Caramia F, et al. Single-cell profiling of breast cancer T cells reveals a tissue-resident memory subset associated with improved prognosis. *Nat Med* (2018) 24:986–93. doi: 10.1038/s41591-018-0078-7

117. Loi S, Michiels S, Adams S, Loibl S, Budczies J, Denkert C, et al. The journey of tumor-infiltrating lymphocytes as a biomarker in breast cancer: clinical utility in an era of checkpoint inhibition. *Ann Oncol* (2021) 32:1236–44. doi: 10.1016/j.annonc.2021.07.007

118. Creelan BC, Wang C, Teer JK, Toloza EM, Yao J, Kim S, et al. Tumor-infiltrating lymphocyte treatment for anti-PD-1-resistant metastatic lung cancer: a phase 1 trial. *Nat Med* (2021) 27:1410–8. doi: 10.1038/s41591-021-01462-y

119. Gueguen P, Metoikidou C, Dupic T, Lawand M, Goudot C, Baulande S, et al. Contribution of resident and circulating precursors to tumor-infiltrating CD8(+) T cell populations in lung cancer. *Sci Immunol* (2021) 6. doi: 10.1126/sciimmunol.abd5778

120. Federico L, Mcgrail DJ, Bentebibel SE, Haymaker C, Ravelli A, Forget MA, et al. Distinct tumor-infiltrating lymphocyte landscapes are associated with clinical outcomes in localized non-small-cell lung cancer. *Ann Oncol* (2022) 33:42–56. doi: 10.1016/j.annonc.2021.09.021

121. Sato E, Olson SH, Ahn J, Bundy B, Nishikawa H, Qian F, et al. Intraepithelial CD8+ tumor-infiltrating lymphocytes and a high CD8+/regulatory T cell ratio are associated with favorable prognosis in ovarian cancer. *Proc Natl Acad Sci U.S.A.* (2005) 102:18538–43. doi: 10.1073/pnas.0509182102

122. Stanton SE, Disis ML. Clinical significance of tumor-infiltrating lymphocytes in breast cancer. *J Immunother Cancer* (2016) 4:59. doi: 10.1186/s40425-016-0165-6

123. Chiba T, Ohtani H, Mizoi T, Naito Y, Sato E, Nagura H, et al. Intraepithelial CD8+ T-cell-count becomes a prognostic factor after a longer follow-up period in human colorectal carcinoma: possible association with suppression of micrometastasis. *Br J Cancer* (2004) 91:1711–7. doi: 10.1038/sj.bjc.6602201

124. Salgado R, Denkert C, Demaria S, Sirtaine N, Klauschen F, Pruneri G, et al. The evaluation of tumor-infiltrating lymphocytes (TILs) in breast cancer: recommendations by an International TILs Working Group 2014. *Ann Oncol* (2015) 26:259–71. doi: 10.1093/annonc/mdu450

125. Fuchs TL, Sioson L, Sheen A, Jafari-Nejad K, Renaud CJ, Andrici J, et al. Assessment of tumor-infiltrating lymphocytes using international TILs working group (ITWG) system is a strong predictor of overall survival in colorectal carcinoma: A study of 1034 patients. *Am J Surg Pathol* (2020) 44:536–44. doi: 10.1097/PAS.0000000000001409

126. Almangush A, Jouhi L, Atula T, Haglund C, Makitie AA, Hagstrom J, et al. Tumour-infiltrating lymphocytes in oropharyngeal cancer: a validation study according to the criteria of the International Immuno-Oncology Biomarker Working Group. *Br J Cancer* (2022) 126:1589–94. doi: 10.1038/s41416-022-01708-7

127. Chaurio RA, Anadon CM, Lee Costich T, Payne KK, Biswas S, Harro CM, et al. TGF-beta-mediated silencing of genomic organizer SATB1 promotes Tfh cell differentiation and formation of intra-tumoral tertiary lymphoid structures. *Immunity* (2022) 55:115–128 e119. doi: 10.1016/j.immuni.2021.12.007

128. Workel HH, Lubbers JM, Arnold R, Prins TM, van der Vlies P, De Lange K, et al. A transcriptionally distinct CXCL13(+)CD103(+)CD8(+) T-cell population is associated with B-cell recruitment and neoantigen load in human cancer. *Cancer Immunol Res* (2019) 7:784–96. doi: 10.1158/2326-6066.CIR-18-0517

129. Yamaguchi K, Ito M, Ohmura H, Hanamura F, Nakano M, Tsuchihashi K, et al. Helper T cell-dominant tertiary lymphoid structures are associated with disease relapse of advanced colorectal cancer. *Oncoimmunology* (2020) 9:1724763. doi: 10.1080/2162402X.2020.1724763

130. Peyraud F, Guegan JP, Rey C, Pulido M, Bompas E, Piperno-Neumann S, et al. High regulatory T cells infiltrate within tertiary lymphoid structure restricts response to immune checkpoint blockers in sarcomas. *Cancer Res* (2022) 82.

131. Zou X, Lin X, Cheng H, Chen Y, Wang R, Ma M, et al. Characterization of intratumoral tertiary lymphoid structures in pancreatic ductal adenocarcinoma: cellular properties and prognostic significance. *J Immunother Cancer* (2023) 11. doi: 10.1136/jitc-2023-006698

132. Tietscher S, Wagner J, Anzeneder T, Langwieder C, Rees M, Sobottka B, et al. A comprehensive single-cell map of T cell exhaustion-associated immune environments in human breast cancer. *Nat Commun* (2023) 14. doi: 10.1038/s41467-022-35238-w

133. Dieu-Nosjean MC. Good prognostic value of tertiary lymphoid structures in human lung cancer. *Ann Rheumatic Dis* (2013) 72:37–8. doi: 10.1136/annrheumdis-2013-eular.164

134. Vella G, Guelfi S, Bergers G. High endothelial venules: A vascular perspective on tertiary lymphoid structures in cancer. *Front Immunol* (2021) 12:736670. doi: 10.3389/fimmu.2021.736670

135. Fleig S, Kapanadze T, Bernier-Latmani J, Lill JK, Wyss T, Gamrekelashvili J, et al. Loss of vascular endothelial notch signaling promotes spontaneous formation of tertiary lymphoid structures. *Nat Commun* (2022) 13. doi: 10.1038/s41467-022-29701-x

136. Zhan Z, Liu SJ, Zhang YR, Liu ZL, Zhao XX, Hui D, et al. High endothelial venules proportion in tertiary lymphoid structure is a prognostic marker and correlated with anti-tumor immune microenvironment in colorectal cancer. *Ann Med* (2023) 55:114–26. doi: 10.1080/07853890.2022.2153911

137. Asrir A, Tardiveau C, Coudert J, Laffont R, Blanchard L, Bellard E, et al. Tumor-associated high endothelial venules mediate lymphocyte entry into tumors and predict response to PD-1 plus CTLA-4 combination immunotherapy. *Cancer Cell* (2022) 40:318–334 e319. doi: 10.1016/j.ccell.2022.01.002

138. Chen Z, Varney ML, Backora MW, Cowan K, Solheim JC, Talmadge JE, et al. Down-regulation of vascular endothelial cell growth factor-C expression using small interfering RNA vectors in mammary tumors inhibits tumor lymphangiogenesis and spontaneous metastasis and enhances survival. *Cancer Res* (2005) 65:9004–11. doi: 10.1158/0008-5472.CAN-05-0885

139. Roberts N, Kloos B, Cassella M, Podgrabinska S, Persaud K, Wu Y, et al. Inhibition of VEGFR-3 activation with the antagonistic antibody more potently suppresses lymph node and distant metastases than inactivation of VEGFR-2. *Cancer Res* (2006) 66:2650–7. doi: 10.1158/0008-5472.CAN-05-1843

140. Burton JB, Priceman SJ, Sung JL, Brakenhielm E, An DS, Pytowski B, et al. Suppression of prostate cancer nodal and systemic metastasis by blockade of the lymphangiogenic axis. *Cancer Res* (2008) 68:7828–37. doi: 10.1158/0008-5472.CAN-08-1488

141. Milutinovic S, Abe J, Godkin A, Stein JV, Gallimore A. The dual role of high endothelial venules in cancer progression versus immunity. *Trends Cancer* (2021) 7:214–25. doi: 10.1016/j.trecan.2020.10.001

142. Whelan TJ, Olivotto IA, Parulekar WR, Ackerman I, Chua BH, Nabid A, et al. Regional nodal irradiation in early-stage breast cancer. *N Engl J Med* (2015) 373:307–16. doi: 10.1056/NEJMoa1415340

143. Andruska N, Mahapatra L, Brenneman RJ, Huang Y, Paniello RC, Puram SV, et al. Regional lymph node irradiation in locally advanced Merkel cell carcinoma reduces regional and distant relapse and improves disease-specific survival. *Radiother Oncol* (2021) 155:246–53. doi: 10.1016/j.radonc.2020.11.003

144. Sawada J, Hiraoka N, Qi R, Jiang L, Fournier-Goss AE, Yoshida M, et al. Molecular signature of tumor-associated high endothelial venules that can predict breast cancer survival. *Cancer Immunol Res* (2022) 10:468–81. doi: 10.1158/2326-6066.CIR-21-0369

145. Zhan Z, Shi-Jin L, Yi-Ran Z, Zhi-Long L, Xiao-Xu Z, Hui D, et al. High endothelial venules proportion in tertiary lymphoid structure is a prognostic marker and correlated with anti-tumor immune microenvironment in colorectal cancer. *Ann Med* (2023) 55:114–26. doi: 10.1080/07853890.2022.2153911

146. Gobert M, Treilleux I, Bendriss-Vermare N, Bachelot T, Goddard-Leon S, Arfi V, et al. Regulatory T cells recruited through CCL22/CCR4 are selectively activated in lymphoid infiltrates surrounding primary breast tumors and lead to an adverse clinical outcome. *Cancer Res* (2009) 69:2000–9. doi: 10.1158/0008-5472.CAN-08-2360

147. Di Caro G, Bergomas F, Grizzi F, Doni A, Bianchi P, Malesci A, et al. Occurrence of tertiary lymphoid tissue is associated with T-cell infiltration and predicts better prognosis in early-stage colorectal cancers. *Clin Cancer Res* (2014) 20:2147–58. doi: 10.1158/1078-0432.CCR-13-2590

148. Hiraoka N, Ino Y, Yamazaki-Itoh R, Kanai Y, Kosuge T, Shimada K. Intratumoral tertiary lymphoid organ is a favourable prognosticator in patients with pancreatic cancer. *Br J Cancer* (2015) 112:1782–90. doi: 10.1038/bjc.2015.145

149. Pages F, Mlecnik B, Marliot F, Bindea G, Ou FS, Bifulco C, et al. International validation of the consensus Immunoscore for the classification of colon cancer: a prognostic and accuracy study. *Lancet* (2018) 391:2128–39. doi: 10.1016/S0140-6736(18)30789-X

150. Kim A, Lee SJ, Ahn J, Park WY, Shin DH, Lee CH, et al. The prognostic significance of tumor-infiltrating lymphocytes assessment with hematoxylin and eosin sections in resected primary lung adenocarcinoma. *PloS One* (2019) 14:e0224430. doi: 10.1371/journal.pone.0224430

151. Deguchi S, Tanaka H, Suzuki S, Natsuki S, Mori T, Miki Y, et al. Clinical relevance of tertiary lymphoid structures in esophageal squamous cell carcinoma. *BMC Cancer* (2022) 22:699. doi: 10.1186/s12885-022-09777-w

152. De Chaisemartin L, Goc J, Damotte D, Validire P, Magdeleinat P, Alifano M, et al. Characterization of chemokines and adhesion molecules associated with T cell presence in tertiary lymphoid structures in human lung cancer. *Cancer Res* (2011) 71:6391–9. doi: 10.1158/0008-5472.CAN-11-0952

153. Barmpoutis P, Di Capite M, Kayhanian H, Waddingham W, Alexander DC, Jansen M, et al. Tertiary lymphoid structures (TLS) identification and density assessment on H&E-stained digital slides of lung cancer. *PloS One* (2021) 16:e0256907. doi: 10.1371/journal.pone.0256907

154. Li R, Huang X, Yang W, Wang J, Liang Y, Zhang T, et al. Tertiary lymphoid structures favor outcome in resected esophageal squamous cell carcinoma. *J Pathol Clin Res* (2022) 8:422–35. doi: 10.1002/cjp2.281

155. Li Z, Jiang Y, Li B, Han Z, Shen J, Xia Y, et al. Development and validation of a machine learning model for detection and classification of tertiary lymphoid structures in gastrointestinal cancers. *JAMA Netw Open* (2023) 6:e2252553. doi: 10.1001/jamanetworkopen.2022.52553

156. Zhang C, Wang XY, Zuo JL, Wang XF, Feng XW, Zhang B, et al. Localization and density of tertiary lymphoid structures associate with molecular subtype and clinical outcome in colorectal cancer liver metastases. *J Immunother Cancer* (2023) 11. doi: 10.1136/jitc-2022-006425

157. Werner F, Wagner C, Simon M, Glatz K, Mertz KD, Laubli H, et al. A standardized analysis of tertiary lymphoid structures in human melanoma: disease progression- and tumor site-associated changes with germinal center alteration. *Front Immunol* (2021) 12:675146. doi: 10.3389/fimmu.2021.675146

158. Cabrita R, Lauss M, Sanna A, Donia M, Skaarup Larsen M, Mitra S, et al. Tertiary lymphoid structures improve immunotherapy and survival in melanoma. *Nature* (2020) 577:561–5. doi: 10.1038/s41586-019-1914-8

159. Lu H, Lou H, Wengert G, Paudel R, Patel N, Desai S, et al. Tumor and local lymphoid tissue interaction determines prognosis in high-grade serous ovarian cancer. *Cell Rep Med* (2023) 4:101092. doi: 10.1016/j.xcrm.2023.101092

160. Coppola D, Nebozhyn M, Khalil F, Dai H, Yeatman T, Loboda A, et al. Unique ectopic lymph node-like structures present in human primary colorectal carcinoma are identified by immune gene array profiling. *Am J Pathol* (2011) 179:37–45. doi: 10.1016/j.ajpath.2011.03.007

161. Zhang BX, Li H, Liu YT, Xiong D, Zhang L, Sun ZJ. Single-cell chemokine receptor profiles delineate the immune contexture of tertiary lymphoid structures in head and neck squamous cell carcinoma. *Cancer Lett* (2023) 558. doi: 10.1016/j.canlet.2023.216105

162. An Y, Sun JX, Xu MY, Xu JZ, Ma SY, Liu CQ, et al. Tertiary lymphoid structure patterns aid in identification of tumor microenvironment infiltration and selection of therapeutic agents in bladder cancer. *Front Immunol* (2022) 13:1049884. doi: 10.3389/fimmu.2022.1049884

163. Hou Y, Qiao S, Li M, Han X, Wei X, Pang Y, et al. The gene signature of tertiary lymphoid structures within ovarian cancer predicts the prognosis and immunotherapy benefit. *Front Genet* (2022) 13:1090640. doi: 10.3389/fgene.2022.1090640

164. Jiang Q, Tian C, Wu H, Min L, Chen H, Chen L, et al. Tertiary lymphoid structure patterns predicted anti-PD1 therapeutic responses in gastric cancer. *Chin J Cancer Res* (2022) 34:365–82. doi: 10.21147/j.issn.1000-9604.2022.04.05

165. Ding GY, Ma JQ, Yun JP, Chen X, Ling Y, Zhang S, et al. Distribution and density of tertiary lymphoid structures predict clinical outcome in intrahepatic cholangiocarcinoma. *J Hepatol* (2022) 76:608–18. doi: 10.1016/j.jhep.2021.10.030

166. Shang T, Jiang T, Lu T, Wang H, Cui X, Pan Y, et al. Tertiary lymphoid structures predict the prognosis and immunotherapy response of cholangiocarcinoma. *Front Immunol* (2023) 14:1166497. doi: 10.3389/fimmu.2023.1166497

167. Sofopoulos M, Fortis SP, Vaxevanis CK, Sotiriadou NN, Arnogiannaki N, Ardavanis A, et al. The prognostic significance of peritumoral tertiary lymphoid structures in breast cancer. *Cancer Immunol Immunother* (2019) 68:1733–45. doi: 10.1007/s00262-019-02407-8

168. Johansson-Percival A, He B, Li ZJ, Kjellen A, Russell K, Li J, et al. *De novo* induction of intratumoral lymphoid structures and vessel normalization enhances immunotherapy in resistant tumors. *Nat Immunol* (2017) 18:1207–17. doi: 10.1038/ni.3836

169. Munoz-Erazo L, Rhodes JL, Marion VC, Kemp RA. Tertiary lymphoid structures in cancer - considerations for patient prognosis. *Cell Mol Immunol* (2020) 17:570–5. doi: 10.1038/s41423-020-0457-0

170. Li H, Liu H, Fu H, Li J, Xu L, Wang G, et al. Peritumoral tertiary lymphoid structures correlate with protective immunity and improved prognosis in patients with hepatocellular carcinoma. *Front Immunol* (2021) 12:648812. doi: 10.3389/fimmu.2021.648812

171. Mai H, Luo J, Hoeher L, Al-Maskari R, Horvath I, Chen Y, et al. Whole-body cellular mapping in mouse using standard IgG antibodies. *Nat Biotechnol* (2023). doi: 10.1038/s41587-023-01846-0

172. Chaffer CL, Weinberg RA. A perspective on cancer cell metastasis. *Science* (2011) 331:1559–64. doi: 10.1126/science.1203543

173. Mustapha R, Ng K, Monypenny J, Ng T. Insights into unveiling a potential role of tertiary lymphoid structures in metastasis. *Front Mol Biosci* (2021) 8:661516. doi: 10.3389/fmolb.2021.661516

174. Remark R, Alifano M, Cremer I, Lupo A, Dieu-Nosjean MC, Riquet M, et al. Characteristics and clinical impacts of the immune environments in colorectal and renal cell carcinoma lung metastases: influence of tumor origin. *Clin Cancer Res* (2013) 19:4079–91. doi: 10.1158/1078-0432.CCR-12-3847

175. Meshcheryakova A, Tamandl D, Bajna E, Stift J, Mittlboeck M, Svoboda M, et al. B cells and ectopic follicular structures: novel players in anti-tumor programming with prognostic power for patients with metastatic colorectal cancer. *PloS One* (2014) 9: e99008. doi: 10.1371/journal.pone.0099008

176. Ahmed A, Halama N. Tertiary lymphoid structures in colorectal cancer liver metastases: association with immunological and clinical parameters and chemotherapy response. *Anticancer Res* (2020) 40:6367–73. doi: 10.21873/anticanres.14657

177. Montfort A, Pearce O, Maniati E, Vincent BG, Bixby L, Bohm S, et al. A strong B-cell response is part of the immune landscape in human high-grade serous ovarian metastases. *Clin Cancer Res* (2017) 23:250–62. doi: 10.1158/1078-0432.CCR-16-0081

178. Lee M, Heo SH, Song IH, Rajayi H, Park HS, Park IA, et al. Presence of tertiary lymphoid structures determines the level of tumor-infiltrating lymphocytes in primary breast cancer and metastasis. *Mod Pathol* (2019) 32:70–80. doi: 10.1038/s41379-018-0113-8

179. Karjula T, Niskakangas A, Mustonen O, Puro I, Elomaa H, Ahtiainen M, et al. Tertiary lymphoid structures in pulmonary metastases of microsatellite stable colorectal cancer. *Virchows Arch* (2023) 483:21–32. doi: 10.1007/s00428-023-03577-8

180. Waldman AD, Fritz JM, Lenardo MJ. A guide to cancer immunotherapy: from T cell basic science to clinical practice. *Nat Rev Immunol* (2020) 20:651–68. doi: 10.1038/s41577-020-0306-5

181. Sun Q, Hong Z, Zhang C, Wang L, Han Z, Ma D. Immune checkpoint therapy for solid tumours: clinical dilemmas and future trends. *Signal Transduct Target Ther* (2023) 8:320. doi: 10.1038/s41392-023-01522-4

182. Pagliaro LC, Williams DL, Daliani D, Williams MB, Osai W, Kincaid M, et al. Neoadjuvant paclitaxel, ifosfamide, and cisplatin chemotherapy for metastatic penile cancer: a phase II study. *J Clin Oncol* (2010) 28:3851–7. doi: 10.1200/JCO.2010.29.5477

183. Yan X, Duan H, Ni Y, Zhou Y, Wang X, Qi H, et al. Tislelizumab combined with chemotherapy as neoadjuvant therapy for surgically resectable esophageal cancer: A prospective, single-arm, phase II study (TD-NICE). *Int J Surg* (2022) 103:106680. doi: 10.1016/j.ijsu.2022.106680

184. Zhang Z, Wu B, Peng G, Xiao G, Huang J, Ding Q, et al. Neoadjuvant chemoimmunotherapy for the treatment of locally advanced head and neck squamous cell carcinoma: A single-arm phase 2 clinical trial. *Clin Cancer Res* (2022) 28:3268–76. doi: 10.1158/1078-0432.CCR-22-0666

185. Chen X, Xu X, Wang D, Liu J, Sun J, Lu M, et al. Neoadjuvant sintilimab and chemotherapy in patients with potentially resectable esophageal squamous cell carcinoma (KEEP-G 03): an open-label, single-arm, phase 2 trial. *J Immunother Cancer* (2023) 11. doi: 10.1136/jitc-2022-005830

186. Birtle A, Johnson M, Chester J, Jones R, Dolling D, Bryan RT, et al. Adjuvant chemotherapy in upper tract urothelial carcinoma (the POUT trial): a phase 3, open-label, randomised controlled trial. *Lancet* (2020) 395:1268–77. doi: 10.1016/S0140-6736(20)30415-3

187. Luke JJ, Rutkowski P, Queirolo P, Del Vecchio M, Mackiewicz J, Chiarion-Sileni V, et al. Pembrolizumab versus placebo as adjuvant therapy in completely resected stage IIB or IIC melanoma (KEYNOTE-716): a randomised, double-blind, phase 3 trial. *Lancet* (2022) 399:1718–29. doi: 10.1016/S0140-6736(22)00562-1

188. Powles T, Tomczak P, Park SH, Venugopal B, Ferguson T, Symeonides SN, et al. Pembrolizumab versus placebo as post-nephrectomy adjuvant therapy for clear cell renal cell carcinoma (KEYNOTE-564): 30-month follow-up analysis of a multicentre, randomised, double-blind, placebo-controlled, phase 3 trial. *Lancet Oncol* (2022) 23:1133–44. doi: 10.1016/S1470-2045(22)00487-9

189. Lu Y, Zhao Q, Liao JY, Song E, Xia Q, Pan J, et al. Complement signals determine opposite effects of B cells in chemotherapy-induced immunity. *Cell* (2020) 180:1081–1097 e1024. doi: 10.1016/j.cell.2020.02.015

190. Van Dijk N, Gil-Jimenez A, Silina K, Hendricksen K, Smit LA, De Feijter JM, et al. Preoperative ipilimumab plus nivolumab in locoregionally advanced urothelial cancer: the NABUCCO trial. *Nat Med* (2020) 26:1839–44. doi: 10.1038/s41591-020-1085-z

191. Lutz ER, Wu AA, Bigelow E, Sharma R, Mo G, Soares K, et al. Immunotherapy converts nonimmunogenic pancreatic tumors into immunogenic foci of immune regulation. *Cancer Immunol Res* (2014) 2:616–31. doi: 10.1158/2326-6066.CIR-14-0027

192. Maldonado L, Teague JE, Morrow MP, Jotova I, Wu TC, Wang C, et al. Intramuscular therapeutic vaccination targeting HPV16 induces T cell responses that localize in mucosal lesions. *Sci Transl Med* (2014) 6:221ra213. doi: 10.1126/scitranslmed.3007323

193. Cottrell TR, Thompson ED, Forde PM, Stein JE, Duffield AS, Anagnostou V, et al. Pathologic features of response to neoadjuvant anti-PD-1 in resected non-small-cell lung carcinoma: a proposal for quantitative immune-related pathologic response criteria (irPRC). *Ann Oncol* (2018) 29:1853–60. doi: 10.1093/annonc/mdy218

194. Van Dijk N, Gil-Jimenez A, Silina K, Van Montfoort ML, Einerhand S, Jonkman L, et al. The tumor immune landscape and architecture of tertiary lymphoid structures in urothelial cancer. *Front Immunol* (2021) 12:793964. doi: 10.3389/fimmu.2021.793964

195. Ryan ST, Zhang J, Burner DN, Liss M, Pittman E, Muldong M, et al. Neoadjuvant rituximab modulates the tumor immune environment in patients with high risk prostate cancer. *J Transl Med* (2020) 18:214. doi: 10.1186/s12967-020-02370-4

196. Campbell MT, Matin SF, Tam AL, Sheth RA, Ahrar K, Tidwell RS, et al. Pilot study of Tremelimumab with and without cryoablation in patients with metastatic renal cell carcinoma. *Nat Commun* (2021) 12:6375. doi: 10.1038/s41467-021-26415-4

197. Ho WJ, Zhu Q, Durham J, Popovic A, Xavier S, Leatherman J, et al. Neoadjuvant cabozantinib and nivolumab converts locally advanced HCC into resectable disease with enhanced antitumor immunity. *Nat Cancer* (2021) 2:891–903. doi: 10.1038/s43018-021-00234-4

198. Chen S, Xie P, Cowan M, Huang H, Cardenas H, Keathley R, et al. Epigenetic priming enhances antitumor immunity in platinum-resistant ovarian cancer. *J Clin Invest* (2022) 132. doi: 10.1172/JCI158800

199. Carril-Ajuria L, Desnoyer A, Meylan M, Dalban C, Naigeon M, Cassard L, et al. Baseline circulating unswitched memory B cells and B-cell related soluble factors are associated with overall survival in patients with clear cell renal cell carcinoma treated with nivolumab within the NIVOREN GETUG-AFU 26 study. *J Immunother Cancer* (2022) 10. doi: 10.1136/jitc-2022-004885

200. Cascone T, Leung CH, Weissferdt A, Pataer A, Carter BW, Godoy MCB, et al. Neoadjuvant chemotherapy plus nivolumab with or without ipilimumab in operable non-small cell lung cancer: the phase 2 platform NEOSTAR trial. *Nat Med* (2023) 29:593–604. doi: 10.1038/s41591-022-02189-0

201. Lee HS, Jang HJ, Ramineni M, Wang DY, Ramos D, Choi JM, et al. A Phase II Window of Opportunity Study of Neoadjuvant PD-L1 versus PD-L1 plus CTLA-4 Blockade for Patients with Malignant Pleural Mesothelioma. *Clin Cancer Res* (2023) 29:548–59. doi: 10.1158/1078-0432.CCR-22-2566

202. Nabbi A, Danesh A, Espin-Garcia O, Pedersen S, Wellum J, Fu LH, et al. Multimodal immunogenomic biomarker analysis of tumors from pediatric patients enrolled to a phase 1-2 study of single-agent atezolizumab. *Nat Cancer* (2023) 4:502–15. doi: 10.1038/s43018-023-00534-x

203. Davies E, Dong M, Gutekunst M, Narhi K, Van Zoggel H, Blom S, et al. Capturing complex tumour biology in *vitro*: histological and molecular characterisation of precision cut slices. *Sci Rep* (2015) 5. doi: 10.1038/srep17187

204. Carter EP, Roozitalab R, Gibson SV, Grose RP. Tumour microenvironment 3D-modelling: simplicity to complexity and back again. *Trends Cancer* (2021) 7:1033–46. doi: 10.1016/j.trecan.2021.06.009

205. Pape J, Emberton M, Cheema U. 3D cancer models: the need for a complex stroma, compartmentalization and stiffness. *Front Bioengineering Biotechnol* (2021) 9. doi: 10.3389/fbioe.2021.660502

206. Farin HF, Mosa MH, Ndreshkjana B, Grebbin BM, Ritter B, Menche C, et al. Colorectal cancer organoid-stroma biobank allows subtype-specific assessment of individualized therapy responses. *Cancer Discovery* (2023) 13(10):2192–2211. doi: 10.1158/2159-8290.CD-23-0050

207. Mcgranahan N, Furness AJ, Rosenthal R, Ramskov S, Lyngaa R, Saini SK, et al. Clonal neoantigens elicit T cell immunoreactivity and sensitivity to immune checkpoint blockade. *Science* (2016) 351:1463–9. doi: 10.1126/science.aaf1490

208. Boumelha J, De Carne Trecesson S, Law EK, Romero-Clavijo P, Coelho MA, Ng KW, et al. An immunogenic model of KRAS-mutant lung cancer enables evaluation of

targeted therapy and immunotherapy combinations. *Cancer Res* (2022) 82:3435–48. doi: 10.1158/0008-5472.CAN-22-0325

209. Ng KW, Boumelha J, Enfield KSS, Almagro J, Cha HG, Pich O, et al. Antibodies against endogenous retroviruses promote lung cancer immunotherapy. *Nature* (2023) 616:563–573. doi: 10.1038/s41586-023-05771-9

210. Turnquist HR, Lin X, Ashour AE, Hollingsworth MA, Singh RK, Talmadge JE, et al. CCL21 induces extensive intratumoral immune cell infiltration and specific anti-tumor cellular immunity. *Int J Oncol* (2007) 30:631–9. doi: 10.3892/ijo.30.3.631

211. Schrama D, Voigt H, Eggert AO, Xiang R, Zhou H, Schumacher TN, et al. Immunological tumor destruction in a murine melanoma model by targeted LTalpha independent of secondary lymphoid tissue. *Cancer Immunol Immunother* (2008) 57:85–95. doi: 10.1007/s00262-007-0352-x

212. Jackson EL, Willis N, Mercer K, Bronson RT, Crowley D, Montoya R, et al. Analysis of lung tumor initiation and progression using conditional expression of oncogenic K-ras. *Genes Dev* (2001) 15:3243–8. doi: 10.1101/gad.943001

213. Jackson EL, Olive KP, Tuveson DA, Bronson R, Crowley D, Brown M, et al. The differential effects of mutant p53 alleles on advanced murine lung cancer. *Cancer Res* (2005) 65:10280–8. doi: 10.1158/0008-5472.CAN-05-2193

214. Dupage M, Dooley AL, Jacks T. Conditional mouse lung cancer models using adenoviral or lentiviral delivery of Cre recombinase. *Nat Protoc* (2009) 4:1064–72. doi: 10.1038/nprot.2009.95

215. Schrama D, Straten PT, Fischer WH, Mclellan AD, Brocker EB, Reisfeld RA, et al. Targeting of lymphotoxin-alpha to the tumor elicits an efficient immune response associated with induction of peripheral lymphoid-like tissue. *Immunity* (2001) 14:111–21. doi: 10.1016/S1074-7613(01)00094-2

216. Fidler IJ. Metastasis: quantitative analysis of distribution and fate of tumor emboli labeled with 125 I-5-iodo-2'-deoxyuridine. *J Natl Cancer Inst* (1970) 45:773–82. doi: 10.1093/jnci/45.4.773

217. Overwijk WW, Restifo NP. B16 as a mouse model for human melanoma. *Curr Protoc Immunol* (2001) Chapter 20:Unit 20 21. doi: 10.1002/0471142735.im2001s39

218. Hingorani SR, Petricoin EF, Maitra A, Rajapakse V, King C, Jacobetz MA, et al. Preinvasive and invasive ductal pancreatic cancer and its early detection in the mouse. *Cancer Cell* (2003) 4:437–50. doi: 10.1016/S1535-6108(03)00309-X

219. Hingorani SR, Wang L, Multani AS, Combs C, Deramaudt TB, Hruban RH, et al. Trp53R172H and KrasG12D cooperate to promote chromosomal instability and widely metastatic pancreatic ductal adenocarcinoma in mice. *Cancer Cell* (2005) 7:469–83. doi: 10.1016/j.ccr.2005.04.023

220. Spear S, Candido JB, Mcdermott JR, Ghirelli C, Maniati E, Beers SA, et al. Discrepancies in the tumor microenvironment of spontaneous and orthotopic murine models of pancreatic cancer uncover a new immunostimulatory phenotype for B cells. *Front Immunol* (2019) 10:542. doi: 10.3389/fimmu.2019.00542

221. Tseng WW, Winer D, Kenkel JA, Choi O, Shain AH, Pollack JR, et al. Development of an orthotopic model of invasive pancreatic cancer in an immunocompetent murine host. *Clin Cancer Res* (2010) 16:3684–95. doi: 10.1158/1078-0432.CCR-09-2384

222. Castino GF, Cortese N, Capretti G, Serio S, Di Caro G, Mineri R, et al. Spatial distribution of B cells predicts prognosis in human pancreatic adenocarcinoma. *Oncoimmunology* (2016) 5. doi: 10.1080/2162402X.2015.1085147

223. Drayton DL, Ying X, Lee J, Lesslauer W, Ruddle NH. Ectopic LT alpha beta directs lymphoid organ neogenesis with concomitant expression of peripheral node addressin and a HEV-restricted sulfotransferase. *J Exp Med* (2003) 197:1153–63. doi: 10.1084/jem.20021761

224. Huang YK, Chen Y, Zhou SL, Chen L, Wang JH, Pei YY, et al. Dual-mechanism based CTLs infiltration enhancement initiated by Nano-sapper potentiates immunotherapy against immune-excluded tumors. *Nat Commun* (2020) 11. doi: 10.1038/s41467-020-14425-7

225. Jia W, Zhang T, Yao Q, Li J, Nie Y, Lei X, et al. Tertiary lymphatic structures in primary hepatic carcinoma: controversy cannot overshadow hope. *Front Immunol* (2022) 13:870458. doi: 10.3389/fimmu.2022.870458

226. Wang X, Asami S, Kitamura D. A novel cancer immunotherapy using tumor-infiltrating B cells in the APCmin/+ mouse model. *PloS One* (2021) 16:e0245608. doi: 10.1371/journal.pone.0245608

227. Neufert C, Heichler C, Brabletz T, Scheibe K, Boonsanay V, Greten FR, et al. Inducible mouse models of colon cancer for the analysis of sporadic and inflammation-driven tumor progression and lymph node metastasis. *Nat Protoc* (2021) 16:61–85. doi: 10.1038/s41596-020-00412-1

228. Wirtz S, Neufert C, Weigmann B, Neurath MF. Chemically induced mouse models of intestinal inflammation. *Nat Protoc* (2007) 2:541–6. doi: 10.1038/nprot.2007.41

229. Overacre-Delgoffe AE, Bumgarner HJ, Cillo AR, Burr AHP, Tometich JT, Bhattacharjee A, et al. Microbiota-specific T follicular helper cells drive tertiary lymphoid structures and anti-tumor immunity against colorectal cancer. *Immunity* (2021) 54:2812–2824 e2814. doi: 10.1016/j.immuni.2021.11.003

230. Varga J, Nicolas A, Petrocelli V, Pesic M, Mahmoud A, Michels BE, et al. AKT-dependent NOTCH3 activation drives tumor progression in a model of mesenchymal colorectal cancer. *J Exp Med* (2020) 217. doi: 10.1084/jem.20191515

231. Kucukkose E, Heesters BA, Villaudy J, Verheem A, Cercel M, Van Hal S, et al. Modeling resistance of colorectal peritoneal metastases to immune checkpoint blockade in humanized mice. *J Immunotherapy Cancer* (2022) 10. doi: 10.1136/jitc-2022-005345

232. Guy CT, Cardiff RD, Muller WJ. Induction of mammary tumors by expression of polyomavirus middle T oncogene: a transgenic mouse model for metastatic disease. *Mol Cell Biol* (1992) 12:954–61. doi: 10.1128/mcb.12.3.954-961.1992

233. Attalla S, Taifour T, Bui T, Muller W. Insights from transgenic mouse models of PyMT-induced breast cancer: recapitulating human breast cancer progression in *vivo*. *Oncogene* (2021) 40:475–91. doi: 10.1038/s41388-020-01560-0

234. Allen E, Jabouille A, Rivera LB, Lodewijckx I, Missiaen R, Steri V, et al. Combined antiangiogenic and anti-PD-L1 therapy stimulates tumor immunity through HEV formation. *Sci Transl Med* (2017) 9. doi: 10.1126/scitranslmed.aak9679

235. Rao T, Ranger JJ, Smith HW, Lam SH, Chodosh L, Muller WJ. Inducible and coupled expression of the polyomavirus middle T antigen and Cre recombinase in transgenic mice: an in *vivo* model for synthetic viability in mammary tumour progression. *Breast Cancer Res* (2014) 16:R11. doi: 10.1186/bcr3603

236. Sekar D, Govene L, Del Rio ML, Sirait-Fischer E, Fink AF, Brune B, et al. Downregulation of BTLA on NKT cells promotes tumor immune control in a mouse model of mammary carcinoma. *Int J Mol Sci* (2018) 19. doi: 10.3390/ijms19030752

237. Sirait-Fischer E, Olesch C, Fink AF, Berkefeld M, Huard A, Schmid T, et al. Immune checkpoint blockade improves chemotherapy in the PyMT mammary carcinoma mouse model. *Front Oncol* (2020) 10:1771. doi: 10.3389/fonc.2020.01771

238. Dankort D, Curley DP, Cartlidge RA, Nelson B, Karnezis AN, Damsky WE Jr., et al. Braf(V600E) cooperates with Pten loss to induce metastatic melanoma. *Nat Genet* (2009) 41:544–52. doi: 10.1038/ng.356

239. Hooijkaas AI, Gadiot J, van der Valk M, Mooi WJ, Blank CU. Targeting BRAFV600E in an inducible murine model of melanoma. *Am J Pathol* (2012) 181:785–94. doi: 10.1016/j.ajpath.2012.06.002

240. Shabaneh TB, Molodtsov AK, Steinberg SM, Zhang P, Torres GM, Mohamed GA, et al. Oncogenic BRAF(V600E) governs regulatory T-cell recruitment during melanoma tumorigenesis. *Cancer Res* (2018) 78:5038–49. doi: 10.1158/0008-5472.CAN-18-0365

241. Iwai Y, Ishida M, Tanaka Y, Okazaki T, Honjo T, Minato N. Involvement of PD-L1 on tumor cells in the escape from host immune system and tumor immunotherapy by PD-L1 blockade. *Proc Natl Acad Sci United States America* (2002) 99:12293–7. doi: 10.1073/pnas.192461099

242. Rodriguez AB, Peske JD, Engelhard VH. Identification and characterization of tertiary lymphoid structures in murine melanoma. *Methods Mol Biol* (2018) 1845:241–57. doi: 10.1007/978-1-4939-8709-2_14

243. Shields JD, Kourtis IC, Tomei AA, Roberts JM, Swartz MA. Induction of lymphoidlike stroma and immune escape by tumors that express the chemokine CCL21. *Science* (2010) 328:749–52. doi: 10.1126/science.1185837

244. Ebert PJR, Cheung J, Yang Y, Mcnamara E, Hong R, Moskalenko M, et al. MAP kinase inhibition promotes T cell and anti-tumor activity in combination with PD-L1 checkpoint blockade. *Immunity* (2016) 44:609–21. doi: 10.1016/j.immuni.2016.01.024

245. Huang KW, Tan CP, Reebye V, Chee CE, Zacharoulis D, Habib R, et al. MTL-CEBPA combined with immunotherapy or RFA enhances immunological anti-tumor response in preclinical models. *Int J Mol Sci* (2021) 22. doi: 10.3390/ijms22179168

246. Yin X, Wang H, Li R, Song X, Zhang T, Liang Y, et al. Tobacco exposure primes the secretion of CCL21 positively associated with tertiary lymphoid structure and response to immunotherapy. *J Immunother Cancer* (2023) 11. doi: 10.1136/jitc-2023-006939

247. Silina K, Soltermann A, Attar FM, Casanova R, Uckeley ZM, Thut H, et al. Germinal centers determine the prognostic relevance of tertiary lymphoid structures and are impaired by corticosteroids in lung squamous cell carcinoma. *Cancer Res* (2018) 78:1308–20. doi: 10.1158/0008-5472.CAN-17-1987

248. Felix J, Savvides SN. Mechanisms of immunomodulation by mammalian and viral decoy receptors: insights from structures. *Nat Rev Immunol* (2017) 17:112–29. doi: 10.1038/nri.2016.134

frontiers | Frontiers in Immunology

TYPE Original Research
PUBLISHED 14 December 2023
DOI 10.3389/fimmu.2023.1244256

OPEN ACCESS

EDITED BY
Ying Ma,
Tianjin Medical University Cancer Institute and Hospital, China

REVIEWED BY
Pei Yang,
Central South University, China
Yaping Xu,
Tongji University, China

*CORRESPONDENCE
Shuanghu Yuan
yuanshuanghu@sina.com

RECEIVED 22 June 2023
ACCEPTED 01 December 2023
PUBLISHED 14 December 2023

CITATION
Xu F, Zhu H, Dong Y, Li L, Liu N and Yuan S (2023) Combined inflammatory parameters and tertiary lymphoid structure predict prognosis in patients with resectable non-small cell lung cancer treated with neoadjuvant chemoimmunotherapy. *Front. Immunol.* 14:1244256. doi: 10.3389/fimmu.2023.1244256

Combined inflammatory parameters and tertiary lymphoid structure predict prognosis in patients with resectable non-small cell lung cancer treated with neoadjuvant chemoimmunotherapy

Fuhao Xu[1], He Zhu[1], Yinjun Dong[2], Li Li[1], Ning Liu[1] and Shuanghu Yuan[1*]

[1]Department of Radiation Oncology, Shandong Cancer Hospital and Institute, Shandong First Medical University and Shandong Academy of Medical Sciences, Shandong Cancer Hospital Affiliated to Shandong First Medical University, Jinan, China, [2]Department of Thoracic Surgery, Shandong Cancer Hospital and Institute Shandong First Medical University and Shandong Academy of Medical Sciences, Jinan, China

Introduction: Neoadjuvant chemoimmunotherapy shows great potential for patients with non-small cell lung cancer (NSCLC), but no clear prognostic markers have been identified. This study investigates the correlation between inflammatory parameters and the expression of tertiary lymphoid structures (TLS) and the predictive ability of inflammatory parameters combined with TLS for disease-free survival (DFS) in patients with resectable NSCLC receiving neoadjuvant chemotherapy.

Materials and methods: We retrospectively analyzed the clinical data and hematological parameters of 117 patients with NSCLC who underwent neoadjuvant chemoimmunotherapy and radical surgery. TLS were evaluated by observing H&E stained and immunohistochemically stained tissue sections. Univariate chi-square and multifactor logistic analyses were used to determine the correlation between hematological parameters and TLS. The Kaplan–Meier method, univariate and multivariate Cox regression analysis and constructed nomogram models were used to assess the prognostic value of the investigated parameters on DFS. Receiver operating characteristic (ROC) curves analyses were used to compare the performances of the three models.

Results: After logistic analysis, it was found that platelet-to-lymphocyte ratio (PLR) ≤288.78 (odds ratio OR=0.122, P=0.009) was an independent predictor of high TLS expression. The Cox regression analyses showed that Histology (HR=0.205, P=0.002), systemic immune inflammation index (SII) (HR=2.758, P=0.042) and TLS (HR=0.057, P<0.05) were independent prognostic factors in patients with NSCLC. The combined SII-TLS model was better than the

single-indicator model in assessing the 1-year and 18-months DFS rates in patients with NSCLC.

Conclusion: Our study showed that PLR was an independent predictor of TLS and that both TLS and SII predicted prognosis in patients with neoadjuvant chemoimmunotherapy-resectable NSCLC; however, combining SII and TLS to assess DFS was more accurate than using either parameter alone.

KEYWORDS

inflammatory parameter, tertiary lymphoid structure, tumor immune microenvironment, immunotherapy, non-small cell lung cancer, prognosis

Introduction

Lung cancer is a global health problem. Approximately 80-85% of lung cancer cases are non-small cell lung cancers (NSCLCs). The latest global cancer statistics indicate that over two million people are newly diagnosed with lung cancer each year. Moreover, recently, lung cancer has become one of the leading causes of cancer-related deaths worldwide (1, 2). Tumor immunotherapy has become one of the most successful approaches in cancer treatment in recent years (3). Immunotherapies for tumors, such as immune checkpoint blockade (ICB), can relieve tumor tolerance to immunity and allow immune cells to recognize and kill the tumor cells. Several ICBs currently undergoing basic and clinical research. Among them, inhibitors targeting the immune checkpoint programmed cell death protein 1 (PD-1) molecule are at the forefront of immunotherapy (4).

The tumor immune microenvironment refers to the microenvironment surrounding a tumor and consists tumor, immune, and mesenchymal cells. Numerous studies have shown that the tumor immune microenvironment has a crucial role in immunotherapy (5). Tertiary lymphoid structures (TLSs) are structured aggregates of immune cells that form in non-lymphoid tissues after birth and are important components of the tumor immune microenvironment (6). TLSs are usually associated with a positive prognosis in most cancer types, and their prognostic value is independent of TNM stage. TLSs have also been shown to be associated with tumor development and progression in certain cancer types (6). A recent study examined on-treatment tumor samples and discovered that ICB treatment stimulates the development of TLSs and that TLSs contribute to the clinical response to immune checkpoint blocking. After neoadjuvant immunotherapy for melanoma and uroepithelial carcinoma, patients who showed immunotherapeutic effects had higher numbers of TLS-associated immune cells in their tumors than before (7). In addition, an increase in the number of TLSs was observed in lesions after neoadjuvant PD-1 blocker treatment for NSCLC (8).

TLSs form in tissues in response to inflammation, require a continuous inflammatory environment to be maintained, and share some structural similarities with lymph nodes; however, TLSs lack a surrounding sealing structure. This structural characteristic may allow cellular components to permeate the surrounding tissues directly, increasing the possibility that immune cells will be affected by components of the inflammatory environment (9). However, not all inflammatory stimuli drive the formation of TLSs, which may depend on specific microenvironmental components. The Systemic Immune Inflammatory Index (SII) is based on a prognostic score of inflammation and immunity, which is calculated as platelet count*neutrophil count/lymphocyte count. The SII, neutrophil-to-lymphocyte ratio (NLR), lymphocyte-to-monocyte ratio (LMR), and platelet-to-lymphocyte ratio (PLR), which reflect the balance between inflammatory factors and immunity in the body, have been shown to be effective in predicting patient prognosis (10–12). This finding indicates that the state of the tumor inflammatory microenvironment may be closely linked to the antitumor immune response and has an important impact on the prognosis of patients with NSCLC.

Despite effective surgical treatment, a proportion of patients with resectable stage IB–IIIA NSCLC still have poor prognosis due to recurrence. Neoadjuvant chemotherapy has shown substantial potential in this group of patients. The use of 2-4 cycles of neoadjuvant immunotherapy combined with platinum-based and paclitaxel-liked chemotherapy before surgery can improve long-term survival, reduce tumor stage, improve resection rates, and provide timely management of micrometastases. Results of the CheckMate-816 phase III trial showed a significant improvement in 3-year disease-free survival with 2-4 cycles of preoperative Nivolumab in combination with chemotherapy compared to surgery alone (63% vs 50%) (13). However, to date, no clear predictive prognostic markers for neoadjuvant chemoimmunotherapy have been identified.

Therefore, this study investigated the effect of hematological parameters (SII, PLR, NLR, and LMR), which represent the inflammatory state of the tumor microenvironment, on TLSs and compared the predictive ability of these hematological parameters, TLSs, and hematological parameters combined with that of TLS alone on disease-free survival (DFS) in patients with NSCLC treated with

neoadjuvant chemoimmunotherapy. Notably, our results provide an accurate model for predicting the prognosis of patients with NSCLC treated with neoadjuvant chemoimmunotherapy.

Materials and methods

Patients and samples

We retrospectively evaluated 117 patients with NSCLC diagnosed *via* surgical pathology at the Shandong Cancer Hospital between January 2020 and June 2022. All patients were driver gene negative and had not received targeted therapy. All patients underwent radical surgery and received at least two cycles of preoperative neoadjuvant therapy. Specific medications: PD-1 ICBs (Pembrolizumab, Sintilimab, Tislelizumab, Camrelizumab) combined with platinum-based drugs (Cisplatin, Carboplatin) and paclitaxel drugs (nab-paclitaxel) or pemetrexed disodium. Administered intravenously on day 1 of a 21-day cycle. R0 resection was obtained in all patients. For early-stage patients, we performed regular follow-up after surgery. For patients with advanced stage and high risk of recurrence factors, we performed immune maintenance therapy after surgery (limited to PD-L1 TC ≥1%). Patients with active autoimmune disease; a previous history of autoimmune disease; or congenital or acquired immune deficiency, such as human immunodeficiency virus infection, active hepatitis B, or hepatitis C, were excluded from the study. The included patients underwent regular follow-up at the outpatient clinic every 3–6 months for 2 years after surgery and annually thereafter. The time of postoperative pathological diagnosis was used as the starting point for observation, and each patient was followed up periodically by outpatient review and telephone until disease progression or death, with a final follow-up date of May 22, 2023. Written informed consents were provided by all participants. It was carried out in accordance with the Helsinki Declaration and approved by the Ethics Review Committee of Shandong Cancer Hospital in China. (SDTHEC2022010006). The process of patient screening is shown in Figure 1.

Data collection

Tissue wax blocks, general clinical data, postoperative pathological data, and laboratory test results, such as routine blood within one week before neoadjuvant immune combination chemotherapy, were collected from patients with NSCLC who met the enrollment criteria by reviewing medical records. The primary data included patient sex, age, type of pathology, TNM stage, neutrophil, monocyte, lymphocyte, and platelet counts. On the basis of the eighth edition of the AJCC cancer staging system, NSCLCs were staged. The tissue wax blocks used in this study were obtained from the Department of Pathology at Shandong Cancer Hospital.

Histopathological analysis

Two or three sections were prepared from each wax block. Sections were stained using hematoxylin and eosin (HE), and the abundance of TLSs in the tumor tissue was scored as 0, 1, or 2: (a) a score of 0 indicates no TLS; (b) a score of 1 indicates that the tumor has less than three TLSs; and (c) a score of 2 indicates that the tumor has at least three TLSs. Based on previous studies, we defined TLSs with active germinal centers (GC) as fully mature secondary follicle-like TLSs (14). We defined patients with an abundance score of 2 and mature TLS as TLS(+) or otherwise as TLS (–). We evaluated the TLSs to an extent of 3 mm at the intertumoral and peritumoral locations. Sections were stained with anti-human

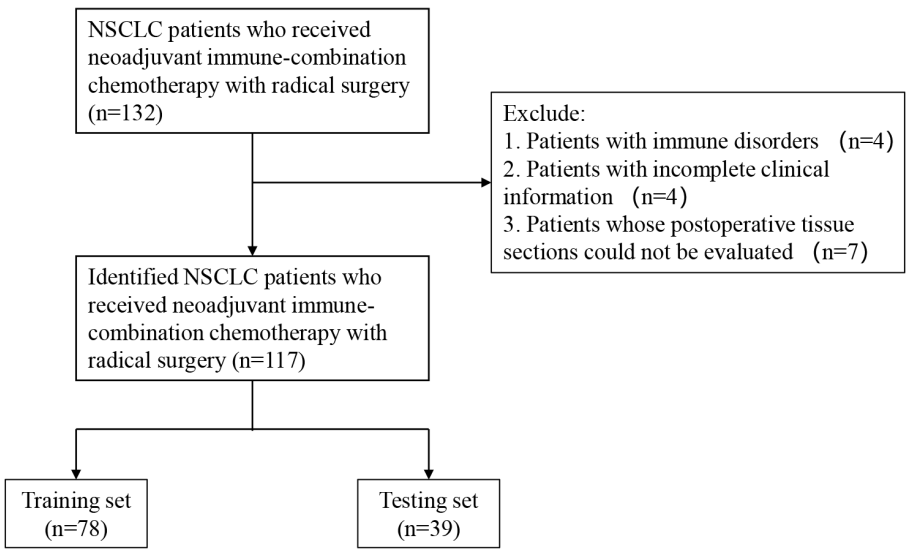

FIGURE 1
Flow chart for the inclusion and exclusion of NSCLC patients and analysis of tumor information. NSCLC, non-small-cell lung cancer.

antibodies against *CD3*, *CD20*, and *CD21* to validate the presence of TLS through T, B, and follicular dendritic cells. TLSs scores were independently assessed by two senior pathologists under double-blind conditions for outcome assessment, and when the pathologist scores differed, the higher score was used.

Statistical analysis

DFS was calculated as the time between postoperative pathological diagnosis and disease progression or death due to NSCLC. Major pathologic response (MPR) was defined as the presence of ≤10% residual tumor cells in the surgical resection specimen, while the non-MPR group included patients who did not achieve MPR. Statistical analyses were performed using RStudio and SPSS software version 25.0. Receiver operating characteristic (ROC) curves and Jamovi statistical software version 2.3.21 were used to determine the optimal cutoff values for blood parameters (SII, PLR, LMR, and NLR). Chi-square and multifactorial binary logistic analyses were used to determine the correlation between blood parameters and TLSs, and Cox proportional hazards regression analysis was used to determine the indicators associated with DFS. DFS was compared using the Kaplan–Meier method, and survival curves were compared using the log-rank test. Differences with p values <0.05 were considered statistically significant. Based on the independent predictors identified, the patients were divided into training and validation sets at a ratio of 2:1. Furthermore, using R language statistical software, nomogram models were constructed to predict DFS based on SII, TLS, and SII combined with TLS. In addition, ROC curves analyses were used to compare the performances of the three models.

Results

Patient characteristics

A total of 117 patients with NSCLC who received neoadjuvant chemo-immunotherapy and underwent radical surgery, were included in the study (96(82.1%) male). The median age at diagnosis was 63 (44–102) years, and the median follow-up duration was 15.5 months. Additionally, 71 (60.7%) patients had squamous cell carcinoma and 46 (39.3%) had adenocarcinoma. Among all patients, 14 (12.0%), 38 (32.5%), and 65 (55.5%) patients scored 0, 1, and 2, respectively, for TLS abundance. By observation, 77 (65.8%) patients had mature TLSs; maturation states are shown in Figure 2. Fifty-eight (49.6%) patients had TLS (+). Other clinical characteristics are shown in Supplementary Table 1.

Systemic inflammation parameters with TLS

The ROC curve analysis was used to determine the optimal cutoff values for the SII, NLR, PLR, and LMR before treatment. This value was used as the threshold value to group inflammatory indicators (Supplementary Table 2). The TLS (+) and TLS (–) subgroups were compared according to cut-off values to investigate the relationship between inflammatory parameters and TLSs. The univariate chi-square analysis indicated that the NLR ($\chi 2$ = 7.873, P=0.005), and PLR ($\chi 2$ = 13.835, P<0.001) significantly correlated with the TLS expression profile. Further inclusion of NLR and PLR in a multifactorial binary logistic analysis revealed that PLR (OR=0.122, 95% CI=0.025-0.592, P=0.009) was an independent predictor of TLS expression level, PLR ≤ 288.78 was considered a protective factor for high TLS expression; lower PLR suggested high TLS expression level (Table 1).

Association between tertiary lymphoid structures and neoadjuvant therapy efficacy and prognosis in NSCLC

TLSs were more readily observed in patients responsive to neoadjuvant immune-chemotherapy; however, were rarely found in non-responders (Figure 3A). Based on the pathological response after treatment, patients with NSCLC were divided into MPR and non-MPR groups. Kaplan-Meier survival curves showed significantly improved DFS in the MPR group compared to the non-MPR group (P=0.019), demonstrating an association between tumor regression induced by neoadjuvant therapy and DFS (Figure 3B). Additionally, the TLS (+) group demonstrated markedly improved DFS compared to the TLS (–) group (P<0.01), validating the advantageous prognostic value of TLSs in NSCLC patients (Figure 3C).

Prognostic survival analysis combining systemic inflammation parameters with TLS

Based on the DFS durations, the optimal cutoff values for inflammatory parameters in patients with NSCLC were determined (SII=1014, PLR=175, LMR=2.22, NLR=3.21) (15). As a result, patients were divided into groups with high and low inflammatory parameters according to the optimal cut-off values. A statistically significant difference in survival between the high and low inflammatory parameters groups was found using Kaplan–Meier survival curves for SII (P<0.01), NLR (P<0.01), PLR (P<0.01) and LMR (P<0.01) groups (Figure 4). In the univariate Cox regression analysis of NSCLC, age, sex, smoking history, T stage, N stage, histology, systemic inflammation parameters, and TLS expression were included. Age, histology, T stage, NLR, PLR, SII, LMR and TLS affected DFS (Table 2). A multivariate Cox regression analysis was subsequently performed; histology, (HR=0.205, P=0.002), SII (HR=2.758, P=0.042) and TLS (HR=0.057, P<0.05) were independent prognostic factors for patients with NSCLC receiving neoadjuvant chemo-immunotherapy (Table 2).

Comparison of nomogram prognostic models

The training set of the combined model included 78 patients, while the validation set included 39 patients. There were no

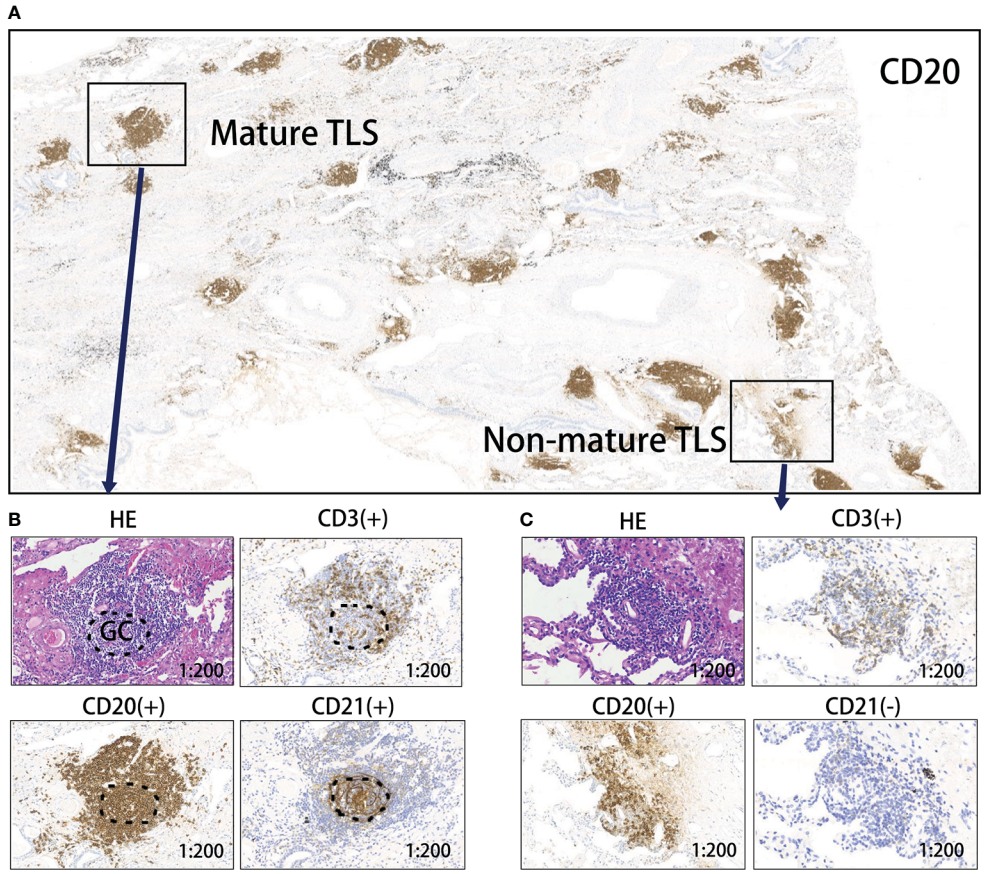

FIGURE 2
Levels of TLS maturity. **(A)** Representative image of CD20 staining of TLSs in a responder after neoadjuvant treatment. **(B)** Mature TLS, dense lymphocytic aggregates (CD3+, CD20+) with follicular dendritic cells (CD21+); **(C)** Immature TLS, dense lymphocytic aggregates (CD3+, CD20+) without follicular dendritic cells (CD21-). TLS, tertiary lymphoid structure; GC, germinal center.

TABLE 1 Univariate and multivariate logistic analyses on inflammatory parameters and the expression profile of TLSs.

Variable	TLS+ (n=58)	TLS-(n=59)	Univariate analysis		Multivariate analysis	
			χ^2	*P*	*P*	*OR (95%CI)*
SII						
≤822.63	40	32	2.681	0.102		
>822.63	18	27				
NLR						
≤3.59	44	30	7.873	0.005	0.168	0.543(0.228-1.292)
>3.59	14	29				
PLR						
≤288.78	56	42	13.835	<0.001	0.009	0.122(0.025-0.592)
>288.78	2	17				
LMR						
≤3.04	30	25	1.027	0.311		
>3.04	28	34				

Statistical significance was set at P < 0.05. The expected count should be <5 to follow the Fisher's exact test results CI, confidence interval; LMR, lymphocyte-to-monocyte ratio; OR, odds ratio; PLR, platelet-to-lymphocyte ratio; NLR, neutrophil-to-lymphocyte ratio; SII, Systemic Inflammatory Index; TLS, tertiary lymphoid structures.

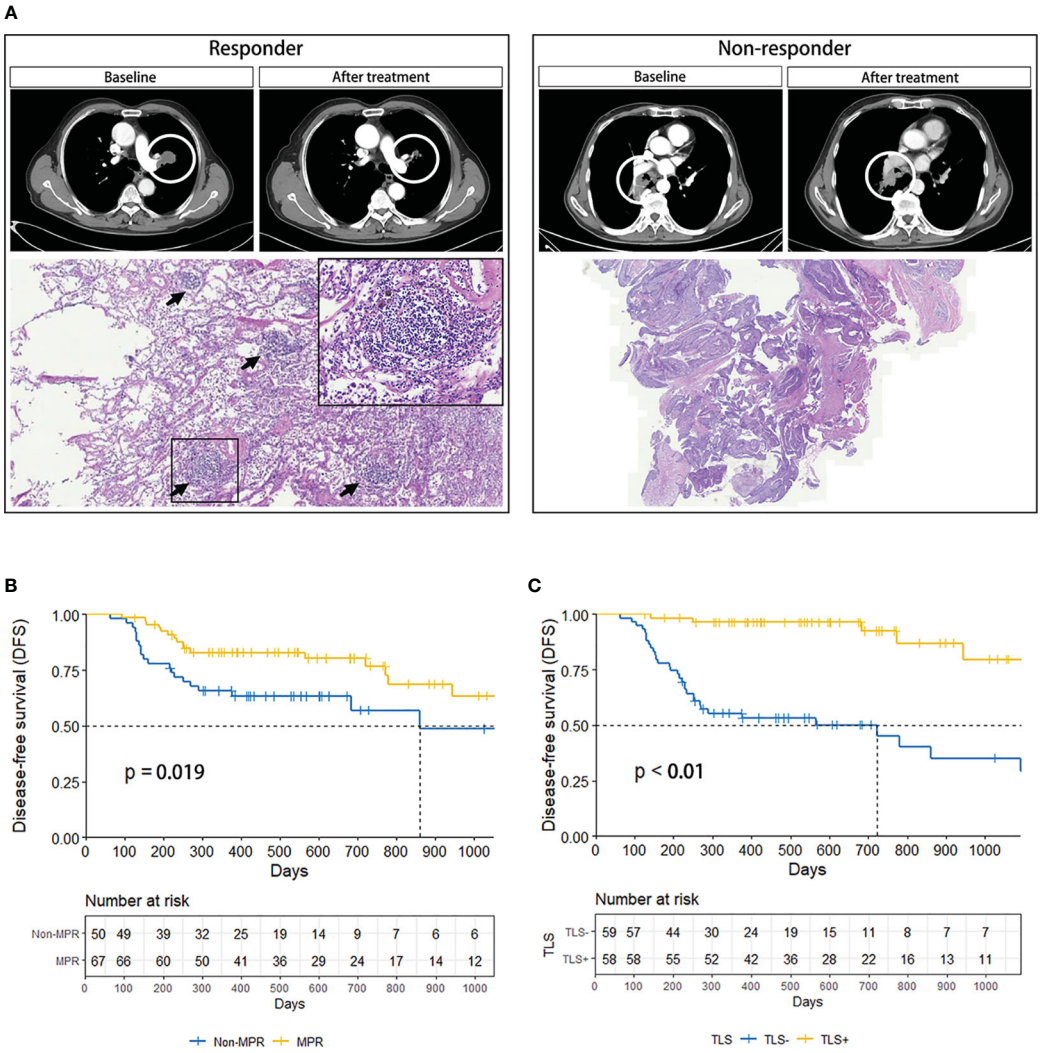

FIGURE 3
(A) Comparison of CT and pathology images of responder (left) and non-responder (right). The black arrow marks the TLSs. **(B)** DFS curves of MPR and Non-MPR in NSCLC patients. **(C)** DFS curves of TLS+ and TLS- in NSCLC patients. CT, computed tomography; DFS, disease-free survival; MPR, major pathologic response; NSCLC, non-small-cell lung cancer; TLS, tertiary lymphoid structure.

significant between-group differences in variables. The validation set comprised 26 (66.7%) patients with squamous cell carcinoma and 13 (33.3%) with adenocarcinoma. Eighteen (49.2%) patients in the validation set tested positive for TLS, while 11 (28.2%) tested positive for SII. The performance of three constructed nomogram models SII (Figure 5A), TLS (Figure 5B), and SII combined with TLS (Figure 5C) was evaluated; the results are displayed in Table 3. The calibration curve of the combined model was close to ideal curve (Figure 5D). A comparison of the area under the ROC curve of the three models revealed that for the 1-year DFS prediction, the combined model had a significantly improved performance compared to the SII- and TLS-based model. Similar results were obtained for the predictive model comparison of the 18-months DFS durations (Table 3). In addition, we perform a validation of the combined model using an independent validation cohort. According to the tertile of the model predicted score, patients were organized into low-, medium-, and high-risk groups. The validation set was stratified by risk scores derived from the training data. Survival curves are presented in Figures 5E, F.

Discussion

In this study, we assessed the immune infiltration status of patients with neoadjuvant chemoimmunotherapy-resectable NSCLC using pretreated peripheral blood and TLSs. Our results indicated that both high expression levels of TLS and low levels of SII were associated with a positive prognosis in patients with NSCLC patients, however, limitations of the single-parameter-based models were observed when predicting the DFS duration of the patients. Therefore, we combined these two factors with basic patient clinical information to design a prognostic model from a more comprehensive perspective. The resulting model was observed to better predict the DFS of patients with NSCLC and thus, will help clinicians treat patients more effectively.

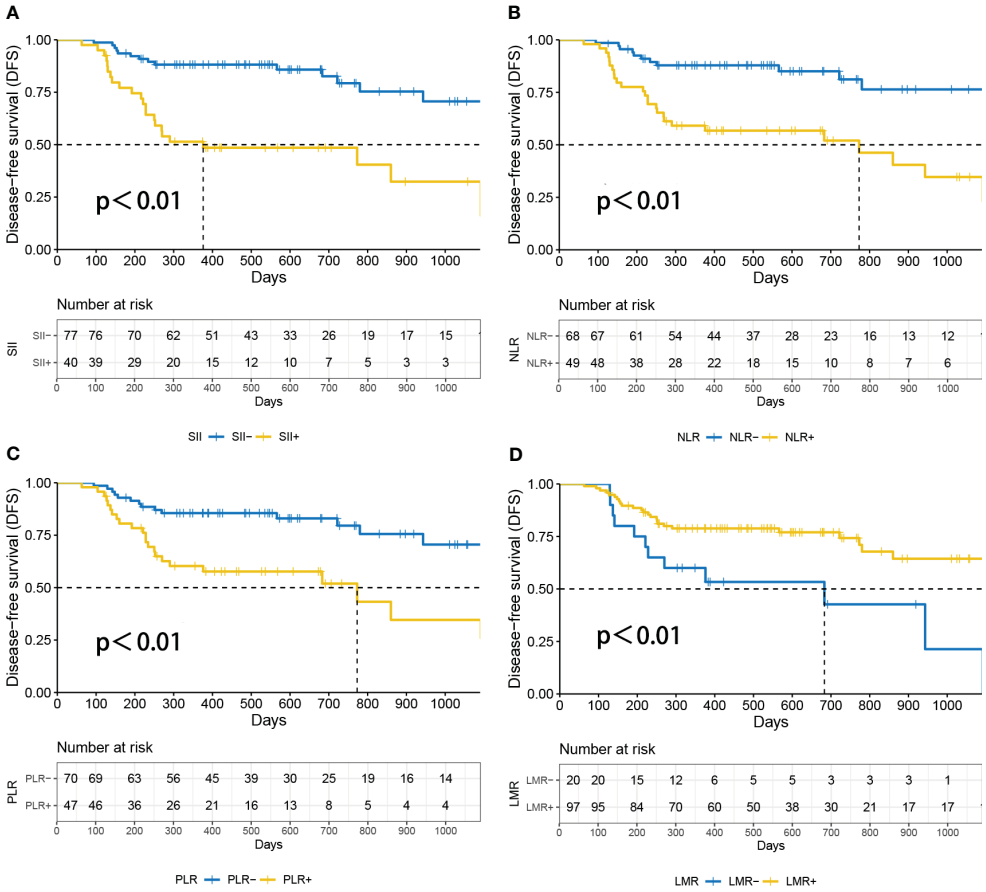

FIGURE 4
Survival analysis according to patients' inflammatory parameters. *P*<0.05 was considered statistically significant. **(A)** DFS curves of SII^{high} and SII^{low} in NSCLC patients. **(B)** Disease-free survival (DFS) curves of NLR^{high} and NLR^{low} in NSCLC patients. **(C)** DFS curves of PLR^{high} and PLR^{low} in NSCLC patients. **(D)** Disease-free survival (DFS) curves of LMR^{high} and LMR^{low} in NSCLC patients. DFS, disease-free survival; LMR, lymphocyte-to-monocyte ratio; NLR, neutrophil-to-lymphocyte ratio; PLR, platelet-to-lymphocyte ratio; SII, Systemic Inflammatory Index.

In recent years, because of the positive predictive performance of TLS in melanoma (16), esophageal cancer (17), lung cancer (18), liver cancer (19) and other tumors, the concept of TLS has gradually become well known to researchers and clinicians and has become a popular prognostic biomarker independent of TNM staging. TLSs are immune cells capable of an anti-tumor immune response (TFH cells, follicular B cells, DC-LAMP+ mature dendritic cells, etc.), and their formation indicates the presence of continuous anti-tumor T and B cell immune responses at the tumor site; thus, their abundance and maturity can reflect the immune infiltration status of patients with NSCLC (20). ICB has been found to increase the abundance of TLSs in several cancer types (7, 21, 22). Therefore, this study was conducted to assess the abundance and maturation of TLSs in patients with NSCLC after immunotherapy, which could reflect the immune status of patients more accurately. These results were consistent with those of the majority of studies, where a higher abundance and maturity of TLSs represented patients with a positive prognosis. It has also been hypothesized that the location of the TLSs affects their prognostic value. A previous study found that in hepatocellular carcinoma, the presence of peritumoral TLSs was associated with a higher risk of cancer recurrence and a poorer prognosis compared with intratumoral TLSs. However, in most cancers, there was no clear association between the location of TLSs and the outcome of treatment (6). Therefore, the location information of the TLSs was not refined for evaluation in this study.

Tumor-associated inflammatory responses have important effects on tumor development. Tumor-associated inflammation can lead to tumorigenesis by inducing genetic mutations, genomic instability, and epigenetic modifications that promote cancer cell proliferation and angiogenesis (23). Additionally, the systemic inflammatory response caused by the tumor accelerates a state of excessive nutritional depletion, which can increase cachexia. The results of this study revealed that low SII levels were associated with favorable DFS in patients with NSCLC who received neoadjuvant immune combination chemotherapy. There are various reasons for this outcome: Firstly, the rise in lymphocytes (CD4+ T cells, CD8+ T cells, et al.) enhances the cytotoxic immune response, which prevents the proliferation, invasion and migration of malignant cells (24). Secondly, the reduction in neutrophils hinders the secretion of pro-angiogenic, growth, and anti-apoptotic factors, thereby suppressing the growth and progression of cancer (25). Additionally, the decrease in platelets increases the susceptibility of

TABLE 2 Univariate and multivariate COX analysis for factors associated with DFS in NSCLC patients with neoadjuvant chemo-immunotherapy.

Variable	Univariate analysis			Multivariate analysis		
	HR	95%CI	*P* value	HR	95%CI	*P* value
Age	1.035	1.004-1.006	0.024	1.029	0.991-1.069	0.134
Sex (vs female)	1.960	0.814-4.723	0.134			
Smoking history (vs never smoker)	1.541	0.789-3.012	0.206			
Histology (vs adenocarcinoma)	0.255	0.113-0.574	0.001	0.205	0.075-0.559	0.002
T Stage (vs 1)			0.023			0.064
2	3.128	0.418-23.387	0.267	1.866	0.217-16.021	0.569
3	8.251	1.063-64.073	0.044	6.032	0.638-57.015	0.117
4	3.630	0.417-31.589	0.243	1.857	0.179-19.220	0.604
N Stage (vs 0)			0.362			
1	0.944	0.347-2.568	0.910			
2	1.011	0.429-2.382	0.981			
3	6.202	0.744-51.727	0.092			
NLR[a]	3.322	1.726-6.393	<0.05	1.937	0.709-5.291	0.198
PLR[b]	3.056	1.614-5.786	0.001	1.866	0.760-4.579	0.173
LMR[c]	0.356	0.178-0.710	0.003	1.056	0.428-2.601	0.906
SII[d]	4.818	2.470-9.398	<0.05	2.758	1.039-7.319	0.042
TLS[e]	0.130	0.054-0.311	<0.05	0.057	0.018-0.182	<0.05

Statistical significance was set at $P < 0.05$. a.Divided into NLR^{High} and NLR^{Low}. b.Divided into PLR^{High} and PLR^{Low}. c.Divided into LMR^{High} and LMR^{Low}. d.Divided into SII^{High} and SII^{Low}. e.Divided into TLS+ and TLS-.

CI, confidence interval; DFS, disease free survival; HR, hazards ratio; LMR, lymphocyte-to-monocyte ratio; OR, odds ratio; PLR, platelet-to-lymphocyte ratio; NLR, neutrophil-to-lymphocyte ratio; NSCLC, non-small-cell lung cancer; SII, Systemic Inflammatory Index; TLS, tertiary lymphoid structures.

circulating tumor cells to shear stress while in circulation, which impedes the initiation of epithelial-mesenchymal transition and mitigates the metastasis of cancer cells (26).

The inflammatory environment is closely associated with the formation and maturation of TLSs. Chronic persistent inflammation caused by tumors leads to the extranodal implantation of lymphoid tissue, which results in the formation of TLSs in the tumor and surrounding sites (27). The development of TLSs is a complicated process in which immune cell-derived pro-inflammatory signals are considered inducers. In this study, we found that a reduction in the inflammatory index PLR facilitated high TLS expression. This may be explained by the fact that the state of platelets and lymphocytes in NSCLC after neoadjuvant immune combination chemotherapy creates a specific inflammatory microenvironment that specifically influences TLSs formation and maturation. Therefore, this study incorporated both inflammatory environmental indicators that affect TLS formation, maturation, and expression into a prognostic model for NSCLC, which accurately predicted DFS durations in patients with NSCLC. More research is expected in the future to clarify the connection between the inflammatory environment of tumors and the anti-tumor immune response to find targets to enhance the effectiveness of immunotherapy.

In clinical practice, we can make a preliminary assessment of a patient's immune therapy response and prognosis based on their inflammatory biomarkers. This assessment can then be combined with a comprehensive analysis of the patient's immune scores and gene expression status to determine if they are suitable for neoadjuvant immune-chemo combination therapy. To our knowledge, this is the first study to investigate the relationship between inflammatory biomarkers with tumor microenvironment TLSs in patients with NSCLC and identify the easily assessable inflammatory index, PLR, as a reflection of TLS status. Changes TLS status, detected through inflammatory biomarkers in the blood, provides a basis for elucidating specific inflammatory microenvironments that promote TLS expression and offers novel insights into immuno-microenvironment research. Additionally, this study demonstrated that TLSs in the tumor microenvironment correlate not only with local factors but also with systemic immune conditions, providing evidence of a novel mechanism by which systemic inflammation aids in regulating tumor microenvironment immunity.

This study has some limitations. First, this was a single-center retrospective study with a small sample size, and the results may have been influenced by individual differences, the geographic area, or specific environmental factors. Second, the follow-up period of this study took place over a limited duration. Therefore, most of the tumor progression of the patients in this study was dominated by recurrence and metastasis, and fewer patients died, making it difficult to study the survival status of the patients. Third, only

10.3389/fimmu.2023.1244256

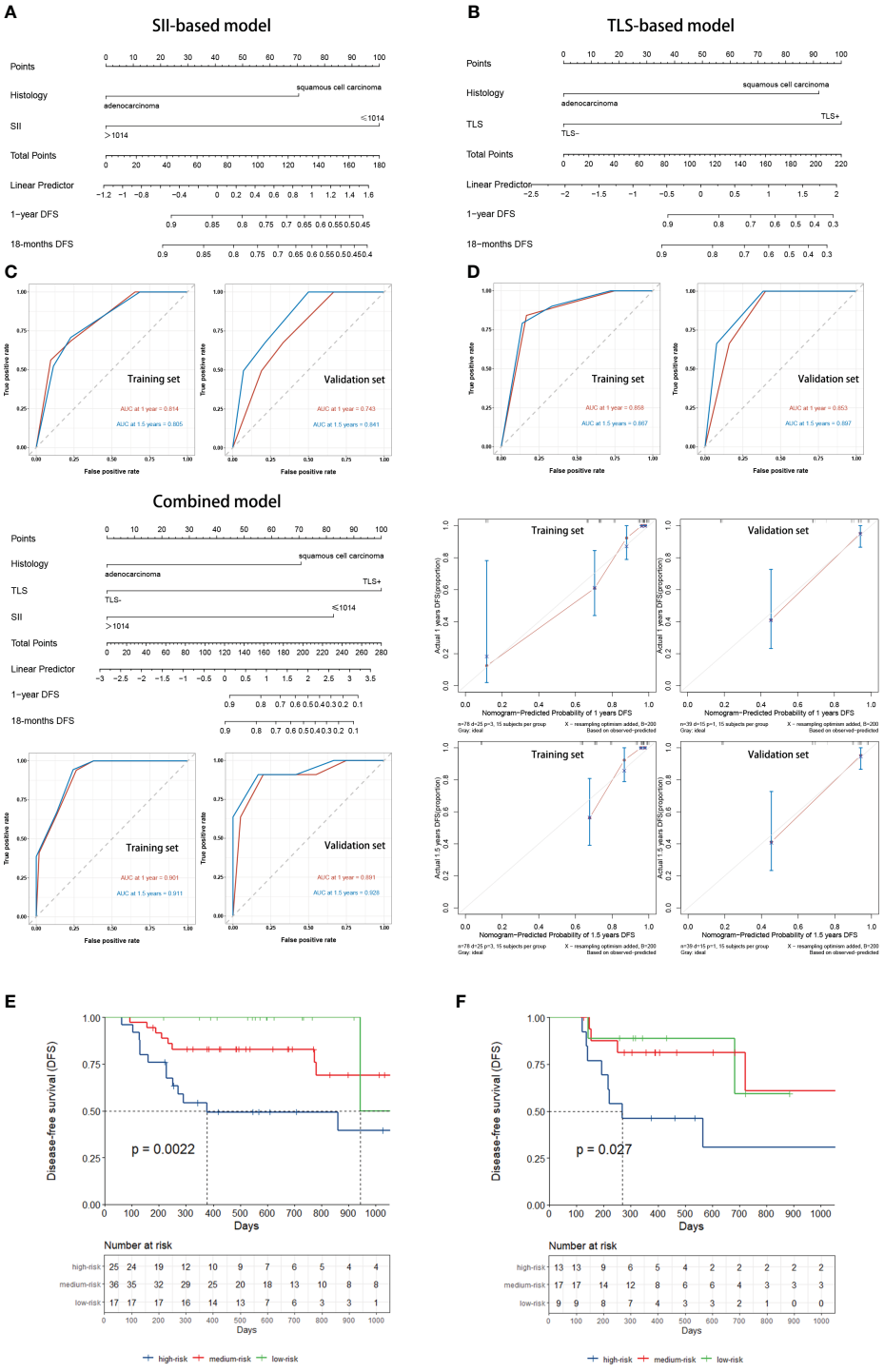

FIGURE 5
(A) SII-based model and ROC curves to predict the DFS of NSCLC patients receiving neoadjuvant chemoimmunotherapy. **(B)** TLSs-based model and ROC curves to predict DFS. **(C)** Combined model and ROC curves to predict DFS. **(D)** The calibration curve was close to ideal. **(E)** Kaplan–Meier curve using the tertile of the model-predicted score (Training set). Patients were grouped into low-, medium-, and high-risk groups. **(F)** Kaplan–Meier curve using the tertile of the model-predicted score (Validation set) with patients grouped into low-, medium-, and high-risk groups. DFS, disease-free survival; NSCLC, non-small-cell lung cancer; ROC, receiver operating characteristic; SII, Systemic Inflammatory Index; TLS, tertiary lymphoid structure.

patients with resectable NSCLC who were treated with neoadjuvant immune combination chemotherapy were included in this study, and the presence of platinum-based and paclitaxel drugs or pemetrexed disodium interfered with and did not allow accurate assessment of the effect of PD-1 inhibitors on TLSs. The PD-1 checkpoint inhibitors and chemotherapeutic drugs used in the study may also have affected the patients' prognosis because they were from different manufacturers. Additionally, the number of

TABLE 3 Comparison of Nomogram Models.

End point	Models	AUC	
		Training cohort	Validation cohort
1-year DFS	Combined model	0.901	0.891
	SII-based model	0.814	0.743
	TLS-based model	0.858	0.853
18-months DFS	Combined model	0.911	0.928
	SII-based model	0.805	0.841
	TLS-based model	0.867	0.897

Combined model: a combined nomogram model based on the expression of TLSs with SII
AUC, area under curve; DFS, disease-free survival; SII, Systemic Inflammatory Index; TLS, tertiary lymphoid sructure.

tissue sections observed for each patient was small and did not allow for a comprehensive assessment of TLS abundance and maturation in and around the entire tumor. Although the study showed a correlation between the inflammatory environment and TLSs, expect more basic experimental studies in the future to further explore their mechanisms.

In conclusion, our study indicated that low PLR was an independent predictor of TLS(+) and that both TLSs and SII predicted prognosis in patients with resectable NSCLC receiving neoadjuvant chemoimmunotherapy. Notably, the combination of SII and TLS to assess DFS duration in patients with NSCLC was more accurate than using either parameter alone.

Data availability statement

The raw data supporting the conclusions of this article will be made available by the authors, without undue reservation.

Ethics statement

Written informed consents were provided by the patients participants/participants. The study was carried out in accordance with the Helsinki Declaration and approved by the Ethics Review Committee of Shandong Cancer Hospital in China. (SDTHEC2022010006).

Author contributions

Study design: SY, FX. Data acquisition and analysis HZ, FX. Interpretation of the data: FX, LL, NL. Drafting of the manuscript: FX. Revision of the manuscript: SY. All authors contributed to the article and approved the submitted version.

Funding

The author(s) declare financial support was received for the research, authorship, and/or publication of this article. This study was supported in part by National Natural Science Foundation of China (grant No. NSFC82073345), Natural Science Foundation of Shandong Province Innovation and Development Joint Fund (ZR202209010002), the Taishan Scholars Program and Jinan Clinical Medicine Science and Technology Innovation Plan (202019060) to SY.

Conflict of interest

The authors declare that the research was conducted in the absence of any commercial or financial relationships that could be construed as a potential conflict of interest.

Publisher's note

Supplementary material

The Supplementary Material for this article can be found online at: https://www.frontiersin.org/articles/10.3389/fimmu.2023.1244256/full#supplementary-material

References

1. Siegel RL, Miller KD, Fuchs HE, Jemal A. Cancer statistics, 2022. *CA Cancer J Clin* (2022) 72(1):7–33. doi: 10.3322/caac.21708

2. Sung H, Ferlay J, Siegel RL, Laversanne M, Soerjomataram I, Jemal A, et al. Global cancer statistics 2020: globocan estimates of incidence and mortality worldwide for 36 cancers in 185 countries. *CA Cancer J Clin* (2021) 71(3):209–49. doi: 10.3322/caac.21660

3. Weiner LM. Cancer immunotherapy–the endgame begins. *N Engl J Med* (2008) 358(25):2664–5. doi: 10.1056/NEJMp0803663

4. Granier C, De Guillebon E, Blanc C, Roussel H, Badoual C, Colin E, et al. Mechanisms of action and rationale for the use of checkpoint inhibitors in cancer. *ESMO Open* (2017) 2(2):e000213. doi: 10.1136/esmoopen-2017-000213

5. Fu T, Dai LJ, Wu SY, Xiao Y, Ma D, Jiang YZ, et al. Spatial architecture of the immune microenvironment orchestrates tumor immunity and therapeutic response. *J Hematol Oncol* (2021) 14(1):98. doi: 10.1186/s13045-021-01103-4

6. Schumacher TN, Thommen DS. Tertiary lymphoid structures in cancer. *Science* (2022) 375(6576):eabf9419. doi: 10.1126/science.abf9419

7. Helmink BA, Reddy SM, Gao J, Zhang S, Basar R, Thakur R, et al. B cells and tertiary lymphoid structures promote immunotherapy response. *Nature* (2020) 577 (7791):549–55. doi: 10.1038/s41586-019-1922-8

8. Cottrell TR, Thompson ED, Forde PM, Stein JE, Duffield AS, Anagnostou V, et al. Pathologic features of response to neoadjuvant anti-pd-1 in resected non-small-cell lung carcinoma: A proposal for quantitative immune-related pathologic response criteria (Irprc). *Ann Oncol* (2018) 29(8):1853–60. doi: 10.1093/annonc/mdy218

9. Ruddle NH. Lymphatic vessels and tertiary lymphoid organs. *J Clin Invest* (2014) 124(3):953–9. doi: 10.1172/jci71611

10. Guo W, Cai S, Zhang F, Shao F, Zhang G, Zhou Y, et al. Systemic immune-inflammation index (Sii) is useful to predict survival outcomes in patients with surgically resected non-small cell lung cancer. *Thorac Cancer* (2019) 10(4):761–8. doi: 10.1111/1759-7714.12995

11. Diem S, Schmid S, Krapf M, Flatz L, Born D, Jochum W, et al. Neutrophil-to-lymphocyte ratio (Nlr) and platelet-to-lymphocyte ratio (Plr) as prognostic markers in patients with non-small cell lung cancer (Nsclc) treated with nivolumab. *Lung Cancer* (2017) 111:176–81. doi: 10.1016/j.lungcan.2017.07.024

12. Zhai B, Chen J, Wu J, Yang L, Guo X, Shao J, et al. Predictive value of the hemoglobin, albumin, lymphocyte, and platelet (Halp) score and lymphocyte-to-monocyte ratio (Lmr) in patients with non-small cell lung cancer after radical lung cancer surgery. *Ann Transl Med* (2021) 9(12):976. doi: 10.21037/atm-21-2120

13. Forde PM, Spicer J, Lu S, Provencio M, Mitsudomi T, Awad MM, et al. Neoadjuvant nivolumab plus chemotherapy in resectable lung cancer. *N Engl J Med* (2022) 386(21):1973–85. doi: 10.1056/NEJMoa2202170

14. Brunet M, Crombé A, Cousin S, Vanhersecke L, Le Loarer F, Bessede A, et al. Mature tertiary lymphoid structure is a specific biomarker of cancer immunotherapy and does not predict outcome to chemotherapy in non-small-cell lung cancer. *Ann Oncol* (2022) 33(10):1084–5. doi: 10.1016/j.annonc.2022.06.007

15. Royston P, Altman DG, Sauerbrei W. Dichotomizing continuous predictors in multiple regression: A bad idea. *Stat Med* (2006) 25(1):127–41. doi: 10.1002/sim.2331

16. Groeneveld CS, Fontugne J, Cabel L, Bernard-Pierrot I, Radvanyi F, Allory Y, et al. Tertiary lymphoid structures marker cxcl13 is associated with better survival for patients with advanced-stage bladder cancer treated with immunotherapy. *Eur J Cancer* (2021) 148:181–9. doi: 10.1016/j.ejca.2021.01.036

17. Ling Y, Zhong J, Weng Z, Lin G, Liu C, Pan C, et al. The prognostic value and molecular properties of tertiary lymphoid structures in oesophageal squamous cell carcinoma. *Clin Transl Med* (2022) 12(10):e1074. doi: 10.1002/ctm2.1074

18. Germain C, Gnjatic S, Tamzalit F, Knockaert S, Remark R, Goc J, et al. Presence of B cells in tertiary lymphoid structures is associated with a protective immunity in patients with lung cancer. *Am J Respir Crit Care Med* (2014) 189(7):832–44. doi: 10.1164/rccm.201309-1611OC

19. Calderaro J, Petitprez F, Becht E, Laurent A, Hirsch TZ, Rousseau B, et al. Intra-tumoral tertiary lymphoid structures are associated with a low risk of early recurrence of hepatocellular carcinoma. *J Hepatol* (2019) 70(1):58–65. doi: 10.1016/j.jhep.2018.09.003

20. Sun X, Liu W, Sun L, Mo H, Feng Y, Wu X, et al. Maturation and abundance of tertiary lymphoid structures are associated with the efficacy of neoadjuvant chemoimmunotherapy in resectable non-small cell lung cancer. *J Immunother Cancer* (2022) 10(11):e005531. doi: 10.1136/jitc-2022-005531

21. Johansson-Percival A, He B, Li ZJ, Kjellén A, Russell K, Li J, et al. *De novo* induction of intratumoral lymphoid structures and vessel normalization enhances immunotherapy in resistant tumors. *Nat Immunol* (2017) 18(11):1207–17. doi: 10.1038/ni.3836

22. Rodriguez AB, Peske JD, Woods AN, Leick KM, Mauldin IS, Meneveau MO, et al. Immune mechanisms orchestrate tertiary lymphoid structures in tumors *via* cancer-associated fibroblasts. *Cell Rep* (2021) 36(3):109422. doi: 10.1016/j.celrep.2021.109422

23. Galdiero MR, Marone G, Mantovani A. Cancer inflammation and cytokines. *Cold Spring Harb Perspect Biol* (2018) 10(8):a028662. doi: 10.1101/cshperspect.a028662

24. Mantovani A, Allavena P, Sica A, Balkwill F. Cancer-related inflammation. *Nature* (2008) 454(7203):436–44. doi: 10.1038/nature07205

25. Paramanathan A, Saxena A, Morris DL. A systematic review and meta-analysis on the impact of pre-operative neutrophil lymphocyte ratio on long term outcomes after curative intent resection of solid tumours. *Surg Oncol* (2014) 23(1):31–9. doi: 10.1016/j.suronc.2013.12.001

26. Schumacher D, Strilic B, Sivaraj KK, Wettschureck N, Offermanns S. Platelet-derived nucleotides promote tumor-cell transendothelial migration and metastasis *via* P2y2 receptor. *Cancer Cell* (2013) 24(1):130–7. doi: 10.1016/j.ccr.2013.05.008

27. Jacquelot N, Tellier J, Nutt Sl, Belz Gt. Tertiary lymphoid structures and B lymphocytes in cancer prognosis and response to immunotherapies. *Oncoimmunology* (2021) 10(1):1900508. doi: 10.1080/2162402x.2021.1900508

frontiers | Frontiers in Immunology

TYPE Review
PUBLISHED 01 February 2024
DOI 10.3389/fimmu.2024.1324093

OPEN ACCESS

EDITED BY
Hui Zhao,
University of Texas MD Anderson Cancer Center, United States

REVIEWED BY
Feng Wei,
Tianjin Medical University Cancer Institute and Hospital, China
Anthony B. Rodriguez,
University of Virginia, United States

*CORRESPONDENCE
E. Ramsay Camp
Ramsay.Camp@bcm.edu

RECEIVED 18 October 2023
ACCEPTED 11 January 2024
PUBLISHED 01 February 2024

CITATION
Gao Z, Azar J, Zhu H, Williams-Perez S, Kang SW, Marginean C, Rubinstein MP, Makawita S, Lee H-S and Camp ER (2024) Translational and oncologic significance of tertiary lymphoid structures in pancreatic adenocarcinoma. *Front. Immunol.* 15:1324093. doi: 10.3389/fimmu.2024.1324093

Translational and oncologic significance of tertiary lymphoid structures in pancreatic adenocarcinoma

Zachary Gao[1], Joseph Azar[2], Huili Zhu[1], Sophia Williams-Perez[1], Sung Wook Kang[1,3,4], Celia Marginean[1], Mark P. Rubinstein[2], Shalini Makawita[1], Hyun-Sung Lee[1,3,4] and E. Ramsay Camp[1,3,5]*

[1]Michael E. DeBakey Department of Surgery, Baylor College of Medicine, Houston, TX, United States, [2]The Pelotonia Institute for Immuno-Oncology, Ohio State University Comprehensive Cancer Center, Columbus, OH, United States, [3]Dan L. Duncan Comprehensive Cancer Center, Baylor College of Medicine, Houston, TX, United States, [4]Systems Onco-Immunology Laboratory, David J. Sugarbaker Division of Thoracic Surgery, Michael E. DeBakey Department of Surgery, Baylor College of Medicine, Houston, TX, United States, [5]Baylor College of Medicine, Michael E. DeBakey VA Medical Center, Houston, TX, United States

Pancreatic adenocarcinoma (PDAC) is an aggressive tumor with poor survival and limited treatment options. PDAC resistance to immunotherapeutic strategies is multifactorial, but partially owed to an immunosuppressive tumor immune microenvironment (TiME). However, the PDAC TiME is heterogeneous and harbors favorable tumor-infiltrating lymphocyte (TIL) populations. Tertiary lymphoid structures (TLS) are organized aggregates of immune cells that develop within non-lymphoid tissue under chronic inflammation in multiple contexts, including cancers. Our current understanding of their role within the PDAC TiME remains limited; TLS are complex structures with multiple anatomic features such as location, density, and maturity that may impact clinical outcomes such as survival and therapy response in PDAC. Similarly, our understanding of methods to manipulate TLS is an actively developing field of research. TLS may function as anti-tumoral immune niches that can be leveraged as a therapeutic strategy to potentiate both existing chemotherapeutic regimens and potentiate future immune-based therapeutic strategies to improve patient outcomes. This review seeks to cover anatomy, relevant features, immune effects, translational significance, and future directions of understanding TLS within the context of PDAC.

KEYWORDS

tertiary lymphoid structures, pancreatic adenocarcinoma, pancreatic cancer, translational ability, immune microenvironment

1 Introduction

Although pancreatic adenocarcinoma (PDAC) accounts for approximately 3% of all cancer in the US, it is projected to become the 2nd leading cause of cancer-related deaths in the US by 2030 (1). The prognosis for patients with PDAC remains poor with <10% five-year overall survival and modest survival benefit from standard treatment regimens (2). Immunotherapy has changed the paradigm in modern oncologic therapy for cancers such as melanoma and non-small cell lung cancer (3–6). Unfortunately, immune checkpoint inhibitor (ICI) therapy has proven ineffective for PDAC outside of the rare few with high microsatellite instability (7–12). Additionally, other strategies such as TCR therapy, CAR-T therapy, tumor-infiltrating lymphocyte (TIL) therapy, and mRNA vaccines are still in their nascency (13–15).

Immunotherapy failure has partially been attributed to the immunosuppressive tumor immune microenvironment (TiME) of PDAC (16). The PDAC TiME is complex and significant tumor immune heterogeneity exists both within the tumor, the peritumoral microenvironment, and across patients (17–20). The cellular constituents of the PDAC TiME consists of multiple immunosuppressive cell lines, including regulatory T cells (Tregs), myeloid-derived suppressor cells (MDSCs), and tumor-associated macrophages (TAMs) (16, 21–30). These features of the TiME contribute to PDAC tumorigenesis, suppression of cytotoxic T cell priming and function (16, 31–34), and T cell exhaustion (29, 35, 36). However, favorable TILs also exist in the TiME such as CD4+ and CD8+ T cell infiltrates (17, 18, 37). Multiple reports have identified an association between higher degrees of CD4+ and CD8+ T cell infiltration with improved survival in PDAC (38–40). Furthermore, the spatial organization of these immune infiltrates impact survival (19, 38), suggesting that a deeper understanding of the architecture and spatial organization of immune cell populations within the PDAC TiME is required to better appreciate their clinical and translational relevance. Tertiary lymphoid structures (TLS) represent an essential component of this immune spatial organization and are organized aggregates of immune cells that arise in nonlymphoid tissue. A growing body of evidence link TLS formation to improved clinical outcomes in a variety of cancers (41–43). This review will define TLS anatomy, the clinical significance, and translational implications for PDAC TLS to establish a deeper understanding of opportunities to harness anti-tumoral immunity that can translate to improved patient outcomes.

2 Anatomy of tertiary lymphoid structures

TLS have been identified in multiple inflammatory disease states (44) such as rheumatoid arthritis (45), Sjogren's disease (46), autoimmune diabetes (47), and various cancers (43). In contrast to lymph nodes, TLS are non-encapsulated organized lymphocyte aggregates that can form in non-lymphoid tissues undergoing chronic inflammatory stress such as infection, transplantation, and cancer (48). In human malignancies, TLS generally contain the major constituents of adaptive immunity, with zones containing B cells, T cells, and a stromal network of follicular dendritic cells (FDCs) (49). High endothelial venules (HEVs) can also surround TLS to allow immune cell trafficking (50). Interestingly, in PDAC, small nerve fibers have been shown to exist in these aggregates and the density of such fibers has been associated with a prolonged overall survival (51).

TLS formation can be broadly defined by three main phases: fibroblast activation, immune cell recruitment, and maturation (52) (Figure 1). Several cytokines such as IL-13, IL-17 and IL-22 are implicated in the initial priming of local fibroblasts by immune cells undergoing inflammatory stress (53, 54). At this stage, immature structures are formed, and their maintenance requires the retention of existing immune cells as well as the recruitment of further immune populations. Continuous local antigen presentation (55) and chemokines such as CXCL13 and others play a key role in these two processes respectively (56). If stressors persist, TLS maturation progresses with the formation of HEVs and germinal centers (GCs). Within PDAC, the B lymphocyte chemoattractant CXCL13 may be of particular relevance, as immunofluorescence studies of PDAC TLS demonstrate an abundance of CXCL13 distributed throughout TLS (57, 58). Furthermore, ectopic CXCL13 expression triggers TLS formation in the pancreas in both cancerous (59) and noncancerous (58) contexts. Other earlier studies also revealed the critical role of chemokines such as TCA4/SLC and CXCL13 (also known as B lymphocyte chemoattractant) (60) in pancreatic lymphoid neogenesis.

3 Mature and immature tertiary lymphoid structures

The maturation from a loose aggregate of B cells and T cells into a mature, functional lymphoid structure impacts the TiME and carries broader clinical significance. TLS can undergo multiple stages of maturity (Figure 2), which have been defined by different criteria from different research groups. Earlier distinctions were typically made based on the presence of GCs within mature TLS compared to immature TLS, which were vaguely organized lymphocytic clusters without GCs (61, 62). More recently, one group defined three phenotypes of TLS maturity in a lung cancer model based on immune cell constituents and anatomical organization (63). Early TLS were dense lymphocytic clusters of $CD21^-$ $CD23^-$ B and T cells without FDCs or GCs localized near CXCL13-expressing perivascular cells, intermediate-stage or "primary follicle-like" TLS contained $CD21^+$ $CD23^-$ FDCs without GCs, and mature or "secondary follicle-like" TLS contained $CD21^+$ $CD23^+$ GCs in addition to the features of TLS in earlier stages of maturation. These maturity phenotypes were later validated in a colorectal cancer model from 109 patient-derived non-metastatic tumor specimens (64). Within studies of PDAC TLS, definitions of immature and mature TLS have varied between studies. Many groups defining PDAC TLS rely upon histological

10.3389/fimmu.2024.1324093

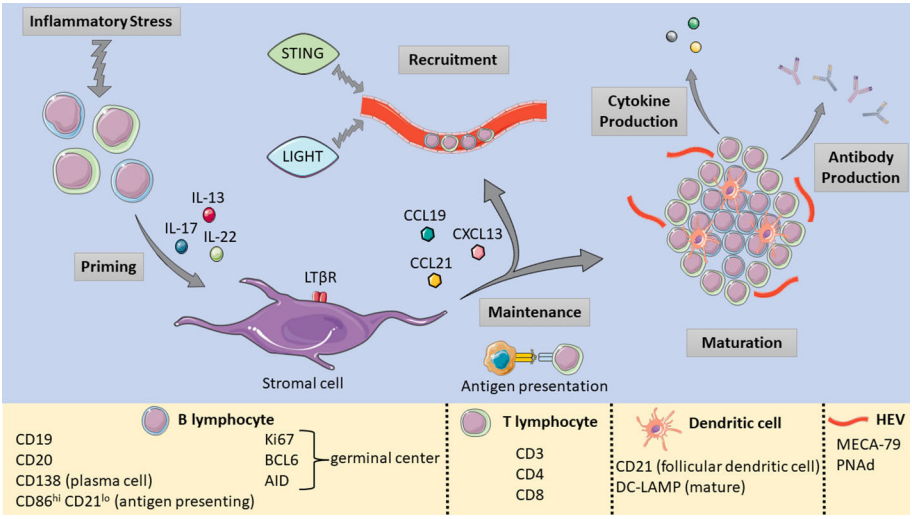

FIGURE 1
Pictorial summary of TLS formation, maturation, and the relevant markers used to identify TLS components. [Shapes and images are imported from Servier Medical Art by Servier (http://smart.servier.com/), accessed on May 19, 2023. Licensed under a Creative Commons Attribution 3.0 Unported License (https://creativecommons.org/licenses/by/3.0/)].

examination with hematoxylin and eosin staining to identify TLS with organized B cell and T cell zones, germinal centers, and HEVs, with immunohistochemical staining of surrogate markers such as peripheral lymph node addressin (PNAd) or Ki67 implying TLS maturity (65, 66), but do not directly identify early or intermediate TLS in comparison to mature TLS. Others fully characterize TLS based on distinct CD3+ and CD20+ B cell and CD8+ T cell zones with CD21+ FDCs and (PNAd+) HEVs (59, 67), providing a more specific definition of PDAC TLS maturity.

GCs are an essential component of peripheral lymphoid organs and important sites of antigen-driven somatic hypermutation and memory B cell and plasma cell maturation (68). Similarly, the GCs of mature TLS contain proliferating B cells and DC-LAMP$^+$ FDCs (69), characterized by Ki67, activation-induced cytidine deaminase (AID) and BCL6 expression (67, 70). HEVs are also present in these structures and are classically identified by the presence of an L-Selectin ligand, MECA-79, and PNAd (71). These HEVs play an essential role in mature TLS function by mediating immune cell trafficking (72) via binding of L-Selectin to PNAd (73).

Evidence from diabetic mice with autoimmune insulitis revealed that functional and mature TLS within the pancreas can harbor differentiated autoreactive B cells that express the activation-induced cytidine deaminase (AID) enzyme which mediates immunoglobulin class switching and affinity maturation (70). As with other neoplasms, expression of Ki67, BCL6 and CD21 in B cell zones is indicative of mature PDAC TLS, with GCs containing B cells undergoing affinity maturation and somatic hypermutation (67). In murine PDAC models, the presence of HEVs in mature TLS have been shown to facilitate lymphocytic infiltration (74) and enhance their activation via LTβR signaling (75).

However, TLS in cancers exhibit significant heterogeneity in maturation, and can also vary in maturity depending on tumor stage (76) or metastatic site (77). PDAC may present a unique challenge in understanding TLS maturity, as the PDAC TiME exhibits considerable immune heterogeneity (78, 79) and lower proportions of TLS are found in PDAC compared to other cancers (43). Relatively few of TLS found in PDAC are mature and possess GCs (67). A timeline of TLS maturity has been proposed (63). Although it remains unclear whether the various phenotypes in PDAC represent a stepwise progression of maturation or are instead terminally differentiated and unable to eventually transform into mature TLS. Understanding these nuances may improve both our knowledge of the PDAC TLS as well as broaden our understanding of the PDAC TiME as a whole.

4 Location and density

TLS can be located either intratumoral or peritumoral. TLS location has significant anatomical and functional implications. In cancers such as melanoma, increased peritumoral mature TLS density is associated with longer survival (74). PDAC TLS formation is more abundant in the invasive front of the tumor and peritumorally compared to the tumor center (80). One study conducted on more than 300 PDAC human samples demonstrated that 84% of the examined samples possessed only peritumoral TLS, while only 16% contained intratumoral TLS (65). Interestingly, a more recent study demonstrated that despite being less plentiful, the intratumoral TLS had a greater B and T cell infiltration, less immunosuppressive populations, a significant Th1 and Th17 pro-inflammatory genetic polarization, and were associated with improved survival (65). The intratumoral TLS were also more mature with intact nerve networks and organized vasculature formed by mature endothelial cells circled by pericytes. PDAC is characterized by a desmoplastic, fibrotic stroma (81–83), which may necessitate a spatial adjacency of TLS to tumor for its anti-tumoral effects to manifest.

10.3389/fimmu.2024.1324093

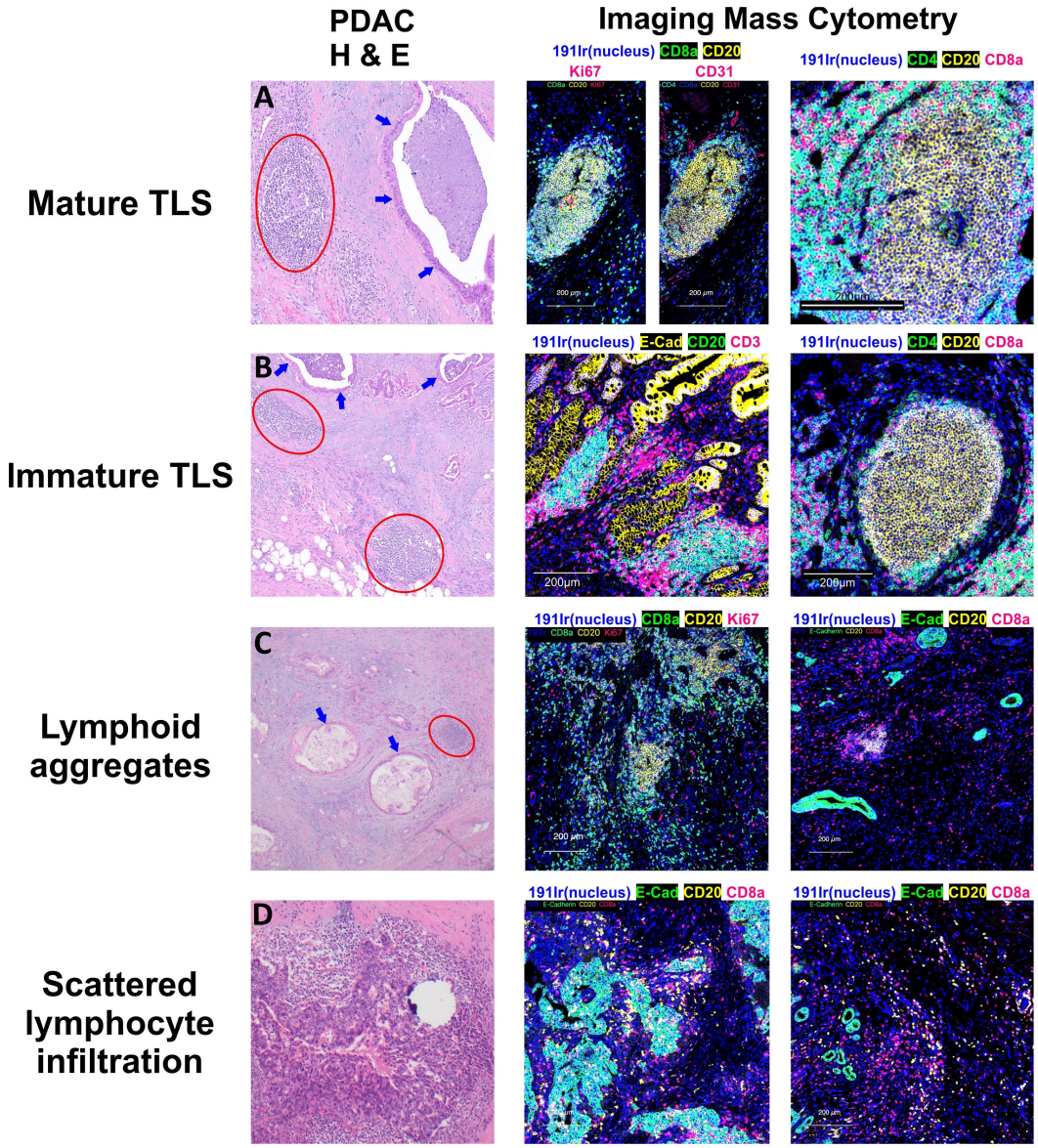

FIGURE 2
Patterns of Lymphocyte Infiltration in Pancreatic Adenocarcinoma. Tertiary lymphoid structures (TLS) in pancreatic adenocarcinoma display varying stages of maturation. **(A)** Mature TLSs comprise B cells, T cells, and follicular dendritic cells, and are distinguished by the presence of germinal centers containing Ki67(+) B cells. **(B)** In contrast, the majority of the observed TLSs are in an immature stage, lacking germinal centers but still exhibiting distinct B cell and T cell zones. **(C)** Apart from these structured aggregates, there are lymphoid aggregates which represent a disorganized accumulation of both B and T lymphocytes. **(D)** Moreover, individual B and T cells can also be observed dispersed within the tumor or surrounding the tumor cells. Circles in red show lymphoid structures, and arrows in blue display invasive adenocarcinoma with luminal necrosis.

5 Relevant cell populations within PDAC TLS

As TLS share morphological and cellular similarities with traditional secondary lymphoid organs, they may also recapitulate some of their functionality. B cells are an essential component of TLS and are present at all stages of TLS maturity (66, 69). Data from the study of TLS in autoimmune disease support the idea that B cells within the TLS GC undergo somatic hypermutation and clonal expansion in rheumatoid arthritis (84), Sjogren's disease (85), myasthenia gravis (86), and autoimmune diabetes. TLS-associated B cells are also capable of terminal differentiation into antibody-secreting plasma cells (87). Similar to the data from autoimmune TLS research, cancer TLS-associated B cells are proliferative, experience somatic hypermutation, and undergo maturation into antibody-secreting plasma cells (69, 88). These plasma cells also produce tumor-specific antibodies (69, 88, 89) capable of binding to tumor cells and enhancing immunotherapy (88), suggesting that the TLS B cell population fulfills an antitumoral niche within the more generalized B cell infiltrate in tumors.

Data from retrospective studies and preclinical models in PDAC highlight the antitumoral function of the TLS-associated B cell population. One group showed that TLS+ PDAC tumors have a higher proportion of memory B cells and memory IgG1 class-

switched B cells compared to TLS- tumors (67), while another group demonstrated that TLS-associated B cell infiltrates in a KPC PDAC murine model exhibited an immunostimulatory phenotype, with upregulation of proinflammatory (SPP1, IL6, CSF2, VEGFA, CCL4, PTGS2) and T cell chemotaxis (CXCL1, CXCL2, CXCL5, CCL2, CXCL12, CCL20) genes, along with downregulation of immunosuppressive genes (CD274 and IL12a) (90, 91).

T cells are an essential component of the TLS (49). As higher CD8 T cell tumor infiltration is associated with increased survival across cancers (92–94), understanding the interaction of CD8 T cell populations and TLS is of particular interest. Preclinical autoimmune diabetes models have linked TLS with naïve T cell recruitment and proliferation (95). Within a cancer-specific context, LIGHT expression in a fibrosarcoma model induced the formation of TLS, naïve T cell recruitment, T cell proliferation and priming, and subsequent tumor regression (96). A preclinical colorectal cancer model showed that TLS were associated with CD3+ T cell infiltration and mediated GFP+ splenocyte recruitment (97), and a preclinical melanoma model demonstrated an association between TLS and tumor-specific T cell responses independent of secondary lymphoid tissue (98).

Multiple retrospective studies from human PDAC samples show an association between TLS formation and increased CD8 T cell infiltration (91, 99, 100). For example, evidence from one group demonstrated that T cells were enriched in mature TLS with PNAd + HEVs, TLS presence correlated with greater intratumoral and circulation CD8 T cell populations, and the TLS+ tumor stroma had a higher CD8/Treg ratio (100). Based on a PDAC tissue microarray, another investigation identified a "TLS rich" immune PDAC subtype with higher expression of T cells (CD8, CD3, and CD4) and B cells (CD20) markers and lower in Treg (FOXP3) markers (101).

The mechanistic interactions between CD8 T cells and the PDAC TLS in PDAC are just beginning to be explored and suggest that PDAC TLS are active participants in T cell maturation and trafficking. Naïve T cell infiltration appears dependent upon PNAd+ CCL21+ HEVs seen in mature TLS (102). Data from a tumor vaccine-induced human PDAC TLS cohort demonstrated high expression of the early T cell activation marker CD69 and T cell trafficking receptor CXCR3 within TLS, implicating their role in T cell activation (103). Furthermore, Vβ2-positive T cells are present in the center of PDAC TLS, suggesting that TLS are sites of T cell clonal expansion (104).

Additional anti-tumoral efficacy may be related to T follicular helper cells (Tfh), which are a component of TLS (105) associated with improved prognosis in cancers (43, 106, 107). PDAC Tfh from patients who received neoadjuvant chemotherapy exhibited increased CD8 T cell and B cell recruitment capability compared to treatment-naïve Tfh (108).

Interestingly, cancer-associated fibroblasts (CAFs) may also play a role in TLS function. PDAC CAFs are typically associated with tumorigenic (109) and immunosuppressive roles (110). However, diverse CAF subpopulations (111, 112) exist within PDAC. Nonspecific ablation of CAFs induces both immune remodeling and a more aggressive tumor phenotype (113, 114), suggesting that an immunologically favorable and tumor suppressive CAF subpopulation exists within PDAC. Similar to other cancers, where CAF subtypes can promote TLS formation (115), a link between PDAC CAFs and PDAC TLS may exist. A recent study described associations between CAF-derived TGF-β with increased TLS gene signatures within PDAC (57). Furthermore, the authors observed that the expression of CXCL13 on CD4 and CD8 T cells occurred in a TGF-β dependent fashion, highlighting the interaction between PDAC TLS and CAFs.

However, this immunologically favorable CAF-TLS interaction in PDAC is still relatively undefined. For one, if the immunologically favorable CAF subtype exists, it is not fully characterized. A potential biomarker of this putative CAF subtype may be podoplanin (PDPN), a lymphatic endothelial and CAF marker (116, 117). PDPN expression on fibroblasts can promote TLS establishment (54), while recent studies in PDAC demonstrated that a PDPN+ CAF subtype (112, 118) was associated with improved prognosis and enrichment of immune-related pathways, However, the role of PDPN in cancer is controversial, and associated with worse outcomes in multiple cancers, including PDAC (119, 120). A more thorough understanding of CAFs and CAF plasticity in PDAC (120) may provide clarification. 6 Clinical significance of PDAC TLS.

In a variety of cancers, mature TLS are associated with improved progression-free survival (41–43, 63, 64, 121) and response to immunotherapy (122). Similarly, a preponderance of data from human PDAC samples have linked TLS with improved survival (Table 1) (65, 67, 91, 99–101, 123, 124). Multiple groups demonstrated a survival benefit with the presence of mature TLS (98, 100, 103). Other have reported the prognostic presence of with intratumoral TLS (123). One of the first groups to report on TLS in PDAC examined surgical specimens from 308 treatment-naïve PDAC patients and identified mature TLS based on histopathological examination (65). Within their study cohort and an additional validation cohort of 226 patients, 84% of samples contained peritumoral TLS, while 16% contained intratumoral TLS. The presence of intratumoral TLS conferred a significant survival benefit, with a median survival of 42.7 months compared to 29.4 months for those with only peritumoral TLS. The presence of intratumoral TLS also correlated with increased CD4 and CD8 T cell infiltration and decreased Treg and M2 macrophage infiltration in the TiME, suggestive of a more anti-tumoral and immunogenic TiME. These findings are corroborated by other retrospective studies examining TLS in surgical PDAC specimens (67, 99, 101).

Importantly, many of these studies describing mature TLS are based upon histological examination and identification of TLS based on the presence of GCs and surrogate markers of maturity such as PNAd+ HEVs (65, 93, 101, 124) and are likely excluding early and immature TLS from analysis. Precise characterization of TLS maturity may have clinical ramifications, as one study reports early PDAC TLS having greater CD8+ T cell infiltration and being enriched for IgG1 class-switched memory B cells and memory CD4 + T cells (67). Using the Cancer Genome Atlas Program PDAC datasets, early TLS are found to harbor decreased tumor molecular burden, but mature TLS expressed more neoantigens and increased B cell somatic hypermutation (78).

TABLE 1 Retrospective analyses of TLS in PDAC and survival outcomes.

Cancer Types	PDAC Stage	# of Patients	TLS Findings	Outcome Measure	Reference
PDAC only	Resectable	534	TLS Grade (based on localization and frequency): grade 1 (49%), grade 2 (35%), grade 3 (14.3%), and grade 4 (1.6%)	mOS (42.7months (intratumor TLS+) vs 15.5 months (TLSneg); p < 0.05)	(65) Hiraoka, N., et al. British Journal of Cancer, 2015. 112(11): p. 1782-1790.
PDAC only	All	140; surgery alone n= 93; NAC n=47	TLO rate (n=128/140) 91.4%; no significant difference between surgery alone and NAC (p=0.058)	5-year OS: 44.2% (NAC) vs 17.7% (surgery alone); p = 0.0017. In NAC group: high TLO/tumor ratio had better prognosis than low TLS/tumor; p = 0.0326	(66) Kuwabara et al. Cancer Science, 2019. 110(6): p. 1853-1862.
PDAC only	Resectable	63	TLS + in n=29 (46%) with at least 2 organized lymphoid aggregates.	mOS (26.3 in TLS+ vs 14.4 months in TLSneg; p = 0.014, HR 1.96)	(67) Gunderson, Andrew J., et al. Oncoimmunology, 2021. 10(1): 1900635.
PDAC only	Resectable	104	CD20-TLT immune reactive area (IRA%) range: 0-23.5% and CD20-TIL IRA% range: <0.05-1.89%	immune signature comprising CD20-TLT^{hi}/CD20-TIL^{lo} with mOS 30.9mo versus 14.1mo (other combos); p = 0.0051	(91) Castino et al. Oncoimmunology, 2016. 5(4): p. e1085147
PDAC only	Resectable	55	TSL + in n=38 (69%)	TLS + had improved OS compared to TLS neg (HR 0.509, 95% CI (0.29-0.89); p = 0.018	(99) Ahmed et al. Oncoimmunology, 2022. 11(1): p. 2027148.
PDAC and pNET	Resectable	27; n=20 PDAC, n=7 pNET	CD20+ TLS in 64% (9/14 PDAC) in tumor stroma (no NAT); TLS infrequent in pNET and rare in PDAC who received NAT (1/6).	mOS TLS+, 755 days; TLSneg, 478 days; HR 0.15, 95% CI, 0.02-1.19, P = 0.07)	(100) Stromnes et al. Cancer Immunology Research, 2017. 5(11): p. 978-991.
PDAC	Resectable	110	TLT presence (17.5% of PDAC) correlated with low-tumor budding and increased OS (p<0.0001) and increased DFS (p = 0.0067)	mOS of Immune-rich with TLTs of 23mo vs. 10mo for immune-escape	(101) Wartenberg et al. Clinical Cancer Research, 2018. 24(18): p. 4444-4454
PDAC	Resectable	127	75% samples had intermediate (100–300 CD3+ cells/mm2) or high (>300 CD3+ cells/mm2) infiltrating T-cells	mOS for TLS+ (n=76) of 27.5mo vs. 14.6mo (n=51) for TLSneg; p=0.0284	(104) Poschke et al. Oncoimmunology, 2016. 5(12): p. e1240859.
PDAC	Resectable	n=380 without NAT; n=136 with NAT	TLS in 80/380 (21.1%) of surgery alone and 21/136 (15.4%) with NAT	Surgery alone: TLS+ had improved OS 24mo vs 12mo in TLSneg p=0.0011 NAT: no significant difference in OS based on TLS.	(123) Xuan et al. Journal for ImmunoTherapy of Cancer, 2023. **11**(6): p. e006698.
PDAC only	Resectable	162	TLS+ in n=112 (69.1%)	Pancreatic cancer-specific survival with adjuvant S-1: HR 0.37; 95% CI 0.25 - 0.56; p < 0.0001	(124) Tanaka et al. Journal of Gastroenterology, 2023. 58(3): p. 277-291
Lung, sarcoma, bladder, colorectal, head/neck, renal, breast, PDAC	All	328	mature TLS positive: 84 cases (25.6%)	anti-PD1 or anti-PDL1 treatment: PFS (6.1 vs 2.7 months; p = 0.015), mOS (24.8 vs 13.3 months; p = 0.016)	(124) Vanhersecke et al. Nature Cancer, 2021. 2 (8): p. 794-802.

*NAC, neoadjuvant chemotherapy; TLO, tertiary lymphoid organ; NAT, neoadjuvant therapy; TLS, tertiary lymphoid structures; TLT, tertiary lymphoid tissue; TIL, tumor infiltrating lymphocytes.

Aside from their impact on CD8 T cells, mature TLS with GCs were enriched for other immunologically relevant immune cell phenotypes, including activated CD4+ memory cells, naïve B cells, and NK cells (67). The interaction between TLS and B cells is noteworthy; in cancers, the role of B cell infiltration is controversial, and has been linked to both pro-tumorigenic (125–127) and anti-tumorigenic (69, 91, 97) states. In human PDAC samples, the spatial distribution of B cells is predominantly within either TLS or at the tumor-stromal interface (91). Interestingly, only TLS-associated B cells were associated with improved prognosis, while an immune signature associated with increased TLS-associated B cells and low B cell TILs predicted longer overall survival (91), supporting the clinical relevance of a TLS-specific subset of B cells within PDAC.

6 Preclinical evidence for targeting TLS

As TLS are associated with favorable TiME characteristics such as an increased level of CD8+ TILs (43, 128), targeting PDAC TLS may improve patient outcomes. Multiple studies (129–132) support the claim that standard of care chemotherapy can favorably alter the PDAC TiME to create an anti-tumoral immune niche. Evidence from matched pre- and post-neoadjuvant treated APC germline mutated hepatoblastoma samples suggested that cisplatin can induced immature TLS formation (133). Within PDAC, a preclinical TLS model established that TLS formation can be induced after intratumor injections of chemokines CXCL13 and CCL21 in an orthotopic pancreatic cancer mouse model (60). Furthermore, coadministration of gemcitabine with these lymphoid chemokines led to significant tumor reduction (60). It should be noted that the sole administration of gemcitabine within this study globally reduced immune cell infiltration within the tumors, while combination chemokine and gemcitabine therapy ameliorated this effect.

Vaccine-based PDAC immunotherapy trials in PDAC also highlight the role of TLS in immunotherapy. Vaccinating mice that spontaneously develop PDAC $Kras^{G12D}$ Pdx1-Cre (KPC) tumors with an α-enolase (ENO1) encoding vector led to a spatial reorganization of the TiME that is marked by TLS induction. These TLS had a higher number of PD-1^{+} germinal center and vaccinated mice had an ameliorated infiltration of antigen-specific T cells (91). A randomized clinical trial with administration of a granulocyte-macrophage colony-stimulating factor (GM-CSF)-allogeneic pancreatic tumor cell vaccine (GVAX) demonstrated the induction of mature TLS formation alone or in combination with low dose cyclophosphamide (134). These vaccine-induced TLS possessed multiple antitumoral attributes such as effector T cell trafficking, T cell activation, and differential expression of immune-regulating pathways. These induced TLS also expressed PD-1 and PD-L1, suggesting the benefit of combination with ICI therapy.

7 PDAC TLS and therapy response

TLS presence is associated with neoadjuvant therapy response in cancers (96, 135, 136). Data on TLS and response to chemotherapy in PDAC remains limited. One group compared a total of 140 resected PDAC specimens from patients who received up-front surgery to those who received neoadjuvant therapy. The TLS from the neoadjuvant therapy group possessed higher proportions of CD8 T cells and lower proportions of PD-1 expressing lymphocytes compared to those from the up-front surgery group, suggesting the induction of an antitumoral niche within TLS through neoadjuvant therapy (66). Another retrospective analysis of 162 patients found that PDAC patients with TLS had longer cancer-specific survival when treated with 5FU-based therapy compared to gemcitabine-based or no adjuvant therapy (124). As platinum-based therapies such as cisplatin and oxaliplatin can interact with the TiME by inducing cytotoxic T cell activity through immunogenic cell death (137–140), the choice of chemotherapy may impact the predictive value of TLS. In contrast, a recent study of 380 treatment-naïve PDAC patients and 136 PDAC patients treated with predominantly gemcitabine-based neoadjuvant chemotherapy demonstrated significant alterations of the neoadjuvant-treated intratumoral TLS (123). The neoadjuvant-treated samples possessed fewer intratumoral TLS compared to the treatment-naïve samples, and the TLS within the neoadjuvant-treated group had significantly lower B cell proportions and higher Treg and macrophage proportions compared to their untreated counterparts (123). Furthermore, in contrast to the treatment-naïve group, the presence of intratumoral TLS within the neoadjuvant-treated group was no longer significantly associated with survival, suggesting that interactions between PDAC TLS and chemotherapy may depend on multiple factors such as the choice of chemotherapy, duration of therapy, or initiation with adjuncts such as corticosteroids (141).

Recent studies have also evaluated the favorable interaction between TLS and immunotherapy across a spectrum of cancers (142–144). As PDAC responds poorly to immune checkpoint inhibitors (ICIs) (9, 10), understanding the anti-tumoral and ICI-potentiating benefit of PDAC TLS becomes critical to improving treatment efficacy. Data from a cohort of 328 patients treated with immunotherapy, including a subset of patients diagnosed with PDAC, identified that mature TLS presence was correlated with increased CD8 T cell density, was predictive of response to ICIs, and an independent predictor of progression free and overall survival (122). These findings also suggest TLS may serve as marker for favorable outcome with FOLFIRINOX and can identify patients for future chemo-immunotherapy trials.

Similarly, as data are beginning to evolve regarding the role of TLS with immunotherapy responses in several aggressive cancer types, a number of clinical trials assessing immunotherapy as an effective treatment strategy for pancreatic ductal adenocarcinoma have been conducted (NCT03214250, NCT03404960, NCT02879318, NCT01836432). However, no trials have also investigated the role of immunotherapy with induction or presence of TLS or in respect to other modulations of the TiME in PDAC. This underscores the need for additional translational studies investigating the role of both TLS and TiME as they relate to immunotherapy responses in PDAC.

8 Future directions to enhance TLS function

As our understanding of the role of TLS in cancers improves, the translational utility of manipulating TLS has become an area of interest as well. As an initial step within the clinical setting, several well-known markers could be used to identify TLS. These could include CD3, CD4 and CD8 for T cells, CD19 or CD20 for B cells, CD21 for FDCs, CD138 for plasma cells, DC-LAMP for mature FDCs, as well as other activation markers (48). Antigen presenting B cells with a high expression of CD86 and a low expression of CD21 have been shown to localize in TLS in several cancers (145).

A chemokine-based "12-CK score" (CXCL9, CXCL10, CXCL11, CXCL13, CCL2, CCL3, CCL4, CCL5, CCL8, CCL18, CCL19 and CCL21) was initially proposed and developed based on colorectal cancer samples (146). Subsequently, this score has been validated as a TLS transcriptomic signature with prognostic significance in several neoplasms (147). A similar 12-chemokine gene signature (CCL2, CCL3, CCL4, CCL5, CCL8, CCL18, CCL19, CCL21, CXCL9, CXCL10, CXCL11, and CXCL13) was derived through metagene analysis and correlated with enhanced patient survival in colorectal cancer (146) independent of tumor stage, location, microsatellite stability status, or treatment. As a single marker, IL-2 levels could be used as a potential biomarker for PDAC TLS formation, as analysis of paired blood and tumor samples from PDAC patients revealed the existence of a "stroma-to-serum" gradient in patients that lack TLS and an association between lower serum IL-2 levels and TLS formation (99). These findings highlight the potential of using serum biomarkers to predict response to immunotherapy; however, additional work needs to be done to determine the optimal time of IL2 monitoring.

Looking ahead, preclinical and clinical studies of the molecular manipulation of TLS may inform PDAC TLS strategies. For example, Tregs play an important role in TLS maintenance and can dampen anti-tumor responses in secondary lymphoid organs, e.g., lymph nodes and spleen. Tregs express high amounts of IL2 receptor as well as immunoinhibitory receptor for PD-1. Infiltration of Tregs into lung adenocarcinoma mouse models was found to suppress anti-tumor responses in TLS; ablation of Tregs induces strong effector T cell responses and tumor destruction (148, 149). Treg deletion may be another promising therapeutic option.

Lymphotoxins belong to the tumor necrosis factor (TNF) superfamily and play an important role in lymphoid tissue organogenesis and may be associated with TLS development (150). Lymphotoxin beta receptor (LTβR) signaling has been shown to mediate the formation of HEVs (72) and FDCs (151). Another lymphotoxin, LIGHT/TNFSF24, increases lymphoid penetration and lead to changes in the TIME, such as the development of TLS (152, 153). Evidence from more than two decades ago revealed that the ectopic expression of chemokines like CCL19 and CCL21 in pancreatic islets led to small-sized infiltrates of lymphocytes with stromal cells and HEVs (154, 155). Other earlier studies also revealed the critical role of chemokines such as TCA4/SLC (60) in pancreatic lymphoid neogenesis. In an orthotopic murine mesothelioma model expressing human mesothelin, treatment with a mesothelin-targeted Fab linked to a toxin eradicated tumors and induced TLS formation (156). Knowing that mesothelin is expressed in almost all pancreatic ductal adenocarcinomas (157), its potential role as a therapeutic target to induce TLS formation in PDAC warrants further investigation.

Looking toward evidence from other preclinical cancer models, other methods to induce TLS formation may be applicable to PDAC. Stimulator of interferon genes, or STING, is a double-stranded DNA sensor, that along with STING agonists, can activate antitumoral immune responses (158). One group demonstrated that intratumoral injection of ADU S-100, a STING agonist, in a preclinical melanoma model promoted formation of CCL19+, CCL21+, PNAd+ TLS, although these TLS did not contain significant B cell infiltration or GCs (159). Similarly, oral administration of an oncolytic virus (160) carrying a vector expressing IL-15 produced similar results in lung cancer and melanoma mouse models (161). This is intriguing not only for the potential of inducing PDAC TLS formation through delivery of lymphogenic cytokines, but the use of oncolytic viruses in PDAC (162) may serve as an effective method to overcome barriers to drug delivery in PDAC (134, 163). This could also be adapted to potentiate the function of existing TLS by inducing immunogenic cell death (164) to enhance T cell mediated immune responses that may originate from pre-existing PDAC TLS.

Other future strategies to potentiate PDAC TLS function may target specific cell populations found within the TLS. The PDAC immune microenvironment possesses immune checkpoint heterogeneity (17), with a distinct subset of exhausted CD8 TILs expressing T-cell immunoglobulin and ITIM domain (TIGIT) (165). A recent study demonstrated the presence of CD8 T cells expressing both PD-1 and TIGIT which were located predominantly within PDAC TLS (166). PD-1+ TIGIT+ Cd8 T cells are associated with worse prognosis in cancer (167), and the relationship between this dual immune checkpoint expressing T cell phenotype and the PDAC TLS have yet to be elucidated. However, dual checkpoint blockade against PD-1 and TIGIT partially restored T cell proliferation and cytokine production (166), suggesting a potential therapeutic avenue for potentiating a TLS-mediated T cell response. CAF-specific therapy strategies targeting CAF plasticity may also be of potential benefit. Multiple phenotypically diverse CAF subtypes have been described in PDAC (112, 116, 118, 121). While the majority of CAF subtypes possess tumorigenic and immunosuppressive capabilities, evidence suggests that a minority of PDAC CAFs are associated with upregulation of immune signatures and TLS formation (57, 112, 118). Strategies involving CAF reprogramming (168, 169) may provide a useful adjunct to TLS-focused strategies in the future.

9 Conclusions

As our understanding of PDAC TLS continues to evolve, it is becoming increasingly evident that they hold promise as a prognostic marker and therapeutic target. The manipulation of TLS may pave the way for novel diagnostic tools, innovative immunotherapeutic strategies, combination treatments, and ultimately improving clinical outcomes for a patient population in need of improved outcomes. Moving forward, further research and clinical trials are warranted to capitalize on the potential of TLS as an integral element in the fight against PDAC.

Author contributions

ZG: Conceptualization, Writing – original draft, Writing – review & editing. JA: Visualization, Writing – review & editing. HZ: Writing – review & editing. SW-P: Writing – review & editing. SK: Data curation, Visualization, Writing – review & editing. CM:

Visualization, Writing – review & editing. MR: Writing – review & editing. SM: Writing – review & editing. H-SL: Visualization, Writing – review & editing. EC: Writing – review & editing, Funding acquisition, Project administration, Supervision.

Funding

The author(s) declare financial support was received for the research, authorship, and/or publication of this article. This work was supported in part by Merit Review Award # I01 CX001880-01A1 from the United States (U.S.) Department of Veterans Affairs Biomedical Laboratory Research and Development Program (ERC), and by an award from the National Pancreatic Cancer Foundation. Additional support was provided by a pilot grant from a Cancer Prevention and Research Institute of Texas grant (Lee: CPRIT RP200443), an NIH R21 (Lee: R1AI159379), a US Department of Defense Impact Award (Lee: W81XWH-22-1-0657), the Helis Medical Research Foundation (Lee), and the Dan L Duncan Comprehensive Cancer Center, which is partly funded by the NIH grant P30 CA125123 (Camp & Lee). This project was also supported by the Cytometry and Cell Sorting Core at Baylor College of Medicine with funding from the NIH (NCI P30CA125123 and NCRR S10RR024574) and CPRIT (RP180672) and the assistance of Joel M. Sederstrom.

Conflict of interest

The authors declare that the research was conducted in the absence of any commercial or financial relationships that could be construed as a potential conflict of interest.

Publisher's note

References

1. Rahib L, Smith BD, Aizenberg R, Rosenzweig AB, Fleshman JM, Matrisian LM. Projecting cancer incidence and deaths to 2030: the unexpected burden of thyroid, liver, and pancreas cancers in the united states. *Cancer Res* (2014) 74(11):2913–21. doi: 10.1158/0008-5472.CAN-14-0155

2. Conroy T, Desseigne F, Ychou M, Bouche O, Guimbaud R, Becouarn Y, et al. FOLFIRINOX versus gemcitabine for metastatic pancreatic cancer. *N Engl J Med* (2011) 364(19):1817–25. doi: 10.1056/NEJMoa1011923

3. Couzin-Frankel J. Cancer immunotherapy. *Science* (2013) 342(6165):1432–3. doi: 10.1126/science.342.6165.1432

4. Topalian SL, Drake CG, Pardoll DM. Immune checkpoint blockade: a common denominator approach to cancer therapy. *Cancer Cell* (2015) 27(4):450–61. doi: 10.1016/j.ccell.2015.03.001

5. Ribas A, Wolchok JD. Cancer immunotherapy using checkpoint blockade. *Science* (2018) 359(6382):1350–5. doi: 10.1126/science.aar4060

6. Farkona S, Diamandis EP, Blasutig IM. Cancer immunotherapy: the beginning of the end of cancer? *BMC Med* (2016) 14(1):73. doi: 10.1186/s12916-016-0623-5

7. Le DT, Durham JN, Smith KN, Wang H, Bartlett BR, Aulakh LK, et al. Mismatch repair deficiency predicts response of solid tumors to PD-1 blockade. *Science* (2017) 357(6349):409–13. doi: 10.1126/science.aan6733

8. Brahmer JR, Tykodi SS, Chow LQ, Hwu WJ, Topalian SL, Hwu P, et al. Safety and activity of anti-PD-L1 antibody in patients with advanced cancer. *N Engl J Med* (2012) 366(26):2455–65. doi: 10.1056/NEJMoa1200694

9. O'Reilly EM, Oh DY, Dhani N, Renouf DJ, Lee MA, Sun W, et al. Durvalumab with or without tremelimumab for patients with metastatic pancreatic ductal adenocarcinoma: A phase 2 randomized clinical trial. *JAMA Oncol* (2019) 5 (10):1431–8. doi: 10.1001/jamaoncol.2019.1588

10. Royal RE, Levy C, Turner K, Mathur A, Hughes M, Kammula US, et al. Phase 2 trial of single agent ipilimumab (anti-CTLA-4) for locally advanced or metastatic pancreatic adenocarcinoma. *J Immunother.* (2010) 33(8):828–33. doi: 10.1097/CJI.0b013e3181eec14c

11. Wong W, Alouani E, Wei A, Ryu YK, Chabot JA, Manji GA. Future of immunotherapy in pancreas cancer and the trials, tribulations and successes thus far. *Semin Oncol* (2021) 48(1):57–68. doi: 10.1053/j.seminoncol.2021.02.007

12. Patel GK, Perry JB, Abdul-Rahim O, Frankel AE, Cameron D, Taylor W, et al. Epidermal growth factor receptor-activating mutation(E746_T751>VP) in pancreatic ductal adenocarcinoma responds to erlotinib, followed by epidermal growth factor receptor resistance-mediating mutation (A647T): A case report and literature review. *J Cancer Res Ther* (2020) 16(4):950–4. doi: 10.4103/jcrt.JCRT_729_18

13. Leidner R, Sanjuan Silva N, Huang H, Sprott D, Zheng C, Shih YP, et al. Neoantigen t-cell receptor gene therapy in pancreatic cancer. *N Engl J Med* (2022) 386 (22):2112–9. doi: 10.1056/NEJMoa2119662

14. Yeo D, Giardina C, Saxena P, Rasko JEJ. The next wave of cellular immunotherapies in pancreatic cancer. *Mol Ther - Oncolytics.* (2022) 24:561–76. doi: 10.1016/j.omto.2022.01.010

15. Rojas LA, Sethna Z, Soares KC, Olcese C, Pang N, Patterson E, et al. Personalized RNA neoantigen vaccines stimulate t cells in pancreatic cancer. *Nature* (2023) 618 (7963):144–50. doi: 10.1038/s41586-023-06063-y

16. Ho WJ, Jaffee EM, Zheng L. The tumour microenvironment in pancreatic cancer - clinical challenges and opportunities. *Nat Rev Clin Oncol* (2020) 17(9):527–40. doi: 10.1038/s41571-020-0363-5

17. Steele NG, Carpenter ES, Kemp SB, Sirihorachai VR, The S, Delrosario L, et al. Multimodal mapping of the tumor and peripheral blood immune landscape in human pancreatic cancer. *Nat Cancer.* (2020) 1(11):1097–112. doi: 10.1038/s43018-020-00121-4

18. Bailey P, Chang DK, Nones K, Johns AL, Patch A-M, Gingras M-C, et al. Genomic analyses identify molecular subtypes of pancreatic cancer. *Nature* (2016) 531 (7592):47–52. doi: 10.1038/nature16965

19. Carstens JL, Correa de Sampaio P, Yang D, Barua S, Wang H, Rao A, et al. Spatial computation of intratumoral t cells correlates with survival of patients with pancreatic cancer. *Nat Commun* (2017) 8(1):15095. doi: 10.1038/ncomms15095

20. Balli D, Rech AJ, Stanger BZ, Vonderheide RH. Immune cytolytic activity stratifies molecular subsets of human pancreatic cancer. *Clin Cancer Res* (2017) 23 (12):3129–38. doi: 10.1158/1078-0432.CCR-16-2128

21. Bayne LJ, Beatty GL, Jhala N, Clark CE, Rhim AD, Stanger BZ, et al. Tumor-derived granulocyte-macrophage colony-stimulating factor regulates myeloid inflammation and t cell immunity in pancreatic cancer. *Cancer Cell* (2012) 21 (6):822–35. doi: 10.1016/j.ccr.2012.04.025

22. Blair AB, Kim VM, Muth ST, Saung MT, Lokker N, Blouw B, et al. Dissecting the stromal signaling and regulation of myeloid cells and memory effector t cells in pancreatic cancer. *Clin Cancer Res* (2019) 25(17):5351–63. doi: 10.1158/1078-0432.CCR-18-4192

23. Clark CE, Hingorani SR, Mick R, Combs C, Tuveson DA, Vonderheide RH. Dynamics of the immune reaction to pancreatic cancer from inception to invasion. *Cancer Res* (2007) 67(19):9518–27. doi: 10.1158/0008-5472.CAN-07-0175

24. Vayrynen SA, Zhang J, Yuan C, Vayrynen JP, Dias Costa A, Williams H, et al. Composition, spatial characteristics, and prognostic significance of myeloid cell infiltration in pancreatic cancer. *Clin Cancer Res* (2021) 27(4):1069–81. doi: 10.1158/1078-0432.CCR-20-3141

25. Dias Carvalho P, Guimaraes CF, Cardoso AP, Mendonca S, Costa AM, Oliveira MJ, et al. KRAS oncogenic signaling extends beyond cancer cells to orchestrate the microenvironment. *Cancer Res* (2018) 78(1):7–14. doi: 10.1158/0008-5472.CAN-17-2084

26. Lee HS, Jang HJ, Choi JM, Zhang J, de Rosen VL, Wheeler TM, et al. Comprehensive immunoproteogenomic analyses of malignant pleural mesothelioma. *JCI Insight* (2018) 3(7). doi: 10.1172/jci.insight.98575

27. Zhang J, Wolfgang CL, Zheng L. Precision immuno-oncology: Prospects of individualized immunotherapy for pancreatic cancer. *Cancers (Basel).* (2018) 10(2). doi: 10.3390/cancers10020039

28. Dougan SK. The pancreatic cancer microenvironment. *Cancer J* (2017) 23 (6):321–5. doi: 10.1097/PPO.0000000000000288

29. Saka D, Gokalp M, Piyade B, Cevik NC, Arik Sever E, Unutmaz D, et al. Mechanisms of t-cell exhaustion in pancreatic cancer. *Cancers (Basel).* (2020) 12(8). doi: 10.3390/cancers12082274

30. Bowers JS, Bailey SR, Rubinstein MP, Paulos CM, Camp ER. Genomics meets immunity in pancreatic cancer: Current research and future directions for pancreatic adenocarcinoma immunotherapy. *Oncol Rev* (2019) 13(2):430. doi: 10.4081/oncol.2019.430

31. Balachandran VP, Beatty GL, Dougan SK. Broadening the impact of immunotherapy to pancreatic cancer: Challenges and opportunities. *Gastroenterology* (2019) 156(7):2056–72. doi: 10.1053/j.gastro.2018.12.038

32. Sharma P, Hu-Lieskovan S, Wargo JA, Ribas A. Primary, adaptive, and acquired resistance to cancer immunotherapy. *Cell* (2017) 168(4):707–23. doi: 10.1016/j.cell.2017.01.017

33. Anderson KG, Stromnes IM, Greenberg PD. Obstacles posed by the tumor microenvironment to t cell activity: A case for synergistic therapies. *Cancer Cell* (2017) 31(3):311–25. doi: 10.1016/j.ccell.2017.02.008

34. Binnewies M, Roberts EW, Kersten K, Chan V, Fearon DF, Merad M, et al. Understanding the tumor immune microenvironment (TIME) for effective therapy. *Nat Med* (2018) 24(5):541–50. doi: 10.1038/s41591-018-0014-x

35. Zheng C, Fass JN, Shih YP, Gunderson AJ, Sanjuan Silva N, Huang H, et al. Transcriptomic profiles of neoantigen-reactive t cells in human gastrointestinal cancers. *Cancer Cell* (2022) 40(4):410–23 e7. doi: 10.1016/j.ccell.2022.03.005

36. Blando J, Sharma A, Higa MG, Zhao H, Vence L, Yadav SS, et al. Comparison of immune infiltrates in melanoma and pancreatic cancer highlights VISTA as a potential target in pancreatic cancer. *Proc Natl Acad Sci USA* (2019) 116(5):1692–7. doi: 10.1073/pnas.1811067116

37. Bailey P, Chang DK, Forget MA, Lucas FA, Alvarez HA, Haymaker C, et al. Exploiting the neoantigen landscape for immunotherapy of pancreatic ductal adenocarcinoma. *Sci Rep* (2016) 6:35848. doi: 10.1038/srep35848

38. Liu L, Zhao G, Wu W, Rong Y, Jin D, Wang D, et al. Low intratumoral regulatory t cells and high peritumoral CD8(+) t cells relate to long-term survival in patients with pancreatic ductal adenocarcinoma after pancreatectomy. *Cancer Immunol Immunother.* (2016) 65(1):73–82. doi: 10.1007/s00262-015-1775-4

39. Fukunaga A, Miyamoto M, Cho Y, Murakami S, Kawarada Y, Oshikiri T, et al. CD8+ tumor-infiltrating lymphocytes together with CD4+ tumor-infiltrating lymphocytes and dendritic cells improve the prognosis of patients with pancreatic adenocarcinoma. *Pancreas* (2004) 28(1):e26–31. doi: 10.1097/00006676-200401000-00023

40. Ino Y, Yamazaki-Itoh R, Shimada K, Iwasaki M, Kosuge T, Kanai Y, et al. Immune cell infiltration as an indicator of the immune microenvironment of pancreatic cancer. *Br J Cancer.* (2013) 108(4):914–23. doi: 10.1038/bjc.2013.32

41. Dieu-Nosjean M-C, Goc J, Giraldo NA, Sautès-Fridman C, Fridman WH. Tertiary lymphoid structures in cancer and beyond. *Trends Immunol* (2014) 35 (11):571–80.

42. Schumacher TN, Thommen DS. Tertiary lymphoid structures in cancer. *Science* (2022) 375(6576):eabf9419.

43. Sautès-Fridman C, Petitprez F, Calderaro J, Fridman WH. Tertiary lymphoid structures in the era of cancer immunotherapy. *Nat Rev Cancer.* (2019) 19(6):307–25. doi: 10.1038/s41568-019-0144-6

44. Aloisi F, Pujol-Borrell R. Lymphoid neogenesis in chronic inflammatory diseases. *Nat Rev Immunol* (2006) 6(3):205–17. doi: 10.1038/nri1786

45. Humby F, Bombardieri M, Manzo A, Kelly S, Blades MC, Kirkham B, et al. Ectopic lymphoid structures support ongoing production of class-switched autoantibodies in rheumatoid synovium. *PloS Med* (2009) 6(1):e1. doi: 10.1371/journal.pmed.0060001

46. Bombardieri M, Barone F, Humby F, Kelly S, McGurk M, Morgan P, et al. Activation-induced cytidine deaminase expression in follicular dendritic cell networks and interfollicular large b cells supports functionality of ectopic lymphoid neogenesis in autoimmune sialoadenitis and MALT lymphoma in sjögren's syndrome. *J Immunol* (2007) 179(7):4929–38. doi: 10.4049/jimmunol.179.7.4929

47. Kendall PL, Yu G, Woodward EJ, Thomas JW. Tertiary lymphoid structures in the pancreas promote selection of b lymphocytes in autoimmune diabetes. *J Immunol* (2007) 178(9):5643–51. doi: 10.4049/jimmunol.178.9.5643

48. Colbeck EJ, Ager A, Gallimore A, Jones GW. Tertiary lymphoid structures in cancer: drivers of antitumor immunity, immunosuppression, or bystander sentinels in disease? *Front Immunol* (2017) 8:1830.

49. Drayton DL, Liao S, Mounzer RH, Ruddle NH. Lymphoid organ development: from ontogeny to neogenesis. *Nat Immunol* (2006) 7(4):344–53. doi: 10.1038/ni1330

50. Martinet L, Garrido I, Filleron T, Le Guellec S, Bellard E, Fournie JJ, et al. Human solid tumors contain high endothelial venules: association with t- and b-lymphocyte infiltration and favorable prognosis in breast cancer. *Cancer Res* (2011) 71(17):5678–87. doi: 10.1158/0008-5472.can-11-0431

51. Heij LR, Tan X, Kather JN, Niehues JM, Sivakumar S, Heussen N, et al. Nerve fibers in the tumor microenvironment are co-localized with lymphoid aggregates in pancreatic cancer. *J Clin Med [Internet]* (2021) 10:3.

52. Gago da Graca C, van Baarsen LGM, Mebius RE. Tertiary lymphoid structures: Diversity in their development, composition, and role. *J Immunol* (2021) 206(2):273–81. doi: 10.4049/jimmunol.2000873

53. Pikor Natalia B, Astarita Jillian L, Summers-Deluca L, Galicia G, Qu J, Ward Lesley A, et al. Integration of Th17- and lymphotoxin-derived signals initiates meningeal-resident stromal cell remodeling to propagate neuroinflammation. *Immunity* (2015) 43(6):1160–73. doi: 10.1016/j.immuni.2015.11.010

54. Nayar S, Campos J, Smith CG, Iannizzotto V, Gardner DH, Mourcin F, et al. Immunofibroblasts are pivotal drivers of tertiary lymphoid structure formation and local pathology. *Proc Natl Acad Sci* (2019) 116(27):13490–7. doi: 10.1073/pnas.1905301116

55. Koscso B, Kurapati S, Rodrigues RR, Nedjic J, Gowda K, Shin C, et al. Gut-resident CX3CR1hi macrophages induce tertiary lymphoid structures and IgA response in situ. *Sci Immunol* (2020) 5(46):10. doi: 10.1126/sciimmunol.aax0062

56. McDonald KG, McDonough JS, Dieckgraefe BK, Newberry RD. Dendritic cells produce CXCL13 and participate in the development of murine small intestine lymphoid tissues. *Am J Pathology.* (2010) 176(5):2367–77. doi: 10.2353/ajpath.2010.090723

57. Kinker GS, Vitiello GAF, Diniz AB, Cabral-Piccin MP, Pereira PHB, Carvalho MLeticiaR, et al. Mature tertiary lymphoid structures are key niches of tumour-specific immune responses in pancreatic ductal adenocarcinomas. *Gut* (2023) 72(10):1927. doi: 10.1136/gutjnl-2022-328697

58. Luther SA, Lopez T, Bai W, Hanahan D, Cyster JG. BLC expression in pancreatic islets causes b cell recruitment and lymphotoxin-dependent lymphoid neogenesis. *Immunity* (2000) 12(5):471–81. doi: 10.1016/s1074-7613(00)80199-5

59. Delvecchio FR, Fincham REA, Spear S, Clear A, Roy-Luzarraga M, Balkwill FR, et al. Pancreatic cancer chemotherapy is potentiated by induction of tertiary lymphoid structures in mice. *Cell Mol Gastroenterol Hepatology.* (2021) 12(5):1543–65. doi: 10.1016/j.jcmgh.2021.06.023

60. Fan L, Reilly CR, Luo Y, Dorf ME, Lo D. Cutting edge: ectopic expression of the chemokine TCA4/SLC is sufficient to trigger lymphoid neogenesis. *J Immunol* (2000) 164(8):3955–9. doi: 10.4049/jimmunol.164.8.3955

61. Finkin S, Yuan D, Stein I, Taniguchi K, Weber A, Unger K, et al. Ectopic lymphoid structures function as microniches for tumor progenitor cells in hepatocellular carcinoma. *Nat Immunol* (2015) 16(12):1235–44. doi: 10.1038/ni.3290

62. Murakami J, Shimizu Y, Kashii Y, Kato T, Minemura M, Okada K, et al. Functional b-cell response in intrahepatic lymphoid follicles in chronic hepatitis c. *Hepatology* (1999) 30(1):143–50. doi: 10.1002/hep.510300107

63. Siliņa K, Soltermann A, Attar FM, Casanova R, Uckeley ZM, Thut H, et al. Germinal centers determine the prognostic relevance of tertiary lymphoid structures and are impaired by corticosteroids in lung squamous cell carcinoma. *Cancer Res* (2018) 78(5):1308–20. doi: 10.1158/0008-5472.CAN-17-1987

64. Posch F, Silina K, Leibl S, Mündlein A, Moch H, Siebenhüner A, et al. Maturation of tertiary lymphoid structures and recurrence of stage II and III colorectal cancer. *OncoImmunology* (2018) 7(2):e1378844. doi: 10.1080/2162402X.2017.1378844

65. Hiraoka N, Ino Y, Yamazaki-Itoh R, Kanai Y, Kosuge T, Shimada K. Intratumoral tertiary lymphoid organ is a favourable prognosticator in patients with pancreatic cancer. *Br J Cancer.* (2015) 112(11):1782–90. doi: 10.1038/bjc.2015.145

66. Kuwabara S, Tsuchikawa T, Nakamura T, Hatanaka Y, Hatanaka KC, Sasaki K, et al. Prognostic relevance of tertiary lymphoid organs following neoadjuvant chemoradiotherapy in pancreatic ductal adenocarcinoma. *Cancer Science.* (2019) 110 (6):1853–62. doi: 10.1111/cas.14023

67. JG A, Rajamanickam V, Bui C, Bernard B, Pucilowska J, Ballesteros-Merino C, et al. Germinal center reactions in tertiary lymphoid structures associate with neoantigen burden, humoral immunity and long-term survivorship in pancreatic cancer. *Oncoimmunology* (2021) 10(1):1900635. doi: 10.1080/2162402x.2021.1900635

68. Klein U, Dalla-Favera R. Germinal centres: role in b-cell physiology and malignancy. *Nat Rev Immunol* (2008) 8(1):22–33. doi: 10.1038/nri2217

69. Germain C, Gnjatic S, Tamzalit F, Knockaert S, Remark R, Goc J, et al. Presence of b cells in tertiary lymphoid structures is associated with a protective immunity in patients with lung cancer. *Am J Respir Crit Care Med* (2014) 189(7):832–44.

70. Astorri E, Bombardieri M, Gabba S, Peakman M, Pozzilli P, Pitzalis C. Evolution of ectopic lymphoid neogenesis and *in situ* autoantibody production in autoimmune nonobese diabetic mice: cellular and molecular characterization of tertiary lymphoid structures in pancreatic islets. *J Immunol* (2010) 185(6):3359–68. doi: 10.4049/jimmunol.1001836

71. Girard JP, Springer TA. High endothelial venules (HEVs): specialized endothelium for lymphocyte migration. *Immunol Today* (1995) 16(9):449–57. doi: 10.1016/0167-5699(95)80023-9

72. Browning JL, Allaire N, Ngam-ek A, Notidis E, Hunt J, Perrin S, et al. Lymphotoxin-β receptor signaling is required for the homeostatic control of HEV differentiation and function. *Immunity* (2005) 23(5):539–50. doi: 10.1016/j.immuni.2005.10.002

73. Jones E, Gallimore A, Ager A. Defining high endothelial venules and tertiary lymphoid structures in cancer. *Methods Mol Biol* (2018) 1845:99–118. doi: 10.1007/978-1-4939-8709-2_7

74. Ladányi A, Kiss J, Somlai B, Gilde K, Fejos Z, Mohos A, et al. Density of DC-LAMP(+) mature dendritic cells in combination with activated t lymphocytes

infiltrating primary cutaneous melanoma is a strong independent prognostic factor. *Cancer Immunol Immunother.* (2007) 56(9):1459–69. doi: 10.1007/s00262-007-0286-3

75. Allen E, Jabouille A, Rivera LB, Lodewijckx I, Missiaen R, Steri V, et al. Combined antiangiogenic and anti-PD-L1 therapy stimulates tumor immunity through HEV formation. *Sci Trans Med* (2017) 9(385). doi: 10.1126/scitranslmed.aak9679

76. Wirsing AM, Ervik IK, Seppola M, Uhlin-Hansen L, Steigen SE, Hadler-Olsen E. Presence of high-endothelial venules correlates with a favorable immune microenvironment in oral squamous cell carcinoma. *Modern Pathology.* (2018) 31 (6):910–22. doi: 10.1038/s41379-018-0019-5

77. Lee M, Heo SH, Song IH, Rajayi H, Park HS, Park IA, et al. Presence of tertiary lymphoid structures determines the level of tumor-infiltrating lymphocytes in primary breast cancer and metastasis. *Mod Pathol* (2019) 32(1):70–80. doi: 10.1038/s41379-018-0113-8

78. Masugi Y, Abe T, Ueno A, Fujii-Nishimura Y, Ojima H, Endo Y, et al. Characterization of spatial distribution of tumor-infiltrating CD8+ t cells refines their prognostic utility for pancreatic cancer survival. *Modern Pathology.* (2019) 32 (10):1495–507. doi: 10.1038/s41379-019-0291-z

79. Liudahl SM, Betts CB, Sivagnanam S, Morales-Oyarvide V, da Silva A, Yuan C, et al. Leukocyte heterogeneity in pancreatic ductal adenocarcinoma: Phenotypic and spatial features associated with clinical outcome. *Cancer Discovery.* (2021) 11(8):2014–31. doi: 10.1158/2159-8290.CD-20-0841

80. Papalampros A, Vailas M, Ntostoglou K, Chiloeches ML, Sakellariou S, Chouliari NV, et al. Unique spatial immune profiling in pancreatic ductal adenocarcinoma with enrichment of exhausted and senescent t cells and diffused CD47-SIRPα expression. *Cancers [Internet]* (2020) 12:7.

81. Binkley CE, Zhang L, Greenson JK, Giordano TJ, Kuick R, Misek D, et al. The molecular basis of pancreatic fibrosis: common stromal gene expression in chronic pancreatitis and pancreatic adenocarcinoma. *Pancreas* (2004) 29(4):254–63.

82. Bachem MG, Schünemann M, Ramadani M, Siech M, Beger H, Buck A, et al. Pancreatic carcinoma cells induce fibrosis by stimulating proliferation and matrix synthesis of stellate cells. *Gastroenterology* (2005) 128(4):907–21.

83. Armstrong T, Packham G, Murphy LB, Bateman AC, Conti JA, Fine DR, et al. Type i collagen promotes the malignant phenotype of pancreatic ductal adenocarcinoma. *Clin Cancer Res* (2004) 10(21):7427–37.

84. Schröder AE, Greiner A, Seyfert C, Berek C. Differentiation of b cells in the nonlymphoid tissue of the synovial membrane of patients with rheumatoid arthritis. *Proc Natl Acad Sci* (1996) 93(1):221–5.

85. Dorner T, Hansen A, Jacobi A, Lipsky P. Immunglobulin repertoire analysis provides new insights into the immunopathogenesis of sjogren's syndrome. *Autoimmun Rev* (2002) 1(3):119–24.

86. Sims GP, Shiono H, Willcox N, Stott DI. Somatic hypermutation and selection of b cells in thymic germinal centers responding to acetylcholine receptor in myasthenia gravis. *J Immunol* (2001) 167(4):1935–44.

87. Kim H-J, Krenn V, Steinhauser G, Berek C. Plasma cell development in synovial germinal centers in patients with rheumatoid and reactive arthritis. *J Immunol* (1999) 162(5):3053–62.

88. Meylan M, Petitprez F, Becht E, Bougoüin A, Pupier G, Calvez A, et al. Tertiary lymphoid structures generate and propagate anti-tumor antibody-producing plasma cells in renal cell cancer. *Immunity* (2022) 55(3):527–41.e5. doi: 10.1016/j.immuni.2022.02.001

89. Montfort A, Pearce O, Maniati E, Vincent BG, Bixby L, Böhm S, et al. A strong b-cell response is part of the immune landscape in human high-grade serous ovarian metastases. *Clin Cancer Res* (2017) 23(1):250–62. doi: 10.1158/1078-0432.Ccr-16-0081

90. Spear S, Candido JB, McDermott JR, Ghirelli C, Maniati E, Beers SA, et al. Discrepancies in the tumor microenvironment of spontaneous and orthotopic murine models of pancreatic cancer uncover a new immunostimulatory phenotype for b cells. *Front Immunol* (2019) 10:542.

91. Castino GF, Cortese N, Capretti G, Serio S, Di Caro G, Mineri R, et al. Spatial distribution of b cells predicts prognosis in human pancreatic adenocarcinoma. *OncoImmunology* (2016) 5(4):e1085147. doi: 10.1080/2162402X.2015.1085147

92. Galon J, Costes A, Sanchez-Cabo F, Kirilovsky A, Mlecnik B, Lagorce-Pagès C, et al. Type, density, and location of immune cells within human colorectal tumors predict clinical outcome. *Science* (2006) 313(5795):1960–4. doi: 10.1126/science.1129139

93. Erdag G, Schaefer JT, Smolkin ME, Deacon DH, Shea SM, Dengel LT, et al. Immunotype and immunohistologic characteristics of tumor-infiltrating immune cells are associated with clinical outcome in metastatic melanoma. *Cancer Res* (2012) 72 (5):1070–80. doi: 10.1158/0008-5472.Can-11-3218

94. Ali HR, Provenzano E, Dawson SJ, Blows FM, Liu B, Shah M, et al. Association between CD8+ t-cell infiltration and breast cancer survival in 12 439 patients. *Ann Oncol* (2014) 25(8):1536–43. doi: 10.1093/annonc/mdu191

95. Lee Y, Chin RK, Christiansen P, Sun Y, Tumanov AV, Wang J, et al. Recruitment and activation of naive t cells in the islets by lymphotoxin β receptor-dependent tertiary lymphoid structure. *Immunity* (2006) 25(3):499–509. doi: 10.1016/j.immuni.2006.06.016

96. Yu P, Lee Y, Liu W, Chin RK, Wang J, Wang Y, et al. Priming of naive t cells inside tumors leads to eradication of established tumors. *Nat Immunol* (2004) 5(2):141–9.

97. Di Caro G, Bergomas F, Grizzi F, Doni A, Bianchi P, Malesci A, et al. Occurrence of tertiary lymphoid tissue is associated with t-cell infiltration and predicts better prognosis in early-stage colorectal cancers. *Clin Cancer Res* (2014) 20(8):2147–58.

98. Schrama D, Voigt H, Eggert AO, Xiang R, Zhou H, Schumacher TN, et al. Immunological tumor destruction in a murine melanoma model by targeted LTalpha independent of secondary lymphoid tissue. *Cancer Immunol Immunother.* (2008) 57 (1):85–95. doi: 10.1007/s00262-007-0352-x

99. Ahmed A, Köhler S, Klotz R, Giese N, Hackert T, Springfeld C, et al. Tertiary lymphoid structures and their association to immune phenotypes and circulatory IL2 levels in pancreatic ductal adenocarcinoma. *OncoImmunology* (2022) 11(1):2027148. doi: 10.1080/2162402X.2022.2027148

100. Stromnes IM, Hulbert A, Pierce RH, Greenberg PD, Hingorani SR. T-cell localization, activation, and clonal expansion in human pancreatic ductal adenocarcinoma. *Cancer Immunol Res* (2017) 5(11):978–91. doi: 10.1158/2326-6066.CIR-16-0322

101. Wartenberg M, Cibin S, Zlobec I, Vassella E, Eppenberger-Castori S, Terracciano L, et al. Integrated genomic and immunophenotypic classification of pancreatic cancer reveals three distinct subtypes with Prognostic/Predictive significance. *Clin Cancer Res* (2018) 24 (18):4444–54. doi: 10.1158/1078-0432.Ccr-17-3401

102. Peske JD, Thompson ED, Gemta L, Baylis RA, Fu Y-X, Engelhard VH. Effector lymphocyte-induced lymph node-like vasculature enables naive t-cell entry into tumours and enhanced anti-tumour immunity. *Nat Commun* (2015) 6(1):7114. doi: 10.1038/ncomms8114

103. Lutz ER, Wu AA, Bigelow E, Sharma R, Mo G, Soares K, et al. Immunotherapy converts nonimmunogenic pancreatic tumors into immunogenic foci of immune regulation. *Cancer Immunol Res* (2014) 2(7):616–31. doi: 10.1158/2326-6066.CIR-14-0027

104. Poschke I, Faryna M, Bergmann F, Flossdorf M, Lauenstein C, Hermes J, et al. Identification of a tumor-reactive t-cell repertoire in the immune infiltrate of patients with resectable pancreatic ductal adenocarcinoma. *OncoImmunology* (2016) 5(12): e1240859. doi: 10.1080/2162402X.2016.1240859

105. Ma Q-Y, Huang D-Y, Zhang H-J, Chen J, Miller W, Chen X-F. Function of follicular helper t cell is impaired and correlates with survival time in non-small cell lung cancer. *Int Immunopharmacology.* (2016) 41:1–7. doi: 10.1016/j.intimp.2016.10.014

106. Duan Z, Gao J, Zhang L, Liang H, Huang X, Xu Q, et al. Phenotype and function of CXCR5+CD45RA–CD4+ t cells were altered in HBV-related hepatocellular carcinoma and elevated serum CXCL13 predicted better prognosis. *Oncotarget* (2015) 6(42).

107. Gu-Trantien C, Loi S, Garaud S, Equeter C, Libin M, de Wind A, et al. CD4+ follicular helper t cell infiltration predicts breast cancer survival. *J Clin Invest* (2013) 123 (7):2873–92. doi: 10.1172/JCI67428

108. Lin X, Ye L, Wang X, Liao Z, Dong J, Yang Y, et al. Follicular helper t cells remodel the immune microenvironment of pancreatic cancer via secreting CXCL13 and IL-21. *Cancers [Internet]* (2021) 13:15.

109. Provenzano PP, Cuevas C, Chang AE, Goel VK, Von Hoff DD, Hingorani SR. Enzymatic targeting of the stroma ablates physical barriers to treatment of pancreatic ductal adenocarcinoma. *Cancer Cell* (2012) 21(3):418–29.

110. Jiang H, Hegde S, Knolhoff BL, Zhu Y, Herndon JM, Meyer MA, et al. Targeting focal adhesion kinase renders pancreatic cancers responsive to checkpoint immunotherapy. *Nat Med* (2016) 22(8):851–60. doi: 10.1038/nm.4123

111. Öhlund D, Handly-Santana A, Biffi G, Elyada E, Almeida AS, Ponz-Sarvise M, et al. Distinct populations of inflammatory fibroblasts and myofibroblasts in pancreatic cancer. *J Exp Med* (2017) 214(3):579–96. doi: 10.1084/jem.20162024

112. Neuzillet C, Tijeras-Raballand A, Ragulan C, Cros J, Patil Y, Martinet M, et al. Inter- and intra-tumoural heterogeneity in cancer-associated fibroblasts of human pancreatic ductal adenocarcinoma. *J Pathology.* (2019) 248(1):51–65. doi: 10.1002/path.5224

113. Özdemir BC, Pentcheva-Hoang T, Carstens JL, Zheng X, Wu C-C, Simpson TR, et al. Depletion of carcinoma-associated fibroblasts and fibrosis induces immunosuppression and accelerates pancreas cancer with reduced survival. *Cancer Cell* (2014) 25(6):719–34.

114. Rhim AD, Oberstein PE, Thomas DH, Mirek ET, Palermo CF, Sastra SA, et al. Stromal elements act to restrain, rather than support, pancreatic ductal adenocarcinoma. *Cancer Cell* (2014) 25(6):735–47.

115. Rodriguez AB, Peske JD, Woods AN, Leick KM, Mauldin IS, Meneveau MO, et al. Immune mechanisms orchestrate tertiary lymphoid structures in tumors *via* cancer-associated fibroblasts. *Cell Rep* (2021) 36(3).

116. Breiteneder-Geleff S, Soleiman A, Kowalski H, Horvat R, Amann G, Kriehuber E, et al. Angiosarcomas express mixed endothelial phenotypes of blood and lymphatic capillaries: podoplanin as a specific marker for lymphatic endothelium. *Am J pathology.* (1999) 154(2):385–94.

117. Pula B, Witkiewicz W, Dziegiel P, Podhorska-Okolow M. Significance of podoplanin expression in cancer-associated fibroblasts: A comprehensive review. *Int J Oncol* (2013) 42(6):1849–57. doi: 10.3892/ijo.2013.1887

118. Neuzillet C, Nicolle R, Raffenne J, Tijeras-Raballand A, Brunel A, Astorgues-Xerri L, et al. Periostin- and podoplanin-positive cancer-associated fibroblast subtypes cooperate to shape the inflamed tumor microenvironment in aggressive pancreatic adenocarcinoma. *J Pathology.* (2022) 258(4):408–25. doi: 10.1002/path.6011

119. Hirayama K, Kono H, Nakata Y, Akazawa Y, Wakana H, Fukushima H, et al. Expression of podoplanin in stromal fibroblasts plays a pivotal role in the prognosis of patients with pancreatic cancer. *Surg Today* (2018) 48:110–8.

120. Boyd LN, Andini KD, Peters GJ, Kazemier G, Giovannetti E. Heterogeneity and plasticity of cancer-associated fibroblasts in the pancreatic tumor microenvironment. In: *Seminars in cancer biology;*. Elsevier (2022). editors.

121. Horeweg N, Workel HH, Loiero D, Church DN, Vermij L, Léon-Castillo A, et al. Tertiary lymphoid structures critical for prognosis in endometrial cancer patients. *Nat Commun* (2022) 13(1):1373. doi: 10.1038/s41467-022-29040-x

122. Vanhersecke L, Brunet M, Guegan JP, Rey C, Bougouin A, Cousin S, et al. Mature tertiary lymphoid structures predict immune checkpoint inhibitor efficacy in solid tumors independently of PD-L1 expression. *Nat Cancer.* (2021) 2(8):794–802. doi: 10.1038/s43018-021-00232-6

123. Xuan Z, Xuan L, He C, Yusheng C, Ruijie W, Mingjian M, et al. Characterization of intratumoral tertiary lymphoid structures in pancreatic ductal adenocarcinoma: cellular properties and prognostic significance. *J ImmunoTherapy Cancer.* (2023) 11(6):e006698. doi: 10.1136/jitc-2023-006698

124. Tanaka T, Masuda A, Inoue J, Hamada T, Ikegawa T, Toyama H, et al. Integrated analysis of tertiary lymphoid structures in relation to tumor-infiltrating lymphocytes and patient survival in pancreatic ductal adenocarcinoma. *J Gastroenterology.* (2023) 58(3):277–91. doi: 10.1007/s00535-022-01939-8

125. Gunderson AJ, Kaneda MM, Tsujikawa T, Nguyen AV, Affara NI, Ruffell B, et al. Bruton tyrosine kinase–dependent immune cell cross-talk drives pancreas cancer. *Cancer Discovery.* (2016) 6(3):270–85. doi: 10.1158/2159-8290.CD-15-0827

126. Pylayeva-Gupta Y, Das S, Handler JS, Hajdu CH, Coffre M, Koralov SB, et al. IL35-producing b cells promote the development of pancreatic neoplasia. *Cancer Discovery.* (2016) 6(3):247–55. doi: 10.1158/2159-8290.CD-15-0843

127. Lee KE, Spata M, Bayne LJ, Buza EL, Durham AC, Allman D, et al. Hif1a deletion reveals pro-neoplastic function of b cells in pancreatic neoplasia. *Cancer Discovery.* (2016) 6(3):256–69. doi: 10.1158/2159-8290.CD-15-0822

128. Fridman WH, Pages F, Sautes-Fridman C, Galon J. The immune contexture in human tumours: impact on clinical outcome. *Nat Rev Cancer.* (2012) 12(4):298–306. doi: 10.1038/nrc3245

129. Mota Reyes C, Teller S, Muckenhuber A, Konukiewitz B, Safak O, Weichert W, et al. Neoadjuvant therapy remodels the pancreatic cancer microenvironment *via* depletion of protumorigenic immune cells. *Clin Cancer Res* (2020) 26(1):220–31.

130. Dias Costa A, Väyrynen SA, Chawla A, Zhang J, Väyrynen JP, Lau MC, et al. Neoadjuvant chemotherapy is associated with altered immune cell infiltration and an anti-tumorigenic microenvironment in resected pancreatic cancer. *Clin Cancer Res* (2022) 28(23):5167–79.

131. Farren MR, Sayegh L, Ware MB, Chen H-R, Gong J, Liang Y, et al. Immunologic alterations in the pancreatic cancer microenvironment of patients treated with neoadjuvant chemotherapy and radiotherapy. *JCI Insight* (2020) 5(1).

132. Peng H, James CA, Cullinan DR, Hogg GD, Mudd JL, Zuo C, et al. Neoadjuvant FOLFIRINOX therapy is associated with increased effector t cells and reduced suppressor cells in patients with pancreatic cancer. *Clin Cancer Res* (2021) 27 (24):6761–71.

133. Morcrette G, Hirsch TZ, Badour E, Pilet J, Caruso S, Calderaro J, et al. APC germline hepatoblastomas demonstrate cisplatin-induced intratumor tertiary lymphoid structures. *OncoImmunology* (2019) 8(6):e1583547. doi: 10.1080/2162402X.2019.1583547

134. Rucki AA, Zheng L. Pancreatic cancer stroma: understanding biology leads to new therapeutic strategies. *World J Gastroenterol* (2014) 20(9):2237–46. doi: 10.3748/wjg.v20.i9.2237

135. Song IH, Heo S-H, Bang WS, Park HS, Park IA, Kim Y-A, et al. Predictive value of tertiary lymphoid structures assessed by high endothelial venule counts in the neoadjuvant setting of triple-negative breast cancer. *Cancer Res treatment: Off J Korean Cancer Assoc* (2017) 49(2):399–407.

136. Sun X, Liu W, Sun L, Mo H, Feng Y, Wu X, et al. Maturation and abundance of tertiary lymphoid structures are associated with the efficacy of neoadjuvant chemoimmunotherapy in resectable non-small cell lung cancer. *J Immunother Cancer.* (2022) 10(11). doi: 10.1136/jitc-2022-005531

137. Dosset M, Vargas TR, Lagrange A, Boidot R, Vegran F, Roussey A, et al. PD-1/PD-L1 pathway: an adaptive immune resistance mechanism to immunogenic chemotherapy in colorectal cancer. *Oncoimmunology* (2018) 7(6):e1433981. doi: 10.1080/2162402X.2018.1433981

138. Tesniere A, Schlemmer F, Boige V, Kepp O, Martins I, Ghiringhelli F, et al. Immunogenic death of colon cancer cells treated with oxaliplatin. *Oncogene* (2010) 29 (4):482–91. doi: 10.1038/onc.2009.356

139. Pfirschke C, Engblom C, Rickelt S, Cortez-Retamozo V, Garris C, Pucci F, et al. Immunogenic chemotherapy sensitizes tumors to checkpoint blockade therapy. *Immunity* (2016) 44(2):343–54. doi: 10.1016/j.immuni.2015.11.024

140. Song W, Shen L, Wang Y, Liu Q, Goodwin TJ, Li J, et al. Synergistic and low adverse effect cancer immunotherapy by immunogenic chemotherapy and locally expressed PD-L1 trap. *Nat Commun* (2018) 9(1):2237. doi: 10.1038/s41467-018-04605-x

141. Cook AM, McDonnell AM, Lake RA, Nowak AK. Dexamethasone co-medication in cancer patients undergoing chemotherapy causes substantial immunomodulatory effects with implications for chemo-immunotherapy strategies. *Oncoimmunology* (2016) 5(3):e1066062. doi: 10.1080/2162402x.2015.1066062

142. Helmink BA, Reddy SM, Gao J, Zhang S, Basar R, Thakur R, et al. B cells and tertiary lymphoid structures promote immunotherapy response. *Nature* (2020) 577 (7791):549–55. doi: 10.1038/s41586-019-1922-8

143. Cabrita R, Lauss M, Sanna A, Donia M, Skaarup Larsen M, Mitra S, et al. Tertiary lymphoid structures improve immunotherapy and survival in melanoma. *Nature* (2020) 577(7791):561–5.

144. Petitprez F, de Reyniès A, Keung EZ, Chen TW-W, Sun C-M, Calderaro J, et al. B cells are associated with survival and immunotherapy response in sarcoma. *Nature* (2020) 577(7791):556–60.

145. Wennhold K, Thelen M, Lehmann J, Schran S, Preugszat E, Garcia-Marquez M, et al. CD86+ antigen-presenting b cells are increased in cancer, localize in tertiary lymphoid structures, and induce specific t-cell responses. *Cancer Immunol Res* (2021) 9 (9):1098–108. doi: 10.1158/2326-6066.CIR-20-0949

146. Coppola D, Nebozhyn M, Khalil F, Dai H, Yeatman T, Loboda A, et al. Unique ectopic lymph node-like structures present in human primary colorectal carcinoma are identified by immune gene array profiling. *Am J Pathol* (2011) 179(1):37–45. doi: 10.1016/j.ajpath.2011.03.007

147. Li R, Berglund A, Zemp L, Dhillon J, Putney R, Kim Y, et al. The 12-CK score: Global measurement of tertiary lymphoid structures. *Front Immunol* (2021) 12:org/10.3389/fimmu.2021.694079. doi: 10.3389/fimmu.2021.694079

148. Joshi N, Akama-Garren E, Lu Y, Lee D-Y, Chang G, Li A, et al. Regulatory t cells in tumor-associated tertiary lymphoid structures suppress anti-tumor t cell responses. *Immunity* (2015) 43(3):579–90.

149. Jing F, Choi EY. Potential of cells and Cytokines/Chemokines to regulate tertiary lymphoid structures in human diseases. *Immune Netw* (2016) 16(5):271–80. doi: 10.4110/in.2016.16.5.271

150. Tang H, Zhu M, Qiao J, Fu YX. Lymphotoxin signalling in tertiary lymphoid structures and immunotherapy. *Cell Mol Immunol* (2017) 14(10):809–18. doi: 10.1038/cmi.2017.13

151. Krautler Nike J, Kana V, Kranich J, Tian Y, Perera D, Lemm D, et al. Follicular dendritic cells emerge from ubiquitous perivascular precursors. *Cell* (2012) 150(1):194–206. doi: 10.1016/j.cell.2012.05.032

152. Ware CF. Targeting lymphocyte activation through the lymphotoxin and LIGHT pathways. *Immunol Rev* (2008) 223:186–201. doi: 10.1111/j.1600-065X.2008.00629.x

153. Filderman JN, Appleman M, Chelvanambi M, Taylor JL, Storkus WJ. STINGing the tumor microenvironment to promote therapeutic tertiary lymphoid structure development. *Front Immunol* (2021) 12:690105. doi: 10.3389/fimmu.2021.690105

154. Luther SA, Bidgol A, Hargreaves DC, Schmidt A, Xu Y, Paniyadi J, et al. Differing activities of homeostatic chemokines CCL19, CCL21, and CXCL12 in lymphocyte and dendritic cell recruitment and lymphoid Neogenesis1. *J Immunol* (2002) 169(1):424–33. doi: 10.4049/jimmunol.169.1.424

155. Chen SC, Vassileva G, Kinsley D, Holzmann S, Manfra D, Wiekowski MT, et al. Ectopic expression of the murine chemokines CCL21a and CCL21b induces the formation of lymph node-like structures in pancreas, but not skin, of transgenic mice. *J Immunol* (2002) 168(3):1001–8. doi: 10.4049/jimmunol.168.3.1001

156. Liu W, Tai CH, Liu X, Pastan I. Anti-mesothelin immunotoxin induces mesothelioma eradication, anti-tumor immunity, and the development of tertiary lymphoid structures. *Proc Natl Acad Sci United States America.* (2022) 119(48): e2214928119. doi: 10.1073/pnas.2214928119

157. Argani P, Iacobuzio-Donahue C, Ryu B, Rosty C, Goggins M, Wilentz RE, et al. Mesothelin is overexpressed in the vast majority of ductal adenocarcinomas of the pancreas: identification of a new pancreatic cancer marker by serial analysis of gene expression (SAGE). *Clin Cancer Res* (2001) 7(12):3862–8.

158. Zhu Y, An X, Zhang X, Qiao Y, Zheng T, Li X. STING: a master regulator in the cancer-immunity cycle. *Mol Cancer.* (2019) 18(1):152. doi: 10.1186/s12943-019-1087-y

159. Chelvanambi M, Fecek RJ, Taylor JL, Storkus WJ. STING agonist-based treatment promotes vascular normalization and tertiary lymphoid structure formation in the therapeutic melanoma microenvironment. *J Immunother Cancer.* (2021) 9(2). doi: 10.1136/jitc-2020-001906

160. Kaufman HL, Kohlhapp FJ, Zloza A. Oncolytic viruses: a new class of immunotherapy drugs. *Nat Rev Drug discovery.* (2015) 14(9):642–62.

161. He T, Hao Z, Lin M, Xin Z, Chen Y, Ouyang W, et al. Oncolytic adenovirus promotes vascular normalization and nonclassical tertiary lymphoid structure formation through STING-mediated DC activation. *OncoImmunology* (2022) 11 (1):2093054. doi: 10.1080/2162402X.2022.2093054

162. Santos J, Heiniö C, Quixabeira D, Zafar S, Clubb J, Pakola S, et al. Systemic delivery of oncolytic adenovirus to tumors using tumor-infiltrating lymphocytes as carriers. *Cells* (2021) 10(5). doi: 10.3390/cells10050978

163. Von Ahrens D, Bhagat TD, Nagrath D, Maitra A, Verma A. The role of stromal cancer-associated fibroblasts in pancreatic cancer. *J Hematol Oncol* (2017) 10(1):1–8.

164. Ma J, Ramachandran M, Jin C, Quijano-Rubio C, Martikainen M, Yu D, et al. Characterization of virus-mediated immunogenic cancer cell death and the consequences for oncolytic virus-based immunotherapy of cancer. *Cell Death Disease.* (2020) 11(1):48. doi: 10.1038/s41419-020-2236-3

165. Manieri NA, Chiang EY, Grogan JL. TIGIT: A key inhibitor of the cancer immunity cycle. *Trends Immunol* (2017) 38(1):20–8. doi: 10.1016/j.it.2016.10.002

166. Pearce H, Croft W, Nicol SM, Margielewska-Davies S, Powell R, Cornall R, et al. Tissue-resident memory t cells in pancreatic ductal adenocarcinoma coexpress PD-1 and TIGIT and functional inhibition is reversible by dual antibody blockade. *Cancer Immunol Res* (2023) 11(4):435–49. doi: 10.1158/2326-6066.Cir-22-0121

167. Liu X, Li M, Wang X, Dang Z, Jiang Y, Wang X, et al. PD-1(+) TIGIT(+) CD8 (+) t cells are associated with pathogenesis and progression of patients with hepatitis b virus-related hepatocellular carcinoma. *Cancer Immunol Immunother*. (2019) 68 (12):2041–54. doi: 10.1007/s00262-019-02426-5

168. Ford K, Hanley CJ, Mellone M, Szyndralewiez C, Heitz F, Wiesel P, et al. NOX4 inhibition potentiates immunotherapy by overcoming cancer-associated fibroblast-mediated CD8 t-cell exclusion from tumors. *Cancer Res* (2020) 80(9):1846–60.

169. Sherman MH, Ruth TY, Engle DD, Ding N, Atkins AR, Tiriac H, et al. Vitamin d receptor-mediated stromal reprogramming suppresses pancreatitis and enhances pancreatic cancer therapy. *Cell* (2014) 159(1):80–93.

frontiers | Frontiers in Immunology

TYPE Original Research
PUBLISHED 07 February 2024
DOI 10.3389/fimmu.2024.1302751

OPEN ACCESS

EDITED BY
Hui Zhao,
University of Texas MD Anderson Cancer Center, United States

REVIEWED BY
Xiangliang Yuan,
University of Texas MD Anderson Cancer Center, United States
Yongkun Wei,
University of Texas MD Anderson Cancer Center, United States

*CORRESPONDENCE
Xiubao Ren
renxiubao@tjmuch.com
Xishan Hao
xishanhao@sina.com

†These authors have contributed equally to this work

RECEIVED 27 September 2023
ACCEPTED 22 January 2024
PUBLISHED 07 February 2024

CITATION
Zhao H, Zhao Y, Zhang S, Wang Z, Yu W, Dong N, Yang X, Zhang X, Sun Q, Hao X and Ren X (2024) Effects of immunogenic cell death-inducing chemotherapeutics on the immune cell activation and tertiary lymphoid structure formation in melanoma. *Front. Immunol.* 15:1302751. doi: 10.3389/fimmu.2024.1302751

Effects of immunogenic cell death-inducing chemotherapeutics on the immune cell activation and tertiary lymphoid structure formation in melanoma

Hua Zhao[1,2,3,4,5†], Yu Zhao[1,2,3,5†], Siyuan Zhang[1,2,3,5†], Zhe Wang[1,2,3,5], Wenwen Yu[1,2,3,5], Nan Dong[1,2,3,5], Xuena Yang[1,2,3,5], Xiying Zhang[1,2,3,5], Qian Sun[1,2,3,4,5], Xishan Hao[1,2,3,4*] and Xiubao Ren[1,2,3,4,5,6*]

[1]Tianjin Medical University Cancer Institute and Hospital, National Clinical Research Center for Cancer, Tianjin, China, [2]Tianjin's Clinical Research Center for Cancer, Tianjin, China, [3]Key Laboratory of Cancer Immunology and Biotherapy, Tianjin, China, [4]Haihe Laboratory of Cell Ecosystem, Tianjin, China, [5]Department of Immunology, Tianjin Medical University Cancer Institute and Hospital, Tianjin, China, [6]Department of Biotherapy, Tianjin Medical University Cancer Institute and Hospital, Tianjin, China

Background: The infiltration and activation of immune cells in the tumor microenvironment (TIME) affect the prognosis of patients with cancer. Tertiary lymphoid structure (TLS) formation favors tumour- infiltrating-lymphocyte (TIL) recruitment and is regarded as an important indicator of good prognosis associated with immunotherapy in patients with tumors. Chemotherapy is currently one of the most commonly used clinical treatment methods. However, there have been no clear report to explore the effects of different types of chemotherapy on TLS formation in the TIME. This study examined the effects of immunogenic cell death (ICD)-inducing chemotherapeutics on immune cells, high-endothelial venules (HEV), and TLSs in mouse melanomas.

Methods: Doxorubicin (an ICD inducer), gemcitabine (non-ICD inducer), and a combination of the two drugs was delivered intra-peritoneally to B16F1-loaded C57BL/6 mice. The infiltration of immune cells into tumor tissues was evaluated using flow cytometry. HEV and TLS formation was assessed using immunohistochemistry and multiple fluorescent immunohistochemical staining.

Results: Doxorubicin alone, gemcitabine alone, and the two-drug combination all slowed tumor growth, with the combined treatment demonstrating a more pronounced effect. Compared with the control group, the doxorubicin group showed a higher infiltration of $CD8^+$ T cells and tissue-resident memory T cells (T_{RM}) and an increase in the secretion of interferon-γ, granzyme B, and perforin in $CD8^+$ T subsets and activation of B cells and dendritic cells. Doxorubicin alone and in combination with gemcitabine decreased regulatory T cells in the TIME. Moreover, doxorubicin treatment promoted the formation of HEV and TLS. Doxorubicin treatment also upregulated the expression of programmed cell death protein (PD)-1 in $CD8^+$ T cells and programmed cell death protein ligand (PD-L)1 in tumor cells.

Conclusions: These results indicate that doxorubicin with an ICD reaction promotes TLS formation and increases PD-1/PD-L1 expression in tumor tissues. The results demonstrate the development of a therapeutic avenue using combined immune checkpoint therapy.

KEYWORDS

immunogenic cell death, chemotherapy, immune cell infiltration, high-endothelial venules, tertiary lymphoid structure, PD-1

1 Introduction

The tumor immune microenvironment (TIME), which comprises abundant immune cells, plays an important role in the antitumor response (1). Tertiary lymphoid structures (TLSs) are organized aggregates of immune cells that form postnatally in non-lymphoid tissues of the TIME (2). The structure is composed of high endothelial venules (HEV) and a variety of immune cells, and is considered the local site where antigen-specific $CD8^+$T cells are generated in the tumor microenvironment (3, 4). The presence of TLSs is associated with better prognosis and clinical outcomes in various carcinomas, including non-small cell lung cancer (5, 6), breast cancer (7, 8), ovarian cancer (9, 10), colorectal cancer (11, 12), and melanoma (4, 13) and can serve as a predictive indicator of clinical efficacy in immune checkpoint inhibitor immunotherapy (14, 15). Currently, chemotherapy is still one of the most commonly used methods in clinical treatment, and no studies have explored the effects of different types of chemotherapeutic drugs on TLS in the tumor microenvironment. Hence, it is clinically significant to explore chemotherapeutic drugs that can promote the formation of TLSs to develop a combination approach with immune checkpoint inhibitors.

Chemotherapeutic drugs can be divided into immunogenic cell death (ICD) and non-ICD drugs based on whether they trigger an immune response (16). When ICD occurs, dying cells produce new antigenic epitopes and release damage-associated molecular patterns (DAMPs), such as calreticulin (CRT), high mobility group protein B1 (HMGB1), and adenosine triphosphate (ATP) and then recruit antigen-presenting cells (APCs) to recognize and present antigens on dying cells to T cells (17). A persistent antitumor immune effect is established by activating the immune response system to eliminate the tumor antigens (18). However, whether ICDs induce the formation of tumor-localized HEV and TLSs remains unclear.

As a representative anthracycline drug, doxorubicin mainly acts on DNA to exert cytotoxicity and acts as a representative chemotherapeutic drug for ICD (18). Gemcitabine is a cytidine analog that inhibits DNA synthesis (19). Although related studies have found that gemcitabine can increase CRT exposure and HMGB1 release *in vitro*, it inhibits DAMPs by triggering the action of prostaglandin E2 *in vivo* (20). Therefore, gemcitabine is still considered a non-ICD inducer. In this study, we observed different effects of doxorubicin and gemcitabine on immune cells in the TIME and further discussed the formation of HEV and TLS, which provided a basis for chemotherapy combined with immunotherapy.

2 Materials and methods

2.1 Cells and culture conditions

Mouse B16-F1 melanoma cells were obtained from the American Type Culture Collection (ATCC). Cells were cultured in RPMI-1640 medium (Cat. L220KJ; Basal Media, Shanghai, China) supplemented with 10% fetal bovine serum (Cat. F801-500; Biocode Biotechnology, Zhejiang, China). The culture conditions involved incubation at 37°C in a humidified incubator containing 5% CO_2.

2.2 *In vivo* mouse tumor model

Female C57BL/6 mice aged between six to eight weeks were purchased from SPF Biotechnology Co. Ltd. (Beijing, China). B16F1 cells were inoculated subcutaneously into C57BL/6 mice at a density of 5×10^5. Nine days after inoculation, mice were divided into four groups (PBS group, doxorubicin group, gemcitabine group, and combined treatment group) and the corresponding groups were PBS (volume 100ul/mice), doxorubicin (5 mg/kg), gemcitabine (25 mg/kg), and a combination of doxorubicin and gemcitabine for six days, respectively. Doxorubicin (S1208) and gemcitabine (S1149) were purchased from Selleck Chemicals (Houston, TX). After initiating the treatment, tumor length and width were measured daily, and tumor volumes were quantified as (length×width×height)/2. All mice were observed, treated, and euthanized according to the protocols of the Animal Ethics and Welfare Committee of Tianjin Medical University Cancer Institute and Hospital. The animal study protocol was approved by the Animal Ethics and Welfare Committee of Tianjin Medical University Cancer Institute and Hospital (protocol code AE-2021030, September 9, 2021).

2.3 Tumor tissue preparation and flow cytometric analysis

The tumor tissues were collected and cut into small pieces of approximately 1 mm^3. The tumor pieces were incubated with a medium containing DNA hydrolase I and collagenase IV for 30 min at 37°C. A 70-μm filter was used to remove non-digested tissue and obtain a single-cell suspension for the following flow cytometry staining. Cells were first stained with Zombie NIR (Fixable Viability kit, BioLegend) to examine live cells and then surface markers staining with the following antibodies at 4°C for 20 min in the dark: anti-CD45-PE (BioLegend, San Diego, CA, USA), anti-CD3-APC (BioLegend), anti-CD4-FITC (BioLegend), anti-CD19-APC (BioLegend), anti-CD11c-FITC (BioLegend), anti-CD86-PerCP/Cyanine5.5 (BioLegend), anti-PD-1-PE/Cyanine7 (BioLegend), anti-PD-L1-PE/Cyanine7 (BioLegend), anti-CD103- PE/Cyanine7 (BioLegend), anti-PNAd-APC (BioLegend). For intracellular markers, cells were fixed and permeabilized using the FoxP3 staining buffer set (eBioscience) and then stained with intracellular antibodies for 30 min at 4°C, including anti-IFN-γ-PerCP/Cyanine5.5 (BioLegend), anti-Granzyme B-APC (BioLegend), anti-Perforin-PE (BioLegend). Flow cytometry analysis was performed using a BD FACSCanto II flow cytometer (BD Biosciences), and the data were analyzed using FlowJo V10 software.

2.4 Immunohistochemistry and multiple immunofluorescence staining

For immunohistochemical analysis, after deparaffinization, rehydration, and antigen repair, tissues were incubated overnight with the primary antibody PNAd (MECA-79, Novus; Shanghai, China). The following day, EIVISON plus (kit-9903, MXB, China) was used for secondary antibody incubation. A DAB kit (ZL1-9019, ZSGB-BIO, China) was used for tissue coloring, hematoxylin was used for nuclear staining, and neutral resin was used to seal the object. Finally, a light-field microscope (Olympus, Tokyo, Japan) was used to examine the stained tumor slices. For multiple immunofluorescence staining, the slides were stained with fluorescently labeled antibodies against CD3 (Abcam, Cambridge, MA, USA), B220 (BioLegend, San Diego, CA, USA), and PNAd (Novus) using a tyramide signal amplification multiplex immunohistochemistry kit (Cat. No. 0004100100; Panovue). According to the immunofluorescence signals, diverse cell types were accurately quantified in each sector of the images using the inForm software (PerkinElmer).

2.5 Statistical analyses

All experimental results were statistically analyzed using GraphPad Prism 8. One-way analysis of variance and Dunnett's test were used to compare the experimental and control groups individually. One-way analysis of variance and Tukey's test were used for comparisons between any two of the four groups. Values with $P<0.05$ were considered statistically significant.

3 Results

3.1 Chemotherapy inhibits tumor growth and influences the expression of HMGB1

We established a melanoma mouse model by subcutaneously inoculating B16F1 tumor cells into the groin region of C57BL/6 mice. The detailed administration schedule and tumor harvest intervals are shown in Figure 1A. Tumor volumes were monitored daily, the data were plotted (Figure 1C), and harvested tumors were photographed (Figure 1B).

The results showed that doxorubicin and gemcitabine alone and the combination of both showed significant tumor growth inhibition effects compared to the control group ($P< 0.001$, $P< 0.01$, and $P< 0.001$, respectively). The combination treatment group showed the most significant inhibitory effect, but no statistically significant difference was noted than that in the other two groups (Figure 1C).

HMGB1 (formerly known as HMG-1), a highly conserved ubiquitous protein, has been described as a nuclear DNA-binding protein involved in nucleosome stabilization and gene transcription. The release of HMGB1 from the nucleus into the surroundings of the dying cells is an important characteristic of ICD (17). Immunohistochemical staining was used to evaluate the cytoplasmic expression of HMGB1 in tumor tissues after different treatments. The results showed that doxorubicin treatment demonstrated an increase in the expression of HMGB1 compared to the control and gemcitabine treatments (5.2% ± 0.45% vs. 3.2% ± 0.45%, P=0.0009, 5.2% ± 0.45% vs. 4.0% ± 1.00%, P=0.0455). In addition, the expression of HMGB1 was also significantly upregulated in the combination treatment group than in the control group (4.6% ± 0.55% vs. 3.2% ± 0.45%,P=0.0175) (Figures 1D, E).

3.2 Effects of doxorubicin on lymphocyte subpopulation

To study the changes in the immune microenvironment after doxorubicin treatment, single-cell suspensions were prepared from tumor tissues for flow cytometry analysis. The results showed that the proportion of $CD3^+$ T cells in doxorubicin group and combination treatment group was significantly higher than that in gemcitabine group (33.2% ± 10.1% vs. 18.1% ± 5.54%, P= 0.0259; 31.9% ± 8.40% vs. 18.1% ± 5.54%, P= 0.0451) (Figure 2A). Doxorubicin alone can significantly promote infiltration of $CD8^+$ T cells compared to control and gemcitabine treatments (20.9% ± 7.77% vs. 11.4% ± 2.85%, P= 0.0300; 20.9% ± 7.77 vs. 9.33% ± 3.02%, P= 0.0080); however, it did not exhibit a significant effect on $CD4^+$ T cells (Figure 2B). Next, we analyzed the levels of cytotoxic cytokines secreted by $CD4^+$ T cells and $CD8^+$ T cells. Compared with the control treatment, both doxorubicin alone and

10.3389/fimmu.2024.1302751

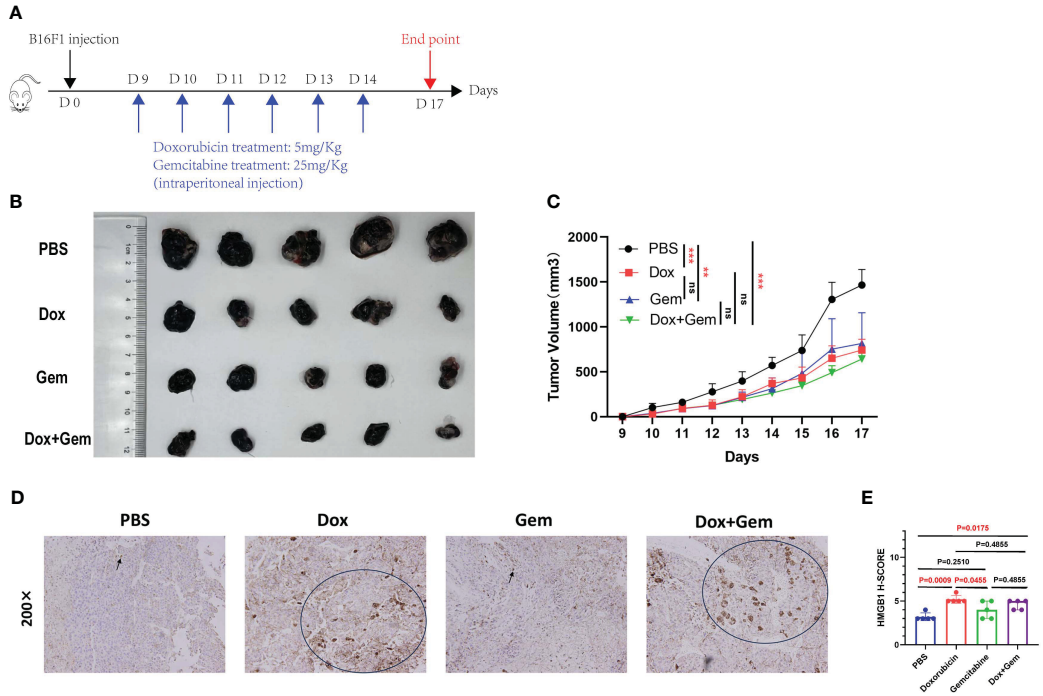

FIGURE 1
Chemotherapy inhibit tumor growth and affect the expression of HMGB1. **(A)** Schematic diagram of the mice tumor model. First, 5×10^5 B16F1 cells were inoculated subcutaneously into C57BL/6 mice. Nine days after inoculation, mice were divided into 4 groups (PBS group, doxorubicin group, gemcitabine group, and combined treatment group), and treated with doxorubicin at 5mg/Kg, gemcitabine at 25mg/Kg, and combination with two for 6 days. **(B)** After 17 days, mice were sacrificed and tumors were photographed. **(C)** Tumor length and width were measured every day, and tumor volumes were quantified as (length×width×width)/2. Results were expressed as mean ± SD (n=5), and represented as tumor volume-time curves (**P<0.01, *** P<0.001). **(D)** Representative images of HMGB1 immunohistochemical staining in the four groups. **(E)** HMGB1 expression levels were calculated by adding the percentage score of positive staining cells (0-25%, 1 point; 26-50%, 2 points; 51-75%, 3 points; 76-100%, 4 points) and the intensity score (negative staining, 1point; light-yellow, 2 points; yellow-brown, 3 points; dark-brown, 4 points) to calculate the total immunohistochemical score. A statistical bar chart was drawn based on the calculated results.

combination treatment promoted the expression of granzyme B (25.9% ± 8.27% vs. 13.9% ± 7.13%, P = 0.0492; 33.1% ± 6.39% vs. 13.9% ± 7.13%, P = 0.0061) and perforin in $CD4^+$ T cells (9.45% ± 4.16% vs. 3.13% ± 2.35%, P = 0.0494; 12.7% ± 5.0% vs. 3.13% ± 2.35%, P = 0.0030). However, the results showed no significant effect on IFN-γ expression (Figure 2C). In $CD8^+$T lymphocytes, compared with the control treatment, doxorubicin increased the expression of IFN-γ (87.5% ± 5.75% vs. 74.4% ± 6.15%, P= 0.0141), granzyme B (86.5% ± 1.30% vs. 68.9% ± 13.3%, P= 0.0142), and perforin respectively. (50.5% ± 10.4% vs. 22.2% ± 8.09%, P= 0.0009; Figure 2D).

Foxp3-expressing regulatory T (Treg) cells suppress effective tumor immunity and are associated with poor prognosis in patients with cancer (21). In this study, the proportion of Tregs in all treatment groups was significantly decreased compared than that in the control group (doxorubicin group:13.6% ± 3.38% vs. 40.2% ± 4.84%,P< 0.0001; gemcitabine group: 29.4% ± 2.49% vs. 40.2% ± 4.84%,P= 0.0078; combined group:15.5% ± 6.29% vs. 40.2% ± 4.84%,P< 0.0001; Figure 2E).

Furthermore, tissue-resident memory T cells (T_{RM}), which are important components of tumor infiltrating lymphocytes (TILs) were also evaluated in this study. T_{RM} cells mediate anti-tumor immunity by producing cytolytic mediators and releasing cytokines and chemokines to recruit and activate immune cells (22). Compared with the control treatment, doxorubicin alone and the combination treatment significantly promoted the infiltration of $CD103^+$ T_{RM} cells (6.43% ± 1.48% vs. 2.24% ± 0.80%, P< 0.0001; 4.15% ± 0.56% vs.2.24% ± 0.80%, P= 0.0186) (Figure 2F).

3.3 Doxorubicin promoted recruitment and activation of antigen-presenting cells

APCs play key roles in the initiation and regulation of innate and adaptive anti-tumor immune responses (23, 24). In the present study, compared with the control treatment, doxorubicin treatment promoted the recruitment of B cells (30.7% ± 5.46% vs. 17.8% ± 3.84%, P= 0.0286) and dendritic cells(DCs) (31.9% ± 3.23% vs. 15.7% ± 5.89%, P= 0.0001) to the tumor tissue site (Figures 3A, C). Furthermore, both the doxorubicin alone and the combination treatment increased the proportion of $CD86^+$ B cells compared to the control treatment (13.2% ± 2.60% vs. 6.57% ± 1.69%, P= 0.0002; 10.8% ± 0.94% vs.6.57% ± 1.69%, P= 0.0105). Gemcitabine treatment did not increase the infiltration or activation of B cells (P > 0.05; Figure 3B). The data showed that only doxorubicin group showed increased proportion of $CD11c^+$DC and $CD86^+$DCs compared to the control group (20.8% ± 2.18% vs.15.1% ± 3.57%, P= 0.0350; Figure 3D).

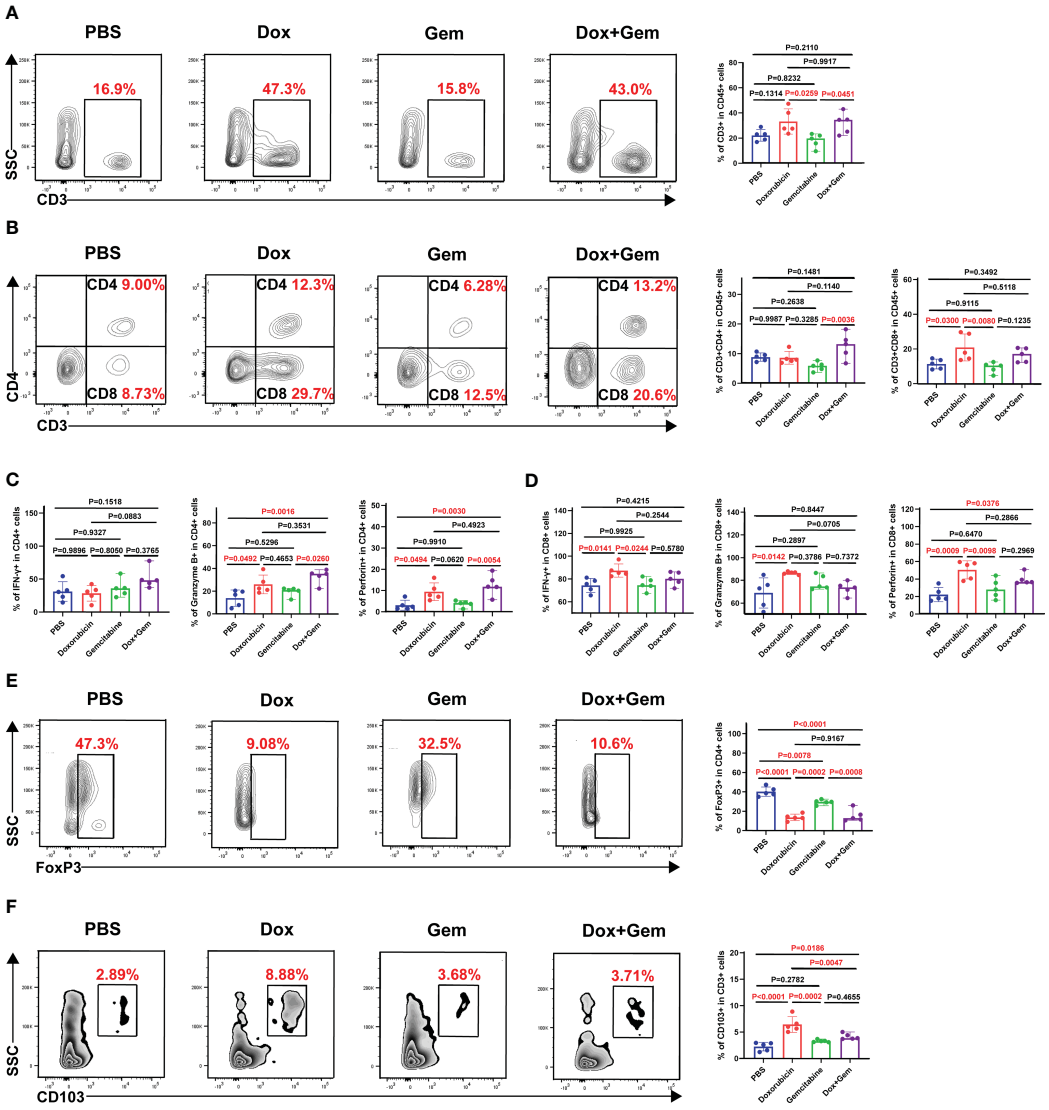

FIGURE 2
Effects of doxorubicin on T cell Subsets. Mice with melanoma were treated with doxorubicin, gemcitabine, and combination of both, and tumors were harvested to produce a single-cell suspension at day 17, which was analyzed by flow cytometry. **(A)** Representative plots of $CD3^+$ cells gated on $CD45^+$ cell population, and histogram of percentage of $CD3^+$ cells in $CD45^+$ cells from the four groups (n=5). **(B)** Representative plots of $CD4^+$ cells, $CD8^+$ cells gated on $CD3^+$ cell population, and histogram of percentage of $CD4^+$ cells and $CD8^+$ cells in $CD3^+$ cells from the four groups (n=5). **(C, D)** Histogram of positive percentage of IFN-γ, granzyme B and perforin in CD4 and CD8 cells, respectively. **(E)** Representative dot plot of $Foxp3^+$ cells within the $CD4^+$ gate and histogram of percentage of $Foxp3^+$ cells in $CD4^+$ cells from the four groups (n=5). **(F)** Representative dot plot of $CD103^+$ cells within the $CD3^+$ gate and histogram of percentage of $CD103^+$ cells in $CD3^+$ cells from the four groups (n=5).

3.4 Doxorubicin promotes HEV and TLS formation

The HEV is the main portal for lymphocytes entering the tumor tissues and is the most important component of TLSs (25). We measured the proportion of $PNAd^+$ HEV in $CD45^-$ cells by flow cytometry. The proportion of $PNAd^+$ HEV in the doxorubicin group was significantly higher than that in the control, gemcitabine, and combination treatment groups ($P< 0.0001$, $P= 0.0002$, and $P= 0.0016$, respectively; Figure 4A).

Multiple immunofluorescence staining was used to evaluate the formation of TLSs (Figure 4B). Five fields were randomly selected from multiple immunofluorescence-stained samples, and the proportion of T and B cells was quantified using the inForm software. The proportion of $CD3^+$ T cells was significantly increased in the doxorubicin group than in the control and gemcitabine groups (1.55% ± 0.83% vs. 0.31% ± 0.35%, $P< 0.0001$; 1.55% ± 0.83% vs. 0.31% ± 0.35%, $P< 0.0001$, Figure 4C). Moreover, the combination treatment group showed similar increase in T-cell infiltration compared with the control group (1.13% ± 0.65% vs.0.31% ± 0.35%, $P< 0.0001$, Figure 4C). The proportion of $B220^+$B cells was significantly increased in the doxorubicin group than in the control, gemcitabine and combination treatment groups (2.67% ± 1.01% vs.0.55% ± 0.42%,$P< 0.0001$; 2.67% ± 1.01% vs.0.68% ± 0.67%,$P<$

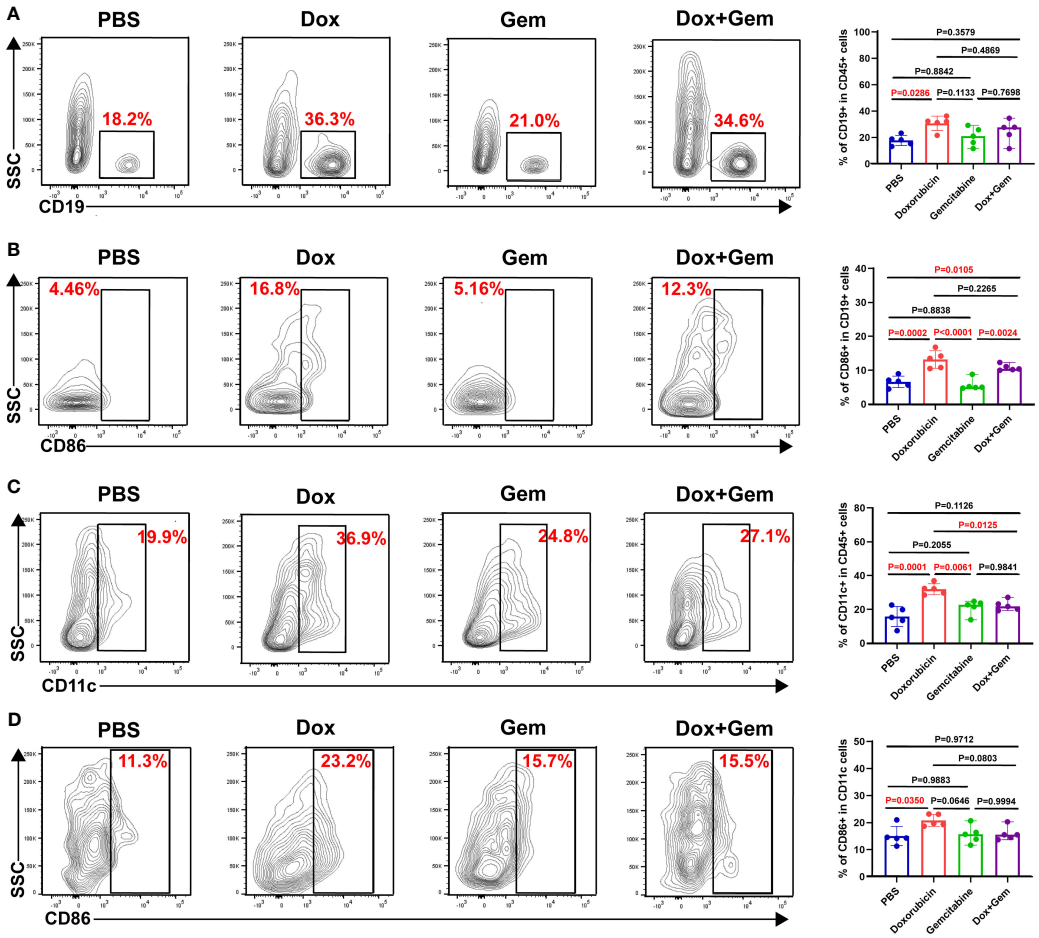

FIGURE 3
Doxorubicin promoted antigen-presenting cells recruitment and activation. B cells, and DCs were gated by CD19, and CD11c respectively. The activated cells were labeled with CD86. **(A)** Representative dot plot of $CD19^+$ cells within the $CD45^+$ gate and histogram of percentage of $CD19^+$ cells in $CD45^+$ cells from the four groups (n=5). **(B)** Representative dot plot of $CD86^+$ cells within the $CD19^+$ gate and histogram of percentage of $CD86^+$ cells in $CD19^+$ cells from the four groups (n=5). **(C)** Representative dot plot of $CD11c^+$ cells within the $CD45^+$ gate and histogram of percentage of $CD11c^+$ cells in $CD45^+$ cells from the four groups (n=5). **(D)** Representative dot plot of $CD86^+$ cells within the $CD11c^+$ gate and histogram of percentage of $CD86^+$ cells in $CD11c^+$ cells from the four groups (n=5).

0.0001; 2.67% ± 1.01% vs.1.16% ± 0.79%,$P< 0.0001$, Figure 4D). We also measured the density of $PNAd^+$ HEV in the samples to quantify the TLS formation. The results showed that doxorubicin treatment significantly promoted TLS formation compared with the control, gemcitabine, and combination treatment (0.91% ± 0.40% vs.0.14% ± 0.07%, $P= 0.0008$; 0.91% ± 0.40% vs.0.17% ± 0.09%, $P= 0.0011$; 0.91% ± 0.40% vs.0.28% ± 0.26%, $P= 0.0050$, Figure 4E). These data are consistent with the flow cytometry results.

3.5 Doxorubicin upregulates PD-1/PD-L1 expression

Finally, we analyzed the changes in PD-1 expression in $CD4^+$ and $CD8^+$ T cells after different treatments. The flow cytometry results showed that doxorubicin significantly increased the expression of PD-1 on $CD8^+$ T cells compared with the control and combination treatments (41.9% ± 7.17% vs.22.1% ± 9.27%, $P= 0.0046$; 41.9% ± 7.17% vs.17.1% ± 7.66%, $P= 0.0006$, Figure 5A). No statistically significant differences were noted in the expression PD-1 in $CD4^+$ T cells among the four groups.

Next, we observed the expression of PD-L1 on $CD45^-$ tumor cells. The results showed that the doxorubicin significantly increased the PD-L1 expression compared with the control and the gemcitabine treatments (15.3% ± 4.83% vs.7.53% ± 1.29%,$P= 0.0022$; 15.3% ± 4.83% vs. 7.10% ± 2.06%,$P= 0.0013$, Figure 5B). The combination treatment group also showed increased proportion of PD-L1 on tumor cells compared with the control and the gemcitabine group (13.0% ± 1.26% vs.7.53% ± 1.29%,$P= 0.0290$;13.0% ± 1.26% vs.7.10% ± 2.06%,$P= 0.0178$, Figure 5B). These findings indicate that combining doxorubicin treatment with anti-PD1 immunotherapy may yield potential benefits.

4 Discussion

The immune system plays a crucial role in the elimination of tumors. In the TIME, TLSs, which include B-cells- and T-cell-

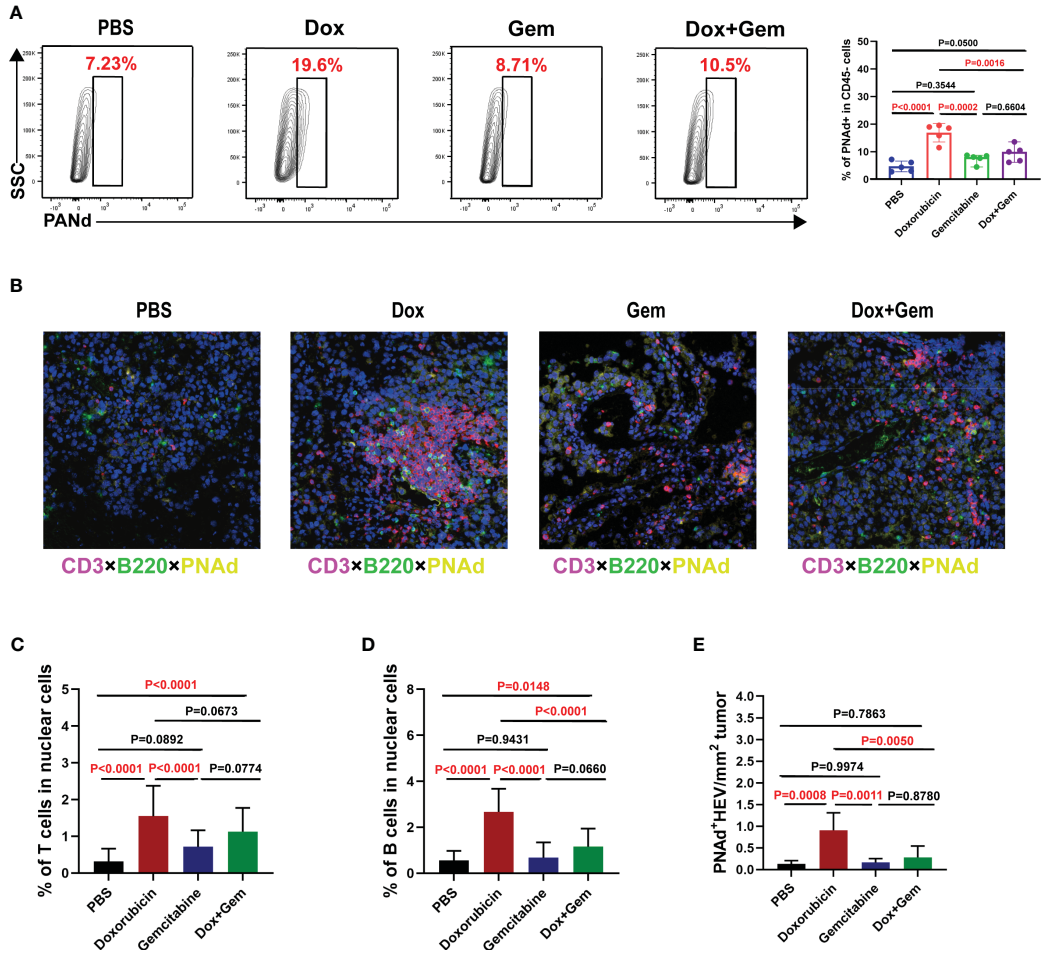

FIGURE 4
Doxorubicin promotes HEV and TLS formation. **(A)** Representative dot plot of PNAd$^+$ cells within the CD45$^-$ gate and histogram of percentage of PNAd$^+$ cells in CD45$^-$ cells from the four groups (n=5). **(B)** Representative images of multiple immunofluorescence staining (magnification, ×200) in control group, doxorubicin group, gemcitabine group, and combination treatment group, respectively. The slide was stained with CD3 (red), B220 (green), PNAd (yellow), and DAPI (blue). **(C-E)** Five fields were randomly selected for each sample, and the proportion of T and B cells occupying nuclear cells was quantified using inForm software (PerkinElmer) based on immunofluorescence signals. **(E)** The density of PNAd$^+$ HEV was used to quantify TLS formation.

enriched areas, may be the local site of initiation and maintenance of humoral and cellular immune responses against cancers (26, 27). Numerous studies have evaluated the formation of TLSs in different cancers and their association with patient prognosis (5–13). Moreover, the presence of TLS in the TIME is an important indicator of the effectiveness of immune checkpoint therapy (28). Therefore, exploring strategies that can induce TLS formation is crucial for proposing combination therapies to improve the efficacy of immune checkpoint therapy.

ICD induction in tumor cells is a promising approach for activating anti-tumor immune responses (16). Chemotherapeutics that can promote ICD can recruit and promote DC maturation and cross-initiation of tumor-specific CD8$^+$ T cells via DAMP release (29, 30). HMGB1 plays a crucial role in this process. Via binding to toll-like receptor 4 (TLR-4) on DCs, HMGB1 promotes DC maturation and releases pro-inflammatory cytokines to trigger an effective immune response (31). Another study showed that HMGB1, synergistically with ATP, could induce DCs to release interleukin-1β (IL-1β), and HMGB1-specific antibodies can block the ability of IL-1β production in DCs after exposure to dying tumor cells (32). In the present study, doxorubicin as a representative chemotherapeutics of ICD was used as the study. Doxorubicin treatment promoted the infiltration and activation of DCs and enhanced the function of infiltrated CD8$^+$ T cells, such as the expression of IFN-γ, granzyme B and perforin, which is consistent with the previous reports (33).

The role of B cells in cancer immunity and their implications in new immunotherapies have garnered significant interest. B cell function includes not only antibody secretion but also antigen presentation to T cells. In human cancers, antigen-presenting B cells are defined as a subset of CD86$^+$CD21$^-$ B cells (34). CD86$^+$ B cells colocalize with T cells in TLSs and are enriched in tumors with increased numbers of TLSs (35). Compared to CD8$^+$ T cells alone, the co-localization of B cells with CD8$^+$ T cells increases patient survival (14, 36). One study showed that oncolytic viruses acting as ICD inducers can increase the

10.3389/fimmu.2024.1302751

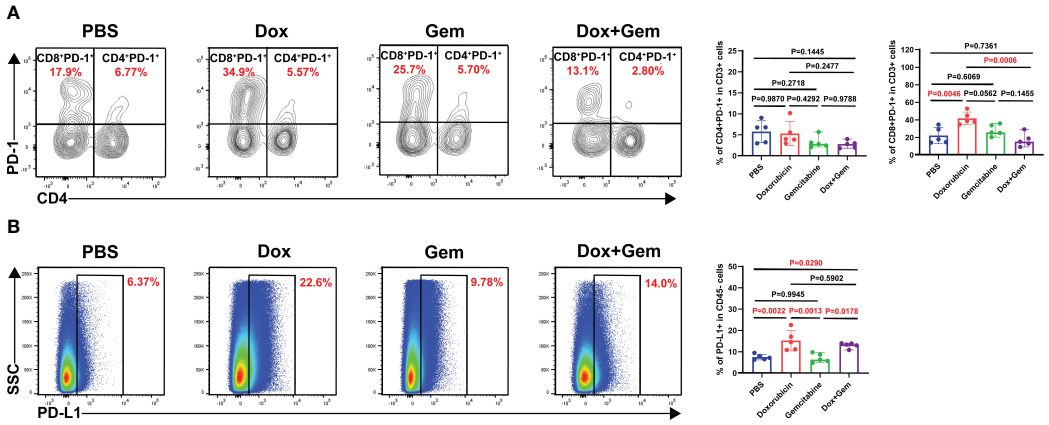

FIGURE 5
Doxorubicin upregulate PD-1/PD-L1 checkpoint expression. **(A)** Representative dot plot of PD-1$^+$ cells within the CD4 and CD8 gates and histogram of percentage of PD-1$^+$ cells in CD4$^+$ and CD8$^+$ cells from the four groups (n=5). **(B)** Representative dot plot of PD-L1$^+$ cells within the CD45- gate and histogram of percentage of PD-L1$^+$ cells in CD45$^-$ cells from the four groups (n=5).

expression of CD86 in B cells; however, it is unclear whether this is related to ICD (37). In this study, the flow cytometry data showed a significant increase in the total number of B and CD86$^+$ B cells after doxorubicin treatment.

Furthermore, the present results showed that doxorubicin treatment can significantly increase the proportion of CD103$^+$ T_{RM}. They can conveniently perform local immune monitoring functions in tumors and exhibit tumor-specific immune protective effects. CD103$^+$ T_{RM} cells can directly kill epithelial-derived tumor cells by producing a large number of cytotoxic particles and cytokines, such as granzyme-B, perforin, and IFN-γ (38). T_{RM} cells may also produce chemokines, leading to the recruitment of XCR1$^+$BATF3$^+$DC and activation of T cells (39). These results further indicate that chemotherapeutics with the capacity of ICD induction might be more beneficial for combination immunotherapy.

PNAd is a hallmark of HEV that facilitates the recruitment of lymphocytes to lymphoid organs and serves as a marker of TLS formation (40). DCs promote the maturation of HEV endothelial cells via lymphotoxin-β, which plays an important role in monitoring the entry of lymphocytes into TLS (41, 42). Whether chemotherapeutics with an ICD induction impact the formation of TLS remains unclear. In the present study, we compared the levels of HEV formation between doxorubicin and gemcitabine and found that doxorubicin induced high PNAd expression and promoted TLS formation. The increased proportion and maturity of DCs in the doxorubicin treatment group confirmed the positive effects of doxorubicin on TLS formation. This may be the link between the onset of ICD and TLS induction.

Additionally, PD-1 expression in CD8$^+$ T cells and PD-L1 expression in tumor cells was elevated after doxorubicin treatment. The high expression of PD-L1 on tumor cells in the TIME may be related to the inflammatory signals, such as IFN-γ, generated during the anti-tumor immune response (43). Our results verify the aforementioned conclusions and provide a theoretical basis for combined anti-PD-1/PD-L1 therapy. In addition, some chemotherapeutics inhibit Treg production with ICD (44–46), which is consistent with our results. This suggests that therapeutics mediating ICD reaction can disrupt the immunosuppressive state of the tumor microenvironment.

Although our experiment showed that doxorubicin promoted the infiltration of immune cells and the formation of TLS simultaneously, this study still has some limitations. First, only one ICD inducer was used. Secondly, the results were examined only using a mouse model of melanoma. Therefore, additional chemotherapeutics with ICD reactions and additional experimental models should be used for further confirmation. In conclusion, the results elucidated that doxorubicin, with an ICD reaction, promoted TLS formation and increased PD-1/PD-L1 expression in tumor tissues, which may be advantageous for combined immune checkpoint therapy.

Data availability statement

The original contributions presented in the study are included in the article/supplementary material. Further inquiries can be directed to the corresponding authors.

Ethics statement

The animal study was approved by the Animal Ethics and Welfare Committee of Tianjin Medical University Cancer Institute and Hospital. The study was conducted in accordance with the local legislation and institutional requirements.

Author contributions

HZ: Project administration, Supervision, Writing – review & editing, Data curation, Writing – original draft. YZ: Data curation, Project administration, Writing – original draft, Writing –

review & editing, Methodology, Validation. SZ: Data curation, Writing – review & editing. ZW: Writing – review & editing. WY: Writing – review & editing. ND: Writing – review & editing. XY: Writing – review & editing. XZ: Writing – review & editing. XH: Writing – review & editing, Funding acquisition, Project administration, Supervision. XR: Writing – review & editing, Funding acquisition, Project administration, Supervision. QS: Writing – review & editing.

Funding

The author(s) declare financial support was received for the research, authorship, and/or publication of this article. This study is funded by National Natural Science Foundation of China (U20A20375, 82372779), Haihe Laboratory of Cell Ecosystem Innovation Fund (22HHXBSS00004), Tianjin Key Medical Discipline (Specialty) Construction Project (TJYXZDXK-009A), Tianjin science technology popularization project (21KPHDRC00150).

Acknowledgments

We sincerely appreciate our colleagues in the Department of Pathology for their help with tumor section preparation.

Conflict of interest

The authors declare that the research was conducted in the absence of any commercial or financial relationships that could be construed as a potential conflict of interest.

Publisher's note

References

1. Sorin M, Rezanejad M, Karimi E, Fiset B, Desharnais L, Perus LJM, et al. Single-cell spatial landscapes of the lung tumor immune microenvironment. *Nature* (2023) 614(7948):548–54. doi: 10.1038/s41586-022-05672-3

2. Sautès-Fridman C, Petitprez F, Calderaro J, Fridman WH. Tertiary lymphoid structures in the era of cancer immunotherapy. *Nat Rev Cancer* (2019) 19(6):307–25. doi: 10.1038/s41568-019-0144-6

3. Ruddle NH. Basics of inducible lymphoid organs. *Curr Top Microbiol Immunol* (2020) 426:1–19. doi: 10.1007/82_2020_218

4. Cabrita R, Lauss M, Sanna A, Donia M, Larsen MS, Mitra S, et al. Tertiary lymphoid structures improve immunotherapy and survival in melanoma. *Nature* (2020) 577(7791):561–5. doi: 10.1038/s41586-019-1914-8

5. Dieu-Nosjean M-C, Antoine M, Danel C, Heudes D, Wislez M, Poulot V, et al. Long-term survival for patients with non-small-cell lung cancer with intratumoral lymphoid structures. *J Clin Oncol* (2008) 26(27):4410–7. doi: 10.1200/JCO.2007.15.0284

6. Goc J, Germain C, Vo-Bourgais TKD, Lupo A, Klein C, Knockaert S, et al. Dendritic cells in tumor-associated tertiary lymphoid structures signal a Th1 cytotoxic immune contexture and license the positive prognostic value of infiltrating CD8+ T cells. *Cancer Res* (2014) 74(3):705–15. doi: 10.1158/0008-5472.CAN-13-1342

7. Prabhakaran S, Rizk VT, Ma Z, Cheng C-H, Berglund AE, Coppola D, et al. Evaluation of invasive breast cancer samples using a 12-chemokine gene expression score: correlation with clinical outcomes. *Breast Cancer Res* (2017) 19(1):71. doi: 10.1186/s13058-017-0864-z

8. Liu X, Tsang JYS, Hlaing T, Hu J, Ni Y-B, Chan SK, et al. Distinct tertiary lymphoid structure associations and their prognostic relevance in HER2 positive and negative breast cancers. *Oncologist* (2017) 22(11):1316–24. doi: 10.1634/theoncologist.2017-0029

9. Kroeger DR, Milne K, Nelson BH. Tumor-infiltrating plasma cells are associated with tertiary lymphoid structures, cytolytic T-cell responses, and superior prognosis in ovarian cancer. *Clin Cancer Res* (2016) 22(12):3005–15. doi: 10.1158/1078-0432.CCR-15-2762

10. Truxova I, Kasikova L, Hensler M, Laco PSJ, Pecen L, Belicova L, et al. Mature dendritic cells correlate with favorable immune infiltrate and improved prognosis in ovarian carcinoma patients. *J Immunother Cancer* (2018) 6(1):139. doi: 10.1186/s40425-018-0446-3

11. Coppola D, Nebozhyn M, Khalil F, Dai H, Yeatman T, Loboda A, et al. Unique ectopic lymph node-like structures present in human primary colorectal carcinoma are identified by immune gene array profiling. *Am J Pathol* (2011) 179(1):37–45. doi: 10.1016/j.ajpath.2011.03.007

12. Posch F, Silina K, Leibl S, Mündlein A, Moch H, Siebenhüner A, et al. Maturation of tertiary lymphoid structures and recurrence of stage II and III colorectal cancer. *Oncoimmunology* (2017) 7(2):e1378844. doi: 10.1080/2162402X.2017.1378844

13. Mattlage AE, Ashenden AL, Lentz AA, Rippee MA, Billinger. Submaximal SA. and peak cardiorespiratory response after moderate-high intensity exercise training in subacute stroke. *Cardiopulm Phys Ther J* (2013) 24(3):14–20. doi: 10.1097/01823246-201324030-00003

14. Petitprez F, de Reyniès A, Keung EZ, Chen TW-W, Sun C-M, Calderaro J, et al. B cells are associated with survival and immunotherapy response in sarcoma. *Nature* (2020) 577(7791):556–60. doi: 10.1038/s41586-019-1906-8

15. Helmink BA, Reddy SM, Gao J, Zhang S, Basar R, Thakur R, et al. and tertiary lymphoid structures promote immunotherapy response. *Nature* (2020) 577(7791):549–55. doi: 10.1038/s41586-019-1922-8

16. Li Z, Lai X, Fu S, Ren L, Cai H, Zhang H, et al. Immunogenic cell death activates the tumor immune microenvironment to boost the immunotherapy efficiency. *Adv Sci (Weinh)* (2022) 9(22):e2201734. doi: 10.1002/advs.202201734

17. Galluzzi L, Vitale I, Aaronson SA, Abrams JM, Adam D, Agostinis P, et al. Molecular mechanisms of cell death: recommendations of the Nomenclature Committee on Cell Death 2018. *Cell Death Differ* (2018) 25(3):486–541. doi: 10.1038/s41418-017-0012-4

18. Ahmed A, Tait SWG. Targeting immunogenic cell death in cancer. *Mol Oncol* (2020) 14(12):2994–3006. doi: 10.1002/1878-0261.12851

19. Casares N, Pequignot MO, Tesniere A, Ghiringhelli F, Roux S, Chaput N, et al. Caspase-dependent immunogenicity of doxorubicin-induced tumor cell death. *J Exp Med* (2005) 202(12):1691–701. doi: 10.1084/jem.20050915

20. Hayashi K, Nikolos F, Lee YC, Jain A, Tsouko E, Gao H, et al. Tipping the immunostimulatory and inhibitory DAMP balance to harness immunogenic cell death. *Nat Commun* (2020) 11(1):6299. doi: 10.1038/s41467-020-19970-9

21. Tanaka A, Sakaguchi S. Targeting Treg cells in cancer immunotherapy. *Eur J Immunol* (2019) 49(8):1140–6. doi: 10.1002/eji.201847659

22. Okła K, Farber DL, Zou W. Tissue-resident memory T cells in tumor immunity and immunotherapy. *J Exp Med* (2021) 218(4):e20201605. doi: 10.1084/jem.20201605

23. Wculek SK, Cueto FJ, Mujal AM, Melero I, Krummel MF, Sancho D, et al. Dendritic cells in cancer immunology and immunotherapy. *Nat Rev Immunol* (2020) 20(1):7–24. doi: 10.1038/s41577-019-0210-z

24. Wennhold K, Thelen M, Lehmann J, Schran S, Preugszat E, Garcia-Marquez M, et al. CD86+ Antigen-presenting B cells are increased in cancer, localize in tertiary lymphoid structures, and induce specific T-cell responses. *Cancer Immunol Res* (2021) 9(9):1098–108. doi: 10.1158/2326-6066.CIR-20-0949

25. Steele KE, Brown C. Multiplex immunohistochemistry for image analysis of tertiary lymphoid structures in cancer. *Methods Mol Biol* (2018) 1845:87–98. doi: 10.1007/978-1-4939-8709-2_6

26. Schumacher TN, Thommen DS. Tertiary lymphoid structures in cancer. *Science* (2022) 375(6576):eabf9419. doi: 10.1126/science.abf9419

27. Zhao H, Wang H, Zhou Q, Ren X. Insights into tertiary lymphoid structures in the solid tumor microenvironment: anti-tumor mechanism, functional regulation, and immunotherapeutic strategies. *Cancer Biol Med* (2021) 18(4):981–91. doi: 10.20892/j.issn.2095-3941.2021.0029

28. Helmink BA, Reddy SM, Gao J, Zhang S, Basar R, Thakur R, et al. B cells and tertiary lymphoid structures promote immunotherapy response. *Nature* (2020) 577:549–55. doi: 10.1038/s41586-019-1922-8

29. Galluzzi L, Humeau J, Buqué A, Zitvogel L, Kroemer G. Immunostimulation with chemotherapy in the era of immune checkpoint inhibitors. *Nat Rev Clin Oncol* (2020) 17(12):725–41. doi: 10.1038/s41571-020-0413-z

30. Pol J, Vacchelli E, Aranda F, Castoldi F, Eggermont A, Cremer I, et al. Trial Watch: Immunogenic cell death inducers for anticancer chemotherapy. *Oncoimmunology* (2015) 4(4):e1008866. doi: 10.1080/2162402X.2015.1008866

31. Apetoh L, Ghiringhelli F, Tesniere A, Criollo A, Ortiz C, Lidereau R, et al. The interaction between HMGB1 and TLR4 dictates the outcome of anticancer chemotherapy and radiotherapy. *Immunol Rev* (2007) 220:47–59. doi: 10.1111/j.1600-065X.2007.00573.x

32. Ghiringhelli F, Apetoh L, Tesniere A, Aymeric L, Ma Y, Ortiz C, et al. Activation of the NLRP3 inflammasome in dendritic cells induces IL-1beta-dependent adaptive immunity against tumors. *Nat Med* (2009) 15(10):1170–8. doi: 10.1038/nm.2028

33. Phung CD, Nguyen HT, Choi JY, Pham TT, Acharya S, Timilshina M, et al. Reprogramming the T cell response to cancer by simultaneous, nanoparticle-mediated PD-L1 inhibition and immunogenic cell death. *J Control Release* (2019) 315:126–38. doi: 10.1016/j.jconrel.2019.10.047

34. Shimabukuro-Vornhagen A, García-Márquez M, Fischer RN, Iltgen-Breburda J, Fiedler A, Wennhold K, et al. Antigen-presenting human B cells are expanded in inflammatory conditions. *J Leukoc Biol* (2017) 101(2):577–87. doi: 10.1189/jlb.5A0416-182R

35. Nielsen JS, Sahota RA, Milne K, Kost SE, Nesslinger NJ, Watson PH, et al. CD20 + tumor-infiltrating lymphocytes have an atypical CD27- memory phenotype and together with CD8+ T cells promote favorable prognosis in ovarian cancer. *Clin Cancer Res* (2012) 18(12):3281–92. doi: 10.1158/1078-0432.CCR-12-0234

36. Wenthe J, Naseri S, Labani-Motlagh A, Enblad G, Wikström KI, Eriksson E, et al. Boosting CAR T-cell responses in lymphoma by simultaneous targeting of CD40/4-1BB using oncolytic viral gene therapy. *Cancer Immunol Immunother* (2021) 70 (10):2851–65. doi: 10.1007/s00262-021-02895-7

37. Mami-Chouaib F, Blanc C, Corgnac S, Hans S, Malenica I, Granier C, et al. Resident memory T cells, critical components in tumor immunology. *J Immunother Cancer* (2018) 6(1):87. doi: 10.1186/s40425-018-0399-6

38. Khalil S, Bardawil T, Kurban M, Abbas O. Tissue-resident memory T cells in the skin. *Inflammation Res* (2020) 69(3):245–54. doi: 10.1007/s00011-020-01320-6

39. Li Q, Liu X, Wang D, Wang Y, Lu H, Wen S, et al. Prognostic value of tertiary lymphoid structure and tumor infiltrating lymphocytes in oral squamous cell carcinoma. *Int J Oral Sci* (2020) 12(1):24. doi: 10.1038/s41368-020-00092-3

40. Moussion C, Girard J-P. Dendritic cells control lymphocyte entry to lymph nodes through high endothelial venules. *Nature* (2011) 479(7374):542–6. doi: 10.1038/nature10540

41. Girard J-P, Moussion C, Förster R. HEVs, lymphatics and homeostatic immune cell trafficking in lymph nodes. *Nat Rev Immunol* (2012) 12(11):762–73. doi: 10.1038/nri3298

42. Pardoll DM. The blockade of immune checkpoints in cancer immunotherapy. *Nat Rev Cancer* (2012) 12(4):252–64. doi: 10.1038/nrc3239

43. Zhu H, Shan Y, Ge K, Lu J, Kong W, Jia C, et al. Oxaliplatin induces immunogenic cell death in hepatocellular carcinoma cells and synergizes with immune checkpoint blockade therapy. *Cell Oncol (Dordr)* (2020) 43(6):1203–14. doi: 10.1007/s13402-020-00552-2

44. Jeong SD, Jung B-K, Lee DY, Ha JH, Chang H-G, Lee J, et al. Enhanced immunogenic cell death by apoptosis/ferroptosis hybrid pathway potentiates PD-L1 blockade cancer immunotherapy. *ACS Biomater Sci Eng* (2022) 8(12):5188–98. doi: 10.1021/acsbiomaterials.2c00950

45. Liang Q, Lan Y, Li Y, Cao Y, Li J, Liu Y. Crizotinib prodrug micelles co-delivered doxorubicin for synergistic immunogenic cell death induction on breast cancer chemo-immunotherapy. *Eur J Pharm Biopharm* (2022) 177:260–72. doi: 10.1016/j.ejpb.2022.07.006

46. Dixon KO, Tabaka M, Schramm MA, Xiao S, Tang R, Dionne D, et al. TIM-3 restrains anti-tumor immunity by regulating inflammasome activation. *Nature* (2021) 595(7865):101–6. doi: 10.1038/s41586-021-03626-9

frontiers | Frontiers in Immunology

TYPE Original Research
PUBLISHED 08 February 2024
DOI 10.3389/fimmu.2024.1302761

OPEN ACCESS

EDITED BY
Hui Zhao,
University of Texas MD Anderson Cancer Center, United States

REVIEWED BY
Tai Hato,
Saitama Medical University, Japan
Hua Wang,
University of Texas MD Anderson Cancer Center, United States

*CORRESPONDENCE
Hua Zhao
huazhao@tmu.edu.cn
Xiubao Ren
renxiubao@tjmuch.com
Feng Wei
fengwei03@tmu.edu.cn

†These authors have contributed equally to this work

RECEIVED 27 September 2023
ACCEPTED 22 January 2024
PUBLISHED 08 February 2024

CITATION
Luo J, Shi X, Liu Y, Wang J, Wang H, Yang X, Sun Q, Hui Z, Wei F, Ren X and Zhao H (2024) Immune checkpoint ligands expressed on mature high endothelial venules predict poor prognosis of NSCLC: have a relationship with CD8$^+$ T lymphocytes infiltration.
Front. Immunol. 15:1302761.
doi: 10.3389/fimmu.2024.1302761

Immune checkpoint ligands expressed on mature high endothelial venules predict poor prognosis of NSCLC: have a relationship with CD8$^+$ T lymphocytes infiltration

Jing Luo[1,2,3,4†], Xiuhuan Shi[1,2,3,4,5†], Yumeng Liu[1,2,3,4], Jian Wang[1,2,3,4], Hao Wang[1,2,3,4,6], Xuena Yang[1,2,3,4], Qian Sun[1,2,3,4,7], Zhenzhen Hui[1,2,3,8], Feng Wei[1,2,3,4,7*], Xiubao Ren[1,2,3,4,7,8*] and Hua Zhao[1,2,3,4,7*]

[1]Tianjin Medical University Cancer Institute and Hospital, National Clinical Research Center for Cancer, Tianjin, China, [2]Tianjin's Clinical Research Center for Cancer, Tianjin, China, [3]Key Laboratory of Cancer Immunology and Biotherapy, Tianjin, China, [4]Department of Immunology, Tianjin Medical University Cancer Institute and Hospital, Tianjin, China, [5]Department of Medical Oncology, Affiliated Hospital of Inner Mongolia Medical University, Huhhot, China, [6]The Affiliated Jiangning Hospital of Nanjing Medical University, Nanjing, China, [7]Haihe Laboratory of Cell Ecosystem, Tianjin, China, [8]Department of Biotherapy, Tianjin Medical University Cancer Institute and Hospital, Tianjin, China

Background: An insufficient number of intratumoral CD8$^+$ T lymphocytes is a major barrier to antitumor immunity and immunotherapy. High endothelial venules (HEVs) are the major sites through which lymphocytes enter tumors; however, the molecular mechanism through which HEVs mediate CD8$^+$ T lymphocyte infiltration remains poorly understood.

Methods: Forty-two patients with stage IIIA lung adenocarcinoma, who underwent surgery, were recruited. Multiplex immunohistochemical staining was conducted on tumor tissues to detect the immune checkpoint ligands (ICLs) expressed in the HEVs, blood vessels, and lymphatics. A new ICL score model was constructed to evaluate ligand expression. The relationship between ICL score, tumor-infiltrating CD8$^+$ T cell frequency, and survival of patients was investigated.

Results: Mature HEVs, but not blood vessels or lymphatics, mediated CD8$^+$ T cell infiltration. However, the ICLs expressed on mature HEVs could negatively regulate CD8$^+$ T cell entry into tertiary lymphoid structures (TLSs). In addition, according to the results obtained using our ICL_{total} score model, the expression of ICLs on HEVs was observed to be a predictor of both CD8$^+$ T cell infiltration and survival, in which a high ICL_{total} score > 1 represent a weak CD8$^+$ T cell infiltration and a high ICL_{total} score > 2 predicts poor survival.

Conclusion: Using the ICL score model, we discovered that ICLs expressed on HEVs are indicative of $CD8^+$ T cell subset infiltration in TLSs, as well as of patient survival with lung cancer.

KEYWORDS

lung cancer, immune checkpoint ligands, high endothelial venules, lymphocytes infiltration, tertiary lymphoid structures

1 Introduction

Since the early 2010s, immunotherapy has achieved monumental breakthroughs in cancer therapy and has revitalized the field of antitumor immunology (1). The clinical responses to immunotherapy have been strong, and the prognosis of patients has improved (1, 2). However, the efficacy of immunotherapy varies, and only specific subsets of patients benefit (3). Immune cell recruitment into the tumor microenvironment (TME) may be a critical factor in antitumor immunity and influence the clinical response and prognoses of cancer patients (4–6). Thus, obtaining an in-depth understanding of the immune infiltrates would be helpful in increasing clinical response and creating new therapeutic strategies for cancer prevention and treatment.

Lymphocyte delivery to tumors is essential for TME and antitumor immunotherapy (7–10). The high infiltration of T cells, especially $CD8^+$ T subsets, into the TME is associated with a clinical response to immunotherapy in several types of cancer (11). Thus, further exploring the mechanisms governing immune cells delivery to tumors is critical. There are several ways in which blood vessels restrict lymphocyte extravasation (12); however, the mechanism of lymphocyte recruitment remains unclear. The chemokines C-X-C motif chemokine ligands 9 and 10 play important roles in T cell infiltration (13–16); however, the exact mechanisms of lymphocyte entry into the TME remain poorly defined.

High endothelial venules (HEVs), structurally and antigenically, are blood vessels that mediate lymphocyte delivery to the lymph nodes and other secondary lymphoid organs (4, 17, 18). HEVs play a critical role in the recruitment of lymphocytes as well as in immune surveillance of foreign invaders (bacteria or viruses) as they facilitate lymphocyte extravasation from the blood (19). The HEV system develops in the immune-stimulated lymph nodes during inflammation and is completely reconstructed in the tumor-draining lymph nodes. HEVs that exist extranodally are characteristically surrounded by lymphocytic forming lymph-nodes-like structures with distinct germinal centers and $CD3^+$ T- and $CD20^+$B-cell-rich areas, referred to as tertiary lymphoid structures (TLSs) (20). The development of TLSs in peripheral tissues is indicative of lymphoid neogenesis that occurs in response to long-term inflammation and they are very common to be found in many types of tumor tissues, according to most solid malignancies investigated thus far, the presence of mature TLSs is associated with a favorable prognosis, however, the degree of TLS maturation can affect immune function significantly, therefore, exploring the TLS maturation is crucial for immunotherapy (21). The periphery of TLSs is located by HEVs, which are the major sites through which lymphocytes enter tumors, govern the delivery of lymphocytes from the blood into the TME and providing specialized vasculature for TLS. HEVs are essential for the immune function and maturation of TLSs (22). As HEVs continue to mature, they mature becoming peripheral-node-addressin (PNAd) expressing HEVs (20), the presence of PNAd is regarded as a sign of maturity. The presence of TLSs with HEVs in human tumors are drawing increased attention owing to the therapeutic potential (22, 23). Both TLSs and HEVs play essential roles in regulating the recruitment of lymphocytes into the TME; however, there are many problems remain to be addressed. As mature HEVs, they have different capacities for delivery T cells, this may contribute to the differences in therapeutical response of immunotherapy between individuals, but the molecular and functional mechanisms remain poorly defined.

In this study, we found the expression of immune checkpoint ligands (ICLs) on mature HEVs negatively regulate the infiltration of $CD8^+$ T cells into the TLSs. In addition, the presence of ICLs on HEVs may be a predictor of $CD8^+$ T cells infiltrating the TLSs as well as of patient survival. This study provides a novel understanding of the HEVs governing lymphocyte delivery into the TLSs, and an index for predicting patient prognosis based on the total ICL (ICL_{total}) score model developed in the study.

2 Materials and methods

2.1 Patients and tumor samples

A total of 49 patients with stage IIIA primary lung adenocarcinoma who had underwent surgery at our hospital between January 2015 and May 2016 were recruited, tumor tissues were collected, and immunohistochemical staining was

performed to detect the TLS. All patients were classified into grades 1–3 based on the maturity level of TLSs as reported in our previous work (24), TLSs in patients of grade 3 were considered the most mature, whereas TLSs in patients of grade 1 were considered naïve. Given that naïve TLSs are PNAd-negative, we exclude patients with TLS maturity grade 1. Only patients with TLS maturity grade 2-3 were recruited. Every patient received 4 cycles of platinum doublet chemotherapy with pemetrexed after surgery, at a frequency of 21 days per cycle. No other treatment was administered. The eligibility criteria were as follows: (I) complete clinical data; (II) age 18–75 years; (III) pathologically confirmed lung adenocarcinoma; (IV) TLS maturity grade 2-3; (V) clinical stage IIIA; (VI) surgical resection of R0; and (VII) received standardized postoperative treatment. Finally, a total of 42 patients are recruited, the clinical characteristics of these patients are provided in Table 1.

TABLE 1 Clinical characteristics in patients with stage IIIA LUAD (n=42).

Characters		N (%)
Age, y		
	≥ 60	18 (42.9)
	< 60	24 (57.1)
Gender		
	Male	18 (42.9)
	Female	24 (57.1)
Smoking		
	Yes	17 (40.5)
	No	25 (59.5)
KPS		
	≥ 60	40 (95)
	< 60	2 (5)
T stage		
	T1	26 (61.9)
	T2	13 (31)
	T3	3 (7.1)
N stage	N1	3 (7.1)
	N2	39 (92.9)
Micropapillary		
	Yes	18 (42.9)
	No	24 (57.1)
Tumor volume		
	≥10 cm^3	15 (35.7)
	<10 cm^3	27 (64.3)
Type of resection		
	Lobectomy	30 (71.4)
	sleeve lobectomy	12 (28.6)

y, year; KPS, Karnofsky performance status.

2.2 Multiplex immunohistochemistry and multispectral analysis

Tumor tissues were collected from 42 patients, and multiplex immunohistochemical staining was conducted using a PerkinElmer Opal 7-color Technology Kit, according to the manufacturer's instructions. Five staining panels were designed and applied to each panel to target different markers. HEVs were defined as $PNAd^+$, while blood vessels and lymphatics were defined as $CD31^+$ or $PDPN^+$. Details of the panels and the relative antibodies are provided in Table 2. Each stained slide was visualized and quantified using a TissueFAXS Spectra System and StrataQuest analysis (TissueGnostics), according to previously described methods (25). The immune checkpoint molecule expression analysis is performed using the contextual tissue cytometry image analysis. Multispectral images were scanned using a 20× objective lens, and 10 fields were randomly selected for each slide. We collected all TLSs from all tumor sections; in total, 821 fields were collected, including 692 TLSs.

The spatial distribution between the cells was quantified using the Dilate algorithm, which defines the cell sociology for each selected area. Finally, we developed the corresponding algorithms based on the analysis requirements, and for each channel, we applied a unified algorithm and threshold to all samples to standardize the expression and fluorescence levels of each marker.

TABLE 2 Details of antibodies used in the multiplex immunohistochemistry staining.

Antibodies	Source	Identifier	Dilution
Recombinant Anti-CD3 antibody	abcam	ab135372	1:400
Anti-CD4 antibody	abcam	ab133616	1:400
Anti-CD8 alpha antibody	abcam	ab101500	1:1000
Anti-CD20 antibody	abcam	ab9475	1:600
Anti-LAG-3 antibody	abcam	ab180187	1:500
Anti-TIM 3 antibody	abcam	ab241332	1:250
Anti-PD1 antibody	abcam	ab137132	1:100
Peripheral Node Addressin Antibody	Novus Biologicals	NB100-77673	1:100
Anti-CD31 antibody	abcam	ab9498	1:500
Anti-Podoplanin antibody	abcam	ab236529	1:200
Anti-galectin 9/Gal-9 antibody	abcam	ab153673	1:100
Anti-HMGB1 antibody	abcam	ab79823	1:1200
Anti-CEACAM1 antibody	abcam	ab108397	1:50
Anti-LSECtin antibody	abcam	ab181196	1:200
Anti-FGL1 antibody	abcam	ab275091	1:400
Anti-Galectin 3 antibody	abcam	ab76245	1:1200
Anti-MHC Class II antibody	abcam	ab55152	1:800
PD-L1 (CD274) Recombinant Rabbit Monoclonal Antibody	Invitrogen	MA5-27896	1:300

Based on previous studies (26, 27), spatial distance was analyzed for radius (r) = 30 μm, representing the proximity distance as the average number of cells distributed from the nuclear center of any reference cell.

2.3 Statistical analysis

Analyses of the results was conducted using SPSS (version 22.0). Kaplan–Meier analyses were used to analyze and compare differences in survival. The clinical characteristics of the patients were analyzed using the chi-square test. Disease-free survival (DFS) was defined as the date of tumor recurrence or diagnosis of metastasis. Statistical tests were two-sided, and a *P*-value < 0.05 was considered statistically significant.

3 Results

3.1 Frequency of CD8$^+$ T cells is high in mature TLSs

Patients with TLS maturity grade 2-3 were recruited in this study, the infiltration of the immune population in the TLSs was evaluated for patients with different TLS maturity grades, and the data indicated that infiltration did not differ among CD3$^+$ T, CD4$^+$ T, and CD20$^+$ B cells, representative images showing T lymphocytes and TLS (defined by B cells) were provided in Supplementary Figure S1. The proportion of only CD8$^+$ T cells was higher in patients with grade 3 TLS maturity than in those with grade 2 TLS maturity (Figures 1A–D). Next, we evaluated the infiltration of CD8$^+$ T cells in whole tumor samples,

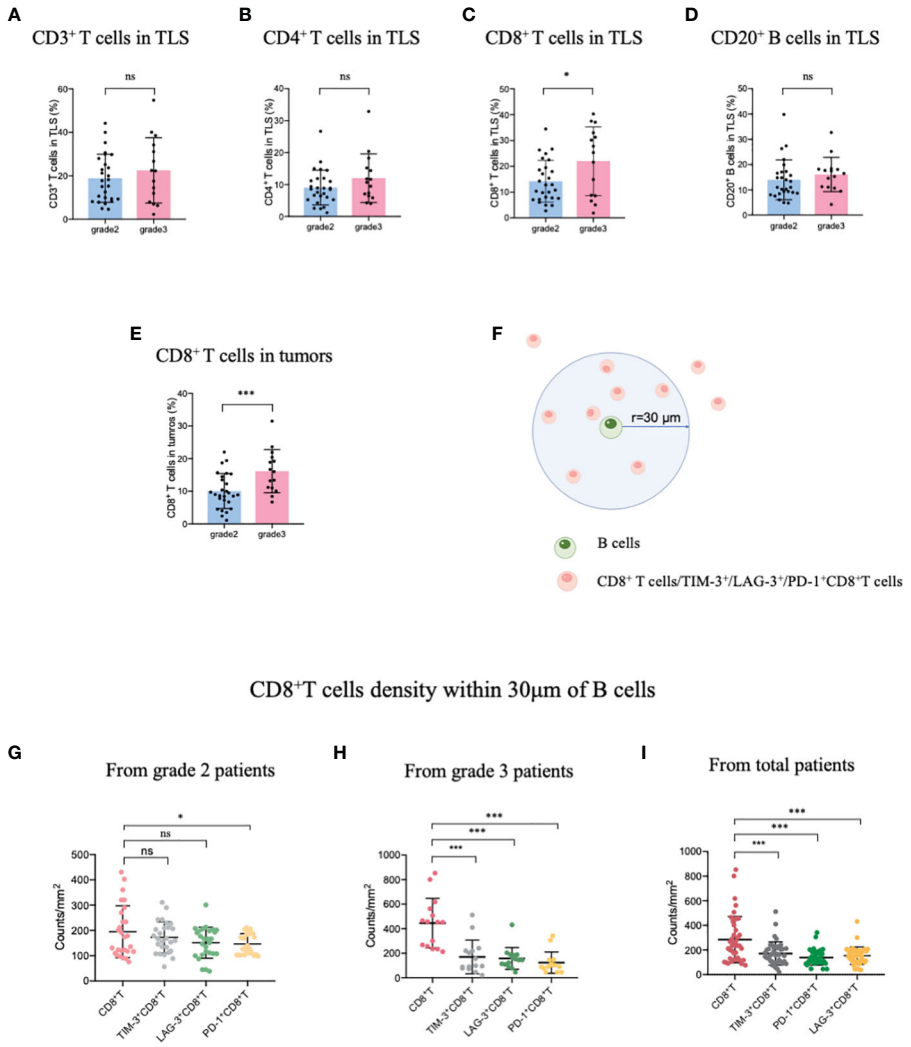

FIGURE 1
Mature HEVs positively affect CD8$^+$ T cell entry into TLSs. The infiltration of **(A)** CD3$^+$ T-, **(B)** CD4$^+$ T-, **(C)** CD8$^+$ T-, and **(D)** CD20$^+$ B-cells into TLSs of patients with different TLS maturity grades. The infiltration of **(E)** CD8$^+$ T cells into tumors of patients with different TLS maturity grades. **(F)** Illustration of spatial analysis methodology. Densities of cells of interest within a certain radius (30 μm) to a reference cell were calculated. Densities of CD8$^+$ T cells and exhausted CD8$^+$ T cells within 30 μm of CD20$^+$ B-cells in patients with **(G)** grade 2, **(H)** grade 3, and **(I)** in all patients. HEVs, high endothelial venules. TLSs, tertiary lymphoid structures. Data are presented as mean ± SD. *P < 0.05; *** P < 0.01; ns, not significant according to unpaired two-tailed Student's t-test.

it was observed that the percentage of $CD8^+$ T cells was higher in patients with grade 3 TLS maturity than in those with grade 2 TLS maturity (Figure 1E). These findings suggested that higher the maturity of the TLSs, higher is the number of $CD8^+$ T cells that infiltrate the TLS or the TME. Based on these results, we analyzed the spatial relationship between $CD8^+$ T/exhausted $CD8^+$ T subsets and the TLSs. The spatial distributions of exhausted $CD8^+$ T cells ($TIM\text{-}3^+/LAG\text{-}3^+/PD\text{-}1^+$ $CD8^+$ T cells) (28) and TLSs ($CD20^+$ B cells) were explored. The bivariate K(r) function (29) was used to describe the spatial distribution of the two cell phenotypes. The radius used (30 μm) is generally considered ideal for calculating the spatial relationship between two cell populations (Figure 1F). In patients with grade 2 TLS maturity, compared with normal $CD8^+$ T cells, only $PD\text{-}1^+$ $CD8^+$ T exhausted cells were found a few reductions around B cells, while other exhausted T cells remained unchanged. However, in patients with grade 3 TLS maturity, a marked decrease in the levels of all exhausted $CD8^+$ T cells around B-cells compared with those of $CD8^+$ T cells was observed, suggesting that exhausted $CD8^+$ T cells were far from mature TLSs (Figures 1G–I). Altogether, these results suggest that the maturity of TLSs is positively correlated with $CD8^+$ T lymphocytes delivery into TLSs.

3.2 Checkpoint ligands expressed in mature HEVs are negatively related to $CD8^+$ T cells infiltrating the TLSs

Next, TIM-3, LAG-3, and PD-1 were chosen as they were the most common immune checkpoints and are very critical for immune regulation (30, 31); we then analyzed their ligands expressed on mature HEVs (PNAd was used as the marker of mature HEVs), blood vessels, and lymphatics, representative images were provided in Figures 2A, B and Supplementary Figures S2, S3. A negative relationship was found between the ligands expressed on mature HEVs and the TLS-infiltrating $CD8^+$ T cell frequency, especially for Gal-9 (ligand of TIM-3), MHC II, Gal-3 (ligand of LAG-3), and PD-L1 (ligand of PD-1) ($P < 0.05$) (Figures 3A–C). When ligands were highly expressed in mature HEVs, the frequency of TLS-infiltrating $CD8^+$ T cells decreased. Notably, these results were observed only for mature HEVs; ligands expressed on blood vessels or lymphatics did not impact TLS-infiltrating $CD8^+$ T cell frequency (Supplementary Figures S4A–C and Supplementary Figures S5A–C). These data indicate the importance of the checkpoint ligands expressed on mature HEVs, which may negatively affect $CD8^+$ T cell entry into tumors. Additionally, not every ligand expressed on HEVs has the ability to substantially affect tumor-infiltrating $CD8^+$ T cells; only Gal-9, MHC II, Gal-3, and PD-L1 play important roles in mediating $CD8^+$ T cell subsets' entry into the TLSs. To further confirm the importance of ICL expressed on mature HEVs, we analyzed the expression of all ICL in the TME and found that patients with high ICL score have a relatively higher expression of ICL in TME than those with low ICL score, but the differences are not statistical (Supplementary Figure S6A). We then investigated the relationship between the 4 important checkpoint ligands (Gal-9, MHCII, Gal-3 and PD-L1) expressed on HEVs and those expressed in TME. Results showed that for the 3 important ligands (MHCII, Gal-3 and PD-L1), correlations were found between their expression levels on HEVs and in TME (Supplementary Figure S6B). Nevertheless, the ICL expressed on other sites of tumors except HEVs might have minimal effects on $CD8^+$T cell delivery (Supplementary Figure S6C).

Considering these results, we constructed an ICL score model to convert the eight ligands into three indices and evaluated the integrative ligand expression level of each immune checkpoint. First, the median value of the expression of each ligand was calculated. When a ligand expression value was larger than its median value, the ligand expression status was defined as "high expression;" otherwise, the status was defined as "low expression." Next, considering the differences in the impacts of each ligand's expression on tumor-infiltrating $CD8^+$ T frequency, for the four important ligands (Gal-9, MHC II, Gal-3 and PD-L1), the item is scored as "2" when any one of them is defined as "highly expression"; otherwise, it is scored as "0". Although the expression of the other four ligands (HMGB1, CEACAM-1, LSECtin, and FGL-1) did not considerably affect the frequency of tumor-infiltrating $CD8^+$ T cells, the negative relationship was consistent for the four important ligands. Thus, when a patient had a high expression of any of the less important four ligands, the patient was assigned an score for the item of "1;" otherwise, the score was "0". The ICL score for each checkpoint was the sum of its ligands scores. The higher the score, the higher the checkpoint ligands expression in the HEVs. We classified patients into three categories (low, moderate, and high checkpoint ligand expression) by their total checkpoint ICL score. The details of the scoring model are shown in Figure 4A. We investigated the frequency of TLS-infiltrating $CD8^+$ T cells for various checkpoint ligand levels. We found that higher expression of TIM-3, LAG-3, or PD-1 ligand on the HEVs, representing a lower percentage of TLS-infiltrating $CD8^+$ T cells; and, lower the ligand expression, higher was the $CD8^+$ T cell infiltration into the TLSs (Figures 4B–D). Differences were statistically significant. According to the maturity level of the TLSs, patients were classified into one of the three grades, as described above (24); the expression of checkpoint ligands for the patients classified as different grades was measured. We found that for patients with grade 3 TLS maturity, who had the most mature TLSs, the expression of checkpoint ligands on HEVs was lower; and for patients with grade 2 TLS maturity, who had less mature, the expression of checkpoint ligands on HEVs was higher (Figures 4E–G). Based on these data, we speculated that the less mature HEVs express a higher number of checkpoint ligands and potentially decrease $CD8^+$ T cell infiltration in TLS, whereas the mature HEVs express fewer ligands, which may increase $CD8^+$ T cell infiltration.

To comprehensively evaluate the checkpoint ligands expressed on mature HEVs, we used the developed ICL score model to convert the three checkpoint ligand expression indicators (TIM-3, LAG-3, and PD-1) into one index representing total checkpoint ligand expression levels. The details are shown in Figure 5A. According to the ICL_{total} scores, we classified patients into three classifications: high, moderate, and low total ligand expression. The effect of total ligand expression on the frequency of TLS-infiltrating $CD8^+$ T cells

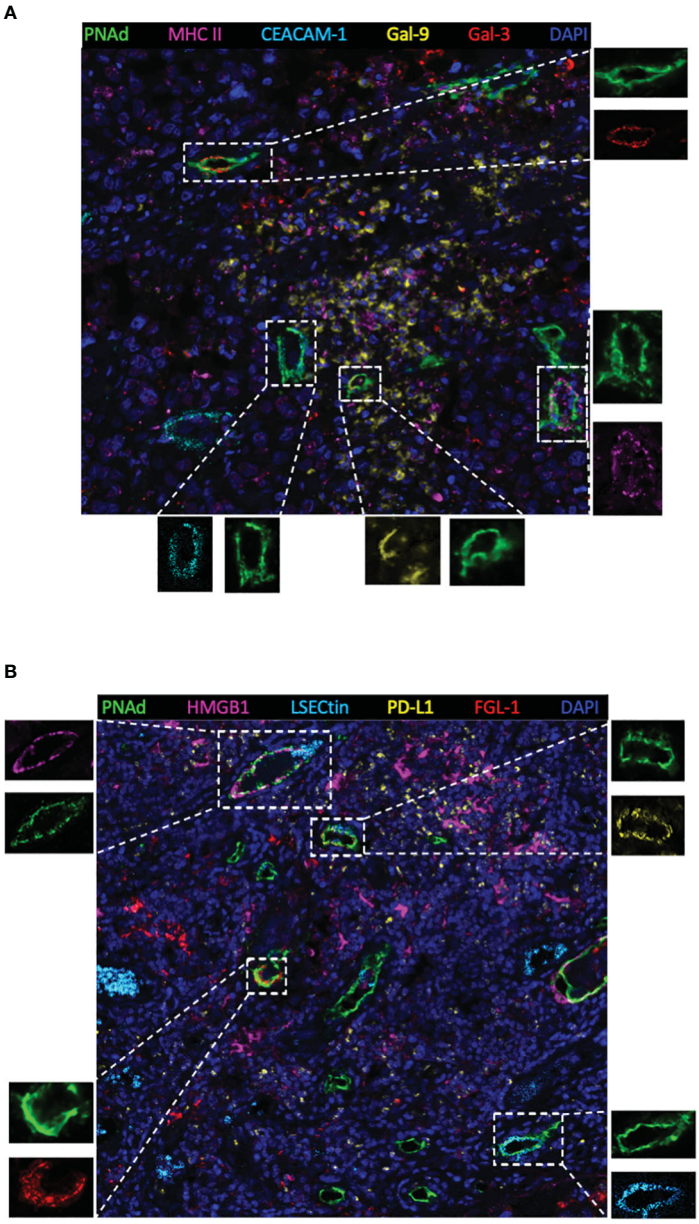

FIGURE 2
Representative multiplex immunohistochemistry staining image (20×) showing ligands expressed on mature HEVs. **(A)** Ligands of MHC II, CEACAM-1, Gal-9 and Gal-3 expressed on mature HEVs. **(B)** Ligands of HMGB1, LSECtin, PD-L1, FGL-1 expressed on mature HEVs.

was investigated, total tumor-infiltrating $CD8^+$ T cells and the exhausted $CD8^+$T cells ($TIM\text{-}3^+/LAG\text{-}3^+/PD\text{-}1^+/PD\text{-}1^+TIM\text{-}3^+CD8^+$T cells) were analyzed, results showed that a higher total checkpoint ligand expression in HEVs represented a lower percentage of TLS-infiltrating $CD8^+$ T cells, whereas a lower total ligand expression indicated increased $CD8^+$ T cell infiltration (Figure 5B), with the differences being statistically significant. The significant associations between the ligands expression levels and clinicopathological parameters were not observed (Table 3). And for the exhausted $CD8^+$T cells, 2 kinds of exhausted $CD8^+$T cells ($PD\text{-}1^+/PD\text{-}1^+TIM\text{-}3^+CD8^+$T cells) were observed an increase in high ICL expression patients (Supplementary Figure S7). This may due to the ICL high expression patients has a weak ability to deliver $CD8^+$T cells into tumors, and those $CD8^+$T cells have to fight against more tumor cells which causing exhaustion. Furthermore, for patients with grade 2 TLSs maturity, the expression of checkpoint ligands was higher in HEVs, whereas for patients with grade 3 TLS maturity, the expression was lower in HEVs (Figure 5C). These results provide evidence that less mature HEVs have higher checkpoint ligand expression, which may negatively affect the $CD8^+$ T cells delivery into TLSs. As the HEVs mature, the ligand expression decreases, and $CD8^+$ T cells can more easily infiltrate the HEVs, as we speculated.

To quantify the negative effect of the ICLs of HEVs on the delivery of $CD8^+$ T cells into TLSs, receiver operating characteristic (ROC) analysis was conducted to assess the

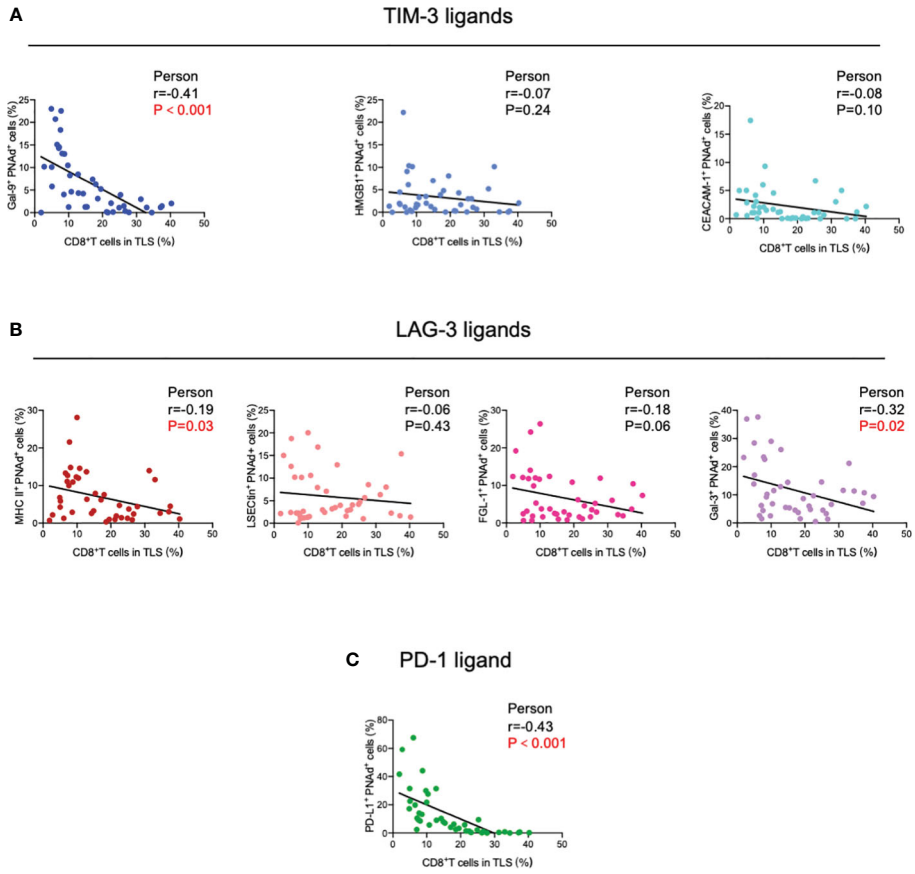

FIGURE 3
Correlation between **(A)** TIM-3, **(B)** LAG-3, and **(C)** PD-1 ligands expressed on mature HEVs and TLS-infiltrating $CD8^+$ T cell frequency. HEVs, high endothelial venules. TLSs, tertiary lymphoid structures. Data are presented as mean ± SD. * $P < 0.05$; *** $P < 0.01$; ns, not significant according to unpaired two-tailed Student's t-test.

accuracy of ICL scores in predicting TLS-infiltrating $CD8^+$ T cell frequency (Figure 5D). Patients with a TLS-infiltrating $CD8^+$ T cell frequency lower than the median value were considered to have "weak $CD8^+$ T cell infiltration;" otherwise, patients were considered "strong $CD8^+$ T cell infiltration." The data showed that all four indices had large area under the curve (AUC) values, especially the ICL_{total} score indicator, which had an AUC value of 0.914 ($P < 0.001$), indicating that the ICL_{total} score could accurately predict TLS-infiltrating $CD8^+$ T cell frequency. The cutoff value for the ICL_{total} score was evaluated, and a value of one was identified as the cutoff value that conferred 91.3% sensitivity and 78.9% specificity, indicating that an ICL_{total} score > 1 leads to weak $CD8^+$ T cell infiltration ($P < 0.001$).

3.3 High ICL expression on HEVs predicts survival loss

After confirming the effects of HEV-expressed ICLs on tumor-infiltrating $CD8^+$ T cells, we analyzed the prognostic predictive ability of ICL levels in patients. The median age of the entire population (57.1% women, 42.9% men) was 57 years, and 95% of the patients had a Karnofsky performance status score ≥ 80. All patients had stage IIIA disease; the median DFS was 15.3 months for the whole population. The results of the survival analysis showed that the survival of patients with higher ICL expression was substantially worse (Figures 6A–D). The median DFS of patients for the low, moderate, and high TIM-3 ligand expression groups was 22.8 months (95% confidence interval (CI), 12.8–32.7), 17.0 months (95% CI, 9.4–24.7), and 7.2 months (95% CI, 5.2–9.1), respectively. The difference between the moderate & low and high TIM-3 ligand expression levels was significant ($P = 0.011$). The median DFS of patients for the low, moderate, and high LAG-3 ligand expression groups was 20.5 months (95% CI, 13.9–27.1), 18.1 months (95% CI, 12.4–23.7), and 7.4 months (95% CI, 0.5–14.4), respectively. The difference between the moderate & low and high LAG-3 ligand expression groups was significant ($P = 0.037$). Additionally, the median DFS of the patients for the low and high PD-1 ligand expression groups was 17.6 months (95% CI, 11.6–23.5) and 7.4 months (95% CI, 0–17.0), respectively. We found no significant difference between the low and high PD-1 ligand expression groups ($P = 0.393$). Finally, we analyzed the total ligand expression; the results indicated that the median DFS of patients for the total low, moderate, and high ligand expression groups was 20.5 months (95% CI, 13.8–27.2), 13.5 months (95% CI,

10.3389/fimmu.2024.1302761

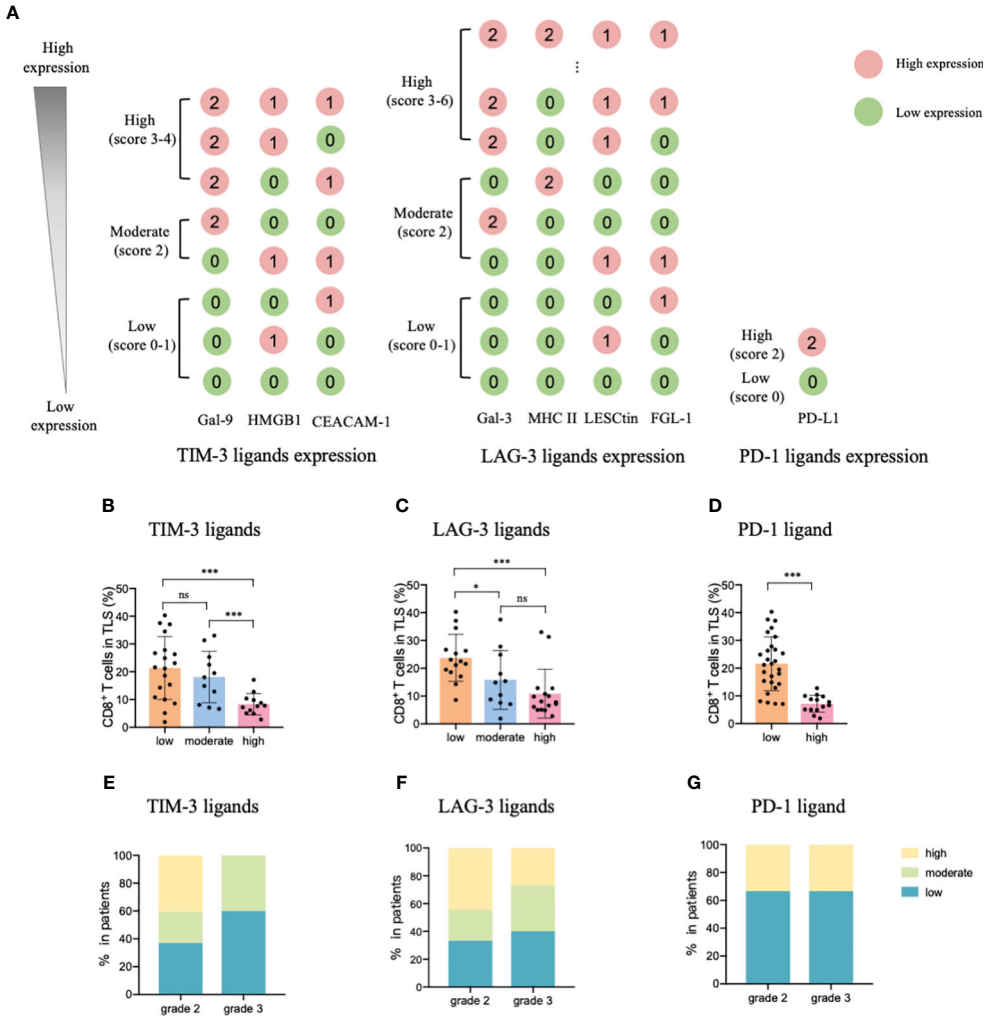

FIGURE 4
TIM-3, LAG-3, and PD-1 ligands expressed on mature HEVs negatively affected the tumor-infiltrating $CD8^+$ T cell frequency. **(A)** The scoring pattern of the developed ICL score model used to calculate the expression levels of three checkpoint ligands. The effect of **(B)** TIM-3, **(C)** LAG-3, and **(D)** PD-1 ligand expression levels on mature HEVs on tumor-infiltrating $CD8^+$ T cell frequency. Comparison of **(E)** TIM-3, **(F)** LAG-3, and **(G)** PD-1 ligand expression levels among patients with different TLS maturity grades. HEVs, high endothelial venules. ICL, immune checkpoint ligand. TLSs, tertiary lymphoid structures. Data are presented as mean ± SD. * $P < 0.05$; *** $P < 0.01$; ns, not significant according to unpaired two-tailed Student's t-test.

2.7–24.2), and 7.4 months (95% CI, 0.3–14.6), respectively. The difference between the low and high ligand expression groups was significant ($P = 0.014$).

To further understand the ICLs expressed on HEVs, we selected four important ligands—Gal-9, MHC II, Gal-3, and PD-L1, which were found to be significantly related to $CD8^+$ T cell entry into the TLSs, and each of which was considered a risk indicator. In patients with a high expression of one or more of the four ligands, the risk level was higher. For patients with a high expression of 1–2 ligands, the risk level was I–II; and for those with a high expression of 3–4 ligands, the risk level was III–IV. For patients with a low expression of all four ligands, the risk level was zero. The survival of patients with different risk levels was studied. We observed that the median DFS of patients for the risk 0, I–II, and III–IV groups was 20.5 months (95% CI, 14.2–26.8), 13.5 months (95% CI, 5.0–21.9), and 7.2 months (95% CI, 3.5–14.6), respectively. The differences between the risk 0 and III–IV groups, and the risk 0 & I–II and III–IV groups were significant ($P = 0.002$, respectively; Figure 6E). Together, these data provide evidence that low ICL expression in mature HEVs is positively associated with better DFS compared with that associated with a high expression on these ligands.

To quantify the negative effect of ICLs of HEVs on survival, the ROC was analyzed to assess the accuracy of ICL scores in predicting survival (Figure 6F). Patients with a DFS shorter than the median (15.3 months) were considered to have survival loss, whereas patients in whom the DFS was longer than the median DFS were considered to have survival benefits. The data showed that among the five indices, only the ICL_{total} score had large AUC values (AUC = 0.705) with a P-value < 0.05 ($P = 0.029$), indicating that the ICL_{total} score had a strong prognostic predictive power. The cutoff value for

10.3389/fimmu.2024.1302761

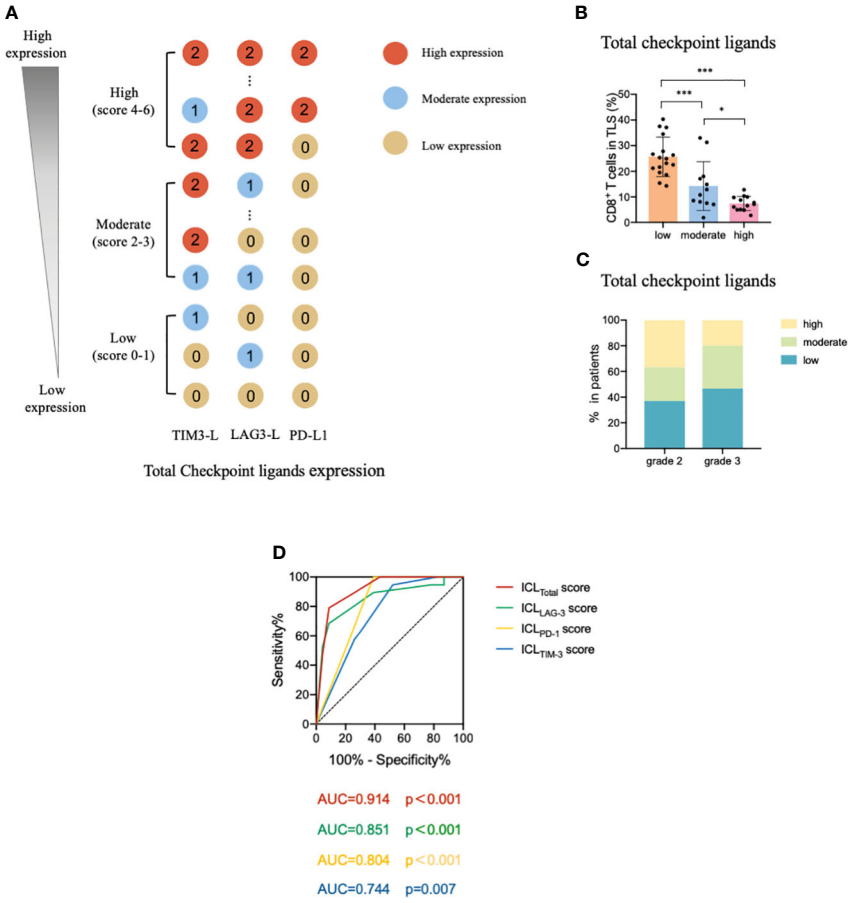

FIGURE 5
Levels of total ligands expressed on mature HEVs have a negative effect on the TLS-infiltrating CD8$^+$ T cell frequency. **(A)** The scoring pattern of the ICL score model used to calculate the total ligand expression level. **(B)** The effect of total ligand expression levels on mature HEVs on the TLS-infiltrating CD8$^+$ T cell frequency. **(C)** Comparison of total ligand expression levels for patients with different TLS maturity grades. **(D)** The ROC curve between TLS-infiltrating CD8$^+$ T cell frequency and ICL scores. HEVs, high endothelial venules. TLSs, tertiary lymphoid structures. ROC, receiver operating characteristic. ICL, immune checkpoint ligand. Data are presented as means ± SD. * $P < 0.05$; *** $P < 0.01$; ns, not significant according to unpaired two-tailed Student's t-test.

the ICL_{total} score was evaluated, and a score of two was identified as the cutoff value that conferred 66.7% sensitivity and 66.7% specificity. Therefore, an ICL_{total} score > 2 predicted poor survival.

4 Discussion

In this study, we found that mature HEVs are participated in regulating the CD8$^+$ T subsets delivery to the TLSs, but the ICLs expressed on mature HEVs (not blood vessels or lymphatics) are capable of affect CD8$^+$ T lymphocytes infiltration negatively. Furthermore, the expression of ligands on HEVs may be an indicator of both CD8$^+$ T cell infiltration and survival, according to our ICL score model, in which a high ICL_{total} score > 1 represent a weak CD8$^+$ T cell infiltration and a high ICL_{total} score > 2 predicts poor survival. Novel foundings of the HEVs controlling lymphocyte delivery into the TLSs are presented in this study, along with a model of the total lymphocyte load (ICLtotal) score that is indicative of patient prognosis. Additionally, an overview was provided to illustrate the present study (Figure 7).

There have been considerable improvements in antitumor immunotherapy due to the immune checkpoint blockade (ICB). However, many patients fail or relapse after ICB treatment, indicating the limitations of antitumor immunotherapy (32, 33). Furthermore, the outcomes of ICB treatment are influenced by the quality and magnitude of the lymphocytes response within the TME (12). In cancer patients, prognosis and outcomes of therapeutic interventions are predicted by tumor-infiltrating lymphocyte levels (34, 35), and increased tumor-infiltrating lymphocyte infiltration may improve patient prognosis. Therefore, the entry of immune cells into the TME has attracted increasing attention. In tumors, lymphocytes are mainly extravasated through HEVs (4). Assia et al. (4) revealed that the maturity of HEVs plays a critical role in their molecular function. The maturity of HEV endothelial cells, in addition to their number, is critical for the lymphocyte delivery mediated by HEVs. Increasing the frequency and maturity of HEV endothelial cells can increase the outcomes and clinical response of ICB treatment. In our study, we uncovered the relationship between TLS maturity and CD8$^+$ T cell infiltration: patients with mature TLSs had higher percentages of TLS-infiltrating CD8$^+$ T, whereas

TABLE 3 Associations between ICL expression levels and important clinicopathological parameters.

		Total ICL expression level			P value
		High	Moderate	Low	
Gender					0.313
	Male	7	3	8	
	Female	6	9	9	
Age, y					0.475
	≥ 60	4	5	9	
	< 60	9	7	8	
Smoking					0.395
	Yes	4	4	9	
	No	9	8	8	
Micropapillary					0.433
	Yes	5	7	6	
	No	8	5	11	
Tumor volume					0.331
	≥10 cm^3	5	6	4	
	<10 cm^3	6	8	13	

y, year; ICL, immune checkpoint ligand.

patients with less mature or naïve TLSs had fewer $CD8^+$ T in the TLSs, suggesting mature HEVs can positively affect $CD8^+$ T cell delivery to the TLSs. Furthermore, the results of our previous study (24) demonstrated that patients with mature TLSs had a longer DFS. Taking our results together, we conclude that the maturity of HEVs/TLSs strongly affects tumor immunity and survival via regulating $CD8^+$ T cell entry. However, the mechanism through which the maturity of HEVs/TLSs influences $CD8^+$ T cell entry into tumors remains unknown, and the underlying molecular mechanisms remain poorly understood.

The results of the multiplex immunohistochemistry analyses in this study revealed that the checkpoint ligand expression on HEVs of mature TLSs is lower, which may be a key factor affecting $CD8^+$ T cell entry into the TLS. There are immune checkpoints that regulate inhibitory or stimulating immune responses through ligand-receptor pairs (31). Immune cells, particularly the T cells express immune checkpoints and their ligands can be found in the TME (36). Ligand expression is essential for triggering signals via immune checkpoint receptors. Immune evasion is the primary function of tumor-associated immune checkpoints, and their suppressive functions mostly depend on ligand-induced signaling (37, 38). When engaged with their ligands, checkpoint signaling can be triggered (37); however, their activity can be easily stopped by preventing ligand-receptor engagement using blocking antibodies (36). Admittedly, a negative relationship was observed between the expression of checkpoint ligands on HEVs and the $CD8^+$ T cell infiltration, this is mostly due to the decrease of $CD8^+$ T cell infiltration, however, the inhibition of the proliferation and activation of $CD8^+$ T cells caused by the expression of the ligands on the HEVs maybe another potential reason. Concerning the HEVs are major vessels that mediate lymphocyte trafficking, and few studies report the HEVs has the ability to affect the proliferation and activation of lymphocyte, we speculate that the HEVs with high expression of checkpoint ligands have a primary effect on negatively influencing the entry of $CD8^+$ T cells into tumors, although they might also inhibit the $CD8^+$ T cells proliferation at the same time. The deep mechanism that how ligands expressed on HEVs affect the $CD8^+$ T cell infiltration is ongoing.

In recent years, many researchers have uncovered the sophisticated regulation of checkpoint-ligand engagement, where different ligands show distinct signaling mechanisms that impact antitumor immunity (37), the molecular functions of immune checkpoints and their ligands remain poorly understood. In this study, we selected TIM-3, LAG-3, and PD-1, the three most common immune checkpoints which are also critical for immune regulation, and analyzed the expression of their corresponding ligands in mature HEVs. Not every ligand was included in the analysis: a ligand of LAG-3, α-syn, was not observed because it is mainly involved in intercellular synaptic transmission and does not substantially participate in immune-related activities (39, 40). Another ligand not included was PD-L2, a PD-1 ligand. The functions of PD-L2 are more sophisticated than those of PD-L1, which is the primary ligand of PD-1; by binding to PD-1, PD-L2 also facilitates the inhibitory functionality of PD-1 (36). In addition, PD-L2 can engage another receptor, RgmB (41), which can activate T cells (41, 42). Considering the uncertainty regarding the function of PD-L2, we excluded PD-L2 in our study. Finally, we found that the ICLs expressed on mature HEVs negatively affect $CD8^+$ T cell

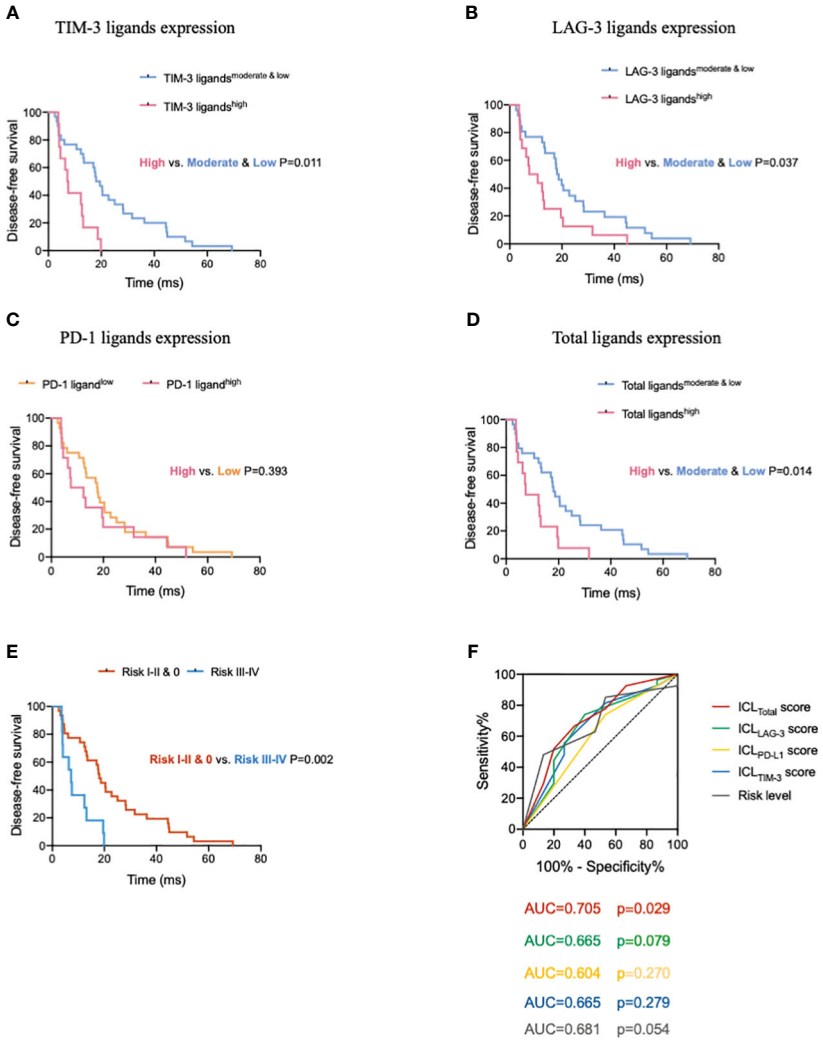

FIGURE 6
High expression of immune checkpoint ligands on mature HEVs predicts poor survival in patients with tumors. Comparison of DFS for patients with different **(A)** TIM-3, **(B)** LAG-3, **(C)** PD-1, and **(D)** total ligand expression levels. **(E)** Comparison of DFS of patients with different risk levels. **(F)** The ROC curve between DFS and the immune checkpoint ligands scores as well as the risk levels. HEVs, high endothelial venules. DFS, disease-free survival. ROC, receiver operating characteristic. Data are presented as means ± SD.

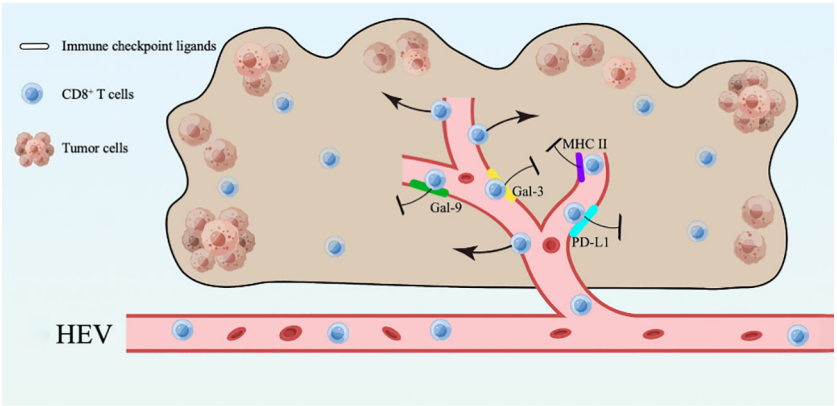

FIGURE 7
An overview of the present study.

entry into the TLSs, which has not been previously reported. Regardless of the ligand expression at the exact checkpoint or the total ligand expression, we observed that lower TLS-infiltrating $CD8^+$ T cell percentages were associated with higher ligand expression, the differences were statistically significant. Additionally, not every ligand was involved in the $CD8^+$ T cell delivery to TLSs; only Gal-9, MHC II, GAL-3, and PD-L1 negatively regulated $CD8^+$ T cell entry into tumors, which also demonstrates the complicated functions of ICLs. Additionally, from the results of survival analysis, we found that DFS was shorter for patients with high ICL expression on HEVs, whereas patients with low expression of these ligands had significantly better DFS. Until now, this is the first study to reveal an association between the expression of ICLs in HEVs and survival. Thus, the value of the ICLs expressed in HEVs was determined.

To quantify the influence of ICL expression on TLS-infiltrating $CD8^+$ T cells and survival, we constructed an ICL score model and performed ROC curve analysis. The AUC of each ICL score was measured, we identified the cut-off value of "1", where an ICL_{total} score greater than "1" predicts weak $CD8^+$ T cell infiltration ($P < 0.001$). Moreover, another cutoff ICL_{total} score was calculated: an ICL_{total} score greater than "2" indicates shorter survival ($P = 0.029$). Based on the ROC curves and their cutoff values, we consider that the ICL_{total} score will help clinicians predict the ICB treatment response and partly predict the DFS of patients.

The present study has several limitations. Only three ICLs were investigated; other immune checkpoints such as TIGIT and CTLA-4 were not considered. Accordingly, further investigations are needed that include ligands of other immune checkpoints. Our study provides preliminary evidence supporting the importance of ICLs expressed on HEVs. Moreover, only 42 patients were recruited; relevant large-scale clinical research is ongoing.

In summary, our study highlights the importance of ICLs in mature HEVs. Mature HEVs (not blood vessels or lymphatics) can positively affect the infiltration of $CD8^+$ T subsets. Additionally, the ICLs expression on mature HEVs may negatively regulate the delivery of $CD8^+$ T population to TLSs. Besides, according to our ICL_{total} score model, the expression of ICLs on HEVs can predict patients' survival, where a high ICL_{total} score predicts a poor prognosis.

Data availability statement

The raw data supporting the conclusions of this article will be made available by the authors, without undue reservation.

Ethics statement

The studies involving humans were approved by Human Investigation Committee of Tianjin Medical University Cancer Institute and Hospital. The studies were conducted in accordance with the local legislation and institutional requirements. Written informed consent for participation in this study was provided by the participants' legal guardians/next of kin.

Author contributions

XR: Project administration, Writing – review & editing. HZ: Supervision, Writing – review & editing. FW: Supervision, Writing – review & editing. JL: Formal analysis, Methodology, Writing – original draft. XS: Methodology, Writing – original draft. YL: Writing – original draft. JW: Writing – original draft. XY: Writing – original draft. HW: Writing – original draft. QS: Writing – original draft. ZH: Writing – original draft.

Funding

The author(s) declare financial support was received for the research, authorship, and/or publication of this article. This study is funded by National Natural Science Foundation of China (82372779, 82303196, 82373279, 82373283, 82302913, U20A20375), Haihe Laboratory of Cell Ecosystem Innovation Fund (22HHXBSS00004) and Tianjin Key Medical Discipline (Specialty) Construction Project (TJYXZDXK-009A).

Conflict of interest

The authors declare that the research was conducted in the absence of any commercial or financial relationships that could be construed as a potential conflict of interest.

Publisher's note

Supplementary material

The Supplementary Material for this article can be found online at: https://www.frontiersin.org/articles/10.3389/fimmu.2024.1302761/full#supplementary-material

References

1. Zhang Y, Zhang Z. The history and advances in cancer immunotherapy: understanding the characteristics of tumor-infiltrating immune cells and their therapeutic implications. *Cell Mol Immunol* (2020) 17(8):807–21. doi: 10.1038/s41423-020-0488-6

2. Dall'Olio FG, Marabelle A, Caramella C, Garcia C, Aldea M, Chaput N, et al. Tumour burden and efficacy of immune-checkpoint inhibitors. *Nat Rev Clin Oncol* (2022) 19(2):75–90. doi: 10.1038/s41571-021-00564-3

3. Lentz RW, Colton MD, Mitra SS, Messersmith WA. Innate immune checkpoint inhibitors: The next breakthrough in medical oncology? *Mol Cancer Ther* (2021) 20 (6):961–74. doi: 10.1158/1535-7163.MCT-21-0041

4. Asrir A, Tardiveau C, Coudert J, Laffont R, Blanchard L, Bellard E, et al. Tumor-associated high endothelial venules mediate lymphocyte entry into tumors and predict response to PD-1 plus CTLA-4 combination immunotherapy. *Cancer Cell* (2022) 40 (3):318–34. doi: 10.1016/j.ccell.2022.01.002

5. Wang S, Sun J, Chen K, Ma P, Lei Q, Xing S, et al. Perspectives of tumor-infiltrating lymphocyte treatment in solid tumors. *BMC Med* (2021) 19(1):140. doi: 10.1186/s12916-021-02006-4

6. Li B. Why do tumor-infiltrating lymphocytes have variable efficacy in the treatment of solid tumors? *Front Immunol* (2022) 13:973881. doi: 10.3389/fimmu.2022.973881

7. Chen DS, Mellman I. Oncology meets immunology: the cancer-immunity cycle. *Immunity* (2013) 39(1):1–10. doi: 10.1016/j.immuni.2013.07.012

8. Ribas A, Wolchok JD. Cancer immunotherapy using checkpoint blockade. *Science* (2018) 359(6382):1350–5. doi: 10.1126/science.aar4060

9. Sharma P, Siddiqui BA, Anandhan S, Yadav SS, Subudhi SK, Gao J, et al. The next decade of immune checkpoint therapy. . *Cancer Discovery* (2021) 11(4):838–57. doi: 10.1158/2159-8290.CD-20-1680

10. Li M, Zhang M, Ye Q, Liu Y, Qian W. Preclinical and clinical trials of oncolytic vaccinia virus in cancer immunotherapy: A comprehensive review. *Cancer Biol Med* (2023) 20(9):646–61. doi: 10.20892/j.issn.2095-3941.2023.0202

11. Tumeh PC, Harview CL, Yearley JH, Shintaku IP, Taylor EJ, Robert L, et al. PD-1 blockade induces responses by inhibiting adaptive immune resistance. *Nature* (2014) 515(7528):568–71. doi: 10.1038/nature13954

12. Paijens ST, Vledder A, de Bruyn M, Nijman HW. Tumor-infiltrating lymphocytes in the immunotherapy era. *Cell Mol Immunol* (2021) 18(4):842–59. doi: 10.1038/s41423-020-00565-9

13. Dangaj D, Bruand M, Grimm AJ, Ronet C, Barras D, Duttagupta PA, et al. Cooperation between constitutive and inducible chemokines enables T cell engraftment and immune attack in solid tumors. *Cancer Cell* (2019) 35(6):885–900:e10. doi: 10.1016/j.ccell.2019.05.004

14. Harlin H, Meng Y, Peterson AC, Zha Y, Tretiakova M, Slingluff C, et al. Chemokine expression in melanoma metastases associated with CD8+ T-cell recruitment. *Cancer Res* (2009) 69(7):3077–85. doi: 10.1158/0008-5472.CAN-08-2281

15. Mikucki ME, Fisher DT, Matsuzaki J, Skitzki JJ, Gaulin NB, Muhitch JB, et al. Non-redundant requirement for CXCR3 signalling during tumoricidal T-cell trafficking across tumour vascular checkpoints. *Nat Commun* (2015) 6:7458. doi: 10.1038/ncomms8458

16. Peng D, Kryczek I, Nagarsheth N, Zhao L, Wei S, Wang W, et al. Epigenetic silencing of TH1-type chemokines shapes tumour immunity and immunotherapy. *Nature* (2015) 527(7577):249–53. doi: 10.1038/nature15520

17. Moussion C, Girard JP. Dendritic cells control lymphocyte entry to lymph nodes through high endothelial venules. *Nature* (2011) 479(7374):542–6. doi: 10.1038/nature10540

18. Girard JP, Moussion C, Forster R. HEVs, lymphatics and homeostatic immune cell trafficking in lymph nodes. *Nat Rev Immunol* (2012) 12(11):762–73. doi: 10.1038/nri3298

19. Blanchard L, Girard JP. High endothelial venules (HEVs) in immunity, inflammation and cancer. *Angiogenesis* (2021) 24(4):719–53. doi: 10.1007/s10456-021-09792-8

20. Jones E, Gallimore A, Ager A. Defining high endothelial venules and tertiary lymphoid structures in cancer. *Methods Mol Biol* (2018) 1845:99–118. doi: 10.1007/978-1-4939-8709-2_7

21. Sautes-Fridman C, Petitprez F, Calderaro J, Fridman WH. Tertiary lymphoid structures in the era of cancer immunotherapy. *Nat Rev Cancer* (2019) 19(6):307–25. doi: 10.1038/s41568-019-0144-6

22. Dieu-Nosjean MC, Giraldo NA, Kaplon H, Germain C, Fridman WH, Sautes-Fridman C. Tertiary lymphoid structures, drivers of the anti-tumor responses in human cancers. *Immunol Rev* (2016) 271(1):260–75. doi: 10.1111/imr.12405

23. Colbeck EJ, Ager A, Gallimore A, Jones GW. Tertiary lymphoid structures in cancer: Drivers of antitumor immunity, immunosuppression, or bystander sentinels in disease? *Front Immunol* (2017) 8:1830. doi: 10.3389/fimmu.2017.01830

24. Zhao H, Wang H, Zhao Y, Sun Q, Ren X. Tumor-resident T cells, associated with tertiary lymphoid structure maturity, improve survival in patients with stage III lung Adenocarcinoma. *Front Immunol* (2022) 13:877689. doi: 10.3389/fimmu.2022.877689

25. Wang T, Zhang J, Li N, Li M, Ma S, Tan S, et al. Spatial distribution and functional analysis define the action pathway of Tim-3/Tim-3 ligands in tumor development. *Mol Ther* (2022) 30(3):1135–48. doi: 10.1016/j.ymthe.2021.11.015

26. Angelova M, Mlecnik B, Vasaturo A, Bindea G, Fredriksen T, Lafontaine L, et al. Evolution of metastases in space and time under immune selection. *Cell* (2018) 175 (3):751–65:e16. doi: 10.1016/j.cell.2018.09.018

27. Wang PC, Hu ZQ, Zhou SL, Yu SY, Mao L, Su S, et al. The spatial distribution of immune cell subpopulations in hepatocellular carcinoma. *Cancer Sci* (2022) 113 (2):423–31. doi: 10.1111/cas.15202

28. Rancan C, Arias-Badia M, Dogra P, Chen B, Aran D, Yang H, et al. Exhausted intratumoral Vdelta2(-) gammadelta T cells in human kidney cancer retain effector function. *Nat Immunol* (2023) 24(4):612–24. doi: 10.1038/s41590-023-01448-7

29. Carstens JL, Correa de Sampaio P, Yang D, Barua S, Wang H, Rao A, et al. Spatial computation of intratumoral T cells correlates with survival of patients with pancreatic cancer. *Nat Commun* (2017) 8:15095. doi: 10.1038/ncomms15095

30. Maruhashi T, Sugiura D, Okazaki IM, Okazaki T. LAG-3: from molecular functions to clinical applications. *J Immunother Cancer* (2020) 8(2). doi: 10.1136/jitc-2020-001014

31. Zhang Y, Zheng J. Functions of immune checkpoint molecules beyond immune evasion. *Adv Exp Med Biol* (2020) 1248:201–26. doi: 10.1007/978-981-15-3266-5_9

32. Li B, Chan HL, Chen P. Immune checkpoint inhibitors: Basics and challenges. *Curr Med Chem* (2019) 26(17):3009–25. doi: 10.2174/0929867324666170804143706

33. Zhang T, Lin Y, Gao Q. Bispecific antibodies targeting immunomodulatory checkpoints for cancer therapy. *Cancer Biol Med* (2023) 20(3):181–95. doi: 10.20892/j.issn.2095-3941.2023.0002

34. Lee HJ, Lee JE, Jeong WG, Ki SY, Park MH, Lee JS, et al. HER2-positive breast cancer: Association of MRI and clinicopathologic features with tumor-infiltrating lymphocytes. *AJR Am J Roentgenol* (2022) 218(2):258–69. doi: 10.2214/AJR.21.26400

35. Azimi F, Scolyer RA, Rumcheva P, Moncrieff M, Murali R, McCarthy SW, et al. Tumor-infiltrating lymphocyte grade is an independent predictor of sentinel lymph node status and survival in patients with cutaneous melanoma. *J Clin Oncol* (2012) 30 (21):2678–83. doi: 10.1200/JCO.2011.37.8539

36. Moon J, Oh YM, Ha SJ. Perspectives on immune checkpoint ligands: expression, regulation, and clinical implications. *BMB Rep* (2021) 54(8):403–12. doi: 10.5483/BMBRep.2021.54.8.054

37. He X, Xu C. Immune checkpoint signaling and cancer immunotherapy. *Cell Res* (2020) 30(8):660–9. doi: 10.1038/s41422-020-0343-4

38. Turley SJ, Cremasco V, Astarita JL. Immunological hallmarks of stromal cells in the tumour microenvironment. *Nat Rev Immunol* (2015) 15(11):669–82. doi: 10.1038/nri3902

39. Guo W, Zhou M, Qiu J, Lin Y, Chen X, Huang S, et al. Association of LAG3 genetic variation with an increased risk of PD in Chinese female population. *J Neuroinflamm* (2019) 16(1):270. doi: 10.1186/s12974-019-1654-6

40. Lashuel HA, Overk CR, Oueslati A, Masliah E. The many faces of alpha-synuclein: From structure and toxicity to therapeutic target. *Nat Rev Neurosci* (2013) 14 (1):38–48. doi: 10.1038/nrn3406

41. Xiao Y, Yu S, Zhu B, Bedoret D, Bu X, Francisco LM, et al. RGMb is a novel binding partner for PD-L2 and its engagement with PD-L2 promotes respiratory tolerance. *J Exp Med* (2014) 211(5):943–59. doi: 10.1084/jem.20130790

42. Solinas C, Aiello M, Rozali E, Lambertini M, Willard-Gallo K, Migliori E. Programmed cell death-ligand 2: A neglected but important target in the immune response to cancer? *Transl Oncol* (2020) 13(10):100811. doi: 10.1016/j.tranon.2020.100811

frontiers | Frontiers in Immunology

TYPE Original Research
PUBLISHED 01 March 2024
DOI 10.3389/fimmu.2024.1302903

OPEN ACCESS

EDITED BY
Hui Zhao,
University of Texas MD Anderson Cancer Center, United States

REVIEWED BY
Yongkun Wei,
University of Texas MD Anderson Cancer Center, United States
Hao Li,
Wuhan University, China

*CORRESPONDENCE
Xiubao Ren
renxiubao@tjmuch.com
Hua Zhao
huazhao@tmu.edu.cn

†These authors have contributed equally to this work

RECEIVED 27 September 2023
ACCEPTED 07 February 2024
PUBLISHED 01 March 2024

CITATION
Feng H, Zhang S, Zhou Q, Han F, Du G, Wang L, Yang X, Zhang X, Yu W, Wei F, Hao X, Ren X and Zhao H (2024) Intratumor tertiary lymphatic structure evaluation predicts the prognosis and immunotherapy response of patients with colorectal cancer.
Front. Immunol. 15:1302903.
doi: 10.3389/fimmu.2024.1302903

Intratumor tertiary lymphatic structure evaluation predicts the prognosis and immunotherapy response of patients with colorectal cancer

Huijing Feng[1†], Siyuan Zhang[2,3,4,5,6†], Qiuru Zhou[2,3,4,5,6,7], Fei Han[8], Gang Du[9], Lin Wang[10], Xuena Yang[2,3,4,5,6], Xiying Zhang[2,3,4,5,6], Wenwen Yu[2,3,4,5,6], Feng Wei[2,3,4,5,6,11], Xishan Hao[2,3,4,5,11], Xiubao Ren[2,3,4,5,6,11,12*] and Hua Zhao[2,3,4,5,6,11*]

[1]Department of Thoracic Oncology, Cancer Center, Shanxi Bethune Hospital, Shanxi Academy of Medical Sciences, Tongji Shanxi Hospital, Third Hospital of Shanxi Medical University, Taiyuan, Shanxi, China, [2]National Clinical Research Center for Cancer, Tianjin, China, [3]Key Laboratory of Cancer Prevention and Therapy, Tianjin, China, [4]Tianjin's Clinical Research Center for Cancer, Tianjin, China, [5]Key Laboratory of Cancer Immunology and Biotherapy, Tianjin, China, [6]Department of Immunology, Tianjin Medical University Cancer Institute and Hospital, Tianjin, China, [7]Wenzhou Central Hospital, Wenzhou, Zhejiang, China, [8]Department of head and neck surgery, Shanxi Province Cancer Hospital/Shanxi Hospital Affiliated to Cancer Hospital, Chinese Academy of Medical Sciences/ Cancer Hospital Affiliated to Shanxi Medical University, Taiyuan, Shanxi, China, [9]Department of Pathology, Shanxi Bethune Hospital, Taiyuan, Shanxi, China, [10]General Surgery Department, Shanxi Bethune Hospital, Taiyuan, Shanxi, China, [11]Haihe Laboratory of Cell Ecosystem, Tianjin, China, [12]Department of Biotherapy, Tianjin Medical University Cancer Institute and Hospital, Tianjin, China

Background: Immune checkpoint therapy, involving the programmed cell death 1 (PD-1) monoclonal antibody, has revolutionized the treatment of cancer. Tertiary lymphatic structure (TLS) serves as an immune indicator to predict the efficacy of PD-1 antibody therapy. However, there is no clear result whether the distribution, quantity, and maturity of TLS can be effective indicators for predicting the clinical efficacy of anti-PD1 immunotherapy in patients with colorectal cancer (CRC).

Methods: Fifty-seven patients who underwent surgical resection and thirty-nine patients who received anti-PD-1 immunotherapy were enrolled in this retrospective study. Immunohistochemical staining and multiple fluorescence immunohistochemistry were used to evaluate the mismatch repair (MMR) subtypes and TLS distribution, quantity, and maturity, respectively.

Results: A comprehensive patient score system was built based on TLS quantity and maturity. We found that the proportion of patients with score >1 was much higher in the deficient mismatch repair(dMMR) group than in the proficient mismatch repair(pMMR) group, and this difference was mainly due to intratumoral TLS. Patient score, based on the TLS evaluation of whole tumor, peritumor, or intratumor, was used to evaluate the efficacy of anti-PD1 immunotherapy. Based only on the intratumor TLS evaluation, the proportion of patients with a score >1 was higher in the response (PR + CR) group than in the non-response (PD) group. Multivariate analysis revealed that patient scores were positively correlated with the clinical efficacy of immunotherapy. Further analysis

of immune-related progression-free survival was performed in patients with CRC who received anti-PD-1 immunotherapy. Patients with score >1 based on the intratumor TLS evaluation had significantly better survival.

Conclusions: These results suggest that the patient score based on intratumor TLS evaluation may be a good immune predictive indicator for PD-1 antibody therapy in patients with CRC.

KEYWORDS

TLS, CRC, dMMR, pMMR, anti-PD1 immunotherapy

1 Introduction

Colorectal cancer (CRC) is a malignant tumor of the colon or rectum that is characterized by poor prognosis and high metastasis (1). According to global cancer statistics, CRC ranked third and second in terms of cancer incidence and mortality, respectively, in 2020 (2). Early CRC can be treated with radical surgical resection; however, surgery and adjuvant chemotherapy are not ideal for the treatment of advanced CRC (1). In recent years, novel immune checkpoint inhibitors (ICIs) have emerged as key therapeutics for patients with metastatic CRC with mismatch repair-deficient (dMMR) and -proficient (pMMR) subtypes according to MMR gene status (3). Although programmed cell death 1 (PD-1) inhibitors have been approved as the first-line treatment for advanced CRC with dMMR as a predictive biomarker for PD-1 ICIs, less than half of the patients with dMMR CRC respond favorably to anti-PD-1 therapy (3). Therefore, exploring the much accurate immune predictive indicators for PD-1 antibody therapy is necessary to guide treatment more accurately in patients with CRC with different MMR subtypes.

Tertiary lymphoid structures (TLSs), also known as ectopic lymphoid organs, develop in non-lymphoid tissues at sites of chronic inflammation, including tumors (4). Tumor-infiltrating lymphocytes, which may originate from the aggregation of ectopic immune cells at the tumor site, have drawn considerable interest because they play an important role in improving anti-tumor immunity (5, 6). Increasing evidence indicates that the presence and maturity of TLSs are correlated with tumor prognosis and can serve as novel prognostic biomarkers (7–10). Furthermore, TLSs can predict the responses to anti-PD-1 immunotherapy and might be a target of PD-1 blockade in several tumors including esophageal carcinoma, bladder cancer, melanoma and head and neck squamous cell carcinoma (HNSCC) (7–9, 11). It has also been demonstrated that high PD-1 expression in the invasive margin of patients was significantly associated with the presence of TLSs, which implies that targeting PD-1 in the immune context might be more effective (12). A recent study in mouse models of spontaneous multi-organ metastasis in MSI-H CRC tumors showed that ICIs of anti-PD-1 treatment significantly reduced the growth of primary tumors and liver metastases, and therapy efficacy correlated with the formation of TLSs in ICI-responding tumors. However, the utility of TLSs as predictive biomarkers for anti-PD-1 treatment of CRC remains unclear (13).

Efficacy of tumor immunotherapy is closely related to the MMR genotype. Greco et al. reported that patients with dMMR CRC have higher objective response rates and longer progression-free survival (PFS) after receiving immunotherapy than patients with pMMR (14). A recent study reported that patients with dMMR bladder cancer with increased tumor-resident memory T cells (T_{RM}) infiltration contributing to TLS formation had improved response rates to neoadjuvant chemotherapy (15). However, the relationship between MMR status and TLS remain unclear.

In this study, we aimed to assess the correlation between MMR status and TLSs in CRC and explore TLSs as predictive biomarkers for anti-PD-1 immunotherapy to facilitate more personalized treatment of patients with CRC with different MMR subtypes.

2 Materials and methods

2.1 Patients and tumor specimens

Fifty-seven patients with CRC who underwent surgical resection between 2016 and 2019 at the Tianjin Medical University Cancer Hospital were enrolled in this retrospective study. Pathological TNM staging was based on the 8th edition of the Union for International Cancer Control TNM classification. Formalin-fixed paraffin-embedded tumor tissue samples of these patients were collected for subsequent multiple immunofluorescence staining, in which 19 patients were dMMR positively expressing mismatch repair proteins, such as MLH1, PMS2, MSH2, and MSH6, and the 38 patients had pMMR-matched basic clinicopathological features with the former. None of the patients had received any therapy before surgery. Thirty-nine patients, comprising 10 dMMR patients and 29 pMMR patients, who received anti-PD1 immunotherapy between 2015 and 2021 at the Shanxi Provincial Cancer Hospital were enrolled in this study. None of the 39 patients ever underwent surgery or other treatments before pathological puncture biopsy.

Specimens from all patients were approved by the Ethics Committee of the Tianjin Medical University Cancer Institute and Hospital (Ek2020214) and the Shanxi Provincial Cancer Hospital (SBQLL-2022-028).

2.2 Multiple immunofluorescence staining and TLS quantification and scoring

A PerkinElmer Opal 7-color Technology Kit (NEL81001KT) was used to conduct immunofluorescence staining according to the manufacturer's protocol. Antibodies against CD20 (1:800, ab9475, Abcam), CD21 (1:800, ab75985, Abcam), CK (1:800, ab215838, Abcam), BCL-6 (1:100, NBP3-07540, NOVUS), and GP2(1:400, D277-3, MBL) were used. Then, 4',6-diamidino-2-phenylindole was used to stain the nuclei after completing all the staining cycles. An Automated Quantitative Pathology Imaging System (Vectra Polaris) was used to scan and visualize the stained slides, and the inForm image analysis software (v2.4.4; PerkinElmer) was used for quantification and scoring.

The method of evaluating TLS quantity and maturity was as follow:

Firstly, according to HE staining results, wax blocks with both normal and tumor tissues were selected to slice. Secondly, mIHC was performed to determinate the number and maturity of TLS.

We collected all TLSs of every tumor section and randomly collected three to five fields from areas outside the TLSs. The early TLS (Grade 1 TLS) was characterized by dense lymphocytic aggregates without CD21 and Bcl-6 expression; primary follicle-like TLS(Grade 2 TLS) was characterized by lymphocytic clusters with central network CD21 expression, but no GC reaction (Bcl-6-); and secondary follicle-like TLS (Grade 3 TLS) was characterized by lymphocytic clusters with GC reaction (CD20+Bcl-6+).

2.3 Statistical analyses

Statistical analyses were performed using SPSS 23.0 and GraphPad Prism (v.9.0). Shapiro Wilktest was used to test the normality of continuous variables, and the data normal distributing was described by mean ± standard deviation; data not subject to normal distribution was described by median and quartile. Comparisons of unpaired numerical variables between the two groups were assessed using Student's *t*-test or Mann–Whitney test. X2 tests or Fisher's exact test were used for comparisons between groups. Statistical significance was set at P value <0.05. When comparing the prognostic differences between the two subgroups after combining TLS quantity and maturity, P value and HR ratio were calculated using the log-rank test in GraphPad Prism software.

3 Results

3.1 Associations between CRC MMR state and TLS quantity and maturity

To explore the TLS difference between dMMR and pMMR, 96 mIHC staining samples of patients with CRC were analyzed (Table 1). TLS with $CD20^{+}CD21^{-}BCL6^{-}$ was defined as grade 1,

TABLE 1 Baseline characteristics of patients (n=96).

		dMMR, n=28 (%)	pMMR, n=68 (%)	*P* value
Age				0.385
	<65	24 (86.0)	53 (78.0)	
	≥65	4 (14.0)	15 (22.0)	
Gender				0.095
	Male	20 (71.0)	36 (53.0)	
	Female	8 (29.0)	32 (47.0)	
Tumor location				0.202
	Right hemicolon	18 (64.0)	34 (50.0)	
	Left hemicolon	10 (36.0)	34 (50.0)	
T stage				0.394
	T1+T2	2 (8.0)	9 (15.0)	
	T3+T4	23 (92.0)	52 (85.0)	
N stage				0.777
	N0	15 (60.0)	34 (57.0)	
	N1+N2	10 (40.0)	26 (43.0)	

(Continued)

TABLE 1 Continued

		dMMR, n=28 (%)	pMMR, n=68 (%)	*P* value
TNM stage				0.855
	I	2 (7.0)	7 (10.0)	
	II	12 (44.0)	24 (36.0)	
	III	10 (37.0)	26 (39.0)	
	IV	3 (12.0)	10 (15.0)	

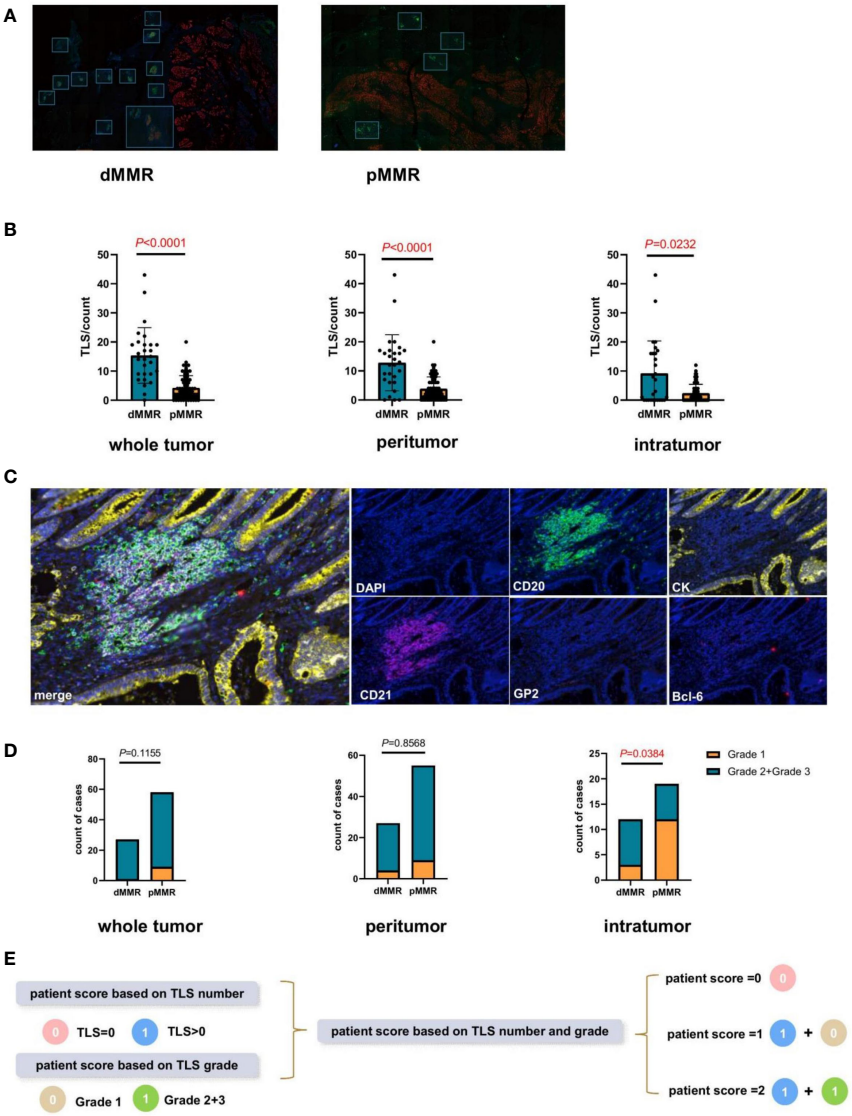

FIGURE 1
Comparison of the tertiary lymphatic structure (TLS) quantity and maturity between patients with dMMR and pMMR CRC (n=96). **(A)** Representative images of TLS number of dMMR and pMMR patient samples (magnification, ×100). The slide was stained with CK, CD21 (red), CD20 (green), Bcl-6 (red), GP2 (orange), and 4′,6-diamidino-2-phenylindole (DAPI; blue). **(B)** Comparison of TLS number between dMMR and pMMR patients in three levels: whole tumor ($P<0.0001$), peritumor ($P<0.0001$), and intratumor ($P<0.0001$) levels. **(C)** Representative images of TLS maturity (magnification, ×100). The slide was stained with GP2 (orange), CD21 (purple), CD20 (green), CK (yellow), Bcl-6 (pink), and DAPI (blue). Grade1-TLS, both CD21 and Bcl-6 markers were negative and GP2 was negative. Grade2-TLS, CD21 was positive and Bcl-6 and GP2 were negative. Grade3-TLS, both CD21 and Bcl-6 markers were positive and GP2 was negative. **(D)** Comparison of the patient proportion between dMMR and pMMR patients based on the TLS grade in the whole tumor ($P=0.1155$), peritumor ($P=0.8568$), and intratumor ($P<0.05$) groups, respectively. **(E)** Establishment of the new patient score system integrating TLS quantity and maturity grade.

10.3389/fimmu.2024.1302903

TLS with $CD20^+CD21^+BCL6^-$ was defined as grade 2, and TLS with $CD20^+CD21^+BCL6^+$ was defined as grade 3 (16). In addition, the $GP2^+$ lymphoid tissue represented a payer patch that was excluded, and CK was used to differentiate the intratumoral and peritumoral regions (Figure 1C). We found that, regardless of the level of intratumor, peritumor, or whole sample, TLS quantity was higher in dMMR than in pMMR (P<0.0001, P<0.0001, P<0.0001; Figures 1A, B), while TLS maturity was higher in dMMR than in pMMR only at the intratumor level (P<0,05; Figures 1C, D).

Therefore, a comprehensive patient scoring system was built based on the TLS quantity and maturity. Scores based on the TLS number were defined as 0 (TLS number=0) or 1(TLS number >0). The score based on TLS maturity was defined as 0 (TLS grade 1) or 1 (TLS grade 2 or 3). Based on the sum of these two scores, the patient scores were calculated and divided into 0, 1, and 2 (Figure 1E).

3.2 Comparison of patient score differences between dMMR and pMMR patients

The proportions of patients with different scores based on the peritumor, intratumor, and whole tumor microenvironment were analyzed separately. Based on the whole tumor, the proportion of patients with a score >1 in the dMMR group was much higher than that in the pMMR group (P=0.0459; Figure 2A). Continuing the analysis, we found that this difference was mainly due to intratumoral TLS, but not peritumoral TLS (P=0.0459, P=0.1510; Figures 2B, C).

In addition, we compared the proportion of peritumor and intratumor patient scores between the dMMR and pMMR groups. In both the dMMR and pMMR groups, the proportion of patients with a score >1 based on the intratumor was much lower than that in the peritumor group (P=0.004, P<0.0001; Figures 2D, E). Since the proportion of patients scoring >1 based on intratumor TLS was very similar to the previously reported clinical response rate (17), it indicated that the patient score based on intratumor TLS might be an effective indicator in anti-PD1 immunotherapy.

3.3 Association between the anti-PD-1 response and patient score

In the present study, 39 patients with CRC received anti-PD-1 immunotherapy were enrolled to further validate the predictive role of the TLS score in the efficacy of PD-1 inhibitor therapy (Table 2). The patients were divided into two groups according to their therapeutic responses. Patients with a partial response (PR) and complete response (CR) were assigned to the response group, and those with progressive disease (PD) were assigned to the non-responsive group. The results showed that based on the intratumor TLS score, the proportion of patients with a score >1 in the PR+CR group was much higher than that in the PD group (P<0.0001;

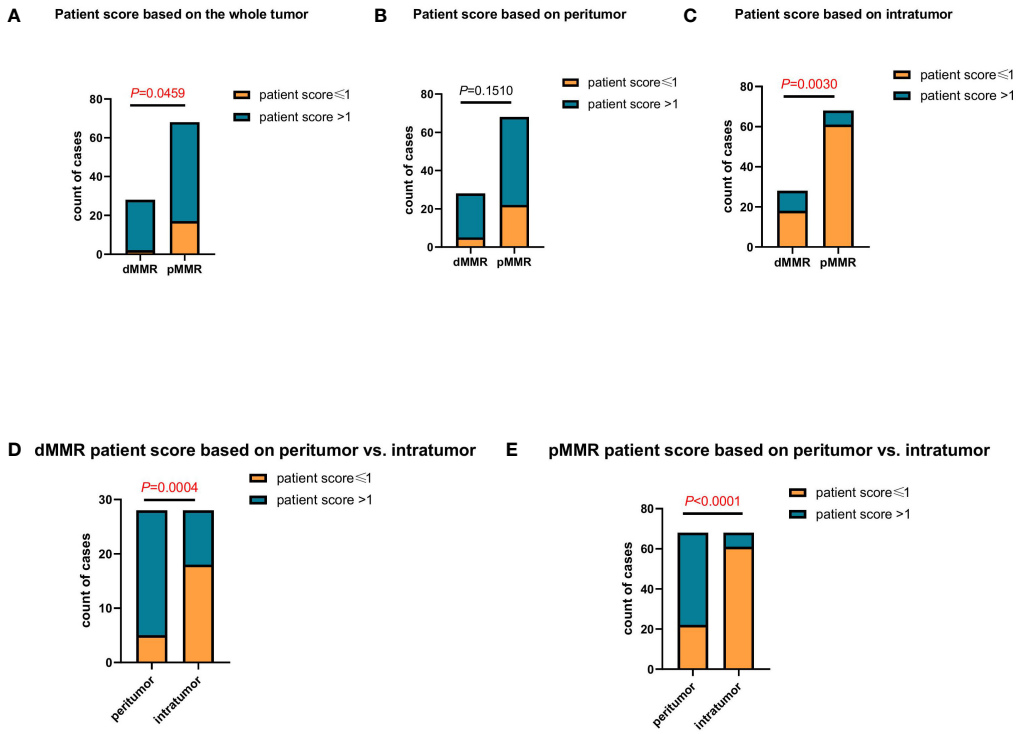

FIGURE 2
Comparing the differences in patient scores between patients with dMMR and pMMR CRC (n=96). **(A–C)** Comparison of patient score between patients with dMMR and pMMR CRC at the whole tumor (P<0.05) **(A)**, peritumor (P=0.1510) **(B)**, and intratumor (P<0.005) **(C)** levels. **(D, E)** Comparison of patient score at the peritumor and intratumor levels between patients with dMMR (P<0.005) **(D)** and pMMR (P<0.0001) **(E)** CRC, respectively.

10.3389/fimmu.2024.1302903

TABLE 2 Baseline characteristics of patients (n=39).

		dMMR, n=10 (%)	pMMR, n=29 (%)	*P* value
Age				0.086
	<65	10 (100.0)	22 (76.0)	
	≥65	0 (0.0)	7 (24.0)	
Gender				0.164
	Male	8 (80.0)	16 (55.0)	
	Female	2 (20.0)	13 (45.0)	
Tumor location				0.105
	Right hemicolon	6 (60.0)	9 (31.0)	
	Left hemicolon	4 (40.0)	20 (69.0)	
T stage				P>0.9999
	T1+T2	0 (0.0)	0 (0.0)	
	T3+T4	7 (100.0)	22 (100.0)	
N stage				0.483
	N0	3 (43.0)	6 (29.0)	
	N1+N2	4 (57.0)	15 (71.0)	
TNM stage				0.429
	II	2 (22.0)	3 (11.0)	
	III	4 (44.0)	15 (54.0)	
	IV	3 (33.0)	10 (35.0)	
In combination with chemotherapy				
	yes	4 (40%)	23 (79%)	0.0202
	no	6 (60%)	6 (21%)	

Figure 3A). Furthermore, we continued to evaluate the treatment response in patients with dMMR and pMMR based on TLS scores, and the data showed similar results to those of all patients. Based only on the intratumor TLS score, the proportion of patients with a score >1 was higher in the response group than in the non-response group (P=0.0384, P=0.0001; Figures 3B, C).

Multiple clinical, pathological, and immune characteristics were investigated to evaluate their impact on the clinical response to anti-PD1 immunotherapy. The results revealed that Patient scores were positively correlated with clinical efficacy in the 39 patients and pMMR group (P=0.004, P=0.012, Tables 3, 4). Multivariate analysis was not performed in the dMMR group because of the small number of enrolled patients.

3.4 Predictive role of patient score in determining the immune-related PFS in anti-PD1 therapy

To further investigate the patient score on clinical efficacy prediction, survival analysis of irPFS and multivariate Cox regression analyses of clinical and immune characteristics in different patient score group was done, which verified that the irPFS of patients score>1 was longer than that of patients score ≤ 1 in pMMR group (P=0.0004; Figure 4A; Table 5). The irPFS in dMMR group did not show any difference, which may have been due to its small sample size (n=10, Figure 4A). Survival analysis of OS was also done, which verified that the OS of patients score>1 was longer than that of patients score ≤ 1 in pMMR group but not the whole 39 patients and dMMR group (P=0.0030, P=0.0576 and P=0.7760, respectively, Figure 4B). In addition, receiver operating characteristic (ROC) curve analysis was performed in pMMR patients, revealing that the patient score had good predictive ability for the clinical efficacy of PD1 treatment (AUC=0.815; Figure 4C). All the results indicated that the patient score based on the intratumor microenvironment can be used as a predictive factor for anti-PD1 immunotherapy in patients with CRC.

4 Discussion

In this study, we first evaluated the associations between MMR typing and TLS distribution, quantity, and maturity, clinical features, and prognosis of 96 patients with stage I–IV CRC.

10.3389/fimmu.2024.1302903

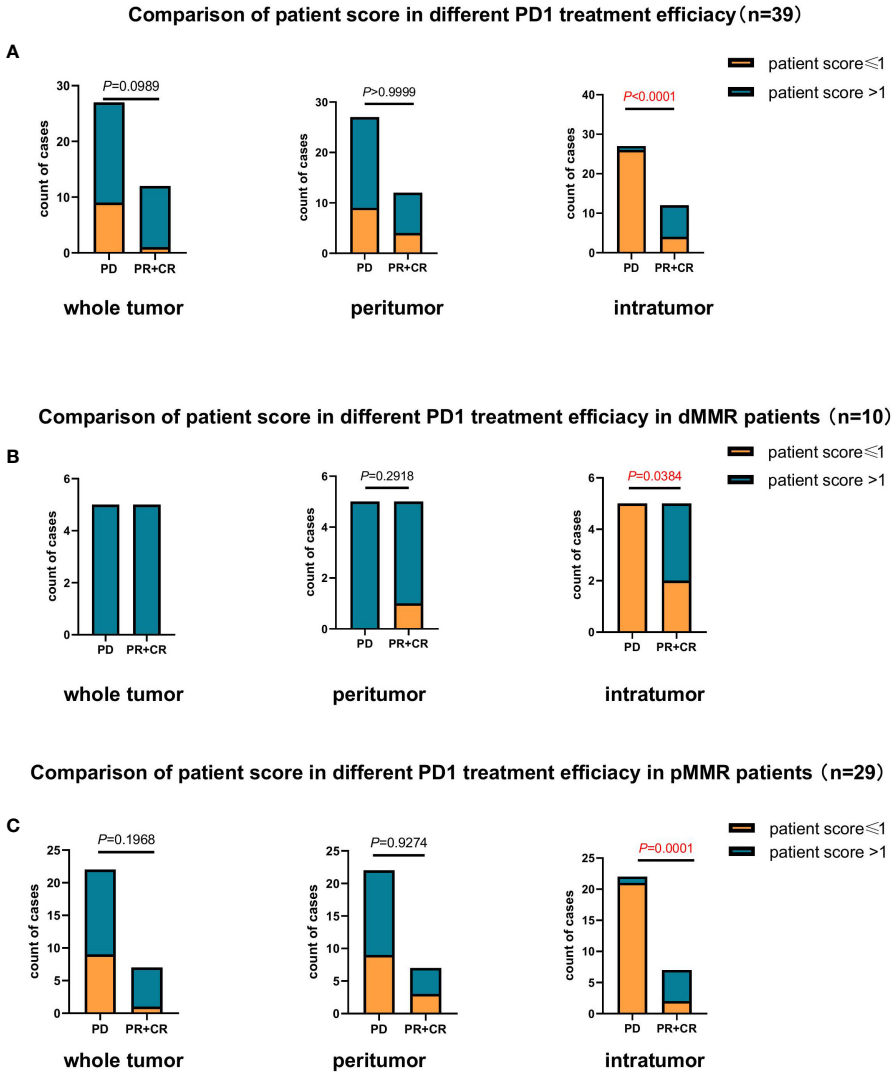

FIGURE 3
Comparison of the association between patient scores based on TLS quantity and maturity and response to anti-PD1 therapy (n=39). **(A)** Comparison of the association between patient score and response to anti-PD1 therapy in patients with CRC (n=39) at the whole tumor (P=0.0989), peritumor (P>0.9999), and intratumor (P<0.0001) levels. **(B)** Comparison of the association between patient score and response to anti-PD1 therapy in patients with dMMR CRC (n=10) at the whole tumor, peritumor (P=0.2918) and intratumor (P<0.05) levels. **(C)** Comparison of the association between patient score and response to anti-PD1 therapy in patients with pMMR CRC (n=29) at the whole tumor (P=0.1968), peritumor (P=0.9274), and intratumor (P=0.0001) levels.

TABLE 3 Multivariate clinical pathological characteristics and immune characteristics affecting response of anti-PD1 immunotherapy in 39 pMMR patients.

	B	S.E.	Wald	df	Sig.	Exp (B)	95% C.I.for EXP (B)	
							Lower	Upper
TLS score	5.153	1.799	8.207	1	0.004	172.872	5.091	5869.952
Gender	2.269	1.586	2.048	1	0.152	9.669	0.432	216.298
Age	2.521	1.921	1.722	1	0.189	12.447	0.288	537.535
Location	1.294	1.384	0.874	1	0.35	3.646	0.242	54.931
Therapy	-0.967	1.536	0.396	1	0.529	0.38	0.019	7.728
TNM stage	-0.105	0.794	0.017	1	0.895	0.901	0.19	4.273
dMMR/pMMR	-1.413	1.432	0.974	1	0.324	0.244	0.015	4.028

10.3389/fimmu.2024.1302903

TABLE 4 Multivariate clinical pathological characteristics and immune characteristics affecting response of anti-PD1 immunotherapy in 29 pMMR patients.

	B	S.E.	Wald	df	Sig.	Exp (B)	95% C.I.for EXP (B)	
							Lower	Upper
TLS score	4.259	1.690	6.351	1	0.012	70.741	2.577	1941.971
Gender	0.930	1.609	0.334	1	0.563	2.535	0.108	59.393
Age	1.405	1.831	0.589	1	0.443	4.076	0.113	147.406
Location	-0.494	1.743	0.080	1	0.777	0.610	0.020	18.599
Therapy	-0.167	2.173	0.006	1	0.939	0.846	0.012	59.832
TNM stage	-0.506	1.035	0.239	1	0.625	0.603	0.079	4.585

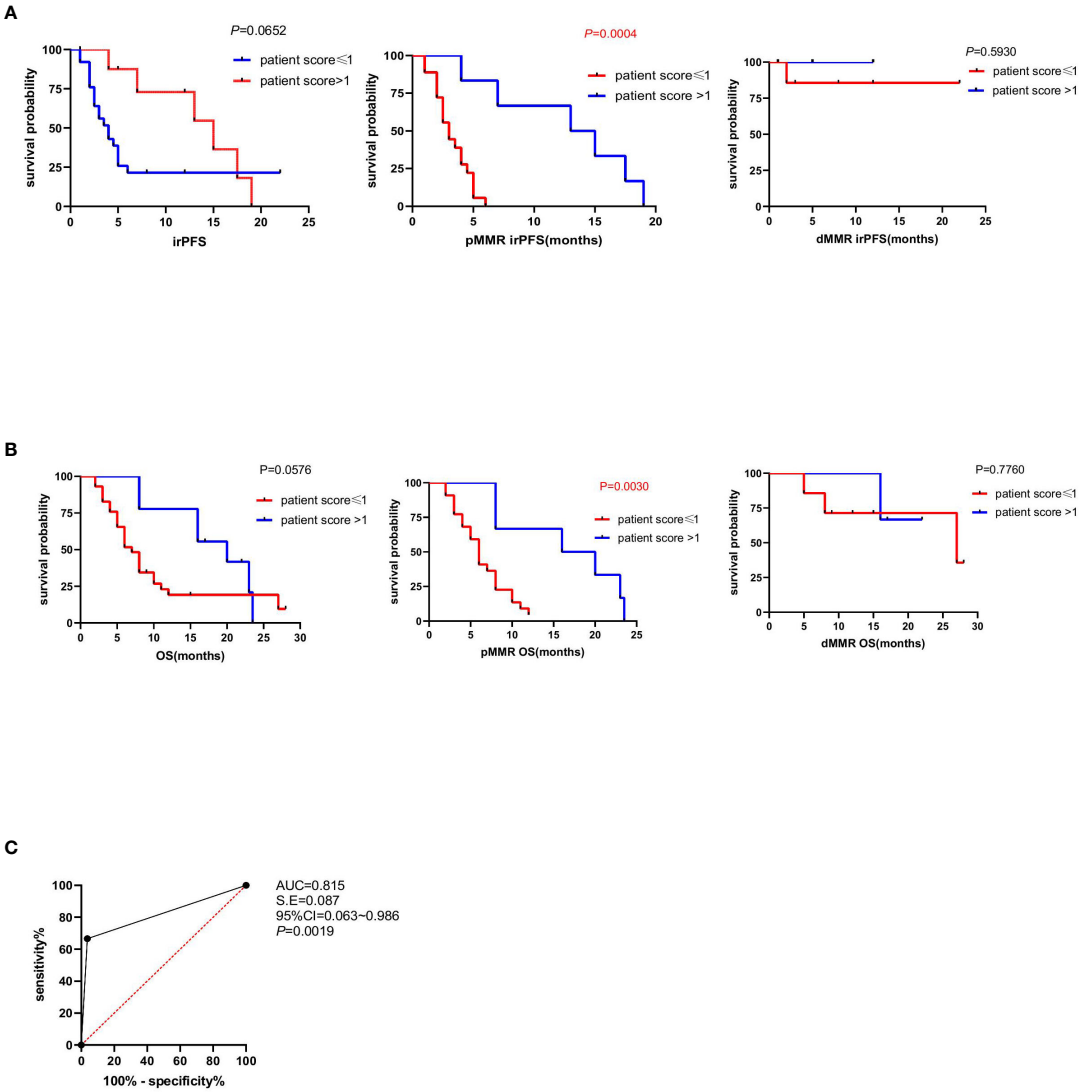

FIGURE 4
Association between patient score and immune-related progression-free survival (irPFS and OS). **(A)** Kaplan–Meier survival curves showing irPFS according to patient score of all the 39 patients, pMMR patients and dMMR patients (P=0.0652, P=0.0004, P=0.5930). P values were calculated by the log-rank test. **(B)** Kaplan–Meier survival curves showing OS according to patient score of all the 39 patients, pMMR patients and dMMR patients. P values were calculated by the log-rank test (P=0.0576, P=0.0030, P=0.7760). **(C)** The ROC curve to evaluate the predictive ability of patient score on anti-PD1 immunotherapy clinical responses (AUC=0.815).

TABLE 5 Multivariate Cox regression analyses of clinical and immune characteristics affecting irPFS of anti-PD1 immunotherapy in 29 pMMR patients.

	B	SE	Wald	df	Sig.	Exp (B)	95.0% CI for Exp (B)	
							Lower	Upper
TLS score	-3.337	1.171	8.127	1	0.004	0.036	0.004	0.352
Gender	-0.198	0.448	0.194	1	0.660	0.821	0.341	1.976
Age	-0.253	0.576	0.193	1	0.660	0.776	0.251	2.400
Location	-0.361	0.575	0.393	1	0.530	0.697	0.226	2.152
Therapy	-1.368	0.729	3.517	1	0.061	0.255	0.061	1.064
TNM stage	0.133	0.375	0.126	1	0.723	1.142	0.548	2.381

In the analysis of TLS quantity difference of the whole tumor, peritumor, or intratumor microenvironment between patients with dMMR and pMMR CRC, the results showed that the number of TLS was much higher in dMMR than in pMMR patients, which was consistent with the results of a study on the immunomicroenvironment characteristics of urachal carcinoma (UrC). They found that the number of TLS tended to be higher in UrC tumor with dMMR (P=0.1919), as well the patients with higher TLS numbers tended to result in a much better prognosis (18). TLS maturity analysis revealed no differences in the whole tumor or peritumor between the dMMR and pMMR groups. In the intratumor-TLS analysis, the proportion of patients with grade 2 +grade 3 pMMR was lower than that of patients with dMMR. The maturity of intratumoral TLS was higher in patients with dMMR than in those with pMMR. This is consistent with the findings of CRC and lung squamous cell carcinoma, in which patients from germinal centers (GCs) had a better prognosis (19, 20). These results further indicated that B cell maturity and humoral immunity play key roles in anti-tumor immune responses (16).

Based on the contribution of TLS quantity and maturity to the anti-tumor response, we used a patient scoring system (PS) to predict the clinical response of patients with CRC to PD-1 antibodies immunotherapy. Using this new score, we analyzed the relationship between TLS and MMR subtype and the results showed both in dMMR and pMMR patients, the proportion of patients score >1 based on intratumor was much lower than that peritumor. Moreover, in either the dMMR group or the pMMR group, the proportion of patients scoring >1 based on intratumoral TLS was similar to the clinical response rate that has been reported (17), and whether the patient score based on intratumoral TLS could be an effective indicator of anti-PD1 immunotherapy.

In this study, we analyzed the correlation between patient scores and clinical responses in 39 patients receiving anti-PD-1 immunotherapy and found that the proportion of patients with intratumoral TLS patient scores > 1 was much higher in the response (PR + CR) group than in the non-responders groups. Similar results were observed in 29 pMMR and 10 dMMR patients. These results suggest that the distribution of TLS affects the efficacy of immunotherapy. Previous studies defined the peritumoral TLS of breast cancer as a range within 5 mm from the invasive edge and divided it into adjacent and distal TLS according to the distance and interval between the normal breast tissue and the invasive edge. The higher the peritumoral TLS (distal TLS) density, the lower is the disease-free survival (DFS), independent of overall survival (OS), and the higher the distal TLS density, the lower is the DFS and OS (21). This is consistent with the results of the present study; however, no similar studies have been reported in CRC to date.

Further analysis of irPFS was performed in 39 patients with CRC who received anti-PD-1 immunotherapy. We found that patients with score > 1 based on the intratumor TLS evaluation had much better survival among the 29 patients with pMMR. Although the same trend was observed in the dMMR group, statistical results are not available because of the small number of cases. The specimens of the 39 patients receiving anti-PD-1 treatment were collected before immunotherapy and the sample size was limited, which might lead to a potential bias. In future research, we will collect more specimens and conduct prospective studies to verify the authenticity and accuracy of the conclusions. In conclusion, our findings indicate the patient score based on intratumor TLS evaluation as a good immune predictive indicator for the efficacy of PD-1 antibody therapy in patients with CRC.

Data availability statement

The original contributions presented in the study are included in the article/supplementary material. Further inquiries can be directed to the corresponding authors.

Ethics statement

The studies involving humans were approved by the Ethics Committee of the Tianjin Medical University Cancer Institute and Hospital and the Ethics Committee of Shanxi Provincial Cancer Hospital. The studies were conducted in accordance with the local legislation and institutional requirements. The human samples used in this study were acquired from primarily isolated as part of your previous study for which ethical approval was obtained. Written

informed consent for participation from the participants or the participants' legal guardians/next of kin was not mentioned in accordance with the national legislation and institutional requirements.

Author contributions

HF: Formal analysis, Methodology, Writing – original draft. SZ: Formal analysis, Methodology, Writing – original draft. QZ: Writing – review & editing. FH: Writing – review & editing. GD: Writing – review & editing. LW: Writing – review & editing. XY: Writing – review & editing. XZ: Writing – review & editing. WY: Writing – review & editing. FW: Writing – review & editing. XH: Writing – review & editing. XR: Project administration, Writing – review & editing. HZ: Project administration, Writing – review & editing.

Funding

The author(s) declare financial support was received for the research, authorship, and/or publication of this article. This study is funded by National Natural Science Foundation of China (82372779, U20A20375), Haihe Laboratory of Cell Ecosystem Innovation Fund (22HHXBSS00004), Tianjin Key Medical Discipline (Specialty) Construction Project (TJYXZDXK-009A), and Shanxi Province "136 Revitalization Medical Project Construction Funds".

Acknowledgments

We sincerely appreciate our colleagues in the Department of Pathology for their help with tumor section preparation.

Conflict of interest

The authors declare that the research was conducted in the absence of any commercial or financial relationships that could be construed as a potential conflict of interest.

Publisher's note

References

1. Dekker E, Tanis PJ, Vleugels JLA, Kasi PM, Wallace MB. Colorectal cancer. *Lancet*. (2019) 394:1467–80. doi: 10.1016/S0140-6736(19)32319-0

2. Sung H, Ferlay J, Siegel RL, Laversanne M, Soerjomataram I, Jemal A, et al. Global cancer statistics 2020: GLOBOCAN estimates of incidence and mortality worldwide for 36 cancers in 185 countries. *CA Cancer J Clin*. (2021) 71:209–49. doi: 10.3322/caac.21660

3. Li J, Wu C, Hu H, Qin G, Wu X, Bai F, et al. Remodeling of the immune and stromal cell compartment by PD-1 blockade in mismatch repair-deficient colorectal cancer. *Cancer Cell*. (2023) 41:1152–69.e7. doi: 10.1016/j.ccell.2023.04.011

4. Sautès-Fridman C, Petitprez F, Calderaro J, Fridman WH. Tertiary lymphoid structures in the era of cancer immunotherapy. *Nat Rev Cancer*. (2019) 19:307–25. doi: 10.1038/s41568-019-0144-6

5. Wang J, Jiang D, Zheng X, Li W, Zhao T, Wang D, et al. Tertiary lymphoid structure and decreased $CD8^+$ T cell infiltration in minimally invasive adenocarcinoma. *iScience*. (2022) 25:103883. doi: 10.1016/j.isci.2022.103883

6. Tokunaga R, Naseem M, Lo JH, Battaglin F, Soni S, Puccini A, et al. B cell and B cell-related pathways for novel cancer treatments. *Cancer Treat Rev*. (2019) 73:10–9. doi: 10.1016/j.ctrv.2018.12.001

7. Hayashi Y, Makino T, Sato E, Ohshima K, Nogi Y, Kanemura T, et al. Density and maturity of peritumoral tertiary lymphoid structures in oesophageal squamous cell carcinoma predicts patient survival and response to immune checkpoint inhibitors. *Br J Cancer*. (2023) 128:2175–85. doi: 10.1038/s41416-023-02235-9

8. Zhou L, Xu B, Liu Y, Wang Z. Tertiary lymphoid structure signatures are associated with survival and immunotherapy response in muscle-invasive bladder cancer. *Oncoimmunology*. (2021) 10:915574. doi: 10.1080/2162402X.2021.1915574

9. Cabrita R, Lauss M, Sanna A, Donia M, Skaarup Larsen M, Mitra S, et al. Tertiary lymphoid structures improve immunotherapy and survival in melanoma. *Nature*. (2020) 577:561–5. doi: 10.1038/s41586-019-1914-8

10. Zhan Z, Shi-jin L, Yi-Ran Z, Zhi-Long L, Xiao-Xu Z, Hui D, et al. High endothelial venules proportion in tertiary lymphoid structure is a prognostic marker and correlated with anti-tumor immune microenvironment in colorectal cancer. *Ann Med*. (2023) 55:114–26. doi: 10.1080/07853890.2022.2153911

11. Li H, Zhu SW, Zhou JJ, Chen DR, Liu J, Wu ZZ, et al. Tertiary lymphoid structure raises survival and immunotherapy in HPV- HNSCC. *J Dent Res*. (2023) 102:678–88. doi: 10.1177/00220345231151685

12. Mokhtari Z, Rezaei M, Sanei MH, Dehghanian A, Faghih Z, Heidari Z, et al. Tim3 and PD-1 as therapeutic and prognostic targets in colorectal cancer: Relationship with sidedness, clinicopathological parameters, and survival. *Front Oncol*. (2023) 13:1069696. doi: 10.3389/fonc.2023.1069696

13. Küçükköse E, Heesters BA, Villaudy J, Verheem A, Cercel M, van Hal S, et al. Modeling resistance of colorectal peritoneal metastases to immune checkpoint blockade in humanized mice. *J Immunother Cancer*. (2022) 10:e005345. doi: 10.1136/jitc-2022-005345

14. Greco L, Rubbino F, Dal Buono A, Laghi L. Microsatellite instability and immune response: From microenvironment features to therapeutic actionability-lessons from colorectal cancer. *Genes (Basel)*. (2023) 14:1169. doi: 10.3390/genes14061169

15. Jin K, Yu Y, Zeng H, Liu Z, You R, Zhang H, et al. $CD103^+CD8^+$ tissue-resident memory T cell infiltration predicts clinical outcome and adjuvant therapeutic benefit in muscle-invasive bladder cancer. *Br J Cancer*. (2022) 126:1581–8. doi: 10.1038/s41416-022-01725-6

16. Zhao H, Wang H, Zhao Y, Sun Q, Ren X. Tumor-resident T cells associated with tertiary lymphoid structure maturity, improve survival in patients with Stage III lung adenocarcinoma. *Front Immunol*. (2022) 13:877689. doi: 10.3389/fimmu.2022.877689

17. Chalabi M, Fanchi LF, Dijkstra KK, Van den Berg JG, Aalbers AG, Sikorska K, et al. Neoadjuvant immunotherapy leads to pathological responses in MMR-proficient and MMR-deficient early-stage colon cancers. *Nat Med*. (2020) 26:566–76. doi: 10.1038/s41591-020-0805-8

18. Zhang X, Wang S, Nie RC, Qu C, Chen J, Yang Y, et al. Immune microenvironment characteristics of urachal carcinoma and its implications for prognosis and immunotherapy. *Cancers (Basel)*. (2022) 14:615. doi: 10.3390/cancers14030615

19. Posch F, Silina K, Leibl S, Mündlein A, Moch H, Siebenhüner A, et al. Maturation of tertiary lymphoid structures and recurrence of Stage II and III colorectal cancer. *Oncoimmunology*. (2018) 7:e1378844. doi: 10.1080/2162402X.2017.1378844

20. Siliņa K, Soltermann A, Attar FM, Casanova R, Uckeley ZM, Thut H, et al. Germinal centers determine the prognostic relevance of tertiary lymphoid structures and are impaired by corticosteroids in lung squamous cell carcinoma. *Cancer Res*. (2018) 78:1308–20. doi: 10.1158/0008-5472.CAN-17-1987

21. Zhao Z, Ding H, Lin ZB, Qiu SH, Zhang YR, Guo YG, et al. Relationship between tertiary lymphoid structure and the prognosis and clinicopathologic characteristics in solid tumors. *Int J Med Sci*. (2021) 18:2327–38. doi: 10.7150/ijms.56347

frontiers | Frontiers in Immunology

TYPE Correction
PUBLISHED 14 June 2024
DOI 10.3389/fimmu.2024.1397764

OPEN ACCESS

APPROVED BY
Frontiers in Editorial Office,
Frontiers Media SA, Switzerland

*CORRESPONDENCE
Xiubao Ren
renxiubao@tjmuch.com
Hua Zhao
huazhao@tmu.edu.cn

†These authors have contributed equally to this work

RECEIVED 08 March 2024
ACCEPTED 31 May 2024
PUBLISHED 14 June 2024

CITATION
Feng H, Zhang S, Zhou Q, Han F, Du G, Wang L, Yang X, Zhang X, Yu W, Wei F, Hao X, Ren X and Zhao H (2024) Corrigendum: Intratumor tertiary lymphatic structure evaluation predicts the prognosis and immunotherapy response of patients with colorectal cancer.
Front. Immunol. 15:1397764.
doi: 10.3389/fimmu.2024.1397764

Corrigendum: Intratumor tertiary lymphatic structure evaluation predicts the prognosis and immunotherapy response of patients with colorectal cancer

Huijing Feng[1†], Siyuan Zhang[2,3,4,5,6†], Qiuru Zhou[2,3,4,5,6,7], Fei Han[8], Gang Du[9], Lin Wang[10], Xuena Yang[2,3,4,5,6], Xiying Zhang[2,3,4,5,6], Wenwen Yu[2,3,4,5,6], Feng Wei[2,3,4,5,6,11], Xishan Hao[2,3,4,5,11], Xiubao Ren[2,3,4,5,6,11,12*] and Hua Zhao[2,3,4,5,6,11*]

[1]Department of Thoracic Oncology, Cancer Center, Shanxi Bethune Hospital, Shanxi Academy of Medical Sciences, Tongji Shanxi Hospital, Third Hospital of Shanxi Medical University, Taiyuan, Shanxi, China, [2]National Clinical Research Center for Cancer, Tianjin, China, [3]Key Laboratory of Cancer Prevention and Therapy, Tianjin, China, [4]Tianjin's Clinical Research Center for Cancer, Tianjin, China, [5]Key Laboratory of Cancer Immunology and Biotherapy, Tianjin, China, [6]Department of Immunology, Tianjin Medical University Cancer Institute and Hospital, Tianjin, China, [7]Wenzhou Central Hospital, Wenzhou, Zhejiang, China, [8]Department of head and neck surgery, Shanxi Province Cancer Hospital/Shanxi Hospital Affiliated to Cancer Hospital, Chinese Academy of Medical Sciences/ Cancer Hospital Affiliated to Shanxi Medical University, Taiyuan, Shanxi, China, [9]Department of Pathology, Shanxi Bethune Hospital, Taiyuan, Shanxi, China, [10]General Surgery Department, Shanxi Bethune Hospital, Taiyuan, Shanxi, China, [11]Haihe Laboratory of Cell Ecosystem, Tianjin, China, [12]Department of Biotherapy, Tianjin Medical University Cancer Institute and Hospital, Tianjin, China

KEYWORDS

TLS, CRC, dMMR, PMMR, anti-PD1 immunotherapy

A Corrigendum on:

Intratumor tertiary lymphatic structure evaluation predicts the prognosis and immunotherapy response of patients with colorectal cancer

By Feng H, Zhang S, Zhou Q, Han F, Du G, Wang L, Yang X, Zhang X, Yu W, Wei F, Hao X, Ren X and Zhao H (2024) *Front. Immunol.* 15:1302903. doi: 10.3389/fimmu.2024.1302903

In the published article, there was an error in affiliation(s) 2, 3, 4, 5, 6, 7, 8, 9, 10, 11, 12, 13. Instead of "[2]Tianjin Medical University Cancer Institute and Hospital, Tianjin China, [3]National Clinical Research Center for Cancer, Tianjin, China, [4]Key Laboratory of Cancer Prevention and Therapy, Tianjin China, [5]Tianjin's Clinical Research Center for Cancer, Tianjin China, [6]Key Laboratory of Cancer Immunology and Biotherapy, Tianjin, China, [7]Department of Immunology, Tianjin Medical University Cancer Institute and Hospital, Tianjin, China, [8]Wenzhou Central Hospital, Wenzhou, Zhejiang, China, [9]Department of Head and Neck Surgery, Shanxi Province Cancer Hospital/ Shanxi Hospital Affiliated to Cancer Hospital, Chinese Academy of Medical Sciences/Cancer Hospital Affiliated to Shanxi Medical University, Taiyuan, Shanxi, China, [10]Department of Pathology, Shanxi Bethune Hospital, Taiyuan, Shanxi, China, [11]General Surgery Department, Shanxi Bethune Hospital, Taiyuan, Shanxi, China, [12]Haihe Laboratory of Cell Ecosystem, Tianjin, China,

[13]Department of Biotherapy, Tianjin Medical University Cancer Institute and Hospital, Tianjin, China.", it should be:" [2]National Clinical Research Center for Cancer, Tianjin, China, [3]Key Laboratory of Cancer Prevention and Therapy, Tianjin, China, [4]Tianjin's Clinical Research Center for Cancer, Tianjin, China, [5]Key Laboratory of Cancer Immunology and Biotherapy, Tianjin, China, [6]Department of Immunology, Tianjin Medical University Cancer Institute and Hospital, Tianjin, China, [7]Wenzhou Central Hospital, Wenzhou, Zhejiang, China, [8]Department of head and neck surgery, Shanxi Province Cancer Hospital/Shanxi Hospital Affiliated to Cancer Hospital, Chinese Academy of Medical Sciences/Cancer Hospital Affiliated to Shanxi Medical University, Taiyuan, Shanxi, China, [9]Department of Pathology, Shanxi Bethune Hospital, Taiyuan, Shanxi, China, [10]General Surgery Department, Shanxi Bethune Hospital, Taiyuan, Shanxi, China, [11]Haihe Laboratory of Cell Ecosystem, Tianjin, China, [12]Department of Biotherapy, Tianjin Medical University Cancer Institute and Hospital, Tianjin, China.".

The authors apologize for this error and state that this does not change the scientific conclusions of the article in any way. The original article has been updated.

In the published article, there was an error regarding the affiliation(s) for Siyuan Zhang, Qiuru Zhou, Fei Han, Gang Du, Lin Wang, Xuena Yang, Xiying Zhang, Wenwen Yu, Feng Wei, Xishan Hao, Xiubao Ren and Hua Zhao.

Instead of Siyuan Zhang[2,3,4,5,6,7†], Qiuru Zhou[2,3,4,5,6,7,8], Fei Han[9], Gang Du[10], Lin Wang[11], Xuena Yang[7], Xiying Zhang[7], Wenwen Yu[7], Feng Wei[7,12], Xishan Hao[12], Xiubao Ren[7,12,13*] and Hua Zhao[7,12*], it should be: Siyuan Zhang[2,3,4,5,6†], Qiuru Zhou[2,3,4,5,6,7], Fei Han[8], Gang Du[9], Lin Wang[10], Xuena Yang[2,3,4,5,6], Xiying Zhang[2,3,4,5,6], Wenwen Yu[2,3,4,5,6], Feng Wei[2,3,4,5,6,11], Xishan Hao[2,3,4,5,11], Xiubao Ren[2,3,4,5,6,11,12*] and Hua Zhao[2,3,4,5,6,11*]

Publisher's note

frontiers | Frontiers in Oncology

TYPE Original Research
PUBLISHED 23 May 2024
DOI 10.3389/fonc.2024.1383096

OPEN ACCESS

EDITED BY
Ying Ma,
Tianjin Medical University Cancer Institute and Hospital, China

REVIEWED BY
Alessandro Poggi,
San Martino Hospital (IRCCS), Italy
Satya Ranjan Dash,
KIIT University, India
Aditya Yashwant Sarode,
Columbia University, United States

*CORRESPONDENCE
Weidong Wang
wangweidong1@scszlyy.org.cn

RECEIVED 12 February 2024
ACCEPTED 06 May 2024
PUBLISHED 23 May 2024

CITATION
Xu Z, Wang Q, Zhang Y, Li X, Wang M, Zhang Y, Pei Y, Li K, Yang M, Luo L, Wu C and Wang W (2024) Exploiting tertiary lymphoid structures gene signature to evaluate tumor microenvironment infiltration and immunotherapy response in colorectal cancer. *Front. Oncol.* 14:1383096. doi: 10.3389/fonc.2024.1383096

Exploiting tertiary lymphoid structures gene signature to evaluate tumor microenvironment infiltration and immunotherapy response in colorectal cancer

Zhu Xu[1,2], Qin Wang[3], Yiyao Zhang[2,4], Xiaolan Li[3], Mei Wang[2,4], Yuhong Zhang[1,2], Yaxin Pei[2,4], Kezhen Li[1], Man Yang[4], Liping Luo[2,4], Chuan Wu[2,4] and Weidong Wang[1,2]*

[1]Department of Oncology, School of Clinical Medicine, Southwest Medical University, Luzhou, China, [2]Department of Radiation Oncology, Sichuan Clinical Research Center for Cancer, Sichuan Cancer Hospital & Institute, Sichuan Cancer Center, Affiliated Cancer Hospital of University of Electronic Science and Technology of China, Chengdu, China, [3]Department of Pathology, QuXian People's Hospital, Dazhou, China, [4]School of Medicine, University of Electronic Science and Technology of China, Chengdu, China

Background: Tertiary lymphoid structures (TLS) is a particular component of tumor microenvironment (TME). However, its biological mechanisms in colorectal cancer (CRC) have not yet been understood. We desired to reveal the TLS gene signature in CRC and evaluate its role in prognosis and immunotherapy response.

Methods: The data was sourced from The Cancer Genome Atlas (TCGA) and the Gene Expression Omnibus (GEO) databases. Based on TLS-related genes (TRGs), the TLS related subclusters were identified through unsupervised clustering. The TME between subclusters were evaluated by CIBERSORT and xCell. Subsequently, developing a risk model and conducting external validation. Integrating risk score and clinical characteristics to create a comprehensive nomogram. Further analyses were conducted to screen TLS-related hub genes and explore the relationship between hub genes, TME, and biological processes, using random forest analysis, enrichment and variation analysis, and competing endogenous RNA (ceRNA) network analysis. Multiple immunofluorescence (mIF) and immunohistochemistry (IHC) were employed to characterize the existence of TLS and the expression of hub gene.

Results: Two subclusters that enriched or depleted in TLS were identified. The two subclusters had distinct prognoses, clinical characteristics, and tumor immune infiltration. We established a TLS-related prognostic risk model including 14 genes and validated its predictive power in two external datasets. The model's AUC values for 1-, 3-, and 5-year overall survival (OS) were 0.704, 0.737, and 0.746. The low-risk group had a superior survival rate, more abundant infiltration of immune cells, lower tumor immune dysfunction and exclusion (TIDE) score, and exhibited better immunotherapy efficacy. In addition, we selected the top important features within the model: *VSIG4*, *SELL* and *PRRX1*.

Enrichment analysis showed that the hub genes significantly affected signaling pathways related to TLS and tumor progression. The ceRNA network: *PRRX1*-miRNA (*hsa-miR-20a-5p*, *hsa-miR-485–5p*) -lncRNA has been discovered. Finally, IHC and mIF results confirmed that the expression level of *PRRX1* was markedly elevated in the TLS- CRC group.

Conclusion: We conducted a study to thoroughly describe TLS gene signature in CRC. The TLS-related risk model was applicable for prognostic prediction and assessment of immunotherapy efficacy. The TLS-hub gene *PRRX1*, which had the potential to function as an immunomodulatory factor of TLS, could be a therapeutic target for CRC.

KEYWORDS

tertiary lymphoid structures, colorectal cancer, tumor microenvironment, prognostic, immunotherapy

1 Introduction

CRC is among one of the most prevalent cancers worldwide. Recent surveys have shown that CRC accounted for 10% of new cancer cases and deaths globally (1, 2). Notwithstanding progress in surgical techniques, chemotherapy, and radiation therapy, a substantial number of patients experience recurrence or metastasis. Immunotherapy has opened new avenue for treatment, particularly for patients with specific genetic mutations like deficient mismatch repair (dMMR) and microsatellite instability-high (MSI-H). Clinical trials, including KEYNOTE-164, CheckMate 142 and others, have shown that the use of programmed cell death protein-1 (PD-1) blockade therapy leads to long-lasting response, especially in advanced-stage patients with MSI-H (3–5). However, immunotherapy is not universally effective; it benefits only a subset of patients and can cause unique side effects, such as autoimmune reactions. The effectiveness of immunotherapy largely depends on the TME and genetic profiles. According to reports, TLS was positively correlated with the expression of immune-related genes in CRC, such as programmed cell death ligand-1 (PD-L1) (6). This suggests that TLS may enhance the effectiveness of immune checkpoint blockade (ICB) therapies by promoting the infiltration of immune cells and remodeling TME.

TLS, also referred to ectopic lymphoid organizations (ELO), serves as a site for immune cells recruitment, activation, and proliferation (7–9). TLS resemble lymph nodes to some extent but with unique features. For example, TLS lack capsules and afferent lymphatic vessels, which distinguishes them from traditional lymph nodes. TLS contains structured zones of immune cells, such as the T cell zone and the B cell germinal center (GC) (10). In summary, TLS is comprised of immune cells, stromal cells, and specialized vascular components (11, 12). TLS has a vital function in local immune responses. Research on TLS is currently flourishing in the fields of cancer, chronic inflammation, and autoimmune diseases (13).

Accumulating evidences suggest that TLS generally associated with favorable prognosis and better immunotherapy efficacy in melanoma, breast cancer and so on (11, 14–16). Patients with TLS tend to have improved OS rates compared to those lacking TLS. TLS can convert an immune cold tumor to a hot tumor by increasing the recognition and clearance of the host immune system to tumors (17). In addition, the latest study found that combining immunotherapies with strategies to promote TLS formation or reorganization may enhance the effectiveness of immunotherapy. Strategies may include using specific cytokines or chemokines to recruit immune cells to TLS.

Despite progress, there remains an incomplete understanding of the precise molecular mechanisms governing TLS growth and maturity. There are still doubts about the interactions between TLS and the tumor immune system. Therefore, our study integrated TRGs and downloaded data from TCGA database to classify patients into two subclusters and develop a novel prognostic model. We also investigated the connection between TLS-hub genes and its molecular mechanisms.

2 Materials and methods

2.1 Data collection and preparation

The data, including gene sequencing data and corresponding clinical data, were obtained from the TCGA and GEO databases. TCGA-CRC dataset functioned as a discovery set for marker selection and model construction, consisting of 558 samples. Samples with survival times under 30 days were removed. GEO datasets GSE38832 and GSE17537 served as external validation sets

to assess the robustness of the model. IMvigor210 immunotherapy cohort was obtained from the original article (18). Clinical information for all samples were detailed in Supplementary Table 1.

2.2 Establish TLS-related molecular subclusters and evaluate the TME

The mutation landscapes of CRC patients were analyzed by the "maftool" R package (19). Unsupervised clustering, via the "ConsensusClusterPlus" R package, segmented patients into two subclusters (20). This segmentation was guided by maximizing intergroup variances and minimizing intragroup variances. The immune infiltration environment in each patient was assessed using CIBERSORT and xCell (21, 22). XCell was also utilized to compare the environment scores in different groups.

2.3 Develop the TLS-related risk model, estimate its prognostic value, and develop a comprehensive nomogram

Using the "DESeq2" package, we obtained differentially expressed genes (DEGs) comparing two clusters, tumor and normal. The Lasso-Cox regression was applied to filter out DEGs that are associated with OS, reduce dimensions, and construct the prognostic model. Patients were classified into two risk groups by the risk score, which was calculated as: $Risk\ Score = \sum_{i=1}^{14} Coef_i * Expr_i$ $Coef_i$ denotes the estimated regression coefficient, while $Expr_i$ denotes the gene's expression level. The model's predictive efficiency and accuracy were evaluated via the "survival", "survminer", "timeROC", and "pheatmap" R packages. MSI status was obtained from the "cBioPoralData" R package. According to the results of multivariate Cox regression, we plotted the forest plot and nomogram.

2.4 Identify TLS-related hub genes, analyze its molecular mechanism and enrichment pathways

The 14 model genes were ranked based on the feature importance calculated through "randomForest" package. All feature importance was normalized to range from 0 to 1. Genes with importance exceeding 0.75 were classified as TLS-related hub genes. To comprehensively analyze the biological pathways of TLS-related genes, a dual approach involving gene set enrichment analysis (GSEA) and gene set variation analysis (GSVA) were used. Gene Ontology (GO), Kyoto Encyclopedia of Genes and Genomes (KEGG), and hallmark annotation were conducted with the "clusterProfiler" and "GSVA" packages (23, 24). The visualization of results using the "ggplot2".

2.5 Estimation of TLS existence in human CRC tissue samples

Human CRC tissue samples were collected from QuXian People's Hospital, including 20 TLS+ tissue samples and 10 TLS- tissue samples (initial diagnosis of CRC, denial of other tumors, unaccepting of neoadjuvant therapy and complete clinical data). Clinical information for all samples was detailed in Supplementary Table 3. The research received approval from the Ethics Committee of the QuXian People's Hospital. Two pathologists independently evaluated the TLS existence in all CRC samples. Questionable results were then co-reviewed for an agreed annotation. TLS were classified into three stages based on maturity: (1) early TLS (compact clumps of lymphocytes without segregated T and B cell zones), (2) primary follicle-like TLS [(have follicular dendritic cell (FDC), lack of GC)] and (3) secondary follicle-like TLS (have an active GC) (25). Samples with TLS were categorized as TLS+ group, while others were deemed TLS- group.

2.6 Using mIF to characterize TLS and related hub gene

Firstly, slides were deparaffinized and placed in the citrate-phosphate buffer (heat them in a microwave at low heat for 15 min). Circled the tissue with an immunohistochemical pen to block endogenous peroxidase. Secondly, incubated the slides in hydrogen peroxide water at room temperature and avoid light for 25 min. Added BSA buffer dropwise onto the slides and sealed for 30 min. After removing the BSA buffer, we added the prepared primary antibody (CD3: ab16669, Abcam, Britain, 1:1000) dropwise and incubated the slides overnight at 4 °C in a wet box. Next, the slides were washed, and horseradish peroxidase (HRP) labelled secondary antibody (Goat anti-mouse/rabbit IgG H&L, RCB054, RecordBio, China) were dripped onto the slides. Tyramide signal amplification (TSA) buffer was used to visualize each biomarker. Dripped corresponding TSA dye onto the slides and incubated them at room temperature in the dark for 10 min to stain the antibody. Repeated the previous steps using different primary antibodies (CD20: ab78237, Abcam, 1:1000; CD21: ab315160, Abcam, 1:1000) and switched different TSA dyes. Finally, stained nucleus with DAPI and coverslipped anti-fluorescence quenching to preserve fluorescence. The slides were digitized using OLYMPUS (OlyVIA, Japan).

Next, we performed IHC to examine the *PRRX1* expression level in TLS+/- CRC formalin-fixed paraffin-embedded (FFPE) samples, using *PRRX1* antibody (ab211292, Abcam, 1:100). Tissues were scored according to the product of stained area percentage (0 = 0%, 1 = 1%–25%, 2 = 26%–50%, 3= 51%–75%, and 4 = more than 75%) and the staining intensity scale [ranged from 0 (no staining) to 3 (strong staining), measured by Halo]. The IHC score for all samples was detailed in Supplementary Table 3.

2.7 Statistical analysis

The data analysis was performed using R software version 4.2.2. For categorical data, the Chi-square test and Fisher's exact test were used to assess differences between groups. For continuous data, if the data are normally distributed and have equal variances, an independent samples T-test was used; if the data do not follow a normal distribution, the Mann-Whitney U test was used. Spearman's correlation analysis was used to identify the relationship between two variables. The threshold for statistical significance was set at $P< 0.05$ (two-tailed).

3 Results

3.1 The genetic and variation characteristics of TRGs in CRC

By integrating current studies and reviews, we identified 42 TRGs, of which 25 were expressed in TCGA-CRC dataset (Supplementary Table 2). Among 517 CRC patients, 94.39% (488) experienced somatic mutations. *APC* and *TP53* had the highest mutation frequencies (Figure 1A). We further analyzed the somatic mutation pattern of TRGs (Figure 1B). 11.41% (59) of patients experienced somatic mutations, predominantly missense mutations.*IL1R1* and *IL1R2* exhibited the highest mutation frequencies, while *CD4* and *LAMP3* primarily underwent frame shift deletions. Using STRING (V12.0), a protein-protein interaction (PPI) network was constructed (Figure 1C). GISTIC2.0 was used to calculate the copy number variations (CNV). The results showed that copy number amplification (including homozygous and heterozygous mutations) was the major mutation (Figure 1D).

3.2 Clinicopathological characteristics and immune cell infiltration of TLS related subclusters

Unsupervised consensus clustering based on TRGs categorized CRC patients into two molecular subclusters. The consensus clustering results indicated that the optimal clustering number was 2 (Supplementary Figures 1A–C). Principal component analysis (PCA) proved the optimal division into two clusters, C1 and C2 (Supplementary Figure 1D). The Kaplan-Meier analysis demonstrated a statistically difference in C1 and C2 ($P<0.01$, Figure 2A). The prognosis for C1 was more favorable compared to C2. Meanwhile, we examined the clinicopathological characteristics of two subclusters. C1 had a higher proportion of males, N0, M0, and stage I/II (Supplementary Figures 1D–I).

Next, we analyzed the TRGs expression profiles of two subclusters in the TCGA-CRC dataset (Figure 2B). We found C1 had higher expression levels of *CCL18*, *CCL21*, *CXCL10* and *CXCL11*. C2 was characterized by the remarkable enrichment in *SDC1* and *CCL20*. In general, TRGs were more highly expressed in C1 than C2. Immune infiltrating cells are a crucial component of TME. We explored the differences in TME infiltration between two subclusters. (Figures 2C, D). B cells, CD8+ T cells, follicular helper T (T_{FH}) cells, activated dendritic cells (DC), neutrophils and granulocyte-macrophage progenitor (GMP) cells were higher in C1, while naive CD4+ T cells and natural killer T (NKT) cells were higher in C2. Both macrophage M1 and macrophage M2 had higher infiltration levels in C1. Besides, we further noticed that C1

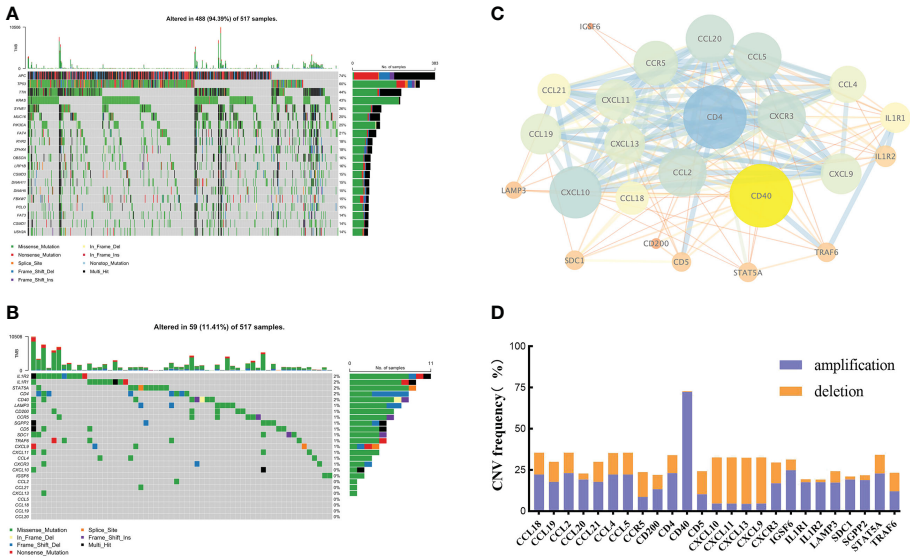

FIGURE 1
The genetic and variation landscapes of TCGA-CRC dataset. **(A)** Somatic mutation of the top 20 genes in CRC. **(B)** Somatic mutation of 25 TRGs. **(C)** PPI network of TRGs. The size and color of the nodes represented the degree of interaction. The edge size and the color showed the combined score of interaction. **(D)** CNV frequency of TRGs.

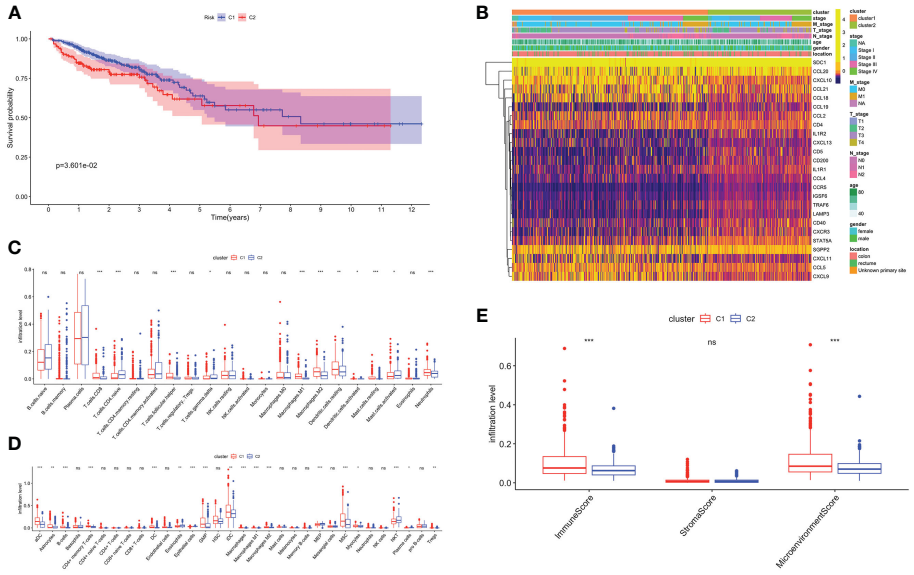

FIGURE 2
Biological characteristics of two TLS related subclusters. **(A)** Kaplan-Meier survival analysis of C1 and C2. **(B)** TRGs expression and clinicopathological characteristics heatmap. Immune cell infiltration patterns by Cibersort **(C)** and xCell **(D)**. **(E)** The immune, stromal and microenvironment scores between two clusters. ns, not significance, *p< 0.05, **p< 0.01, ***p< 0.001.

correlated positively with higher immune and microenvironment scores, while there was no difference between two subclusters in stroma scores (Figure 2E).

3.3 Biological functional enrichment analysis of TLS molecular subclusters

Volcano map was used to demonstrate DEGs between C1 and C2, with 639 genes upregulated in C1 and 86 in C2 (Supplementary Figure 2A). Firstly, we performed over-representation analysis (ORA) to determine the biological behavior behind these DEGs. The GO enrichment analysis revealed that immune receptor activity enrichment in molecular function (MF); plasma membrane signaling receptor complex and immunological synapse enrichment in cellular component (CC); T cell proliferation and activation enrichment in biological process (BP) (Figure 3A). The KEGG analysis indicated predominantly enrichment in cytokine-cytokine receptor interaction, calcium signaling pathway, and cell adhesion molecules (Figure 3B). GSEA showed that C1 was enriched in immune response, activation, and antigen presentation, including immunoglobulin mediated immune response, Th1 and Th2 cells differentiation, and Toll-like receptor signaling pathway (Figures 3C, D). Metabolic processes and biosynthesis related pathways were enriched in C2, such as glucuronate metabolic process, and biosynthesis of amino acids and steroid hormone (Figures 3E, F). GSVA showed differentially active signaling pathways and immune responses between two clusters (Figure 3G). Taken together, this suggested that TLS-enriched subcluster, C1, may inhibit tumor progression by activating non-specific anti-tumor immune responses. While TLS-depleted subcluster, C2, was for hypermetabolic and immunosuppression state.

3.4 Development and verification of the TLS-related risk model

To further analyze and quantify the TLS characteristics, a TLS-related prognostic model was established. TCGA-CRC dataset served as the training set, while GSE38832 and GSE17537 were utilized for the external validation. DEGs between tumor and normal samples were measured with the "DESeq2" (Supplementary Figure 2B). There were 508 intersection genes left (Supplementary Figure 2C, Supplementary Table 2). After univariable Cox regression analysis, we found 43 OS-related DEGs. Ultimately, 14 genes were selected for the risk model: *CAVIN2*, *CCL19/21*, *CD8A*, *CXCL5*, *FHL1*, *IGHG1*, *MMP1*, *MRC1*, *NEXN*, *MOTUM*, *PRRX1*, *SELL* and *VSIG4* (Supplementary Figures 2D, E). The model genes displayed a distinct expression pattern between two groups (Supplementary Figure 2F).

Based on the optimum cutoff value, patients were divided into two risk groups. Kaplan-Meier curves indicated lower mortality and better prognosis in the low-risk group (P<0.001, Figures 4A, B). Furthermore, the AUC revealed the 1-, 3-, and 5-year survival rates were all above 0.7, which proved the accuracy of this model was wonderful (Figure 4C). External validation datasets GSE38832 and GSE17537 also demonstrated the model's excellent prognostic performance (Figures 4D–I).

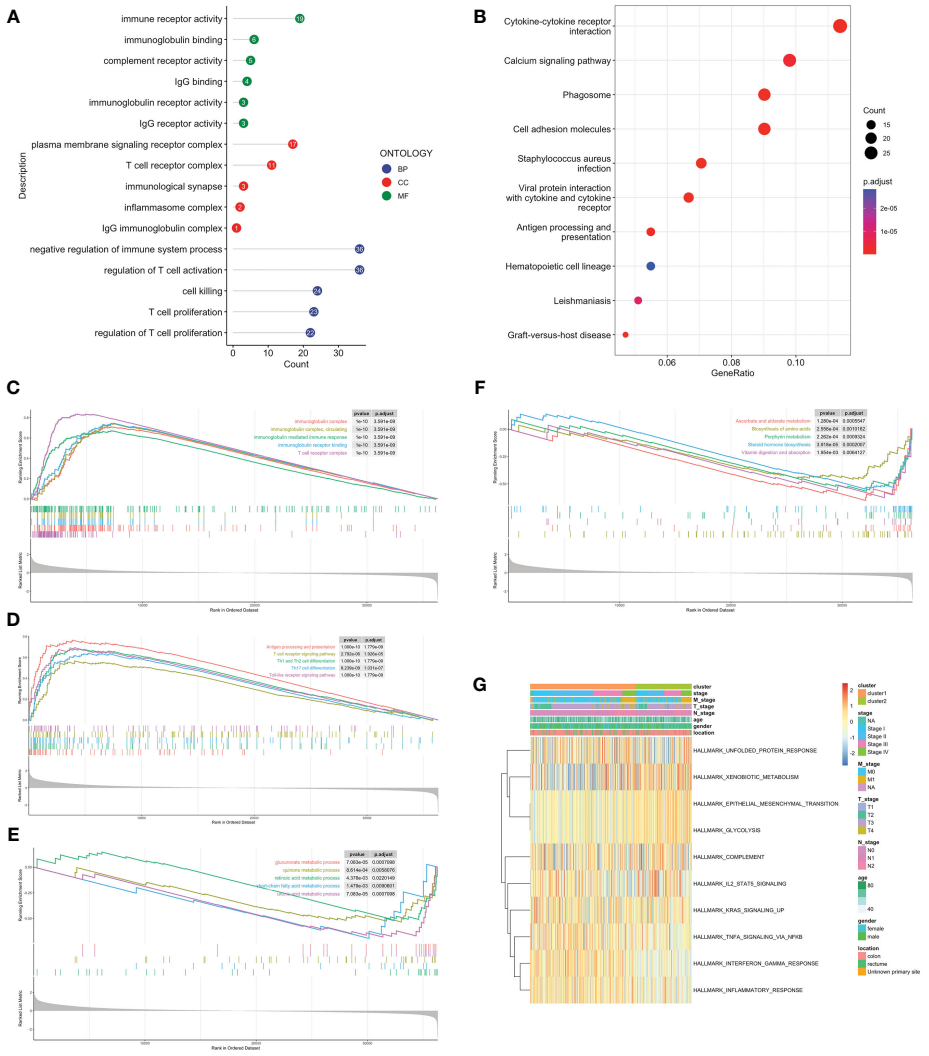

FIGURE 3
Biological functional enrichment analysis. GO **(A)** and KEGG **(B)** enrichment analyses based on DEGs. GSEA of C1 by GO **(C)**, KEGG **(D)**. GSEA of C2 by GO **(E)**, KEGG **(F)**. **(G)** GSVA of two clusters by Hallmark database.

3.5 Immune infiltration of TLS-related risk model

Different kinds of immune cell infiltration were estimated using CIBERSORT (Figure 5A). Plasma cells, macrophages and follicular helper T cells were higher in high-risk group. Additionally, we estimated the proportion of each cell in TME (Figure 5B). There were remarkably positive associations between risk score and CD8+ T cells, CD4+ naive T cells, macrophages and activated mast cells ($P<0.01$, Figure 5C). Further analysis revealed that there were more patients with KRAS mutations and fewer patients with BRAF mutations in the high-risk group (no statistically significant, Figures 5D, E). Next, we estimated the association between immune checkpoint genes and 14 model genes (Figure 5F). We found that the vast majority of model genes were positively correlated with immune related genes, except NOTUM.

3.6 Predict the efficacy of immunotherapy

Our above findings demonstrated a potential correlation between risk score and immunotherapy response. The low-risk group had higher stroma, immune, and TIME scores (Supplementary Figures 3A–C). TIDE score has been extensively employed to assess the likelihood of immune evasion and resistance to immunotherapy. We discovered the high-risk group had a much higher TIDE score (Supplementary Figure 3D). A higher TIDE score was linked to worse ICB effectiveness as well as shorter OS with ICB therapies. The IMvigor210 dataset, involving patients treated with atezolizumab, was utilized to validate these observations. In IMvigor210, low-risk patients had a greater prognosis and higher disease control rate ($p<0.05$, Supplementary Figures 3E, F).

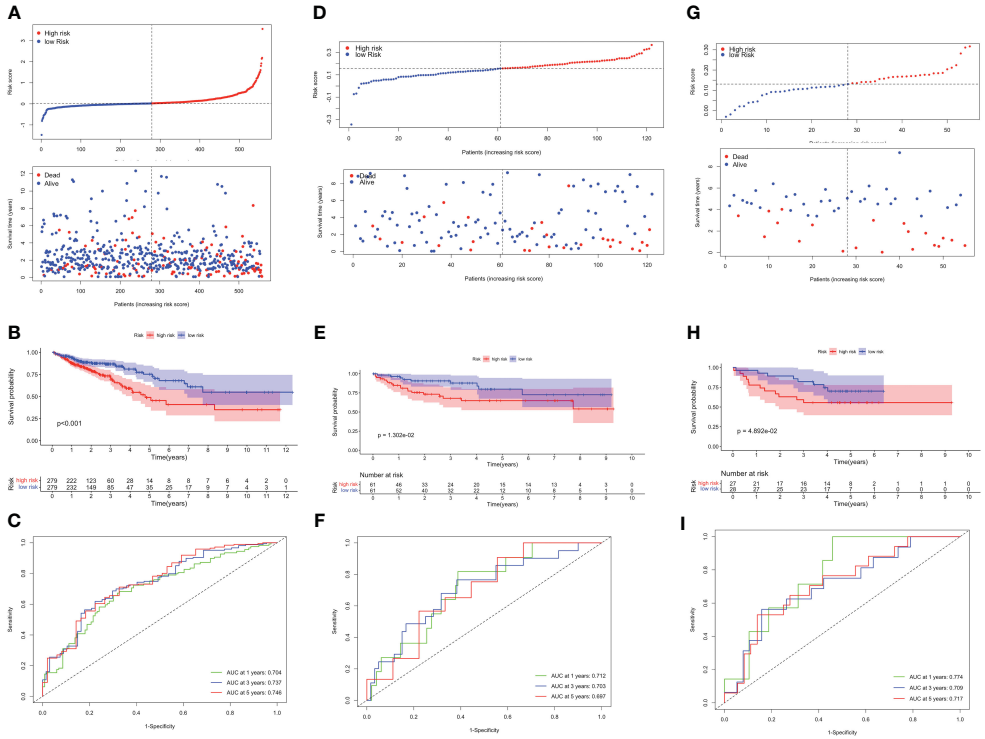

FIGURE 4
Validation of the TLS-related prognostic model in TCGA-CRC, GSE38832 and GSE17537 datasets. **(A)** Risk score distribution (up) and survival status (down) between high- and low-risk groups. **(B)** Kaplan–Meier survival analysis. **(C)** Time-dependent ROC analysis of risk scores. Risk score distribution and survival status **(D)**, Kaplan–Meier survival analysis **(E)**, and Time-dependent ROC analysis **(F)** in GSE38832. Risk score distribution and survival status **(G)**, Kaplan–Meier survival analysis **(H)**, and Time-dependent ROC analysis **(I)** in GSE17537.

3.7 Construction of a comprehensive nomogram to predict prognosis

MSI status was used to be an effective predictor for patients receiving ICB treatment. Typically, patients with high level of MSI were classified as MSI-High, indicating genomic instability resulting from repeated microsatellite expansions or contractions. Conversely, patients with low or no MSI were classified as microsatellite instability-low (MSI-L)/Microsatellite Stability (MSS). We analyzed the relationship between patients with different MSI status and risk score, and found no significant correlation (Figure 6A). Then, we combined the risk score with MSI status for stratified survival analysis (Figure 6B). Investigations indicated that MSI-H and low-risk scores patients had the best prognosis, followed by those with MSI-L and low-risk scores. Univariate and multivariate Cox regression confirmed the risk score as an independent prognostic factor for CRC (HR=3.706, 95%CI=2.552–5.380, Figures 6C, D). Exploiting these Clinicopathological characteristics, a new-type nomogram was constructed to assess the clinical prognostic more accurately (Figure 6E).

3.8 TLS-related hub gene identification

Random forest analysis was used to determine the feature importance of 14 model genes, among which three genes—*VSIG4*, *SELL* and *PRRX1*—stood out with importance scores exceeding 0.75 (Supplementary Figure 4A). In the high-risk group, the expression level of *VSIG4*, *SELL* and *PRRX1* were higher (Supplementary Figure 4B). Correlation analysis revealed that the vast majority of model genes were significantly positively correlated with hub genes (Supplementary Figure 4C). We conducted a further study to explore the correlation between the expression of TLS-related hub genes and the infiltration of immune cells in TME (Supplementary Figure 4D). *VSIG4*, *SELL* and *PRRX1* exhibited a positive relationship with macrophages M2 and neutrophils.

3.9 Explore the potential molecular mechanisms of TLS-related hub genes

GSEA and GSVA were conducted to investigate the molecular mechanisms and immune functions of the three hub genes. Results indicated that *VSIG4* was positively correlated with signaling pathways such as NF-kappa B signaling pathways, PI3K-AKT signaling pathways, and cytokine-cytokine receptor interaction (Figures 7A, B). High expression of *SELL* primarily enriched in the intestinal immune network for IGA production, oxidative phosphorylation, arginine and proline metabolism, Fc epsilon signaling pathway, and others (Figures 7C, D). GSEA of *PRRX1* subsequently uncovered that *PRRX1* was significantly linked to

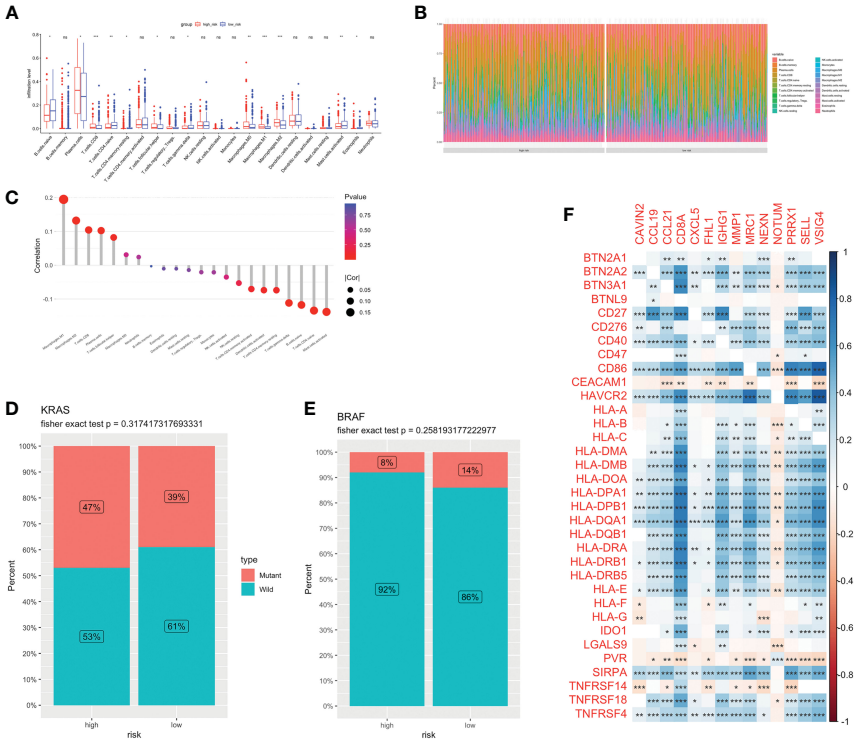

FIGURE 5
Immune infiltration and TME of low-and high-risk groups. Immune cell infiltration **(A)** and percentage **(B)** between two groups. **(C)** Correlation analysis between risk score and infiltration level. Risk score and CRC molecular features: KRAS **(D)** and BRAF **(E)**. **(F)** The correlations between immune genes and model genes. ns, not significance, *p< 0.05, **p< 0.01, ***p< 0.001.

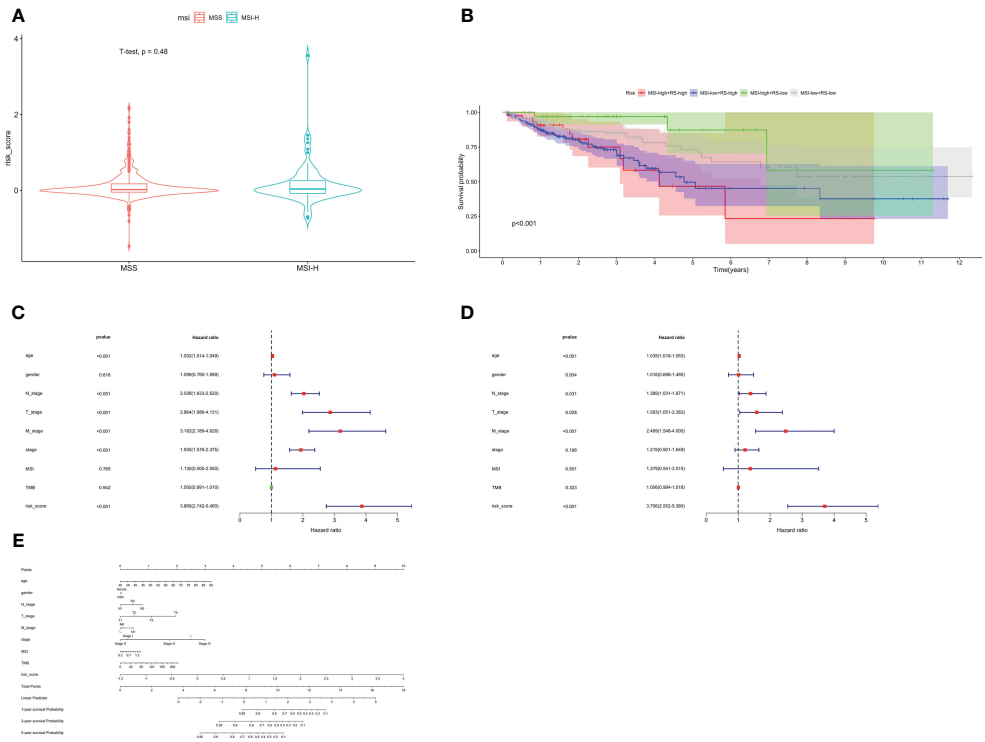

FIGURE 6
Stratified survival analysis and nomogram. **(A)** The relationship between risk score with different MSI status. **(B)** Stratified survival analysis combined with MSI status and risk score. Univariate Cox **(C)** and multivariate Cox **(D)** regression analyses. **(E)** The nomogram containing age, gender, T, N, M, stage, TMB and risk score.

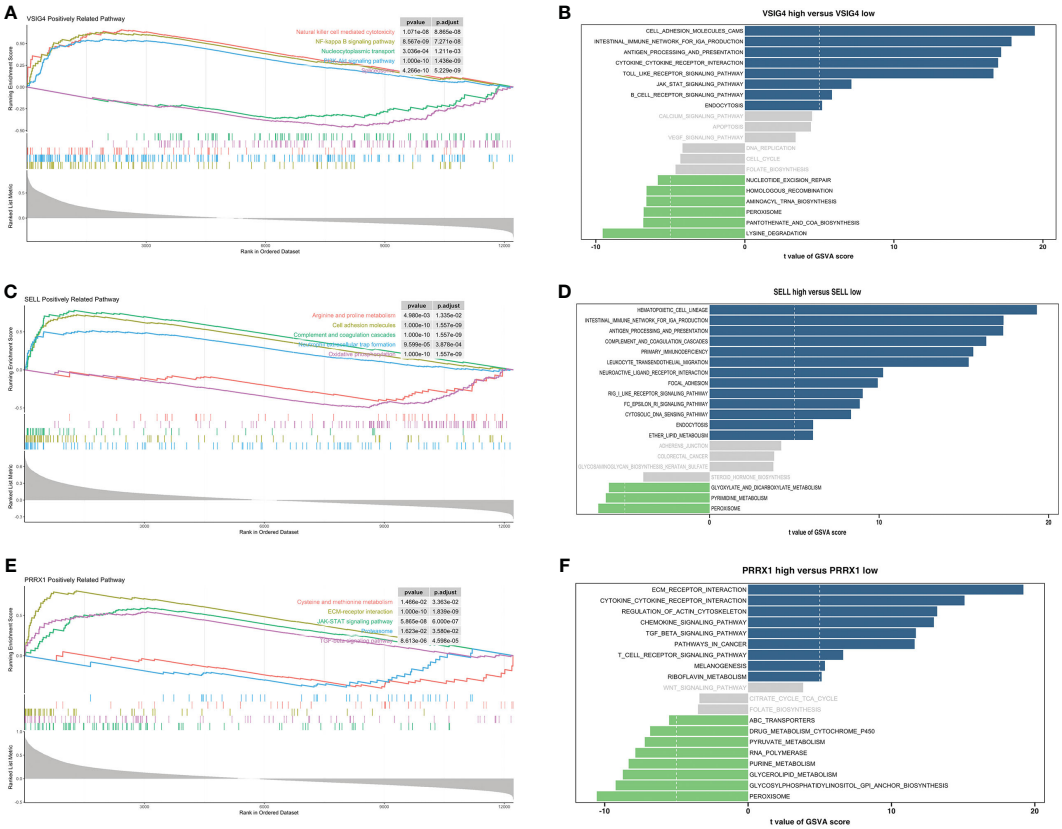

FIGURE 7
Enrichment analyses of *VSIG4*, *SELL* and *PRRX1*. **(A)** GSEA of *VSIG4*. **(B)** GSVA of *VSIG4*. **(C)** GSEA of *SELL*. **(D)** GSVA of *SELL*. **(E)** GSEA of *PRRX1*. **(F)** GSVA of *PRRX1*.

epithelial-mesenchymal transition (ECM) -receptor interaction, proteasome and TGF-beta signaling pathway (Figure 7E). High expression of *PRRX1* was mainly enriched in riboflavin metabolism, regulation of actin cytoskeleton, and others (Figure 7F). The low expression of *PRRX1* was enriched in pyruvate metabolism, purine metabolism, peroxisome, etc. In addition, *PRRX1* may serve as a prominent regulatory factor in tumorigenesis and progression.

3.10 Identification of a hub gene related ceRNA network

Increasing evidence has shown that the mutual regulatory patterns between mRNA, lncRNA, miRNA, and downstream target genes are intimately related to tumors. Our study exploited the Human MicroRNA Disease Database (HMDD) and miRNA Walkthrough (miRWalk) databases to identify the miRNA and lncRNA associated with CRC. Excluding interactions unrelated to disease, only two mRNA (*SELL*, *PRRX1*) and eight miRNA were retained (Figure 8A). Secondly, those mRNA-miRNA interactions were validated in the ENCORI database, *hsa-miR-485–5p* and *hsa-miR-20a-5p* regulated *PRRX1* were discovered. Utilizing Cytoscape, we constructed a ceRNA network, including 1 mRNA, 2 miRNA and 127 lncRNA (56 for *hsa-miR-20a-5p*, 71 for *hsa-miR-485–5p*) interaction pairs (Figure 8B).

3.11 Experimental validation

Using IHC to assess the *PRRX1* expression in the TLS+/- groups. Firstly, we observed TLS images through hematoxylin-eosin (H&E) and mIF (Figure 9A). The lymphocyte aggregates containing CD3+T cells, CD20+B cells, and CD21+FDCs that form corresponding regions are considered secondary follicle-like TLS, also known as mature TLS. To further validate the expression of *PRRX1*, we performed IHC on TLS+/- CRC tissues (Figures 9B, C). *PRRX1* was significantly higher in the TLS- group (Figure 9D). Through these above findings, we speculate that *PRRX1* may be a negative regulator of TLS and play a crucial role in tumor metastasis and immunocompetence.

4 Discussion

With the continuous development of anti-tumor therapy, immunotherapy has gradually become a common treatment method in clinical practice (26, 27). However, effective biomarkers to identify potential beneficiaries remain limited. PD-L1 and tumor mutation burden (TMB) are considered to be insufficient. Some patients receiving ICB treatments do not derive benefit, mainly due to the heterogeneity of TME and the complexity of immune mechanisms (28). TLS, as a particular component of

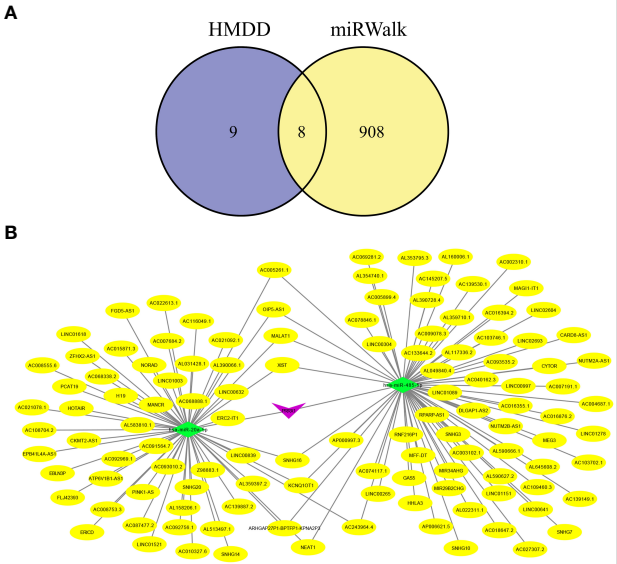

FIGURE 8
Hub genes-related ceRNA network analysis. **(A)** Intersection miRNAs of HMDB and miRWalk databases. **(B)** A hub genes-related ceRNA network of mRNA (*PRRX1*)-miRNA (hsa-miR-485–5p, hsa-miR-20a-5p)-lncRNA.

TME, has been proven to independently predict the response to ICB, regardless of the PD-L1 expression and MSI status (15, 17, 29). In this research, we conducted a detailed analysis of the variations in immune infiltration and potential mechanisms caused by TLS, and developed a novel model for evaluating the prognosis and the effectiveness of immunotherapy in CRC.

Firstly, we integrated a large number of reviews and articles to recruit TRGs. TRGs including various TLS signatures relevant to CRC, melanoma, breast cancer, gastric cancer, ovarian cancer, soft tissue sarcoma, and others (13, 30–37). We initially investigated the expression and mutation patterns of TRGs in CRC. *IL1R1* and *IL1R2* had the highest mutation frequencies, *CD40* and *IGSF6* had the highest CNV amplification mutation frequencies. CD40 is a member of TNF receptor superfamily. The high mutation rate of CD40 is related to its structural changes and TRAF (TNF-α Receptor Associated Factor)-binding domain exposure induced by a residue mutation of its ligand CD40L. CD40-CD40L interaction promotes GC formation and maintenance, and Th1 (T helper 1) response conversion (38).

Unsupervised consensus clustering, as one of the methods of consensus clustering, can be used to distinguish various subclusters. According to TRGs, 2 TLS related subclusters (TLS-enriched/TLS-depleted) were identified. Survival analysis revealed that C1 had a more favorable prognosis. We further analyzed the immune infiltration patterns between two clusters. The abundance of B cells, CD8+ T cells, T_{FH} cells, neutrophils and DC were higher in C1. Studies by Qin F et al. indicated that anti-TGF-β facilitates neutrophils recruitment and polarizes neutrophils towards an anti-tumor phenotype (N1) in CRC (39). Meanwhile, tumor infiltrating neutrophils can exert the role of antigen-presenting cells and heighten T cell proliferation (40). T_{FH} cells are usually accompanied by high *CXCR5*, *CD40*, and *CXCL13* expression.

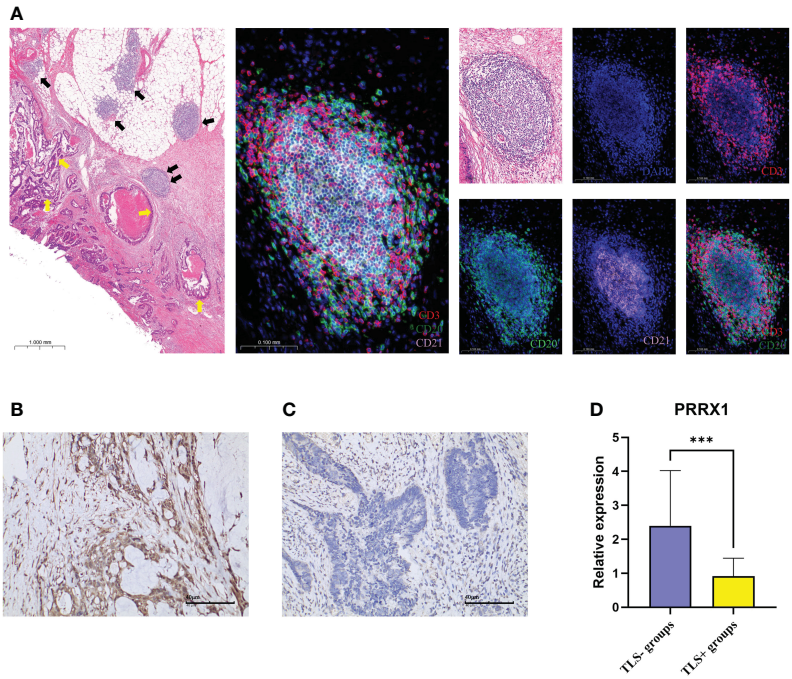

FIGURE 9
mIF and IHC characterized TLS and PRRX1 expression in CRC. **(A)** Representative images of secondary follicle-like TLS. The yellow arrows in the left image represented tumor tissue, the black arrows represented TLS. The TLS pointed by the two black arrows indicated the enlarged TLS in the subsequent image. The images contained H&E staining, mIF staining, and single IF under each marker (DAPI, CD3, CD20, CD21). IHC images (×200) of PRRX1 expression in the TLS- group **(B)** and TLS+ group **(C)**. **(D)** Differences in the expression of PRRX1 between TLS+/- groups. ***p< 0.001.

CXCL13/*CXCR5* signaling axis is a critical signaling pathway for TLS formation (41). Research has shown that T_{FH} controls the proliferation of B cells in GC (42). Patients with a substantial fraction of T_{FH} cells usually have a more favorable clinical outcome (33). The GC with *CD20*+ B cells is considered a mature feature of TLS. B cells has the ability to generate antibodies and also enhance cytotoxic CD8+ T cell response by secreting various cytokines in TME, such as interleukin-2 (IL-2) and interferon-γ (IFN-γ) (43, 44). Various studies demonstrated a strong correlation between B cells, especially those in TLS, and the efficacy of immunotherapy (45, 46). Inducing the formation and maturation of TLS by enhancing B cell expression may improve the treatment response rates and OS in CRC. Immune and environment scores also indicate that C1 has an inflammatory immune phenotype and stands in an immune-activated state. Thereby, we infer that C1 is the TLS-enriched cluster, while C2 is the TLS-depleted cluster.

In addition, a prognostic risk model related to TLS was developed. The AUC values for OS at 1–3-5 years were 0.704, 0.737, and 0.746, as well. The external validation datasets GSE38832 and GSE17537 also demonstrated their excellent prognostic ability. Next, we further analyzed the immune infiltration landscapes, molecular mutation features and immunotherapy efficacy of the two risk groups. Based on risk score, TMB and other clinical features, we constructed a new-type nomogram to comprehensively evaluate the prognosis.

According to the random forest analysis, we selected TLS-related hub genes in the model: *VSIG4*, *SELL* and *PRRX1*. *VSIG4*, fully defined as V-set and immunoglobulin domain-containing 4, is a complement receptor of the B7 immunoglobulin superfamily. *VSIG4* is mainly expressed in macrophages. *VSIG4*-expressing tumor-associated macrophages (TAMs) can inhibit tumor-specific CD8+ T cell proliferation and cytokines production, which function as a suppressor of anti-tumor immune response (47, 48). Recent studies indicates that *VSIG4* could activate the PI3K-AKT-STAT3 pathway, upregulating PDK2 and thereby inhibiting mitochondrial pyruvate metabolism and mitochondria ROS secretion (49). The relationship between *VSIG4* and poor prognosis has been confirmed in lung cancer (50), ovarian cancer (51), and glioma (52). *SELL*, an adhesion molecule, regulates the transport of immune cells to lymphocyte aggregates in TME (53). Tumor cells may utilize *SELL* to facilitate their detachment from the primary tumor, thereby promoting tumor metastasis and dissemination. Research by Liao et al. has inferred that *SELL* is involved in regulating the generation of PNAd and MAdCAM-1+ HEVs in TLS (54). These studies indicate that *SELL* may have a pivotal function in the initial stage of TLS formation. Research on this aspect is still lacking currently.

PRRX1, named as paired related homeobox 1 and *PRX1*, works as a primary transcription factor of cancer-associated fibroblasts (CAFs) (55). Prior research has established a robust link between elevated *PRRX1* expression and the progression and recurrence of CRC, breast cancer, and esophageal cancer, leading to poor prognosis and drug resistance (55–57). Zhong et al. discovered that *PRRX1* promotes tumor cells to migrate and invade by targeting the IL-6/JAK3/STAT3 axis (58). Silencing of *PRRX1* may indirectly influence the proliferation and differentiation of TLS in CRC by inhibiting this axis (59). We checked the expression of *PRRX1* in the TLS+/- groups through IHC in this study. In summary, *PRRX1* may function as a therapeutic target for CRC treatment and be a negative immunomodulatory regulator of TLS.

Our research provided an innovative perspective for exploring the crosstalk between TLS and CRC TME. Nevertheless, our research still has some weaknesses. The data bias caused by retrospective studies is inevitable. TCGA and GEO cannot provide MRI imaging and hematological data. Furthermore, applying spatial transcriptomics to analyze TLS *in situ* may bring new insights.

5 Conclusion

Based on TRGs and DEGs, we discriminated the TLS related subclusters, constructed a prognostic risk model, and explored the potential mechanisms of hub genes to regulate TLS and CRC progression. Low-risk group exhibited a more favorable clinical outcome, richer immune infiltration, and better immunotherapy efficacy. Moreover, a preliminary exploration of the mechanisms of hub genes could help identify potential therapeutic targets.

Data availability statement

The original contributions presented in the study are included in the article/Supplementary Material. Further inquiries can be directed to the corresponding author.

Ethics statement

The studies involving human participants were reviewed by and approved by Institutional Ethics Committee of QuXian People's Hospital. The participants provided their written informed consent to participate in this study. The studies were conducted in accordance with the local legislation and institutional requirements. The participants provided their written informed consent to participate in this study.

Author contributions

ZX: Conceptualization, Data curation, Funding acquisition, Writing – original draft, Writing – review & editing. QW: Data curation, Investigation, Resources, Writing – original draft. YYZ: Conceptualization, Funding acquisition, Software, Supervision, Validation, Writing – original draft. XL: Conceptualization, Methodology, Project administration, Resources, Validation, Writing

– original draft. MW: Conceptualization, Methodology, Project administration, Resources, Software, Writing – review & editing. YHZ: Conceptualization, Investigation, Methodology, Resources, Visualization, Writing – original draft. YP: Investigation, Methodology, Project administration, Writing – review & editing. KL: Data curation, Methodology, Software, Supervision, Writing – review & editing. MY: Investigation, Supervision, Validation, Writing – original draft. LL: Conceptualization, Supervision, Validation, Writing – review & editing. CW: Project administration, Software, Validation, Writing – review & editing. WW: Conceptualization, Funding acquisition, Investigation, Resources, Software, Supervision, Validation, Visualization, Writing – original draft, Writing – review & editing.

Funding

The author(s) declare financial support was received for the research, authorship, and/or publication of this article. This work was supported by the Key Projects of Sichuan Natural Science Foundation (2022NSFSC0051), the Clinical Scientist Program of Sichuan Cancer Hospital (YB2022003), and the Chengdu Technology Innovation R&D Project (2021YF0501659SN).

Conflict of interest

The authors declare that the research was conducted in the absence of any commercial or financial relationships that could be construed as a potential conflict of interest.

Publisher's note

Supplementary material

The Supplementary Material for this article can be found online at: https://www.frontiersin.org/articles/10.3389/fonc.2024.1383096/full#supplementary-material

References

1. Bien J, Lin A. A review of the diagnosis and treatment of metastatic colorectal cancer. *Jama-J Am Med Assoc*. (2021) 325:2404–5. doi: 10.1001/jama.2021.6021

2. Sung H, Ferlay J, Siegel RL, Laversanne M, Soerjomataram I, Jemal A, et al. Global cancer statistics 2020: globocan estimates of incidence and mortality worldwide for 36 cancers in 185 countries. *Ca-a Cancer J Clin*. (2021) 71:209–49. doi: 10.3322/caac.21660

3. Le DT, Kim TW, Van Cutsem E, Geva R, Jager D, Hara H, et al. Phase ii open-label study of pembrolizumab in treatment-refractory, microsatellite instability-high/mismatch repair-deficient metastatic colorectal cancer: keynote-164. *J Clin Oncol*. (2020) 38:11–9. doi: 10.1200/jco.19.02107

4. Diaz LA, Shiu KK, Kim TW, Jensen BV, Jensen LH, Punt C, et al. Pembrolizumab versus chemotherapy for microsatellite instability-high or mismatch repair-deficient metastatic colorectal cancer (Keynote-177): final analysis of a randomized, open-label, phase 3 study. *Lancet Oncol*. (2022) 23:659–70. doi: 10.1016/s1470–2045(22)00197–8

5. Lenz HJ, Van Cutsem E, Limon ML, Wong KYM, Hendlisz A, Aglietta M, et al. First-line nivolumab plus low-dose ipilimumab for microsatellite instability-high/mismatch repair-deficient metastatic colorectal cancer: the phase ii checkmate 142 study. *J Clin Oncol*. (2022) 40:161–70. doi: 10.1200/jco.21.01015

6. Galon J, Costes A, Sanchez-Cabo F, Kirilovsky A, Mlecnik B, Lagorce-Pagès C, et al. Type, density, and location of immune cells within human colorectal tumors predict clinical outcome. *Science*. (2006) 313:1960–4. doi: 10.1126/science.1129139

7. van de Pavert SA, Mebius RE. New insights into the development of lymphoid tissues. *Nat Rev Immunol*. (2010) 10:664–74. doi: 10.1038/nri2832

8. Meier D, Bornmann C, Chappaz S, Schmutz S, Otten LA, Ceredig R, et al. Ectopic lymphoid-organ development occurs through interleukin 7-mediated enhanced survival of lymphoid-tissue-inducer cells. *Immunity*. (2007) 26:643–54. doi: 10.1016/j.immuni.2007.04.009

9. Colbeck EJ, Ager A, Gallimore A, Jones GW. Tertiary lymphoid structures in cancer: drivers of antitumor immunity, immunosuppression, or bystander sentinels in disease? *Front Immunol*. (2017) 8:1830. doi: 10.3389/fimmu.2017.01830

10. Drayton DL, Liao S, Mounzer RH, Ruddle NH. Lymphoid organ development: from ontogeny to neogenesis. *Nat Immunol*. (2006) 7:344–53. doi: 10.1038/ni1330

11. Di Caro G, Bergomas F, Grizzi F, Doni A, Bianchi P, Malesci A, et al. Occurrence of tertiary lymphoid tissue is associated with T-cell infiltration and predicts better prognosis in early-stage colorectal cancers. *Clin Cancer Res*. (2014) 20:2147–58. doi: 10.1158/1078–0432.Ccr-13–2590

12. Bergomas F, Grizzi F, Doni A, Pesce S, Laghi L, Allavena P, et al. Tertiary intratumor lymphoid tissue in colo-rectal cancer. *Cancers*. (2011) 4:1–10. doi: 10.3390/cancers4010001

13. Sautes-Fridman C, Petitprez F, Calderaro J, Fridman WH. Tertiary lymphoid structures in the era of cancer immunotherapy. *Nat Rev Cancer*. (2019) 19:307–25. doi: 10.1038/s41568–019-0144–6

14. Germain C, Gnjatic S, Tamzalit F, Knockaert S, Remark R, Goc J, et al. Presence of B cells in tertiary lymphoid structures is associated with a protective immunity in patients with lung cancer. *Am J Respir Crit Care Med*. (2014) 189:832–44. doi: 10.1164/rccm.201309-1611OC

15. Cabrita R, Lauss M, Sanna A, Donia M, Larsen MS, Mitra S, et al. Tertiary lymphoid structures improve immunotherapy and survival in melanoma. *Nature*. (2020) 577:561. doi: 10.1038/s41586–019-1914–8

16. Martinet L, Garrido I, Filleron T, Le Guellec S, Bellard E, Fournie JJ, et al. Human solid tumors contain high endothelial venules: association with T- and B-lymphocyte infiltration and favorable prognosis in breast cancer. *Cancer Res*. (2011) 71:5678–87. doi: 10.1158/0008–5472.Can-11–0431

17. Helmink BA, Reddy SM, Gao JJ, Zhang SJ, Basar R, Thakur R, et al. B cells and tertiary lymphoid structures promote immunotherapy response. *Nature*. (2020) 577:549–55. doi: 10.1038/s41586–019-1922–8

18. Necchi A, Joseph RW, Loriot Y, Hoffman-Censits J, Perez-Gracia JL, Petrylak DP, et al. Atezolizumab in platinum-treated locally advanced or metastatic urothelial carcinoma: post-progression outcomes from the phase ii imvigor210 study. *Ann Oncol*. (2017) 28:3044–50. doi: 10.1093/annonc/mdx518

19. Mayakonda A, Lin DC, Assenov Y, Plass C, Koeffler HP. Maftools: efficient and comprehensive analysis of somatic variants in cancer. *Genome Res*. (2018) 28:1747–56. doi: 10.1101/gr.239244.118

20. Wilkerson MD, Hayes DN. Consensusclusterplus: A class discovery tool with confidence assessments and item tracking. *Bioinformatics*. (2010) 26:1572–3. doi: 10.1093/bioinformatics/btq170

21. Newman AM, Liu CL, Green MR, Gentles AJ, Feng WG, Xu Y, et al. Robust enumeration of cell subsets from tissue expression profiles. *Nat Meth*. (2015) 12:453. doi: 10.1038/nmeth.3337

22. Aran D, Hu ZC, Butte AJ. Xcell: digitally portraying the tissue cellular heterogeneity landscape. *Genome Biol*. (2017) 18(1):220. doi: 10.1186/s13059–017-1349–1

23. Yu GC, Wang LG, Han YY, He QY. Clusterprofiler: an R package for comparing biological themes among gene clusters. *Omics-a J Integr Biol*. (2012) 16:284–7. doi: 10.1089/omi.2011.0118

24. Hänzelmann S, Castelo R, Guinney J. Gsva: gene set variation analysis for microarray and rna-seq data. *BMC Bioinf*. (2013) 14:7. doi: 10.1186/1471–2105-14–7

25. Posch F, Silina K, Leibl S, Mundlein A, Moch H, Siebenhuner A, et al. Maturation of tertiary lymphoid structures and recurrence of stage II and III colorectal cancer. *Oncoimmunology*. (2018) 7(2):e1378844. doi: 10.1080/2162402x.2017.1378844

26. Galluzzi L, Humeau J, Buqué A, Zitvogel L, Kroemer G. Immunostimulation with chemotherapy in the era of immune checkpoint inhibitors. *Nat Rev Clin Oncol*. (2020) 17:725–41. doi: 10.1038/s41571-020-0413-z

27. Vaddepally RK, Kharel P, Pandey R, Garje R, Chandra AB. Review of indications of fda-approved immune checkpoint inhibitors per nccn guidelines with the level of evidence. *Cancers*. (2020) 12:738. doi: 10.3390/cancers12030738

28. O'Donnell JS, Teng MWL, Smyth MJ. Cancer immunoediting and resistance to T cell-based immunotherapy. *Nat Rev Clin Oncol*. (2019) 16:151–67. doi: 10.1038/s41571–018-0142–8

29. Vanhersecke L, Brunet M, Guégan JP, Rey C, Bougouin A, Cousin S, et al. Mature tertiary lymphoid structures predict immune checkpoint inhibitor efficacy in solid tumors independently of pd-L1 expression. *Nat Cancer*. (2021) 2:794–802. doi: 10.1038/s43018–021-00232–6

30. Coppola D, Nebozhyn M, Khalil F, Dai HY, Yeatman T, Loboda A, et al. Unique ectopic lymph node-like structures present in human primary colorectal carcinoma are identified by immune gene array profiling. *Am J Pathol*. (2011) 179:37–45. doi: 10.1016/j.ajpath.2011.03.007

31. Messina JL, Fenstermacher DA, Eschrich S, Qu XT, Berglund AE, Lloyd MC, et al. 12-chemokine gene signature identifies lymph node-like structures in melanoma: potential for patient selection for immunotherapy? *Sci Rep*. (2012) 2:765. doi: 10.1038/srep00765

32. Finkin S, Yuan DT, Stein I, Taniguchi K, Weber A, Unger K, et al. Ectopic lymphoid structures function as microniches for tumor progenitor cells in hepatocellular carcinoma. *Nat Immunol*. (2015) 16:1235–44. doi: 10.1038/ni.3290

33. Gu-Trantien C, Loi S, Garaud S, Equeter C, Libin M, de Wind A, et al. Cd4+ Follicular helper T cell infiltration predicts breast cancer survival. *J Clin Invest*. (2013) 123:2873–92. doi: 10.1172/jci67428

34. Hennequin A, Derangere V, Boidot R, Apetoh L, Vincent J, Orry D, et al. Tumor infiltration by tbet plus effector T cells and cd20+B cells is associated with survival in gastric cancer patients. *Oncoimmunology*. (2016) 5:e1054598. doi: 10.1080/2162402x.2015.1054598

35. Kroeger DR, Milne K, Nelson BH. Tumor-infiltrating plasma cells are associated with tertiary lymphoid structures, cytolytic T-cell responses, and superior prognosis in ovarian cancer. *Clin Cancer Res*. (2016) 22:3005–15. doi: 10.1158/1078–0432.Ccr-15–2762

36. Hou Y, Qiao SJ, Li M, Han X, Wei X, Pang YX, et al. The gene signature of tertiary lymphoid structures within ovarian cancer predicts the prognosis and immunotherapy benefit. *Front Genet*. (2023) 13:1090640. doi: 10.3389/fgene.2022.1090640

37. Becht E, de Reynies A, Giraldo NA, Pilati C, Buttard B, Lacroix L, et al. Immune and stromal classification of colorectal cancer is associated with molecular subtypes and relevant for precision immunotherapy. *Clin Cancer Res*. (2016) 22:4057–66. doi: 10.1158/1078–0432.Ccr-15–2879

38. Sarode AY, Jha MK, Zutshi S, Ghosh SK, Mahor H, Sarma U, et al. Residue-specific message encoding in cd40-ligand. *iScience*. (2020) 23:101441. doi: 10.1016/j.isci.2020.101441

39. Qin F, Liu X, Chen J, Huang S, Wei W, Zou Y, et al. Anti-tgf-β Attenuates tumor growth via polarization of tumor associated neutrophils towards an anti-tumor phenotype in colorectal cancer. *J Cancer*. (2020) 11:2580–92. doi: 10.7150/jca.38179

40. Awasthi D, Sarode A. Neutrophils at the crossroads: unraveling the multifaceted role in the tumor microenvironment. *Int J Mol Sci*. (2024) 25(5):2929. doi: 10.3390/ijms25052929

41. Tian C, Li C, Zeng YL, Liang JY, Yang QF, Gu FF, et al. Identification of cxcl13/cxcr5 axis's crucial and complex effect in human lung adenocarcinoma. *Int Immunopharmacol*. (2021) 94:107416. doi: 10.1016/j.intimp.2021.107416

42. Noël G, Fontsa ML, Garaud S, De Silva P, De Wind A, Van den Eynden GG, et al. Functional th1-oriented T follicular helper cells that infiltrate human breast cancer promote effective adaptive immunity. *J Clin Invest*. (2021) 131:e139905. doi: 10.1172/jci139905

43. Jacquelot N, Tellier J, Nutt SL, Belz GT. Tertiary lymphoid structures and B lymphocytes in cancer prognosis and response to immunotherapies. *Oncoimmunology*. (2021) 10:1900508. doi: 10.1080/2162402x.2021.1900508

44. Bruno TC, Ebner PJ, Moore BL, Squalls OG, Waugh KA, Eruslanov EB, et al. Antigen-presenting intratumoral B cells affect cd4+ Til phenotypes in non-small cell lung cancer patients. *Cancer Immunol Res*. (2017) 5:898–907. doi: 10.1158/2326–6066.Cir-17–0075

45. Phanthunane C, Wijers R, de Herdt M, Langeveld TPM, Koljenovic S, Dasgupta S, et al. B-cell clusters at the invasive margin associate with longer survival in early-stage oral-tongue cancer patients. *Oncoimmunology*. (2021) 10(1):1882743. doi: 10.1080/2162402x.2021.1882743

46. Petitprez F, de Reyniès A, Keung EZ, Chen TWW, Sun CM, Calderaro J, et al. B cells are associated with survival and immunotherapy response in sarcoma. *Nature*. (2020) 577:556–60. doi: 10.1038/s41586–019-1906–8

47. Huang W, Doucet M, Sen R, Pardoll A, Ganguly S. The role of vsig4 as an immuno-regulatory protein in cancer. *J Immunother Cancer*. (2022) 10:A508–A. doi: 10.1136/jitc-2022-SITC2022.0487

48. Jung K, Seo SK, Choi I. Endogenous vsig4 negatively regulates the helper T cell-mediated antibody response. *Immunol Lett*. (2015) 165:78–83. doi: 10.1016/j.imlet.2015.04.004

49. Li JL, Diao B, Guo S, Huang XY, Yang CY, Feng ZQ, et al. Vsig4 inhibits proinflammatory macrophage activation by reprogramming mitochondrial pyruvate metabolism. *Nat Commun*. (2017) 8(1):1322. doi: 10.1038/s41467–017-01327–4

50. Liao YM, Guo S, Chen YW, Cao DY, Xu H, Yang CY, et al. Vsig4 expression on macrophages facilitates lung cancer development. *Lab Invest*. (2014) 94:706–15. doi: 10.1038/labinvest.2014.73

51. Byun JM, Jeong DH, Choi IH, Lee DS, Kang MS, Jung KO, et al. The significance of vsig4 expression in ovarian cancer. *Int J Gynecol Cancer*. (2017) 27:872–8. doi: 10.1097/igc.0000000000000979

52. Xu T, Jiang Y, Yan Y, Wang HX, Lu CY, Xu HC, et al. Vsig4 is highly expressed and correlated with poor prognosis of high-grade glioma patients. *Am J Transl Res*. (2015) 7:1172–80.

53. Ivetic A, Green HLH, Hart SJ. L-selectin: A major regulator of leukocyte adhesion, migration and signaling. *Front Immunol*. (2019) 10:1068. doi: 10.3389/fimmu.2019.01068

54. Liao S, Ruddle NH. Synchrony of high endothelial venules and lymphatic vessels revealed by immunization. *J Immunol*. (2006) 177:3369–79. doi: 10.4049/jimmunol.177.5.3369

55. Lee KW, Yeo SY, Gong JR, Koo OJ, Sohn I, Lee WY, et al. Prrx1 is a master transcription factor of stromal fibroblasts for myofibroblastic lineage progression. *Nat Commun*. (2022) 13(1):2793. doi: 10.1038/s41467–022-30484–4

56. Takahashi Y, Sawada G, Kurashige J, Uchi R, Matsumura T, Ueo H, et al. Paired related homoeobox 1, a new emt inducer, is involved in metastasis and poor prognosis in colorectal cancer. *Br J Cancer*. (2013) 109:307–11. doi: 10.1038/bjc.2013.339

57. Cazet AS, Hui MN, Elsworth BL, Wu SZ, Roden D, Chan CL, et al. Targeting stromal remodeling and cancer stem cell plasticity overcomes chemoresistance in triple negative breast cancer. *Nat Commun*. (2018) 9:2897. doi: 10.1038/s41467–018-05220–6

58. Zhong LZ, Tan WL, Yang QQ, Zou ZW, Zhou R, Huang YS, et al. Prrx1 promotes colorectal cancer stemness and chemoresistance via the jak2/stat3 axis by targeting il-6. *J Gastrointestinal Oncol*. (2022) 13(6):2989–3008. doi: 10.21037/jgo-22–1137

59. Nairismägi ML, Gerritsen ME, Li ZM, Wijaya GC, Chia BKH, Laurensia Y, et al. Oncogenic activation of jak3-stat signaling confers clinical sensitivity to prn371, a novel selective and potent jak3 inhibitor, in natural killer/T-cell lymphoma. *Leukemia*. (2018) 32:1147–56. doi: 10.1038/s41375-017-0004-x

frontiers | Frontiers in Immunology

TYPE Original Research
PUBLISHED 13 August 2024
DOI 10.3389/fimmu.2024.1423775

OPEN ACCESS

EDITED BY
Ying Ma,
Tianjin Medical University Cancer Institute and Hospital, China

REVIEWED BY
Feng Wei,
Tianjin Medical University Cancer Institute and Hospital, China
Luis Munoz-Erazo,
The University of Auckland, New Zealand

*CORRESPONDENCE
Hui Zhao
zhaohui@dmu.edu.cn

†These authors have contributed equally to this work

RECEIVED 26 April 2024
ACCEPTED 24 July 2024
PUBLISHED 13 August 2024

CITATION
Xin S, Wen S, He P, Zhao Y and Zhao H (2024) Density of tertiary lymphoid structures and their correlation with prognosis in non-small cell lung cancer. *Front. Immunol.* 15:1423775. doi: 10.3389/fimmu.2024.1423775

Density of tertiary lymphoid structures and their correlation with prognosis in non-small cell lung cancer

Shuyue Xin[1†], Shuang Wen[2†], Peipei He[1†], Yulong Zhao[1] and Hui Zhao[1*]

[1]Department of Health Examination Center, The Second Affiliated Hospital of Dalian Medical University, Dalian, China, [2]Department of Pathology, The Friendship Hospital of Dalian, Dalian, China

Background: Tertiary lymphoid structures (TLS), ordered structure of tumor-infiltrating immune cells in tumor immune microenvironment (TIME), play an important role in the development and anti-tumor immunity of various cancers, including liver, colon, and gastric cancers. Previous studies have demonstrated that the presence of TLS in intra-tumoral (IT), invasive margin (IM), and peri-tumoral (PT) regions of the tumors at various maturity statuses. However, the density of TLS in different regions of non-small cell lung cancer (NSCLC) has not been extensively studied.

Methods: TLS and tumor-infiltrating immune cells were assessed using immunohistochemistry (IHC) staining in 82 NSCLC patients. Tumor samples were divided into three subregions as IT, IM and PT regions, and TLS were identified as early/primary TLS (E-TLS) or secondary/follicular TLS (F-TLS). The distribution of TLS in different maturity statuses, along with their correlation with clinicopathological characteristics and prognostic value, was assessed. Nomograms were used to predict the probability of 1-, 3-, and 5-year overall survival (OS) in patients with NSCLC.

Results: The density of TLS and proportion of F-TLS in the IT region (90.2%, 0.45/mm^2, and 61.0%, respectively) were significantly higher than those in the IM region (72.0%, 0.18/mm^2, and 39.0%, respectively) and PT region (67.1%, 0.16/mm^2, and 40.2%, respectively). A lower density of TLS, especially E-TLS in the IM region, was correlated with better prognosis in NSCLC patients. CD20+ B cells, CD3+ T cells, CD8+ cytotoxic T cells, and CD68+ macrophages were significantly overexpressed in the IM region. CD20+ B cells and CD3+ T cells in the IM region were significantly correlated with the density of E-TLS, while no statistically significant correlation was found with F-TLS. The E-TLS density in the IM region and TNM stage were independent prognostic factors for NSCLC patients. The nomogram showed good prognostic ability.

Conclusions: A higher density of E-TLS in the IM region was associated with a worse prognosis in NSCLC patients, potentially due to the inhibition of TLS maturation caused by the increased density of suppressive immune cells at the tumor invasion front.

KEYWORDS

tertiary lymphoid structures (TLS), non-small cell lung cancer (NSCLC), prognosis, tumor immune microenvironment (TIME), nomogram

Introduction

Lung cancer is the second most common cancer and the leading cause of cancer-related death (1), and non-small cell lung cancer (NSCLC) accounting for more than 85% of all cases (2). In recent years, with more detailed studies of the tumor immune microenvironment (TIME), immunotherapy has become the most promising treatment method for NSCLC. However, despite the potential for prolonged survival in some patients, only 20-40% of NSCLC patients ultimately benefit from immunotherapy (3), and many more patients suffer from poor outcomes due to immune unresponsiveness or drug resistance. Therefore, it is crucial to further explore the characteristics of TIME and seek better directions for NSCLC immunotherapy.

Tertiary lymphoid structures (TLS) were first identified in inflammation-related tissues, named for their structural resemblance to secondary lymphatic organs (4). In the TIME, TLS are ordered structures of tumor-infiltrating immune cells, mainly consisting of T cell (CD3+) colonies surrounding B cell (CD20+) colonies, with macrophages, dendritic cells, stromal cells, and high endothelial venules at the periphery (5–8). It has been reported that the density and structure of tumor-associated TLS may be related to the clinical outcome of patients with various cancers, such as lung cancer, hepatocellular carcinoma, and melanoma, etc (9–11). TLS can exist in different maturity statuses, which influence prognosis differently. Mature TLS, also known as secondary/follicular TLS, appear to have the same germinal center (GC) as secondary lymphatic organs, with an organized follicular dendritic cell (CD21+) network as its characteristic component. The TLS in their mature state are important sites for initiating or maintaining local and systemic B and T cell responses to tumors (12, 13). High densities of mature TLS-containing GC correlate with favorable clinical prognosis in several cancers, including hepatocellular carcinoma (14), colorectal cancer (15), pancreatic cancer (16), pancreatic neuroendocrine tumor (17), NSCLC (18, 19), and oral cancer (20). In contrast, a higher proportion of immature TLS, also known as primary TLS (without GC), located in tumors, may be associated with poor prognosis (19).

The spatial distribution of TLS within tumors plays different roles in anti-tumor immunity and outcomes. For example, in intrahepatic cholangiocarcinoma, more TLS, especially mature TLS in the tumor core, are associated with improved survival and better responses to immunotherapy. However, more mature TLS in the peri-tumoral regions can lead to worse prognoses (21). Two other studies on liver cancer reached the opposite conclusions. Finkin et al. found that the presence of TLS in the intra-tumor region provided energy for the growth of tumor cells and promoted the progression of liver cancer, leading to worse prognosis in patients (22). Li et al. found that only 30% of TLS were present in the tumor, while higher density of TLS was expressed in peri-tumoral tissues, which was significantly correlated with a good prognosis for patients (23). As such, the density and maturity of TLS vary in different regions of liver cancer and display different prognostic implications. It is important to note that TLS also exist at the invasive margin, the front line of tumor invasion and anti-tumor immunity. In several studies based on tumors of the digestive system, higher densities of immune cells such as CD8+ T cells and Treg immunosuppressor cells were found in the IM regions than in the IT and PT regions, suggesting that invasive margin may have important research value in anti-tumor immunity (24–26). Therefore, the density and maturity of TLS in tumors may differ depending on the pathological type and tissue site. However, it remains unclear whether TLS exhibit spatial heterogeneity in NSCLC and their clinical significance (27).

In this study, we investigated the density and the maturity status of TLS in the intra-tumor, peri-tumor, and invasive margins of NSCLC patients. We also assessed the correlation between TLS density and tumor-infiltrating immune cells and explored the relationship between TLS and prognosis. Our aim is to comprehensively analyze the function of TLS, gain a deeper understanding of their role in the progression of NSCLC, and provide important insights for enhancing immunotherapy as well as identifying a new reference marker for predicting prognosis in NSCLC patients.

Materials and methods

Clinicopathologic characteristics of patients

This retrospective study included 95 patients with NSCLC who were diagnosed and underwent resection of their primary lung tumors between January 2011 and November 2018 at Dalian Friendship Hospital. All patients were aged 18 or older, had no prior malignant disease, and did not receive preoperative neoadjuvant chemotherapy

and/or radiotherapy. Two patients were excluded because of a history of renal clear cell carcinoma and thyroid carcinoma. Additionally, 11 patients were excluded due to inadequate peritumor content for assessment. Consequently, 82 patients were included in the study cohort and subjected to further analyses (Table 1). The study protocol was approved by the Institutional Review Board of the hospital (IRB No. KY-2023 (009)-001). As this is a noninterventional retrospective study, informed consent was waived by the IRB. This study was conducted in accordance with the principles of the Declaration of Helsinki.

Clinical and pathological data, including age, sex, smoking history, and tumor size, were retrieved from electronic hospital records. Tumors were staged according to the 8th edition of the Union for International Cancer Control (UICC) tumor-node-metastases (TNM) classification and pathological staging guidelines. Follow-up information was collected through telephone surveys, with the last follow-up conducted in December 2022. A total of 80 patients were followed-up, with a median follow-up time of 59.1 months. Overall survival (OS) was defined as the time from resection to death, loss to follow-up, or the last follow-up date. Recurrence-free survival (RFS) was defined as the time from surgical resection to the diagnosis of recurrence or the last follow-up.

Immunohistochemistry

Formalin-fixed, paraffin-embedded (FFPE) tumor tissues were retrieved from pathology archives. A consecutive series of tissue specimens were collected from FFPE and prepared at a thickness of 5 μm. Max Vision staining was performed manually. The tissues were deparaffinized and rehydrated in graded ethanol to water. Antigen retrieval was achieved by pressure cooker treatment for 2 minutes, followed by cooling to room temperature. Endogenous peroxidases were inactivated using 0.3% H_2O_2/methanol for 15 minutes at room temperature. Sequential tissue sections were incubated overnight with primary monoclonal antibodies, anti-CD47 (A11382, 1:100, ABclonal) and ready-to-use antibodies from MXB Biotechnologies, including anti-CD8 (MAB-0021), anti-CD3 (MAB-0740), anti-CD20 (kit-0001), anti-CD21 (RMA-0811), and anti-CD68 (kit-0026). Subsequently, the slides were washed three times with PBS for 3 minutes each and then incubated with secondary antibody for 15 minutes. Specific signals were visualized with 3,3′-diaminobenzidine (DAB) for 3-10 minutes (controlled under a microscope), and then washed with PBS for 10 minutes. The sections were counterstained with hematoxylin for 20 seconds, dehydrated and mounted. Necrotic areas were excluded from the analysis.

Quantification of TLS

TLS were assessed by an expert pathologist (SW) and two observers (SYX and XPH), who were blinded to clinicopathological data. They were trained to identify the pathologic features of TLS in full section slides containing the intra-tumor (IT), invasion margin (IM), and peri-tumor (PT) regions (Figures 1A–C). The IM region was defined as 500 μm on each side of the border between the tumor and

TABLE 1 Clinicopathologic characteristics of 82 NSCLC patients.

Clinicopathologic characteristics		Number (%)
Age, years		
	< 65	38(46.3%)
	≥ 65	44(53.7%)
Sex		
	Female	29(35.4%)
	Male	53(64.6%)
Histology		
	Squamous cell carcinoma	23(28.0%)
	Adenocarcinoma	59(72.0%)
TNM		
	I	45(54.9%)
	II	20(24.4%)
	III	17(20.7%)
Tumor size		
	<3cm	54(65.9%)
	≥3cm	28(34.1%)
Tumor location		
	left	30(36.6%)
	right	52(63.4%)
Tumor number		
	Solitary	80(97.6%)
	Multiple	2(2.4%)
Lymph node metastasis		
	Yes	13(15.9%)
	No	69(84.1%)
Differentiation		
	Well/Moderate	26(56.5%)
	Poor	20(43.5%)
Smoking		
	Yes	31(37.8%)
	No	51(62.2%)
Ki67		
	positive	77(93.9%)
	negative	5(6.1%)
P53		
	positive	34(48.6%)
	negative	36(51.4)

normal lung tissue (28). TLS was identified by CD3/CD20 staining on consecutive slides for whole FFPE tumor tissue sections (7, 23). A patient was considered TLS-positive (TLS+) if at least one TLS was observed (19). TLS maturity status was categorized into early TLS (E-TLS) and follicle-formed TLS (F-TLS). E-TLS exhibited diffuse lymphocyte aggregation with scarce CD21+ cells (Figure 1D), while F-TLS showed follicular morphology with CD21+ follicular dendritic cells (FDCs) (Figure 1E) (27, 29). TLS density was calculated as the number of TLS per mm^2 tissue area in IT, IM, and PT regions (30). ROC curves were constructed based on the overall survival and TLS density, with the maximum Youden's index used to determine the optimal TLS density cutoff (Youden's index = sensitivity + specificity -1). Patients were then divided into high and low density groups according to TLS density in each region (23).

Quantification of tumor-infiltrating immune cells

The density of infiltrating lymphocytes was evaluated by two observers (SYX and XPH) using digital slide review. Digital images were scanned using an MVC3000 slide scanner (Mydream Electronic, Shanghai, China) and quantified using the ImageJ software (NIH). Five randomized microscopic fields (20× magnification) were selected and captured from the IT, IM, and PT regions. Cell density was calculated as the mean number of positive cells per field (23).

CD47 expression

To further explore immune characteristics, CD47 expression was assessed. Tumor cells express high levels of CD47 during tumorigenesis, binding to macrophage receptors and leading to immune escape (31, 32). The expression rate of CD47 was calculated as the percentage of CD47-positive cells in the corresponding section area (0-100%). Staining intensity of CD47 was categorized as weak (assignment = 1), moderate (assignment = 2), and strong (assignment = 3). The expression score of CD47 was calculated as (32):

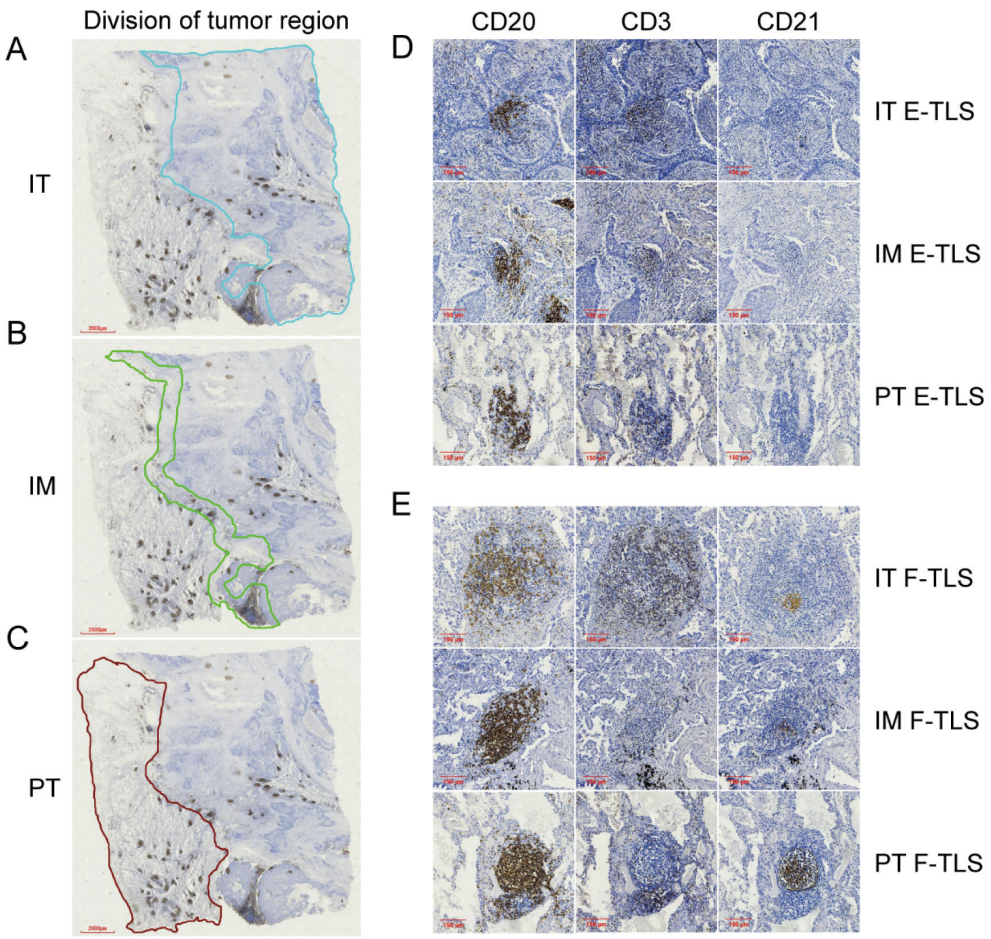

FIGURE 1
The division of tumor region and the maturity of TLS in subregions. **(A)** The region enclosed by the blue line shown is the IT region (4×). **(B)** The region enclosed by the green line shown is the IM region (4×). **(C)** The region enclosed by the brown lines shown is the PT region (4×). **(D)** Image of E-TLS in IT, IM and PT regions (10×). **(E)** Image of F-TLS in IT, IM and PT regions (10×). IT, intratumor region; IM, invasive margin region; PT, peritumor region; F-TLS, secondary TLS; E-TLS, primary TLS.

CD47 score = (percentage of CD47 stained at weak intensity × 1)
+ (percentage of CD47 stained at moderate intensity × 2)
+ (percentage of CD47 stained at strong intensity × 3)

Scores ranged from 0 to 300, with a score of 300 indicating 100% strong positive expression in the tumor region.

Statistical analysis

Statistical analyses were conducted using SPSS 26.0 (IBM) and GraphPad Prism 9 (San Diego, California, USA). Measurement data were expressed as mean ± standard deviation (SD), and counting data were expressed as median (quartile). The t-test or Mann-Whitney U test was used to compare differences in the counting data. Chi-square and continuous correction chi-square tests were used to analyze categorical variables. The optimal TLS density threshold for each subregion was identified using the area under the curve (AUC) of the receiver operating characteristics (ROC) curve. Spearman's rank correlation was used to analyze the correlations between TLS maturation and immune cells. Kaplan-Meier method was used to plot OS and PFS curves, with the log-rank test for comparison. Prognostic risk for NSCLC patients was assessed using univariate and multivariate Cox regression models. Statistical significance was set as $P<0.05$. Based on multivariate Cox regression analyses, a nomogram including the age, sex, IM E-TLS, and tumor-node-metastasis (TNM) stage was used to predict 1-, 3-, and 5-year overall survival probabilities in NSCLC patients.

Results

Density of TLS in different subregions in NSCLC patients

The presence and location of TLSs were initially assessed in IHC-stained sections of NSCLC patients. Out of the 82 patients, only one had no detectable TLS in the specimen. To further evaluate TLS expression, TLS density was examined in various subregions, revealing significant differences in TLS density frequency. The positive rate of TLS in the IT region (90.2%, 74/82) was significantly higher than in the IM (72.0, 59/82) and PT regions (67.1%, 55/82) (Figures 2A–C). As shown in Figure 2D, the average TLS density in the IT region (0.45/mm2) was significantly higher than in the IM (0.18/mm2) and PT regions (0.16/mm2) (P<0.00). Regardless of maturity grade, the density was much higher in the IT region (P<0.001, Figures 2E, F). Additionally, F-TLS had the highest proportion of TLS in the IT region (61.0%, 50/82) compared to the IM (39.0%, 32/82) and PT regions (40.2%, 33/82; P<0.001, Figure 2G).

Association of TLS and clinicopathologic characteristics of patients

The relationship between TLS density and clinicopathological characteristics was further analyzed (Table 2). Higher TLS density in the IT region was detected in tumors with lower TNM stage (P=0.002) or no lymph node metastasis (P=0.034), suggesting an anti-tumor

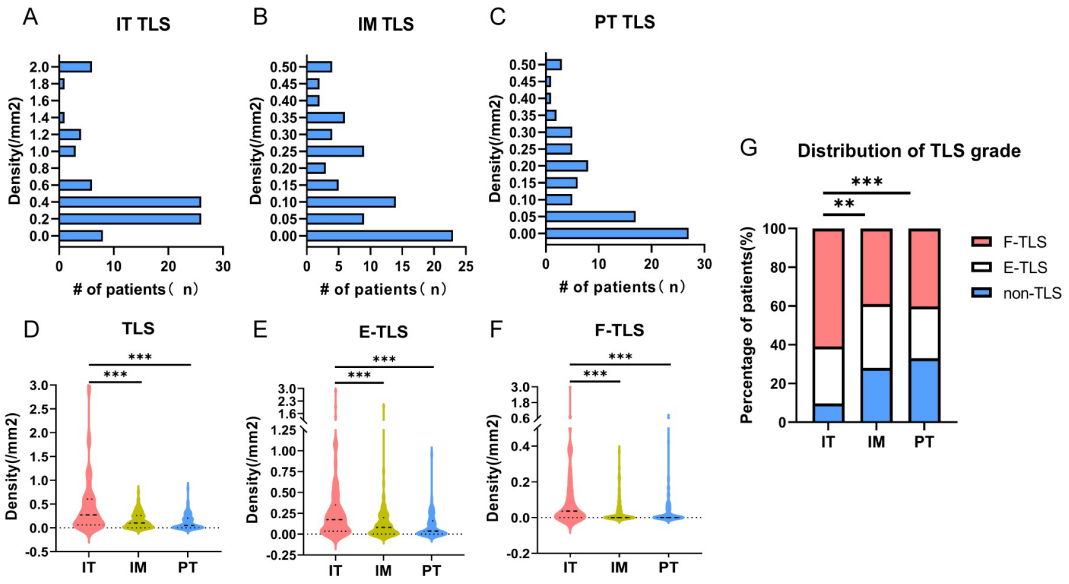

FIGURE 2
Density of TLS in different maturity grades. **(A)** TLS density and frequency of corresponding patients in IT region. **(B)** TLS density in IM region and frequency of corresponding patients. **(C)** TLS density in PT region and frequency of corresponding patients. **(D)** TLS density and differences in IT, IM and PT regions. **(E)** The density and differences of E-TLS in IT, IM and PT regions. **(F)** The density and differences of F-TLS in IT, IM and PT regions. **(G)** Statistics on the proportion of patients without TLS and with E-TLS and F-TLS in IT, IM and PT regions. IT, intratumor region; IM, invasive margin region; PT, peritumor region; F-TLS, secondary TLS; E-TLS, primary TLS; non-TLS, absence of TLS. ** is $P<0.01$, *** is $P<0.001$.

immune identity for TLS in the IT region. Concurrently, increased TLS density in the IM region was associated with squamous cell carcinoma (P=0.005), lymph node metastasis (P=0.013), and smoking history (P=0.045), while higher PT TLS density was mainly in male patients (P=0.001), associated with squamous cell carcinoma (P=0.000), large tumor diameter (P=0.013), smoking history (P=0.004), and absence of P53 (P=0.015), which may indicate that TLS density in the IM and PT regions was associated with adverse factors like tumor growth, invasion, and metastasis. These findings suggest that the density of TLS may be involved in various pathways in the different subregions.

Association between density of TLS and prognosis of NSCLC patients

Given the high positive rates of TLS in the IT, IM, and PT regions (90.2%, 72.0%, and 67.1%, respectively), we first analyzed the impact of TLS presence or absence on patient prognosis but found no clear correlation (Supplementary Figure 1). We then conducted a prognostic analysis of the TLS density, stratifying patients into high and low groups based on the optimal cutoff of the ROC. Only the AUC for IM TLS density reached 0.6 (AUC=0.643, 95%*CI*: 0.521-0.764, Figure 3A). Kaplan-Meier analysis showed that the low IM TLS group was significantly correlated with longer OS and PFS (Figures 3B, C). Considering the different maturity grades of TLS, we further conducted a binary classification of the density of TLS with different maturity grades, revealing that lower density of E-TLS in the IM region was associated with better OS and PFS (Figures 3D–F).

The density of tumor-infiltrating immune cells and its relationship with TLS in subregions

TLS structures and tumor-infiltrating immune cells are important components of the TIME, playing crucial roles in tumor immunity. We

TABLE 2 Relationship between clinicopathologic characteristics and density of TLS in NSCLC patients.

Clinical features		Density of IT TLS (/mm2)	*P* value	Density of IM TLS (/mm2)	*P* value	Density of PT TLS (/mm2)	*P* value
Age, years			0.967		0.959		0.842
	<65	1.52		0.21		0.13	
	≥ 65	0.65		0.15		0.18	
Sex			0.684		0.351		0.001
	Male	1.28		0.21		0.19	
	Female	0.63		0.13		0.10	
Histology			0.606		0.005		0.000
	Squamous cell carcinoma	0.73		0.30		0.30	
	Adenocarcinoma	1.18		0.13		0.10	
TNM			0.002		0.125		0.242
	I	1.74		0.18		0.10	
	II	0.26		0.17		0.21	
	III	0.17		0.20		0.25	
Tumor size			0.118		0.051		0.013
	<3cm	1.33		0.14		0.11	
	≥3cm	0.52		0.27		0.23	
Tumor location			0.885		0.546		0.220
	Left	0.56		0.18		0.12	
	Right	1.34		0.18		0.18	
Tumor number			0.489		0.597		0.939
	Single	1.07		0.18		0.16	
	Multiple	0.16		0.09		0.06	

(Continued)

10.3389/fimmu.2024.1423775

TABLE 2 Continued

Clinical features		Density of IT TLS (/mm2)	*P* value	Density of IM TLS (/mm2)	*P* value	Density of PT TLS (/mm2)	*P* value
Lymph node metastasis			0.034		0.013		0.323
	Yes	0.16		0.30		0.18	
	No	1.22		0.16		0.15	
Differentiation			0.756		0.238		0.088
	Well/Moderate	0.61		0.19		0.14	
	poor	0.25		0.29		0.24	
Smoking			0.368		0.045		0.004
	Yes	0.78		0.26		0.20	
	No	1.22		0.13		0.13	
Ki67			0.764		0.296		0.450
	Positive	1.09		0.18		0.15	
	Negative	0.46		0.11		0.18	
P53			0.837		0.948		0.015
	Positive	1.6		0.17		0.23	
	Negative	0.81		0.22		0.61	

analyzed the density of immune cells in the subregions of NSCLC tumors, revealing that the density of CD20+ B cells, CD3+ T cells, CD8 + cytotoxic T cells, and CD68+ macrophages was higher in the IM region than in the IT and PT regions (Figure 4). Patients were grouped into TLS+ and TLS- categories based on TLS presence in subregions, and differences in immune cells were compared. No significant differences were found between the IT TLS+ and IT TLS- groups (Figure 5A). However, the IM TLS+ group had significantly higher

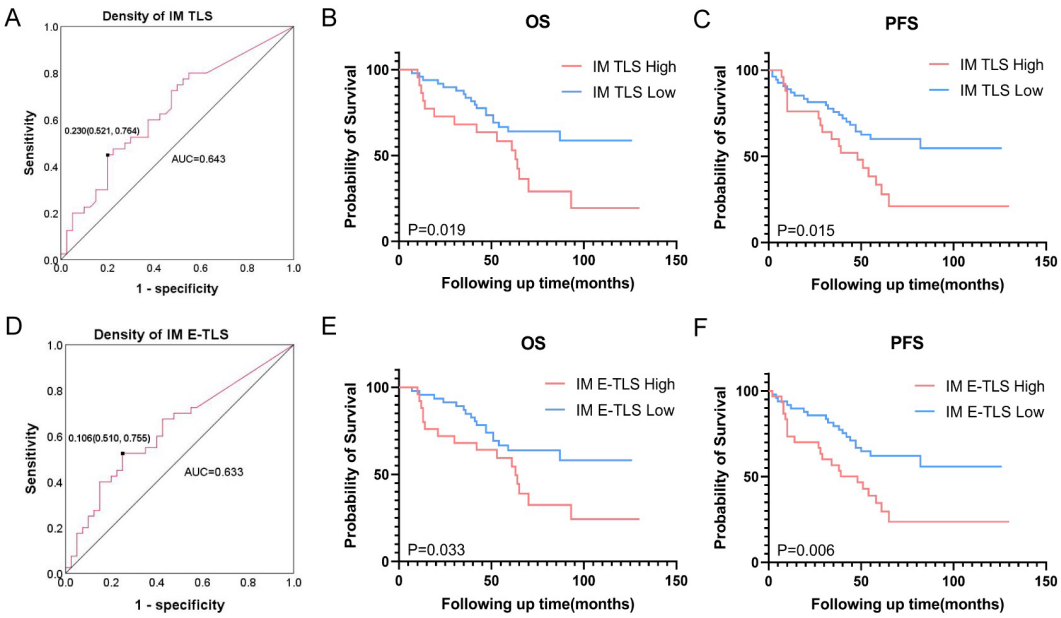

FIGURE 3
Association between density of TLS and prognosis of NSCLC patients. **(A)** ROC curve based on the overall survival rate of NSCLC patients and TLS density in the IM area, the black dot is the best cut-off value. **(B)** Effect of TLS density in IM region on overall survival. **(C)** Effect of TLS density in IM region on progression-free survival. **(D)** ROC curve based on the overall survival rate of NSCLC patients and E-TLS density in the IM area, the black dot is the best cut-off value. **(E)** Effect of E-TLS density in IM region on overall survival. **(F)** Effect of E-TLS density in IM region on progression-free survival. IT, intratumor region; IM, invasive margin region; PT, peritumor region; F-TLS, secondary TLS; E-TLS, primary TLS.

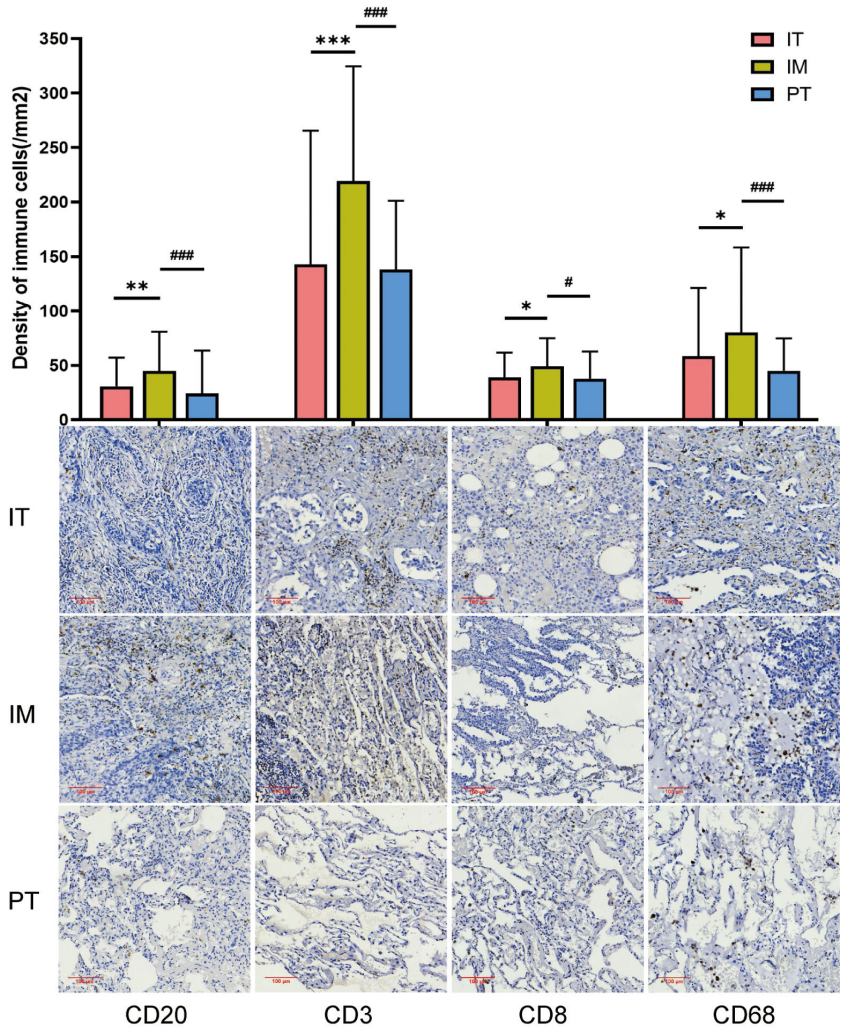

FIGURE 4
The density of immune cells in different regions. IT, intratumor region; IM, invasive margin region; PT, peritumor region; F-TLS, secondary TLS; E-TLS, primary TLS. *: compared with IT region, $P<0.05$; **: compared with IT region, $P<0.01$; ***: compared with IT region, $P<0.001$; #: compared with IM region, $P<0.05$; ###: compared with IM region, $P<0.001$.

densities of CD20+ B cells and CD3+ T cells than the IM TLS- group ($P=0.000$ and $P=0.047$, Figure 5B). The PT TLS+ group had significantly higher densities of CD20+ B cells, CD3+ T cells, CD8+ cytotoxic T cells, and CD68+ macrophages than the PT TLS- group ($P=0.004$, $P=0.003$, $P=0.049$, $P=0.000$, Figure 5C).

Association between tumor-infiltrating immune cells and different maturity status of TLS in subregions

We further analyzed the role of tumor-infiltrating immune cells in TLS maturation by comparing immune cell densities between E-TLS and F-TLS groups in subregions. As shown in Figure 6A, in the IT region, the densities of CD20+ B cells and CD8+ T cells were significantly higher in the F-TLS group than in the E-TLS group ($P=0.004$ and $P=0.024$, respectively). No statistical difference was observed in the IM and PT regions (Figures 6B, C).

Correlation between TLS and immune cells

We further analyzed the correlation between immune cell densities and TLS density to determine their connection. CD20+ B cell density was significantly correlated with TLS density in the IM and PT regions ($R^2 = 0.31$, $P<0.0001$; $R^2 = 0.53$, $P<0.0001$; Figures 7A–C). The correlation was more significant between the E-TLS (Supplementary Figure 2). CD3+ T cell density was significantly correlated with TLS density in all three regions ($R^2 = 0.08$, $P=0.0115$; $R^2 = 0.07$, $P=0.0129$; $R^2 = 0.26$, $P<0.0001$; Figures 7D–F). Further analysis revealed significant correlations between CD20+ B cells, CD3+ T cells, and TLS density in the three regions, while CD8+ T cells correlated significantly with total TLS and F-TLS density in the IT region, and CD68+ macrophages with total TLS and E-TLS density in the PT region (Figure 7H). Prognostic analysis showed that none of the immune cells was associated with prognosis in the IT region. In the IM region, lower density of CD20+ B cells, lower CD8/CD3 ratio, and higher density

10.3389/fimmu.2024.1423775

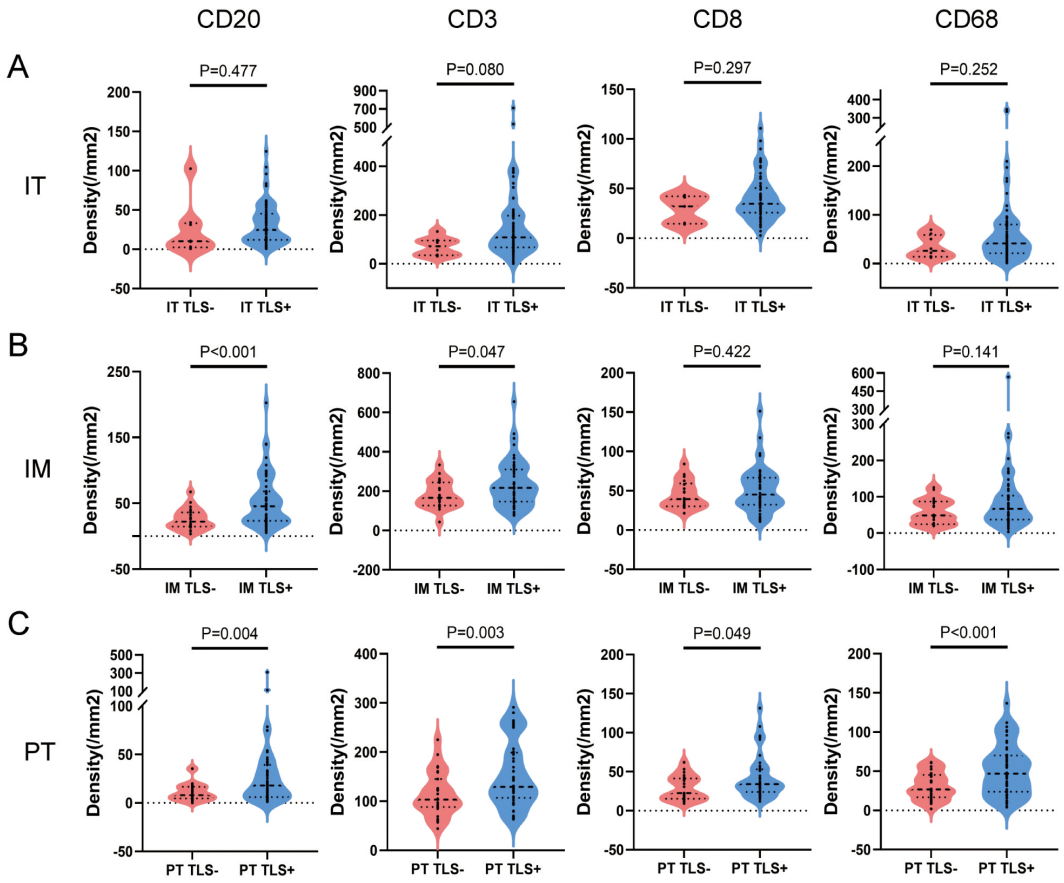

FIGURE 5
The difference of immune cells between TLS+ and TLS- patients in subregions. **(A)** Patients were divided into IT TLS+ group and IT TLS- group according to the presence or absence of TLS in IT area. Independent sample T test was conducted to analyze the density differences of CD20+ B cells, CD3+ T cells, CD8+ T cells and CD68+ macrophages in IT area between the two groups. **(B)** Patients were divided into IM TLS+ group and IM TLS- group according to the presence or absence of TLS in IM region. Independent sample T test was conducted to analyze the density differences of CD20+ B cells, CD3+ T cells, CD8+ T cells and CD68+ macrophages in IM region between the two groups. **(C)** Patients were divided into the TLS+ group and the TLS- group according to the presence or absence of TLS in the PT area. The density differences of CD20+ B cells, CD3+ T cells, CD8+ T cells and CD68+ macrophages in the PT area were analyzed by independent sample T test. IT, intratumor region; IM, invasive margin region; PT, peritumor region.

of CD3+ T cells were associated with better prognosis. In the PT region, lower density of CD20+ B cells was associated with better prognosis (Supplementary Figure 3).

CD47 scores, associated with the immune escape, were significantly higher in the IT (mean score 36.34) and IM regions (mean score 39.02) than in the PT region (mean score 6.59), with no significant difference between IT and IM regions (Figure 7G). No significant correlation was observed between CD47 scores and TLS density in the IT, IM, and PT regions (Figure 7H).

Density of IM E-TLS as an independent prognostic factor for overall survival

Univariate Cox regression analysis identified histology, lymph node metastasis, tumor size, TNM stage, and IM TLS and IM E-TLS density as significant prognostic factors. Multivariate analysis confirmed that TNM stage and IM E-TLS can serve as independent prognostic factors for overall survival (all $P<0.05$), while other clinicopathological variables showed no consistent significance (Figure 8).

Nomogram predicted 1-, 3- and 5-year OS in NSCLC patients

Based on multivariate Cox regression analysis, a nomogram prognostic model was established, including IM E-TLS and TNM stage as predictors, along with patient age and sex based on our clinical experience (Figure 9A). The nomogram demonstrated good predictive performance for overall survival in NSCLC patients (Figures 9B–E).

Discussion

Our study comprehensively analyzed the density of TLS at different maturity statuses across various subregions and their

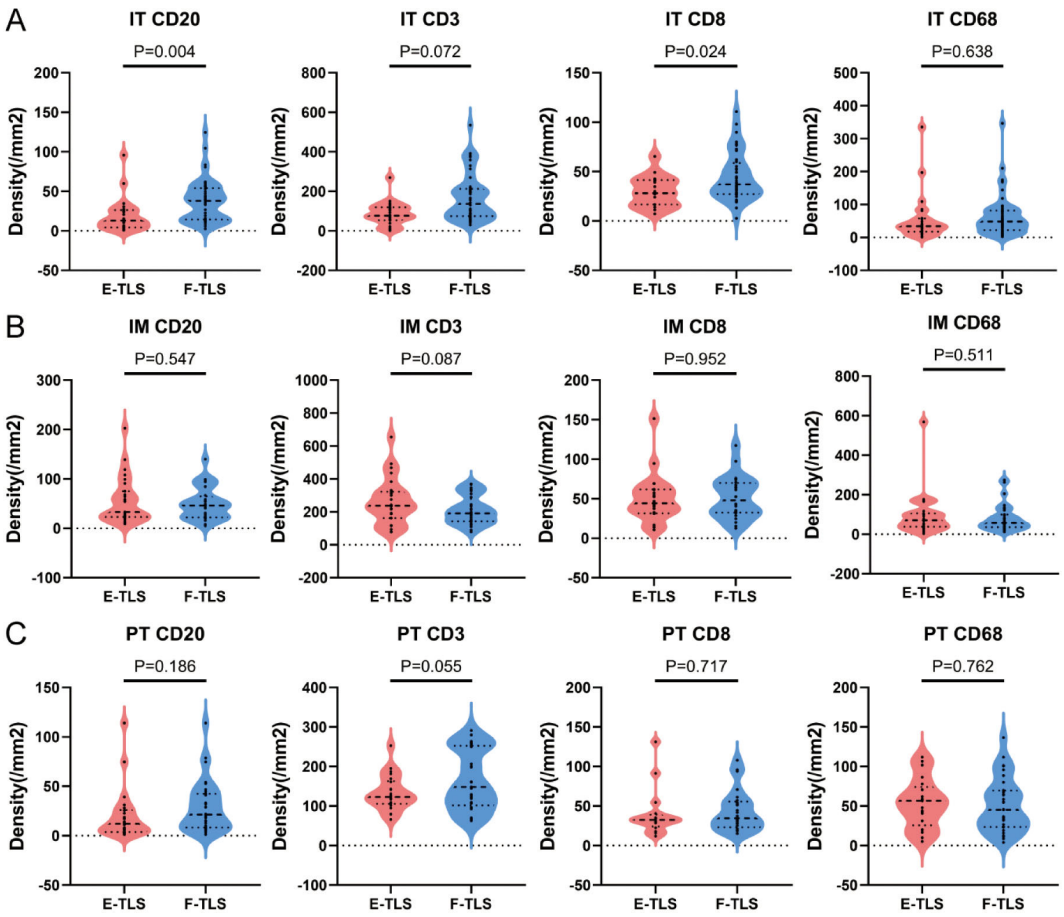

FIGURE 6
The difference between immune cells with different maturity of TLS. **(A)** Patients were divided into E-TLS group and F-TLS group according to TLS maturation status in IT region. Independent sample T test was conducted to analyze the density differences of CD20+ B cells, CD3+ T cells, CD8+ T cells and CD68+ macrophages in IT area between the two groups. **(B)** Patients were divided into E-TLS group and F-TLS group according to TLS maturation status in IM region. Independent sample T test was conducted to analyze the density differences of CD20+ B cells, CD3+ T cells, CD8+ T cells and CD68+ macrophages in IM region between the two groups. **(C)** Patients were divided into E-TLS group and F-TLS group according to TLS maturation status in the PT region. Independent sample T test was conducted to analyze the density differences of CD20+ B cells, CD3+ T cells, CD8+ T cells and CD68+ macrophages in the PT region between the two groups. IT, intratumor region; IM, invasive margin region; PT, peritumor region; F-TLS, secondary TLS; E-TLS, primary TLS.

correlation with the prognosis of NSCLC patients. Moreover, we plotted a nomogram incorporating IM E-TLS, TNM stage, age, and sex to predict patient prognosis. We found a high detection rate of TLS in NSCLC patients (98.8%), with higher density in the IT region compared to the IM and PT regions. Mature TLS had a significantly higher proportion in the IT region than in the other two regions. Based on previous studies, the presence of GC in mature TLS is an important starting point for anti-tumor immune response, we hypothesized that the anti-tumor immunity in the IT region of tumors is stronger than in the other two regions (33).

Our analysis of clinical data from NSCLC patients demonstrated that higher TLS density in the IT region was associated with lower TNM stage and absence of lymph node metastasis, indicating an accumulation of TLS in early-stage NSCLC and better prognosis. By contrast, increased TLS density in the IM and PT regions was associated with adverse prognostic factors such as tumor growth, invasion, and metastasis, suggesting a negative impact on prognosis. Intriguingly, while many studies have argued for a positive prognostic effect of TLS in lung cancer (34, 35), our study found that IT and PT TLS density at any maturity status was not predictive of prognosis. Higher density of TLS in the IM region was associated with worse prognosis in NSCLC patients. Furthermore, high density of E-TLS in the IM region was an independent risk factor for overall survival, possibly due to the absence of a germinal center, rendering TLS less effective (19, 36).

Tumor-infiltrating immune cells may play an important role in TIME and TLS development. We observed the highest proportion of these cells in the IM region, consistent with the findings by Zhu et al. (37). The IM region, as the interface between intra-tumor and peri-tumor tissues, is the front line of tumor invasion. When immune aggregation occurs here, it reflects an active anti-tumor immune response. Although previous studies proposed that the infiltration of immune cells within tumors was higher than that in the peri-tumor region and could be further correlated with better prognosis (38–40), we found higher densities of CD20+ B cells, CD3+ T cells, CD8+ cytotoxic T cells, and CD68+ macrophage cells

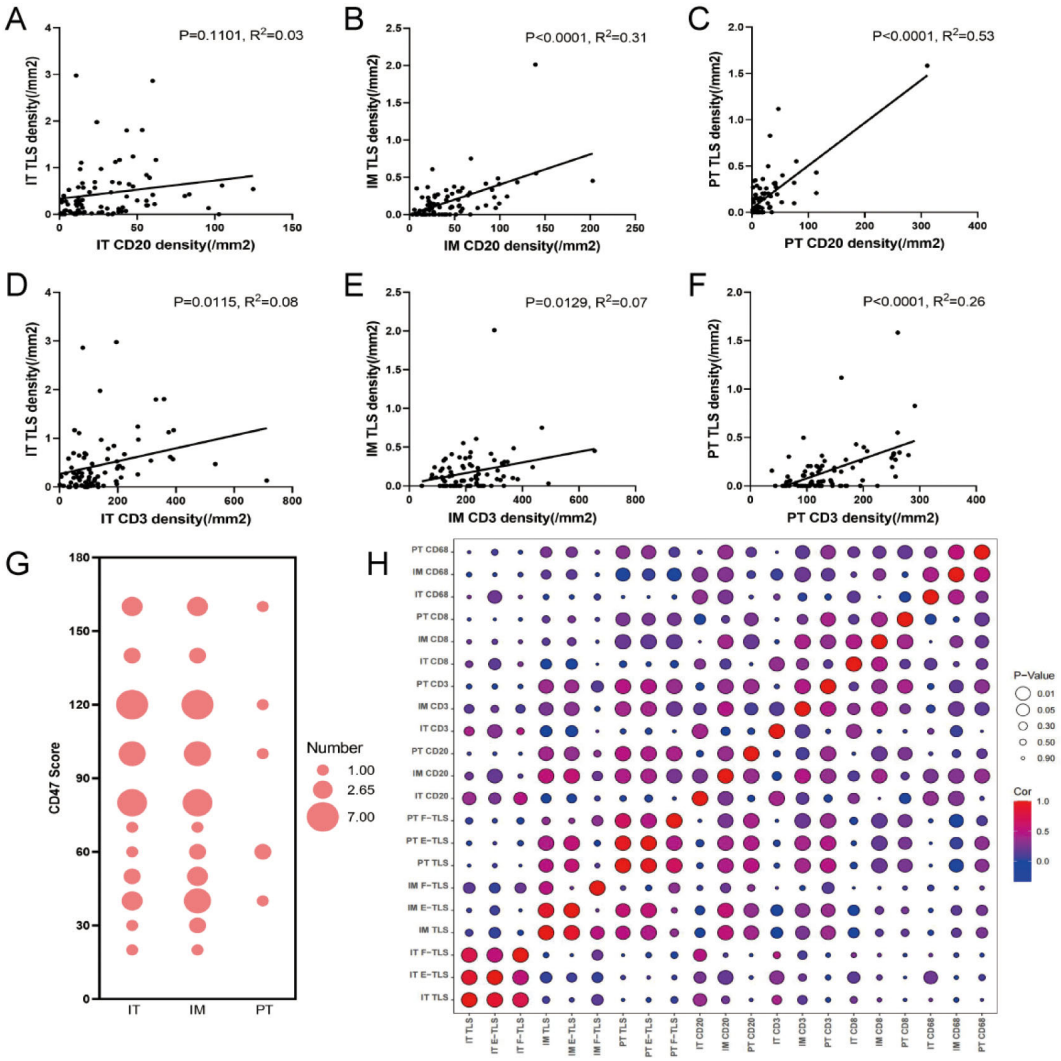

FIGURE 7
Correlation between the density of immune cells and TLS. **(A–C)** General linear regression analysis was performed to determine the correlation between CD20+ B cells in IT, IM and PT regions and TLS density in the corresponding regions. **(D–F)** General linear regression analysis was performed to determine the correlation between CD3+ T cells in IT, IM and PT regions and TLS density in the corresponding regions. **(G)** The bubble chart shows the CD47 scores in the IT, IM and PT regions (the size of the circle indicates the score frequency). **(H)** The bubble map shows the correlation between TLS at different maturation states in IT, IM and PT regions and immune cells in each region (red indicates positive correlation coefficient, blue indicates negative correlation coefficient, and purple indicates close to 0 correlation coefficient; The larger the circle, the more significant the correlation, and the smaller the circle, the weaker the correlation). IT, intratumor region; IM, invasive margin region; PT, peritumor region; F-TLS, secondary TLS; E-TLS, primary TLS.

in the IM region compared to the IT and PT regions, with CD20+ B cell density associated with better prognosis and CD8+/CD3+ ratio with poorer prognosis. We hypothesize that previous studies merging the invasive edge (IM region) with the IT region might have led to different findings. Therefore, in this study, when the IM region was separated from the IT region, a high number of immune cells could be detected in this region.

Given that the IM region had significant association with patient prognosis and obvious immune cell infiltration, our study focused on this region. Just like some of the previous studies, we also found that the density of CD20+ B cells and CD3+ T cells was most closely related to prognosis and immunotherapy response (41–43). These cells were significantly correlated with the presence of TLS, suggesting their role in TLS formation. Notably, the density of CD20+ B cells and CD3+ T cells in the IM region was only positively correlated with the density of E-TLS but not with the presence or density of F-TLS, suggesting that these immune cells are not involved in the maturation of TLS in this region. However, in the PT region, the density of these cells was higher in the tissues in the presence of F-TLS and positively correlated with the density of F-TLS, implying their involvement in TLS development and maturation in peri-tumoral tissues. This contrast highlights that CD20+ B cells and CD3+ T cells participate in TLS formation but are inhibited in TLS maturation in the IM region, leading to high E-TLS density in the IM region.

This study suggests a potential immunosuppressive state in the IM region, based on two main observations. Firstly, the IM region

Variables	Categories	Univariate analysis		Multivariate analysis	
		HR (95% CI)	*P* value	*HR* (95% CI)	*P* value
Age, y	⩾ 65 vs < 65	1.517(0.799-2.879)	0.203		
Sex	Male vs Female	0.870(0.454-1.669)	0.675		
Tumor location	Right vs Left	0.760(0.407-1.416)	0.387		
Tumor number	Multiple vs Solitary	0.047(0.000-140.725)	0.454		
Differentiation	Well/Moderate vs Poor	0.541(0.250-1.173)	0.12		
Smoking	Yes vs No	1.430(0.766-2.672)	0.262		
Ki67	Positive vs Negative	0.623(0.150-2.593)	0.515		
P53	Positive vs Negative	0.937(0.483-1.820)	0.848		
IM F-TLS	High vs Low	1.540(0.817-2.904)	0.182		
Histology	LUSC vs LUAD	0.514(0.274-0.964)	0.038		
Lymphnode metastasis	Yes vs No	2.435(1.187-4.996)	0.015		
Tumor size	⩾ 3cm vs < 3cm	1.987(1.066-3.704)	0.031		
IM TLS	High vs Low	2.067(1.106-3.861)	0.023		
TNM			0.01		0.042
	I vs II+III	0.925(0.416-2.055)	0.848	0.982(0.440-2.194)	0.965
	III vs I+II	2.519(1.116-5.687)	0.026	2.328(1.112-4.868)	0.025
IM E-TLS	High vs Low	2.188(1.174-4.079)	0.014	1.951(1.031-3.689)	0.040

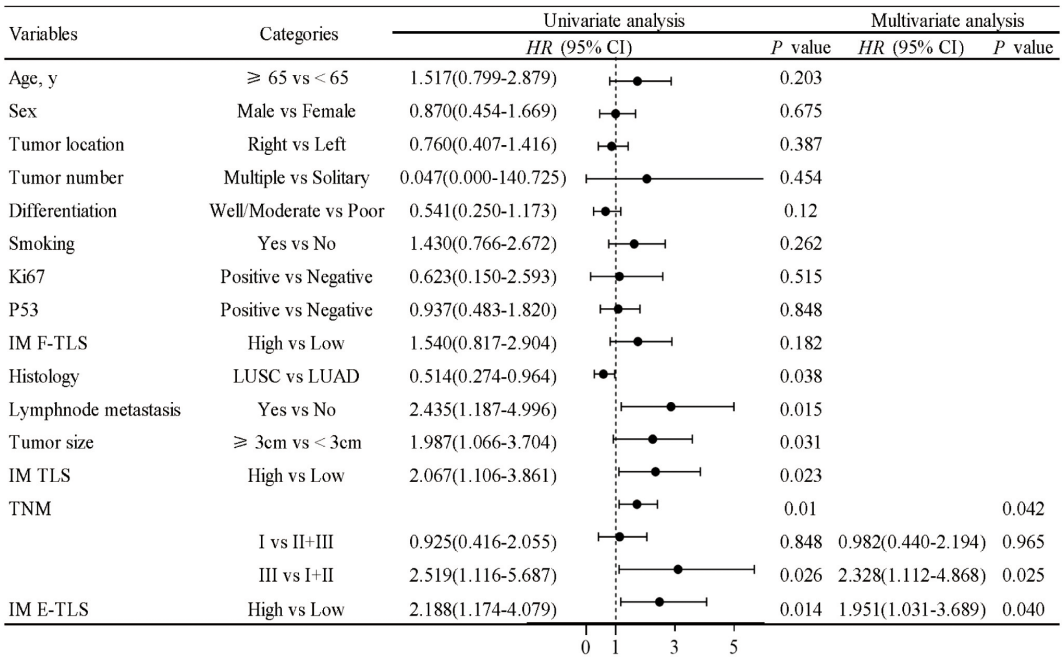

FIGURE 8
COX proportional hazard regression model for overall survival of NSCLC. A univariate Cox regression analysis was performed on the clinical characteristics and the density of TLS in NSCLC patients. P<0.05 was taken as the threshold to screen out prognostic factors. The relevant factors were included in the multivariate analysis for predicting overall survival (all *P*<0.05).

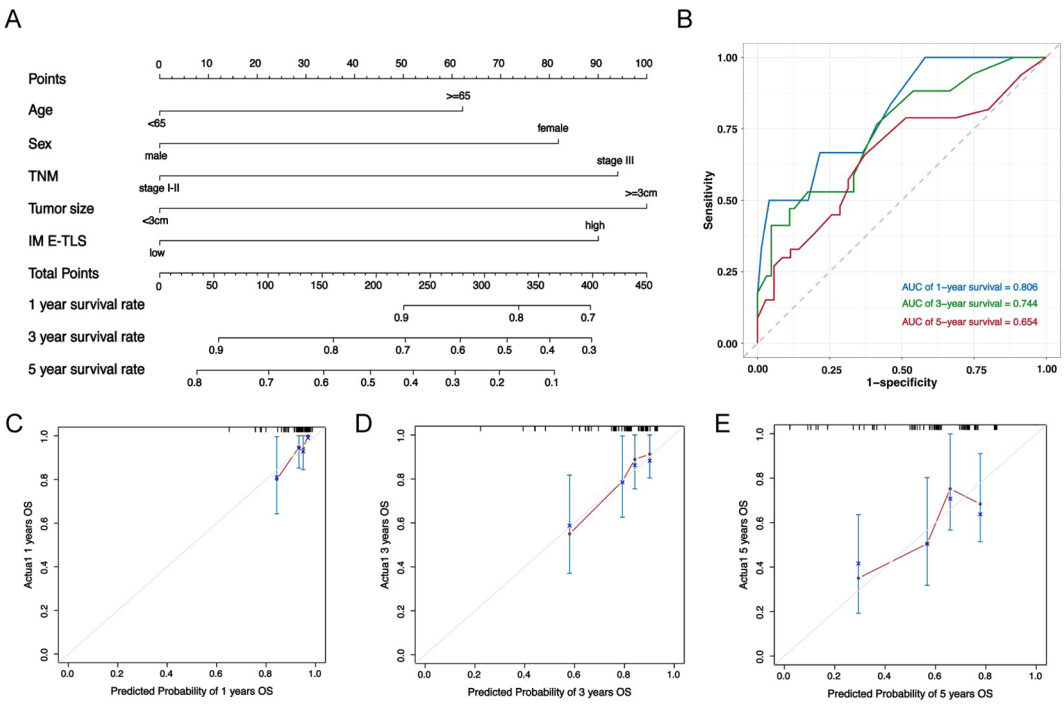

FIGURE 9
Nomogram predicted the overall survival of NSCLC patients. **(A)** Nomogram was plotted based on four factors: age, sex, density of IM E-TLS and TNM grade, and 1-, 3- and 5-years of OS could be predicted. The probabilities were estimated as the sum of points for each variable as a function of total points. Each variable obtained an integral by drawing a line up from the corresponding value to the 'point' line. On the "total points" line, the total sum of points added by each variable was shown. A line was drawn downward to read the associated probability forecasts. The Bootstrap method was used for internal validation, with 200 repeat samples. **(B)** ROC curve to verify nomogram model performance. **(C–E)** Calibration curves of a nomogram to predict OS at 1-, 3- and 5 years in this data set.

displayed high density of E-TLS. Previous studies have shown that the presence of E-TLS is associated with the immunosuppressive state of the tumor immune microenvironment. When E-TLS is formed in large quantities, immature immune cells often differentiate into immunosuppressive cells (such as regulatory B cells), and in the early stage of disease or after immunotherapy, the production of E-TLS in tumor microenvironment is associated with the expression of immunosuppressive genes and poor prognosis (44–46). CD8+ T cells are the main anti-tumor immune cells associated with favorable prognosis in various tumors, and their immune function can be inhibited by regulatory B cells, which further contributes to the functional suppression of anti-tumor immune cells in the IM region (47, 48). Secondly, we observed a high H-score for CD47 in the IM region. As a marker of immunologically privileged cells, CD47 can be expressed by stromal cells, red blood cells, endothelial cells and other body cells. During tumor progression, high density of tumor cells express CD47 and bind to the corresponding receptors on macrophages to evade the immune system (49). The high density of CD47 in the IM region suggests an immunosuppressive state in this region (50).

Our study demonstrated a correlation between the density of E-TLS in the IM region and prognosis in NSCLC patients, as well as the immune characteristics of the IM region. Studies have found that the IM region of liver cancer is the lesion front for tumor invasion of normal tissues, where the density of immunosuppressive genes is significantly increased (46). Our study found a high density of immune cells and high expression of CD47 in the IM region, suggesting that the anti-tumor immune ability of immune cells may be inhibited, and also proved that the immunosuppressive state of the IM region of NSCLC tumors, and proposed that this immunosuppressive state may be related to the abnormal participation of B cells and T cells in the high density of E-TLS during TLS maturation in the IM region. Currently, it is not clear why large amounts of E-TLS are produced in such early tissue lesions. However, the causal relationship between E-TLS and local immunosuppression remains uncertain. It is also unclear whether E-TLS is the cause or result of local suppression of immune cells in the tissue, whether the mass aggregation of tumor-infiltrating immune cells in the IM region is a manifestation of anti-tumor immunoactivation or compensatory proliferation after immunosuppression, and whether its density can represent the expression and function of cells. These questions require further investigation in future research.

Due to the non-specific early clinical manifestations of NSCLC and the low diagnostic rate, obtaining early tissue samples from patients for research is challenging. We believe that in the future, we can verify our conclusions by multicenter studies and expanding the sample size to discuss the expression and distribution characteristics of TLS in early and advanced NSCLC patients, especially patients at TNM stage I, to clarify the density and distribution characteristics of TLS in the tumor tissues of early NSCLC lesions. Another limitation of this study was the lack of external validation for the nomogram prediction model and the absence of sample data for tumor tripartite in the online database. This again calls for multicenter clinical studies that should be performed to validate our findings. Our study also suggested that future studies should sequence the expression of immune-related genes in the IT, IM, and PT regions. Comparing the upregulation or inhibition of immune-related genes among the three regions, rather than relying solely on immune cell density as a functional indicator, would enable a more comprehensive evaluation of the immunomodulatory effects of tumor-related tissues during tumor development and invasion. This would offer a valuable reference for improving NSCLC immunotherapy.

Conclusion

In summary, we found that TLS had a high positivity rate in patients with NSCLC. Although TLS had the highest density in the IT region, its density in the IM region was most closely associated with the patient prognosis. A nomogram, including age, sex, IM E-TLS, and tumor-node-metastasis (TNM) stage, was created to predict 1-, 3-, and 5-year overall survival probabilities in NSCLC patients. A higher density of E-TLS in the IM region was associated with poorer prognosis of NSCLC patients, which we believe is linked to the immunosuppressive state in the IM region.

Data availability statement

The raw data supporting the conclusions of this article will be made available by the authors, without undue reservation.

Ethics statement

The studies involving humans were approved by Dalian Friendship Hospital Ethics Committee. The studies were conducted in accordance with the local legislation and institutional requirements. The ethics committee/institutional review board waived the requirement of written informed consent for participation from the participants or the participants' legal guardians/next of kin because this is a noninterventional retrospective study.

Author contributions

SX: Data curation, Formal analysis, Investigation, Methodology, Software, Writing – original draft. SW: Data curation, Methodology, Visualization, Writing – review & editing. PH: Data curation, Formal analysis, Investigation, Software, Writing – review & editing. YZ: Data curation, Investigation, Methodology, Software, Writing – review & editing. HZ: Conceptualization, Funding acquisition, Investigation, Methodology, Project administration, Resources, Writing – review & editing.

Funding

The author(s) declare financial support was received for the research, authorship, and/or publication of this article. This work was supported by the United Fund of the Second Hospital of Dalian Medical University and Dalian Institute of Chemical Physics,

Chinese Academy of Sciences (UF-ZD-202011), and Project of Science and Technology of Liaoning Province (2023-MS-272).

Acknowledgments

The authors thank the staff in the Department of Pathology, The Friendship Hospital of Dalian, and all patients involved in this study for their support.

Conflict of interest

The authors declare that the research was conducted in the absence of any commercial or financial relationships that could be construed as a potential conflict of interest.

Publisher's note

Supplementary material

The Supplementary Material for this article can be found online at: https://www.frontiersin.org/articles/10.3389/fimmu.2024.1423775/full#supplementary-material

References

1. Duma N, Santana-Davila R, Molina JR. Non-small cell lung cancer: epidemiology, screening, diagnosis, and treatment. *Mayo Clin Proc*. (2019) 94(8):1623–40. doi: 10.1016/j.mayocp.2019.01.013

2. Huang J, Deng Y, Tin MS, Lok V, Ngai CH, Zhang L, et al. Distribution, risk factors, and temporal trends for lung cancer incidence and mortality: A global analysis. *Chest*. (2022) 161:1101–11. doi: 10.1016/j.chest.2021.12.655

3. Kamer I, Bab-Dinitz E, Zadok O, Ofek E, Gottfried T, Daniel-Meshulam I, et al. Immunotherapy response modeling by ex-vivo organ culture for lung cancer. *Cancer Immunol Immunother*. (2021) 70:2223–34. doi: 10.1007/s00262-020-02828-w

4. Hwang JY, Randall TD, Silva-Sanchez A. Inducible bronchus-associated lymphoid tissue: taming inflammation in the lung. *Front Immunol*. (2016) 7:258. doi: 10.3389/fimmu.2016.00258

5. Ruddle NH. Basics of inducible lymphoid organs. *Curr Top Microbiol Immunol*. (2020) 426:1–19. doi: 10.1007/82_2020_218

6. Rodriguez AB, Peske JD, Woods AN, Leick KM, Mauldin IS, Meneveau MO, et al. Immune mechanisms orchestrate tertiary lymphoid structures in tumors via cancer-associated fibroblasts. *Cell Rep*. (2021) 36:109422. doi: 10.1016/j.celrep.2021.109422

7. Sautès-Fridman C, Petitprez F, Calderaro J, Fridman WH. Tertiary lymphoid structures in the era of cancer immunotherapy. *Nat Rev Cancer*. (2019) 19:307–25. doi: 10.1038/s41568-019-0144-6

8. Dieu-Nosjean MC, Giraldo NA, Kaplon H, Germain C, Fridman WH, Sautès-Fridman C. Tertiary lymphoid structures, drivers of the anti-tumor responses in human cancers. *Immunol Rev*. (2016) 271:260–75. doi: 10.1111/imr.12405

9. Germain C, Gnjatic S, Tamzalit F, Knockaert S, Remark R, Goc J, et al. Presence of B cells in tertiary lymphoid structures is associated with a protective immunity in patients with lung cancer. *Am J Respir Crit Care Med*. (2014) 189:832–44. doi: 10.1164/rccm.201309-1611OC

10. Germain C, Devi-Marulkar P, Knockaert S, Biton J, Kaplon H, Letaïef L, et al. Tertiary lymphoid structure-B cells narrow regulatory T cells impact in lung cancer patients. *Front Immunol*. (2021) 12:626776. doi: 10.3389/fimmu.2021.626776

11. Jacquelot N, Tellier J, Nutt SL, Belz GT. Tertiary lymphoid structures and B lymphocytes in cancer prognosis and response to immunotherapies. *Oncoimmunology*. (2021) 10:1900508. doi: 10.1080/2162402X.2021.1900508

12. Delvecchio FR, Fincham REA, Spear S, Clear A, Roy-Luzarraga M, Balkwill FR, et al. Pancreatic cancer chemotherapy is potentiated by induction of tertiary lymphoid structures in mice. *Cell Mol Gastroenterol Hepatol*. (2021) 12:1543–65. doi: 10.1016/j.jcmgh.2021.06.023

13. Dieu-Nosjean MC, Goc J, Giraldo NA, Sautès-Fridman C, Fridman WH. Tertiary lymphoid structures in cancer and beyond. *Trends Immunol*. (2014) 35:571–80. doi: 10.1016/j.it.2014.09.006

14. Wen S, Chen Y, Hu C, Du X, Xia J, Wang X, et al. Combination of tertiary lymphoid structure and neutrophil-to-lymphocyte ratio predicts survival in patients with hepatocellular carcinoma. *Front Immunol*. (2021) 12:788640. doi: 10.3389/fimmu.2021.788640

15. Posch F, Silina K, Leibl S, Mündlein A, Moch H, Siebenhüner A, et al. Maturation of tertiary lymphoid structures and recurrence of stage ii and iii colorectal cancer. *Oncoimmunology*. (2018) 7:e1378844. doi: 10.1080/2162402X.2017.1378844

16. JG A, Rajamanickam V, Bui C, Bernard B, Pucilowska J, Ballesteros-Merino C, et al. Germinal center reactions in tertiary lymphoid structures associate with neoantigen burden, humoral immunity and long-term survivorship in pancreatic cancer. *Oncoimmunology*. (2021) 10:1900635. doi: 10.1080/2162402X.2021.1900635

17. Zhang WH, Wang WQ, Han X, Gao HL, Xu SS, Li S, et al. Infiltrating pattern and prognostic value of tertiary lymphoid structures in resected non-functional pancreatic neuroendocrine tumors. *J Immunother Cancer*. (2020) 8(2):e001188. doi: 10.1136/jitc-2020-001188

18. Fukuhara M, Muto S, Inomata S, Yamaguchi H, Mine H, Takagi H, et al. The clinical significance of tertiary lymphoid structure and its relationship with peripheral blood characteristics in patients with surgically resected non-small cell lung cancer: A single-center, retrospective study. *Cancer Immunol Immunother*. (2022) 71:1129–37. doi: 10.1007/s00262-021-03067-3

19. Siliņa K, Soltermann A, Attar FM, Casanova R, Uckeley ZM, Thut H, et al. Germinal centers determine the prognostic relevance of tertiary lymphoid structures and are impaired by corticosteroids in lung squamous cell carcinoma. *Cancer Res*. (2018) 78:1308–20. doi: 10.1158/0008-5472.CAN-17-1987

20. Li K, Guo Q, Zhang X, Dong X, Liu W, Zhang A, et al. Oral cancer-associated tertiary lymphoid structures: gene expression profile and prognostic value. *Clin Exp Immunol*. (2020) 199:172–81. doi: 10.1111/cei.13389

21. Ding GY, Ma JQ, Yun JP, Chen X, Ling Y, Zhang S, et al. Distribution and density of tertiary lymphoid structures predict clinical outcome in intrahepatic cholangiocarcinoma. *J Hepatol*. (2022) 76:608–18. doi: 10.1016/j.jhep.2021.10.030

22. Finkin S, Yuan D, Stein I, Taniguchi K, Weber A, Unger K, et al. Ectopic lymphoid structures function as microniches for tumor progenitor cells in hepatocellular carcinoma. *Nat Immunol*. (2015) 16:1235–44. doi: 10.1038/ni.3290

23. Li H, Liu H, Fu H, Li J, Xu L, Wang G, et al. Peritumoral tertiary lymphoid structures correlate with protective immunity and improved prognosis in patients with hepatocellular carcinoma. *Front Immunol*. (2021) 12:648812. doi: 10.3389/fimmu.2021.648812

24. Derks S, de Klerk LK, Xu X, Fleitas T, Liu KX, Liu Y, et al. Characterizing diversity in the tumor-immune microenvironment of distinct subclasses of gastroesophageal adenocarcinomas. *Ann Oncol*. (2020) 31:1011–20. doi: 10.1016/j.annonc.2020.04.011

25. Deguchi S, Tanaka H, Suzuki S, Natsuki S, Mori T, Miki Y, et al. Clinical relevance of tertiary lymphoid structures in esophageal squamous cell carcinoma. *BMC Cancer*. (2022) 22:699. doi: 10.1186/s12885-022-09777-w

26. Lin JR, Wang S, Coy S, Chen YA, Yapp C, Tyler M, et al. Multiplexed 3d atlas of state transitions and immune interaction in colorectal cancer. *Cell*. (2023) 186:363–81.e19. doi: 10.1016/j.cell.2022.12.028

27. Schumacher TN, Thommen DS. Tertiary lymphoid structures in cancer. *Science*. (2022) 375:eabf9419. doi: 10.1126/science.abf9419

28. Hu C, Zhao L, Liu W, Fan S, Liu J, Liu Y, et al. Genomic profiles and their associations with tmb, pd-L1 expression, and immune cell infiltration landscapes in synchronous multiple primary lung cancers. *J Immunother Cancer*. (2021) 9(12):e003773. doi: 10.1136/jitc-2021-003773

29. Fridman WH, Sibéril S, Pupier G, Soussan S, Sautès-Fridman C. Activation of B cells in tertiary lymphoid structures in cancer: anti-tumor or anti-self? *Semin Immunol*. (2023) 65:101703. doi: 10.1016/j.smim.2022.101703

30. Sofopoulos M, Fortis SP, Vaxevanis CK, Sotiriadou NN, Arnogiannaki N, Ardavanis A, et al. The prognostic significance of peritumoral tertiary lymphoid structures in breast cancer. *Cancer Immunol Immunother*. (2019) 68:1733–45. doi: 10.1007/s00262-019-02407-8

31. Hu LY, Zhuang WT, Chen MJ, Liao J, Wu DF, Zhang YX, et al. Egfr Oncogenic Mutations in Nsclc Impair Macrophage Phagocytosis and Mediate Innate Immune Evasion through up-Regulation of Cd47. *J Thorac Oncol*. (2024) 19(8):1186–200. doi: 10.1016/j.jtho.2024.03.019

32. Yordanov A, Shivarov V, Kostov S, Ivanova Y, Dimitrova P, Popovska S, et al. Prognostic utility of cd47 in cancer of the uterine cervix and the sensitivity of immunohistochemical scores. *Diagnostics (Basel)*. (2022) 13(1):52. doi: 10.3390/diagnostics13010052

33. Ng KW, Boumelha J, Enfield KSS, Almagro J, Cha H, Pich O, et al. Antibodies against endogenous retroviruses promote lung cancer immunotherapy. *Nature*. (2023) 616:563–73. doi: 10.1038/s41586-023-05771-9

34. Xu X, Gao Y, Duan S, Ding Q, Wang X, Dai X, et al. Clinical implications and molecular features of tertiary lymphoid structures in stage I lung adenocarcinoma. *Cancer Med*. (2023) 12:9547–58. doi: 10.1002/cam4.5731

35. Zhao H, Wang H, Zhao Y, Sun Q, Ren X. Tumor-resident T cells, associated with tertiary lymphoid structure maturity, improve survival in patients with stage iii lung adenocarcinoma. *Front Immunol*. (2022) 13:877689. doi: 10.3389/fimmu.2022.877689

36. de Chaisemartin L, Goc J, Damotte D, Validire P, Magdeleinat P, Alifano M, et al. Characterization of chemokines and adhesion molecules associated with T cell presence in tertiary lymphoid structures in human lung cancer. *Cancer Res*. (2011) 71:6391–9. doi: 10.1158/0008-5472.CAN-11-0952

37. Zhu W, Germain C, Liu Z, Sebastian Y, Devi P, Knockaert S, et al. A high density of tertiary lymphoid structure B cells in lung tumors is associated with increased cd4(+) T cell receptor repertoire clonality. *Oncoimmunology*. (2015) 4:e1051922. doi: 10.1080/2162402X.2015.1051922

38. Federico L, McGrail DJ, Bentebibel SE, Haymaker C, Ravelli A, Forget MA, et al. Distinct tumor-infiltrating lymphocyte landscapes are associated with clinical outcomes in localized non-small-cell lung cancer. *Ann Oncol*. (2022) 33:42–56. doi: 10.1016/j.annonc.2021.09.021

39. Dai F, Liu L, Che G, Yu N, Pu Q, Zhang S, et al. The number and microlocalization of tumor-associated immune cells are associated with patient's survival time in non-small cell lung cancer. *BMC Cancer*. (2010) 10:220. doi: 10.1186/1471-2407-10-220

40. Wu J, Li L, Zhang H, Zhao Y, Zhang H, Wu S, et al. A risk model developed based on tumor microenvironment predicts overall survival and associates with tumor immunity of patients with lung adenocarcinoma. *Oncogene*. (2021) 40:4413–24. doi: 10.1038/s41388-021-01853-y

41. Phanthunane C, Wijers R, de Herdt M, Langeveld TPM, Koljenovic S, Dasgupta S, et al. B-cell clusters at the invasive margin associate with longer survival in early-stage oral-tongue cancer patients. *Oncoimmunology*. (2021) 10:1882743. doi: 10.1080/2162402X.2021.1882743

42. Oliveira G, Wu CJ. Dynamics and specificities of T cells in cancer immunotherapy. *Nat Rev Cancer*. (2023) 23:295–316. doi: 10.1038/s41568-023-00560-y

43. Edin S, Kaprio T, Hagström J, Larsson P, Mustonen H, Böckelman C, et al. The prognostic importance of cd20(+) B lymphocytes in colorectal cancer and the relation to other immune cell subsets. *Sci Rep*. (2019) 9:19997. doi: 10.1038/s41598-019-56441-8

44. Fridman WH, Meylan M, Petitprez F, Sun CM, Italiano A, Sautès-Fridman C. B cells and tertiary lymphoid structures as determinants of tumour immune contexture and clinical outcome. *Nat Rev Clin Oncol*. (2022) 19:441–57. doi: 10.1038/s41571-022-00619-z

45. Zhao X, Yue D, Qian J, Zhang L, Song J, Zhang B, et al. Case report: sarcoid-like reactions and tertiary lymphoid structures following dual checkpoint inhibition in a patient with early-stage lung adenocarcinoma. *Front Immunol*. (2022) 13:794217. doi: 10.3389/fimmu.2022.794217

46. Meylan M, Petitprez F, Lacroix L, Di Tommaso L, Roncalli M, Bougoüin A, et al. Early hepatic lesions display immature tertiary lymphoid structures and show elevated expression of immune inhibitory and immunosuppressive molecules. *Clin Cancer Res*. (2020) 26:4381–9. doi: 10.1158/1078-0432.CCR-19-2929

47. Hashimoto M, Kamphorst AO, Im SJ, Kissick HT, Pillai RN, Ramalingam SS, et al. Cd8 T cell exhaustion in chronic infection and cancer: opportunities for interventions. *Annu Rev Med*. (2018) 69:301–18. doi: 10.1146/annurev-med-012017-043208

48. Paijens ST, Vledder A, de Bruyn M, Nijman HW. Tumor-infiltrating lymphocytes in the immunotherapy era. *Cell Mol Immunol*. (2021) 18:842–59. doi: 10.1038/s41423-020-00565-9

49. Zhang W, Huang Q, Xiao W, Zhao Y, Pi J, Xu H, et al. Advances in anti-tumor treatments targeting the cd47/sirpα Axis. *Front Immunol*. (2020) 11:18. doi: 10.3389/fimmu.2020.00018

50. Jiang Z, Sun H, Yu J, Tian W, Song Y. Targeting cd47 for cancer immunotherapy. *J Hematol Oncol*. (2021) 14:180. doi: 10.1186/s13045-021-01197-w

frontiers | Frontiers in Immunology

TYPE Original Research
PUBLISHED 20 September 2024
DOI 10.3389/fimmu.2024.1422206

OPEN ACCESS

EDITED BY
Ying Ma,
Tianjin Medical University Cancer Institute and Hospital, China

REVIEWED BY
Wenji Ma,
Columbia University, United States
Ali Roghanian,
University of Southampton, United Kingdom

*CORRESPONDENCE
Helen K. Angell
helen.angell@astrazeneca.com

RECEIVED 23 April 2024
ACCEPTED 26 August 2024
PUBLISHED 20 September 2024

CITATION
Berthe J, Poudel P, Segerer FJ, Jennings EC, Ng F, Surace M, Andoni A, Testori M, Saraiya M, Vuko M, Hessel H, Heininen-Brown M, Blando J, Jones EV, Willis SE, Galon J, van de Ven R, de Gruijl TD and Angell HK (2024) Exploring the impact of tertiary lymphoid structures maturity in NSCLC: insights from TLS scoring. *Front. Immunol.* 15:1422206. doi: 10.3389/fimmu.2024.1422206

Exploring the impact of tertiary lymphoid structures maturity in NSCLC: insights from TLS scoring

Julie Berthe[1], Pawan Poudel[2], Felix J. Segerer[3], Emily C. Jennings[4], Felicia Ng[2], Michael Surace[5], Alma Andoni[5], Marco Testori[3], Megha Saraiya[3], Miljenka Vuko[3], Harald Hessel[3], Mari Heininen-Brown[3], Jorge Blando[5], Emma V. Jones[1], Sophie E. Willis[1], Jérôme Galon[6,7,8], Rieneke van de Ven[9,10,11], Tanja D. de Gruijl[10,11,12] and Helen K. Angell[1]*

[1]Translational Medicine, Oncology R&D, AstraZeneca, Cambridge, United Kingdom, [2]Oncology Data Science, Oncology R&D, AstraZeneca, Cambridge, United Kingdom, [3]Computational Pathology, Oncology R&D, AstraZeneca, Munich, Germany, [4]Oncology Data Science, Oncology R&D, AstraZeneca, Waltham, MA, United States, [5]Translational Medicine, Oncology R&D, AstraZeneca, Gaithersburg, MD, United States, [6]INSERM, Laboratory of Integrative Cancer Immunology, Paris, France, [7]Sorbonne Université, Université Paris Cité, Centre de Recherche des Cordeliers, Paris, France, [8]Equipe Labellisée Ligue Contre le Cancer, Paris, France, [9]Department of Otolaryngology, Head and Neck Surgery, Amsterdam UMC, Vrije Universiteit Amsterdam, Amsterdam, Netherlands, [10]Cancer Center Amsterdam, Cancer Biology and Immunology Theme, Amsterdam, Netherlands, [11]Amsterdam Institute for Immunology and Infectious Diseases, Amsterdam, Netherlands, [12]Department of Medical Oncology, Amsterdam UMC, Vrije Universiteit Amsterdam, Amsterdam, Netherlands

Tertiary Lymphoid Structures (TLS) are lymphoid structures commonly associated with improved survival of cancer patients and response to immunotherapies. However, conflicting reports underscore the need to consider TLS heterogeneity and multiple features such as TLS size, composition, and maturation status, when assessing their functional impact. With the aim of gaining insights into TLS biology and evaluating the prognostic impact of TLS maturity in Non-Small Cell Lung Carcinoma (NSCLC), we developed a multiplex immunofluorescent (mIF) panel including T cell (CD3, CD8), B cell (CD20), Follicular Dendritic cell (FDC) (CD21, CD23) and mature dendritic cell (DC-LAMP) markers. We deployed this panel across a cohort of primary tumor resections from NSCLC patients (N=406) and established a mIF image analysis workstream to specifically detect TLS structures and evaluate the density of each cell phenotype. We assessed the prognostic significance of TLS size, number, and composition, to develop a TLS scoring system representative of TLS biology within a tumor. TLS relative area, (total TLS area divided by the total tumor area), was the most prognostic TLS feature (C-index: 0.54, p = 0.04). CD21 positivity was a marker driving the favorable prognostic impact, where $CD21^+$ $CD23^-$ B cells (C-index: 0.57, p = 0.04) and $CD21^+$ $CD23^-$ FDC (C-index: 0.58, p = 0.01) were the only prognostic cell phenotypes in TLS. Combining the three most robust prognostic TLS features: TLS relative area, the density of B cells, and FDC $CD21^+$ $CD23^-$ we generated a TLS scoring system that demonstrated strong prognostic value in NSCLC when considering the effect of age, sex, histology, and smoking status. This TLS Score also demonstrated significant association with Immunoscore, EGFR mutational status and gene expression-based B-cell

and TLS signature scores. It was not correlated with PD-L1 status in tumor cells or immune cells. In conclusion, we generated a prognostic TLS Score representative of the TLS heterogeneity and maturity undergoing within NSCLC tissues. This score could be used as a tool to explore how TLS presence and maturity impact the organization of the tumor microenvironment and support the discovery of spatial biomarker surrogates of TLS maturity, that could be used in the clinic.

KEYWORDS

NSCLC, tertiary lymphoid structures, tissue scoring, tumor immunity, multiplex immunofluorescence

Introduction

Several spatial biomarkers, predictive of improved patient survival and response to immuno-therapies, have been identified over the last decade. One example is the density and location of immune cells within the tumor microenvironment. In particular, the presence of tumor-infiltrating lymphocytes (TILs) has been correlated to a better prognosis and response to immunotherapy in various cancer types, including melanoma, non-small cell lung cancer, and bladder cancer (1, 2). Other studies have demonstrated similar prognostic and predictive impact of immune cell density within the tumor center or the invasive margin (2, 3). Additionally, the spatial organization of immune cells within the tumor microenvironment can be of major importance. For example, the presence of highly organized ectopic lymphoid structures, called tertiary lymphoid structures (TLS) found in inflamed or tumor tissues, have been linked with better prognosis and response to immunotherapy in many cancer types (4–9).

While TLS are associated with favorable outcomes in tumor indications such as lung, colorectal, and pancreatic cancers, their relationship with histopathological and clinical parameters is complex and can vary across tumor types. In other tumor indications, TLS impact can be controversial, for instance in invasive breast cancer, bladder cancer, and gastric tumors where the presence of TLS has been correlated with poor prognostic value (8, 9). These conflicting observations suggest that not all lymphoid aggregates are functionally equivalent, and minimal characteristics may be required to define a functional TLS. Many cell types are recruited and segregated in two distinct B cell and T cell areas that typically comprise a TLS, including immune cells such as B cells, T cells, mature dendritic cells (mDC), Follicular helper T cells (TFH) and macrophages, differentiated stromal components (follicular dendritic cells (FDC), fibroblastic reticular cells (FRC), marginal reticular cells (MRC)), and high endothelial venules (HEV) (8). This complex TLS structural organization is critical for immune activation, as it enables the interaction of immune cells and antigens, leading to the generation of effective anti-tumor immune responses (8). The presence or absence of some cellular components may reflect different levels of organization, maturation stages or even types of lymphoid aggregates (10–13) which may impact their clinical significance.

Furthermore, it is of importance to note that there is no single, universally accepted definition of TLS, and different groups may define them differently based on their research question or tissue type. Moreover, various methods are used to evaluate and classify TLS, including histology H&E staining, immunohistochemistry (IHC), multiplex immunofluorescence (multiplex IF) and gene expression profiling, each method having its strengths and limitations (8, 9). Using different methods or single IHC markers to identify TLS may lead to variations in the classification of TLS and in the assessment of their clinical impact, with each method focusing on a specific TLS feature.

Variable numbers of lymphoid aggregates can be present within a tumor tissue, each one of these structures displaying unique characteristics (such as the size, cellular composition, location, maturation stage), and each feature having a potential impact on the clinical outcome. A better understanding of TLS impact on patient survival would thus require characterizing them at a high-resolution level by considering their functional, compositional, and spatial characteristics.

The objective of this study was to assess the prognostic value of TLS in Non-Small Cell Lung Cancer (NSCLC), by establishing a TLS Score that reflected the diversity of lymphoid clusters within a tissue. This scoring method considers various factors, including the size of the TLS relative to the tumor size, their cellular composition, and their prevalence.

Materials and methods

Acquisition of samples

All human tissues were obtained with fully informed consent and transferred to AstraZeneca. AstraZeneca has a governance framework and processes to ensure that commercial sources have appropriate patient consent and ethical approval in accordance with the principles outlined in the Declaration of Helsinki, in place for

collection of the samples for research purposes including use by for-profit companies. The AstraZeneca Biobank in the UK is licensed by the Human Tissue Authority (License No. 12109) and has National Research Ethics Service Committee (NREC) approval as a Research Tissue Bank (RTB) (REC No 17/NW/0207) which covers the use of the samples for this project.

Immunohistochemistry staining

Immunohistochemistry (IHC) staining was used as a Gold Standard to validate the multiplex immunofluorescence staining. IHC was performed on 4 µm thick sections of FFPE tissues and carried out on BOND RX using the following pre-programmed protocols and ready-to-use reagents (Leica Biosystems): dewax, ER1 citrate-based pH 6 retrieval (CD8, CD20, CD21, and CD23) or ER2 EDTA based pH 9 retrieval (CD3 and DC-LAMP) at 100°C for 20 mins. A blocking step using Protein Block Serum-Free reagent (Agilent) preceded the 'F standard' staining protocol, with post-primary (CD8, CD20, CD21 stains) or without (CD3, CD23 stains), poly-HRP-IgG and DAB refine (Polymer refine detection kit, Leica Biosystem). Primary antibodies used were as follows: anti-DC-LAMP (clone 1010E1.01, Dendritics, at 1 µg/mL), anti-CD3 (clone 2GV6, Roche, at 0.1 µg/mL), anti-CD8 (clone C8/144 B, Dako, at 1.5 µg/mL), anti-CD20 (clone L26, Abcam, at 0.1 µg/mL), anti-CD21 (clone 2G9, Cell Marque, at 0.5 µg/mL), anti-CD23 (clone SP23, Abcam, at 0.25 µg/mL). The antibodies were diluted in Dako antibody diluent (Agilent) and incubated for 15 mins. For DC-LAMP staining, ER2 retrieval incubation time was 40 mins, primary antibody incubation 40 mins and the secondary antibody used was a donkey anti-rat IgG H&L HRP (Abcam) at 1/200 dilution incubated 16 mins. Digital slide images were acquired with the Aperio AT2 scanner (Leica) using a 20x or 40x objective.

PD-L1 and immunoscore (CD3 and CD8) immunohistochemistry

Tumor sections were stained by IHC using the VENTANA PD-L1 (SP263) assay and scored by a pathologist for the proportion of membrane staining tumor cells and immune cells as described in Scorer et al. (14). CD3 and CD8 IHC Immunoscore Gold Standard assays were performed using the VENTANA, in conformity with Pages et al. (15). The T cells $CD8^+$ density in the tumor center and the invasive margin is used to provide an Immunoscore 'I'. It ranges from Immunoscore 0 'I0' to Immunoscore 4 'I4' depending on the T cell density in both tumor regions.

Multiplex immunofluorescence staining and multispectral image acquisition

Multiplex IF staining was conducted on 4 µm thick sections from FFPE NSCLC tissues using the Opal 6-Plex Detection Kit for Whole Slide Imaging (Akoya Biosciences). The BOND RX automated stainer was used for the pretreatment and staining of the tissues using ER2 retrieval at 100°C for 40 mins (Leica Biosystems). The endogenous peroxidase was blocked using the Peroxidase Block Novocastra (Leica) for 7 mins, before staining the tissues through repeated staining cycles for each marker. Each staining step cycle was composed of 5 steps: protein blocking using the Antibody Diluent/Block reagent for 5 mins (Akoya Biosciences), primary antibody incubation for 45 mins to 60 mins, secondary antibody incubation for 10 mins, Opal dye incubation for 10 mins, and an antibody denaturation step using ER1 retrieval at 97°C for 20 min to 30 mins. Identical primary antibody clones and concentrations were used for both chromogenic IHC and multiplex IF staining. The staining order and antibody-TSA reagent combination were as follows: 1) anti-DC-LAMP visualized with Opal480 (1/200 dilution), 2) anti-CD3 with Opal690 (1/100 dilution), 3) anti-CD8 with Opal520 (1/150 dilution), 4) anti-CD20 with Opal570 (1/100 dilution), 5) anti-CD21 with Opal620 (1/100 dilution), and 6) anti-CD23 with TSA-DIG (1/100 dilution) and Opal780 (1/50 dilution). Every TSA reagent was double dispensed. The Opal polymer anti-Ms + Rb HRP secondary antibody (Akoya Biosciences) was used for CD3, CD20, CD21 and CD23 stainings, the anti-mouse HRP SignalStain Boost IHC Detection Reagent (Cell Signaling Technologies) for CD8 staining, and the donkey anti-rat IgG H&L HRP (Abcam) for DC-LAMP staining. At the end of the protocol, the stained slides were counterstained with DAPI. The slides were scanned at 20x using the PhenoImager automated imaging system (Phenoptics; Akoya Biosciences) and multispectral images were unmixed using the InForm software version 2.4.8 and the synthetic spectral library (Akoya Biosciences).

Image analysis and TLS/B-cell cluster detection

A robust, standardized, and scalable image analysis pipeline has been developed and applied to analyze the 406 resection images stained with our panel across the entire tissue area (Supplementary Figure 1). To account for variability in staining intensities across staining batches we initially normalized intensities utilizing batch controls from the same tissue block (Supplementary Figure 1A). We adjusted equalization settings for each of the control slides such that the individual markers in the control block appear at the same intensity across all staining batches. Afterwards, the equalization settings of each control slide were applied to all slides of the corresponding staining batch. This was followed by image analysis (Supplementary Figure 1B), where, in an initial step, annotations of the tumor center "TC" and invasive margin "IM" were manually drawn by a pathologist for each image. These annotations served as regions of interest (ROIs) for further analysis. The denominated Annotated Area "AA" corresponds to the entire tumor tissue which includes IM and TC areas. Afterwards, we applied several deep-learning-based segmentation

and detection models across the whole slides for purposes of: (i) detection of nuclei, (ii) detection of positive cells for all markers in the panel, (iii) segmentation of analyzable tissue, and (iv) segmentation of parenchymal regions based on synthetically generated PANCK staining (16). Afterwards, TLS were segmented through the detection of $CD20^+$ cell clusters and enlarging these regions into the surrounding areas of high $CD3^+$ densities to detect both the TLS B-cell ($CD20^+$) and T-cell ($CD3^+$) zones (Supplementary Figure 1C). Clusters containing less than 20 $CD20^+$ cells arbitrarily were not considered as TLS. Image analysis results for regions and detected cells were then combined into a single segmentation map and cells were classified such that information about marker positivity and region associations were available for each detected cell. Finally, readouts were calculated across different ROIs, as summarized in Table 1.

Heatmap visualization and principal component analysis of multiplex IF density readouts

The cell density of each cell phenotype (N=10) within the regions labelled 'AA' (entire tumor annotated area), 'AA-TC' (tumor center area), 'TLS-AA' (TLS within the 'AA' area) and 'TLS-TC' (TLS within the 'TC' area) were $\log_{10}$ transformed and scaled to normalize the data. 'TLS-AA' and 'TLS-TC' correspond to TLS specific areas detected by the image analysis solution. Hence, when no TLS were detected within the tissue (TLS negative cases), cell densities were treated as missing values (*NA*) in those TLS specific areas. Principal component analysis was performed using the R package – *FactoMineR* (17). Spearman's correlation was used to assess the correlation between TLS readouts, including densities of immune phenotypes and TLS features, with the first five principal components.

Immune gene expression profiling and gene signature calculation

5–10 µm thick sections from 375 primary FFPE NSCLC tumor tissues were used for NanoString gene expression (GE) analysis. Tumor macro-dissected and RNA extracted with RNeasy FFPE extraction kit (Qiagen). NanoString transcriptomics using both the PanCancer Immune Profiling Panel and Myeloid Innate Immunity Panel (770 genes each) was carried out following manufacturer's instructions. The data obtained were processed using the nSolver Analysis Software version 4.0 (https://www.nanostring.com/products/analysis-software/nsolver) (NanoString). The processed NanoString data were used to estimate the signature scores associated with the B cells and TLS chemokine using the R package GSVA (18).

EGFR mutation status

EGFR mutation status was determined as described in Tu et al. (19). Briefly, *EGFR* mutant tumors were identified by annotation from the tissue vendors or verified internally by whole exome sequencing.

Statistical analysis

All the statistical analyses in this study were performed using R software (version 4.1.0). Differences between groups (or clusters) were tested with the Wilcoxon rank sum test and the Kruskal–Wallis test for comparisons between two or more groups, respectively. To identify the optimal cut-off points for converting the continuous TLS score into categorical scores, an iterative log-rank test was performed using the Python package *lifelines* (20). All other survival analyses were done using the R package – *survival* (21). Survival plots were generated using the R package – *survminer* (22). *Concordance index was estimated using R package – dynpred* (23).

Results

Multiplex IF panel deployment across 408 primary NSCLC tissue resections

In order to work towards a more standardized characterization of TLS, we here assessed the clinical impact of TLS parameters such as their size, cellular composition, and maturity status, understand the added value of each parameter and highlight any overlap in the information carried by these parameters. To this end, we developed a multiplex IF panel that enabled simultaneous detection of the TLS main cellular components: CD20 for B cells (TLS B-cell zone), CD3 for T cells and CD8 for cytotoxic T cells (TLS T-cell zone), and maturation markers such as DC-LAMP for activated conventional dendritic cells, CD21 for follicular dendritic cells (FDC) and CD23 for mature B cells. It is important to note that CD21 and CD23 markers can be expressed on both FDC and B cell populations (8, 24–26) (Table 1). The multiplex IF protocol was validated by comparing the IF staining against the single IHC chromogenic staining which was considered as the Gold Standard reference, performed on consecutive tissue sections (Figure 1A). The panel was then deployed across a cohort of 408 primary NSCLC baseline tumor resections, from patients treated with standard of care agents. Two cases were excluded from the analysis due to staining quality issues. The cohort clinicopathological characteristics are detailed in Table 2.

A visual inspection conducted by pathologists revealed a large variety of B-cell clusters/TLS located within the tumor tissue

10.3389/fimmu.2024.1422206

TABLE 1 Image analysis readouts.

<table>
<tr><td colspan="2">Tissue detection</td><td colspan="2">Tissue areas detected:
 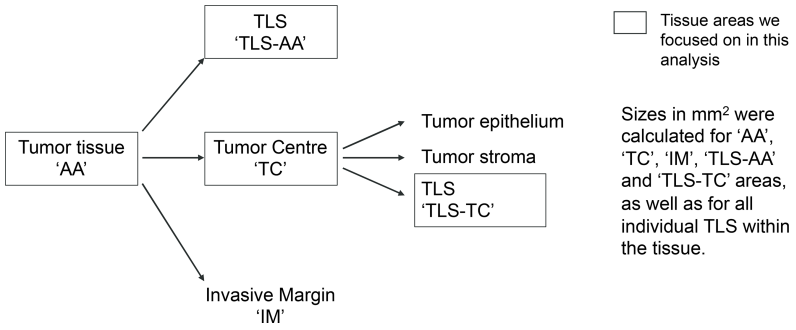
</td></tr>
<tr><td rowspan="13">B-cell cluster / TLS composition and maturation status</td><td rowspan="9">B-cell zone</td><td colspan="2">B-cell zone and Germinal centre staining: CD20, CD21 and CD23 markers</td></tr>
<tr><td colspan="2">CD20: pan B-cell marker
CD21 and CD23: B cells and Follicular Dendritic Cells (FDC) (8)</td></tr>
<tr><td colspan="2">TLS maturation stage according to CD21 and CD23 positivity status: (10)
TLS CD21$^-$ CD23$^-$: B-cell cluster
TLS CD21$^+$ CD23$^-$: Primary follicle-like TLS ('immature TLS')
TLS CD21$^+$ CD23$^+$: Secondary follicle-like TLS ('mature TLS')</td></tr>
<tr><td>B cell phenotyping</td><td>B cell populations</td></tr>
<tr><td>CD20$^+$ CD21$^-$ CD23$^-$</td><td>B cells CD21$^-$ CD23$^-$</td></tr>
<tr><td>CD20$^+$ CD21$^+$ CD23$^-$</td><td>B cells CD21$^+$ CD23$^-$</td></tr>
<tr><td>CD20$^+$ CD21$^-$ CD23$^+$</td><td>B cells CD21$^-$ CD23$^+$</td></tr>
<tr><td>CD20$^+$ CD21$^+$ CD23$^+$</td><td>B cells CD21$^+$ CD23$^+$</td></tr>
<tr><td>FDC phenotyping</td><td>FDC populations</td></tr>
<tr><td>CD3$^-$ CD20$^-$ CD21$^+$ CD23$^-$</td><td>FDC CD21$^+$ CD23$^-$</td></tr>
<tr><td>CD3$^-$ CD20$^-$ CD21$^-$ CD23$^+$</td><td>FDC CD21$^-$ CD23$^+$</td></tr>
<tr><td>CD3$^-$ CD20$^-$ CD21$^+$ CD23$^+$</td><td>FDC CD21$^+$ CD23$^+$</td></tr>
<tr><td rowspan="4">T-cell zone</td><td colspan="2">T-cell zone staining: CD3, CD8 and DC-LAMP markers</td></tr>
<tr><td>T cell phenotyping</td><td>T cell populations</td></tr>
<tr><td>CD8$^+$</td><td>Cytotoxic CD8$^+$ T cells</td></tr>
<tr><td>CD3$^+$ CD8$^-$</td><td>Surrogate for CD4$^+$ T cells</td></tr>
<tr><td rowspan="3">DC-LAMP$^+$</td><td>Dendritic cell phenotyping</td><td>DC population</td></tr>
<tr><td>mature dendritic cells (mDC) DC-LAMP$^+$</td></tr>
<tr><td>* readouts within TLS area only (to limit the challenge of the expression in both mDC and epithelial pneumocytes II cells)</td></tr>
<tr><td colspan="3">The density of each cell population was analysed per tissue area and per TLS.</td></tr>
</table>

exhibiting different sizes, organizational patterns, and cellular composition (Figures 1B, C). Despite diameter sizes varying from approximatively 150-200 mm to > 500 mm, all clusters presented a clear CD20$^+$ B-cell zone surrounded by a CD3$^+$ T-cell zone containing CD3$^+$ CD8$^+$ cytotoxic T cells and a high density of CD3$^+$ CD8$^-$ cells considered as CD4$^+$ T cells (Figure 1B). We found the degree of maturity of an aggregate, assessed by the presence of positive cells for CD21 and CD23 markers, to be independent of their size. Example images of both large (> 500 mm) and small (150-200 mm) B-cell clusters are presented in Figures 1B, C, respectively. Figure 1B shows two large clusters, (Cluster #1 and Cluster #2), describing different levels of maturation. Cluster #1 presented a central area with high prevalence of CD21$^+$ and CD23$^+$ cells, corresponding to the follicular dendritic cells network and the germinal center, also known as site of an ongoing local B cell activation process that leads to the differentiation of specific

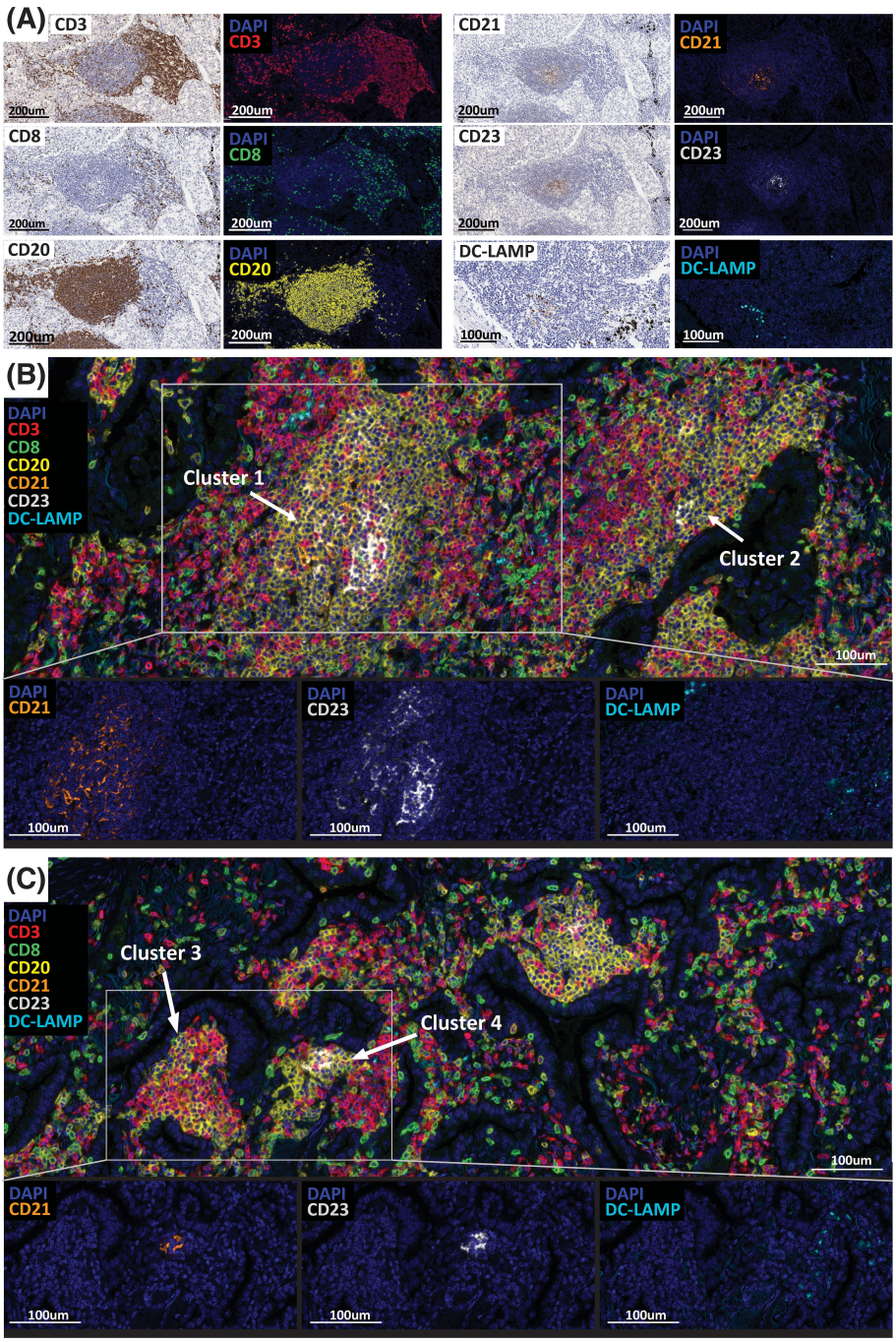

FIGURE 1
TLS detection and maturity assessment in 406 NSCLC cases. **(A)** Multiplex immunofluorescence assay validation (CD3, CD8, CD20, CD21, CD23, DC-LAMP) by comparing the IF to the chromogenic IHC staining performed on serial tissue sections. CD3 (T cells, red), CD8 (CTL T cells, green), CD20 (B cells, yellow), CD21 (FDC, orange), CD23 (GC B cells, white), DC-LAMP (mDC, cyan). **(B, C)** Representative images of large **(B)** and small **(C)** TLS/B-cell clusters positive for the maturation markers CD21, CD23 and DC-LAMP detected in NSCLC cases. Slides were imaged using the PhenoImager HT automated imaging system. Scale bars are indicated.

memory B cells and plasma cells. In contrast, while located in the same tumor area, Cluster #2 shows a very low prevalence of cells positive for those maturity markers. Both aggregates are positive for DC-LAMP, suggesting the presence of mature dendritic cells. However, it is important to note that the image analysis of DC-LAMP in NSCLC was challenged by the presence of pneumocytes type II epithelial cells that could also express this marker. Thus, we cannot be certain that the DC-LAMP$^+$ cells detected are all activated dendritic cells, and the results should be interpreted carefully. Similar to large clusters, small structures (Figure 1C) show

10.3389/fimmu.2024.1422206

TABLE 2 Clinical and histologic characteristics of the NSCLC patient cohort (N = 406).

Clinical characteristics		Prognostic variables	
Characteristic	N = 406	Characteristic	N = 406
Diagnosis category[1]		**Survival status**[1]	
adenocarcinoma	214 (53%)	Alive	171 (42%)
adenosquamous	1 (0.2%)	Deceased	188 (46%)
bronchioalveolar	1 (0.2%)	Unknown	47 (12%)
large cell	6 (1.5%)	**Overal survival (months)**[2]	23 (9, 45)
other	9 (2.2%)	Unknown	48
sarcomatoid	1 (0.2%)	**Progression free survival**[2]	19 (8, 40)
squamous cell	142 (35%)	Unknown	66
Unknown	32 (7.9%)	**Censoring status (PFS)**[1]	101 (30%)
Tumor grade[1]		Unknown	67
G1	9 (2.2%)	**Recurrence**[1]	
G1-2	8 (2.0%)	Never disease-free	4 (1.0%)
G2	69 (17%)	No	239 (59%)
G2-3	10 (2.5%)	Unknown	57 (14%)
G3	83 (20%)	Yes	106 (26%)
Unknown	227 (56%)	[1] n (%); [2] Median (IQR)	
T Category[1]			
T1	106 (26%)		
T2	191 (47%)	**Patient demographic and data information**	
T3	59 (15%)	**Characteristic**	**N = 406**
T4	10 (2.5%)	**Age**[2]	67 (61, 74)
TA	1 (0.2%)	Unknown	32
Unknown	39 (9.6%)	**Sex**[1]	
M category[1]		Female	166 (41%)
M0	59 (15%)	Male	208 (51%)
M1	6 (1.5%)	Unknown	32 (7.9%)
Unknown	341 (84%)	**Race**[1]	
N category[1]		Asian	11 (2.7%)
N0	234 (58%)	Caucasian	49 (12%)
N1	69 (17%)	Unknown	346 (85%)
N2	46 (11%)	**Smoking history**[1]	
Unknown	57 (14%)	Current	110 (27%)
Stage[1]		Never	38 (9.4%)
I	83 (20%)	Past	175 (43%)
II	58 (14%)	Unknown	83 (20%)
III	17 (4.2%)	**Alcohol history**[1]	
IV	3 (0.7%)	Heavy Drinker	2 (0.5%)
Unknown	245 (60%)	Never	18 (4.4%)

(Continued)

10.3389/fimmu.2024.1422206

TABLE 2 Continued

Clinical characteristics		Prognostic variables	
Characteristic	N = 406	Characteristic	N = 406
Chemo treatment history[1]		Social or Occasional Drinker	21 (5.2%)
No	48 (12%)	Unknown	365 (90%)
Unknown	249 (61%)	**Exome Profiling**[1]	273 (67%)
Yes	109 (27%)	**Nanostring Profiling**[1]	375 (92%)
Radiation treatment history[1]		[1] n (%); [2] Median (IQR)	
No	46 (11%)		
Unknown	309 (76%)		
Yes	51 (13%)		
TLS status[1]			
TLS Negative	134 (33%)		
TLS Positive	272 (67%)		
TLS count[2]	2 (0, 8)		

[1] n (%); [2] Median (IQR).

different maturation levels. Indeed, whilst Cluster #3 does not contain any positive cells for CD21, CD23 and DC-LAMP, Cluster #4 presents high densities of $CD21^+$, $CD23^+$ and $DC\text{-}LAMP^+$ cells. These observations suggest that a high organizational and maturation degree of B-cell clusters, with the presence of a follicular dendritic cells network and a germinal center, is independent of their size.

Moreover, if each lymphoid aggregate displays unique features that could result in different anti-tumor immune functions and clinical outcomes (8, 9, 27), it is worth noting that a tumor tissue can contain multiple aggregates, all describing specific size, cellular composition, organization and maturation levels (Figures 1B, C). Thus, when assessing the clinical value of B-cell aggregates, it is important to consider all types of aggregates present within a tissue.

Following this visual assessment identifying small B-cell aggregates positive for CD21, CD23 and DC-LAMP, and with the objective of evaluating how the size, cellular composition and maturation degree impact the immune cell activity and clinical outcomes, we developed an image analysis solution that specifically detects B-cell aggregates containing at least 20 $CD20^+$ cells (Supplementary Figure 1C). These aggregates were segmented by detecting clusters of high density $CD20^+$ cells and enlarging these regions into the surrounding areas of high $CD3^+$ densities. The specificity of this algorithm was confirmed after pathologist visual assessment. Furthermore, in the absence of a universal and specific definition for TLS, we designated 'TLS' as large lymphoid aggregates exhibiting a germinal center and displaying CD21, CD23 and DC-LAMP positive cells. The remaining aggregates detected were referred to as 'B cell aggregates' or 'B cell clusters'.

In addition to TLS area, the segmentation of tumor epithelium and the cell phenotyping analysis required the development and deployment of several additional deep-learning-based segmentation and detection models (Supplementary Figure 1B). Information about marker positivity and region association were available for each detected cell, hence allowing us to evaluate the impact of TLS composition in an accurate way. Using these data, we calculated densities of each cell type and sub-type within the segmented regions described in Table 1. Owing to the considerable dynamic ranges observed in the densities of all cell types within both the total tumor area and the TLS regions, log10 transformation was applied to these densities for subsequent analysis. This transformation was undertaken to normalize the data and stabilize the variance, as illustrated in Supplementary Figure 2A.

NSCLC cohort immune profiling

In our effort to understand the level of B-cell cluster and TLS heterogeneity within the tumor TME of NSCLC patients, we generated a heatmap using the TLS multiplex IF readouts (Figure 2A). These readouts, summarized in Table 1, consisted of the densities of 10 cell phenotypes in different tissue areas and described as the main cellular components of the TLS B-cell zone (B cells and follicular dendritic cells) and the TLS T-cell zone (T cells and mature dendritic cells).

B cells and FDC cell types were segregated into different subsets based on the positivity of specific markers CD20, CD21 and CD23, commonly used to evaluate TLS impact and maturation status in the clinic (5, 7–10, 28, 29). The CD20 antigen is expressed on the surface of B-cells starting from the pre-B cell stage, with the exception of plasmablasts and plasma cells. In contrast, the proteins CD21 and CD23 are expressed at later stages in the activation process. CD21 positivity can be observed from the transitional B cell stage 1, and CD23 expression is typically detected from the transitional B cell stage 2. These markers are commonly used to identify germinal center B cells (25, 30, 31). In

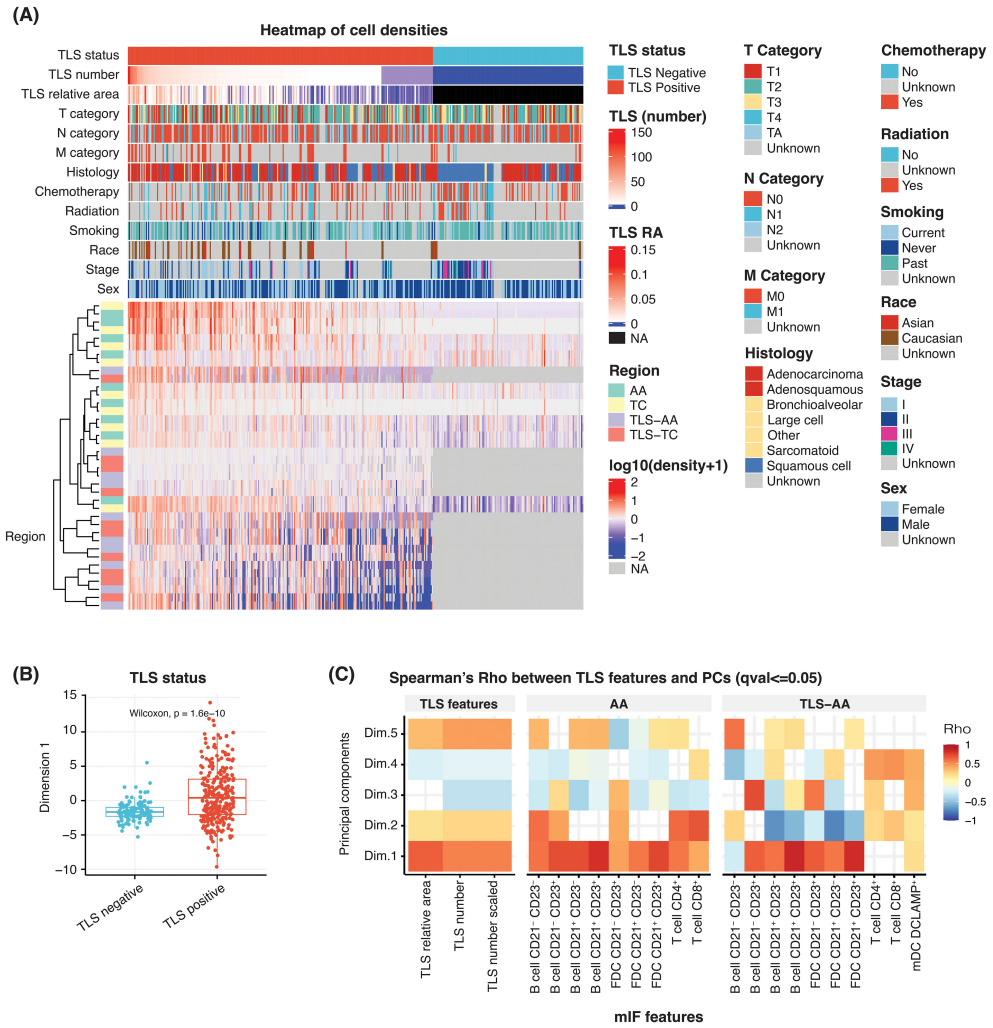

FIGURE 2
Heatmap of multiplex IF features to identify the key cell phenotypes associated with TLS structures. **(A)** Heatmap showing the scaled (following the $\log_{10}$ transformation) density of 10 cell phenotypes and their association with sex, stage, race, smoking status, therapy (radiation and chemotherapy), histology, TNM categories, TLS relative area (RA), TLS number and TLS status. Individual patients are represented in each column. Each row represents the cell density of a specific cell phenotype located within the indicated tissue region. For cases TLS negative, TLS RA and cell densities are treated as missing value *NA*. **(B)** A box plot comparing the first principal component scores according to the TLS status of the NSCLC cases. **(C)** A heatmap showing the correlation between multiple multiplex IF features, namely: TLS relative area, TLS number (unscaled), TLS number (scaled), densities of 10 cell phenotypes in 'AA' and 'TLS-AA' (*x-axis*), with the first principal component (*y-axis*).

this context, B cells were segregated into four B cell subsets depending on CD21 and CD23 positivity status. The subsets are the following: B cells $CD21^{-}$ $CD23^{-}$, B cells $CD21^{+}$ $CD23^{-}$, B cells $CD21^{-}$ $CD23^{+}$ and B cells $CD21^{+}$ $CD23^{+}$. Similarly, we categorized the follicular dendritic cells, which are stromal cells involved in the structure and organization of TLS and which can express both CD21 and CD23, into three subsets based on their positivity status for both CD21 and CD23. Three subtypes were assessed: FDC $CD21^{+}$ $CD23^{-}$, FDC $CD21^{-}$ $CD23^{+}$ and FDC $CD21^{+}$ $CD23^{+}$. Furthermore, the T cell population was divided into two cell populations: cytotoxic T cells $CD3^{+}$ $CD8^{+}$ (CTL) and T cells $CD3^{+}$ $CD8^{-}$ considered as a surrogate of T helper cells $CD4^{+}$.

The densities of B cells, FDC and T cells were analysed in different tissue areas including: the tumor annotated area 'AA' corresponding to the entire tumor area, the tumor centre 'TC', TLS within the tumor annotated area 'TLS-AA' and TLS within the tumor centre 'TLS-TC'. Finally, mature dendritic cells were assessed using the DC-LAMP marker, commonly used to study this cell population. However, lung tissues may contain type II pneumocytes epithelial cells, which exhibit positivity for this antigen. Consequently, we restricted its analysis to TLS areas, specifically 'TLS-AA' and 'TLS-TC', mature dendritic cells being more likely to be located within TLS (Table 1).

The heatmap analysis considered the TLS multiplex IF cell densities readouts within the tissue areas 'AA', 'TC, 'TLS-AA' and 'TLS-TC'. Individual patients were represented in each column (Figure 2A). This analysis predominantly separated the cohort according to the presence or absence of TLS within the tissue, which was an expected result as the assay is specific to the main TLS immune cell components. Additionally, TLS positive cases were segregated according to diverse TLS features such as the TLS number, the immune cell densities and the TLS relative area, the

latter corresponding to the total TLS area within a tumor tissue divided by the tumor area (Supplementary Figure 2B).

We then proceeded with a principal component analysis (PCA) to understand and identify the key TLS variables driving the observed heterogeneity within tumor tissues. Our analysis revealed that the first dimension effectively distinguished NSCLC cases based on their TLS status, whether TLS-positive or TLS-negative (Figure 2B). This first dimension was also significantly correlated with TLS features such as the TLS relative area and TLS number both in unscaled and scaled values (Figure 2C). Similarly, most cell densities exhibited a significant correlation with this first dimension and displayed Spearman's Rho values over 0.5 (Figure 2C). We particularly focused on the whole tumor area 'AA' and TLS-specific regions within the tumor 'TLS-AA' to assess the TLS cellular diversity throughout the entire tissue. Moreover, although additional PCA dimensions allowed us to further explain the variance, the common trend observed among multiplex IF cell density readouts in the first component suggested a shared mechanism influencing their presence in TLS regions (Figure 2C).

These heatmap and PCA results supported the TLS heterogeneity observed during the visual inspection amongst this NSCLC cohort and confirmed the need of further characterizing the TLS biology – TLS number, TLS relative area, TLS composition – within a tissue to accurately evaluate their impact on clinical outcomes.

Prognostic value of TLS features and cell densities

Following the heatmap visualization and PCA analysis, we aimed to understand how the prevalence of each TLS main component, such as B cells, T cells, FDC and dendritic cells, TLS maturation status and location within the tumor tissue, can impact the prognostic relevance of these structures.

The proportion of B cells was significantly increased in the TLS compared to the tumor areas (Figures 3A, B). These cells represented approximately 55% and 20% of the total cell population detected within the TLS areas and the tumor, respectively (Figure 3A). This result was in coherence with B cells being the main immune component of TLS and our subsequent image analysis strategy to develop a TLS detection algorithm based on the CD20 marker positivity. As shown in Figure 3B, all B cell subtypes displayed higher densities in TLS specific areas. Similarly, we evaluated the distribution of different follicular dendritic cell subsets. The density of all FDC subsets was significantly increased in TLS compared to the entire tissue area, the FDC population representing approximately 3% and 6% of the analysed cells within the tumor and TLS specific areas, respectively (Figures 3A, B). After evaluating the overall proportion of B cells and FDC, which are the two main cell phenotypes that compose TLS B-cell zone and germinal centre, we assessed the prevalence of the main TLS T-cell zone components, T cells and mature dendritic cells DC-LAMP$^+$. We observed a considerably higher proportion of T cells – including both CTL and CD4$^+$ cells – in the tumor areas compared to the TLS areas, the T cell population representing approximately 80% of the phenotyped cells within the tumor tissue and 40% in the TLS areas (Figure 3A). Interestingly, the density of both CTL and CD4$^+$ cell subsets was significantly higher in TLS areas compared to the entire tumor area (Figure 3B). Finally, a low prevalence of mature dendritic cells DC-LAMP+ was observed within TLS areas, these cells representing less than 1% of the total TLS cellular population (Figure 3A).

We next conducted a comprehensive analysis and calculated the Concordance Index (C-index) of TLS features (Figure 3C) and cell densities within two distinct tissue areas, the tumor tissue 'AA' (Figure 3D) and TLS-specific areas 'TLS-AA' (Figure 3E), to evaluate their associations with patient survival in our study cohort. The C-index, ranging from 0 to 1, evaluates survival model performance. A score of 1 signifies perfect discrimination between survivors and non-survivors, while 0.5 indicates performance similar to random guessing. The C-index, Hazard ratio, 95% Confidence interval, and p-values of all parameters assessed in multiple tissue areas are also indicated in Supplementary Table 1. Surprisingly, we showed that among the two TLS features considered, scaled TLS relative area (scaled) and TLS number, only the TLS relative area demonstrated a significant prognostic power with a C-index of 0.54 (p-value = 0.04) (Figure 3C and Supplementary Table 1). Moreover, our analysis revealed the importance of considering the location within the tissue when understanding the contribution of specific cell phenotypes to survival outcomes. Among the densities (in $\log_{10}$ scaled) (Supplementary Figure 2A) of the nine cell phenotypes assessed within the tissue area 'AA', we identified four namely B cells CD21$^-$ CD23$^-$, B cells CD21$^-$ CD23$^+$, B cells CD21$^+$ CD23$^-$ and T cells CD4$^+$ which demonstrated significant associations with patient survival, as evidenced by their high concordance indices and significant -$\log_{10}$(p-values). Notably, the density of B cells CD21$^-$ CD23$^-$ and B cells CD21$^+$ CD23$^-$ exhibited strongest predictive capabilities, with C-index values of 0.57 and 0.58, respectively, and robust statistical significance (p = 0.001 and p = 0.002, respectively). The cellular density of B cells CD21$^+$ CD23$^+$, of the three different FDC subsets FDC CD21$^-$ CD23$^+$, FDC CD21$^+$ CD23$^-$ and FDC CD21$^+$ CD23$^+$, and of T cells CD8$^+$ did not show statistically significant associations with patient survival when the entire tumor area was considered (Figure 3D and Supplementary Table 1). Interestingly, only two cell phenotypes exhibited a significant prognostic impact in TLS specific areas. The density of B cells CD21$^+$ CD23$^-$ within the TLS regions remained a significant predictor of patient survival with a C-index of 0.57 despite displaying a slightly lower p-value compared to the 'AA' area counterpart. Additionally, FDC CD21$^+$ CD23$^-$ emerged as a second cell phenotype significantly impacting the survival of patient when located in TLS areas (C-index: 0.58), whereas B cells CD21$^-$ CD23$^-$, B cells CD21$^-$ CD23$^+$ and T cells CD4$^+$ significant prognostic impact was lost (Figure 3E and Supplementary Table 1). Finally, we demonstrated that the density of DC-LAMP$^+$ cells within TLS was not of prognostic value in this cohort (Figure 3E and Supplementary Table 1). The survival analysis results of additional parameters such as TLS relative area (unscaled), TLS number (scaled), and of cell densities within different tumor areas are indicated in Supplementary Table 1.

10.3389/fimmu.2024.1422206

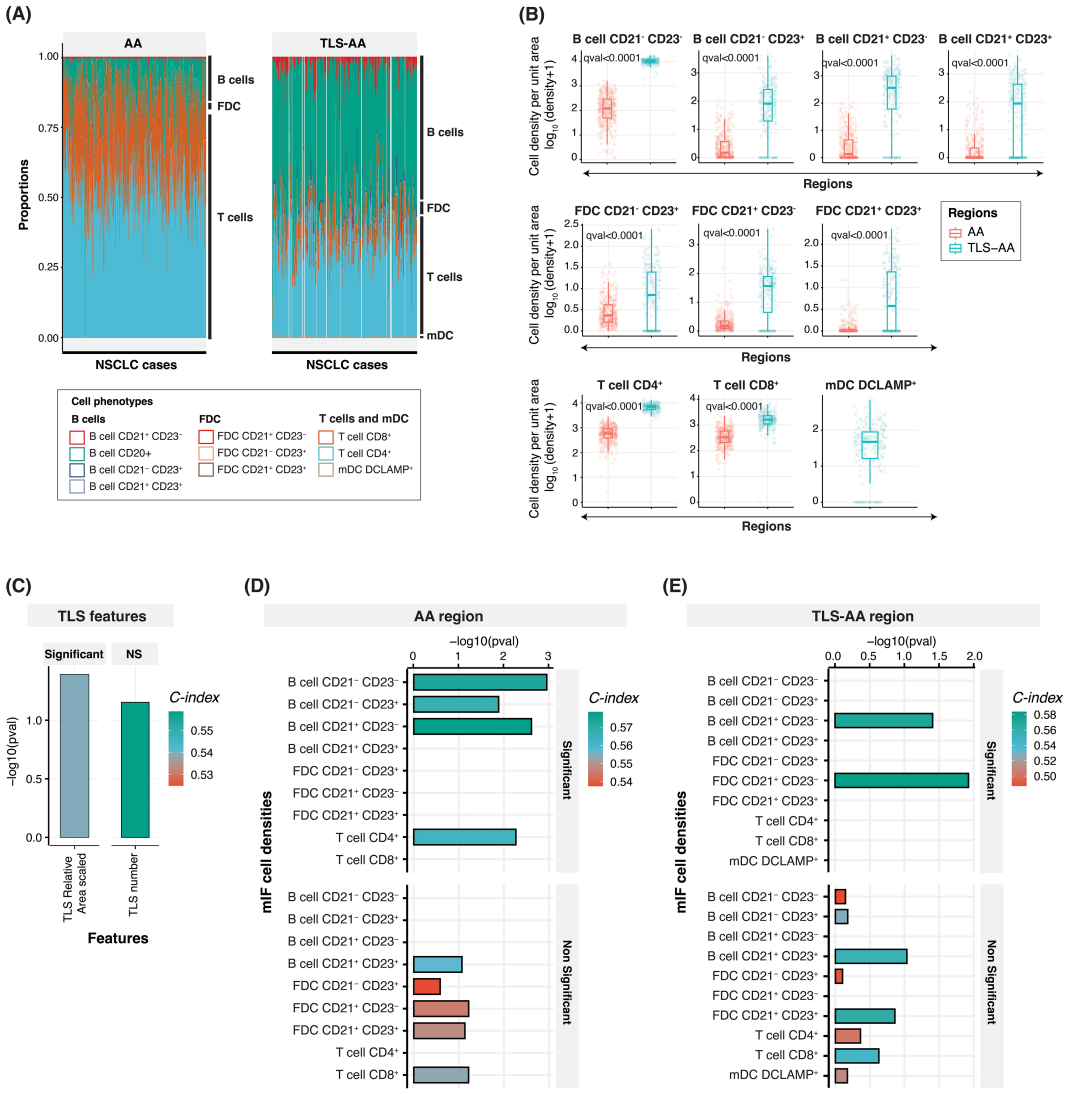

FIGURE 3
Cell densities within the tumor and TLS-specific area, and prognostic relevance. **(A)** Bar plot showing the relative proportion of ten cell phenotypes captured using the multiplex IF panel in the tumor 'AA' (left panel) and TLS-specific area 'TLS-AA' (right panel) regions. The proportion has been calculated by dividing the specific cell type density by the total cell density. **(B)** Box plots comparing the densities (number of cells per unit area) of these ten cell phenotypes between the 'AA' and 'TLS-AA' regions. The q-value in the plot refers to the FDR adjusted p-value from Wilcoxon rank sum test. **(C–E)** Bar plots showing concordance index (C-index), and -$\log_{10}$(p-values) for TLS relative area (scaled) and TLS number **(C)** and cell phenotypes within the tumor area 'AA' **(D)** or within TLS specific areas 'TLS-AA' **(E)**. NS, Non-significant.

In conclusion, our results suggested that both TLS relative area and TLS composition should be considered when evaluating TLS prognostic benefit, both features showing prognostic value. Moreover, while the presence of lymphoid aggregates is frequently associated with an improved prognostic value in multiple cancer indications (8, 9), tools need to be developed to better characterize, score these TLS structures at a tissue level, and evaluate their real impact on the survival of cancer patients.

TLS score aim and calculation

In this context, we aimed to generate a TLS tissue scoring system, called TLS Score, which would reflect the TLS biology within the tumor tissue. In many cancer types, TLS maturation status, commonly assessed by DC-LAMP positivity or the presence of CD21$^+$ FDC network and a CD23$^+$ Germinal Centre, is described as one of the main drivers of TLS prognostic value (8, 9). Although generating a TLS Score based on the TLS knowledge we have from the literature was an attractive option, the TLS biology complexity and different prognostic values of TLS components highlighted in Figures 2 and 3 led us to generate a data-driven scoring system. Figure 4A summarizes the strategy and multi-step process to generate a TLS Score based on our TLS multiplex IF data: step 1- heatmap of mIF density features to identify common trends (Figure 2A), step 2- PCA analysis to identify key TLS multiplex IF features (Figures 2B, C), step 3- Concordance index analysis to select the most prognostic TLS features (Figures 3C–E) and step 4-

10.3389/fimmu.2024.1422206

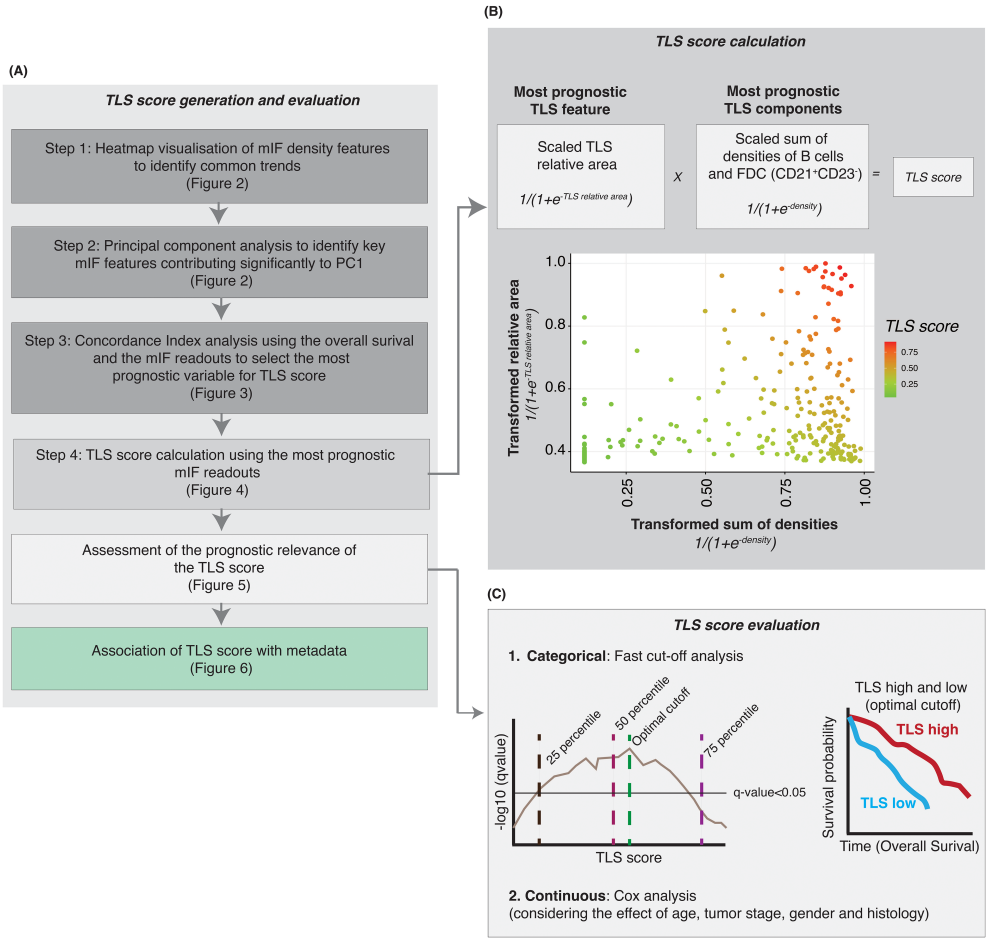

FIGURE 4
Generation of a TLS score after identifying the most consistently prognostic TLS mIF features. **(A)** Steps performed to identify the key multiplex IF cell phenotypes and TLS features to generate a TLS score with prognostic value. **(B)** Based on the results from heatmap, principal component analysis and survival analysis we selected the most prognostic (i) TLS feature (relative area of the TLS) and (ii) TLS components (densities of B cells and follicular dendritic cells CD21$^+$ CD23$^-$) to generate a TLS score. The TLS relative area was scaled, and the logistic function was applied. For the CD21$^+$ CD23$^-$ cells (B cells and FDC), cell densities were scaled and summed followed by transformation of data using the logistic function. The TLS score is the product of (i) and (ii). **(C)** A log-rank test was performed to assess the prognostic relevance of TLS score, at multiple cut-off points, and the optimal cut-off was selected to categorize the NSCLC samples into TLS-high and -low groups. The optimal cut-off was selected based on two criteria – minimizing the FDR-adjusted p-value and balancing the number of samples in the TLS-high and TLS-low categories. Kaplan-Meier survival analysis was performed to assess the survival difference between the TLS-high and TLS-low samples, using the optimal cut-off-based TLS stratification.

TLS Score calculation using the most relevant and prognostic multiplex IF readouts.

As previously described, the PCA analysis (step 2) revealed that these readouts contained similar information, requiring the selection of optimal readouts for generating a TLS Score to avoid using redundant information (Figure 2). The subsequent concordance index analysis conducted aimed to identify the most prognostic TLS features and cell density readouts (Figure 3 and Supplementary Table 1). These analyses highlighted the three most prognostic TLS parameters selected to generate a TLS tissue score (step 3): TLS scaled relative area, B cell CD21$^+$ CD23$^-$ and FDC CD21$^+$ CD23$^-$ cell densities. The TLS Score uses (i) the scaled TLS relative area and (ii) the scaled sum of B cells CD21$^+$ CD23$^-$ and FDC CD21$^+$ CD23$^-$ densities (in $\log_{10}$ scale, see the methods section). It is important to emphasize that in order to consistently generate a TLS Score for all the patients within this cohort and include TLS negative cases for which TLS data were absent (resulting in missing values marked as NA for TLS relative area and cell densities within TLS), we addressed these missing values by treating them as 0. Furthermore, the data underwent a $\log_{10}$ transformation for normalization and variance stabilization and scaling to ensure consistent scales for the maximum and minimum values across multiple TLS features. The scaled sum of B cells and FDC densities and the scaled relative area were transformed using a logistic function and then multiplied to generate the TLS score (Figure 4B). The calculated TLS Score values ranged from 0 to 1 (Figure 4B) and can be used as a categorical or continuous variable. As indicated in Figure 4C, we then assessed the TLS Score prognostic relevance through an iterative log-rank test analysis and a univariate Cox analysis which considered the effect other metadata variables such as age, sex, smoking status and histology categories. The results are presented in Figures 5 and 6 and described below.

10.3389/fimmu.2024.1422206

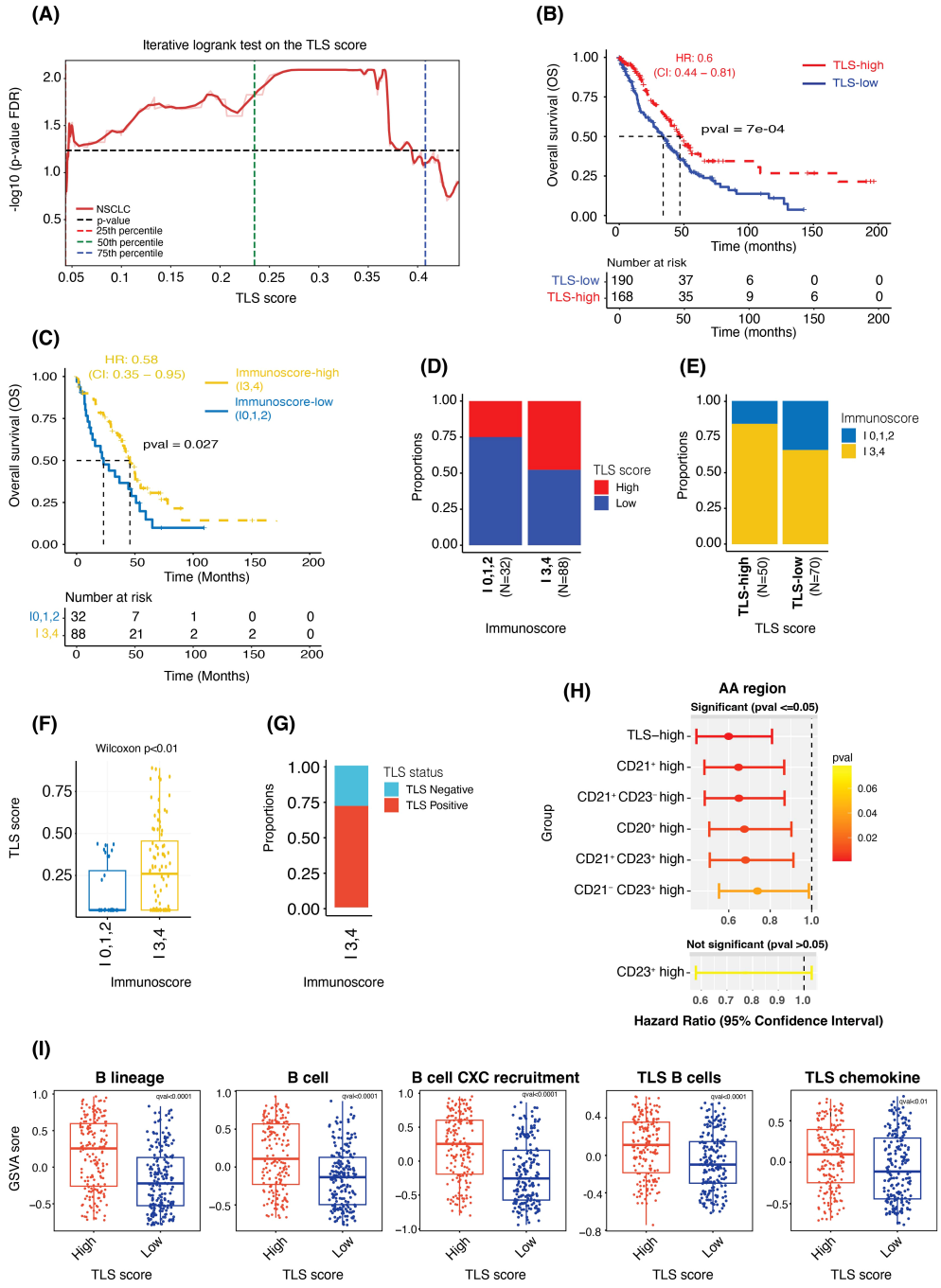

FIGURE 5
TLS score is prognostic independent of the cutoff used to categorize the data and shows significant association with Immunoscore and gene expression-based signature scores. **(A)** Plot showing FDR-adjusted p-values (from the log-rank test) observed at multiple cut-off points between the TLS-high and TLS-low samples. **(B, C)** Kaplan-Meier survival curves showing the difference in overall survival between the TLS-high and -low groups **(B)** and between the Immunoscore-high (I3,4) and Immunoscore-low (I0,1,2) groups **(C)**. **(D, E)** Bar plots showing the proportions of TLS-high and TLS-low samples in the Immunoscore-high and -low groups **(D)** and the proportions of Immunoscore-high and -low samples in TLS-high and TLS-low groups **(E)**. **(F)** Box plot comparing the TLS Score (as a continuous value) between Immunoscore-high and Immunoscore-low groups. **(G)** Bar plot showing the proportions of TLS-high and TLS-low samples in the Immunoscore-high group. **(H)** A plot showing hazard ratios, the 95% confidence interval of HR and the p-value from the Wald test of TLS-high (vs TLS-low, used as reference), $CD21^+$ high (vs $CD21^+$ low), $CD21^+$ $CD23^-$ high (vs $CD21^+$ $CD23^-$ low), $CD20^+$ high (vs $CD20^+$ low), $CD21^+$ $CD23^+$ high (vs $CD21^+$ $CD23^+$ low), $CD21^-$ $CD23^+$ high (vs $CD21^-$ $CD23^+$ low) and $CD23^+$ high (vs $CD23^+$ low) cases. **(I)** Box plots showing the difference in the gene expression-based enrichment scores of B cells and TLS signatures between the TLS-high and TLS-low groups.

10.3389/fimmu.2024.1422206

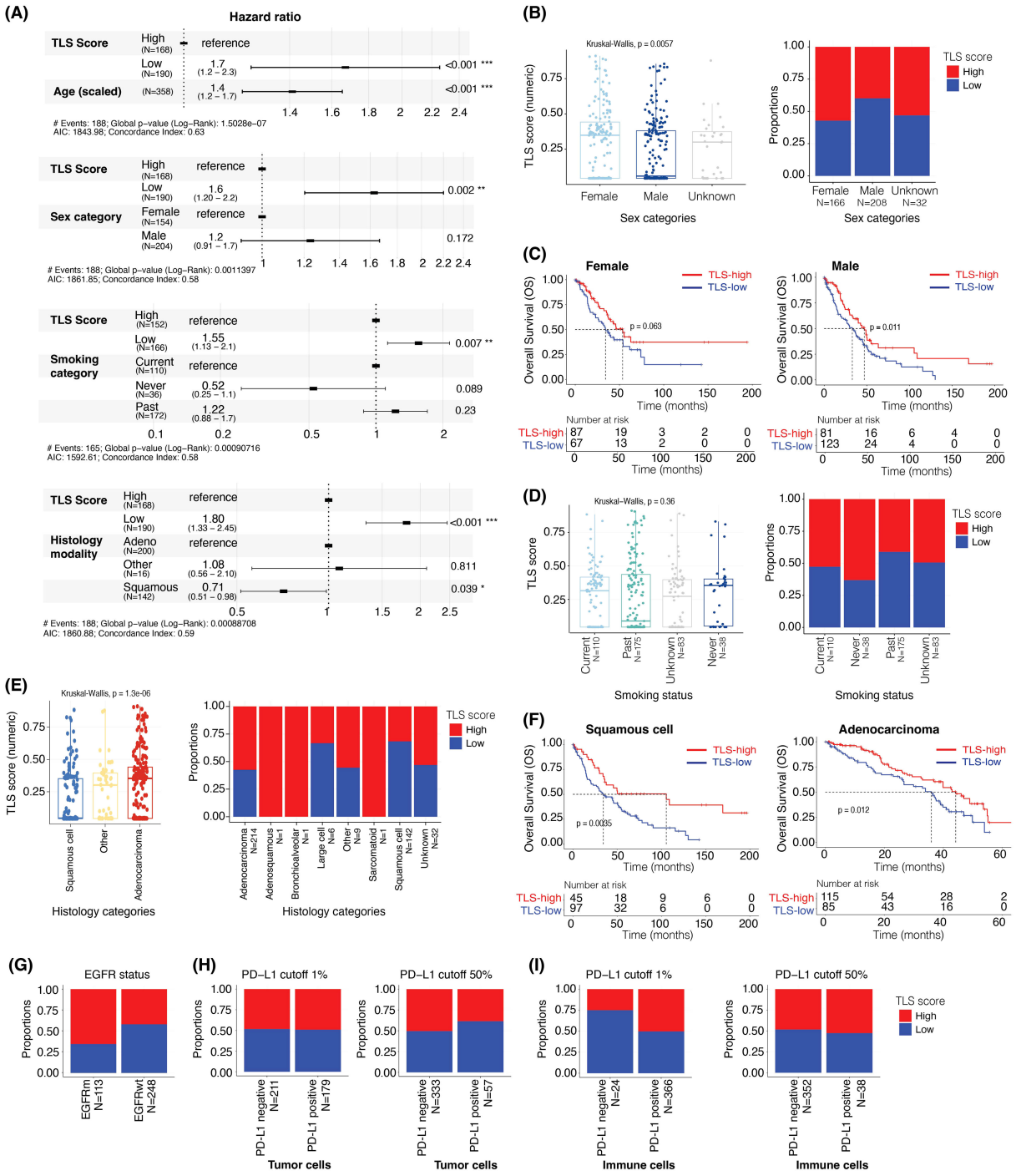

FIGURE 6
TLS score is prognostic after adjusting for age, sex, smoking status, and is associated with EGFR mutational status but not PD-L1 positivity status. **(A)** The hazard ratios and 95% confidence interval of TLS scores adjusted for the effect of **(i)** age, **(ii)** sex, **(iii)** smoking status, and (iv) histology using multivariable Cox regression analysis and overall survival data. **(B)** Box plot showing the difference in TLS scores (as a continuous value) in male and female samples (left panel). Bar plot showing the proportions of TLS-high and -low samples in male and female (right panel). **(C)** Kaplan-Meier plots showing the difference in overall survival between TLS-high and TLS-low groups in female (left panel) and male (right panel). **(D)** Box plot comparing the TLS scores (as a continuous value) by smoking status (left panel). Bar plot showing the proportions of TLS-high and -low samples in current, never, and past smokers (right panel). **(E)** Box plot comparing the TLS score (as a continuous value) in different histological subtypes of NSCLC (left panel). Bar plot showing the proportions of TLS-high and -low in different histological subtypes of NSCLC samples (right panel). **(F)** Kaplan-Meier plots showing the difference in overall survival between the TLS-high and TLS-low groups in squamous cell carcinoma (left panel) and adenocarcinoma (right panel). **(G)** Bar plot showing the proportions of TLS-high and -low samples in EGFR mutant and wildtype samples. **(H, I)** Bar plots showing the proportions of TLS-high and TLS-low groups in PD-L1 staining positive and negative samples in tumor cells 'TC' **(H)** and immune cells 'IC' **(I)** at 1% (left panels) or 50% (right panels) PD-L1 positivity cut-offs.

10.3389/fimmu.2024.1422206

TLS score correlation with immunoscore and TLS gene expression signatures

After the TLS Score generation, we first wanted to evaluate its prognostic impact in NSCLC. The iterative log-rank test, where each cut-off point contained at least 10% of the total observation in each category, demonstrated that the TLS score was significantly prognostic independently of the cut-off used to categorize the data (Figure 5A). In the downstream analyses, we hence used the optimal cut-off value of 0.28 to divide the NSCLC cohort (N = 358) into two groups: TLS-high (TLS Score ≥ 0.28) and TLS-low (TLS Score < 0.28) and considered this score as a categorical variable, TLS-high versus -low. Survival analysis between the TLS-high (N = 168) and -low (N = 190) groups indicated that the TLS-high group had a longer overall survival compared to the TLS-low group (median OS of 46.2 months and 33.8 months, respectively, $p < 0.001$ from log-rank test, HR: 0.6, 95% CI: 0.44 - 0.81) (Figure 5B), confirming the prognostic power of this TLS scoring system in NSCLC.

Another immune cell scoring system, known as Immunoscore and which quantifies tumor infiltrating lymphocytes (TILs) using CD3 and CD8 markers, has already proven to be highly valuable in clinic. It has indeed been shown to be more powerful than the traditional staging system and is now considered as a prognostic indicator (1, 2). In this regard, we wanted to confirm the clinical value of the Immunoscore (N = 120) in this cohort and assess if there was any correlation between Immunoscore and TLS score status. Due to the low number of samples in I0 (N = 10), I1 (N = 1), I2 (N = 21), I3 (N = 25) and I4 (N = 63) after considering the survival data, we consolidated the Immunoscore classification into two major groups – Immunoscore-high and Immunoscore-low – to mitigate the sample size challenge. Survival analysis comparing Immunoscore-high group (I3 and I4; N = 88) to Immunoscore-low group (I0, I1, and I2; N = 32) revealed that indeed Immunoscore-high patients had longer overall survival compared to Immunoscore-low patients (median OS of 46.2 months in the -high group versus 23.8 months in the -low group, $p < 0.03$ from log-rank test; HR: 0.58, 95% CI: 0.35 - 0.95) (Figure 5C). Overall, these results showed that both TLS Score and Immunoscore -high values were associated with better survival. Additional univariate Cox analysis confirmed these observations, greater and significant hazard ratios being obtained for both TLS-high and Immunoscore-high groups compared to their respective -low categories (Supplementary Figures 3A, B).

Next, we evaluated the association between TLS score and Immunoscore. Despite observing a significant increase in the proportion of TLS-high samples in the Immunoscore-high compared to the -low samples, only 53% of the Immunoscore-high samples were also TLS-high (Figure 5D). Conversely, high proportions of Immunoscore-high were found in both TLS-high and TLS-low cases. Immunoscore-high represented indeed 83% of the TLS-high and 65% of the TLS-low cohorts (Figure 3E). These results suggested that despite observing a positive trend between the Immuno- and TLS- scores, there was no absolute concordance between these two scoring systems, possibly due to the fact that they are primarily based on two different immune cell populations, T cells and B cells, respectively. These findings were further confirmed in Figures 5F, G, where a high range of TLS Score values was observed within Immunoscore-high samples (Figure 5F), with more than 25% of these samples being TLS negative (Figure 5G).

Multiple histology methods and assays are used to detect TLS and assess their maturity levels, including single IHC assays for the CD20, CD21 and CD23 markers. In this regard, we wanted to assess the prognostic value of the TLS Score, which considers multiple TLS features based on the positivity status of these markers taken all together and compare it with the prognostic value of each marker considered as a single marker, as we would do for single IHC assays data. As presented in Figure 5H, we calculated the total density of positive cells for single markers (CD20, CD21 and CD23) and the combined markers for CD21 and CD23 ($CD21^+$ $CD23^-$, $CD21^-$ $CD23^+$, and $CD21^+$ $CD23^+$) located within the entire tumor area 'AA'. For each density results, the cohort was divided into two groups, high and low density based on the median cut-off. For TLS Score classification, we used the previously described optimal cut-off. Subsequently, we conducted univariate Cox analyses to assess the hazard ratio, measuring the relative risk of death, between (i) density-high versus density-low (reference) category for each individual marker, (ii) TLS-high versus -low (reference) category and (iii) density-high versus density-low (reference) group for combined markers $CD21^+$ $CD23^-$, $CD21^-$ $CD23^+$, and $CD21^+$ $CD23^+$. Outstandingly, the TLS-high group demonstrated the most pronounced and significant impact on survival outcomes, confirming the added value of the TLS tissue score. No significant result was obtained for the $CD23^+$ density high, probably due to the lower prevalence of these cells within the tumor tissues.

Another way commonly used to assess TLS is by evaluating gene expression (GE) signatures specific to TLS. Thus, we first wanted to assess how our TLS Score correlated with the two main and commonly used '12-chemokine TLS' and 'TLS T_H1 B cell' GE signatures (8) (N = 375 samples). The 12-chemokine TLS signature includes *CCL2, CCL3, CCL4, CCL5, CCL8, CCL18, CCL19, CCL21, CXCL9, CXCL10, CXCL11* and *CXCL13* genes (12/12 genes overlap with our GE data), and TLS T_H1 B cell signature contains *CD4, CCR5, CXCR3, CSF2, IGSF6, IL2RA, CD38, CD40, CD5, MS4A1, SDC1, GFI1, IL1R1, IL1R2, IL10, CCL20, IRF4, TRAF6* and *STAT5A* genes (15/19 genes overlap, *IGSF6, SDC1, GFI1* and *STAT5A* genes were missing). B cells being the major TLS immune component, we also assessed the expression of multiple B-cell gene signatures, named 'B cell' (*CD19, MS4A1, CD22* and *CD79A* genes) (32), 'B lineage' (*CD19, MS4A1, CD22, CD79A* and *CXCL13* genes) and 'B cell CXC recruitment' (*CD19, MS4A1, CD22, CD79A* and *CXCL13*). Using gene set variation analysis (GSVA), we observed a significant difference in the enrichment of these five signatures when comparing TLS-high with TLS-low tissues (Figure 5I), but also when comparing TLS negative samples to TLS positives cases (Supplementary Figure 3C). Indeed, while TLS-high and TLS positive tissues demonstrated higher GSVA scores for all GE signatures, TLS-low and TLS negative samples showed a lower GSVA scores.

Together, these results confirmed the prognostic relevance of the Immunoscore in NSCLC but also demonstrated the clinical potential of this TLS Score, which was associated with an improved overall survival and was positively associated with published TLS gene expression signatures.

TLS score association with clinical and demographical parameters

Next, we aimed to determine the relationships between TLS Score and clinicopathological features of the overall population. We performed Cox regression analyses to investigate the prognostic relevance of TLS score, along with several other variables including age, sex category, smoking status, and NSCLC histology. However, due to a substantial amount of missing data overlapping for sex, smoking status, and histology categories, we were unable to include all these variables in a single survival model.

Consequently, we employed four distinct survival models to assess the prognostic value of the TLS Score while adjusting for the impact of the following variables: (i) age, (ii) sex, (iii) smoking status, and (iv) histology. Additionally, we examined the association between the TLS groups (-high and -low) and other covariates such as *EGFR* (Epidermal Growth Factor Receptor) mutational status and PD-L1 (Programmed Death-Ligand 1) positivity status.

In Figure 6A, we showed that although the age of the patient had a significant impact on the overall survival (N = 358) (HR: 1.42, 95% CI: 1.21 – 1.67, p < 0.001, with age scaled data), this did not affect the prognostic value of the TLS Score, with a hazard ratio of 0.32 (95% CI: 0.16 – 0.63, p < 0.001). Moreover, even when considering the sex category (N = 358), smoking status (N = 318) and NSCLC histology (N = 358) factors, the TLS Score impact on the overall survival remained significant (Figure 6A). Interestingly, the female category exhibited a significantly higher TLS Score than the male category, with TLS score median values of 0.35 and 0.05, respectively (Kruskal-Wallis, p = 0.0057) (Figure 6B, left panel). This could be explained by higher proportion of TLS-high cases in the Female category, as they represented approximately 68% of the female population, whereas this number fell at 40% in the male population (Figure 6B, right panel). We then segregated the two gender categories into two sub-groups according to their TLS Score status, TLS-high or TLS-low, to assess how this score impacted the overall survival in each group. Whereas the median OS increased by 19.3 months in the female category (Figure 6C, left panel) and by 14.1 months in the male category (Figure 6C, right panel) when we compared TLS-high with TLS-low cases, only the male group result was significant (p = 0.011), the female group describing a p-value of 0.063.

When considering the smoking status, the TLS Score still had a significant association with survival (HR: 0.38, 95% CI: 0.19 – 0.77, p = 0.008) while the impact of the smoking category was not significant in this analysis (Figure 6A). Furthermore, although we did not observe a statistically significant relationship between the TLS Score value and the smoking categories (Kruskal-Wallis, p = 0.0057) (Figure 6D, left panel), the proportion of TLS-high cases tended to be higher in patients who never smoked at the time of the survey (63%), compared to the current (52%) and past smokers (43%) (Figure 6D, right panel).

We then evaluated the impact of NSCLC histology on the overall patient survival and TLS Score repartition within different lung cancer sub-types. This cohort contains 214 adenocarcinoma, 1 adenosquamous, 1 bronchioalveolar, 1 large cell, 142 squamous cell, 1 sarcomatoid, 9 "other", and 29 "unknown" cases. Due to the low number of tissues in some categories, we focused on the adenocarcinoma (N = 214) and squamous cell (N = 142) categories for the subsequent analyses. In Figure 6A, we observed a significant impact of the histological modality, the squamous cell category reducing the risk of death by 28% (HR: 0.72, 95% CI: 0.52 – 0.99, p = 0.043) compared to the adenocarcinoma category when taken as reference. Furthermore, considering the histology type and TLS Score as covariate did not impact the prognostic relevance of this tissue score which described a hazard ratio of 0.27 (95% CI: 0.14 – 0.56, p < 0.001) (Figure 6A). Interestingly, we observed lower TLS Score values in the squamous cell category than in the adenocarcinoma category, with TLS score median values of 0.04 and 0.37, respectively (Kruskal-Wallis, p = 1.3e-06) (Figure 6E, left panel). This could be explained by a lower proportion of TLS-high cases in the squamous cell compared to the adenocarcinoma subtype, with 30% of squamous cell and 58% of adenocarcinoma cases being TLS-high (Figure 6E, right panel). A high TLS Score was however associated with a better outcome in both categories (Figure 6F). Indeed, when comparing TLS-high with TLS-low cases, the median OS was increased by 70.5 months in squamous cell (34.2 vs 104.7 months, p = 0.0035) (Figure 6F, left panel), and by 8.3 months in adenocarcinoma (35.4 vs 43.7 months, p = 0.012) (Figure 6F, right panel).

These NSCLC cases have also been characterized for *EGFR* mutation status and PD-L1 expression levels. We thus wanted to assess the prevalence of TLS-high and TLS-low cases within each drug segment category. Interestingly, approximately 66% of the *EGFR* mutant samples (N = 113) were TLS-high against 43% of the *EGFR* wild-type cohort (N = 248) (Figure 6G), suggesting an impact of the mutational status on the TLS Score value (hypergeometric test, qval <0.001, Supplementary Figure 3D).

Finally, we evaluated the TLS Score repartition according to PD-L1 categories characterized by different PD-L1 positivity cut-off (>1% or >50% positivity) on the surface of the tumor cells (Figure 6H) or immune cells (Figure 6I). These categories were as follow: PD-L1 1% TC (PD-L1 cut-off >1% on tumor cells) (Figure 6H, left panel), PD-L1 50% TC (PD-L1 cut-off >50% on tumor cells) (Figure 6H, right panel), PD-L1 1% IC (PD-L1 cut-off >1% on immune cells) (Figure 6I, left panel) and PD-L1 50% IC (PD-L1 cut-off >50% on immune cells) (Figure 6I, right panel).

We did not observe a significant impact of PD-L1 status on the TLS Score proportions, approximately 50% of cases describing TLS-high scores in all the PD-L1 positive cohorts and independently of the PD-L1 cut-off used (Figures 6H, I). However, it is interesting to note that change in this cut-off had a slight impact on the TLS Score proportion within PD-L1-negative cohorts, TLS-high cases representing 50% of the PD-L1-negative cases among the PD-L1 50% IC cohort and 25% among the PD-L1 1% IC cohort (Figure 6I). We found that the TLS score is prognostic after adjusting for PD-L1 status in tumor and immune cells. (Supplementary Figure 4). As a summary, although this analysis did not demonstrate any impact of the PD-L1 status on the TLS Score, it highlighted the importance of keeping the same analysis cut-off across studies and when comparing data.

Discussion

TLS are commonly associated with favorable prognosis in many cancer types. However, conflicting studies suggest that not all aggregates are functionally equivalent and minimal characteristics may be required to form a functional TLS (8–13). Moreover, variable numbers of TLS can be present within a tumor tissue, each one of these structures describing unique characteristics (such as the size, cellular composition, location, maturation stage), each feature having a potential impact on the collective clinical power. In this context, we aimed at evaluating the prognostic value of TLS in NSCLC by establishing a TLS Score that captures the diversity of TLS within a tumor, considering functional and compositional features.

We observed a large variety of TLS and B-cell aggregates within tumor tissues, each differing in size, organization level and cellular composition. Interestingly, high density of $CD21^+$ and $CD23^+$ cells, markers considered as TLS maturity markers, were observed in both small and large aggregates, suggesting that a high degree of TLS organization and maturation is independent of aggregate size.

Based on our observations and the image analysis readouts, we considered multiple ways for calculating a tissue score capturing TLS compositional, functional, and organizational diversity within tissues. We initially considered (i) TLS relative area and (ii) the density of each cell phenotype, for each TLS, and combined these data into a unique TLS tissue score. However, this idea was challenged by the Concordance index survival analysis which demonstrated a prognostic significance of only specific cells within TLS, particularly B cells and FDC $CD21^+$ $CD23^-$. A parallel can be made with the three TLS maturation stages first identified by Karīna Siliņa et al. in human lung squamous cell carcinoma, which are: (i) early TLS ($CD21^-$ $CD23^-$); (ii) primary follicle-like TLS with differentiated FDC ($CD21^+$ $CD23^-$); (iii) and mature secondary follicle-like TLS with a germinal center reaction ($CD21^+$ $CD23^+$) (10). Moreover, the germinal center reaction, crucial for B cell activation and differentiation, has demonstrated significant relevance for patient survival in various cancer types (8–10, 33–37). In lymph nodes in mice, the long-term retention of antigens in germinal centers is controlled by the spatial organization of the follicular dendritic cell network and notably high levels of CD21 expression on their surface (38), thus supporting our findings.

The other cell phenotypes assessed did not show significant impact when located within TLS, thus questioning the relevance of including them into a TLS scoring system which aimed at evaluating the clinical value of these structures. In light of these findings, we refined our TLS Score calculation strategy to generate a data-driven score, that would only include the readouts identified as the most prognostic and robust. The final score was calculated using (i) the scaled sum of B cells and FDC $CD21^+$ $CD23^-$ densities (log_{10}), and (ii) the TLS scaled relative area, which were the three most prognostically relevant and robust TLS features in this NSCLC cohort.

Excitingly, this TLS Score demonstrated a strong prognostic power, independently of the cut-off used, and added value over the commonly used TLS markers CD20, CD21 and CD23 when assessed as single markers in the context of single IHC analysis. These results highlighted the relevance of using combination of markers specific to TLS, such as a TLS tissue score, instead of single markers, to accurately evaluate how the TLS biology and heterogeneity within a tumor tissue impact patients' prognosis. Nevertheless, this score being generated based on the specific detection of TLS structures in tumor resections, it would not solve the challenge of TLS detection and assessment in tumor biopsies, fewer number of TLS or none being detected due to the small size of the tumor cores.

We could also question the reproducibility of the TLS Score values and subsequent prognostic results if different tissue sections of the same tumors were stained. Small TLS observed in one section could indeed correspond to larger TLS cut near the surface and thus displaying different sizes, maturation status and cellular composition – parameters used to calculate the TLS Score values. In this context, it would be relevant to further explore the TME organization in tissues TLS-high compared to TLS-low cases with the aim of highlighting TLS TME spatial signatures that could be used as TLS surrogate in tumor biopsies. We could for example describe the spatial characteristics of areas outside TLS, understand the distribution of immune cells within the tissue, how they interact with each other and with tumor cells. In this regard, we assessed if there was any correlation between TLS Score and Immunoscore, another tissue scoring system focusing on the T cell population using CD3 and CD8 markers and now considered as a prognostic indicator in multiple tumor types (1, 2). While we demonstrated higher TLS Score values in Immunoscore-high cases overall, in agreement with the literature reporting that a high $CD8^+$ T cell infiltration is significantly correlated with the presence of mature TLS (5, 8, 9, 39–43), this result should be interpreted carefully and would require additional investigations, since one quarter of the Immunoscore-high cases were TLS-negative. We could thus hypothesize that this T cell sub-population might not be the optimal one to be considered as a TLS surrogate, and evaluating other cell populations or combinations of different cell types as potential TLS surrogates is necessary. We could assess the distribution of another T cell sub-population, such as $CD4^+$ T cells, but also myeloid cells, such as dendritic cells, macrophages, or lymphatic vessels and high endothelial venules for which increased densities have been described in TLS-positive tissues (8, 13, 44–47). Additionally, it is important to note the lack of Immunoscore data for 286 out of 406 NSCLC cases, which might affect these results.

Genomic technologies are another common way to evaluate TLS presence within tumor tissues in the clinic, using gene expression (GE) signatures specific to TLS, the main two being the '12-chemokine signature' and 'T_H1 cell and B cell signature' first published by Sautès-Fridman et al. (8, 33, 48). GSVA analyses revealed significantly higher TLS GE signature scores in TLS-high compared to TLS-low cases, despite a large proportion of samples having low signature score, thus supporting the clinical potential of this TLS Score. One possible explanation for the low GSVA scores obtained could be the fact that transcriptomic data were generated using tumor bulk tissues, whereas the TLS Score was based on multiplex IF data specific to the TLS structures within the tumor and hence reflected the power of spatial over tumor bulk

technologies. Furthermore, TLS GE signatures are related to either chemokines or cell populations involved in TLS neogenesis and considered as pan-cancer signatures (8); hence, refining TLS GE signatures with the support of spatial transcriptomic technologies, or defining new ones that show greater specificity to the TLS maturation degrees might be of relevance to improve our understanding of TLS impact in the clinic. Another explanation could be related to the fact that this TLS Score has been developed based on multiplex IF data obtained from one cohort of NSCLC patients which includes different histology types, tumor stages, and demographical characteristics, with missing information for many patients. Thus, we cannot exclude the fact that the TLS Score results obtained, and its promising prognostic value may be specific of one sub-category of the NSCLC patient population. It will thus be necessary to confirm the impact of this scoring system in other lung cancer cohorts as well as in different tumor indications.

These observations about the NSCLC cohort, which can be considered as limitations, are particularly relevant and should be taken into account when interpreting the results assessing whether clinical and demographical features such as age, sex, smoking status, histology category, *EGFR* mutational and PD-L1 positivity status contributed to TLS heterogeneity and correlated with our TLS Score. We indeed demonstrated that the TLS Score prognostic value was independent of age, sex, smoking category, and histology modality features. Besides, we revealed a higher prevalence of TLS-high cases in (i) the female compared to the male category, (ii) the adenocarcinoma compared to the squamous cell subtype, and (iii) *EGFR* mutant compared to *EGFR* wild-type samples. No correlation with PD-L1 expression levels was observed. Interestingly, and in coherence with our findings, a study reported a higher frequency of *EGFR* mutations in tumors enriched with mature dendritic cells, cell subset considered as a hallmark of TLS (49). A parallel can also be made with a study which highlighted a predictive value of mature TLS to immune checkpoint inhibitor in solid tumors, independently of PD-L1 expression (5). In contrast, multiple studies evaluating the impact of TLS in lung adenocarcinoma did not find a correlation between TLS density and maturity and features such as age, sex, *EGFR* mutation, pathological types or smoking status (50–52).

Furthermore, these NSCLC cases being baseline tumors coming from patients having received chemotherapy or radiotherapy treatments, a fundamental next step would be to evaluate the clinical value of this TLS Score for patients treated with immunotherapies. The identification of reliable predictive biomarkers of response to immunotherapies is indeed a current unmet medical need. In this context, Vanhersecke et al. recently demonstrated that the presence of mature TLS $CD23^+$ is predictive of response to immunotherapies in multiple tumor types, independently of PD-L1 expression status and $CD8^+$ T cell density (5). The calculation of the TLS Score relying on the density of cells composing the germinal center, which is a feature characterizing mature TLS, evaluating and comparing the predictive values of (i) TLS Score and (ii) presence of mature TLS would inform us further on the clinical benefit of combining multiple TLS features into one unique tissue score.

In conclusion, we developed and demonstrated the prognostic value of a TLS tissue score in NSCLC which allows a better representation and characterization of the TLS biology and heterogeneity undergoing within a tumor. Our aim being the identification of biomarkers which could be used in the clinic to select patients who are more likely to benefit from immunotherapies, the next step is to evaluate the predictive power of this TLS Score in cohorts of patients treated with immune checkpoint inhibitors. Finally, this TLS scoring system could be used as a tool to assess how TLS impact the organization of the tumor microenvironment, thus supporting the discovery of TLS TME spatial biomarkers, surrogates of mature TLS, to help overcome the challenge of TLS detection and assessment in tumor biopsies in the clinic.

Data availability statement

The original contributions presented in the study are included in the article/Supplementary Material, further inquiries can be directed to the corresponding author.

Ethics statement

The studies involving humans were approved by The AstraZeneca Biobank in the UK is licensed by the Human Tissue Authority (License No. 12109) and has National Research Ethics Service Committee (NREC) approval as a Research Tissue Bank (RTB) (REC No 17/NW/0207) which covers the use of the samples for this project. The studies were conducted in accordance with the local legislation and institutional requirements. The participants provided their written informed consent to participate in this study.

Author contributions

JuB: Conceptualization, Data curation, Formal analysis, Investigation, Methodology, Writing – original draft, Writing – review & editing. PP: Data curation, Formal analysis, Writing – original draft, Writing – review & editing. FS: Writing – original draft, Writing – review & editing, Data curation, Formal analysis. EJ: Formal analysis, Writing – original draft, Writing – review & editing. FN: Data curation, Formal analysis, Methodology, Writing – original draft, Writing – review & editing. MSu: Supervision, Writing – original draft, Writing – review & editing. AA: Data curation, Writing – original draft, Writing – review & editing. MT: Validation, Data curation, Writing – original draft, Writing – review & editing. MSa: Data curation, Writing – original draft, Writing – review & editing. MV: Data curation, Methodology, Writing – original draft, Writing – review & editing. HH: Formal analysis, Writing – original draft, Writing – review & editing. MH-B: Project administration, Writing – original draft, Writing – review & editing. JoB: Validation, Writing – original draft, Writing – review & editing. EJ: Methodology, Writing – original draft, Writing – review & editing. SW: Methodology, Writing – original draft, Writing – review & editing. JG: Data curation, Writing – original draft, Writing – review & editing. RV: Conceptualization,

Writing – original draft, Writing – review & editing. TG: Conceptualization, Writing – original draft, Writing – review & editing. HA: Conceptualization, Funding acquisition, Resources, Supervision, Writing – original draft, Writing – review & editing.

Funding

The author(s) declare financial support was received for the research, authorship, and/or publication of this article. JB was supported by an AstraZeneca post-doc fellowship funding. The authors affiliated with AstraZeneca were provided financial support in the form of salaries, research materials by AstraZeneca and are shareholders in AstraZeneca.

Acknowledgments

We thank Damian Bikiel for his iterative log-rank test code.

Conflict of interest

Authors JB, HA, PP, EJ, SW, JB, MSa, FN and MSu were employed by the company AstraZeneca and are shareholders. Authors FS, EJ, MV, TG, AA, HH and MH-B were employed by the company AstraZeneca. Author JG was employed by the company Veracyte.

The remaining author declares that the research was conducted in the absence of any commercial or financial relationships that could be construed as a potential conflict of interest.

The authors declare that this study received funding from AstraZeneca. Additionally, Author TG received research funding from Idera Pharmaceuticals, consulting fees from Mendus, LAVA Therapeutics and GE Health, and is shareholder of LAVA Therapeutics. Author RV received research funding from Genmab BV. However, none of these funders, except AstraZeneca, were involved in the study design, data collection and analysis, decision to publish, or preparation of the manuscript.

The author(s) declared that they were an editorial board member of Frontiers, at the time of submission. This had no impact on the peer review process and the final decision.

Publisher's note

Supplementary material

The Supplementary Material for this article can be found online at: https://www.frontiersin.org/articles/10.3389/fimmu.2024.1422206/full#supplementary-material.

References

1. Galon J, Mlecnik B, Bindea G, Angell HK, Berger A, Lagorce C, et al. Towards the introduction of the 'Immunoscore' in the classification of Malignant tumours. *J Pathol*. (2014) 232:199–209. doi: 10.1002/path.4287

2. Bruni D, Angell HK, Galon J. The immune contexture and Immunoscore in cancer prognosis and therapeutic efficacy. *Nat Rev Cancer*. (2020) 20:662–80. doi: 10.1038/s41568-020-0285-7

3. Bai R, Lv Z, Xu D, Cui J. Predictive biomarkers for cancer immunotherapy with immune checkpoint inhibitors. *biomark Res*. (2020) 8:34. doi: 10.1186/s40364-020-00209-0

4. Cabrita R, Lauss M, Sanna A, Donia M, Skaarup Larsen M, Mitra S, et al. Tertiary lymphoid structures improve immunotherapy and survival in melanoma. *Nature*. (2020) 577:561–5. doi: 10.1038/s41586-019-1914-8

5. Vanhersecke L, Brunet M, Guegan JP, Rey C, Bougouin A, Cousin S, et al. Mature tertiary lymphoid structures predict immune checkpoint inhibitor efficacy in solid tumors independently of PD-L1 expression. *Nat Cancer*. (2021) 2:794–802. doi: 10.1038/s43018-021-00232-6

6. Helmink BA, Reddy SM, Gao J, Zhang S, Basar R, Thakur R, et al. B cells and tertiary lymphoid structures promote immunotherapy response. *Nature*. (2020) 577:549–55. doi: 10.1038/s41586-019-1922-8

7. Petitprez F, de Reynies A, Keung EZ, Chen TW, Sun CM, Calderaro J, et al. B cells are associated with survival and immunotherapy response in sarcoma. *Nature*. (2020) 577:556–60. doi: 10.1038/s41586-019-1906-8

8. Sautès-Fridman C, Petitprez F, Calderaro J, Fridman WH. Tertiary lymphoid structures in the era of cancer immunotherapy. *Nat Rev Cancer*. (2019) 19:307–25. doi: 10.1038/s41568-019-0144-6

9. Fridman W, Meylan M, Petitprez F, Sun CM, Italiano A, Sautès-Fridman C. B cells and tertiary lymphoid structures as determinants of tumour immune contexture and clinical outcome. *Nat Rev Clin Oncol*. (2022) 19:441–57. doi: 10.1038/s41571-022-00619-z

10. Silina K, Soltermann A, Attar FM, Casanova R, Uckeley ZM, Thut H, et al. Germinal centers determine the prognostic relevance of tertiary lymphoid structures and are impaired by corticosteroids in lung squamous cell carcinoma. *Cancer Res*. (2018) 78:1308–20. doi: 10.1158/0008-5472.CAN-17-1987

11. Kroeger DR, Milne K, Nelson BH. Tumor-infiltrating plasma cells are associated with tertiary lymphoid structures, cytolytic T-cell responses, and superior prognosis in ovarian cancer. *Clin Cancer Res*. (2016) 22:3005–15. doi: 10.1158/1078-0432.CCR-15-2762

12. Koti M, Xu AS, Ren KYM, Visram K, Ren R, Berman DM, et al. Tertiary lymphoid structures associate with tumour stage in urothelial bladder cancer. *Bladder Cancer*. (2017) 3:259–67. doi: 10.3233/BLC-170120

13. Yamaguchi K, Ito M, Ohmura H, Hanamura F, Nakano M, Tsuchihashi K, et al. Helper T cell-dominant tertiary lymphoid structures are associated with disease relapse of advanced colorectal cancer. *Oncoimmunology*. (2020) 9:1724763. doi: 10.1080/2162402X.2020.1724763

14. Scorer P, Scott M, Lawson N, Ratcliffe MJ, Barker C, Rebelatto MC, et al. Consistency of tumor and immune cell programmed cell death ligand-1 expression within and between tumor blocks using the VENTANA SP263 assay. *Diagn Pathology*. (2018) 13:47. doi: 10.1186/s13000-018-0725-9

15. Pagès F, Mlecnik B, Marliot F, Bindea G, Ou F-S, Bifulco C, et al. International validation of the consensus Immunoscore for the classification of colon cancer: a prognostic and accuracy study. *Lancet*. (2018) 391:2128–39. doi: 10.1016/S0140-6736(18)30789-X

16. Segerer FJ, Nekolla K, Rognoni L, Kapil A, Schick M, Angell HK, et al. Novel deep learning approach to derive cytokeratin expression and epithelium segmentation from DAPI (2022). Available online at: https://arxivorg/abs/220808284.

17. Lê S, Josse J, Husson F. FactoMineR: an R package for multivariate analysis. *J Stat Software*. (2008) 25:1–18. doi: 10.18637/jss.v025.i01

18. Hänzelmann S, Castelo R, Guinney J. GSVA: gene set variation analysis for microarray and RNA-Seq data. *BMC Bioinf*. (2013) 14. doi: 10.1186/1471-2105-14-7

19. Tu E, McGlinchey K, Wang J, Martin P, Ching SL, Floc'h N, et al. Anti-PD-L1 and anti-CD73 combination therapy promotes T cell response to EGFR-mutated NSCLC. *JCI Insight*. (2022) 7. doi: 10.1172/jci.insight.142843

20. Davidson-Pilon C. lifelines: survival analysis in Python. *J Open Source Software*. (2019) 4. doi: 10.21105/joss.01317

21. Therneau T. A Package for Survival Analysis in R. *R package version 3.7-0*, (2024). Available at: https://CRAN.R project.org/package=survival.

22. Alboukadel K. survminer: Drawing Survival Curves using 'ggplot2'. *R package version 0.4.9*. (2016) Available at: https://cran.r-project.org/web/packages/survminer.

23. Harrell FE, Lee KL, Mark DB. Multivariable prognostic models: issues in developing models, evaluating assumptions and adequacy, and measuring and reducing errors. *Stat Med*. (1995) 15:361–87.

24. Kurshumliu F, Sadiku-Zehri F, Qerimi A, Vela Z, Jashari F, Bytyci S, et al. Divergent immunohistochemical expression of CD21 and CD23 by follicular dendritic cells with increasing grade of follicular lymphoma. *World J Surg Oncol*. (2019) 17:115. doi: 10.1186/s12957-019-1659-8

25. Suryani S, Fulcher DA, Santner-Nanan B, Nanan R, Wong M, Shaw PJ, et al. Differential expression of CD21 identifies developmentally and functionally distinct subsets of human transitional B cells. *Blood*. (2010) 115:519–29. doi: 10.1182/blood-2009-07-234799

26. Allen CD, Cyster JG. Follicular dendritic cell networks of primary follicles and germinal centers: phenotype and function. *Semin Immunol*. (2008) 20:14–25. doi: 10.1016/j.smim.2007.12.001

27. Dieu-Nosjean MC, Goc J, Giraldo NA, Sautes-Fridman C, Fridman WH. Tertiary lymphoid structures in cancer and beyond. *Trends Immunol*. (2014) 35:571–80. doi: 10.1016/j.it.2014.09.006

28. Le Rochais M, Hemon P, Ben-Guigui D, Garaud S, Le Dantec C, Pers JO, et al. Deciphering the maturation of tertiary lymphoid structures in cancer and inflammatory diseases of the digestive tract using imaging mass cytometry. *Front Immunol*. (2023) 14:1147480. doi: 10.3389/fimmu.2023.1147480

29. Italiano A, Bessede A, Pulido M, Bompas E, Piperno-Neumann S, Chevreau C, et al. Pembrolizumab in soft-tissue sarcomas with tertiary lymphoid structures: a phase 2 PEMBROSARC trial cohort. *Nat Med*. (2022) 28:1199–206. doi: 10.1038/s41591-022-01821-3

30. Levesque MC, St. Clair EW. B cell–directed therapies for autoimmune disease and correlates of disease response and relapse. *J Allergy Clin Immunol*. (2008) 121:13–21. doi: 10.1016/j.jaci.2007.11.030

31. Chung JB, Sater RA, Fields ML, Erikson J, Monroe JG. CD23 defines two distinct subsets of immature B cells which differ in their responses to T cell help signals. *Int Immunol*. (2002) 14:157–66. doi: 10.1093/intimm/14.2.157

32. Danaher P, Warren S, Dennis L, D'Amico L, White A, Disis ML, et al. Gene expression markers of Tumor Infiltrating Leukocytes. *J Immunother Cancer*. (2017) 5:18. doi: 10.1186/s40425-017-0215-8

33. Sautès-Fridman C, Verneau J, Sun C, Moreira M, Chen T, Meylan M, et al. Tertiary Lymphoid Structures and B cells: Clinical impact and therapeutic modulation in cancer. *Semin Immunol*. (2020) 48. doi: 10.1016/j.smim.2020.101406

34. Hayashi Y, Makino T, Sato E, Ohshima K, Nogi Y, Kanemura T, et al. Density and maturity of peritumoral tertiary lymphoid structures in oesophageal squamous cell carcinoma predicts patient survival and response to immune checkpoint inhibitors. *Br J Cancer*. (2023) 128:2175–85. doi: 10.1038/s41416-023-02235-9

35. Liang H, Zhang Z, Guan Z, Zheng S, Lou J, Liu W, et al. Follicle-like tertiary lymphoid structures: A potential biomarker for prognosis and immunotherapy response in patients with laryngeal squamous cell carcinoma. *Front Immunol*. (2023) 14:1096220. doi: 10.3389/fimmu.2023.1096220

36. Lynch KT, Young SJ, Meneveau MO, Wages NA, Engelhard VH, Slingluff CL Jr., et al. Heterogeneity in tertiary lymphoid structure B-cells correlates with patient survival in metastatic melanoma. *J Immunother Cancer*. (2021) 9. doi: 10.1136/jitc-2020-002273

37. He M, He Q, Cai X, Liu J, Deng H, Li F, et al. Intratumoral tertiary lymphoid structure (TLS) maturation is influenced by draining lymph nodes of lung cancer. *J Immunother Cancer*. (2023) 11. doi: 10.1136/jitc-2022-005539

38. Martinez-Riano A, Wang S, Boeing S, Minoughan S, Casal A, Spillane KM, et al. Long-term retention of antigens in germinal centers is controlled by the spatial organization of the follicular dendritic cell network. *Nat Immunol*. (2023) 24:1281–94. doi: 10.1038/s41590-023-01559-1

39. Gao J, Navai N, Alhalabi O, Siefker-Radtke A, Campbell MT, Tidwell RS, et al. Neoadjuvant PD-L1 plus CTLA-4 blockade in patients with cisplatin-ineligible operable high-risk urothelial carcinoma. *Nat Med*. (2020) 26:1845–51. doi: 10.1038/s41591-020-1086-y

40. Hiraoka N, Ino Y, Yamazaki-Itoh R. Tertiary lymphoid organs in cancer tissues. *Front Immunol*. (2016) 7:244. doi: 10.3389/fimmu.2016.00244

41. Goc J, Germain C, Vo-Bourgais TK, Lupo A, Klein C, Knockaert S, et al. Dendritic cells in tumor-associated tertiary lymphoid structures signal a Th1 cytotoxic immune contexture and license the positive prognostic value of infiltrating CD8+ T cells. *Cancer Res*. (2014) 74:705–15. doi: 10.1158/0008-5472.CAN-13-1342

42. Behr DS, Peitsch WK, Hametner C, Lasitschka F, Houben R, Schönhaar K, et al. Prognostic value of immune cell infiltration, tertiary lymphoid structures and PD-L1 expression in Merkel cell carcinomas. *Int J Clin Exp Pathology*. (2014) 7:7610–21.

43. Di Caro G, Bergomas F, Grizzi F, Doni A, Bianchi P, Malesci A, et al. Occurrence of tertiary lymphoid tissue is associated with T-cell infiltration and predicts better prognosis in early-stage colorectal cancers. *Clin Cancer Res*. (2014) 20:2147–58. doi: 10.1158/1078-0432.CCR-13-2590

44. Kang W, Feng Z, Luo J, He Z, Liu J, Wu J, et al. Tertiary lymphoid structures in cancer: the double-edged sword role in antitumor immunity and potential therapeutic induction strategies. *Front Immunol*. (2021) 12:689270. doi: 10.3389/fimmu.2021.689270

45. Han J, Dong L, Wu M, Ma F. Dynamic polarization of tumor-associated macrophages and their interaction with intratumoral T cells in an inflamed tumor microenvironment: from mechanistic insights to therapeutic opportunities. *Front Immunol*. (2023) 14:1160340. doi: 10.3389/fimmu.2023.1160340

46. Bobik A, Kyaw TS, Tipping P, Toh BH. M1 macrophages, key contributors to lymphoid neogenesis in atherosclerotic aorta. *Cardiovasc Res*. (2014) 101:339–41. doi: 10.1093/cvr/cvu019

47. Koscsó B, Kurapati S, Rodrigues RR, Nedjic J, Gowda K, Shin C, et al. Gut-resident CX3CR1hi macrophages induce tertiary lymphoid structures and IgA response in situ. *Sci Immunol*. (2020) 5.

48. Li R, Berglund A, Zemp L, Dhillon J, Putney R, Kim Y, et al. The 12-CK score: global measurement of tertiary lymphoid structures. *Front Immunol*. (2021) 12:694079. doi: 10.3389/fimmu.2021.694079

49. Biton J, Mansuet-Lupo A, Pecuchet N, Alifano M, Ouakrim H, Arrondeau J, et al. TP53, STK11, and EGFR mutations predict tumor immune profile and the response to anti-PD-1 in lung adenocarcinoma. *Clin Cancer Res*. (2018) 24:5710–23. doi: 10.1158/1078-0432.CCR-18-0163

50. Xu X, Gao Y, Duan S, Ding Q, Wang X, Dai X, et al. Clinical implications and molecular features of tertiary lymphoid structures in stage I lung adenocarcinoma. *Cancer Med*. (2023) 12:9547–58. doi: 10.1002/cam4.5731

51. Ren F, Xie M, Gao J, Wu C, Xu Y, Zang X, et al. Tertiary lymphoid structures in lung adenocarcinoma: characteristics and related factors. *Cancer Med*. (2022) 11:2969–77. doi: 10.1002/cam4.4796

52. Domblides C, Rochefort J, Riffard C, Panouillot M, Lescaille G, Teillaud JL, et al. Tumor-associated tertiary lymphoid structures: from basic and clinical knowledge to therapeutic manipulation. *Front Immunol*. (2021) 12:698604. doi: 10.3389/fimmu.2021.698604

frontiers | Frontiers in Immunology

TYPE Systematic Review
PUBLISHED 31 October 2024
DOI 10.3389/fimmu.2024.1414884

OPEN ACCESS

EDITED BY
Ying Ma,
Tianjin Medical University Cancer Institute and Hospital, China

REVIEWED BY
Kaili Yang,
Peking Union Medical College Hospital (CAMS), China
Ipsita Guha,
Children's Hospital of Philadelphia, United States

*CORRESPONDENCE
Xueying Yang
yangxueying@cmu.edu.cn

RECEIVED 09 April 2024
ACCEPTED 11 October 2024
PUBLISHED 31 October 2024

CITATION
Jiang B, Wu Z, Zhang Y and Yang X (2024) Associations between tertiary lymphoid structure density and immune checkpoint inhibitor efficacy in solid tumors: systematic review and meta-analysis. *Front. Immunol.* 15:1414884. doi: 10.3389/fimmu.2024.1414884

Associations between tertiary lymphoid structure density and immune checkpoint inhibitor efficacy in solid tumors: systematic review and meta-analysis

Bin Jiang, Zhuo Wu, Yang Zhang and Xueying Yang*

Department of Thoracic Surgery, The Fourth Affiliated Hospital of China Medical University, Shenyang, China

Background: Tertiary lymphoid structures (TLS) play a crucial role in tumor immunity, yet their relationship with the efficacy of immune checkpoint inhibitors (ICI) in cancer therapy is not fully understood. This study aims to systematically evaluate how TLS density influences treatment outcomes in cancer patients receiving ICI therapy.

Methods: The PubMed, Embase, Cochrane Library, and Web of Science databases were searched for eligible studies published before January 22, 2024. Our analysis encompassed odds ratios (ORs) for response rates (RRs) and hazard ratios (HRs) for progression-free survival (PFS), each with their respective 95% confidence intervals (CIs).

Results: Our meta-analysis, including 19 clinical trials with 1,752 patients, identified a strong correlation between high TLS density and increased RR to ICIs (OR= 2.99, 95% CI: 2.14-4.18, $P < 0.001$). Furthermore, a higher TLS density was associated with prolonged PFS (HR=0.75, 95% CI: 0.63-0.88, $P < 0.001$). Specifically, in the context of non-small cell lung cancer (NSCLC), breast cancer (BC), renal cell carcinoma (RCC), esophageal cancer (EC), and urothelial carcinoma (UC), a significant relationship was observed between high TLS density and better ICI efficacy. Publication bias did not affect the integrity of our conclusions. Sensitivity analysis further reinforced the reliability of our aggregated outcomes.

Conclusion: Our meta-analysis underscores the predictive role of TLS density in determining the RR and PFS among cancer patients undergoing ICI therapy. These results highlight the prognostic significance of TLS, suggesting its potential as a biomarker for guiding treatment decisions, even in tumor types traditionally considered ICI-resistant. Clinicians are recommended to assess TLS density as a part of patient evaluation to optimize ICI therapy initiation.

Systematic review registration: https://www.crd.york.ac.uk/prospero/, identifier CRD42023439875.

KEYWORDS

tertiary lymphoid structures (TLS), immune checkpoint inhibitors, immunotherapy, solid tumors, PD1/PDL1

Introduction

Since their introduction, immune checkpoint inhibitors (ICIs) have emerged as a critical treatment for cancer, supplementing traditional approaches such as surgery, chemotherapy, and radiation therapy. However, the efficacy of ICIs remains limited, with response rates for most tumors lying between 10% and 40% (1). This disparity underscores the need for reliable biomarkers to predict ICI therapy outcomes, making precision in immunotherapy a critical area of clinical research. Initially, PD-1/PD-L1 expression was explored for this purpose, yet predictive accuracy has been suboptimal (2). Tertiary lymphoid structures (TLS)—comprising lymphocyte and myeloid cell aggregations within inflamed tissues, akin to secondary lymphoid organs and frequently observed in tumor proximity— have shown promise. Notably, the presence of TLS in pre-treatment biopsy samples has been linked with increased ICI responses across various cancers (3–6). For instance, in the study by Lucile Vanherske, patients with mature TLS, regardless of PD-L1 expression, exhibited a 40.3% response rate to ICI therapy (7). Despite these indications of TLS as a potential ICI efficacy predictor, substantial epidemiological evidence remains scarce. Our meta-analysis aims to demonstrate that TLS density can effectively predict the response and therapeutic effect of ICI.

Methods

Protocol and registration

This systematic review and meta-analysis adhered to the PRISMA guidelines (http://www.prisma-statement.org/) and was registered on PROSPERO (CRD42023439875) (Supplementary Table S1).

Data sources and search strategy

We conducted our search across four primary databases: PubMed, Embase, Cochrane Library, and Web of Science, supplemented by additional internet searches to locate further relevant studies. The search was last updated on January 22, 2024. The following search terms were used: (Supplementary Table S2).

Selection criteria

Studies were selected based on the following criteria:

Participants

Patients with advanced malignant tumors (any solid tumor) undergoing ICI therapy were included.

Intervention

We included studies that assessed the use of ICIs, either as monotherapy or in combination with other anticancer agents, irrespective of the administration route.

Outcomes

We included studies that evaluated potential correlations between TLS and treatment outcomes in cases where ICIs were part of the regimen.

Study design

We included observational cohort and case–control studies, excluded reviews, meta-analyses, case reports, or guidelines. We excluded studies in which a 2×2 table between TLS density and the outcome of ICI treatment could not be constructed. We also excluded studies with insufficient data or no relevant information provided.

Two independent reviewers screened the titles and abstracts, and the full texts of the studies that met the inclusion criteria were obtained. Any disagreements encountered during the screening process were resolved through discussion and, if necessary, with the assistance of a third reviewer.

Data extraction

The extracted variables, when available, included: Name of the first author, Year of publication, Study sample size, Ratio of patients with high/low TLS, Number of responding patients, Type of cancer, TLS determination method, Cut-off criteria for TLS, Cut-off value, Stage of tumor, ICI application, ICI therapy, Response rate (RR) and survival analysis for TLS status subgroups, including hazard ratios (HRs) and 95% CIs for progression-free survival (PFS). In cases where HRs and 95% CI were not provided, Engauge Digitizer software version 4.1 was employed to analyze Kaplan– Meier curves, facilitating the extraction of multiple survival rates to estimate HRs and 95% CIs. Data extraction was independently conducted by two researchers, with any discrepancies resolved through discussion with a third researcher.

We performed comparative analyses between high and low TLS groups based on historical data. We classified TLS-high and TLS-low subgroups using three distinct cutoff criteria (presence, density, and signature score). The included studies provided specific TLS detection method, such as hematoxylin and eosin (H&E) staining, immunohistochemistry (IHC), etc.

For classifications based on presence and density, two detection methods for TLS were employed: H&E staining, and IHC. In H&E staining, TLS is generally defined as dense lymphocyte aggregation, while in IHC, CD20-enriched areas occasionally accompanied by CD3, CD21, or CD8 were defined as TLS. We ensured that TLS at all stages of maturity (both mature and immature) were included in each study.

We evaluated the impact of TLS on the response to ICI therapy by assessing the patient RR. Complete response, partial response, and objective response were classified as responses, Objective response included both complete response and partial response. Complete response was defined as complete disappearance of all measurable disease, partial response as a reduction in tumor size comparable to that defined by Response Evaluation Criteria in Solid Tumors (RECIST) criteria.

Stable disease, absence of progression, and progressive disease were considered non-responses. Progressive disease was either clinical progression or tumor growth, stable disease or absence of progression was patients who did not meet RECIST criteria for either disease progression or objective response.

The overall proportion of responses was defined as the RR. In studies where only the objective response rate (ORR) was calculated, ORR was considered equivalent to RR.

Statistical analysis

We calculated ORs using random-effects Mantel-Haenszel meta-analysis models, based on the TLS content in patients' biopsy specimens. PFS outcomes were reported as HRs with 95% CIs.

Statistical analyses were conducted using Review Manager 5.4 (Cochrane Collaboration, Oxford, UK) and STATA 17.0 (StataCorp LP, College Station, Texas). To evaluate heterogeneity across all meta-analyses, the Cochrane QP -value and I^2 statistic were employed. Significant heterogeneity was indicated by a P-value < 0.05 or I^2 > 50%, prompting the use of a random-effect model to integrate the results. In the absence of significant heterogeneity, a fixed-effect model was applied. Statistical significance was set at a P-value < 0.05. Publication bias was examined through Egger's test, and the trim and fill method was applied to amend the results in the presence of significant publication bias.

Quality evaluation

The quality of included studies was evaluated using the Newcastle-Ottawa Scale, while the level of evidence was assessed according to the standards set by the Oxford Centre for Evidence-Based Medicine. Each study received independent ratings from two researchers, with scores up to a maximum of 9, focusing on patient selection, outcome assessment, and comparability. This independent evaluation by two researchers aimed to minimize bias. In cases of scoring discrepancies, the study was re-evaluated and a consensus reached through discussion among the authors.

Results

Search results

A total of 871 studies were identified through electronic searches. From these, 341 duplicates were removed, along with 460 studies deemed irrelevant based on their titles and abstracts. After a detailed review of the full texts, 51 studies were further excluded. Consequently, 19 studies encompassing 1,752 patients with solid tumors who received ICI treatment were selected for inclusion in our meta-analysis. The entire selection process is illustrated in the provided PRISMA flowchart (Figure 1).

Study characteristics and quality assessment

The studies included in this meta-analysis are detailed in (Table 1). The compilation features five studies on non-small cell lung cancer (NSCLC), three on urothelial carcinoma (UC), two each dedicated to gastric cancer (GC) and renal cell carcinoma (RCC), and one study each on breast cancer (BC), esophageal carcinoma (EC), thoracic tumors, hepatocellular carcinoma (HCC), nasopharyngeal carcinoma (NPC), and melanoma. TLS-high and TLS-low subgroups using three distinct cutoff criteria (presence, density and signature score) as enumerated in (Table 1).

All studies provide RR data, while only seven studies provide PFS data. They are all cohort studies, with quality ratings between six to eight stars out of nine, with none omitted from the meta-analysis.

Effect of TLS-high on RR

Our analysis revealed a statistically significant correlation between high TLS and increased RR in patients treated with ICIs (OR=2.99; 95% CI: 2.14-4.18, P < 0.001), as depicted in (Figure 2).

Effect of TLS-high on PFS

Data from seven cohorts, covering 769 patients, provided insights into PFS. Our analysis highlighted a significant and positive relationship between elevated TLS density and extended PFS in patients undergoing ICI therapy (HR=0.75, 95% CI: 0.63-0.88, P < 0.001), as illustrated in (Figure 3).

Effect of high TLS on RR according to presence, density and signature score

Subgroup analyses revealed a distinct association between elevated TLS levels and increased RR, categorized by presence (OR=3.19; 95% CI: 1.94-5.25, P < 0.001) and density (OR=3.48; 95% CI: 1.86-6.49, P < 0.001). However, these analyses found no significant association in the subgroup defined by signature score, (OR =4.06, 95% CI: 0.38-43.42, P=0.247), as depicted in (Figure 4).

Effect of high TLS on RR according to tumor classification

Our detailed analysis focused on specific cancers showed: UC (OR=2.38, 95% CI: 1.09-5.19, P=0.029), BC (OR= 7.50, 95% CI: 1.61-34.95, P=0.01), HCC (OR=27.00 95% CI: 0.85-856.53, P=0.062), NSCLC (OR=3.47, 95% CI: 1.53-7.87, P=0.003), GC (OR=16.06, 95% CI: 1.56-165.20, P=0.020), EC (OR=14.22, 95% CI: 1.52-132.73, P=0.02), RCC (OR=2.60, 95% CI: 1.25-5.37, P=0.01), NPC (OR=1.94, 95% CI: 0.32- 11.76, P=0.469),

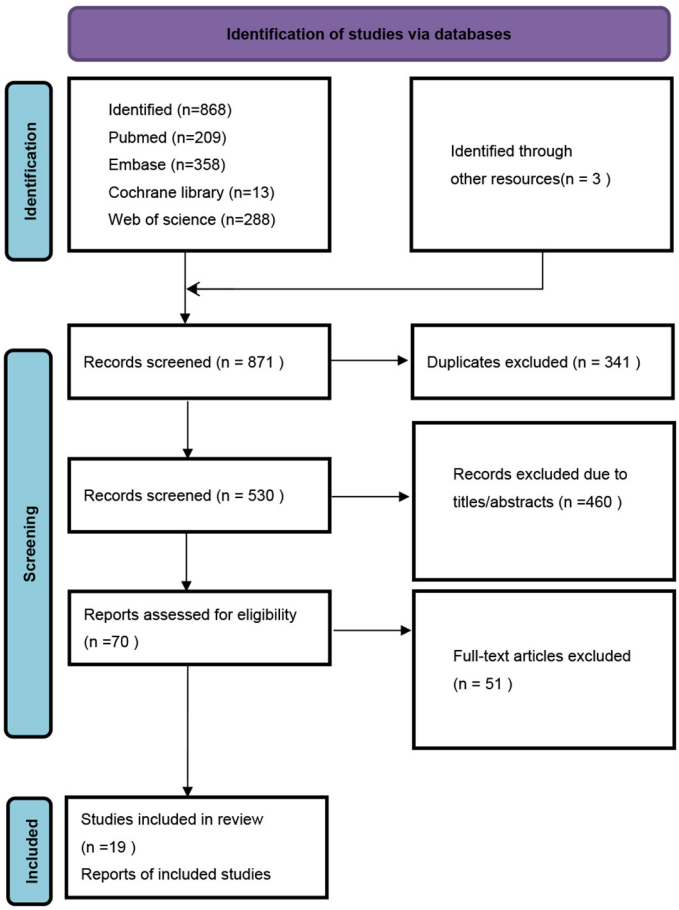

FIGURE 1
The flow diagram of identifying eligible studies.

melanoma (OR=35.00, 95% CI: 0.95-1292.43, *P*=0.053) as shown in (Figure 5). This indicates that TLS density is a strong predictor of ICI response in NSCLC. However, there wasn't a significant association between TLS density and response rates in HCC, NPC, and melanoma.

Subgroup analyses based on ICI application settings (adjuvant therapy, neoadjuvant therapy, systemic therapy) and ICI therapy approaches (ICI monotherapy, ICI combined with chemotherapy, ICI combined with other anticancer drugs) revealed no significant differences between subgroups, with low heterogeneity. (Supplementary Figures S1, S2).

Effect of high TLS on PFS according to tumor classification

Subgroup analysis on the association between high TLS density and PFS showed significant findings in RCC (HR=0.84, 95% CI: 0.74-0.96, *P*=0.011), UC (HR=0.60, 95% CI: 0.39-0.92, *P*=0.020), and EC (HR=0.50, 95% CI: 0.25-0.99, *P*=0.048), as well as NSCLC (HR=0.47, 95% CI: 0.28-0.79, *P*=0.004), as illustrated in (Figure 6). However, in GC patients, the link between high TLS density and prolonged PFS did not reach statistical significance (HR=0.91, 95% CI: 0.46- 1.81, *P*=0.787).

Publication bias

To assess the potential for publication bias, we constructed a funnel plot correlating each trial's effect size with its standard error (see appendix). Funnel plot asymmetry was evaluated using Egger's tests, with significant publication bias defined by a *P*-value < 0.1. We employed the trim-and-fill method to estimate the influence of publication bias on the interpretation of our findings. The studies exhibited mild heterogeneity, indicated by an I^2 value of 28.5% for the OR. (Supplementary Figure S3).

In addition, in 7 articles providing PFS, Egger tests indicated no significant publication bias. The analysis suggested minimal heterogeneity among the studies, with an I^2 value of 29.3% for the HR.

In the various subgroup analyses, the study's stability remained unaffected by differences in cut-off criteria (I^2=28.5%, *P*=0.120), tumor classification (I^2=29.5%, *P*=0.157), ICI application (I^2=28.5%, *P*=0.120) or ICI therapy (I^2=30.8%, *P*=0.137), thereby ensuring the reliability of our findings.

TABLE 1 Characteristics of 1752 patients with solid tumors treated with ICI.

Study	Region	Sample size	TLS-high/low	Response number	Cancer types	Determination method of TLS	Cut-off criteria	Cut-off value	NOS scores	Outcome measures	Stage of tumor	ICI application	ICI therapy
Jianjun Gao.2020 (8)	USA	26	13/13	13	UC	IHC	Density	0.155 TLS mm−2	6	RR, PFS	N. A	Neoadjuvant therapy	Anti-PD-L1 plus anti-CTLA-4
Lucile Vanherseck. 2021 (7)	France	328	105/223	78	Malignant tumor	H&E+IHC	Presence	0	8	RR	Stage IV	Systemic therapy	Anti-PD1/PD-L1 monoclonal antibodies
Xiaoyan Sun.2022 (9)	China	40	34/6	18	NSCLC	H&E+IHC	Density	TLS score	6	RR	Stage II-IIIA	Neoadjuvant therapy	Anti-PD-1 antibody plus chemotherapy
Takuya Mori.2022 (10)	Japan	19	9/10	3	GC	IHC	Density	Median percentage area (1.24%)	8	RR, PFS	Stage I-IV	Adjuvant therapy	Nivolumab
Jieqiong Liu. 2022 (11)	China	34	14/20	15	BC	IHC	Density	Mean area ≥30,000μm2	6	RR	Unresectable recurrent or metastatic	Systemic therapy	Camrelizumab combined with Apatinib and Eribulin
Y. Hayashi. 2023 (12)	Japan	34	17/17	9	EC	H&E+IHC	Density	0.325/mm2	8	RR, PFS	Stage I-IV	Adjuvant therapy	Anti-PD-1 antibody monotherapy
T. R. Cottrell. 2018 (13)	USA	20	11/9	16	NSCLC	H&E	Presence	0	6	RR	Stage I–IIIA	Neoadjuvant therapy	Nivolumab (anti- PD-1)
Justine Gantzer.2022 (14)	France	4	1/3	1	Thoracic tumors	IHC	Presence	0	6	RR	N. A	Systemic therapy	Immune checkpoint inhibitor
Shu D.H. 2022 (15)	USA	9	5/4	4	HCC	12-chemokine gene signature	Signature score	Hierarchical clustering	6	RR	Locally advanced	Neoadjuvant therapy	Nivolumab and cabozantinib
Xingchen Li. 2022 (16)	USA	298	78/220	69	UC	12-chemokine gene signature	Signature score	Top 25%	6	RR	Locally advanced or metastatic	Systemic therapy	Atezolizumab administration
Lucia Carril Ajuria.2022 (17)	France	274	126/148	66	RCC	IHC	Density	2 TLS	6	RR, PFS	Metastatic	Systemic therapy	Nivolumab monotherapy
Li Yuan.2023 (18)	China	21	10/11	13	NPC	H&E+IHC	Density	Mean area	6	RR	Recurrent/ metastatic	Systemic therapy	Immunotherapy combined with antiangiogenic targeted therapy
Kazumasa Komura. 2023 (5)	Japan	97	23/74	22	UC	IHC	Presence	0	6	RR, PFS	Metastatic	Systemic therapy	Checkpoint inhibitors Pembrolizumab

(Continued)

10.3389/fimmu.2024.1414884

TABLE 1 Continued

Study	Region	Sample size	TLS-high/low	Response number	Cancer types	Determination method of TLS	Cut-off criteria	Cut-off value	NOS scores	Outcome measures	Stage of tumor	ICI application	ICI therapy
Nicole L. Edmonds. 2022 (3)	USA	19	1/18	2	Melanoma	IHC	Presence	0	6	RR	Advanced melanoma	Systemic therapy	PD-1 blockade Pembrolizumab
Karlijn Hummelink. 2022 (19)	Netherlands	91	30/61	20	NSCLC	IHC	Presence	0	6	RR	Stage IV	Systemic therapy	PD-1 blockade Monotherapy
Takuya Mori.2021 (20)	Japan	10	3/7	2	GC	IHC	Density	CD20+ B cells (1.59 per field)	8	RR	Stage II-IV	Adjuvant therapy	PD-1 blockade with nivolumab
Wenhao Xu.2023 (21)	China	230	65/165	39	RCC	H&E+IHC	Presence	0	6	RR, PFS	Metastatic	Adjuvant therapy	Tyrosine kinase inhibitors (TKIs) and ICIs combination therapy
Fuhao Xu.2023 (4)	China	106	93/13	64	NSCLC	H&E+IHC	Presence	0	6	RR	Stage IB to IIIB	Neoadjuvant therapy	PD-1 inhibitors combined with taxanes and platinum-based drugs
Ying Liu.2023 (6)	China	80	37/43	30	NSCLC	H&E	Density	5 TLSs	6	RR, PFS	Stage IB- IIIB	Neoadjuvant therapy	Immune checkpoint inhibitors plus platinum-based chemotherapy

NSCLC, non-small cell lung cancer; UC, urothelial carcinoma; GC, gastric cancer; RCC, renal cell carcinoma; BC, breast cancer; EC, esophageal carcinoma; thoracic tumors, HCC, hepatocellular carcinoma; NPC, nasopharyngeal carcinoma; hematoxylin/eosin (H&E) staining, IHC, immunohistochemistry; RR, response rate; PFS, progression-free survival; N.A, not available.

10.3389/fimmu.2024.1414884

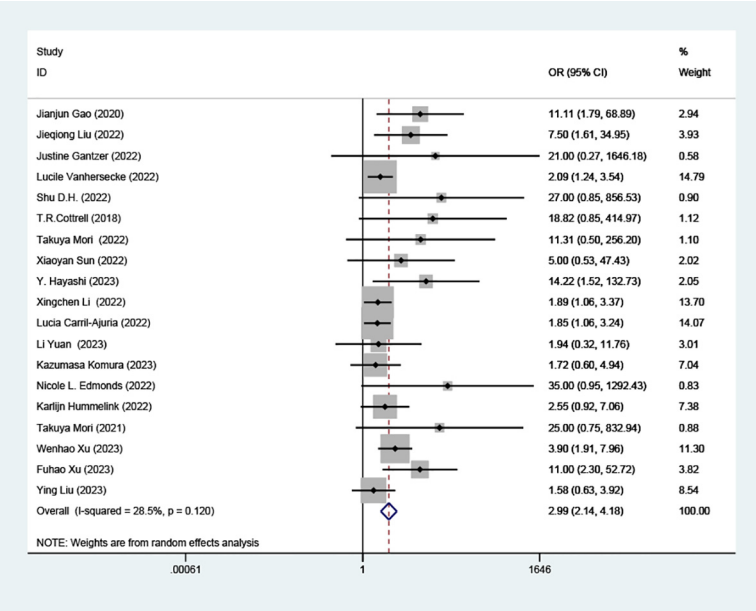

FIGURE 2
Comparison of response rates between TLS-high and TLS-low patients treated with ICI. OR, odd ratio; CI, confidence interval.

Discussion

Our study establishes a strong connection between TLS density and the efficacy of ICI therapy, highlighting the significant role of TLS density as a predictive marker for ICI response. Through rigorous analysis, our findings have been consistently validated across different cut-off criteria and a diverse array of cancer types, particularly demonstrating solid applicability in UC and RCC. The methods used to classify TLS— specifically presence and density—were found to strongly support our conclusions, underscoring their relevance in predicting therapy outcomes. This research positions TLS density as an indispensable tool for clinicians in devising personalized immunotherapy strategies, aiming to predict both the response rates and prognoses of patients.

TLS is an important component of the tumor microenvironment (TME). Its underlying mechanism involves augmenting tumor-related immunity. TLS contributes to the activation of anti-tumor immune responses by promoting an inflamed tumor microenvironment,

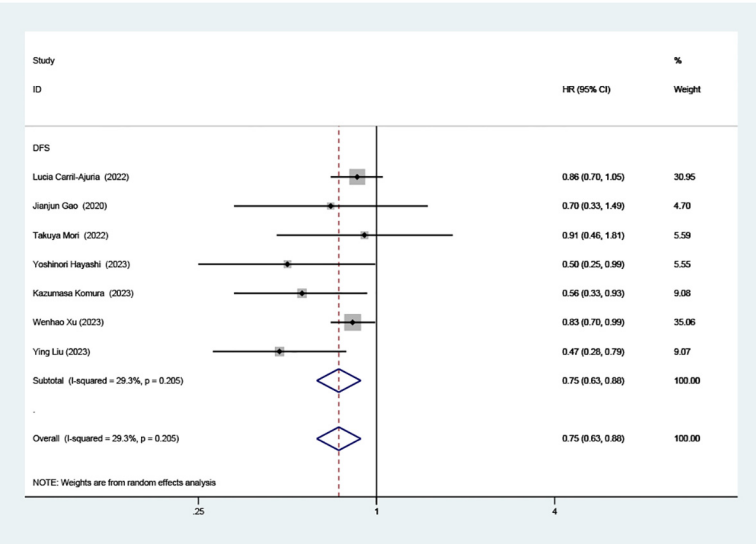

FIGURE 3
Estimates of progressive-free survival in patients treated with ICI and high TLS. HR, hazard ratios; CI, confidence interval.

10.3389/fimmu.2024.1414884

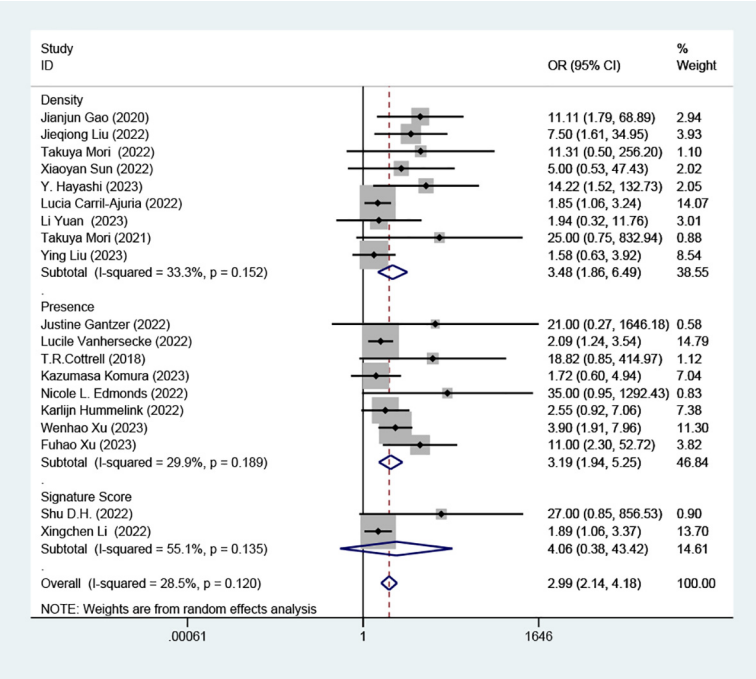

FIGURE 4
Comparison of response rates between TLS-high and TLS-low patients treated with ICI according to presence, density and signature score.

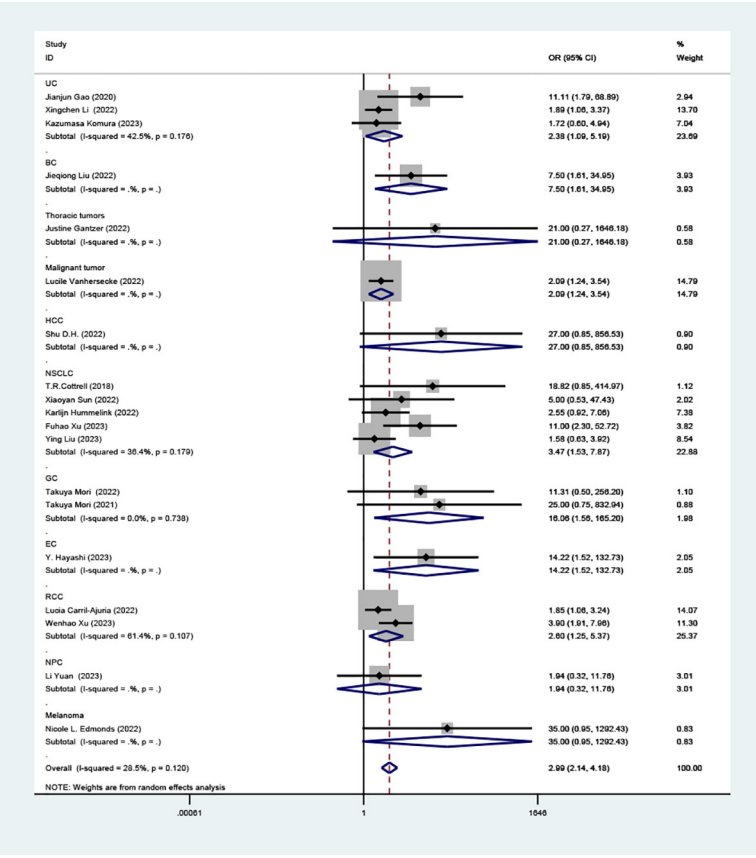

FIGURE 5
Comparison of response rates between TLS-high and TLS-low patients treated with ICI as subgroups according to tumor classification.

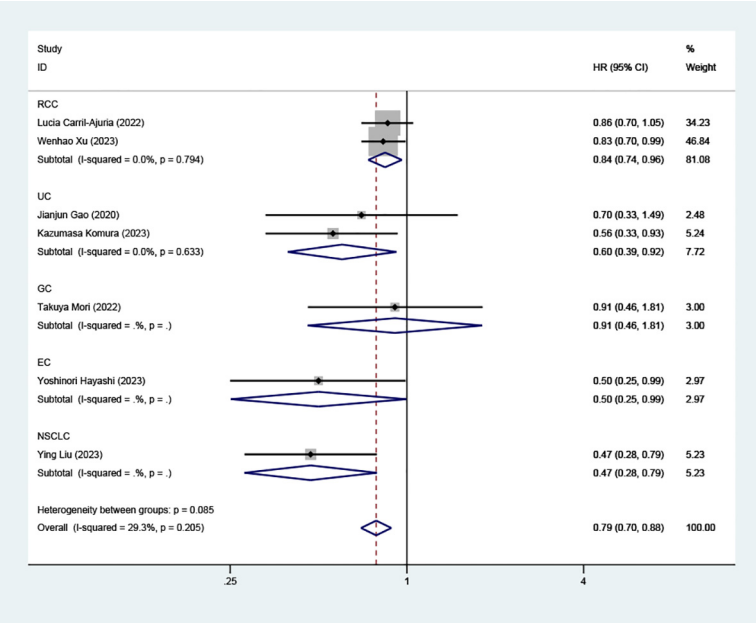

FIGURE 6
Comparison of progressive-free survival between TLS-high and TLS-low patients treated with ICI as subgroups according to tumor classification.

characterized by increased immune signatures including cytolytic activity, IFN-γ signaling, and MHC expression (16). Additionally, TLS is associated with a higher degree of immune cell infiltration within various tumor types, encompassing cytotoxic T lymphocytes, natural killer cells, and gamma delta T cells (22). Furthermore, the presence of mature dendritic cells, helper T cells, and B cells within TLS serves as a persistent source of stimulation for T cells linked to TLS (23).

It is worth noting that the presence of these immune cells also influences TLS activity. In a study on tumor-induced TLS in NSCLC patients, a higher density of Treg cells within TLS was associated with shorter patient survival, diminishing the favorable prognostic value of TLS (24). In another NSCLC study, the negative impact of high Treg cell density on patient survival was mitigated by a high density of B cells within TLS, with patients exhibiting a high B cell to low Treg cell ratio in TLS showing the best clinical outcomes (25). During the maturation of TLS, myeloid cells (such as mature dendritic cells), stromal cells (including follicular dendritic cells and follicular reticular cells), high endothelial venules, as well as B cells and T cells, all play indispensable roles (26). The functional differences of TLS are determined by the composition and proportion of its constituent cell types.

Interestingly, in a study on advanced-stage bladder cancer, CXCL13 was demonstrated as a surrogate marker for tumor TLS (27). As a chemoattractant, CXCL13 facilitates the formation of TLS and plays an important role in anti-tumor activity through the CXCL13/CXCR5 axis (28) and T follicular helper cells (29). However, further research is needed to explore its role in other solid tumors.

TLSs are ectopic lymphoid structures with a cellular composition similar to that of secondary lymphoid organs (SLOs), and therefore have comparable anti-tumor functions. However, TLSs also exhibit distinct characteristics that differentiate them from SLOs. Notably, unlike SLOs, TLSs are not encapsulated and are located within or around tumors, allowing them to exert a more direct and potent impact on the TME (26). This proximity may offer significant advantages in enhancing the effectiveness of ICI therapy.

TLS represents the continuous activation of the immune system during the anti-tumor immune process, thereby enhancing the body's overall immune response to the tumor. TLS, while linked to improved anti-tumor responses post-ICI therapy, is also closely associated with the incidence of immune-related adverse events (irAEs). In clinical research, TLS has been observed in the tissues of patients experiencing acute interstitial nephritis (AIN), a severe form of irAE (30). Additionally, studies have shown that in aged, tumor-bearing mice, therapy targeting the programmed death receptor (PD)-1 can induce irAE-like symptoms and multiorgan dysfunctions characterized by TLS-like lymphocytic infiltration in affected organs, suggesting a correlation between TLS presence and irAE incidence in patients treated with immune checkpoint blockade (ICB) (31). This evidence underscores the importance for clinicians to actively monitor TLS density and be especially vigilant for irAEs in patients with high TLS levels, enhancing patient care by anticipating and managing potential adverse reactions.

In the studies we included, we sought to identify the similarities and differences of TLS across different tumor types. However, discrepancies in the detection methods of TLS pose significant challenges. We hope that future research will employ consistent histological markers for TLS identification.

Our findings showed that higher TLS density is linked to prolonged PFS. However, overall survival (OS) is also a common cancer survival index. OS is usually assessed alongside PFS to evaluate therapeutic efficacy in clinical research. In the currently

available studies, high TLS density was consistently associated with longer OS (8, 10, 21).

Anti-PD1/PD-L1 antagonists are the most commonly used ICI treatments. However, in two studies on NSCLC and EC (12, 19), PD-L1 TPS/CPS did not show significant predictive value for ICI treatment efficacy. In contrast, our study found that TLS density is a significant predictor of ICI therapy effectiveness. This may be because TLS better reflects an individual's immune status, which is crucial in determining response to ICI therapy. The ICI-insensitive state is essentially an immune condition independent of tumor type, highlighting the importance of individual immune characteristics (32). Compared to markers like PD-L1 TPS/CPS and tumor mutational burden (TMB), TLS provides a more personalized assessment of immune status (33). Despite this, no studies have directly compared the predictive value of PD-L1 TPS/CPS with that of TLS, leaving it uncertain which marker is more reliable for predicting ICI therapy efficacy. Further research is needed to clarify this issue.

Apart from acting as markers of therapeutic efficacy, TLSs present significant potential as direct targets for immunotherapy. Current research efforts are investigating ways to induce the formation of TLS through diverse approaches, such as employing STING agonists, inhibiting endothelial Notch signaling, and implementing systemic delivery of αCD40 (34–36). These exploratory studies are designed to synthesize and assess the resulting data, aiming to lay the groundwork for the creation of more dynamic and potent treatments. This forward-thinking strategy seeks to transform cancer management by more effectively leveraging the body's immune system, offering a promising avenue for enhancing patient outcomes through immunologically centered interventions.

This study has several limitations. Primarily, our statistical analysis and validation efforts are centered on PD-L1, owing to the restricted use of other immune checkpoint inhibitors (ICIs) such as EGFR and HER2. This specificity suggests that our conclusions may not be universally applicable to treatments involving these other ICIs, advising a degree of caution in their broader application. Secondly, there is publication bias, but after statistical analysis, there is no effect on the stability of the results. Finally, the included studies and patients are limited, and our analyses are all based only on observational studies, potentially leaving some variables uncontrolled, highlighting the necessity for these results to be corroborated through large-scale, prospective studies dedicated to this area of research in the future.

Conclusion

Our research demonstrates a significant correlation between TLS density and the efficacy of ICI therapy, underscoring the potential of TLS density as a valuable predictor for treatment outcomes. Given these findings, we advocate for clinicians to routinely assess TLS density in cancer patients. Those identified with high TLS density may particularly benefit from ICI treatment. This approach could enable more personalized and effective immunotherapy strategies, potentially improving patient responses and outcomes.

Data availability statement

The original contributions presented in the study are included in the article/Supplementary Material. Further inquiries can be directed to the corresponding author.

Author contributions

BJ: Conceptualization, Data curation, Formal analysis, Investigation, Methodology, Project administration, Supervision, Validation, Visualization, Writing – original draft, Writing – review & editing. ZW: Data curation, Formal analysis, Methodology, Software, Validation, Visualization, Conceptualization, Funding acquisition, Writing – review & editing. YZ: Data curation, Investigation, Project administration, Software, Validation, Visualization, Formal analysis, Methodology, Supervision, Writing – original draft. XY: Data curation, Software, Validation, Visualization, Writing – review & editing, Investigation, Project administration, Resources.

Funding

The author(s) declare financial support was received for the research, authorship, and/or publication of this article. The work was supported by Liaoning Provincial Natural Science Foundation (2023020799-JH2/202).

Conflict of interest

The authors declare that the research was conducted in the absence of any commercial or financial relationships that could be construed as a potential conflict of interest.

Publisher's note

Supplementary material

The Supplementary Material for this article can be found online at: https://www.frontiersin.org/articles/10.3389/fimmu.2024.1414884/full#supplementary-material

References

1. Ma W, Xue R, Zhu Z, Farrukh H, Song W, Li T, et al. Increasing cure rates of solid tumors by immune checkpoint inhibitors. *Exp Hematol Oncol*. (2023) 12:10. doi: 10.1186/s40164-023-00372-8

2. Davis AA, Patel VG. The role of PD-L1 expression as a predictive biomarker: an analysis of all US Food and Drug Administration (FDA) approvals of immune checkpoint inhibitors. *J Immunother Cancer*. (2019) 7:278. doi: 10.1186/s40425-019-0768-9

3. Edmonds NL, Flores SE, Mahmutovic A, Young SJ, Mauldin IS, Slingluff CL Jr, et al. CD103 and periplakin are potential biomarkers for response of metastatic melanoma to pembrolizumab. *Melanoma Res*. (2022) 32:440–50. doi: 10.1097/cmr.0000000000000855

4. Xu F, Zhu H, Xiong D, Wang K, Dong Y, Li L, et al. Tertiary lymphoid structures combined with biomarkers of inflammation are associated with the efficacy of neoadjuvant immunochemotherapy in resectable non-small cell lung cancer: A retrospective study. *Thorac Cancer*. (2023) 15:172–81. doi: 10.1111/1759-7714.15175

5. Komura K, Tokushige S, Ishida M, Hirosuna K, Yamazaki S, Nishimura K, et al. Tertiary lymphoid structure and neutrophil-lymphocyte ratio coordinately predict outcome of pembrolizumab. *Cancer Sci*. (2023) 114:4622–31. doi: 10.1111/cas.15976

6. Liu Y, Xiong L, Chen Y, Cai R, Xu X, Wang T, et al. Complete pathological remission and tertiary lymphoid structures are associated with the efficacy of resectable NSCLC receiving neoadjuvant chemoimmunotherapy: A double-center retrospective study. *Hum Vaccines Immunotherapeutics*. (2023) 19:2285902. doi: 10.1080/21645515.2023.2285902

7. Vanhersecke L, Brunet M, Guégan JP, Rey C, Bougouin A, Cousin S, et al. Mature tertiary lymphoid structures predict immune checkpoint inhibitor efficacy in solid tumors independently of PD-L1 expression. *Nat Cancer*. (2021) 2:794–802. doi: 10.1038/s43018-021-00232-6

8. Gao J, Navai N, Alhalabi O, Siefker-Radtke A, Campbell MT, Tidwell RS, et al. Neoadjuvant PD-L1 plus CTLA-4 blockade in patients with cisplatin-ineligible operable high-risk urothelial carcinoma. *Nat Med*. (2020) 26:1845–51. doi: 10.1038/s41591-020-1086-y

9. Sun X, Liu W, Sun L, Mo H, Feng Y, Wu X, et al. Maturation and abundance of tertiary lymphoid structures are associated with the efficacy of neoadjuvant chemoimmunotherapy in resectable non-small cell lung cancer. *J immunotherapy Cancer*. (2022) 10. doi: 10.1136/jitc-2022-005531

10. Mori T, Tanaka H, Deguchi S, Yamakoshi Y, Miki Y, Yoshii M, et al. Clinical efficacy of nivolumab is associated with tertiary lymphoid structures in surgically resected primary tumors of recurrent gastric cancer. *PloS One*. (2022) 17. doi: 10.1371/journal.pone.0262455

11. Liu JQ, Wang Y, Tian ZL, Lin Y, Li H, Zhu Z, et al. Multicenter phase II trial of Camrelizumab combined with Apatinib and Eribulin in heavily pretreated patients with advanced triple-negative breast cancer. *Nat Commun*. (2022) 13:3011. doi: 10.1038/s41467-022-30569-0

12. Hayashi Y, Makino T, Sato E, Ohshima K, Nogi Y, Kanemura T, et al. Density and maturity of peritumoral tertiary lymphoid structures in oesophageal squamous cell carcinoma predicts patient survival and response to immune checkpoint inhibitors. *Br J Cancer*. (2023) 128:2175–85. doi: 10.1038/s41416-023-02235-9

13. Cottrell TR, Thompson ED, Forde PM, Stein JE, Duffield AS, Anagnostou V, et al. Pathologic features of response to neoadjuvant anti-PD-1 in resected non-small-cell lung carcinoma: a proposal for quantitative immune-related pathologic response criteria (irPRC). *Ann oncology: Off J Eur Soc Med Oncol*. (2018) 29:1853–60. doi: 10.1093/annonc/mdy218

14. Gantzer J, Davidson G, Vokshi B, Weingertner N, Bougouin A, Moreira M, et al. Immune-desert tumor microenvironment in thoracic SMARCA4-deficient undifferentiated tumors with limited efficacy of immune checkpoint inhibitors. *Oncologist*. (2022) 27:501–11. doi: 10.1093/oncolo/oyac040

15. Shu DH, Danilova L, Yuan L, Zhu Q, Wang H, Kagohara L, et al. 12-chemokine gene signature identifies major pathologic response in patients with hepatocellular carcinoma treated with neoadjuvant nivolumab and cabozantinib. *Cancer Res*. (2022) 82:1323–1323. doi: 10.1158/1538-7445.AM2022-1323

16. Li XC, Wan ZY, Liu X, Ou K, Yang L. A 12-chemokine gene signature is associated with the enhanced immunogram scores and is relevant for precision immunotherapy. *Med Oncol*. (2022) 39:43. doi: 10.1007/s12032-021-01635-2

17. Carril-Ajuria L, Desnoyer A, Meylan M, Dalban C, Naigeon M, Cassard L, et al. Baseline circulating unswitched memory B cells and B-cell related soluble factors are associated with overall survival in patients with clear cell renal cell carcinoma treated with nivolumab within the NIVOREN GETUG-AFU 26 study. *J Immunotherapy Cancer*. (2022) 10. doi: 10.1136/jitc-2022-004885

18. Yuan L, Jia GD, Lv XF, Xie SY, Guo SS, Lin DF, et al. Camrelizumab combined with apatinib in patients with first-line platinum-resistant or PD-1 inhibitor resistant recurrent/metastatic nasopharyngeal carcinoma: a single-arm, phase 2 trial. *Nat Commun*. (2023) 14:4893. doi: 10.1038/s41467-023-40402-x

19. Hummelink K, van der Noort V, Muller M, Schouten RD, Lalezari F, Peters D, et al. PD-1T TILs as a predictive biomarker for clinical benefit to PD-1 blockade in patients with advanced NSCLC. *Clin Cancer Res*. (2022) 28:4893–906. doi: 10.1158/1078-0432.Ccr-22-0992

20. Mori T, Tanaka H, Suzuki S, Deguchi S, Yamakoshi Y, Yoshii M, et al. Tertiary lymphoid structures show infiltration of effective tumor-resident T cells in gastric cancer. *Cancer Sci*. (2021) 112:1746–57. doi: 10.1111/cas.14888

21. Xu W, Lu J, Tian X, Ye S, Wei S, Wang J, et al. Unveiling the impact of tertiary lymphoid structures on immunotherapeutic responses of clear cell renal cell carcinoma. *MedComm*. (2024) 5:e461. doi: 10.1002/mco2.461

22. Wang M, Zhai R, Wang M, Zhu W, Zhang J, Yu M, et al. Tertiary lymphoid structures in head and neck squamous cell carcinoma improve prognosis by recruiting CD8(+) T cells. *Mol Oncol*. (2023) 17:1514–30. doi: 10.1002/1878-0261.13403

23. Ladányi A, Kiss J, Somlai B, Gilde K, Fejős Z, Mohos A, et al. Density of DC-LAMP(+) mature dendritic cells in combination with activated T lymphocytes infiltrating primary cutaneous melanoma is a strong independent prognostic factor. *Cancer immunology immunotherapy: CII*. (2007) 56:1459–69. doi: 10.1007/s00262-007-0286-3

24. Devi-Marulkar P, Fastenackels S, Karapentiantz P, Goc J, Germain C, Kaplon H, et al. Regulatory T cells infiltrate the tumor-induced tertiary lymphoïd structures and are associated with poor clinical outcome in NSCLC. *Commun Biol*. (2022) 5:1–16. doi: 10.1038/s42003-022-04356-y

25. Germain C, Devi-Marulkar P, Knockaert S, Biton J, Kaplon H, Letaïef L, et al. Tertiary lymphoid structure-B cells narrow regulatory T cells impact in lung cancer patients. *Front Immunol*. (2021) 12:626776. doi: 10.3389/fimmu.2021.626776

26. Teillaud JL, Houel A, Panouillot M, Riffard C, Dieu-Nosjean MC. Tertiary lymphoid structures in anticancer immunity. *Nat Rev Cancer*. (2024) 24:629–46. doi: 10.1038/s41568-024-00728-0

27. Groeneveld CS, Fontugne J, Cabel L, Bernard-Pierrot I, Radvanyi F, Allory Y, et al. Tertiary lymphoid structures marker CXCL13 is associated with better survival for patients with advanced-stage bladder cancer treated with immunotherapy. *Eur J Cancer*. (2021) 148:181–9. doi: 10.1016/j.ejca.2021.01.036

28. Gu X, Li D, Wu P, Zhang C, Cui X, Shang D, et al. Revisiting the CXCL13/CXCR5 axis in the tumor microenvironment in the era of single-cell omics: implications for immunotherapy. *Cancer Lett*. (2024) 605:217278. doi: 10.1016/j.canlet.2024.217278

29. Gutiérrez-Melo N, Baumjohann D. T follicular helper cells in cancer. *Trends Cancer*. (2023) 9:309–25. doi: 10.1016/j.trecan.2022.12.007

30. Singh S, Long JP, Tchakarov A, Dong Y, Yee C, Lin JS, et al. Tertiary lymphoid structure signatures are associated with immune checkpoint inhibitor related acute interstitial nephritis. *JCI Insight*. (2022). doi: 10.1172/jci.insight.165108

31. Tsukamoto H, Komohara Y, Tomita Y, Miura Y, Motoshima T, Imamura K, et al. Aging-associated and CD4 T-cell-dependent ectopic CXCL13 activation predisposes to anti-PD-1 therapy- induced adverse events. *Proc Natl Acad Sci USA*. (2022) 119:e2205378119. doi: 10.1073/pnas.2205378119

32. Santiago-Sánchez GS, Fabian KP, Hodge JW. A landscape of checkpoint blockade resistance in cancer: underlying mechanisms and current strategies to overcome resistance. *Cancer Biol Ther*. (2024) 25:2308097. doi: 10.1080/15384047.2024.2308097

33. Sautès-Fridman C, Petitprez F, Calderaro J, Fridman WH. Tertiary lymphoid structures in the era of cancer immunotherapy. *Nat Rev Cancer*. (2019) 19:307–25. doi: 10.1038/s41568-019-0144-6

34. Filderman JN, Appleman M, Chelvanambi M, Taylor JL, Storkus WJ. STINGing the tumor microenvironment to promote therapeutic tertiary lymphoid structure development. *Front Immunol*. (2021) 12:690105. doi: 10.3389/fimmu.2021.690105

35. Fleig S, Kapanadze T, Bernier-Latmani J, Lill JK, Wyss T, Gamrekelashvili J, et al. Loss of vascular endothelial notch signaling promotes spontaneous formation of tertiary lymphoid structures. *Nat Commun*. (2022) 13:2022. doi: 10.1038/s41467-022-29701-x

36. van Hooren L, Vaccaro A, Ramachandran M, Vazaios K, Libard S, van de Walle T, et al. Agonistic CD40 therapy induces tertiary lymphoid structures but impairs responses to checkpoint blockade in glioma. *Nat Commun*. (2021) 12:4127. doi: 10.1038/s41467-021-24347-7

Frontiers in Immunology

Explores novel approaches and diagnoses to treat immune disorders.

The official journal of the International Union of Immunological Societies (IUIS) and the most cited in its field, leading the way for research across basic, translational and clinical immunology.

Discover the latest Research Topics

See more →

Frontiers

Avenue du Tribunal-Fédéral 34
1005 Lausanne, Switzerland
frontiersin.org

Contact us

+41 (0)21 510 17 00
frontiersin.org/about/contact